

Lecture Notes in Mechanical Engineering

Sanjay Yadav

Prashant Kumar Jain

Pavan Kumar Kankar

Yogesh Shrivastava *Editors*


Advances in Mechanical and Energy Technology

Select Proceedings of ICMET 2021

 Springer

Lecture Notes in Mechanical Engineering

Editorial Board

Francisco Cavas-Martínez , Departamento de Estructuras, Construcción y Expresión Gráfica Universidad Politécnica de Cartagena, Cartagena, Murcia, Spain

Francesca di Mare, Institute of Energy Technology, Ruhr-Universität Bochum, Bochum, Nordrhein-Westfalen, Germany


Mohamed Haddar, National School of Engineers of Sfax (ENIS), Sfax, Tunisia

Young W. Kwon, Department of Manufacturing Engineering and Aerospace Engineering, Graduate School of Engineering and Applied Science, Monterey, CA, USA

Justyna Trojanowska, Poznan University of Technology, Poznan, Poland

Series Editors

Fakher Chaari, National School of Engineers, University of Sfax, Sfax, Tunisia

Francesco Gherardini , Dipartimento di Ingegneria “Enzo Ferrari”, Università di Modena e Reggio Emilia, Modena, Italy

Vitalii Ivanov, Department of Manufacturing Engineering, Machines and Tools, Sumy State University, Sumy, Ukraine

Lecture Notes in Mechanical Engineering (LNME) publishes the latest developments in Mechanical Engineering—quickly, informally and with high quality. Original research reported in proceedings and post-proceedings represents the core of LNME. Volumes published in LNME embrace all aspects, subfields and new challenges of mechanical engineering. Topics in the series include:

- Engineering Design
- Machinery and Machine Elements
- Mechanical Structures and Stress Analysis
- Automotive Engineering
- Engine Technology
- Aerospace Technology and Astronautics
- Nanotechnology and Microengineering
- Control, Robotics, Mechatronics
- MEMS
- Theoretical and Applied Mechanics
- Dynamical Systems, Control
- Fluid Mechanics
- Engineering Thermodynamics, Heat and Mass Transfer
- Manufacturing
- Precision Engineering, Instrumentation, Measurement
- Materials Engineering
- Tribology and Surface Technology

To submit a proposal or request further information, please contact the Springer Editor of your location:

China: Ms. Ella Zhang at ella.zhang@springer.com

India: Priya Vyas at priya.vyas@springer.com

Rest of Asia, Australia, New Zealand: Swati Meherishi at swati.meherishi@springer.com

All other countries: Dr. Leontina Di Cecco at Leontina.dicecco@springer.com

To submit a proposal for a monograph, please check our Springer Tracts in Mechanical Engineering at <https://link.springer.com/bookseries/11693> or contact Leontina.dicecco@springer.com

Indexed by SCOPUS. All books published in the series are submitted for consideration in Web of Science.

More information about this series at <https://link.springer.com/bookseries/11236>

Sanjay Yadav · Prashant Kumar Jain ·
Pavan Kumar Kankar · Yogesh Shrivastava
Editors

Advances in Mechanical and Energy Technology

Select Proceedings of ICMET 2021

 Springer

Editors

Sanjay Yadav
Physico-Mechanical Metrology
CSIR—National Physical Laboratory
New Delhi, Delhi, India

Pavan Kumar Kankar
Department of Mechanical Engineering
Indian Institute of Technology Indore
Indore, Madhya Pradesh, India

Prashant Kumar Jain
Design and Manufacturing
PDPM Indian Institute of Information
Technology
Jabalpur, Madhya Pradesh, India

Yogesh Shrivastava
Galgotias College of Engineering
and Technology
Greater Noida, Uttar Pradesh, India

ISSN 2195-4356

ISSN 2195-4364 (electronic)

Lecture Notes in Mechanical Engineering

ISBN 978-981-19-1617-5

ISBN 978-981-19-1618-2 (eBook)

<https://doi.org/10.1007/978-981-19-1618-2>

© The Editor(s) (if applicable) and The Author(s), under exclusive license to Springer Nature Singapore Pte Ltd. 2023

This work is subject to copyright. All rights are solely and exclusively licensed by the Publisher, whether the whole or part of the material is concerned, specifically the rights of translation, reprinting, reuse of illustrations, recitation, broadcasting, reproduction on microfilms or in any other physical way, and transmission or information storage and retrieval, electronic adaptation, computer software, or by similar or dissimilar methodology now known or hereafter developed.

The use of general descriptive names, registered names, trademarks, service marks, etc. in this publication does not imply, even in the absence of a specific statement, that such names are exempt from the relevant protective laws and regulations and therefore free for general use.

The publisher, the authors, and the editors are safe to assume that the advice and information in this book are believed to be true and accurate at the date of publication. Neither the publisher nor the authors or the editors give a warranty, expressed or implied, with respect to the material contained herein or for any errors or omissions that may have been made. The publisher remains neutral with regard to jurisdictional claims in published maps and institutional affiliations.

This Springer imprint is published by the registered company Springer Nature Singapore Pte Ltd. The registered company address is: 152 Beach Road, #21-01/04 Gateway East, Singapore 189721, Singapore

Preface

International Conference on Mechanical and Energy Technologies (ICMET-2021) has been the second international conference of its series organized by the Department of Mechanical Engineering of Galgotias College of Engineering and Technology, Greater Noida, Uttar Pradesh, India. It was considered a forum to bring together scientists, university professors, graduate students, and mechanical engineers, presenting new science, technology, and engineering ideas and achievements.

The conference attracted many participants working in various fields of engineering: design, mechanics, materials, energy, etc. More than 200 manuscripts were submitted to the conference, topics ranging from the latest research in the field of aerodynamics and fluid mechanics, artificial intelligence, rapid manufacturing technologies, remanufacturing, refrigeration and air conditioning, renewable energies technology, I.C. engines, turbo machinery metrology, and computer-aided design and inspection, etc.

Furthermore, we thank the management and director of Galgotias College of Engineering and Technology, Greater Noida, India, for their cooperation and support. We are thankful to all the members of the organizing committee for their contribution to organizing the conference. Last but not least, we thank Springer for its professional assistance and particularly Miss Priya Vyas who supported this publication.

New Delhi, India
Jabalpur, India
Indore, India
Greater Noida, India

Dr. Sanjay Yadav
Dr. Prashant Kumar Jain
Dr. Pavan Kumar Kankar
Dr. Yogesh Shrivastava

Contents

Application of Taguchi Approach to Optimize the Robot Spot Welding Parameters of JSC590RN Mild Steel	1
Abhishek Tyagi, Mukesh Kumar, Gaurav Kumar, Kapil Kumar Goyal, Eram Neha, and Mohd Atif Wahid	
Taguchi with GRA Based Optimization of Machining Parameters for End Milling of SS-304	11
Gaurav Kumar, Kapil Kumar Goyal, Mukesh Kumar, Ankit Tomer, Mohd Atif Wahid, and Eram Neha	
Design and Analysis of Knuckle Pin Using Different Materials in ANSYS	23
Birendra Kumar, Avaneet Kumar, Brahma Nand Agrawal, and Pawan Kumar Singh Nain	
The Current State and Potential of Canal Top Solar Power Plants in India	33
Chandrabhushan Vishwakarma, Ananya Dwivedi, and Devendra Yadav	
Weapon Detection Rope Roaming Human Safety Robot	43
Praveen Kumar Maduri, Priyanka Sharma, Himanshu Saini, Pradyuman Mani Tripathi, and Sakshi Singh	
Review and Real-World Usability of Magnetic Levitation Trains	53
Anshuman Srivastava, Anurag Chaturvedi, and S. Kennedy	
Entrepreneurial Women in the Culture of Cear�: The Case of Cearens Literature	63
Thais Helena Costa da Silva, Tatiana Monteiro Holanda, Janina Mirtha Gladys Moquillaza Sanchez, Matloobullah Khan, Sandeep Kumar Gupta, and Rohit Kaushik	

Machining of Composite Materials Using Different Conventional and Unconventional Machining Processes: A Short Review	75
Ankit Jain, Cheruku Sandesh Kumar, and Yogesh Shrivastava	
An Investigation on Effect of Hybrid Nanofluids in End Milling of Aluminium 6061 Alloy	85
Ravi Shanker Tiwari, Prameet Vats, Tushar Singh, Vineet Dubey, Pawan Kumar Arora, and Anuj Kumar Sharma	
Classification Methods for Labelled Data in Machine Learning	99
Ashish Kannojiya, Anuj Singh Rajput, and Anurag Shanu	
A Review of Solar Refrigeration for Cooling Applications	109
Sudhanshu Sharma, Aayush Tiwari, Abdur Rehman, Arbaz Ahmad Siddiqui, and Himanshu Yadav	
Experimental Analysis on Different Terrains Using Proprioceptive Information of One Leg of Quadruped Robot	119
Avinash Bhashkar and Anuj Kumar Sharma	
Advanced Cooling System Using Graphite Foam Heat Exchangers for Automobile	131
Kapil Rajput, Nayan Kumar Roy, and Aakash Crispin Martin	
Additive Manufacturing: A State of Art Review	139
Rahul Jain, Sudhir Kumar Singh, and Rajeev Kumar Upadhyay	
Investigation of Machining Parameters in Turning of AISI 316 Steel Using Palm Oil-Enriched Cutting Fluid	155
Tushar Singh, Prameet Vats, Vineet Dubey, Pawan Kumar Arora, Harish Kumar, and Anuj Kumar Sharma	
Real-Time Medical Infusion Set Drip Monitoring and Controlling Healthcare System	165
Praveen Kumar Maduri, Mohd. Alamgir Khan, and Rajesh Yadav	
Design and Fabrication of CNC Lathe Fixture for Cone	177
Sanjay Rathaur, Rishi Sanoria, Syed Haider Abbas Abidi, and Abdul Gani	
Utilization of Reinforced Palm Fibers Used for Composite Materials—A Review	187
Shailendra Kumar Verma, Vijay Kumar Dwivedi, and S. P. Dwivedi	
Development of Mathematical Model of Chiller System Considering Pressure as Well as Heat Losses Using C++ Programming	197
Pradeep Barnwal, Anil. P. Singh, Subhash Mishra, Neeraj Kumar, Sourabh Joshi, and Vikas Tiwari	

Generation of Electricity from Sound Waves 209
 Praveen Kumar Maduri, Avinash Kaushal Awasthi, Sachin Pandey,
 and Rajneesh Mishra

**Identification of Process Parameter Combination for Maximum
 Tensile Strength in 3D Printed Polylactic Acid Specimens Using
 Regression and ANOVA** 217
 Manohar Singh and Pushpendra S. Bharti

**Flammability and Moisture Absorption Behavior of Sugarcane
 Bagasse with Epoxy-Based Composite** 227
 Nitin Mukesh Mathur, Yashpal, and Akshay Jain

Progressive Collapse: A Review and Bibliometric Analysis 235
 Md Osaid Arshad, Shilpa Pal, and Mohammad Umair

**Analysis of Double Wishbone Suspension System Using
 MechAnalyzer** 245
 Abhay Dhar Dubey, Shubham Verma, and Pramod Kumar

**A Review and Emphasis on the Relevance of the Aluminum Based
 Hybrid Composite** 257
 Mohammad Arshad Jamal, Praveen Pachauri,
 and Shailendra Kumar Verma

**Descriptive Analysis of Performance and Emissions Characteristics
 of Diesel with Palm Oil and WCO** 267
 Sunny Kumar, Param Verma, Ranjeet Sharma, Satendra Choudhary,
 and Raj Kumar

**Influence of Process Parameter of Die-Sinking Electric Discharge
 Machining on Machining of Grade-2 Type Titanium** 277
 Kuwar Mausam

**A Broad Review of Biodiesel Feedstocks with Competency
 to Replace Diesel** 285
 Ashish Dewangan, Anand Bahadur Singh, Anurag Srivastava,
 Amartya Srivastava, Ankush Patel, and Ashok Kumar Yadav

Aerodynamic Drag Reduction Using Biomimics Inspired Surface 297
 Shubbhesh Ranjan and Faisal Shameem

**Effect of Social Network System (Peer Inputs) in Influencing
 the Consumer Conformity Behavior in Product Customization
 System** 307
 Anitha Nallasivam, C. Selvaraj, K. S. Kalavathy, Prabha Kiran,
 and Trupti Dandekar Humnekar

CFD Based Investigation of Thermophoresis Effect on Microparticles in Micro Channel	323
Niraj Kumar, Ashok Kumar Yadav, Ashish Dewangan, and Mukesh Kumar	
Design and Analysis of the Effect Through Different Aspect Ratio on Performance of VAWT	333
Ashish and P. Suresh	
Parametric Optimization of Fused Filament Fabrication Process	341
Sourabh Anand and M. K. Satyarthi	
A Perspective on Third-Generation Medium-Mn Steels for Automotive Application	351
Isha Apurwa, Jeetendra Kumar Yadav, and Ashok Kumar	
Review on Drag Reduction Using Biomimics Surface	359
Shubhesh Ranjan and Faisal Shameem	
Solar Industrial Process Heating Prospects in Indian Cement Industries	367
Niranjan Sahoo, Anil Kumar, and Samsher	
Recent Progress in the Design of Sustainable Thermoelectric Cooling Systems	375
Jitendra Mohan Giri and Pawan Kumar Singh Nain	
Solar Photovoltaic System (SPV) Installation in Indian Rural Households	387
Suyash Sharma, Affan Khan, Kapil Rajput, and Shrikant Vidya	

About the Editors

Dr. Sanjay Yadav is a Senior Principal Scientist and Head of the Pressure, Vacuum, and Ultrasonic Metrology Section and Professor of Academy of Scientific and Innovative Research (AcSIR), National Physical Laboratory, New Delhi, India. He received his Ph.D. in Physics from Meerut University in 1990. He has published more than 280 papers in international journals and conference proceedings and serves as Editor-in-Chief of the journal *MAPAN/Journal of Metrology Society of India*, published by Springer.

Dr. Prashant Kumar Jain is currently working as Associate Professor at Department of Mechanical Engineering, Indian Institute of Information Technology, Design and Manufacturing, Jabalpur. He obtained his Ph.D. from Indian Institute of Technology, Delhi. His major research interests include additive manufacturing, geometric modeling, CAD/CAM integration, and computational geometry. He has more than 85 publications to his credit, published in international peer-reviewed journals, and national and international conferences in India and abroad.

Dr. Pavan Kumar Kankar is currently working as an Associate Professor in Discipline of Mechanical Engineering, Indian Institute of Technology Indore. He has more than 14 years of teaching and research experience. Dr. Pavan has obtained his Ph.D. from Indian Institute of Technology Roorkee, India. He has published more than 100 papers in refereed journals and conferences. He had served as a guest editor in the special issue of various journals. He is a member of professional bodies like the American Society of Mechanical Engineers, Society for Reliability and Safety, Tribology Society of India, and International Institute of Acoustics and Vibration.

Dr. Yogesh Shrivastava has a result-oriented profile with more than 40 research papers in various journals of repute and conferences. Dr. Shrivastava has completed his Ph.D. in 2019 with specialization in manufacturing technology and has research interest in Fault diagnosis in machinery using signal processing techniques, unconventional machining of advanced materials, and fiber-reinforced plastic composite. He has reviewed many articles that are published in renowned journals. Currently,

he is working as Assistant Professor and Research Coordinator in the Department of Mechanical Engineering at Galgotias College of Engineering and Technology, Noida, India.

Application of Taguchi Approach to Optimize the Robot Spot Welding Parameters of JSC590RN Mild Steel



Abhishek Tyagi, Mukesh Kumar, Gaurav Kumar, Kapil Kumar Goyal, Eram Neha, and Mohd Atif Wahid

Abstract This research focuses on using a KUKA robot to spot weld low carbon steel JSC 590RN cold-rolled sheet. This paper aims to determine the influence of welding input factors on T-S strength. To analyze, the impact of various input parameters, namely electrode dia., electrode force, current, and weld time on tensile-shear (T-S) strength of spot welding, joints are produced on low carbon steel. Taguchi L18based design was utilized to conduct this experiment. Ratio of signal and noise was enforced to measure the impact of welding input factor on the T-S strength. To find out the contributing roles of every parameter ANOVA and F-test were applied. A1B2C2D3 are the optimum spot-welding parameters to maximize the T-S strength. The outcomes of ANOVA test predict that the current (50.67%) is a significant contributing factor ensued by the electrode force (7.21%), electrode diameter (6.01%), and weld time (4.32%). The result is confirmed and validated by a confirmation experiment that indicates it is feasible to increase the spot joint standard up to 2.06%.

Keywords JSC590RN · Taguchi · KUKA robot · Tensile strength

1 Introduction

Electrical spot welding is the earliest resistance welding method applied in the manufacturing world for a long time due to more considerable electrical resistance and lower thermal conductivity (λ) [1]. Due to several advantages such as low cost of

A. Tyagi · M. Kumar · G. Kumar (✉)
Vidya College of Engineering, Meerut, India
e-mail: gaurav.me86@gmail.com

K. K. Goyal
Dr. B. R. Ambedkar National Institute of Technology, Jalandhar, Punjab, India

E. Neha
Galgotias College of Engineering and Technology, Greater Noida, India

M. A. Wahid
Delhi Technical Campus, Greater Noida, India

joining, easy process, and high productivity, RSW is used in many industries. If the level of current (I) and nugget size increases, then the joint's strength also decreases [2]. In the RSW process, mainly aluminum and low carbon steel sheet is utilized for coalescence. Various essential parameters manage the spot-welding procedure, i.e., dia. of the electrode, electrode pressure; weld current, weld time, electrode, and sheet materials. The best qualitative parameters of spot welding are the size of nugget diameter, the value of heat affected zone, and tensile load. The outcomes of such output characteristics depend on the RSW input factors [3]. During the RSW process, a large amount of current is needed for melting and joining the metal sheet, which will cause to warm the electrode and reduce the continuance of the electrode cover. So, to reduce this issue of extreme electrode heating, water is utilized as a coolant [4]. RSW is a regular coalescence process in the automobile and manufacturing industry, and it supersedes the other. In the RSW process, steel and other light sheet alloys faced many difficulties. These difficulties are extra heating, flushing, and melting [5]. It is the metal sheet amalgamating procedure in many areas, like automobiles, aircraft, railways, spacecraft fabrication, and domestic appliances. There are three to six thousand spot welds used in any automotive body, indicating the RSW [6].

Tutar et al. [7] have selected an aluminum compound (AA3003-H12) sheet to optimize the FSSW parameters by applying the L_9 Taguchi technique. They selected plunge time (second), dwell time (second), and rotation speed (revolution per minute) are the three process parameters to determine the optimization outcomes of T-S strength and found that the plunge depth was the essential parameter among the entire factor. Miland and Ghogale [8] used Taguchi methodology to improve the quality of MIG welding. This investigation aims to find the excellent value of penetration by taking the main process factor of MIG welding, such as current, voltage, and flow of gas. Ananda [9] also used the Taguchi design to determine the influence of input factors on T-S load. The ANOVA test is conducted to examine the outcomes and found that the current contributes more than other parameters. Muthu [10] experimented on SS 316 sheet to improve the RSW parameters by Taguchi L_{27} design. As reported in this research, it has been found that the electrode diameter is the very crucial factor of T-S strength relative to others parameters. Dhawale and Name [11] have done an investigation to predict the tensile and shear strength of spot welding by applying the L_{27} arrays of Taguchi design. Input factors and selected input factors are chosen to investigate the T-S load. Singh et al. [12] presented a review paper to discuss the contribution of the Taguchi and GRA approaches to the improvement of milling input factors. They did the shoulder milling on AA6063 T6 by using Taguchi and GRA. Kumar et al. [13] experimented with optimizing the end milling on SS 304 by the Taguchi method. Muhammad et al. [14] presented an investigation to optimize the input factor of RSW to increase the weld quality. They took nugget size and HAZ as quality parameters and applied the Taguchi L_9 OA technique. Ghazali et al. [15] have investigated the optimization of the RSW factor by using the Taguchi L_9 design. They took three input parameters to determine quality characteristics, i.e., tensile-shear strength and nugget diameter. Their research indicates that the weld current (I) was the supreme factor that affected the load strength and nugget diameter. Sao and Banchor [16] experimented with optimizing the spot-welding factor by applying the

GRA method. They conclude that the current is the very vital parameter to find out the optimized weld characteristics. Goel et al. [17, 18] have done friction stir welding to join the two different materials, namely AA-7475-T761 and AISI 304, using the L_8 Taguchi technique. They used various parameters to determine the highest value of UTS and found rotational tool speed is the most contributing factor.

The research paper analysis indicates that the RSW issue of mild steel (JSC 590RN) has many problems: melting of electrode, ruptured, porousness, weld area, and challenging to find out the standard of welds like T-S load. The difficulty related to the coalescence of JSC 590RN by the KUKA robot was the primary objective for selecting the job metals. The effect of input factors of RSW on T-S load was observed. Taguchi L_{18} design was enforced for the optimization of electrical spot welding.

2 Materials and Method

2.1 Workpiece Design

Low carbon steel (JSC590RN), CR sheets with a thickness of 1.2 mm, was exercised to weld the workpiece. $160 \times 50 \times 1.2$ mm is the size of one sample with a lapping of forty millimeters on other samples having a similar size as illustrated in Fig. 1. Present material sheet (description–JSC590RN, Commodity–cold-rolled sheet, Bureau of Indian standard category–IS 513(Part II), ISC 590 LA) is mainly consumed for producing automotive equipment, mainly used in cross-member dash (upper side) of the automobile.

For the chemical composition test, a small part is removed from the JSC590RN sheet. The constitution of the sheet materials is shown below in Table 1.

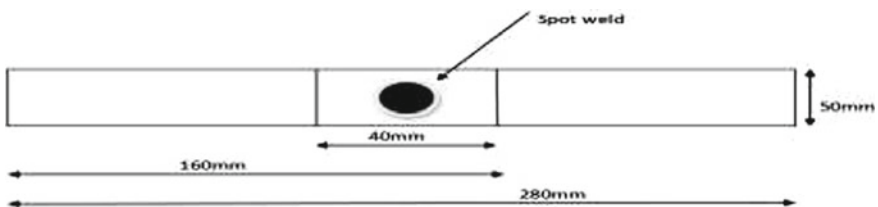


Fig. 1 Lap joint for spot welding

Table 1 JSC590RN chemical composition

Content	Value %
C	0.144
Mn	1.37
Si	0.240
P	0.013
S	0.003

2.2 Experimental Procedure

Four input factors are selected in the present work. Their values are under the Taguchi L18 technique design illustrated in Table 2.

All experimental trials are conducted in VEEGEE Industrial Enterprises, Faridabad, by KUKA robot. And The Taguchi L18 technique was used to conduct all of the experiments. A UTM (TUE-C-400) was used to determine the T-S strengths of all samples (illustrated in Fig. 3). Failure of the specimen before and after testing is also shown in Fig. 4. (Fig. 2).

The working prerequisite of this research is illustrated in Table 3.

Table 2 Spot-welding factors at various scales

Symbol	Factors	Scale1	Scale2	Scale3
A	Electrode (dia./L) (mm)	13/23	16/23	–
B	Electrode force (N)	2650	2750	2850
C	Weld current (Ampere)	9700	9800	9900
D	Welding time (cycle)	10	12	14

Fig. 2 Kuka robot

Fig. 3 UTM**Fig. 4** Failure of the specimen**Table 3** Spot-welding prerequisite

Prerequisite	Specification
Materials	Low carbon steel (JSC 590RN) size 160 mm × 50 mm × 1.2 mm
Welding instrument	Kuka robot
Calibrating appliances	UTM

3 Outcomes and Discussion

3.1 S/N Ratio [Signal-To-Noise Ratio]

Acceptable and unacceptable values are determined by the ratio of “signal” to “noise” [19]. The features are grouped into three groups based on quality engineering (QE): larger is better, smaller is better, and nominal is best. The T-S strength needs to be increased. Likewise, Heat affected zone (HAZ) requires a lesser value [20]. The descriptions of this equation are referred to in [21]. In this investigation, for T-S strength is higher is better is chosen. Equation (1) is used for maximization of T-S strength.

$$S/N = -10 \times \log\left(\sum(1/Z^2)/n\right) \quad (1)$$

where n is the no. of the test, Z = observed data.

Taguchi L18 experimental method was used for all 18 experimental trials. The T-S strength of all the joints can be determined by the UTM. The measured values of T-S strength and their S/N ratio are illustrated in Table 4.

Table 4 Taguchi OA with T-S strength and their S/N ratio

Run No.	A	B	C	D	T-S (kN)	S/N ratio
1.	1	1	1	1	11.31	21.07
2.	1	1	2	2	19.91	25.98
3.	1	1	3	3	21.09	26.48
4.	1	2	1	1	14.41	23.17
5.	1	2	2	2	24.47	27.77
6.	1	2	3	3	23.93	27.58
7.	1	3	1	2	13.50	22.61
8.	1	3	2	3	16.58	24.39
9.	1	3	3	1	14.77	23.39
10.	2	1	1	3	12.23	21.75
11.	2	1	2	1	15.75	23.95
12.	2	1	3	2	13.35	22.51
13.	2	2	1	2	10.46	20.39
14.	2	2	2	3	17.20	24.71
15.	2	2	3	1	20.09	26.06
16.	2	3	1	3	15.76	23.95
17.	2	3	2	1	18.65	25.41
18.	2	3	3	2	17.13	24.68

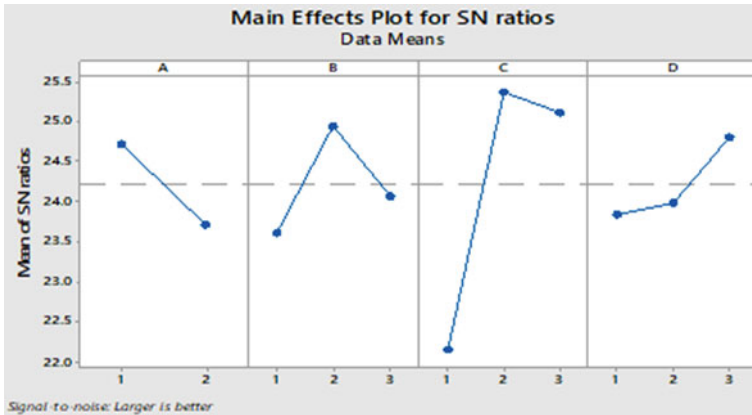


Fig. 5 Average of S/N ratio

Table 5 S/N ratio response table

Symbol	Input parameters	Scale1	Scale2	Scale3	Maxi-Mini
A	Electrode diameter	24.72	23.71	-	-1.01
B	Electrode force	23.62	24.95	24.07	-1.32
C	Welding current	22.16	25.36887	25.11539	0.25
D	Weld time	23.84	23.98895	24.80992	0.15

The total average of S/N ratio = 24.21

From Fig. 5, it was noticed that the S/N value of electrode diameter is reducing on raising their levels. Although the S/N values of electrode force, weld current, and welding time raised their second levels. A dashed line shows the average of S/N value, i.e., 24.21. Table 5 illustrated that the distinction among the maximum and minimum levels of the S/N values of parameters C (0.25) was the maximum, chased by the parameters D (0.15), A (-1.01), and B (-1.32). Figure 5 further shows that the signal-to-noise values are highest at first, second, second, and third levels of input parameters. So $A_1B_2C_2D_3$ is the most acceptable conjunction of quality features for spot-welding procedures.

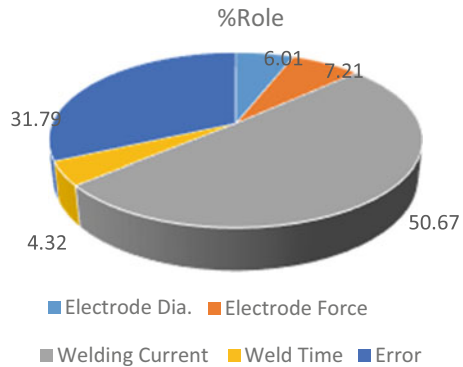
3.2 ANOVA

The outcomes of the Taguchi method are analyzed using an ANOVA analysis. It provides the relative influences of each researched parameter as well as the impact of parameter interactions. The outcomes of ANOVA illustrated in Table 6 verify that out of all input parameters of spot welding, welding current contributes more in contrast to remains input factors. Besides, electrode diameter, electrode force, and

Table 6 Outcomes of ANOVA

Input factor	SS	Dof	MS	F ratio	Percentage role
Electrode dia	4.55	1	4.55	1.89	6.01
Electrode force	5.45	2	2.72	1.13	7.21
Welding current	38.30	2	19.15	7.97	50.67
Weld time	3.27	2	1.63	0.68	4.32
Error	24.02	10	2.40		31.79
Total	75.58	17			100.00

Fig. 6 A % Contribution of input factors



weld time have a minor impact on T-S strength because for these input factors, the value of the F ratio is lesser than 4. The error measured was 31.79%.

Distinguish coefficient (α) lies between 0 and 1, i.e., and here $\alpha = 0.5$, then the confidence level of ANOVA was 95%.

From ANOVA, the most contributing factor is welding current, i.e., 50.67% chased by the electrode force (F), electrode diameter (d), and weld time (t) are 7.21%, 6.01%, and 4.32%, respectively. As shown in Fig. 6, the weld current is the utmost vital process parameter when it comes to collating with another process factor.

3.3 Confirmation Test

To determine the optimization result of this research, the Taguchi L_{18} method was used. Table 7 illustrates that the investigation outcomes of tensile-shear strength is in most excellent deal with the prediction of the investigation design.

According to Table 7, the signal-to-noise ratio changed from 27.20 to 27.77 (an increment of 2.06%) due to an increase of tensile strength from 22.91 KN to 24.47 KN (an increment of 6.38%), which illustrates that the best combination (A1B2C2D3) is good enough for maximize the tensile-shear strength (T-S strength).

Table 7 Outcomes of confirmation experiment

	Predication	Experiment	% Change
Level	A ₁ B ₂ C ₂ D ₃	A ₁ B ₂ C ₂ D ₃	
T-S (KN)	22.91	24.47	6.38
S/N ratio	27.20	27.77	2.06

4 Conclusions

On formulated the observation and result outcome, the various conclusions can be made:

- The best combination for the T-S strength of the spot-welding process is A₁B₂C₂D₃.
- From ANOVA, the most contributing factor is welding current, i.e., 50.67% chased by the electrode force (F), electrode diameter (d), and weld time (t) are 7.21%, 6.01%, and 4.32%, respectively. This implies that, in contrast to the other input factor, the weld current is the most important process parameter. According to this technique, the outcomes can be enhanced by up to 2.06%.

In the upcoming time, it is possible to increase the outcomes by applying different optimization methods.

References

1. Raut M, Achwal V (2014) Optimization of spot-welding process parameters for maximum tensile strength. *Int J Mech Eng Robo Res* 3(4):507–517
2. Mat Yasin NA, Alisibramulisi A, Salleh Z, Ghazali FA, Pawan A (2020) Optimization of resistance spot welding (RSW) parameters by using Taguchi method. *Int J Innov Technol Explor Eng* 9(3):2795–2800
3. Thakur AG, Rao TE, Mukhedkar MS, Nandedkar VM (2010) Application of Taguchi method for resistance spot welding of galvanized steel. *ARNP J Eng App Sci* 5(11):22–26
4. Rawal MR, Kolhapure RR, Sutar SS, Shinde VD (2016) Optimization of resistance spot welding of 304 steel using GRA. *Int J* 3(9):492–499
5. Bilici MK (2012) Application of Taguchi approach to optimize friction stir spot welding parameters of polypropylene. *Mat Des* 35:113–119
6. Pandey AK, Khan MI, Moeed KM (2013) Optimization of resistance spot welding parameters using Taguchi method. *Int J Eng Sci Tech* 5(2):234–241
7. Tutar M, Aydin H, Yuce C, Yavuz N, Bayram A (2014) The optimisation of process parameters for friction stirs spot-welded AA3003-H12 aluminium alloy using a Taguchi orthogonal array. *Mat Des* 63:789–797
8. Ghogale MM, Patil SA (2013) Optimisation of process parameters of MIG welding to improve quality of weld by using Taguchi methodology. *Int J Eng Res Tech* 2(12):3677–3685
9. Ananda KV (2013) Analysis of effect of process parameters on resistance spot welding shear strength. *Int J Sci Res* 2(11):224–227
10. Muthu P (2019) Optimization of the process parameters of resistance spot welding of AISI 316l sheets using Taguchi method. *Mechan Mech Eng* 23(1):64–69

11. Dhawale PA, Name BR (2019) Prediction of weld strength by parametric optimization of resistance spot welding using Taguchi method. *AIP Conf Proc* 2200(1):020287
12. Singh OP, Kumar G, Kumar M (2019) Multi performance optimization shoulder milling process parameters of AA6063 T6 aluminum alloy by Taguchi based GRA. *Int J Innov Technol Explor Eng* 8(10S):420–425
13. Kumar G, Kumar M, Tomer A (2021) Optimization of end milling machining parameters of SS 304 by Taguchi technique. *Record advance mechanics engineering Springer, Singapore*, pp 683–689
14. Muhammad N, Manurung YH, Hafidzi M, Abas SK, Tham G, Haruman E (2012) Optimization and modeling of spot-welding parameters with simultaneous multiple response consideration using multi-objective Taguchi method and RSM. *J Mech Sci Tech* 26(8):2365–2370
15. Ghazali FA, Manurung YH, Mohamed MA (2014) Multi-response optimization using Taguchi method of resistance spot welding parameters. In: *Application mechanics materialy transactions technology Pub. Ltd.* vol 660, pp 120–124
16. Sao M, Banchor R (2016) Optimization of resistance spot weld parameters using grey relational analysis. *Int J Sci Res Dev* 4(10):375–378
17. Goel P, Saxena AK, Wahid MA, Rathore S, Sharma N, Mishra KM (2020) Influence of friction stir welding parameters on mechanical properties of dissimilar AA7475 to AISI 304. *IOP Conf Ser: Mat Sci Eng* 802(1):012010
18. Goel P, Mohd AW, Sharma N, Siddiquee AN, Khan ZA (2019) Effect of Welding parameters in friction stir welding of stainless steel and aluminum alloy. In: *Advances in industrial and production engineering. Springer, Singapore*, pp 815-823
19. Tyagi A, Kumar G, Kumar M, Neha E, Wahid MA (2021) Experimental investigation for optimization of robot spot welding parameters on low carbon steel JSC 590RN. *Production material science*
20. Tyagi A, Kumar G, Kumar M, Wahid MA (2021) Analysis the effect of process parameters on robot spot welding of JSC 590RN mild steel using Taguchi based GRA. *Production material science*
21. Siddiquee AN, Khan ZA, Mallick Z (2010) Grey relational analysis coupled with principal component analysis for optimisation design of the process parameters in in-feed centerless cylindrical grinding. *Int J Adv Manuf Tech* 46(9):983–992

Taguchi with GRA Based Optimization of Machining Parameters for End Milling of SS-304



Gaurav Kumar, Kapil Kumar Goyal, Mukesh Kumar, Ankit Tomer, Mohd Atif Wahid, and Eram Neha

Abstract A mechanical component has to experience variable loads during operation, which causes fatigue failure. High tool wear, surface roughness, and low material removal rate (MRR) are associated with stainless steel machining (SS-304). This work performed 18 end milling operations on SS-304 according to Taguchi's L_{18} orthogonal array (O.A.). The analysis was completed using Taguchi, Gray relational analysis (GRA), and Analysis of Variance (ANOVA). A validation test was performed to check the results related to the surface integrity. The outcomes of the study reveal that the machining conducted with coolant, feed rate (2500 mm/min), depth of cut (0.4 mm), and speed (1500 r.p.m) resulted in the best multi-performance features achieved for end-milling of SS-304. In addition, ANOVA's results show that all four processing parameters significantly affect multiple performances, with the most significant contribution of feed (39.97%) followed by the depth of cut (24.98%), coolant (13.52%), and speed (7.97%). Under the set of parameters after optimization, it seems that response parameters, i.e., SR, and MRR were affected favorably.

Keywords Surface roughness (SR) · MRR · End milling · Optimization · Multi-performance

G. Kumar (✉) · M. Kumar · A. Tomer
Vidya College of Engineering, Meerut, India
e-mail: gaurav.me86@gmail.com

K. K. Goyal
Dr. B. R. Ambedkar National Institute of Technology, Jalandhar, Punjab, India

M. A. Wahid
Delhi Technical Campus, Greater Noida, India

E. Neha
Galgotias College of Engineering and Technology, Greater Noida, India

1 Introduction

Machining surfaces that are exclusively considered in Surface integrity (SI) requires a gathered information on changes during machining under lower conditions. Material processing conditions are assessed by surface integrity in respect of safety, dependability and to satisfy the needs of complex service circumstances [1]. One of the main reasons for fatigue failure which is associated with stress concentration and endurance strength is poor surface integrity of component [2].

In present scenario, milling is a very cooperative method that is vastly used in manufacturing of mechanical components used in buildings, farming machines, mining, automobile, earthmovers, etc. all such components are normally composed of stainless steel 304(SS-304). SI can be defined using microhardness, MRR, SR, and strain developed in machine surface and these all-outcomes changes are responsible for change in microstructure of surface after machining. Important studies of stainless steel have been further explained.

Sun et al. [3] improved surface roughness of Ti-6Al-4 V through end milling. Sijo et al. [4] discovered that it is difficult and time-consuming to perform turning process for optimization. Taguchi is used to perform the optimization. Karnwal et al. [5] used GRA (Gray relational analysis) along with Taguchi to find performance features of diesel engines. Lin and Ho [6] discovered that Taguchi process data might be used with GRA to estimate the affecting order of machining parameters. Siddiquee et al. [7] performed deep drilling optimization process for improving the surface quality. Singh et al. [8, 9] improved the surface integrity of AA6060T6 alloy through shoulder milling. Microstructure testing was performed before and after milling in 18 trials based on Taguchi-based GRA. Kumar et al. [10] have done end milling on VMM to improve the surface quality of SS 304 using L_{18} Taguchi technique. Kumar et al. [11] have done deep drilling on SS 321 for improving machining properties. To optimize the drilling settings, the Taguchi-based GRA was utilized. Goel et al. [12, 13] have done friction stir welding to join the two different materials, namely AA-7475-T761 and AISI 304, using the L_8 Taguchi technique. They used various parameters to determine the highest value of UTS and found rotational tool speed is the most contributing parameter.

After reviewing numerous research publications, which revealed that depth of cut, feed, tool size, speed, coolant, and other machining factors affect surface integrity, tool wear, MRR, microhardness, and surface strain in the end milling of stainless steel. As a result, in this research, a plan of experiment has been designed for improving surface roughness (SR) and material removal rate (MRR) by considering end milling factors like coolant, spindle speed, feed rate, and depth of cut, taking resource availability and feasibility into account.

Fig. 1 SS-304 pieces

2 Investigational Details

2.1 Sample Details

18 Pieces of stainless steel 304 were opted for investigation as shown in Fig. 1. Result of constituent test is shown in Table 1.

2.2 Experimental Setup

End milling operations on the SS-304 pieces were performed using a vertical milling machine (VMM). Table 2 depicts the working settings in this study. Figure 2 illustrates an overview of the process used in the current study.

Table 1 Spectroscopy Test Result for SS-304 Sample

Name of constituents	Fe	C	Si	Mn	S	Cr	Al	Cu	Nb	V
(% by wt)	70.37	0.042	0.345	1.76	<0.005	18.38	<0.01	0.361	0.049	0.066

Table 2 Working settings

Settings	Description
Size of sample	SS-304 (80 × 50 × 10 mm ³)
Cutting tool used	Solid Carbide tool (M, Ø12, CR 2.5)
Machine used	VMM (BMV 60 T.C. 24)
Coolant	Blastocut-4000
Tester	Roughness tester



Fig. 2 Experimental setup for end milling operation

Table 3 End milling parameters with their values

Notation	A	B	C	D
Parameter	Coolant	Feed (mm/min.)	DOC (mm)	Speed (r.p.m.)
1	On	1500	0.2	1500
2	Off	2000	0.3	2500
3	–	2500	0.4	3500

2.3 Plan of Experiment

Milling machining parameters like end milling with their scales are illustrated in Table 3.

2.4 Recording of Response Characteristics

Each sample had an average of three roughness levels determined using a roughness tester. The MRR is calculated as follows:

$$\text{Material Removal Rate} = \frac{w \times f \times d}{60} \text{mm}^3/\text{sec} \quad (1)$$

where f is feed measured in millimeters per minute, w is block width measured in millimeters (in this study, 10 mm), and d is depth of cut in millimeters.

Values of SR (Ra) and MRR are illustrated in Table 4.

Table 4 Plan of L₁₈ orthogonal array

Experiments	A	B	C	D	Ra (μm)	MRR (mm ³ /s)
1	P	1500	0.2	1500	1.91	50
2	P	1500	0.3	2500	1.21	75
3	P	1500	0.4	3500	1.75	100
4	P	2000	0.2	1500	2.35	66.66
5	P	2000	0.3	2500	2.3	100
6	P	2000	0.4	3500	2.18	133.33
7	P	2500	0.2	2500	1.96	83.33
8	P	2500	0.3	3500	1.79	125
9	P	2500	0.4	1500	2.15	166.66
10	A	1500	0.2	3500	1.5	50
11	A	1500	0.3	1500	1.45	75
12	A	1500	0.4	2500	1.38	100
13	A	2000	0.2	2500	1.41	66.66
14	A	2000	0.3	3500	1.08	100
15	A	2000	0.4	1500	1.81	133.33
16	A	2500	0.2	3500	1.83	83.33
17	A	2500	0.3	1500	1.98	125
18	A	2500	0.4	2500	1.61	166.66

3 Methods

3.1 Taguchi Technique (Signal to Noise (S/N) Ratio)

Three signals to noise ratios are usually used, with the response characteristics determining which one is used. The “lower is better” criterion will be used to choose the S/N ratio for roughness, while “higher is better” criterion will be used to choose the MRR [14–16].

3.2 Gray Relational Analysis (GRA)

3.2.1 Normalization

Data pre-processing is a technique for transforming an original series into a series that is comparable to the original. This is accomplished by the use of a 0 to 1 scale when analyzing experimental findings [17–19].

3.2.2 Gray Relational Grade and Coefficient Evaluation

Gray Relational Analysis is a technique for determining the ideal state of numerous input parameters in order to acquire the best quality features. Gray Relational analysis is commonly used to evaluate or judge the success of a complex project with limited data. Because this research experimental design is orthogonal, i.e., likely to find separate impacts of all end milling parameters at the numerous values used in the research, and the Grades are calculated by averaging the gray coefficient as shown below [8]:

$$\xi_i(l) = \frac{\nabla_{\min i} + \xi \cdot \nabla_{\max i}}{\nabla_{0i}(l) + \xi \cdot \nabla_{\max i}} \quad (2)$$

$$\Delta_{0i}(l) = \|a_0^*(l) - a_i^*(l)\| \quad (3)$$

$$\Delta_{\max i} = \forall \Delta \in i \quad \min_l \|a_0^*(l) - a_i^*(l)\| \quad (4)$$

$$\Delta_{\min i} = \forall \Delta \in i \quad \min_l \|a_0^*(l) - a_i^*(l)\| \quad (5)$$

$$\gamma_i = \frac{1}{n} \sum_{l=1}^n \xi_i(l) \quad (6)$$

However, the influence of each factor is not the same in practice. Equation 6 can so be rewritten as follows:

$$\gamma_i = \frac{1}{n} \sum_{l=1}^n w_l \xi_i(l) \sum_{l=1}^n w_l \quad (7)$$

4 Results

4.1 Optimum Combination of Parameters

Normalized values of gray relational coefficient (GRC) and gray relational grade (GRG) with their ranks are depicted in Table 5.

Table 6 demonstrates that feed is ranked first due to its highest max–min value of 0.2205, rest three parameters have their different max–min values as depth of cut (0.1718), coolant (0.1086), and speed (0.0903) in decreasing order. The scales first for coolant, third for feed, third for depth of cut, and first for speed have the most

Table 5 Normalized, GRC and GRG values with their ranks

Exp. No.	Normalized values		GRC		GRG	Ranks
	SR	MRR	SR	MRR		
1	0.7333	0.0000	0.6522	0.3333	0.4928	12
2	0.1462	0.3368	0.3693	0.4298	0.3996	17
3	0.6208	0.5757	0.5687	0.5410	0.5548	10
4	1.0000	0.2389	1.0000	0.3965	0.6982	5
5	0.9723	0.5757	0.9476	0.5410	0.7443	4
6	0.9034	0.8147	0.8381	0.7296	0.7838	2
7	0.7666	0.4243	0.6817	0.4648	0.5733	9
8	0.6499	0.7611	0.5882	0.6767	0.6324	8
9	0.8856	1.0000	0.8138	1.0000	0.9069	1
10	0.4225	0.0000	0.4641	0.3333	0.3987	18
11	0.3789	0.3368	0.4460	0.4298	0.4379	14
12	0.3153	0.5757	0.4220	0.5410	0.4815	13
13	0.3430	0.2389	0.4321	0.3965	0.4143	16
14	0.0000	0.5757	0.3333	0.5410	0.4372	15
15	0.6642	0.8147	0.5982	0.7296	0.6639	7
16	0.6783	0.4243	0.6085	0.4648	0.5367	11
17	0.7796	0.7611	0.6941	0.6767	0.6854	6
18	0.5136	1.0000	0.5069	1.0000	0.7534	3

Table 6 Max–Min table for grade

Particulars	End milling parameter	Scale 1	Scale 2	Scale 3	Maxi–Mini
A	Coolant	0.6429	0.5343	–	0.1086
B	Feed rate	0.4609	0.6236	0.6813	0.2205
C	Depth of cut	0.5190	0.5561	0.6907	0.1718
D	Speed	0.6475	0.5611	0.5573	0.0903

significant gray relationship grade. As a result, $A_1B_3C_3D_1$ is the best alternative for improving end milling parameters.

In Fig. 3 the value of GRG decreases when coolant and speed levels rise, it rises as feed and depth of cut scales rise. Thick dashed lines show the average value of GRG.

4.1.1 ANOVA

The outcome of ANOVA helps to judge the essential factors in the quality features of end milling. A statistical tool, F-Test, was applied to find out the influence of these

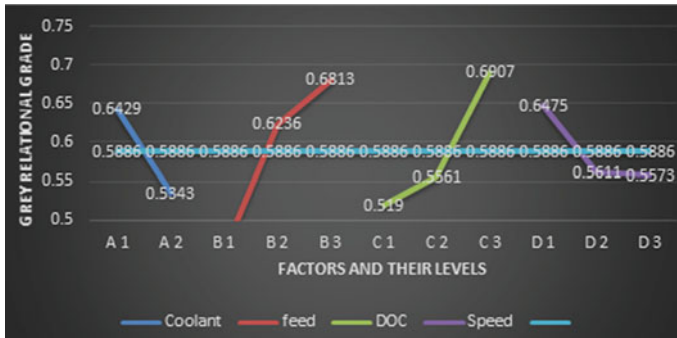


Fig. 3 Different gray relational grade with end machining parameters [14, 16]

Table 7 ANOVA result

Particulars	Source	Dof	Sum of squares	Mean square	F value	%C
A	Coolant	1.00	0.0530	0.0530	9.9695	13.52
B	Feed rate	2.00	0.1568	0.0784	14.736	39.97
C	Doc	2.00	0.0980	0.0490	9.2085	24.98
D	Speed	2.00	0.0313	0.0156	2.9381	7.97
Error		10.0	0.0532	0.0053		13.56

input factors on quality features. When its value is higher than four, this implies that modification in end milling factors has more impact on quality features. In ANOVA, the null hypothesis states that no difference in means exists. The research or alternative hypothesis is that the means are not all equal, and it is frequently expressed in words rather than mathematical symbols. The study hypothesis captures any variation in means, including situations where all four standards are unequal, one is different from the other three, two are different, and so on. As illustrated above, the alternative hypothesis captures all possible scenarios other than the null hypothesis’s specification of equality of all means.

Distinguish coefficient (ζ) lies between 0 and 1, i.e., and here $\zeta = 0.5$, then confidence level of ANOVA was 95%.

As indicated in Table 7, the feed has the highest contribution of 39.97%, depth of cut has 24.98%, and coolant and speed are third and fourth with 13.52% and 7.97%, respectively. Figure 4 depicts the contributions of all parameters.

4.1.2 Validation Test

To determine the optimization result of this research, the Taguchi L_{18} method was used. Table 8 illustrates that the investigation outcomes as the most excellent deal with the prediction of the investigation design.

Fig. 4 % Contribution of end milling parameters

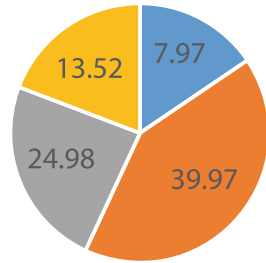


Table 8 Validation test outcomes

Optimum machining parameter			
	Prediction	Experiment	% Change
Level	A ₁ B ₃ C ₃ D ₁	A ₁ B ₃ C ₃ D ₁	
SR		0.8138	
MRR		1.0000	
GRG	0.8966	0.9069	1.14

Table 8 depicts that the GRG increases by 1.14%, ensuring the present end milling process settings are optimally suited to satisfy the prerequisite.

5 Microstructure

Microstructure testing of the ninth experimental workpiece found the most consistent and best approach to detect micro-cracks, micro-defects, and variations in microstructure associated changes. The machining condition influences many defects on the specimen’s surface, such as micro-cracks and flaws. As a result, superior metallographic techniques and an optical microscopy tool should be used to inspect surface characteristics. The behavior of the workpiece surfaces is not replicated by simply finishing of material. The elementary research was performed in order to study microstructure potentials on stainless steel 304. In addition to the given data, a microstructure analysis was carried out, with the maximum strain of the surface being detected. Figure 5a, b shows microstructure photos were obtained by 600 X capabilities optical microscopy (Make Rsamet Unitron).

Pearls and polygonal ferrite particles make up the structure in Fig. 5a (before end milling). Pearls and polygonal ferrite particles may be seen in the microstructure of the construction in Fig. 5b (after end milling). Particle sizes were small and the quantity of particles observed ranged from 4 to 5.

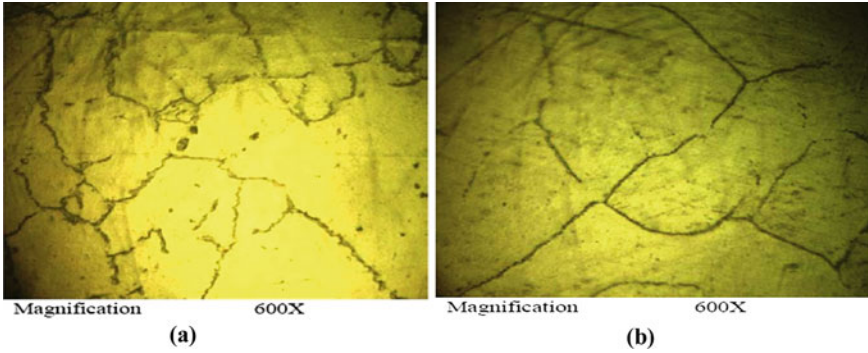


Fig. 5 **a** Microstructure (Before end milling). **b** Microstructure (After end milling)

6 Conclusions and Future Scope

Based on the observation and result outcome, the following conclusion can be made:

- Multi-performance features for end milling process parameters, the best combination is $A_1B_3C_3D_1$, which includes coolant on, 2500 mm per minute feed rate, 0.4-mm depth of cut, and 1500 revolution per minute machining speed.
- ANOVA states that the percentages involvement for feed rate, depth of cut, coolant, and machining speed are 39.97, 24.98, 13.52, and 7.97%, respectively. This approach detects various performance optimum improvements of 1.14%. On the other hand, the validation experiments reveal a variance of $\pm 10\%$ at the optimal setting, indicating good result reproducibility.
- Pearls and polygonal ferrite particles may be seen in the micrographs (before and after milling). There were a few rough surfaces with coarse particles as well. Particle sizes were small and the quantity of particles observed ranged from 4 to 5.

In the future, a Surface integrity study may be carried out for machined surfaces of different machined materials by a cutting tool other than the one used in the current study. Surface integrity study may be performed on different machine-like CNC Lathe and other responses like surface strain, microhardness, etc. In the upcoming time, it is possible to increase the outcomes by applying different optimization methods.

References

1. Jawahir IS, Brinksmeier E, M'saoubi R, Aspinwall DK, Outeiro JC, Meyer D, Umbrello D, Jayal AD (2011) Surface integrity in material removal processes: recent advances. *CIR Ann* 60(2):603–626
2. Field M, Kahles JF (1971) Review of surface integrity of machined components. *Ann CIR* 20(2):153–163

3. Sun J, Guo YB (2009) A comprehensive experimental study on surface integrity by end milling Ti-6Al-4V. *J Mat Proc Tech* 209(8):4036–4042
4. Sijo MT, Biju N (2011) Taguchi method for optimization of cutting parameters in turning operations. *Int J Manuf Mat Sci* 1(1):44
5. Karnwal A, Hasan MM, Kumar N, Siddiquee AN, Khan ZA (2011) Multi-response optimization of diesel engine performance parameters using thumba biodiesel-diesel blends by applying the Taguchi method and grey relational analysis. *Int J Auto Tech* 12(4):599–610
6. Ho CY, Lin ZC (2003) Analysis and application of grey relation and ANOVA in chemical-mechanical polishing process parameters. *Int J Adv Manuf Tech* 21(1):10–14
7. Siddiquee AN, Khan ZA, Goel P, Kumar M, Agarwal G, Khan NZ (2014) Optimization of deep drilling process parameters of AISI 321 steel using Taguchi method. *Price Mater Sci* 6:1217–1225
8. Singh OP, Kumar G, Kumar M (2019) Multi-performance optimization shoulder milling process parameters of AA6063 T6 aluminum alloy by Taguchi based GRA. *Int J Innov Technol Explore Eng* 8(10S):420–425
9. Singh OP, Kumar G, Kumar M (2019) Role of Taguchi and grey relational method in optimization of machining parameters of different materials: a review. *Acta Electronica Malays* 3(1):19–22
10. Kumar G, Kumar M, Tomer A (2021) Optimization of end milling machining parameters of SS 304 by Taguchi technique. In: *Recent advances in mechanical engineering*. Springer, Singapore, 683–689
11. Kumar M, Kumar G, Singh OP, Tomer A (2021) Multi performance optimization of parameters in deep drilling of SS-321 by Taguchi-based GRA. In: *Recent advances in mechanical engineering*. Springer, Singapore, pp 675–681
12. Goel P, Saxena AK, Wahid MA, Rathore S, Sharma N, Mishra KM (2020) Influence of friction stir welding parameters on mechanical properties of dissimilar AA7475 to AISI 304. *IOP Conf Ser: Mat Sci Eng* 802(1):012010
13. Goel P, Mohd AW, Sharma N, Siddiquee AN, Khan ZA (2019) Effect of welding parameters in friction stir welding of stainless steel and aluminum alloy. In: *Advances in industrial and production engineering*. Springer, Singapore, pp 815–823
14. Siddiquee AN, Khan ZA, Mallick Z (2010) Grey relational analysis coupled with principal component analysis for optimization design of the process parameters in in-feed centerless cylindrical grinding. *Int J Adv Manuf Tech* 46(9):983–992
15. Kumar G, Goel P, Kumar M, Tomer A, Wahid MA (2021) Role of end-milling process parameters on surface integrity of SS-304: Integrated taguchi-grey approach. *Pro Mat Sci*
16. Sharma K, Kumar G, Kumar M (2021) Application of taguchi method coupled with GRA for optimization of drilling process parameters. *IOP Conf Ser: Mat Sci Eng* 1149(1):012032
17. Khan ZA, Kamaruddin S, Siddiquee AN (2010) Feasibility study of recycled high-density polyethylene and multi-response optimization of injection moulding parameters using combined grey relational and principal component analyses. *Mat Des* 31(6):2925–2931
18. Jangra KK, Sharma N, Khanna R, Matta D (2016) An experimental investigation and optimization of friction stir welding process for AA6082 T6 (cryogenic treated and untreated) using an integrated approach of Taguchi, grey relational analysis and entropy method. *Proc Inst Mech Eng, Part L: J Mat: Des App* 230(2):454–69
19. Sharma N, Khanna R, Sharma YK, Gupta RD (2019) Multi-quality characteristics optimization on WEDM for Ti-6Al-4V using Taguchi-grey relational theory. *Int J Mach Machin Mat* 21(1–2):66–81

Design and Analysis of Knuckle Pin Using Different Materials in ANSYS



Birendra Kumar, Avaneet Kumar, Brahma Nand Agrawal, and Pawan Kumar Singh Nain

Abstract This paper aims to calculate the stresses and factors of safety in knuckle pins using regular country analysis for different materials and out of that one material is selected as optimal which provides better results than others. The knuckle joint is analyzed for structural metallic, general aluminum alloy, and aluminum alloy 6061. It is determined that aluminum alloy 6061 is first-class optimizing material out of the selected fabric. The knuckle pin is proposed to increase within the present examine is for an implemented force of 900 KN. Since ANSYS does not provide aluminum alloy 6061 that is why this paper defines custom material with the same property as aluminum alloy 6061. It has been determined that shear stresses developed for knuckle joints fabricated from general aluminum alloy, aluminum alloy 6061, and structural steel is are nearly the same. But the factor of safety varying for these three materials and aluminum alloys 6061 shows a larger factor of safety among these three.

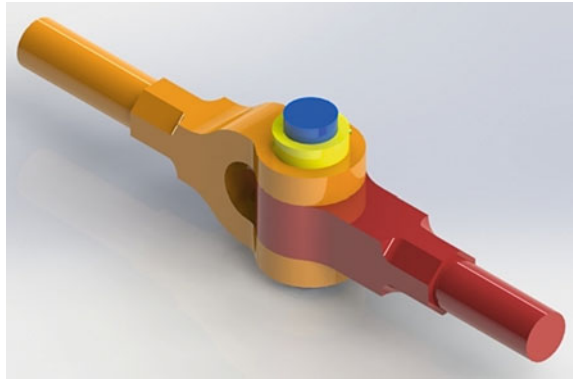
Keywords Knuckle pin · Factor of safety · ANSYS · Stress · Structural steel · Aluminum

1 Introduction

A knuckle joint is mainly used to connect two rods that are under tensile forces. It is essentially a tensile joint. However, sometimes joint is guided in such a way that it can be used under a compressible load. This joint has high demand in industries because it can be easily disconnected for adjustments or repairment. Some of the examples are link of a curler chain, anxiety hyperlink used in a bridge frame, roof truss tie rod, jib crank tie rod, and many more.

Figure 1 shows a model of knuckle joint made using solid works. A typical knuckle joint basically consists of five different parts. They are as follows:

B. Kumar (✉) · A. Kumar · B. N. Agrawal · P. K. S. Nain
Department of Mechanical Engineering, Galgotias University, Greater Noida, India
e-mail: birendrakum.119@gmail.com

Fig. 1 Knuckle joint

1. Double-eye or fork
2. Single eye
3. Collar
4. Taper pin
5. Knuckle pin

An ordinary knuckle joint consists of three parts: a fork, Single eye and a knuckle pin. One end of the rod is shaped into an eye and the cease of another rod is fashioned into fork with each fork having an eye. The pin is inserted into the fork eye, after aligning the holes in the eye and fork, the knuckle pin is inserted through single eye. The knuckle pinhead at one end gets fixed and at the other end it is fixed via a collar and a taper pin is inserted through the hole of pin and collar. The basic definition of pressure is the force per unit area.

If the pressure is perpendicular to the area and pulling the body, the pressure is called tensile. If the pressure is perpendicular to the body and pushing in the direction of each other, the force is called compressive. It was reported by john that shear failure due to torsional loading is generally the normal failure mechanism of the components. However, friction is the main cause of failure in many cases [1, 2]. Generally, stainless steel and cast iron are used to make knuckle pins but aluminum can also be used for making pins because of many advantages over stainless steel like aluminum is lighter than steel which reduces about approx. 35–45% and also aluminum is naturally non-corrosive while stainless steel goes under treatment to make it corrosion-free. So, in this study aluminum made knuckle pin is compared with stainless steel knuckle pin. Also, aluminum of two different types is taken and compared successfully. This study helps the manufacturers to select best material for making knuckle pins.

The failure of knuckle joints may cause accidents. So, it is necessary to design knuckle joints to withstand load under given tension without failing. A knuckle joint failure occurs at part of joint as given below [3, 4].

1. Shear failure of Knuckle pin (single or double shear).
2. Crushing of pin.

3. Failure of eye.
4. Tensile failure of flat end bar.

1.1 Structural Steel

Structural steel mainly consists of carbon as main constituent which is why it is generally called carbon steel; the content of carbon is approx. up to 2.1% by weight. By altering the carbon content in steel, desired properties are achieved. For example, increasing carbon content results in increase in strength and low ductility. Depending on the situation or area where steel will be used, will determine the level of carbon content in it. To decrease the amount of impurity, technological melting process is used [5, 6]. Mild steel which is also known as low-carbon steel is considered as best choice for industries because of its property and have high demand in construction areas. In low-carbon steel, carbon percentage is approx. between 0.04 and 0.30%, that is why its strength is high and ductility is low when compared with other forms of steel. Although both medium as well as high-carbon steel can be considered structural steel and are typically used for mechanical engineering purposes.

1.2 Aluminum Alloy

Aluminum is the metal that comprises about 8% of earth crust and is the 3rd most common element present in earth's crust. Aluminum's property and versatility make it 2nd the most widely used metal after steel [7]. Mineral Bauxite contains aluminum, which is extracted through process. First step in this process is to convert the bauxite into aluminum oxide named as alumina through the Bayer Process. Electrolytic cells and the Hall-Heroult Process convert alumina into aluminum metal. Pure aluminum develops the property of being soft, ductile, corrosion-resistant and has a high electrical conductivity [8, 9]. Some of the uses are foil and conductor cables. But alloying aluminum with other elements can be used in many other applications like automobile parts, machinery parts, etc. Aluminum is one of the lightest metals and has high strength, that is why aluminum, when alloyed with different materials, proves superior to steel.

2 Problem Identification

- (a) To determine the high-quality suitable material for Knuckle pin from available materials for equal load-carrying capability.
- (b) To study the stresses of different materials by using the ANSYS software.

3 Methodology

3.1 Modeling and Mesh

Design of knuckle joint is modeled using solid works. For analysis, ANSYS is used and first step is to create a mesh of knuckle joints. It is necessary to create a high-quality mesh for better analysis, so we set the size type to hex dominant and set the size value to 2 mm.

Figure 2 shows the meshed model of knuckle joint. It is done using ANSYS hexahedral feature. The meshing feature of ANSYS divides the whole section into many smaller elements, high the mesh quality better will result. This will enable us to analyse the stress of the components at distinct locations.

Now next step is to find shear stress on the knuckle pin using the theoretical formula. The stress obtained theoretically, we are going to compare with the stress obtained from analysis using different materials, i.e., Structural Steel, Aluminum alloy, and aluminum alloy 6061. As the knuckle pin is under tension load by two sides.

Nomenclature:

D = Rod diameter,

d_1 = Pin diameter,

d_2 = Eye outer diameter,

t = Single eye thickness,

t_1 = Fork Thickness.

The Diameter of the rod (d) = 20 mm.

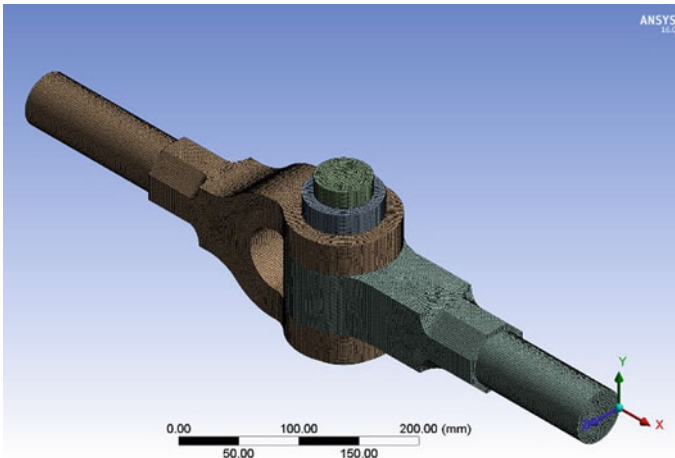


Fig. 2 Mesh of knuckle joint

Outer diameter of eye = 100 mm and inner diameter of eye = 50 mm.

Diameter of Knuckle pin = 50 mm.

The thickness of single eye (t) = 60 mm.

Thickness of fork (t_1) = 120 mm.

3.2 The Material Selected in the Present Investigation on Structural Steel, Aluminum Alloy, and Aluminum Alloy 6061

Structural Steel

1. Young's modulus = 200,000 MPa
2. Poisson's ratio = 0.3
3. Yield strength = 350 MPa to 1793 MPa.

Aluminum Alloy

1. Young's modulus = 71,000 MPa
2. Poisson's ratio = 0.33
3. Yield strength = 280 MPa.

Aluminum Alloy 6061

1. Young's modulus = 70,000 GPa
2. Poisson's ratio = 0.33
3. Yield strength = 276 MPa.

Table 1 shows a detailed data about the knuckle joint parts like length on all three-axis, mass, density, etc. Every column represents one part of knuckle joint.

3.3 Analysis Parameters

Now after that, finite element analysis or structural analysis is done on the knuckle joint. FEM is the most commonly used method for solving differential equations and analyzing load, stress, deformation, etc. for the mechanical components [4, 10]. FEM method divides the model into small elements for performing analysis [11].

Table 2 shows analysis parameter set for the study. Two forces are defined, i.e., Force1 and Force2 and are applied on double-eye end in negative x-direction and on single eye end in positive x-direction, respectively. The top of the pin and bottom are provided with fixed support.

Table 1 Bounding box and properties of knuckle joint

Bounding box					
Length X	39.783 mm	70.0 mm		400.0 mm	350.12 mm
Length Y	6.0 mm	20.0 mm	169.0 mm	120.0 mm	60.0 mm
Length Z	66.063 mm	70.0 mm		100.0 mm	100.11 mm
Properties					
Volume	2035.5 mm ³	37,129 mm ³	3.53e + 005 mm ³	1.238e + 006 mm ³	1.038e + 006 mm ³
Mass	1.5979e-002 kg	0.29146 kg	2.7711 kg	9.7185 kg	8.1486 kg
Centroid X	32.868 mm	32.388 mm	32.386 mm	-88.362 mm	134.11 mm
Centroid Y	238.5 mm		175.75 mm	168.5 mm	
Centroid Z	263.43 mm	264.31 mm		264.3 mm	264.31 mm
Moment of Inertia Ip1	6.906 kg·mm ²	142.09 kg·mm ²	7631.5 kg·mm ²	13,421 kg·mm ²	5560.0 kg·mm ²
Moment of Inertia Ip2	6.906 kg·mm ²	268.47 kg·mm ²	966.74 kg·mm ²	1.1387e + 005 kg·mm ²	77,178 kg·mm ²
Moment of Inertia Ip3	7.1223e-002 kg·mm ²	146.05 kg·mm ²	7633.6 kg·mm ²	1.1959e + 005 kg·mm ²	75,797 kg·mm ²

Table 2 Analysis parameters

Parameters	Force1	Force 2	Fixed support	Fixed support 2
State	Fully defined	Fully defined	Fully defined	Fully defined
Definition				
Parameters	Force1	Force 2		
Define by	Components	Components		
Vector	Defined	Defined		
Value	900,000. N	900,000. N		
Direction	Negative x-axis	Positive x-axis		

4 Results

Structural Steel

See Figs. 3 and 4.

For Aluminum Alloy

See Figs. 5 and 6.

For Aluminum Alloy 6061

See Figs. 7 and 8.

The knuckle joint is a part that undergoes maximum stress when the load is applied. Therefore, the material selection should be done in such a way that it could withstand and handle the stresses that develop in the joint without failing and could go under elastic deformation when load is high. ANSYS software provides the feature which can effectively measure the amount of deformation, i.e., change in length of the joints which are shown in above Figure for different materials. Every material goes under

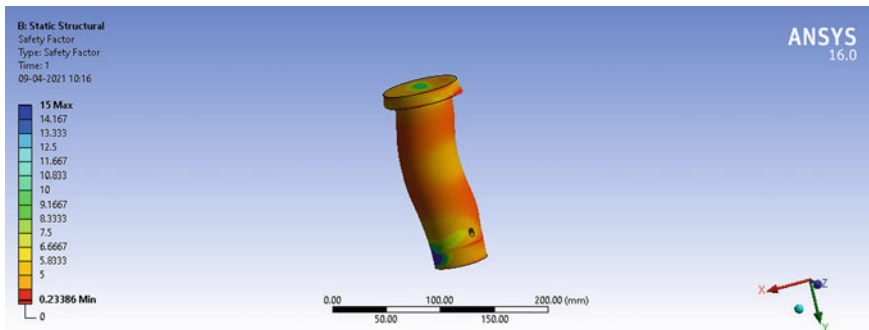


Fig. 3 Factors of safety in structural steel

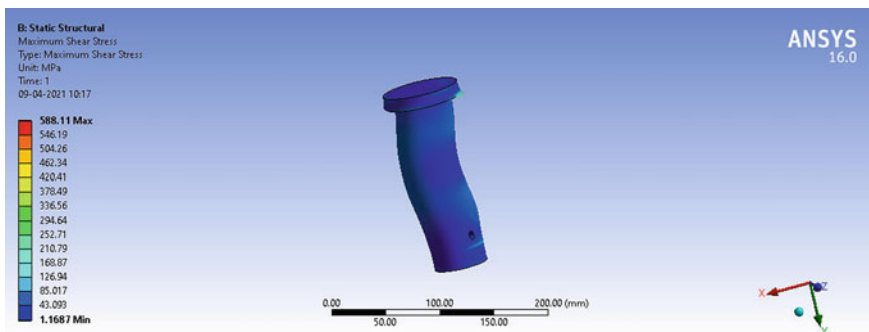


Fig. 4 Max shear stress for structural steel

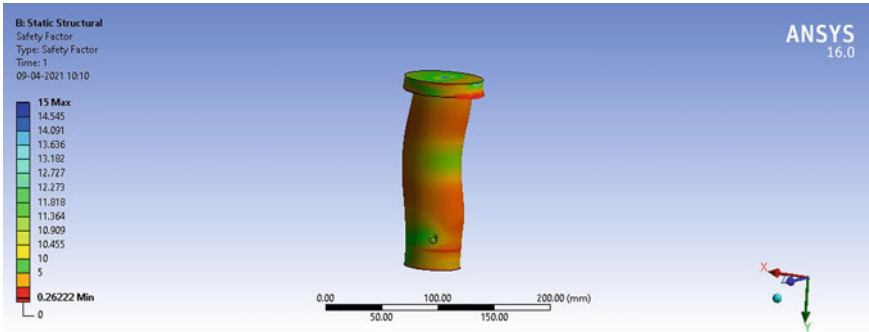


Fig. 5 Factor of safety in aluminum alloy

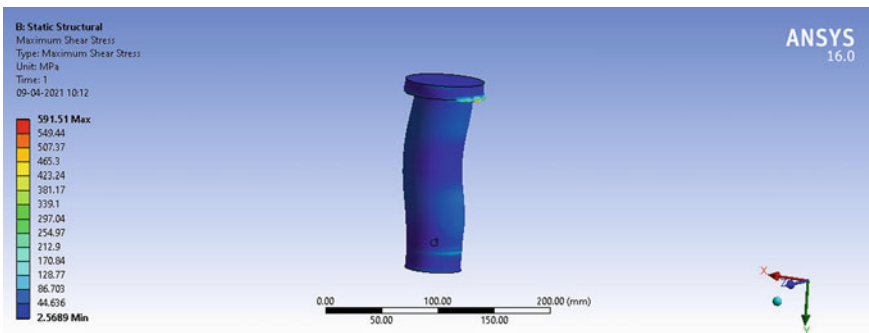


Fig. 6 Max shear stress for aluminum alloy

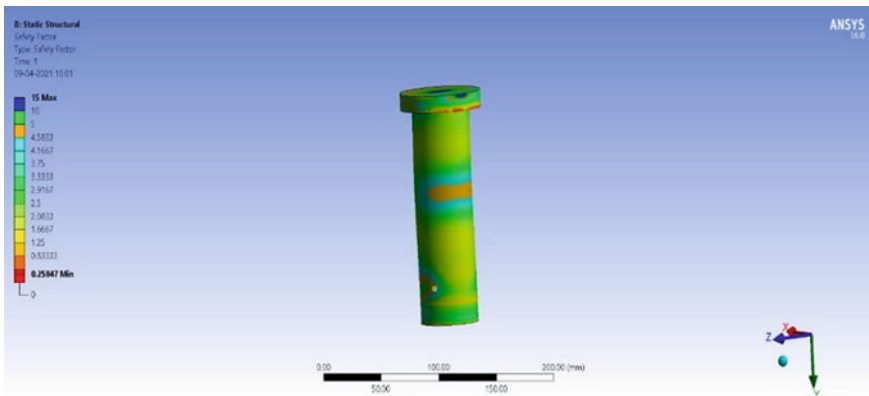


Fig. 7 Factor of safety in aluminum alloy 6061

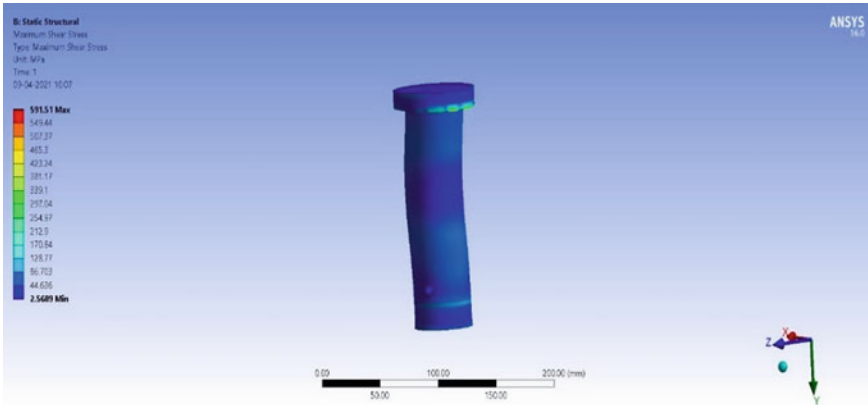


Fig. 8 Max shear stress for aluminum alloy 6061

two types of analysis that are a factor of safety and max shear stress. Figure 8 shows aluminum alloy 6061 has very little deformation or has the max factor of safety among these materials. Figure 6 shows general aluminum alloy shows less deformation when compared with structural steel. Figure 4 shows the highest deformation among the three. Max Shear stress developed for different materials are as follows:

1. Structural steel: 588.11 MPa
2. Aluminum alloy: 591.51 MPa
3. Aluminum alloy 6061: 591.51 MPa.

In Fig. 3, the factor of safety of structural steel varies from 0.23386 to 15 max. However maximum body parts have a factor of safety approx. between 0.2 and 5. Similarly, Fig. 5 shows that in general aluminum alloy has a factor of safety approx. between 1 and 9 while min is 0.26222 and max is 15 and the best result obtained in aluminum alloy 6061 has a factor of safety approx. between 2 and 12 while min is 0.25487 and max is 15 which is at top of the pin from Fig. 7. Factor of safety in pin is given below.

1. Structural steel: 0.2 – 5
2. Aluminum alloy: 1 – 9
3. Aluminum alloy 6061: 2 – 12.

Although shear stress developed are nearly the same, Aluminum and its alloy shows that it can handle more shear stress. From the factor of safety analysis, it is observed that the aluminum is safer than structural steel because in structural steel almost the body of the pin has very less factor of safety approx. 0.2 – 5 and in the case of aluminum almost the body of pin shows a factor of safety approx between 2 and 10. It is clear that aluminum performs better in the analysis and between the two types of aluminum alloy, aluminum alloy 6061 has a factor of safety approx between 2 and 10 and general aluminum alloy have a factor of safety approx between 1 and 9.

5 Conclusion

This study concludes as follows:

- The shear stress developed in three different materials, i.e., structural steel, aluminum alloy, and aluminum alloy 6061, are nearly the same.
- Aluminum alloy 6061 shows very less deformation as compared to other two materials. While Structural steel shows highest deformation among these three materials.
- Aluminum alloy 6061 found max factor of safety among these materials.

So, from this study, it revealed that it is suitable to use aluminum alloy 6061 for building knuckle pins. Although aluminum is costlier than steel its lightweight and many more advantages over steel make it more suitable choice.

References

1. Pantazopoulos G, Sampani A, Tsagaridis E (2007) Torsional failure of a knuckle joint of a universal steel coupling system during operation—a case study. *Eng Fail Anal* 14:73–84. <https://doi.org/10.1016/j.engfailanal.2005.12.005>
2. Liu Y, Zhang X, Wang X, et al (2020) Failure analysis on friction and wear of tool joints. *Mater Sci Forum* 993 MSF:1118–1123. <https://doi.org/10.4028/www.scientific.net/MSF.993.1118>
3. Raj SY, Dayalan HP, Shrivardhan M (2018) Investigation of knuckle joint and its importance—a literature case study. 2018 7th Int Conf Ind Technol Manag ICITM 2018 2018–Janua: 62–70. <https://doi.org/10.1109/ICITM.2018.8333921>
4. Rao AY (2018) Structural analysis of Knuckle joint with different materials. 5:14–22
5. Pantazopoulos G, Antoniou S (2004) Wear-related failures of nitrocarburized steels: some microstructural and morphological observations. *J Fail Anal Prev* 4:51–57. <https://doi.org/10.1361/15477020421755>
6. Bannykh OA, Sorokin AM, Bannykh IO, Lukin EI (2018) Structure and mechanical properties of high-strength structural steels. *Russ Metall* 2018:528–532. <https://doi.org/10.1134/S0036029518060046>
7. Patil SS, Patil S, Sunil Kumar S, Saviraj AS (2018) A review on influence of various technological processes on mechanical properties of aluminum alloys. *IOP Conf Ser Mater Sci Eng* 376. <https://doi.org/10.1088/1757-899X/376/1/012043>
8. Al-Qutub AM, Khalil A, Saheb N, Hakeem AS (2013) Wear and friction behavior of Al6061 alloy reinforced with carbon nanotubes. *Wear* 297:752–761. <https://doi.org/10.1016/j.wear.2012.10.006>
9. Gurcan AB, Baker TN (1995) Wear behaviour of AA6061 aluminium alloy and its composites. *Wear* 188:185–191. [https://doi.org/10.1016/0043-1648\(95\)06639-X](https://doi.org/10.1016/0043-1648(95)06639-X)
10. Bhardwaj R (2020) Design and analysis of knuckle
11. Liu Y (2008) ANSYS and LS-DYNA used for structural analysis. *Int J Comput Aided Eng Technol* 1:31–44. <https://doi.org/10.1504/IJCAET.2008.021254>

The Current State and Potential of Canal Top Solar Power Plants in India



Chandrabhushan Vishwakarma, Ananya Dwivedi, and Devendra Yadav 

Abstract India is the world's second-most populous country, with an ever-increasing energy need. Harnessing renewable energy is best suited for India in order to meet the country's electricity demand while also achieving the country's sustainability goals. The majority of India's land receives sufficient incoming direct normal irradiation from the sun, making it suitable for the installation of solar power plants. One of the most difficult aspects of installing solar power plants is the huge amount of land required by PV solar panels. Because the area of the canal top is unused, installing PV on the canal top might be a viable solution to this land-use issue. The paper demonstrates the present state of power demand and fulfillment utilizing various energy sources. The different canal top solar power plant installations throughout nations, their workings, scope, and concerns about technological adaptation are discussed in this paper.

Keywords Solar power · Canal top solar power · CSP technology · Solar panels

1 Introduction

India has a population of 136.64 billion people and contributes 16.9% of the global population. India is expected to overtake China as the world's most populous country by 2050, accounting for 17.2% of the global population [1]. Due to our fast-rising population and industrial growth, the country has been experiencing an energy crisis for the past year. Total gross electricity generated in FY2019-20 was 1383.5 TWh. Traditional energy sources such as fossil fuels are used in the country's energy sector. India emits 2.65GT (Gigatons) of carbon, which must be reduced to meet the energy needs of a population confronting dangerous concerns like climate change. India's energy needs are currently met by its abundant coal reserves, crude oil, natural gas, and renewable energy. Figure 1 shows the growth of electricity generation in different fields of energy sources in India. This graph shows that thermal energy meets the

C. Vishwakarma · A. Dwivedi · D. Yadav (✉)
Department of Mechanical Engineering, Galgotias College of Engineering and Technology,
Greater Noida, Uttar Pradesh, India
e-mail: ydevendra393@gmail.com

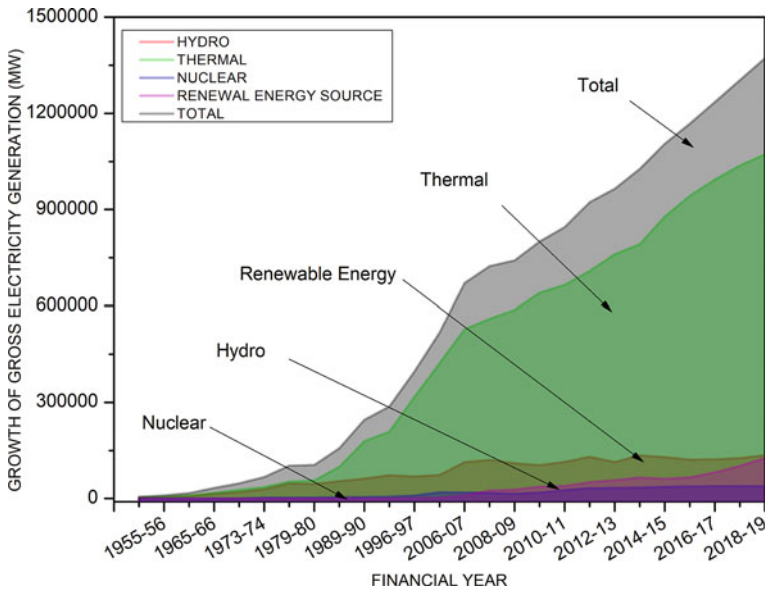


Fig. 1 Growth in electricity generation in the various energy field in India

majority of the country's energy consumption and that it has risen quickly since independence. On the other side, we can witness the increase of renewable energy generation on the country's grid electric supply, but not at the same rate as thermal energy.

Because of rising wages and rising living standards, India is now the world's third-largest energy consumer. Since 2000, energy consumption has more than doubled, with coal, oil, and solid biomass still meeting 80% of demand. The industry sector consumed the most energy in India, followed by the domestic sector as shown in Fig. 2.

In 2020, it is predicted that coal reserves will be 344.02 billion tons, crude oil reserves will be 603.37 million tons, natural gas reserves will be 1371.89 billion cubic meters, and renewable energy potential will be 1,097,465 MW. In which, Solar power has a potential of 748,990 MW (68.25%), wind power has a potential of 302,251 MW (27.54%) at 100 m hub height, small hydropower has a potential of 21,134 MW (27.54%), and biomass has a potential of 17,536 MW (1.60%) [2–4]. India's overall capacity mix (including large hydro) increased marginally to 36.2% in the first quarter of 2020, up from 35.9% at the end of the calendar year 2019. Despite our potential, we are experiencing energy shortages. In India's geographical area of 3.287 million km², energy amount should be 657.4 million MW [5]. Forests, agriculture, fallow land, and other uses account for 87.5% of the land. The housing industry uses 6.7%, and 5.8% is used in either desert, snowbound, or generally inhabitable areas, therefore solar energy installations use 12.5% of the land area of

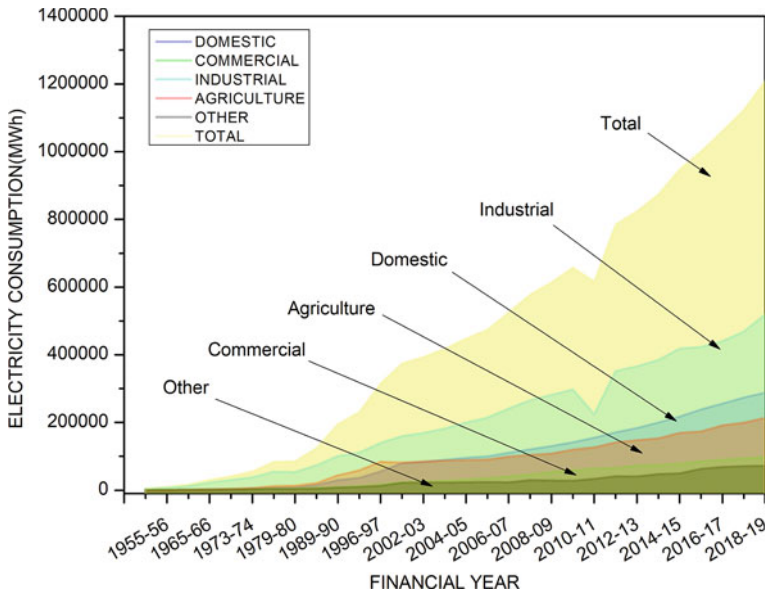


Fig. 2 Electricity consumption by various sectors in India

0.413 million km². In theory, if we could use only 10% of the land area, we could get 8 million MW [6].

Despite contributing only a little proportion to global greenhouse gas emissions thus far, India is already feeling the consequences of climate change. India may transition to renewable energy sources, resulting in a rapid reduction in emissions. Around the world, there has been an increase in solar energy-based power plants. It is currently recognized as a huge potential sector for renewable energy. The goal of this research is to provide an overview of the present state of solar energy, particularly as it relates to canals and agriculture. Many countries are quickly adopting this concept. There have been several canal top solar power plants constructed in India, which are summarized in this paper. The many elements of this technology are thoroughly addressed. This paper also proposes a method for improving solar energy conversion efficiency using concentrated solar technology which can be integrated into this system.

2 Solar Potential in India

The solar photovoltaic cell, which creates energy, is proportional to the amount of global insolation received and the area exposed [7]; it is defined by [8]:

$$\eta = A/B \tag{1}$$

whereas; A = max power output, B = power input.

The power input is a standard test condition (STC) of 1000 W/m^2 global isolation, a module temperature of 250 C , and an air mass of 1.5 . (AM). India receives 2600 to 3200 h of annual sunshine, and the country's solar irradiance is $4\text{--}7 \text{ KWh/m}^2/\text{day}$ or 200 MW/km^2 of average solar ingratiation. If solar energy is gathered from a 1 m^2 collector in a day, it is roughly equivalent to the energy released by burning 1 kg of coal or $1/2 \text{ L}$ of kerosene. Rooftop PV systems, floating PV systems, and ground-mounted PV are cultural techniques for harvesting solar energy with such potential.

In the upcoming sections, we will look at the possibility of canal top solar plants, which are already in use in a few Indian states. Furthermore, when compared to other PV plants, this power plant has greater potential, as well as superior resource usability and performance. But first, it is essential to understand how this plant works and what drives it.

3 Canal Top Solar Power Plant

It is a relatively new notion of harnessing our solar energy potential. India is an agricultural country, and many farmers rely on a canal system to irrigate their fields. During $2008\text{--}09$, the canal watered about half of the 165.97 lakh hectares of land. If the region above the canal is used to generate energy, we will be able to produce clean energy and supply them to a local area without the need for a long transmission cable. These solar plants can avoid the expense of the huge land necessary to construct the solar plants and even meet the canal's energy needs. The canal top solar plant also has the benefit of not requiring a separate cooling system because the canal water serves this purpose.

3.1 Canal Top Solar Power Technology

The solar power plant necessitates the utilization of a huge area of land. The cost of the land can be decreased by constructing the solar power plants above the canal. Canals are built in two directions: north–south and east–west. The interspacing between the solar arrays can be avoided in the East–West canal, but in the North–South canal, the interspacing is supplied and the panels are angled (Fig. 3) to avoid shade on the neighboring panel [8, 9].

Using simple trigonometry, the maximum shadow distance can be calculated;

$$D' = \frac{h}{\tan \alpha} \quad (2)$$

$$D = D' \cos \psi \quad (3)$$

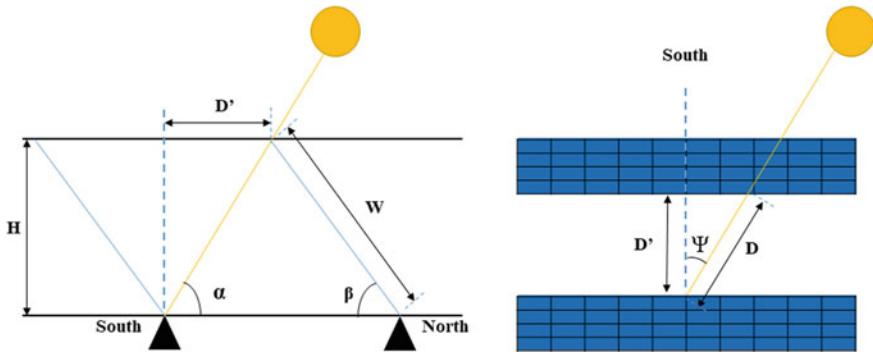


Fig. 3 Layout of the solar arrays on the canal top

where; α —Solar attitude angle, Ψ —Solar azimuth angle, h —height of the obstruction, D' —Maximum length of the shadow, D —minimum distance between the panel, β —tilt angle of the panel.

4 Major Successfully Installed Solar Power Plant in India

India is primarily an agricultural country. In many regions of the nation, farming is the primary source of income. Canals supply water to huge agricultural fields for irrigation. A vast number of canals are formed by diverting water from neighboring rivers. India has a huge network of canals, which are mostly used to irrigate crops. The canal is built across a broad region, and the top section of the canal is left unfinished. This section is used to generate energy by the canal top solar power plant.

Gujarat’s first canal top solar power pilot project (Fig. 4a), worth Rs. 177.1 million, was launched in Kadi. The project was completed on the Narmada canal network, which is 532 km long. The plant’s total power output was 1 MW, which saved 9,000,000 gallons of water. Because the canal ran north–south, the panels are slanted [10].

In November 2014, a 10 MW canal top solar grid-connected power plant in Vadodara, Gujarat, was commissioned (Fig. 4b). In this power plant, crystalline silicon photovoltaic cells are used. 33,816 solar panels and 14 630 KW inverters are utilized to produce 10 MW of electricity. This top solar power plant in Vadodara, Gujarat, has a total length of 3.6 Kindling and a total of four canals. Because the canal ran east–west, no tilting of the panels was necessary [11]. In March 2017, a 5.25 MW canal top solar power plant was built in Sangrur and Ludhiana, Punjab (Fig. 4c). This project uses 16,680 REC 315 PE 72 type solar panels, with an annual capacity of 8,414,000 kWh [12–16].

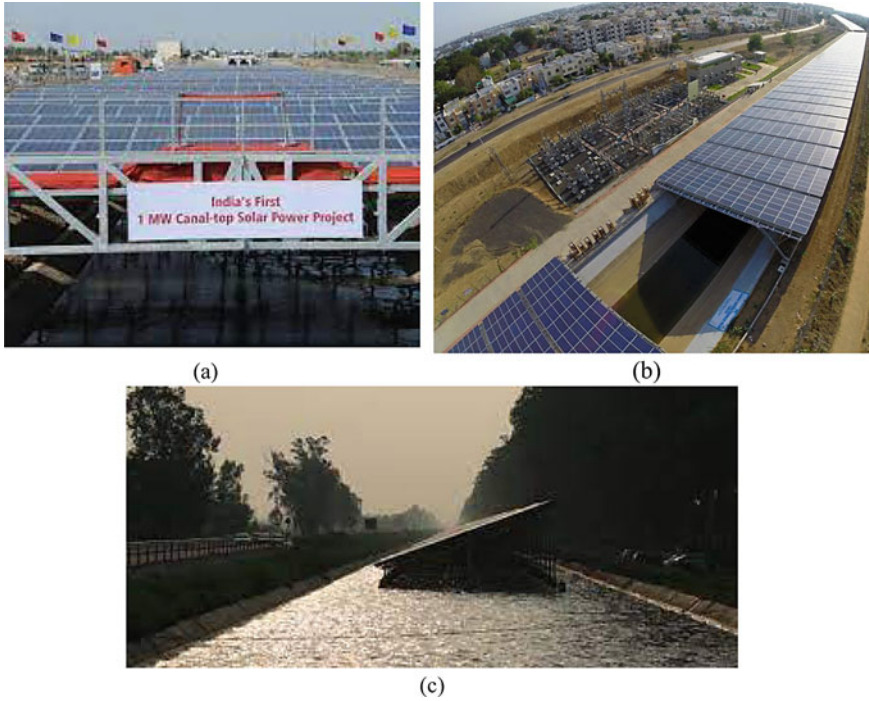


Fig. 4 a Gujarat’s first canal top solar power pilot project (India’s first) b 10 MW Canal top solar plant in Vadodara, Gujrat c Canal top solar plant in Ludhiana, Punjab

4.1 Different Canal Top Solar Power Plants in India

Canal top solar is an innovative method that has already been adopted by many Indian states. This provides a renewable energy source for agricultural and on grid activity while preserving agricultural land. Table 1 shows a list of several canal top projects.

5 Benefits of a Canal Top Solar Power Plant

We currently have a rooftop solar power plant and a ground-mounted solar power plant. The development, installation, and maintenance of a ground-mounted solar plant are all challenging. For construction, we must first select a place and buy acres of land, which requires legal formalities, bureaucracy, and occasional disagreements with the landlord. The infrastructure for rooftop solar power plant energy is not large enough to connect to the national electrical grid. All of these problems can be solved with a canal top solar power plant. With so much potential, solar plants can offer a constant supply of electricity during the day, when demand is greatest, and there

Table 1 Different solar projects in India [13]

Solar project	Location	Type	Technology	Cost of installation (USD)	Land area (Acres)	Installed capacity (MWh)
Bhadla solar park	Bhadla, Rajasthan	Land-based	Flat-panel PV	1.4b	14,000	2245
Kurnool ultra-mega solar plant	Kurnool, Andhra Pradesh	Land-based	Flat-panel PV	980 m	2974.11	1000
Adani Kamuthi solar plant	Ramanathapuram, Tamil Naidu	Land-based	Flat-panel PV	720 m	2500	648
Pavagada solar park	Pavagada, Karnataka	Land-based	Flat-panel PV	2.1b	13,000	2050
Kadapa solar power plant	Kadapa, Andhra Pradesh	Land-based	Flat-panel PV		5927.76	1000
Canal solar power project	Narmada branch canal, Gujrat	Canal top	Concentrating solar power	2.5 m	532 km of the Narmada Canal, Gujrat	1
Canal top solar grid-connected power plant	Vadodara branch canal, Vadodara	Canal top	Crystalline silicon PV	14.7 m	19.659	

is no need for fuel, which reduces maintenance and distribution, and transmission losses. For example, the length of the open canal in Gujarat is 458 km, but if we add sub-branches, it is around 19,000 km at the present, and when SSNNL completes the canal network, it would be about 85,000 km long. If we can only use 10% of the current canal network of 19,000 km, we can build a 2,200 MW solar power plant, save 11,000 acres of land, and save 20 billion liters of water each year. In comparison to ground-mounted solar panels, canal top solar photovoltaic panels not only save space but also make use of the space above the canal. India has to expand its industrial, agricultural, and residential areas to accommodate its expanding population, yet the cost of land is high. Because it exploits free space above a canal, a canal top solar plant offers a new solution to these problems. There would be no land costs, but we may save thousands of liters of water.

The canal top solar plant lowers evaporation and saves water that may be used in a variety of industries. The annual quantity of water evaporated is provided by:

$$E = 43.3 + T4.5 \tag{4}$$

where as E —Evaporation (cm/year), T —average yearly temperature ($^{\circ}C$).

By applying the above equation, Gujarat’s first model 1 MW plant can save 9 million liters of water.

The panel is positioned on the canals, which can improve the plant's efficiency. Because of the water underneath, it will assist to reduce the temperature of the panel, and feather it will gain confidence and if we use reflectors in plant efficiency can also be boosted.

6 Conclusion

The canal is the oldest and cheapest form of irrigation and has a long network that occupies a vast area, but we were unable to make use of those lands due to a lack of innovative ideas. Canal top solar plants may use such lands to generate clean energy with better efficiency by utilizing solar panels. More renewable energy projects all across the rest of the canal are needed in India. The canal top solar power plant takes up less space, saves a million liters of water, and lowers transmission and distribution line losses. A solar power plant on the top of a canal could help India's national grid become more environmentally friendly. Because the water below the panels reduces the temperature and boosts the energy conversion efficiency, this canal top power plant has higher efficiencies. This power plant may also be utilized for agricultural water pumping stations, which can reduce the cost and CO₂ emissions associated with traditional energy generating methods.

References

1. Samir KC, Wurzer M, Springer M, Lutz W (2018) Future population and human capital in heterogeneous India. *Proc Nat Acad Sci* 115(33):8328–8333
2. Kumar NM, Gupta RP, Mathew M, Jayakumar A, Singh NK (2019) Performance, energy loss, and degradation prediction of roof-integrated crystalline solar PV system installed in Northern India. *Case Stud Therm Eng* 13:100409
3. Usman O, Iorember PT, Olanipekun IO (2019) Revisiting the environmental Kuznets curve (EKC) hypothesis in India: the effects of energy consumption and democracy. *Environ Sci Pollut Res* 26(13):13390–13400
4. Shahbaz M, Van Hoang TH, Mahalik MK, Roubaud D (2017) Energy consumption, financial development and economic growth in India: new evidence from a nonlinear and asymmetric analysis. *Energy Econ* 63:199–212
5. Madurai Elavarasan R, Selvamanohar L, Raju K, Vijayaraghavan RR, Subburaj R, Nurunnabi M, Khan IA, Afridhis S, Hariharan A, Pugazhendhi R, Subramaniam U (2020) A holistic review of the present and future drivers of the renewable energy mix in Maharashtra, state of India. *Sustainability* 12(16):6596
6. Kiesecker J, Baruch-Mordo S, Heiner M, Negandhi D, Oakleaf J, Kennedy C, Chauhan P (2020) Renewable energy and land use in India: a vision to facilitate sustainable development. *Sustainability* 12(1):281
7. Ramachandra TV, Jain R, Krishnadas G (2011) Hotspots of solar potential in India. *Renew Sustain Energy Rev* 15(6):3178–3186
8. Augustin D, Chacko R, Jacob J (2016) Canal top solar PV with reflectors. In: 2016 IEEE international conference on power electronics, drives and energy systems (PEDES). IEEE, pp 1–5

9. Sajimon A, Chacko R (2017) Design of reflectors for a canal top solar power plant. In: 2017 IEEE international conference on intelligent techniques in control, optimization and signal processing (INCOS). IEEE, pp 1–4
10. Sumaiah Naz P (2017) Generation of solar energy developed in different states of India. *Int J Eng Res Technol* 6(6)
11. Elavarasan RM, Shafiullah GM, Manoj Kumar N, Padmanaban S (2020) A state-of-the-art review on the drive of renewables in Gujarat, state of India: present situation, barriers and future initiatives. *Energies* 13:40
12. Singh BR, Singh O (2016) Future scope of solar energy in India. *Samriddhi: J Phys Sci, Eng Technol* 8(01):20–25
13. Buckley T, Shah KJ (2018) Financial analysis, solar is driving a global shift in electricity markets: rapid cost deflation and broad gains in scale
14. Belyakov N (2019) Sustainable power generation: current status, future challenges, and perspectives. Academic Press
15. Breeze P (2016) Parabolic trough and fresnel reflector solar power plants. 25–34
16. Gharbi NEI, Derbal H, Bouaichaoui S, Said NJEP (2011) A comparative study between parabolic trough collector and linear Fresnel reflector technologies 6, 565–572

Weapon Detection Rope Roaming Human Safety Robot



Praveen Kumar Maduri, Priyanka Sharma, Himanshu Saini,
Pradyuman Mani Tripathi, and Sakshi Singh

Abstract This paper is proposing a human safety robot which will be roaming on the rope above the ground including camera to surveillance particular area, road or any other premises. It is designed for areas which are unsafe or where crime rate is high. As era changes the necessity of modern technologies is must to secure everyone, so this problem is proposed for focusing strongly on the human safety during day and night. It introduces with a new mechanism which will be proved as a guard during un-happening or abnormal incidents. For improving the accuracy of the project we will use CNN model algorithms. This roaming robot moves on the rope or wires at particular time intervals with the mounted HD camera with sound sensors with the weapon detection. It works on predefined back–forth path for surveillance. It is designed in the way that it moves on the predefined forward and backward direction. It roams to that direction from where the incidental sound is received and clicks 360 degrees pictures and videos of that area to detect and identify the human and weapon. It instantly sends whole data on the designed online platform. It has ability to detect the weapon like gun or knife at the incident place; here we are using raspberry pi local area network for transmission of the footages with alerting sound. It is fully automatic human safety robot which secures and monitors the premises or area with weapon detection (knife/gun etc.).

Keywords Human safety · Raspberry Pi · Machine learning · CNN · Weapon detection · Centered shaft motor · Pi cam · Internet of things

1 Introduction

In the modern era, human safety is the major concern in different areas of the world, the technology has transformed but humans are not safe due to increase in crime rate as no one feels safe in night at public place. To enhance the protection of less secure areas a model is implemented which runs on the wire/rope connected on pales, and

P. K. Maduri · P. Sharma · H. Saini (✉) · P. M. Tripathi · S. Singh
Galgotias College of Engineering and Technology (AKTU), Lucknow, India
e-mail: himanshusainiisd@gmail.com

it also can detect weapon clearly. Convolution neural network (CNN), ML model is used in this project for weapon detections [1]. It is designed in the way that two sound sensors are attached to both opposite sides of the robot also the HD camera is used with servo motor for capturing the images of all sides. It will be patrolling to that side from where the sound of particular predefined frequency value is detected then it will analyze incident, detect the weapons and monitor the situation with the capturing of pictures of the incident and transmit it to particular designed platform [2].

Here Raspberry PI microcontroller is used to control and manage all their module sensors used by this device for better performance. It monitors the premises road and other areas from a specific height on the rope connected on poles, on which robot will be patrolling and surveillance that area [3]; prototype is shown in the Fig. 1. It is fixed on a specific height so no one can touch or harm the robot, and the robot can easily scan area and roam without obstacle on its path, we have used R-pi local area network for transmission of image to the predefined IOT dashboard thus we are eager to implement fully automatic human safety robot which can work 24×7 tirelessly and can surveillance large specific area [4]. Various machine learning models are used for detecting the weapons and sound of human so it can easily identify the direction and human voice for immediate approach to the incident place. Two motors with pulley are fixed in the way that they can roam on the rope or steel wire in both directions.

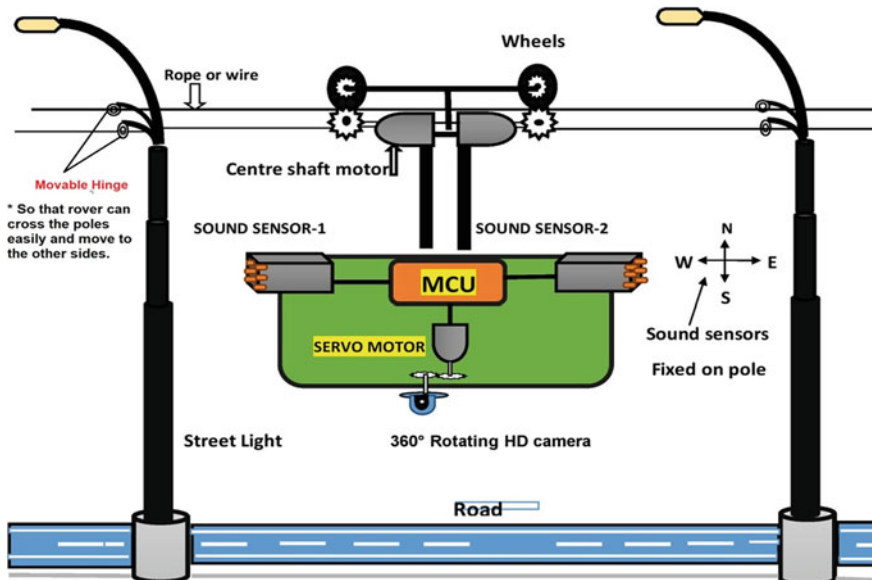


Fig. 1 Project prototype

2 Literature Review

In this era, there are many research and inventions going on to fulfill today's necessities and comfort of citizens. So with focusing on security topic in high-tech cities also to enhance the security features a weapon detection rope roaming robot is designed and implemented. Till now, road patrolling rowers are used due to roaming on road, many problems were faced e.g. traffic problem, system harm etc. [5]. Some gadgets based on geo-locations have been implemented by some authors which are IOT based systems. Whenever button is pressed then it will alert to the parents and nearest police station with the real-time location of that person, it is specially made for children and women so they can feel secure every time. In these systems, crime areas were pointed with criminal pattern based on particular areas [6]. As per day, crime rate is going up, harassment, accident murders, women security is the major concern in weight as they should feel secure whether in day or night; also for the women safety some ML modules are used in road patrolling power, raspberry pi model with pi can be used in this model to capture the required image for transmission [7].

This project uses HD camera with 360 degree rotation which will be patrolling continuously and this uses sound detection technology for surveillance of the particular area premises it will send all the clicked pictures and videos and detect information on the designed available IOT dashboard, so that assigned officer can receive the robot, the weapon detection technology is used in it with the CNN model [8] to differentiate whether the offender is normal or with weapon (e.g. gun, knife); OpenCV, dark net and YOLO applications are used to perform the weapon detection task. And this whole data is monitored and controlled by administration with the designed platform remotely.

3 Methodology

3.1 Monitoring and Controlling Part

Whenever the sound will be detected from any directions, then it is received through sound sensors. Four sound sensors are fixed at the poles with the range of 200 m between the poles, facing toward each direction (e.g., north, south, east and west). Each of them will transmit data with direction indication. So that rover can click the photo of particular direction. Accordingly, it can move to received direction for performing its operation. As per matching of accidental sounds with predefined values (e.g., crash, firing, vehicle accident etc.) and start capturing the picture of that direction as shown in Fig. 1. Also, two sound sensors are fixed back and front side and fix the HD camera at the bottom facing downward with servo motor battery is set with in the acrylic box. Center shaft motor with pulleys they can move on the wire or rope provided to roam and rope is clipped at poles. Four sound sensors are fixed at pole having distance of approx. 200 m which are used to signal the direction



Fig. 2 Pictures of implemented rover moving on rope

of the incident to the microcontroller, so that robot moves quickly to that received direction and can monitor it fastly.

When incidence occur within the area then sound sensor detects human voice with a range of defined frequency, robot will start moving to that direction immediately with the help of rope roaming pulleys connected to CSM. Then it will analyze the event, then PI camera will face toward it and click the pictures and send them immediately to the platform provided. It will roam on the rope or wire smoothly so the pictures will be clear and out of reach of human. Through IOT, its transmission and communication are carried out in the supervision of administrator. After sound detection sensor sent the signal to R. Pi and it allows the PI. Cam is mounted on servo motor to click the images forwarded to R. Pi and transmit to predefined base station. Also, signal is received by CSM to move in advised direction immediately. It will be patrolling with some duration according to received signal, and work from a specific height as shown in Fig. 2.

3.2 *Weapon Detection Part*

It detects the weapon using machine learning with open CV and YOLO (You Only Look Once), an advanced technology used for object detection in the in the image or video received from the HD camera mounted on the servo motor. Dark net is used for neural network implementation with advanced detection frameworks for image or video classification for weapon detection. YOLO focuses on entire video or image received and detects object after going through the network. Deep neural network used openCV_contrib with the ability to run an interface on pre-trained DCM with OpenCV.

This operation of clicking images and videos is carried out with the Pi cam with Raspberry Pi microcontroller which will analyze the whole data and send it to the designed dashboard for further monitoring and controlling of algorithms used as shown in Fig. 4. This is performed using YOLO and CNN measuring weights of the detected data with neural network with complexity and good observation speed. Complexity will increase for calculating the combinations of weight correctly. The

difference of desired target vector and output vector are used to update the weights of neural network, and continues till their difference becomes minimum. The calculation of gradient of given error function is carried out at each iteration as shown in Figs. 3 and 4.

If U is the input vector, W is the weight of given hidden layers and T is the output vector then,

$$T_k = \sum U_b W_c \tag{1}$$

where T_k is the k th layer output of given input U_b and b will be $c - 1$.

Fig. 3 Working flowchart

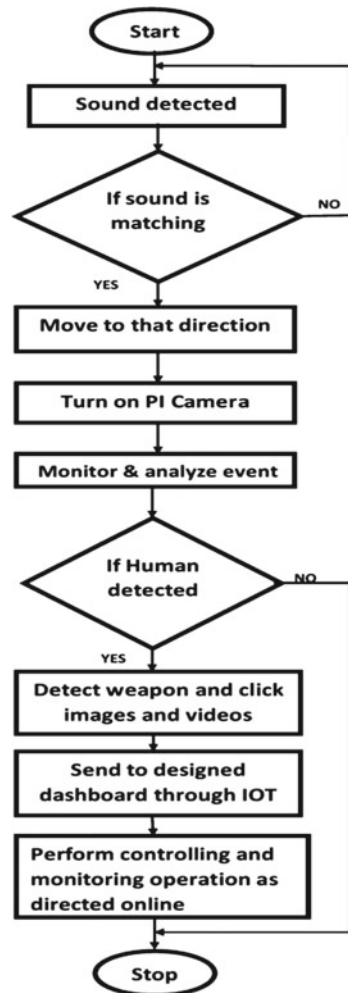
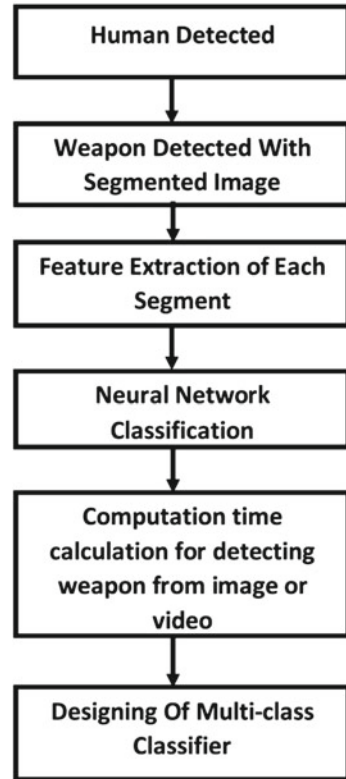


Fig. 4 Weapon detection algorithm



4 Working

Robot detects sound with sound sensors and checks with already predefined values of frequency used, if sound is matching then it starts run to that direction, turns ON Camera, monitor and analyze the incident. Also detects human if found then check for weapon otherwise no action will be taken. It will click images and videos and sends to the controlling department so that monitoring, controlling and further actions can be taken by administration regarding the incident as shown in Fig. 5. The data frame is analyzed whether it is set in that given pixel frame then neural network classification performed after receiving data from camera. An input image or video is inserted into its frame with tensor flow and YOLO, dark net. It is built with setting n -fold cross validation of data then builds the training of neural network model with the help of sampling of each weight by normal distribution as shown in Fig. 3.

Each node is having three attributes and processes:

1. Forward-Passing, each node's output is calculated as a weighted node with sum of previous layer data input with following sigmoid transfer function.



Fig. 5 Captured images transmitted to dashboard

2. Backward-passing, the classification of errors is performed for updating deltas node provided current node weights with delta rule eqn. which is derived from gradient descent of loss function.
3. The forward-pass is performed for updating current weights which uses deltas and node outputs both, for further recognition.

The class making prediction is started which provides approximations of detection of predefined patterns so that the accuracy score will be more to recognize the object pattern. Then computation time is calculated to know the time taken for completing the detection process and will be indicated with colored rectangular box, then received object data is categorized into multi-class classifiers with available labels in dataset, techniques applied for classification as one v/s all and one v/s one to check the different types of objects available in fetched images or videos. This whole information is monitored by the assigned officers and whole incident can be analyzed so that robot can be controlled for taking further suitable actions required immediately for human safety as shown in Fig. 4.

5 Results and Outcomes

The proposed model works nicely with weapon detection successfully, and quality of monitoring, controlling and weapon detection is so fine and results are shown in the Fig. 6. The output of detected weapon is seen on screen as (weapon detected in frame) and whenever not detected provide no output as blank space in brackets (). The videos or images fetched from HD camera are automatically configured with this machine learning model and shows a command message (received file for weapon detection) as shown in Fig. 7.

Finally, each and every video/image is detected nicely with the convolution neural network and YOLO (You Only Look Once) which is a real-time weapon detection algorithm, identifiers objects in images, videos or live feed. Dark net is used in this system which is an open-source platform, faster and works on python easily with neural networks. For mass surveillance to protect the citizens from criminals with

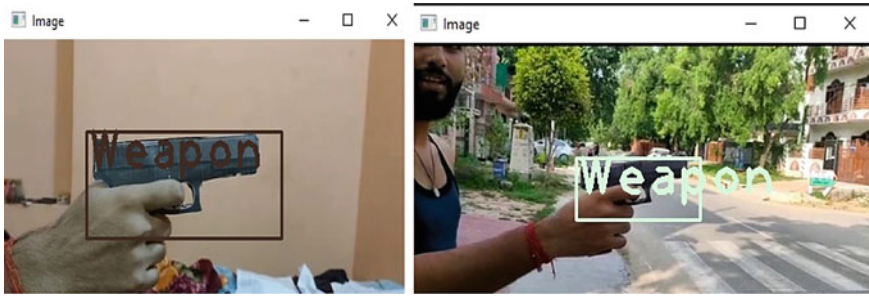


Fig. 6 Weapons detected with by robot

Fig. 7 Program o/p of detected weapons

```
Received file for weapon detection :  
gunn2.mp4  
[[0]]  
weapon detected in frame  
[[0]]  
weapon detected in frame  
  
Process finished with exit code -1
```

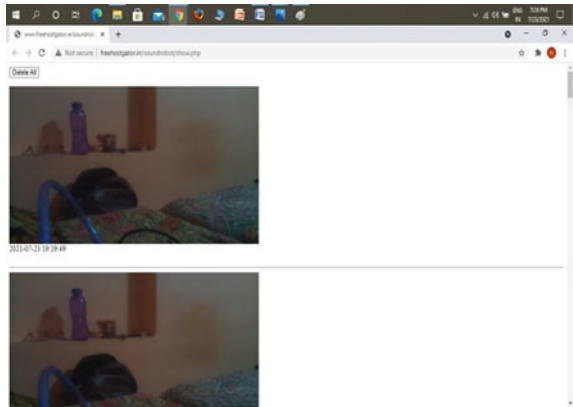
the CNN models used which detects weapon containing human and sends signal with the indication of weapon in colorful rectangular box for further identification of offender.

In real-time the live feeds, images or videos pass through this algorithm and recognize human executing crime or any illegal activity society, road or within any premises. And this whole information is shared with the linked platform designed for monitoring and controlling the robot so that suitable actions can be taken accordingly taken by assigned administration shown in Fig. 8.

6 Conclusion and Future Scope

In this model security problems of society and a perfect solution with advanced technology proposed so, human can feel free to have outside independently with this implemented system, the crime rate can be classified scientifically, it will reach immediately detect weapon, click images with different angles then send to predefined administration's dashboard. It will facilitate more security features with the R. Pi which can be modified later. It will surveillance and secure the premises or area completely which will help in the modern era to reduce crime rate. It also detects

Fig. 8 Monitoring and controlling dashboard



weapon for easier detection type of event so that multiple controlling operations can be performed immediately. Anyone can feel secure while going to anywhere and make administration to find out and detect the criminal easily which will affect in reducing crime rate. It is above from ground so no traffic problem, out of human reach (no obstacle in its work), detect the weapon easily, used IOT technology for transmission (fast and secure), less power consumption (due to moving on rope). It can be a better model when we inclined the full automation, (reducing the effort of monitoring by authorities. It should take actions on its own to manage the incident. It is safe for environment; no harmful effect is ejected and need no maintenance for a long period of time.

References

1. Delgado E, Tapia L (2021) Robotics research during a pandemic [Women in Engineering]
2. Gopalakrishnan K, Thiruvenkatasamy S, Prabhakar E, Aarthi R (2019) Night vision patrolling rover navigation system for women's safety using machine learning. *Int J Psychosoc Rehabil* 23(4):1136–1148
3. Hermawan H (2019) Experimental vision robot for general working application using raspberry Pi and single camera with python-openCV. *ACMIT Proc* 3(1):231–238
4. Scherer J, Rinner B (2020) Multi-robot patrolling with sensing idleness and data delay objectives. *J Intell Rob Syst* 99(3–4):949–967
5. Lengare M (2019) A review on night vision robot patrolling and monitoring system. *Int J Res Appl Sci Eng Technol* 7(1):341–344
6. Devakunchari R, Bhowmick S, Bhutada SP, Shishodia Y (Jan 2019) Analysis of crimes against women in India using regression. *Int J Eng Adv Technol (IJEAT)* ISSN: 2249-8958. 8(2S2)
7. Verma GK, Dhillon A (2017) A handheld gun detection using faster R-CNN deep learning. In: *Proceedings of the 7th international conference on computer and communication technology*. ACM, pp 84–88
8. Bochkovskiy A, Wang C-Y, Liao H-YM (2020) YOLOv4: optimal speed and accuracy of object detection. arXiv preprint [arXiv:2004.10934](https://arxiv.org/abs/2004.10934)

Review and Real-World Usability of Magnetic Levitation Trains



Anshuman Srivastava, Anurag Chaturvedi, and S. Kennedy

Abstract This literature involves the design, equipment, dexterity, purpose, and future uses of “Maglev Trains”. It is a much more reliable, efficient, and more futuristic mode of transportation. They are currently used in applications such as carriage, high-speed trains, and their construction. There is no use of conventional means of equipment like bearing, axles, etc. instead magnetic propulsion is used to drive the vehicle. In magnetic levitation, the pod is put above the rails using a strong magnetic field to a short distance with which frictionless motion is made possible. There have been clashes between contemporary and modern means of transport nowadays because of lower efficiency. While Europeanized air travel has increased in the later decades. The (Hyperloop) is a fairly modern transport technology that is in wide experimental process and it has claimed to provide superior performances to backdated and somewhat modern rail and air transport systems in terms of safety, reliability, and time-saving manner.

Keywords HL (Hyperloop) system · Magnetic induction efficiency · Long-distance transport · Modeling · Assessment · Electromagnetic suspension

1 Introduction

Magnetic Levitation vehicles (trains) move much more efficiently than conventional trains. They are free of any contact friction and traction, also they have better capabilities of much higher acceleration and decelerations. The power used mostly consists of powering those electromagnets as well as reducing the air drag as maglev trains move with very high velocities. Magnetic levitation also improves efficiency and longevity of systems as there is comparably very less wear and tear. It also minimizes the operation cost of the system. Competition between conventional and modern trains

A. Srivastava (✉) · A. Chaturvedi · S. Kennedy
School of Mechanical Engineering, Galgotias University, Greater Noida, India
e-mail: anshumansri98@gmail.com

S. Kennedy
e-mail: kennedy.s@galgotiasuniversity.edu.in

has lasted over a decade [1]. However, in European countries instead, air transport has gained a popular demand with industries. The hyperloop system aims to improve running to high-speed rails and air travelers, particularly in terms of travel time, transportation costs, energy efficiency, and freight safety. Existing studies have not been very successful in demonstrating the uses and have proposed significant models. This research aims at giving new insights into various aspects of working, commercial, and communal, ecological, performances of the hyperloop technique and contrast them to popular means of transport in the present [2]. The results of these differences are intended to support the discussion about the overall achievability of the maglev vehicles.

2 Literature Review

This concept was first proposed by Elon Musk in 2013 in his release of the Alpha paper. It outlined hyperloop, in a particular way of putting the pod (Moving part) inside a vacuum tube which could achieve high velocities with little to no loss. He also conducted a hyperloop competition to popularize the idea of hyperloop with fundings of his own company called SpaceX [3]. It centered on the evolution and prototype experiment of a subscale model of hyperloop. It was named as one of the most successful teams in that competition, the hyperloop team from (MIT) revealed the first mini-scaled prototype in May 2016 and later demonstrated the working scale model on Jan 17. Since the release of the Alpha paper, several other hyperloop firms in North America and Europe have assembled and have carried on to develop their own HL technologies, with a vision of taking it to the level of commercial maneuver.

2.1 *Scale of Readiness*

It can be shown in the given table indicating the ergonomics and the technology on hand to dispose of on various grounds related to this review (Fig. 1).

2.2 *Magnetic Levitation Technology*

This specialization uses single rail tracks with in-line motors, such trains move on specialized tracks instead of earlier gauge tracks. They float about 1–10 cm above the path over a magnetic field. Once the train is shifted to the next segment the magnetism changes so that the train is withdrawn again. The electromagnets run throughout the entire length of the mono track.



Fig. 1 Proposed scale of readiness showing general trends in various stages of development [4]

2.3 High-Speed Rail (HSR)

Development of the High-Speed Rail System has been developed in Europe and the United States, these developments have been taken into account to enhance rail transportation and achieve efficiency in conventional means. The system has had different meanings and roles in the particular region of the world.

2.4 The HL (Hyperloop) System

Historically, several models and hypothetical prototypes have been introduced of maglev trains which were only at hypothetical level, mainly aiming to reduce substantial travel time when set against previous modes, and therefore being taken on in the transport system. The Hyperloop has the potential to convey people and freight just like an ordinary rail transport system at very updated and hypersonic speeds while being ultimately energy efficient when compared to the present HSR systems.

2.5 Theory and Operations

Reducing friction and air drag have been the obstacles while designing high-speed rail systems, both of which are tangible issues when vehicles commence to hypersonic velocities. The proposed idea has overridden such limitations as there will be no contact friction as well as the resulting air drag would also be zero. However, it incurs high cost of maintenance when there has to be fulfilled one of the required conditions of making the tubes vacuumed throughout over large distances which will be then and only then we can achieve the target of operating the vessel at hypersonic

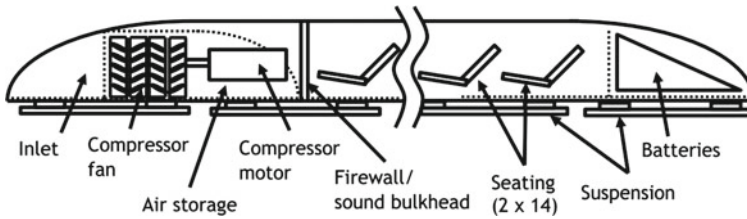


Fig. 2 Proposed design for Hyperloop pod construction [5]

speed. The Hyperloop system requires air pressure of less than 100mb (millibars) when compared to atmospheric pressure of 1 kPa.

2.6 Working

Large-scale vacuum pumps are required to first create a low pressure and then displace small particles around the tube by heating process, especially carried around the first and the third chamber relative to the pod position. Such pumps draw huge amounts of energy at the initial stage of evacuating the air inside but later after a sustained level is met, the overall power consumption is fairly low (Fig. 2).

2.7 Modeling Performance

The main human capital required to carry on operations are of two types basically, the first one is technical and component care and second being the quality of services provided. Mainly focusing on the performance front while the system is under development and the latter is opted when a commercial-scale production is met, so as to provide better facility to consumers [6].

2.8 Vacuum and Power

The vacuum tubes are the fundamental component in the design of hyperloop systems, other functioning parts consist of power units and air evacuating vacuum stations. Other electronic components will be connected to the power grid via Small power subunits. The system would require power delivery in a sustained manner to function in various numbers of subdivided departments for e.g., Propulsion systems, power transfer mechanism, etc. [7] (Fig. 3).



Fig. 3 Image showing vacuum power generation unit [8]

2.9 Levitation and Guidance

The basic maglev trains are distinguished from hyperloop as the latter also include an almost zero air drag which further lowers the power needed for a forceful propulsion in order to break the inertia of rest. Some conventional maglev technology is being used in Japanese model of bullet trains where there is less contact friction with the rail tracks but hyperloop being a superior technology is way ahead in terms of efficiency. Notably, initial Hyperloop models were designed in such a way that the compressed air could be used to create an air bearing beneath the capsule so that any external power is not required to levitate the pod [9]. However, with later development in literature on hyperloop technology, this approach is now considered more of an impractical one, as there was an estimation that moving pods would not be displacing a very significant amount of air. It is likely not possible to design and maintain a track system of such dimensions to meet the required thrust to uplift a vehicle.

2.10 Engineering Problems

On propulsion with permanent and electromagnets.

Advantages: This new mode of transport will be more technologically advanced as it uses the most enhanced and efficient propulsion technology, levitation with lower drag distance, and also less bulky vehicles with more capacity to carry passengers and freight. This system can be used conveniently on the existing MagLev concepts and does not require breakthroughs in its basic technology, which is transportation within a tube.

Disadvantages: A major disadvantage listed for a successful and effective propulsion and levitation is continuous supply of energy for a seamless transmission of the vehicle. Also, there will be a need for a permanent Human Resource to do inspection in the area of in-efficiency. This process would be difficult while reducing resilience and it would be a lot costly to maintain [10]. A minor fault might lead to an enormous amount of damage to basically every part of the pod vessel especially when it will be moving at hypersonic velocity and it also could create panic among people commuting with a strong feeling of claustrophobia as a high-speed train inside a sealed tube! Some failure in the levitation mechanism would require a landing ground for the vehicle too.

2.11 Engineering Review Conclusions

In this part, we are revisiting the Technology Readiness Level (TRL) of some most important elemental technologies related to the Hyperloop system using retrievable facts present in published journals and few expert judgments. We have also look forward to the existing literatures and other published studies by taking into account various available solutions for the basic study of our literature (e.g., propulsion, levitation and rail track aspects, and various power delivery techniques) to send away the highlighted nitpick in the technology that today’s competitive firms on Hyperloop have thought to commercialize [11]. The below diagram shows how much progress has been met to the present date (Fig. 4).

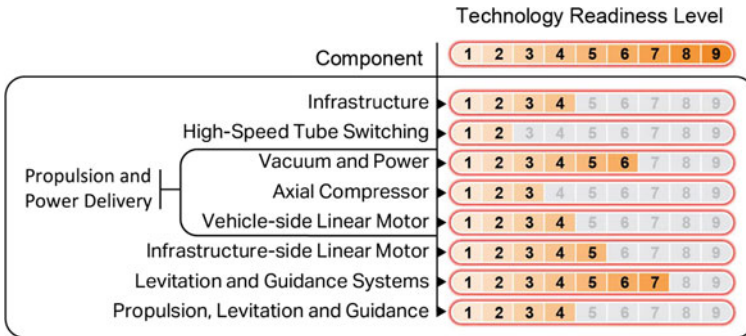


Fig. 4 Technology readiness level schematic for Hyperloop development [12]

Description	Capital Cost (Million)
Guideway, Tubes & Switches	\$12,080
Stations & Depots	\$1,100
Support Facilities	\$1,630
Sitework	\$1,480
Systems	\$3,330
Vehicles	\$650
ROW & Land Acquisition	N/A
Professional Services	\$4,260
Unallocated Contingency	\$3,670
Total	\$28,200

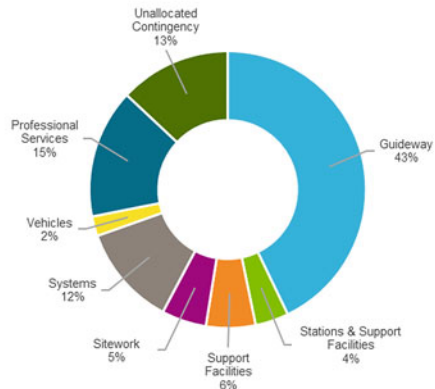


Fig. 5 Table with pie chart showing economical aspects for development [15]

3 Conclusion

3.1 Capital Cost Assessment

The economic side of our study has two key aspects. The first tool estimates the engineering obstacles on propulsion, levitation, material requirement and power consumption of the pod vehicle to be achieved effectively without spending more than the allowed budget and also keeping in mind competitiveness [13]. Because all these futuristic technologies are proposed by keeping in mind their usability on a commercial scale. The second model estimates all other expenditures in the field of construction, infrastructure pod vehicles, and other facilities that will be required to provide their clients (Individual/industrial) all the desired services that they get in today’s conventional transport systems. There’s also a third model for human capital requirements but that is not the focus of our study [14] (Fig. 5).

3.2 Summary of Capital and Operating Costs

This particular part consists of our capital and manufacturing costs for hyperloop. While assessing the capital cost we have considered for experimental purposes a 500 km route to test the feature set of various of its mechanism. This analysis of the capital cost tells us an estimated expenditure of \$56.4 Million/km, which is much greater than the Alpha paper proposed by Musk which estimated one-third of cost incurred in our assessment [16]. Though some macroeconomic factors did play a role for example inflation and rising labor wages, etc. It did not come as a surprise

as the actual prototype had much more complexity in real-life situations. Still, some technology that is being incorporated into real-world modeling of several improved components has made our predictions more difficult [17, 18].

3.3 Final Words

Hyperloop is still a very new piece of technology that is highly capable of transforming how we look at our transportation infrastructure. Given mankind's achievements over the past few decades, there are lesser doubts that we can achieve the goal of developing Hyperloop as the fifth mode of transport. However, there are few concerns about safety, reliability, and the huge cost of infrastructure development. We will be needing more technological enhancements to overcome engineering hurdles. It is still in its infancy stage but with time the hurdles would be crossed. Still, there is some time left to put the concept on commercial scale, a decade or so would be the earliest possible prediction.


References

1. Van Goeverden CD, Van Arem B, Van Nes R (2016) Volume and GHG emissions of long-distance travelling by western Europeans. *Transp Res D* 45:28–47. <https://doi.org/10.1016/j.trd.2015.08.009>
2. Lee DS, Fahey DW, Forster PM, Newton PJ, Wit RCN, Lim LL, Owen B, Sausen R (2009) Aviation and global climate change in the 21st century. *Atmos Environ* 43:3520–3537. <https://doi.org/10.1016/j.atmosenv.2009.04.02>
3. Commission E (2014) EU Energy, transport and GHG emissions, trends to 2050, reference scenario 2013. Publications Office of the European Union, Luxembourg
4. Musk E (2013) Hyperloop alpha. SpaceX, Texas http://www.spacex.com/sites/spacex/files/hyperloop_alpha-20130812.pdf
5. Abdelrahman AS, Sayeed J, Youssef MZ (2018) Hyperloop transportation system: analysis, design, control, and implementation. *IEEE Trans Ind Electron* 65(9):7427–7436. <https://doi.org/10.1109/TIE.2017.2777412>
6. Braun J, Sousa J, Pekardan C (2017) Aerodynamic design and analysis of the hyperloop. *AIAA J* 55(12):4053–4060. <https://doi.org/10.2514/1.J055634>
7. Hyperloop commercial feasibility analysis: high level overview. Report. Arup, BCI, TNO & VINU (2017). Main report: hyperloop in The Netherlands. Report
8. Catapult Transport System (2018) Hyperloop—opportunity for UK supply chain. Report Delft Hyperloop (2019)
9. Werner M, Eissing K, Langton S (2016) The future of Hyperloop. Report shared value potential of transporting Cargo via Hyperloop. Article
10. Ross P (2015) Hyperloop: no pressure. Article. *TransPod* (2017) Initial order of magnitude analysis for TransPod hyperloop system infrastructure. Report
11. Paczek P (2017) The hyperloop concept compared to the economic performance of other means of transportation. Article
12. Gonzalez-Gonzalez E, Nogues S (2017) Railways of the future evolution and prospects of high-speed, MAGLEV and Hyperloop (PART1). Article

13. Gonzalez-Gonzalez E, Nogues S (2017) Railways of the future evolution and prospects of high-speed, MAGLEV and hyperloop (PART 2). Article; Janic M (2018) Multicriteria evaluation of the high speed rail. TransRapid Maglev Hyperloop Syst
14. MIT Hyperloop Team 2017 (2017) MIT Hyperloop final report. Report
15. Ji W-Y, Jeong G, Park C-B, et al (2018) A study of non-symmetric double-sided linear induction motor for hyperloop all-in-one system (Propulsion, Levitation, and Guidance). Article
16. https://www.tapecon.com/hubfs/MRL_blog-01.svg
17. <https://www.frontiersin.org/articles/10.3389/fbuil.2016.00017/full>
18. Federal railroad administration—capital cost estimating guidance for project sponsors (30 August 2016)

Entrepreneurial Women in the Culture of Ceará: The Case of Cearens Literature



Thais Helena Costa da Silva, Tatiana Monteiro Holanda,
Janina Mirtha Gladys Moquillaza Sanchez, Matloobullah Khan,
Sandeep Kumar Gupta , and Rohit Kaushik

Abstract This article aims to know about women's entrepreneurship in the field of culture, specifically in the literature area. The study object is the case of the Aquiraz Literary Party promoter, Terezinha Holanda and also two Ceará highlight writers of the Literature Academy of Ceará are interviewed, we aim to understand their motivations and challenges. Our research hypothesizes that society preserves "machista" notions that influence women's entrepreneurship. This research adopts Hisrich entrepreneurship notions, the idea of intrinsic motivation of Cecilia Bergamini, and the debate of Maria Ritha Kehl about the *feminine*. For a better understanding of women's entrepreneurship action in this country, we recurred to Mary Del Priore and her studies about the history of active women in Brasil. The methodology of this research is quali-quantitative; formularies were applied and data collected were analyzed so as the interviews. We finally found that cearense society believes that women entrepreneurship innovate, they are creative and in this process, they promote social changes.

Keywords Entrepreneur women · Cearense literature · Culture · Motivation

1 Introduction

The purpose of this research is to learn about women entrepreneurs in the context of Ceará culture, specifically in the area of literature, and to seek to understand their motivations and challenges. This study aims to know how the female entrepreneur

T. H. C. da Silva · T. M. Holanda · J. M. G. M. Sanchez
Centre Christ University, Fortaleza, Brazil

M. Khan
Jamia Hamdard, New Delhi, India

S. K. Gupta (✉)
IIMT College of Engineering, Greater Noida, India
e-mail: skguptabhu@gmail.com

R. Kaushik
G. L. Bajaj Institute of Technology and Management, Greater Noida, India

is perceived by society in the culture of Ceará and to analyze how they undertake in the literature of Ceará.

Theoretically, Cecília Bergamini's concept of intrinsic motivation was adopted [1] because according to the author, motivation is always internal, internal to the person, and independent of external stimuli. For a better understanding of the action of women entrepreneurs, the theory of entrepreneurship by Hisrich [2] was also adopted, which maintains that the entrepreneur is the one who is "between", that is, he is an intermediary that promotes a process of creation in the sense of creating something new, of value. The entrepreneurial process involves more than a simple solution to administrative problems, the entrepreneur must find, evaluate, and develop opportunities, overcoming the forces, the challenges that resist the creation of something new. For the discussion on femininity, contributions by Kehl [3] were adopted, and for a better understanding of the action of Brazilian entrepreneurial women, Priore [4] and her studies on the history of active women in Brazil were used. The methodology of this research is quantitative and qualitative. As part of the GEP—Anthropology of Administration and Entrepreneurship of Women, the group held a seminar on entrepreneurship of women from Ceará, with the participation of businesswomen awarded by SEBRAE in previous years, having been able to listen and learn from their experiences. We visited EDISCA, having interviewed Dora Andrade, a third sector businesswoman who also told us about her experience. We participated in an event at the Academy of Letters of the Municipalities of Ceará, ALMECE, in which women who work in the literary sector were awarded. We visited the Aquiraz Education Secretariat, interviewing the Education Secretary who carries out the FLAQ Project—Aquiraz Literary Festival. Through the quantitative methodology, data were collected through the questionnaire to know what the society of Ceará women thinking. Presently, the results found demonstrated that the society of Ceará believes that the entrepreneurial woman innovates, creates, and changes society in her entrepreneurial process [1, 2, 5].

2 Literature Review: From Resistance to Entrepreneurship

"Sociologists and everyone else can be scandalized: for the twenty-first century, I foresee the social victory of women. Women will cease to be the secondary element in society and the family, to assume the vanguard of all acts and all events ..." (Rachel de Queiroz 1940). Priore [4], when studying the woman in the history of Brazil, the author found an abundant production of works praising women. According to the author, this was intended to cover up the true intentions behind the words, which aimed at better "taming them" for the life of the home and creating a model of an obedient, modest female body and of "sad meats" [3, 6].

Diogo de Paiva de Andrade (1782) "Instruction to married ladies to live in peace with their husbands" referring to what the husband was allowed to advise his wife and punish her if he found that she deserved it, which made us realize that the physical and mental purity of women went beyond sacred and profane texts invading

colonial communication. The author maintains (Idem) that the ideal model of women that society tried to impose adhered to hypocrisy. However, resisting the power of the church and the society ruled by men, women resorted to ecclesiastical courts to separate themselves from their husbands, fiancés, lovers, and boyfriends; also resisting the exclusive model of marriage they responded with adultery and through wills revealed other faces of their behavior in making known bastard children. Mary Del Priore also quotes Nísia Floresta Brasileira Augusta, from the Northeast, married at the age of 13, despised by the family for having separated from her husband a year after marriage, and even so she continued to help her family financially by teaching at a school [7]. She was responsible for a publication on the prejudice of Brazilian society against women “Women’s Rights and Injustices of Men” published in 1832. The author denounced that “if we asked the opinion of men about women they would say that old concept that already it is rooted in the culture of the society that women only serve to care for children and the home and to satisfy and obey male desires (...)” (S/d, p. 144).

In fact, in Western industrialized societies, they were seen as objects for satisfying men, looking after the home, and having strong and healthy children. According to Khel [3, p. 48] women were seen as beasts who had characteristics peculiar to their nature and needed to be tamed by the society that had already determined their destiny from birth, motherhood, and imposing them to occupy a unique social place that it was the family and the domestic space. Around the world, these claims to try to reaffirm the true place of women caused concern among women who began to be aware of their autonomy and caused them to react causing what was seen in the seventeenth century as the beginning of a social disorder that exploded in the eighteenth century in the French revolution when they took to the streets to claim their civic participation and revolutionary disobedience which, according to the monarchist De Bonald, these extreme attitudes ruined the natural society where the woman was seen as a subject, someone who is there to serve and submit to the will of the man who held power [3, p. 49–50]. In England and later in Germany, women did not accept submission to marriage or the idea that they should be at home imprisoned taking care of their children and trying to cultivate another way of living. Encyclopedists preached equality between the sexes, an idea that was respected in the status of women in marriage and the family, for example with children who heard early on that father and mother should have the same rights and the same authority. Rousseau already said in his work “Social Contract” that women should be free to choose the husband they want and that these choices should be based on even romantic criteria, based on love [3, p. 51]. Kehl quotes Condorcet who says that women can spend a good part of their lives feeling the same as men but could only be considered as such if they had not been excluded from male experiences by education and social conventions. Faced with this subjective equation, Wollstonecraft also said that human qualities were independent of sex, stating that “there is no sex in souls” [3, p. 56]. Later, many women made similar statements in support of Wollstonecraft’s ideals, the English feminist Frances Wright wrote to her friend Lafayette that “the mind has no sex except the one that it inhabits and education gives it”. In 1837 the French writer Aurore Dupin wrote to her friend Frédéric Girard that “she could do many important

things if she had not had the misfortune to be born a woman". In 1856 Louise May Scott wrote in her diary that she had the soul of a man in the body of a woman, that her spirit was masculine, and that she was born with the wrong gender [3, p. 56]. São Paulo philosopher Marilena Chauí [5, p. 92], Brazilian society has a dominant class that spares no effort to defend the public sphere from any claim, which caused a lot of resistance to accept the claims arising from women, because in social relations there are always those who believe they are superior who, have powers to exploit physically and psychically those who believed to be inferior, in this case, women, made to obey, subject themselves to always being in the condition of unprotected (p. 89). When talking about Brazilian society, it is crucial to highlight that it always believes that authoritarianism is a political event, always accuses and places the blame on dominant politics, however, it does not stop to reflect that the background of political behavior is itself [5, p. 90]. According to Chauí, social divisions are always accepted as something natural, as it would be interesting to keep women at a lower level. All of this led to the naturalization of the belief in violence that often ends up being "invisible" in the eyes of society and justice since all of this is a reflection of the acceptance of women as someone without the right to speak and the right to justice (Ibid).

Marilena Chauí completes emphasizes that: For the great, the law is a privilege; for the popular strata, repression. For this reason, laws are necessarily abstract and appear as innocuous, useless, or incomprehensible, designed to be transgressed and not to be enforced or, much less, transformed [5, p. 90]. These beliefs conditioned women to live without any other prospects than to marry and manage their home. A short time ago women were still treated as inferior beings, until after the manifestations of the 60s of the twentieth century they claimed to be heard, to be treated like men, after all, they are all human beings. In Brazil, the struggles for the recognition of citizenship in the 60s, resulted in obtaining the right to attend higher education institutions and strive for academic education, even against the criticisms of society that held strong cultural beliefs, imposing the concept that women would be fortunate only if she married and had children to look after [4].

It is worth mentioning that, in Brazil, until recently, women were legally represented by a man, she had no voice, that is, the law itself conditioned women to men, thus neglecting their right to citizenship. According to the authors Anna Luiza Matos Coêlho and Janina Sanchez—based on the Civil Code—only in 2002, the woman start to be recognized as a being with full conditions of law to express her voice and be legally responsible for herself, thus eliminating their dependence on being represented by their father, husband or eldest son, confirming a new order of equality (2014, p. 146). In this way, the woman legally obtained her autonomy, her freedom, being justified. Anna Luiza Matos Coêlho and Janina Sanchez, when discussing the gender issue, mention: When Article 1 of the Civil Code of 2002, Chap. "[Application of Taguchi Approach to Optimize the Robot Spot Welding Parameters of JSC590RN Mild Steel](#)", Personality and Capacity, Title I, Of Natural People, stating that: "Everyone is capable of rights and duties in the civil order" it went beyond just offering historical redress to women; replacing the word man for a person, treating women as citizens, just like men, subject to rights and duties that account

for their actions and are no longer at the mercy and shadow of a man (father, then husband, or son older), article 1 broke the chain between the woman and her destiny pre-determined by femininity (year, p. 147).

In this sense, according to the authors (*ibid*), after this change in article 1, it was necessary to understand that if, on the one hand, women are no longer understood in the term man, as the representative of Humanity, from then on, men and women started to be mentioned for the difference: Brazilians. On the other hand, having been deprived for a long time of the written representation of her voice, of her wills, in short, to what extent has the woman inhibited the effective function of the Self concerning decision-making? How would a woman make her voice count, given that it has been represented by men for centuries? It is understood that not always what is in the law is effectively applied, the historical, political, and legal change where that woman who was placed as a background, who was in the meeting room talking to men just to serve tea or coffee passed to be the one in the law who held her right and would not need to ask any man to represent her now she would do that. But the change happened and the woman was not prepared to resolve important issues on her own, how could she be? Having no training, I taught, because culturally she was educated to believe that it was men who exercised this legal role. They grew up with the idea that only the tasks that society deems “easy” such as: being responsible for education and the administration of any home activities were up to women. With this background, it is assumed that not even they believed in their potential. It is evident that despite so many struggles the woman uses her internal strength to overcome challenges and turn things around. In this sense, the authors Coêlho and Sanchez (based on the Federal Constitution of 1988 and the Civil Code of 2002) mention: The woman found space for her voice in the legal system, even though she was not used to exposing her speech and finally having her voice respected, whether in the domestic space or for continuity in the political sphere, even in a situation that she does not see conditions for. exercise their rights, they started to feel more protected by the law, now they do not feel alone anymore.

With that, the woman has had a lot of determination and has been conquering her place in society and, consequently, in the job market. In this context, there are still many differences between men in terms of treatment and salary. In this sense, according to Chauí, citing José de Souza Martins, [5, p. 92], wage inequalities between men and women are considered normal by society. The author maintains that the Brazilian society has the popular strata in absolute decay, with another bias for a dominant group of men, with absolute privilege (*Ibid*). According to Malena Oliveira (The State of São Paulo, 2014), Brazil is a signatory to a global pact that denounces the promotion of unjust differences between men and women, however, few changes can be noticed in the business environment, considering that for more than a decade continues in the same way. For every hundred existing posts in high positions of Brazilian companies listed on the stock exchange, only eight positions are held by women. It is worth mentioning that this statistic has undergone few changes in the last 15 years, according to a study by a group of researchers from the School of Law of the Getúlio Vargas Foundation in São Paulo (*Ibid*). It is noticed that the female figure has been the target of studies and research in all areas and we

feel the need for a greater explanation for the case of the Woman from Ceará who undertakes in the scope of literature.

Rachel de Queiroz is one of the most important figures in Brazilian and Ceará literature, she was the first woman to occupy a chair at the Academia Brasileira de Letras. Rachel at the age of seven went with her parents to the Ria de Janeiro to escape one of the worst droughts in the Northeast that occurred in 1915, which served as the theme for her first work *O Quinze*, which drew attention from São Paulo and Rio de Janeiro, received criticism from several important writers from Ceará and which earned him the Graça Aranha Foundation award. Later she published several works and received many significant awards that made her one of the most important women in Brazil.

3 The Methodological Process

Having as objectives to know about women entrepreneurs in the scope of culture, specifically in the literary area, and the hypothesis that women entrepreneurs are seen by the society of Ceará still from the sexist perspective, the hypotheses presented contributed to our study, in the sense of knowing better about actions women entrepreneurs.

The quantitative part of this research was developed, through the application of two hundred and sixty-six forms and data analysis, seeking to understand what the society of Ceará thinks of women entrepreneurs and it was found that the majority emphasized that the macho society is still one of the main oppositions that prevent women from the undertaking. As for the previously defined indicators, that is, those aspects that we decided to observe, in the quantitative research, were: what are the main characteristics that women entrepreneurs have, what are the oppositions that prevent them from undertaking, and what examples does Ceará society have as an entrepreneur woman? As for the qualitative aspect of the research, about the symbolic cultural system of women, it was noticed that in the process of undertaking the same, in general, she has support from her family.

- 3.1. As part of the GEP—Group for the Study and Research of Anthropology of Administration and Women's Entrepreneurship, a seminar was held on the entrepreneurship of women from Ceará, organized by professor Janina Sanches in the third day UNICHRISTUS, with the participation of business-women awarded by SEBRAE in previous years, having been able to hear the experiences of four women entrepreneurs: Barbara Linard, Maria de Fatima, Renata Ary and Graça Maria Rebouças de Oliveira, where they described the challenges they had to face in their professional trajectory.
- 3.2. We participated in an event at the Academy of Letters of the Municipalities of Ceará, ALMECE, in which women who undertake in the literary sector were awarded prizes. This is an event that adds value to women entrepreneurs, present at the ceremony was Mrs. Eliane Arruda, current president of the

Academia de Letras Juvenal Galeno, and former president of the Academia Brasileira de Letras do Ceará.

- 3.3. We visited the Aquiraz Education Department, interviewing the Education Secretary Terezinha Holanda Costa de Freitas, who wanted to encourage children, young people, and the population of Aquiraz to also get involved in the world of literature. She idealized FLAQ together with two other women, promoted with initial difficulty the FLAQ—Festa Literária de Aquiraz event that aims to encourage the population to learn more about Ceará literature, which has the participation of great poets from Ceará and is one among other similar cases in Brazil, of events of this nature, such as FLIP—International Literary Festival of Paraty, FLIPORTO—International Literary Festival of Pernambuco and FESTIPOA—Literary Festival of Porto Alegre, among others.

The event invites intellectuals from all over Brazil to FLAQ—Literary Festival of Aquiraz, where everyone from the municipality of Aquiraz and even from neighboring municipalities can honor great works that are exposed and have the opportunity to attend tributes that are made for great poets, teachers, and writers who are invited to give lectures and talk about their works, in addition to being surprised by some young people from the city, who write poems and stories inspired by the trajectory of those guests. The interview with the Secretary of Education made it possible to identify that the women of the twenty-first century are more independent of extrinsic prejudices, that is, the woman no longer cares about how she is seen in society and currently her motivation comes from herself, from his claw, he is no longer convinced that the woman would serve only to take care of household chores.

Terezinha is a woman of great determination and with enough resilience to face several difficulties. Since her childhood, she was passionate about literature and reported how difficult it was to be able to afford her studies, due to her humble origin. However, since he was a child, he felt a thirst for knowledge in his heart, he knew he had a lot to learn. Her mother was so motivating in these difficult times that she was a self-taught teacher, without training. She is still her greatest supporter and her greatest example of life and overcoming that, even living in rural areas, she did not allow herself to be overcome by the difficulties that the family faced with education. Her mother was instrumental in the development of her knowledge and made her have a passion for books since childhood, having completed a very rich curriculum: Degree in pedagogy from the state university of the Acaraú valley, Specialist in school administration from UVA, Specialist in reading and training from the reader, from the Federal University of Ceará and Specialist in public school administration—UDESC. Terezinha is a very important figure for the Municipality of Aquiraz, before reaching the position of Secretary of Education she went through all sectors of the municipal government, analyzing and seeing the individual needs of each sector. As a result of her knowledge and due to meritocracy she became Secretary of Education of Aquiraz T. Other women entrepreneurs could be mentioned in the literary field, we chose to highlight.

- (1) **Maria Argentina, ex-resident of the Female Academy of Letters of Ceará (AFELCE)** gave us an interview with four questions:

The first question: Entrepreneurship is considered to be transforming for the better. How do you see the entrepreneurship of women who, like you, undertook in literature? “I think women’s entrepreneurship in Ceará’s literature is a very positive point because people need a culture, especially of literature, the change of the human being begins with the culture that is where everyone learns to be citizens.” The second question: What do you consider to be the greatest challenge for women who undertake in literature? “Nowadays it is the dissemination of his works, showing and taking his art to people since the editorials of magazines and newspapers are expensive and the government’s culture department does not invest in literature. “The Third Question: Who is an example of an entrepreneurial woman for you?” Yolanda Queiroz for being a hardworking and resilient woman who does not let herself be overwhelmed by challenges and Giselda Medeiros a very talented writer, with a natural talent and for having a poetic streak”.

The Fourth Question: Who do you think was your biggest supporter? “My husband, I got married very young and soon after I lost my parents and he was always by my side supporting me in all the decisions of my life like when I went to four colleges and then when I decided to do specializations. Another person I admire a lot is Juarez Leitão, a wonderful and very talented historian and teacher.

- (2) **Giselda Medeiros teacher, coordinator and poet.** She started in poetry at just 10 years old and gave us a four-question interview. The first question was: Entrepreneurship is considered to be transforming for the better. How do you see the entrepreneurship of women who, like you, undertook in literature? “I see it satisfactorily because women have suffered a lot of discrimination in the past where to write or publish something they used codenames of men and today they overcome challenges and are growing more and more in the field of literature.” The second question: What do you consider to be the greatest challenge for women who undertake in literature? “To win a readership, because there is no point in writing a book and not having readers to read it, what is not read is not remembered, what gives life to books is the readers”.

The Third Question: Who is an example of an entrepreneurial woman for you? “Rachel de Queiroz for being a battling woman and since she was very young she already wrote and at the age of eighteen she wrote her first book *O Quinze*, which won several very important awards and later became the first woman to occupy a seat at the Academia Brasileira de Letras.”

*The Fourth Question: Who do you think was your biggest supporter? “In my personal life, it was my mother who always supported me and encouraged me to like literature since I was very young because as a teacher she always gave me good books and good examples and so I started to like poetry more and more and had already decided that I would become: writer. This year I will launch the book: *Caminho de Sol* in honor of the centenary of Raimunda de Sousa Fernandes my mother. In the literary field that encouraged me to write, Artur Eduardo Benevides was the prince of the poets and because of him, I am called the princess of the poets”.*

These women stand out for their contributions to the literature of Ceará, their life trajectories, and especially for the determination and attitude with which they faced their challenges, since most come from a humble families and fought from an early age to be able to finance their studies and grow professionally, but they never let themselves be shaken by these difficulties. As Bergamini [1] says even though external factors conspired against it, they sought internal motivation and found within themselves the strength they lacked to face challenges and let their potential emerge for literature. Women are increasingly looking for their space in society, which has a dominant class and goes to great lengths to defend the public sphere from any claim, [5, p. 92], which caused a lot of resistance to accepting the rights claimed by women. As for the motivations for Entrepreneurship, we believe that wanting to be part of the labor market and society, led women, in general, to want to gain a voice in society, starting with the family environment.

3.1 Results Found on What Culture Thinks of Entrepreneurial Women

About how a local culture seen women entrepreneurs, using the quantitative methodology, we collected data through the application of forms to know what the society of Ceará thinks of women entrepreneurs, currently. In the quantitative research, it was noticed that women entrepreneurs currently do not give the same importance that they used to in the past to the opposition or prejudices in the process of entrepreneurship and face challenges to carry out their projects, as seen in the Figs. 1, 2, 3 and 4.

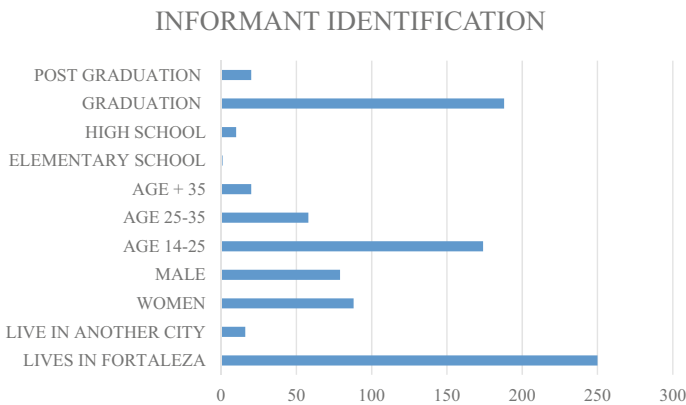


Fig. 1 Characteristics of interviews

CHARACTERISTICS OF THE ENTREPRENEURIAL WOMAN

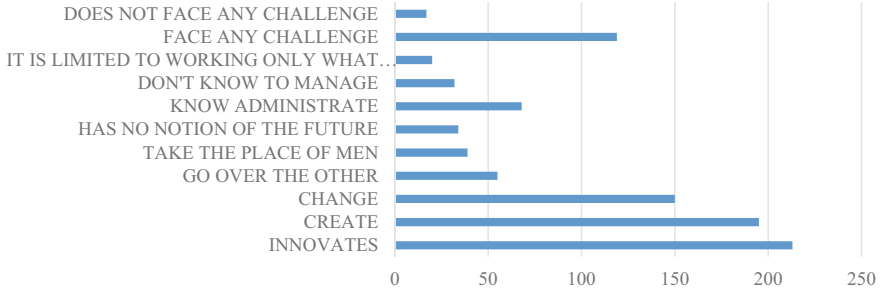


Fig. 2 How culture characterizes entrepreneurial women

EXAMPLES OF ENTREPRENEURIAL WOMAN

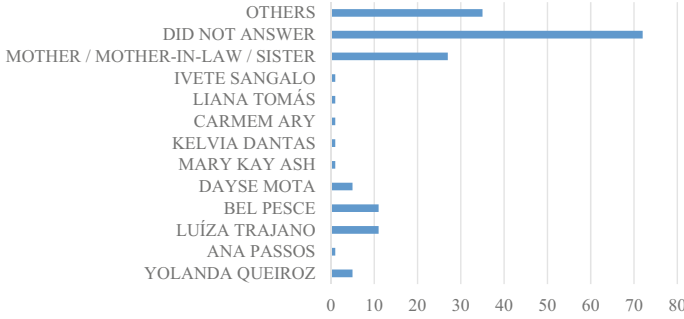


Fig. 3 How the cultural symbolic system perceives women

HOW SOCIETY PERCEIVES WOMEN

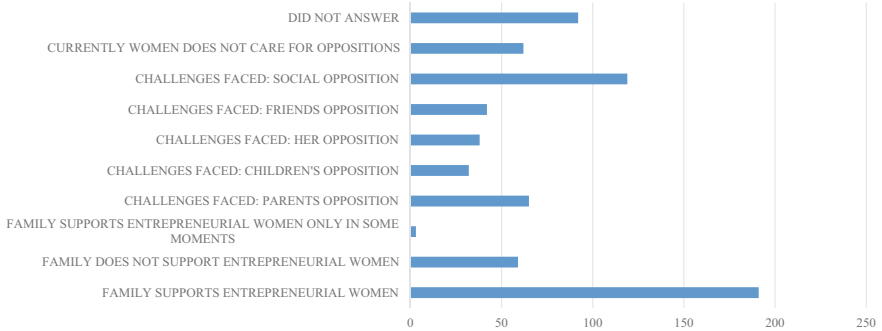


Fig. 4 Example of entrepreneurial woman

4 Results

Through quantitative research aimed at revealing what culture thinks of women entrepreneurs, forms were applied and it was identified that the largest number of respondents live in Fortaleza, the majority being female, aged between 14 and 25 years old, the majority being students of higher education. Most responded that the woman has support from her family when she seeks to undertake, and most responded that the greatest opposition they face is opposition from the society they believe to be sexist. Regarding the characteristics of the entrepreneurial woman, most of them answered that women are innovative, create and change in the entrepreneurial process, emphasizing also that women face any challenge to achieve their goals, however, there was a small portion that emphasized that women do not know how to manage. About an example of an entrepreneurial woman most did not respond and this choice for omission caught our attention, also because some had difficulty in responding or did not have an example of an entrepreneurial woman in mind.

Through qualitative research and interviews with women who have undertaken in the culture, their speeches revealed that they are women of great persistence, having overcome and are overcoming the challenges that presented themselves about their projects. Their intrinsic motivation favors them to fight for the realization of their projects and through their actions, they have in common the fact that they benefit other people and show these people the value of culture and literature, have been able to perceive that they are women of great determination and determination in your endeavor.

5 Conclusion

We conclude that women have the support of their families in the entrepreneurial process, however, paradoxically, in culture, the society of Ceará is the one that most opposes the entrepreneurial woman in preserving behaviors from previous, sexist times, such as the lack of confidence in women's entrepreneurship... low wages are observed in comparison with men, lack of great opportunities in the labor market, among others. In entrepreneurship, women are innovative, and create and change administrative scenarios. This work confirms the hypothesis launched that the woman from Ceará is a woman who faces challenges to reach her goals, having been a revealing experience for us, business students, which showed us in the first place the surprising opinion of society, has enabled us to perceive the points of view of different women entrepreneurs and in the interviews, we also noticed the common points. For the future, we recommend deepening studies on the importance of the new positioning that women are adopting, of greater independence in the face of the pressures of culture and society.

References

1. Bergamini CW (Apr–Jun 1990) Motivation: myths, beliefs and misunderstandings. *RAE-Revista de Administração de Empresas* 30(2)
2. Hisrich RD (2007) *Entrepreneurship*. Translation: Teresa Felix de Souza, 7th edn. Sao Paulo: Bookman, pp 30–31. ISBN 978-0-07-321056-8
3. Kehl MR (2008) *Female shifts*, 2nd edn. Rio de Janeiro: Imago. pp 47–51, ISBN 978-85-312-1012-7
4. del Priore M (1994) *Women in the history of Brazil*, 4th edn. São Paulo: Contexto, (collection rethinking history), pp 16, 17, 20. ISBN 85-85134-11-9
5. Chauí M (2000). *Brazil: founding myth and authoritarian society*, 1 edn. São Paulo: Perseu Abramo Foundation, pp 89–93. ISBN 8586469270
6. Mattos C, Sanches AL, Janina (1988a/2002a) *Constitutionalization of Brazilian civil law*, 1st edn. Fortaleza: Unichristus, (2014). pp 146–147. ISBN 978-85-99562-46-8
7. Oliveira M (2014) Quotas for women in management positions divide opinions. São Paulo: The State of São Paulo, Nov. Disponível em: <http://economia.estadao.com.br/noticias/governanca,cotas-para-mulheres-em-cargos-de-gestao-dividem-opinioes,1589058>. Acesso em: 14 Setp 2014

Machining of Composite Materials Using Different Conventional and Unconventional Machining Processes: A Short Review



Ankit Jain, Cheruku Sandesh Kumar, and Yogesh Shrivastava

Abstract Due to the object's diversity and heat sensitivity, as well as the high combativeness of the fibers, machining composite materials is challenging. As a consequence, the workpiece is damaged and the tool wear is quite high. Because of its outstanding physical and mechanical characteristics, the application of Metal Matrix Composite is growing. The major challenge is to keep their costs under control while preserving qualities like lightweight, high strength, and durability. Natural fiber composites are a viable substitute for synthetic fiber because of their enhanced characteristics and, more significantly, since they are biodegradable and inexpensive. The study shows these features make it feasible for modern engineering and related technologies which is usual and more effective in present era. Furthermore, due to the limitations in the manufacture and machining, large-scale production of natural composites is prone. Because of their heterogeneous and an-isotropic conduct, fiber composites have poor machinability features. Various processes and new techniques in order to achieve excellent machining in composites with natural fiber were created to solve this challenge.

Keywords Metal matrix composites · Fiber-matrix composites · Conventional · Unconventional machine tools

A. Jain
Amity University, Rajasthan Jaipur, India

C. S. Kumar (✉)
Amity University, Rajasthan Jaipur, India
e-mail: sandeshkumarc7@gmail.com

Y. Shrivastava
Department of Mechanical Engineering, Galgotias College of Engineering and Technology,
Greater Noida, Uttar Pradesh, India

1 Introduction

Composite materials are materials with more than one phase, exhibiting diverse qualities, like high strength, high rigidity, low friction, lightweight, etc. Nowadays, a composite hybrid metal matrix is also utilized in the automotive and aerobatic industries and is typically produced by stir casting. Aluminum 6061 is typically utilized as a matrix above zirconium dioxide, as it has characteristics such as strong wear, high defensive compatibility, and automotive compatible. Metal matrix Composite has various applications, such as compressor blades, trains, satellites, sports goods, bike frames, etc. Metal matrix composite's machinability is influenced by characteristics such as feed rate, cutting speed, tool shape, tool material, [1]. For the milling of metal matrix composites, many types of traditional machining, etc. techniques are utilized, such as boiling, turning, grinding, milling, etc. (MMCs). While non-Conventional Machining Proceedings (EDM), Electrochemical Machining (ECM), etc. are used to machine MMCs, Abrasive Water Jet (AJM). Through the ages, this development in materials began with the discoveries of iron, copper, metal, and polymers. In recent times, due to its excellent features, the application and use of composite materials have been aggressively increased. The composite materials are two or more chemically distinct materials, generally a matrix and strengthening. In the composite, the matrix material is present in a continuous phase, whereas the strengthening is intermittent. The matrix material can be in any form either a polymer or a metal, or a ceramic. The polymer matrix is the plastics that may be thermoplastic or thermoset. In polymer composites, fiber is the material that is used as reinforcement, in some cases, filler materials are also used as reinforcement [2].

2 Metal Matrix Composites

The composites of the metal matrix (MMC) are a type of material consisting of one metal that is fused to another. The two components are chemically and physically separate in different periods [3]. The basic material is a metal matrix, whereas the other component appears to be working as fibers or particles. The objective of making this material is to improve, as with other metal matrix composites, the existing characteristics of the metal matrix, by adding additional functionality provided by the reinforcement, as shown in Fig. 1.

3 Fiber-Matrix Composites

The best and most promising material in this century has been determined to be composites. Composite materials with synthetic or natural material fibers currently take on more relevance as requirements are rising for lightweight materials of

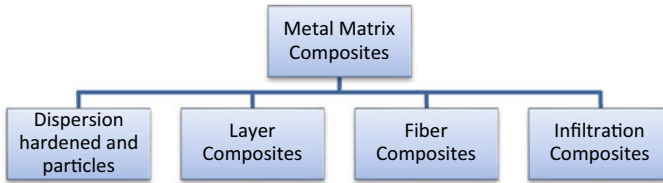


Fig. 1 Different composite material

high durability for specific purposes. Composite Fiber-reinforced polymer offers not only a high strength/weight ratio but also great durability, steadiness, damping characteristics, bending strength and corrosion resistance, wear, impact, and firing. These varieties of properties have led to the development of composite materials in the automotive, building, aviation, automotive, pharmaceutical, and marine sectors [4–16].

4 Conventional Machining of Metal Matrix Composites

Uncoated carbide tools are not appropriate for MMC machining, and Keyon and Silicon Nitride tools are also not used for serious surface roughness. They are analyzed. They also determined that workpiece polishing provides a superior finish on the surfaces. Investigated wear rate tools, borders, and cornered dots, when the use of Al matrix composites in sic particles has been cut. As Sic content grows, the likelihood of flank wear is increased, thereby reducing tool life. Low speed is usually suitable for the production, of course, Sic Particles, and Developed Edge, while the cutting of fine Silicon Carbide Particles reinforced MMC is permitted at high speed. During the processing of metal particles, wear mechanism is prevalent (PMMCs). The degree of flank wear also rises as feed force increases while PMMCs is boiling. They have also created a mathematical method that will optimize the situation during PMMC drilling. Thus, this model was used to create several objectives in order to evaluate the influence of various machining factors [5]. In the machining of MMC by diamonds tool abrasive wear play a vital function. PCD insertion tool durability And K10 diamonds instruments are achieved using the equation of tool life. PCD insert tools are usually utilized in the machining of MMCs enhanced with silicon carbide particles for extended tool life and a superior surface finishing. It takes longer to impose flank wear on PCDs, while CVD instruments require less time to attain wear mechanisms. A rougher grinding of aluminum composites is favored by Sic wheels, since their particles are more difficult and less expensive than diamonds, while by fine grinding of alumina composites, diamond wheels are preferable. The study also discovered that the grinding force reduces for rough grinding with an improvement in grinding speed while the rough grinding decreases owing to varied sizes and adhesives. The rate of flank wear on the device likewise rises with a cutting

speed. As the cutting speed of the tool increases, the temperature increases and the material adhesion to the tool diminishes. The lower the cutting speed, on the other hand, lowers the temperature and therefore produces stress hardening. BUE formation preserves the tool surface from abrasion and decreased adhesive wear and size of the tool by increasing the tool's cut speed. A Mechanical framework for prediction of forces when working with ceramic particles reinforced alloy-based metal matrix composite [6]. And it was also discovered that cutting and thrust forces, which were based on slip-line set theory, shear-plane analyses from Merchant, and the Griffith concept, were estimated for the production of a chip. From perspective of physical and mechanical characteristics, MMCs are superior to non-enhanced alloys. Because they have good abrasion characteristics, they are thus classified as tough materials. As the wear rate changes linearly with the average particle size and in the case of 2-body and 3-body abrasions the rate of cut-off and feed rises. The influence of several factors like tool surface, dimensional deviation, processed surface, etc. on the machine tools of the Si—MMC by various types of PCD tools at changing velocity. They observed in their experiments that during machining using PCD instruments, good surface finishing is acquired. We also studied how coolant lowers the surface polish by adhering to particulates. Micro MMCs played an essential role in the machining of particles, the size of particles, and their position when nano MMC's are being machined. During the processing of micro MMCs, continuous chips were produced whereas interrupted chips were generated while micro MMCs were machined. Better finish is achieved when nano MMCs are processed [7].

5 Unconventional Machining of MMCs

Cast aluminum metal matrix composite machinability enhanced with Sic (Silicon Carbide). The Alloy matrix protected from degrading the effect of sparks produced during electrocutting hazard processing by Silicon Carbide. With the use of special gravity and TEM, the thermal zone concerned was analyzed (Transmission Electron Microscopy). EDM was generally preferably selected for the production of complicated forms over other processes. Boiling of blind hole followed by EDM in order to assess machining performances of Al₂O₃/6061 Al. Large voltage and other electrical factors impacted MRR. According to its data, the MRR rises with the speed of the rotation, the flushing pressure, and two eccentric holes inside the electrodes. The electrode increases. The modifications happened while processing Al-10% SiCp, as cast MMC, in the metal removal rate. The source of current rises also increased the wear rate and the rate of metal loss. And MRR also rises owing to a lower risk of short circuits due to reductions in the flushing pressures due to the delay in inflammation. The impact of the grain-specific surface area of Silicon Carbide (Sic), the electrode rotation speed, layer thickness, the tool wear rate (TWR), and the radial cut (ROC). And it was observed that MRR and TWR increase the wall thickness of the electrode, the speed of the electrode rises as well as the grain size of Silicon Carbide particles decreases [8]. This process was carried out with the aid of EDM followed

by rotating brass electrodes to machine Silicon Carbide Particulates composites of 7075A–10 wt%. Furthermore, a degradation was due to the surface morphology that was caused by the thermal division for the removal of ceramic particles and re-solidified layer development. Non-conventional machining is used for the machining of MMI like Electric Discharge Machining (EDM), Laser Beam Machining (LBM), or Abrasive Water Jet Machining (AWJM). However, issues like the development of recasting layer in case of EDM hinder the process in order to enhance surface finishing by using powder mixed EDM and therefore reduce the difficulties of tool wear and tool distortion. The AWJM has played an important role in the surface finishing of workpieces in the size of abrasive and reinforced particles [2, 9].

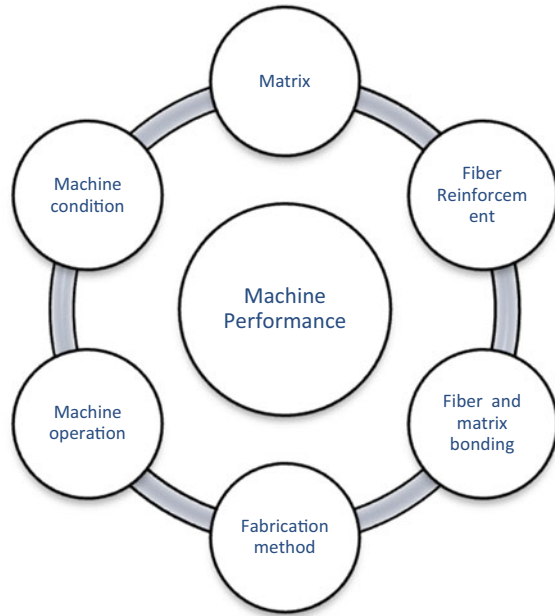
6 Conventional Machining of Fiber-Matrix Composites

The diverse characteristics of the composites of the fiber-matrix challenge the traditional method. Conventional machinery such as boiling, friction, rotation polishing, and milling of composite materials creates further matrix and reinforcing material failures. In addition to the material characteristics, material failure also affects the machining parameters. In determining the cutting force, the orientation of natural fibers is essential. The natural fiber reinforcements are resistant to tool penetrating, resulting in fiber pull out and delamination. Furthermore, the surface fiber injuries produce surface waviness [10]. In fiber-matrix composites the production of chips is not predictable; the cutting process is difficult to detect. The increasing temperature during the drilling process melts the matrix, producing a poor surface area and affecting material performance. With the exception of material failure of machining, traditional machining impairs the worker's assistance owing to the production of dust during milling. The equipment is one of the most essential factors in the traditional machining operation. The tool is usually worn during machining and even plastic deformation takes place. The tool material is worn during chopping due to the destructive fiber nature of the fiber reinforcement, as shown in Fig. 2.

7 Unconventional Machining of Fiber-Matrix Composites

The unconventional machining method is being increasingly used in the machining of fiber composites with a goal to produce high-quality machining in fiber-matrix composites. Modern technologies of machining have increased machined quality characteristics, decreased machining time, and flaws in various composite fibers. In an unusual machining operations material is removed by the phase transformation mechanism, i.e., using specific equipment, which is entirely different from traditional material removal procedures by using high, medium, and high-frequency vibration temperatures. While a variety of unusual processes are practically applicable such as water jet processing, ultrasonic machine tools, laser machining, and electrochemical

Fig. 2 Different machine operations



machining, only a restricted method for the machining of fiber-matrix composites is employed. In particular, several researchers have examined the abrasive waterjet process effect (AWJM) of fiber-matrix composites [9, 11].

8 Equivalence of Conventional and Unconventional Machining Processes

Most individuals do not realize that two groups, main and secondary processes, constitute the manufacturing process. The fundamental form and size of the material are created by the primary process, while the secondary—sometimes known as the machining process—ensures a greater control of measurements, surfaces, etc. You need to grasp the distinction between conventional and non-conventional processes to comprehend the secondary manufacturing processes [12].

- **Accurateness:** The conventional process has a lesser consistency and surface finish, whereas a better accuracy and surface finish is provided for non-conventional processing.
- **Used Tool:** Conventional machining must always be provided with a mechanical equipment. For example, in a Lathe machine, a cutting tool. However, in a non-conventional machining process, there may be no physical tool available.

For instance, laser beams do the work in laser machinery while electrochemical milling demands a physical instrument.

- **Machining Process:** Conventional machining generally includes altering the form of a workpiece using a hard-working tool. Using conventional methods for machining hard metals and alloys, time and energy consumption are raised and prices are therefore enhanced. In some instances, it may not be possible to work conventionally.
- **Conventional machining adds:** consequences in terms of tool wear and product quality loss due to generated stress distribution during production. Evermore attention to non-conventional machining processes has increased with the rising demand for production of hard alloys and metals.
- **Contact tool and part of work:** The conventional technique of machining includes direct tool-work part contact while the non-conventional approach does not need direct tool-work part contacts.
- **Waste Material:** The conventional machining method is also likely to produce more waste because of the high surface contact and wear of tools with lower lifetime. Non-conventional machining has reduced waste products because of little or no wear using tools having a longer life [3, 13].

Limitations of Machining Process have Been Listed in Table 1.

The latest machining methods such as NC, CNC, DNC, FMS, etc. have been developed to overcome these drawbacks [6, 14].

Advantages of machining process have been listed in Table 2.

Table 1 Limitations of machining process

1	The precision of the produced components depends on the operator’s effectiveness
2	There is no uniformity in production. Therefore, the element must be inspected at 100%
3	The operator’s subjective requirements decrease output rates
4	The labor difficulty will also be considered because of the enormous number of workers employed
5	Extreme systems are difficult to produce, such as parabolic curvature components and cube curvature components
6	The present arrangement cannot include frequent modifications in the component

Table 2 Advantages of machining process

1	You may get a high surface polish
2	Machining is conducted on wood, plastic, composites, and materials, but not simply on metals
3	Various geometrical characteristics like screw threads, high straight edges, precise circular trapezoids, etc. are conceivable
4	Good size precision

9 How Unconventional Machining Process is Better Than Conventional Machining Process

On the other side, non-conventional machines are those having computer-based operations autonomously and no human interaction or operator is necessary. Usually, these are operated by an automated robot or computer [15]. For examples vehicle painting in automotive production facilities, soldering car units, and production procedures, where the severe heat and the extremely low temperature are involved that people are unable to resist are activities that employ non-conventional machinery [16]. The conventional machining process requires that the tool and the work material have a direct contact. For example, for cutting an aluminum bar, a quick spinning iron cutter is essential [17]. This procedure involves direct contact between the cutting instrument and the substance to be sliced. In contrast, the method of non-conventional machining uses state-of-the-art optimization algorithms. No-touch between tools and material is involved in this procedure. Examples of utilized tools that are not traditional are infra-rot, laser beam, electric arc, plasma cutting, and electric beam [18]. The two differences are as follows.

10 Results and Discussion

The term “conventional machining” refers to a technique that employs mechanical force various forms of technologies are used in non-traditional machining. Thermal, chemical, and electrical energy are the three primary types of energy utilized in non-conventional machining. Turning, boring, milling, shaping, broaching, slotting, grinding, and other traditional machining techniques are examples. Similarly, non-traditional machining methods include Abrasive Jet Machining (AJM), Ultrasonic Machining (USM), Water Jet and Abrasive Water Jet Machining (WJM and AWJM), and Electro-discharge Machining (EDM). Non-conventional machines, across the other hand, are those that perform computer-based activities without the need for human contact or operation. These are generally controlled by a computer or a robot. Non-conventional machinery is used in activities such as automobile painting in automobile manufacturing facilities welding automobile units, and manufacturing processes where high heat and extremely low temperature are engaged and employees are unable to withstand.

11 Conclusion

A comprehensive examination of the processing of metal matrix combinations and fiber-matrix composites has been carried out in this article. The review highlighted the differences between conventional and unconventional machining and highlighted

benefits and limitations. The study describes the standard methods of machining of both composites and unusual machining processes of the two composites. Finally, we will illustrate how unconventional processes are superior to traditional processes.

References

1. Ashby MF, Jones DR (2012) *Engineering materials 1: an introduction to properties, applications and design*, vol 1. Elsevier
2. Chawla KK (2012) *Composite materials: science and engineering*. Springer Science and Business Media
3. Chawla N, Chawla KK (2006) Microstructure-based modeling of the deformation behavior of particle reinforced metal matrix composites. *J Mater Sci* 41(3):913–925
4. Ferry M, Munroe PR (2003) Recrystallized grain size prediction in a particulate reinforced metal matrix composite. *J Mater Sci* 38(9):1925–1930
5. Hung NP, Yang LJ, Leong KW (1994) Electrical discharge machining of cast metal matrix composites. *J Mater Process Technol* 44(3–4):229–236
6. Jain A, Pandey AK (2017) Multiple quality optimizations in electrical discharge drilling of mild steel sheet. *Mater Today: Proc* 4(8):7252–7261
7. Jain A, Pandey AK (2019) Modeling and optimizing of different quality characteristics in electrical discharge drilling of titanium alloy (grade-5) sheet. *Mater Today: Proc* 18:182–191
8. Jain A, Yadav AK, Shrivastava Y (2020) Modelling and optimization of different quality characteristics in electric discharge drilling of titanium alloy sheet. *Mater Today: Proc* 21:1680–1684
9. Matthews FL (2003) *Composites manufacturing: materials, product and process engineering*. SK Mazumdar. CRC Press, 2000 NW Corporate Blvd., Boca Raton, FL 33431, USA. 2002. p 392. Illustrated. £ 69.99. ISBN 0-8493-0585-3. *Aeronaut J* 107(1071):274–274
10. Mazumdar S (2001) *Composites manufacturing: materials, product, and process engineering*. CRC press
11. Nunes JP, Silva JF (2016) Sandwiched composites in aerospace engineering. In: *Advanced composite materials for aerospace engineering*. Woodhead Publishing, pp 129–174
12. Paliwal S, Rao PS (2019) Study of different machining process on metal matrix composites. *Studies* 5(05)
13. Panwar V, Sharma DK, Kumar KP, Jain A, Thakar C (2021) Experimental investigations and optimization of surface roughness in turning of en 36 alloy steel using response surface methodology and genetic algorithm. *Mater Today: Proc*
14. Purohit R, Verma CS, Shekhar P (2012) Electric discharge machining of 7075Al-10 wt.% SiCp composites using rotary tube brass electrodes. *Int J Eng Res Appl (IJERA)*, 2(2):411–423
15. Wang CC, Yan BH (2000) Blind-hole drilling of Al₂O₃/6061Al composite using rotary electro-discharge machining. *J Mater Process Technol* 102(1–3):90–102
16. Wang RM, Zheng SR, Zheng YG (2011) *Polymer matrix composites and technology*. Elsevier
17. Yan BH, Tsai HC, Huang FY, Lee LC (2005) Examination of wire electrical discharge machining of Al₂O₃p/6061Al composites. *Int J Mach Tools Manuf* 45(3):251–259
18. Yi XS (2018) An introduction to composite materials. In: *Composite materials engineering*, vol 1. Springer, Singapore, pp 1–61

An Investigation on Effect of Hybrid Nanofluids in End Milling of Aluminium 6061 Alloy



Ravi Shanker Tiwari, Prameet Vats, Tushar Singh, Vineet Dubey, Pawan Kumar Arora, and Anuj Kumar Sharma

Abstract In machining operations, the coolant contributes a major cost of production, therefore now days the studies toward reducing the lubricant or complete elimination of lubricant are targeted. Reduction or elimination can improve the environment, machining performances and reduce the cost of machining also. The Minimum quantity lubrication technique reduces the lubrication cost as well as poses less harm to human health. This study investigated the effect of depth of cut, spindle speed and cutting feed parameters in end milling of aluminium 6061 on cutting force in MQL with base fluid as well as hybrid nanofluid conditions using SINOMILL VMC300 with HSS end mill tool on three different spindle speed (1000, 2000 and 3000 rpm), three different cutting feeds (100, 200 and 300 mm/min) and three depth of cuts (0.5, 0.75 and 1.0 mm). Response surface methodology is used for experimental design. The findings reveal that cutting force is less in milling operation of aluminum 6061 using hybrid nanofluid in comparison to base fluid under MQL condition. Depth of cut is dominating parameter than cutting speed and feed rate in cutting force analysis. The improvement in cutting forces is reported as 15.98% with hybrid nanofluid in comparison to base fluid.

Keywords MQL · Cutting forces · Aluminium alloy · Optimization · Hybrid nanofluids

1 Introduction

Machinability is degree of difficulty or convenience to process that material. This can be defined by factors such as cutting force, surface finish and tool life. Maximum the tool life minimum the cutting force representing good machinability. Power consumption is most important factor of production cost in machining processes.

R. S. Tiwari · P. Vats · T. Singh · V. Dubey (✉) · A. K. Sharma
Centre for Advanced Studies, Lucknow 226031, India
e-mail: dubey.vin1324@gmail.com

P. K. Arora
Galgotias College of Engineering & Technology, Greater Noida 201310, India

The cutting force is very important factor to determine the power consumption. The cutting force is also important to detect the surface roughness, tool wear and vibrations therefore, the research on this cutting force has most significant value [1]. The conventional cutting fluids have very bad effect on human health, environment and production costs. For all the above reasons nowadays the research is going on to reduce the use of coolant. The MQL can improve the total production cost by up to 15% [2]. The MQL uses 10 to 100 ml/h oil with pressurized air [3]. MQL reduce the loss due to thermal shocks, reduce heat between tool and workpiece interfaces, reduces tool wear and production cost [4]. In the machining process, the cost of lubrication may be up to 20% of total machining costs [5]. Dubey et al. [6] reviewed different cooling methodologies in machining processes. MQL machining reported better results among other techniques. In another study, Dubey et al. [7] studied various methods of estimating the cutting temperature in machining. The thermocouple technique was found favorable in comparison to others. Dry machining can be also used if the product quality and tool wear are considerable, and when the dry processes are not possible, minimum quantity of lubrication technique can be applied for considerable product quality and tool life. It is seen that the coolant affects the surface roughness and thermal deformation. Obikawa et al. [8] do comparative studies between normal and micro spraying and found that micro spraying is very effective to increase tool life over normal. Wang et al. [9] do a comparative study between MQL and dry machining in milling process with Inconel 182. They stated that MQL is very effective in the terms of cutting force in the up milling process. Li et al. [10] investigated that in MQL the cutting force decreased by 24% on comparing with dry and 32% with wet. Rabiei et al. [11] do study on MQL in grinding process for hard and soft steel, compared with dry and wet machining and found MQL is better over the dry and wet. The performance of MQL could be improved by adding nanotubes, carbon nanotubes give better results [12]. Khettabi et al. [13] conducted a study to optimize MQL and dry processes, using aluminium alloy 2024, 6061 and 7075 as a workpiece and carbide coated end mill tool on four different rates of flow of mist on Nexus 3 axis high-speed CNC vertical center and found that MQL can be used on the consideration of force and surface roughness but if considering the particle emission dry machining should be preferred. Yildirim et al. [14] conduct a study to optimize the parameters of MQL, using as alloy as workpiece and uncoated carbide insert on DELTA SEIKI CNC 1050 vertical center, taking cutting force and tool life as a parameter and finding that minimum cutting force and maximum tool life obtained by vegetable oil combination MQL on 100 ml/h flow rate and 25 mm spray distance in up milling. Mia et al. [15] conduct a study to improve the performance of MQL, using hardened steel HRC40 as a workpiece and a carbide tool in vertical machining center applying Taguchi methodology taking parameters cutting force and surface roughness. It was also found that flow rate of 150 ml/h gives cutting force and surface roughness minimum. Pandey et al. [16] studied the tribological effect of nanofluids in machining and reported that the MQL machining enhanced the tribological properties significantly. Joshua et al. [17] conducted a study to test effect of cutting parameters in MQL on surface roughness using aluminium 6061 as workpiece and 12 mm HSS end milling tool in V 645 CNC vertical machining

center. ANOVA analysis uses for analysis taking surface roughness as a parameter find that machining using MQL apart from being environmentally good reduced the surface roughness value to about 20% toward a better surface finish.

Tosun and Pihili [18] studied to analyse performance characteristics of MQL milling of aluminium 7075 with HSS end mill tool in VMC Lagun Ft-2 applying Taguchi taking surface finish and MRR as a parameter. Find that the order of importance of parameters is feed rate > cutting speed > material of tool > and cooling technique. Mishra et al. [19] reviewed the potential of different metal oxides for application in different machining operations. Tosun and Huseyinoglu [20] do study to test effect of MQL in milling of aluminium 7075 on surface finish. Using aluminium 7075 as workpiece and HSS tool in the VMC applying ANOVA taking surface finish as a main parameter and find that best surface finish can be achieved by higher the spindle speed and lowering the feed of cutting. Uysal et al. [21] apply MQL with MOS_2 nanoparticle in milling of martensitic stainless steel using SPHN120404 WC uncoated tool in MCV 300CNC milling, taking surface finish and tool wear as parameter, find that MQL with nanofluids can increase surface finish and decrease tool wear simultaneously. Li et al. [22] do study on TC4 alloy as workpiece and carbide tool in TH5650 4-axis VMC end milling operation using MQL with graphene nanofluids, taking tool temperature and tool wear as response parameters find that in graphene MQL conditions the tool life increase, milling temperature decrease and cutting force decrease because graphene particle works as an antifriction element. Mia and Dhar [23] studied medium carbon steel with carbide tool insert at lathe machine of 7.5 kW applying Taguchi, taking response parameters as tool wear and surface finish find that for the surface roughness the cutting speed 161 m/m and the feed rate 0.12 mm/rev is optimum while 81 m/m cutting speed and same feed rate is optimum for tool wear. Speeds of spray, distance of spray, angle of spray, rate of flow and types of nozzle are various factors of MQL system, optimizing these variables makes more efficient MQL system.

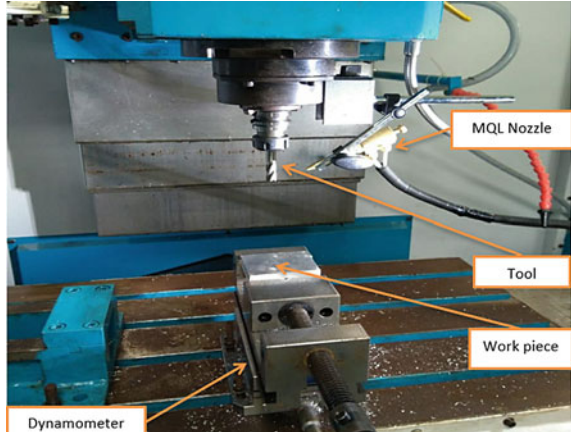
In this study the effect of cutting parameters like depth of cut, spindle speed and cutting feed on the cutting forces in end milling of 6061 aluminium alloy end milling under MQL condition with base fluid and hybrid nanofluid.

2 Materials and Methodology

Aluminium alloy 6061 is a hardened alloy of aluminium, which has silicon and magnesium as major elements of alloying. Nowadays this material is widely used in aircraft's wings and fuselages, 6061 is more resistant to corrosion than other aluminium alloys. It is also used in yacht construction. It has very good mechanical properties. Here the workpiece used in experiments is 100*80*16 mm in dimensions. Before starting the experiments, each sample was cleaned properly to remove surface oxidation. The chemical composition of 6061 is given in Table 1. For machining the workpiece, HSS type-N end mill tools are used, having 12 mm diameter.

Table 1 6061 Aluminium alloy composition

Al	Mg	Cu	Cr	Si	Fe	Zn	Ti	Mn
96–98.56	0.8–1.2	0.15–0.40	0.04–0.35	0.40–0.8	0.0–0.70	0.0–0.25	0.0–0.25	0.0–0.15

Fig. 1 Milling experimental setup

The SINOMIL300 vertical machining center is used for the all experiments, Fig. 1 shows the details of the machining center. Different cutting parameters were taken based on design of experiment. All experiments with base fluid MQL and hybrid nanofluid MQL experiments were performed on same setup.

In the experiments to measure the cutting forces, the KISTLER 9257B a piezo-electric dynamometer was used. The measurements of cutting forces were taken for the end milling of 100 mm length at various machining conditions. The cutting forces was taken into consideration from middle section to avoid engagement and disengagement of tool jerks. The MQL system was used at four bar pressure and the nozzle distance was 40 mm. The base fluid was made with 5% volume of vegetable oil and 1% volume of liquid detergent into 94% volume of water. And the nanofluid was prepared by mixing 1% volume in the base fluid. The hybrid nanofluids were mixture of Al₂O₃ and graphene in 90:10 ratio.

2.1 Methodology of Experiment Design

Response surface methodology is a technique to analyze the data in which one or more responses depend upon many variables as shown below:

$$y = f(x_1, x_2, x_3, \dots) \quad (1)$$

where f is multivariable function and all x are variables. This type of relation in RSM is defined by a curved surface. Equation (1) is first-order equation of this methodology, when this first-order fails then comes second order equation as given below:

$$y = a_0 + \sum_{i=1}^n a_i x_i^1 + \sum_{i=1}^n a_{ii} x_i^2 + \sum_{i=1}^n \sum_{j=1}^n a_{ij} x_i^1 x_j^1, i < j \tag{2}$$

In RSM box behnken design is used for optimization of input variables at which the response variable is optimized. Taking three variables of machining parameter containing three levels as in Table 2. Design of Experiment was generated in MINITAB as shown in Table 3 and all 15 different experiments were performed for both (Base fluid MQL and NMQL) conditions. Each experiment were performed thrice and the average value of all responses was considered.

Table 2 Machining parameters

Cutting speed (rpm)	Feed (mm/min)	Depth of cut (mm)
1000	100	0.5
2000	200	0.75
3000	300	1.00

Table 3 Design of experiment

Run order	Depth of cut	Feed rate	Velocity
1	0.75	200	2000
2	0.75	200	2000
3	0.75	100	1000
4	0.75	300	1000
5	1	300	2000
6	0.75	300	3000
7	0.75	100	3000
8	0.5	100	2000
9	0.5	200	1000
10	1	200	1000
11	0.5	200	3000
12	1	200	3000
13	0.75	200	2000
14	0.5	300	2000
15	1	100	2000

3 Results and Discussion

The experimental data of cutting forces were analyzed in MINITAB we find all regression relations and ANOVA of data as well as surface plots showing relation between forces and all parameters. Table 4 shows the DOE with responses.

3.1 Forces in MQL of Base Fluid

MQL milling of base fluid shows the forces F_x and F_y in Tables 5 and 6 with ANOVA and regression analysis as well as coefficient of determination and adjusted coefficient of determination.

Here in F_x the coefficient of determination (R^2) and adjusted R^2 are 96.38% and 89.85%, respectively and in F_y the coefficient of determination (R^2) and adjusted R^2 are 95.33% and 86.92%, respectively. It should be closer to 100 and above the 90 values are acceptable. And the regression equation for F_x and F_y are given below as Eqs. (3) and (4)

Table 4 Cutting forces in different environments

Run order	MQL with base fluid			MQL with hybrid nanofluid		
	F_x MQL	F_y MQL	F_z MQL	F_x NMQL	F_y NMQL	F_z NMQL
1	104.2	88.3	59.7	88.6	80.6	43.8
2	103.4	90.2	60.2	85.3	74.9	46.5
3	81.2	89.5	61	74.3	66.6	45.1
4	109.3	121.9	34.2	103.6	116.6	26.1
5	131.6	131.5	81.6	112.6	125.6	76.8
6	66.7	130.6	47	61.9	110.6	37.4
7	78.3	106.5	46.2	72.7	83.7	31.2
8	103	101.5	126.9	95	74.2	115.4
9	118.5	89.1	109	103.5	69.6	85.45
10	108.3	101	88.2	89	77.1	83.9
11	79.4	92.3	109.5	65.4	67.4	91.1
12	130.2	131.2	88.9	120.1	101.5	91.35
13	92.3	86.9	58.4	74.1	72.19	49.4
14	109.8	92.4	90.5	92.3	98.2	63.1
15	119.3	101.1	60.2	101.2	90.7	49.9

Table 5 ANOVA of F_x in MQL milling

Source	Degree of freedom	Adj SS	Adj MS	F-value	P-value	
Model	9	5057.59	561.95	14.77	0.004	
Linear	3	1424.04	474.68	12.48	0.009	
Depth of cut	1	774.21	774.21	20.35	0.006	Significant
Feed	1	158.42	158.42	4.16	0.097	
Velocity	1	491.41	491.41	12.92	0.016	Significant
Square	3	2301.71	767.24	20.17	0.003	
Depth of cut * Depth of cut	1	1565.60	1565.60	41.15	0.001	Significant
Feed * Feed	1	79.27	79.27	2.08	0.208	
Velocity * Velocity	1	484.78	484.78	12.74	0.016	Significant
2-Way Interaction	3	1331.83	443.94	11.67	0.011	
Depth of cut * Feed	1	7.56	7.56	0.20	0.674	
Depth of cut * Velocity	1	930.25	930.25	24.45	0.004	Significant
Feed * Velocity	1	394.02	394.02	10.36	0.024	Significant
Error	5	190.22	38.04			
Lack-of-fit	3	101.74	33.91	0.77	0.609	
Pure error	2	88.49	44.24			
Total	14	5247.81				

$$\begin{aligned}
 F_x \text{ MQL} = & 258.2 - 587.9 \text{ Depth of cut} + 0.387 \text{ Feed} + 0.0121 \text{ Velocity} \\
 & + 329.5 \text{ Depth of cut} * \text{Depth of cut} - 0.000463 \text{ Feed} * \text{Feed} \\
 & - 0.000011 \text{ Velocity} * \text{Velocity} + 0.055 \text{ Depth of cut} * \text{Feed} \\
 & + 0.0610 \text{ Depth of cut} * \text{Velocity} - 0.000099 \text{ Feed} * \text{Velocity} \quad (3)
 \end{aligned}$$

$$\begin{aligned}
 F_y \text{ MQL} = & 249.2 - 201.4 \text{ Depth of cut} - 0.695 \text{ Feed} - 0.0496 \text{ Velocity} \\
 & + 75.5 \text{ Depth of cut} * \text{Depth of cut} + 0.001344 \text{ Feed} * \text{Feed} \\
 & + 0.000010 \text{ Velocity} * \text{Velocity} + 0.395 \text{ Depth of cut} * \text{Feed} \\
 & + 0.0270 \text{ Depth of cut} * \text{Velocity} - 0.000021 \text{ Feed} * \text{Velocity} \quad (4)
 \end{aligned}$$

3.2 Forces in MQL of Hybrid Nanofluid

The ANOVA of F_x and F_y are shown in Tables 7 and 8 in case of milling with hybrid nanofluid. The last column of ANOVA shows that it is significant or not, when P-value is less than 0.050 then it will be considered to be significant.

Table 6 ANOVA of F_y in MQL milling

Source	Degree of freedom	Adj SS	Adj MS	F-Value	P-Value	
Model	9	3798.54	422.06	11.34	0.008	
Linear	3	2194.49	731.50	19.66	0.003	
Depth of cut	1	1001.28	1001.28	26.90	0.004	Significant
Feed	1	756.61	756.61	20.33	0.006	Significant
Velocity	1	436.60	436.60	11.73	0.019	Significant
Square	3	1014.52	338.17	9.09	0.018	
Depth of cut * Depth of cut	1	82.14	82.14	2.21	0.198	
Feed * Feed	1	667.12	667.12	17.93	0.008	Significant
Velocity * Velocity	1	385.40	385.40	10.36	0.024	Significant
2-Way interaction	3	589.53	196.51	5.28	0.052	
Depth of cut * Feed	1	390.06	390.06	10.48	0.023	Significant
Depth of cut * Velocity	1	182.25	182.25	4.90	0.078	
Feed * Velocity	1	17.22	17.22	0.46	0.527	
Error	5	186.08	37.22			
Lack-of-fit	3	180.59	60.20	21.94	0.044	
Pure error	2	5.49	2.74			
Total	14	3984.62				

Here in F_x the coefficient of determination (R^2) and adjusted R^2 are 92.39% and 88.70%, respectively and in F_y the coefficient of determination (R^2) and adjusted R^2 are 98.15% and 94.82%, respectively. It should be closer to 100 and above the 90 values are acceptable. And the regression equation for F_x and F_y are given below as Eqs. (5) and (6)

$$\begin{aligned}
 F_x \text{ in Hybrid nanofluid MQL} = & 283.0 - 541 \text{ Depth of cut} + 0.104 \text{ Feed} \\
 & - 0.0175 \text{ Velocity} + 271.9 \text{ Depth of cut} \\
 & * \text{ Depth of cut} + 0.000062 \text{ Feed} * \text{ Feed} \\
 & - 0.000005 \text{ Velocity} * \text{ Velocity} \\
 & + 0.141 \text{ Depth of cut} * \text{ Feed} \\
 & + 0.0692 \text{ Depth of cut} * \text{ Velocity} \\
 & - 0.000100 \text{ Feed} * \text{ Velocity}
 \end{aligned}
 \tag{5}$$

Table 7 *F_x* of hybrid nanofluid milling

Source	DF	Adj SS	Adj MS	F-value	P-value	
Model	9	3835.21	426.13	6.75	0.024	
Linear	3	964.85	321.62	5.09	0.056	
Depth of cut	1	556.11	556.11	8.81	0.031	Significant
Feed	1	92.48	92.48	1.46	0.280	
Velocity	1	316.26	316.26	5.01	0.075	
Square	3	1221.49	407.16	6.45	0.036	Significant
Depth of cut * Depth of cut	1	1066.03	1066.03	16.88	0.009	Significant
Feed * Feed	1	1.40	1.40	0.02	0.887	
Velocity * Velocity	1	98.25	98.25	1.56	0.267	
2-Way interaction	3	1648.86	549.62	8.70	0.020	
Depth of cut * Feed	1	49.70	49.70	0.79	0.416	
Depth of cut * Velocity	1	1197.16	1197.16	18.96	0.007	Significant
Feed * Velocity	1	402.00	402.00	6.37	0.053	
Error	5	315.70	63.14			
Lack-of-fit	3	200.18	66.73	1.16	0.495	
Pure error	2	115.53	57.76			
Total	14	4150.91				

Table 8 *F_y* of hybrid nanofluid milling

Source	DF	Adj SS	Adj MS	F-value	P-value	
Model	9	4960.23	551.14	29.50	0.001	
Linear	3	3357.60	1119.20	59.90	0.000	
Depth of cut	1	913.78	913.78	48.91	0.001	Significant
Feed	1	2305.21	2305.21	123.38	0.000	Significant
Velocity	1	138.61	138.61	7.42	0.042	Significant
Square	3	1262.63	420.88	22.53	0.002	
Depth of cut * Depth of cut	1	31.09	31.09	1.66	0.254	
Feed * Feed	1	1246.90	1246.90	66.74	0.000	Significant
Velocity * Velocity	1	0.04	0.04	0.00	0.966	
2-way interaction	3	339.99	113.33	6.07	0.040	
Depth of cut * Feed	1	29.70	29.70	1.59	0.263	
Depth of cut * Velocity	1	176.89	176.89	9.47	0.028	Significant
Feed * Velocity	1	133.40	133.40	7.14	0.044	Significant
Error	5	93.42	18.68			
Lack-of-fit	3	56.56	18.85	1.02	0.529	
Pure error	2	36.85	18.43			
Total	14	5053.64				

$$\begin{aligned}
 F_y \text{ Hybrid nanofluid MQL} = & 134.7 - 101.9 \text{ Depth of cut} - 0.532 \text{ Feed} \\
 & - 0.0046 \text{ Velocity} + 46.4 \text{ Depth of cut} \\
 & * \text{Depth of cut} + 0.001838 \text{ Feed} * \text{Feed} \\
 & + 0.000000 \text{ Velocity} * \text{Velocity} \\
 & + 0.1090 \text{ Depth of cut} * \text{Feed} + 0.02660 \text{ Depth of cut} \\
 & * \text{Velocity} - 0.000058 \text{ Feed} * \text{Velocity} \quad (6)
 \end{aligned}$$

3.3 Relation Between Cutting Force and Machining Parameter

Cutting forces in MQL milling—In the following surface plot the forces on Z-axis are in Newton and depth of cut is in mm at x-axis while feeding on y-axis in mm/min. It shows that the F_x is minimum at 100 mm/min feed and 0.75 mm D.O.C. while the F_y is minimum at feed 200 and DOC 0.5 mm [15] (Fig. 2).

Cutting forces in NMQL Milling—In the following surface plot the forces on Z-axis are in Newton and depth of cut is in mm at x-axis while feeding on y-axis in mm/min. It shows that the F_x is minimum at 100 mm/min feed and 0.75 mm D.O.C. while the F_y is minimum at feed 200 and DOC 0.5 mm. [17, 24] (Fig. 3).

3.4 Confirmatory Experiment for Cutting Forces

In MINITAB, the F_y (Feed force) was analyzed to minimize its value and find the following parameter at which F_y was minimum in (MQL, NMQL) milling conditions separately.

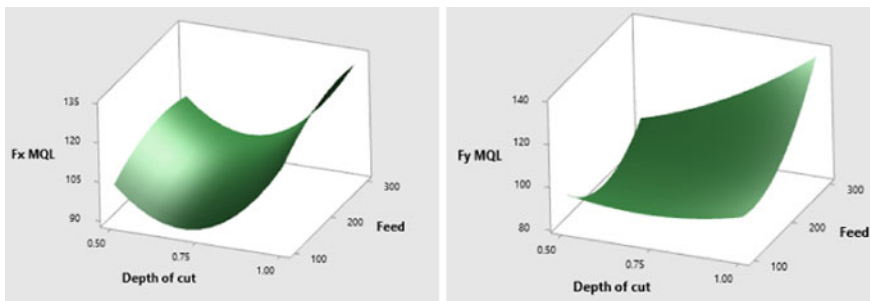


Fig. 2 Surface plot of MQL milling

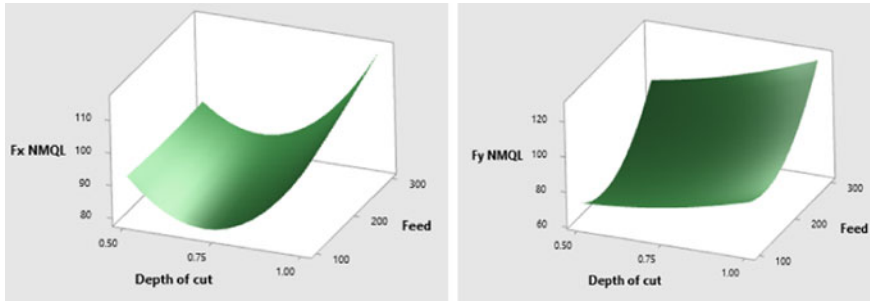


Fig. 3 Surface plot of NMQL milling

Table 9 Optimum parameters for machining

Solution	Depth of cut	Feed	Velocity	F_y -MQL fit	F_y -NMQL fit	Composite desirability
Predicted	0.5	188.889	2633.20	86.824	65.62	1
Experimented	0.5	188.889	2633.20	95.54	70.68	
Percentage deviation				9.12%	7.15%	

The above Table 9 shows the at which F_y will be minimum. The study shows that the optimum parameter of machining is 0.5 depth of cut, 188.88 mm/min feed and 2633.20 rpm spindle speed in end milling of Al6061.

4 Conclusions

- The cutting forces in NMQL are low as compared to MQL milling with base fluid.
- As per the ANOVA analysis, depth of cut showed a major contribution in cutting force analysis in both conditions, i.e., with base fluid and hybrid nanofluid, respectively.
- In case of hybrid nanofluid, there is 15.98% decrement in cutting force with respect to machining with base fluid in MQL milling.
- The cutting force was optimized in all three milling conditions at 0.5 depth of cut, 188.889 mm/min feed and 2633.20 rpm spindle speed for Al6061 milling with HSS tool.

References

1. Tazehkandi AH, Shabgard M, Kiani G, Pilehvarian F (2016) Investigation of the influences of polycrystalline cubic boron nitride (PCBN) tool on the reduction of cutting fluid consumption and increase of machining parameters range in turning Inconel 783 using spray mode of cutting fluid with compressed air. *J Clean Prod* 135(2016):1637–1649. <https://doi.org/10.1016/j.jclepro.2015.12.102>
2. Shokrani A, Dhokia V, Newman ST (2012) Environmentally conscious machining of difficult-to-machine materials with regard to cutting fluids. *Int J Mach Tools Manuf* 57:83–101. <https://doi.org/10.1016/j.ijmactools.2012.02.002>
3. Maruda RW, Feldshtein E, Legutko S, Krolczyk GM (2016) Analysis of contact phenomena and heat exchange in the cutting zone under minimum quantity cooling lubrication conditions. *Arab J Sci Eng* 41(2):661–668. <https://doi.org/10.1007/s13369-015-1726-6>
4. Sharma J, Sidhu BS (2014) Investigation of effects of dry and near dry machining on AISI D2 steel using vegetable oil. *J Clean Prod* 66:619–623. <https://doi.org/10.1016/j.jclepro.2013.11.042>
5. Weinert K, Inasaki I, Sutherland JW, Wakabayashi T (2004) Dry machining and minimum quantity lubrication. *CIRP Ann—Manuf Technol* 53(2):511–537. [https://doi.org/10.1016/S0007-8506\(07\)60027-4](https://doi.org/10.1016/S0007-8506(07)60027-4)
6. Dubey V, Kumar Sharma A, Kumar Singh R (2019) Study of various cooling methodology used in machining processes. *Mater Today Proc* 21:1572–1576. <https://doi.org/10.1016/j.matpr.2019.11.092>
7. Dubey V, Sharma AK, Singh RK (2021) A technological review on temperature measurement techniques in various machining processes. In: *Lecture notes in mechanical engineering*, pp 55–67. https://doi.org/10.1007/978-981-15-5151-2_6
8. Obikawa T, Kamata Y, Asano Y, Nakayama K, Otieno AW (2008) Micro-liter lubrication machining of Inconel 718. *Int J Mach Tools Manuf* 48(15):1605–1612. <https://doi.org/10.1016/j.ijmactools.2008.07.011>
9. Wang C, Li K, Chen M, Liu Z (2018) Evaluation of minimum quantity lubrication effects by cutting force signals in face milling of Inconel 182 overlays. *J Clean Prod* 145–157. <https://doi.org/10.1016/j.jclepro.2015.06.095>
10. Li KM, Liang SY (2007) Performance profiling of minimum quantity lubrication in machining. *Int J Adv Manuf Technol* 35(3–4):226–233. <https://doi.org/10.1007/s00170-006-0713-1>
11. Rabiei F, Rahimi AR, Hadad MJ, Ashrafiyou M (2015) Performance improvement of minimum quantity lubrication (MQL) technique in surface grinding by modeling and optimization. *J Clean Prod* 86:447–460. <https://doi.org/10.1016/j.jclepro.2014.08.045>
12. Sharma P, Sidhu BS, Sharma J (2015) Investigation of effects of nanofluids on turning of AISI D2 steel using minimum quantity lubrication. *J Clean Prod* 108:72–79. <https://doi.org/10.1016/j.jclepro.2015.07.122>
13. Khettabi R, Nouioua M, Djebara A, Songmene V (2017) Effect of MQL and dry processes on the particle emission and part quality during milling of aluminium alloys. *Int J Adv Manuf Technol* 92(5–8):2593–2598. <https://doi.org/10.1007/s00170-017-0339-5>
14. Yıldırım ÇV, Kıvak T, Erzincanlı F (2019) Tool wear and surface roughness analysis in milling with ceramic tools of Waspaloy: a comparison of machining performance with different cooling methods. *J Brazilian Soc Mech Sci Eng* 41(2). <https://doi.org/10.1007/s40430-019-1582-5>
15. Mia M, Al Bashir M, Khan MA, Dhar NR (2017) Optimization of MQL flow rate for minimum cutting force and surface roughness in end milling of hardened steel (HRC 40). *Int J Adv Manuf Technol* 89(1–4):675–690. <https://doi.org/10.1007/s00170-016-9080-8>
16. Pandey K, Dubey V, Sharma AK, Mital A (2019) State of art on tribological behaviour of nanoparticle enriched cutting fluid. *Mater Today: Proc* 26:2586–2589. <https://doi.org/10.1016/j.matpr.2020.02.547>
17. Joshua OS, David MO, Sikiru IO (2015) Experimental investigation of cutting parameters on surface roughness pretidicon during end milling of aluminium 6061 under MQL (Minimum

- quantity lubrication). *J Mech Eng Autom* 5(1):1–13. <https://doi.org/10.5923/j.jmea.20150501.01>
18. Tosun N, Pihili H (2010) Gray relational analysis of performance characteristics in MQL milling of 7075 Al alloy. *Int J Adv Manuf Technol* 46(5–8):509–515. <https://doi.org/10.1007/s00170-009-2118-4>
 19. Mishra S, Dubey V, Sharma AK (2022) Potential of various metal-oxide nanofluids for sustainable machining application—a review. *Lect Notes Mech Eng* 23–34. https://doi.org/10.1007/978-981-16-3330-0_2
 20. Tosun N, Huseyinoglu M (2010) Effect of MQL on surface roughness in milling of AA7075-T6. *Mater Manuf Process* 25(8):793–798. <https://doi.org/10.1080/10426910903496821>
 21. Asiltürk I, Neşeli S, Ince MA (2016) Optimisation of parameters affecting surface roughness of Co28Cr6Mo medical material during CNC lathe machining by using the Taguchi and RSM methods. *Meas J Int Meas Confed* 78:120–128. <https://doi.org/10.1016/j.measurement.2015.09.052>
 22. Li M, Yu T, Zhang R, Yang L, Li H, Wang W (2018) MQL milling of TC4 alloy by dispersing graphene into vegetable oil-based cutting fluid. *Int J Adv Manuf Technol* 99(5–8):1735–1753. <https://doi.org/10.1007/s00170-018-2576-7>
 23. Mia M, Dhar NR (2017) Optimization of surface roughness and cutting temperature in high-pressure coolant-assisted hard turning using Taguchi method. *Int J Adv Manuf Technol* 88(1–4):739–753. <https://doi.org/10.1007/s00170-016-8810-2>
 24. Okafor AC, Nwoguh TO (2020) Comparative evaluation of soybean oil-based MQL flow rates and emulsion flood cooling strategy in high-speed face milling of Inconel 718. *Int J Adv Manuf Technol* 107(9–10):3779–3793. <https://doi.org/10.1007/s00170-020-05248-3>

Classification Methods for Labelled Data in Machine Learning



Ashish Kannojiya, Anuj Singh Rajput, and Anurag Shanu

Abstract In the fast-growing web technology and breakthrough techniques of acquiring data from the user without letting them know and using this data to tackle any other problem, data scientist often has to go through a lot of hustles to get the correct and meaningful data. To minimize the efforts and work efficiently there are various ways in machine learning algorithms to do so and one of them is classification. The motive of this paper is to help and enlighten how one can work with labelled data and classification models and make the best use out of them either for study or for working on live projects which can be as sensitive as detecting cancer in a patient.

Keywords Regression · Dummy variable · Classification · Sigmoid · Nodes · Logistic · Vector

1 Introduction

The main motive of this is to learn about various methods used for classification of labelled data. It is a subset of what we call a Binary Classification in Machine Learning [1–8]. Here the discussion is about how one can use labelled data to classify it and use as per the convince and efficiency. A binary classification is the simplest method that we still use and is one the most efficient one too which consists of two classes [1] i.e., 1 and 2 or in other words either True or False. Some of the very basic examples of classification problems consist of detecting an e-mail to be in spam folder or in ham folder, whether someone is eligible for a loan or not, diagnosing a disease such as cancer [9, 10]. There has been many major breakthroughs in machine learning since the start of 21st Century.

In sigmoid function aka logistic function one can give whatever input that he/she feels like and the system will provide answer in 0 and 1 [9]. We often use a confusion matrix along with Logistic Regression to cross check and evaluate our results.

A. Kannojiya · A. S. Rajput · A. Shanu (✉)
Department of Mechanical Engineering, Galgotias University, Greater Noida, India
e-mail: anurag.shanu@galgotiasuniversity.edu.in

$$S(x) = \frac{1}{1 + e^{-x}} \quad (1)$$

Equation (1) Mathematical representation of sigmoid function.

2 Literature Review

Machine Learning was first saw in a computer programme in the form of a checkers game created by Samuel [11]. In 1958, Frank Rosenblatt formulated the first artificial neural network, called perceptron. The objective of this approach was to recognize pattern and shapes [12–20].

After these major incidents there was no major development and research in the field till early 90's. In 1997, the IBM computer Deep Blue, came into notice as it was a chess playing computer which defeated the world chess champion at that time [21–30]. After this incident there were many advances and research done to the field by many IT giants and from the start of this century many tech giants have realized that machine learning will increase calculation potential.

Recent breakthrough includes.

- i. For clinical pleural effusion categorization, machine learning was used to near-infrared spectra [17].
- ii. A platform for estimating anti-SARS-CoV-2 actions using machine learning [13].
- iii. Data from short pilot investigations employing deep generative models on synthetic single cell RNA sequencing [16].
- iv. Using a deep neural network and optical coherence tomography, distinguishing retinal angiomas from polypoidal choroidal vasculopathy. And many more [14].

All these things were possible by using various data either it is labelled or unlabelled (most of the time it is labelled data only) [22]. So, now the question arises what is meant by labelled data and why it is used and how it is used in various methods of classification in machine learning. We are going to discuss all about that in this paper and give a brief yet complete layout of how one can use classification techniques in machine learning [31].

3 Logistic Regression with Python

In machine learning the language we use is Python so we have to write the algorithms in Python language. To get a better view of what we are conveying in our work of this research paper we here consider an example of testing for a disease in a patient of which the symptoms we already know, for instance cancer or covid-19 [29].

Table 1 Data of 165 trails for a disease outcome

$N = 165$	Predicted: NO	Predicted: YES
Actual NO	50 (Tn)	10 (Fp)
Actual YES	5 (Fn)	100 (Tp)

Suppose we have a model for predicting the outcome of the disease which consist of 165 trials and we want to run Logistic Regression on it to make it more accurate.

Table 1 shows an example of 165 trails for a disease outcome.

Here the NO signifies Negative test = False = 0.

YES, signifies Positive test = True = 1.

Tn implies True negative that means the model predicted True and the test was negative [25].

Tp implies True positive that means the model predicted True and the test was also positive.

Fp implies False positive that means the model predicted False and the test was positive.

Fn implies False negative that means the model predicted False and the test was also negative.

These are the terms that we usually use when dealing with machine learning particularly dealing with Logistic Regression or any other type of classification [2].

In the Table 1 we can find the accuracy and error rate to find out how our model is working without the use of Logistic Regression.

3.1 Code Used

To train and visualize the data

```

Train = pd.read_csv('cancer_patients.csv')
Train.head()
Train.isnull()
Sns.heatmap (train.isnull(), yticklabels = False, cbar = False, cmap = 'viridis')
Sns.set_style('white_grid')
Sns.countplot(x = 'survived', data = train, hue = 'Pclass')
Sns.countplot(x = 'survived', data = train, hue = 'sex' palette = 'RdBu_r')
Train['Fare']. hist (bins = 40, figsize = (10,4))
Plt.figure(figsize = (10,7))
Sns.boxplot(x = 'pclass', y = 'age', data = train)
    
```

Now that we have trained our data, we have to do cleaning of the data. This includes filling the missing data and then drop or eliminate the null values. The method of dropping and filling the missing data all depends on the programmer that which type of information is useful to them in the given perspective. [28].

For instance, in this particular example, we are not concerned about the age column, so we are going to eliminate it or drop it.

3.2 Code Used

```

Def impute_age(cols):
Age = cols [0]
Pclass = cols [1]
If pd.isnull(Age):
If pclass == 1:
Return 37
If pclass == 2:
Return 29
Else:
Return 24
Train['age'] = train [['age', 'pclass']]. apply(impute_age, axis = 1)
Now to drop null values
Train.drop ('cabin', axis = 1, inplace = True)
Train.dropna(inplace = True).

```

3.3 Creating Dummy Variable

Now that we have done data pre-processing and our data is ready, we need to create a dummy variable in order to implement logistic regression. The idea behind dummy variable is that the machine learning doesn't understand the laymen language that we use it only understands 0's and 1's. So, for every type of data that is not in the form of binary digits we create a dummy variable [24].

For instance, let's say we have been working on a data frame in which we need to distinguish between gender but the data is stored in the form of either male or female.

In order to overcome this problem, we will create variable for male and female in the form of 0's and 1's [23].

3.4 Predicting the Data

Now that we have done all the feature engineering and creating dummy variables now, we can use the model to predict the data and use our logistic function to get the predicted outcome more accurate [26].

4 Decision Trees and Random Forests with Python

A decision tree is just a basic concept that divides the initial output into various corresponding components with the motive of gaining an output while accounting for all the possible outcomes [18].

As the name implies decision tree, all the data is supervised as we would see how a tree is that is, we have roots and stem and then the branches [3]. In machine learning we call them nodes, edges, roots and leaves.

In this tree we have:

- i. Nodes—This is the input which then further splits for the value of a certain attribute. Like here in the above diagram Weather is a node and then further Humidity and Wind are also nodes as they have subdivisions for each of them [19].
- ii. Edges—Edges are the outcome of a split to next node
- iii. Root—The node that performs the first split is known as root. In Fig. 1 weather is a root
- iv. Leaves—Terminal nodes that predict the outcomes are referred to leaves like No and Yes [27].

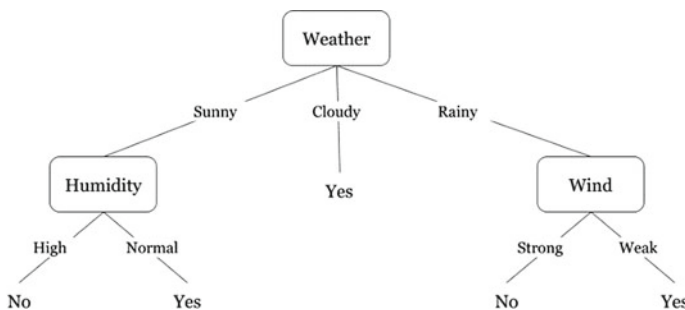


Fig. 1 Decision tree

4.1 *Benefits of Using Tree Method*

To enhance the production, one can split the tree into many trees using a random selection of attributes. At each split, a new random sample of attributes is selected for each tree. The square root of p is commonly used as m in categorization [15].

4.2 *Code Used*

Random Forest Classifier with Python

```
From sklearn.ensemble import RandomForestClassifier
```

```
Rfc = RandomForestClassifier(n_estimators = 200)
```

```
Rfc.fit(X_train, y_train)
```

```
Rfcpred = rfc.predict(X_test)
```

```
Print(classification_report(y_test, rfcpred))
```

```
Print(confusion_matrix(y_test,rfcpred)).
```

5 Support Vector Machines

SVMs are coordinated learning models with related learning computations that dissect data and perceive plans, used for order and backslide examination [6]. Given a bunch of getting ready delineations, each stepped for a having a spot to one of the two classifications, a SVM planning estimation besides constructs a show that allocates unused case into one class or the other, making it a non-probabilistic equal straight classifier [21] (Fig. 2).

6 K Nearest Neighbours

KNN is a classification algo which we are very simple and predicts the data quite efficiently [7]. First, we store all the data then we calculate the distance from x to all points in your data thus, the name nearest Neighbour. Then, we sort the points in our data by gradually increasing distance from x [5]. And, finally predicting the majority label of the ' k ' closes points.

This method is very simple to use and the training is trivial but it comes with the con of high prediction cost and even worse with large data sets [4]. It can work with any number of classes and comes handy to add more data while it is not good with

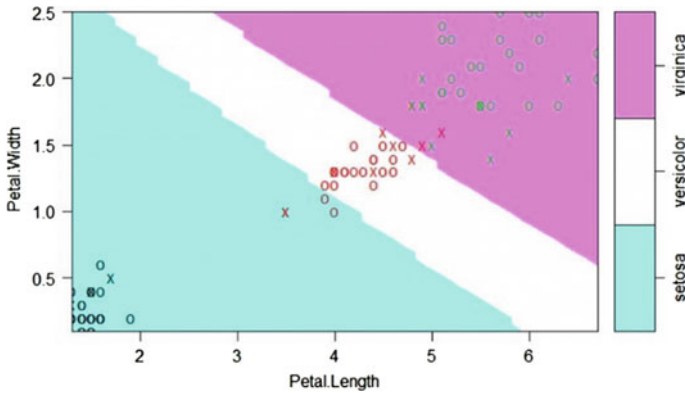
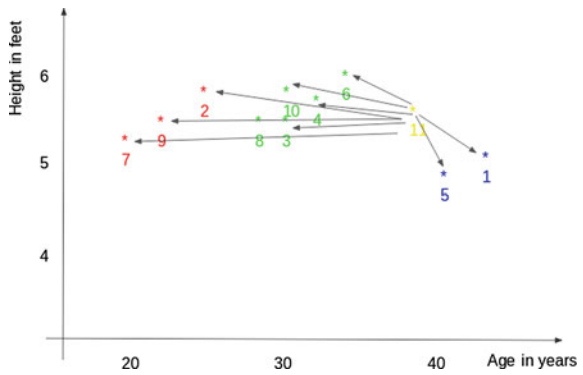


Fig. 2 Support vector machine

Fig. 3 K nearest neighbour



high dimensional data and even for categorical features. Although it is widely used till date due to it few parameters requirement and ease of use (Fig. 3).

7 Conclusion

All these methods that we discussed are majorly used while dealing with the labelled data. With the use of such methods, we can make the models more accurate and efficient. It's not like the machine learning algorithm won't work without these methods but to get the best out of these prediction models we need to use such approaches like we have discussed above. We do have a choice to use a certain method, it all depends on the data that we are working on. In machine learning there is no good or bad models and there is no way of setting any benchmark on how efficient a model is as we are just predicting the outcome so it all comes down to the data that we are going to work on. These methods assure us that the model is pushed

to its limits especially when we are dealing with sensitive data like cancer diagnosis etc. This will surely help in making system more efficient and there will be less chances of an error or failure in the machine learning. Although in machine learning error is equally important and only because of an error we can test our algorithm is working properly and predicting both the outcomes (like yes or no). Further there is a much greater scope in this field and many other ways can be found out to increase efficiency while predicting an outcome.

References

1. Pang B, Lee L (2008) Opinion mining and sentiment analysis. *Found Trends Inf Retrieval* 2(1–2):1–135
2. Pang B, Lee L, Vaithyanathan S (2002) Thumbs up? Sentiment classification using machine learning techniques. In: *Proceedings of the conference on empirical methods in tongue processing (EMNLP)*, pp 79–86
3. Go A, Bhayani R, Huang L Twitter sentiment classification using distant supervision
4. Read J (2005) Using emoticons to scale back dependency in machine learning techniques for sentiment classification. *Association for linguistics*
5. Nigam K, Lafferty J, McCallum A (1999) Using maximum entropy for text classification. In: *IJCAI-99 workshop on machine learning for information filtering*, pp 61–67. [Mikheev, 1999] Andrei Mikheev. Feature lattices and maximum entropy models. *Machine learning*, 1999.
6. Wang J, Yu L, Lai KR, Zhang X (2016) Dimensional sentiment analysis employing a regional CNN-LSTM model. In: *Proceedings of the 54th annual meeting of the association for linguistics*, vol 2 short papers. <https://doi.org/10.18653/v1/p16-2037>
7. Han J, Kamber M *Data mining concept and techniques*, Copyright 2006, Second edition
8. Jin C, De-Lin L, Fen-Xiang M An improve ID3 decision tree algorithm. In: *IEEE 4th international conference on computer science & education*
9. Quinlan JR (1986) Induction of decision trees. *Mach Learn* 1–1:81–106
10. Breimann L, Friedman JH, Olshen RA, Stone CJ (1984) *Classification and regression trees*. Wadsworth international group, Belmont, California
11. Bartlett P, Shawe-Taylor J (1998) Generalization performance of support vector machine and other pattern classifiers. In: *Burges C, Scholkopf B (ed) Advances in kernel methods--support vector learning*. MIT press
12. Bottou L, Vapnik V (1992) Local learning algorithms. *Neural Comput* 4(6):888–900
13. A tutorial on support vector machines for pattern recognition (1998) In *Data Mining and Knowledge Discovery*. Kluwer academic publishers, Boston, (vol 2)
14. Hand D, Mannila H, Smyth P (2001) *Principles of data mining*. The MIT press
15. Wang H (2002) Nearest neighbours without k: a classification formalism based on probability, technical report, faculty of informatics, University of Ulster. N. Ireland, UK
16. Sebastiani F (2002) Machine learning in automated text categorization. *ACM Computing Surveys* 34(1):1–47
17. Wang H, Düntsch I, Bell DA (1998) Data reduction based on hyper relations. In: *proceedings of KDD98*, pp 349–353, New York
18. Hart P (1968) The condensed nearest neighbour rule. *IEEE Trans Inf Theory* 14:515–516
19. Sorrower MS (2010) A literature survey on algorithms for multi-label learning. *Oregon State University, Corvallis*, p 18
20. Utku A, Karacan H, Yildiz O, Akcayol M (2015) Implementation of a new recommendation system based on decision tree using implicit relevance feedback. *J Softw* 10(12):1367–74
21. Gershman A, Meisels A, Lüke KH, Rokach L, Scholar A, Sturm A (2010) A decision tree based recommender system. In: *2010 IICS*, pp 170–179

22. Jadhav SD, Channe HP (2016) Efficient recommendation system using decision tree classifier and collaborative filtering. *Int Res J Eng Technol* 3:2113–2118
23. Beel J, Langer S, Genzmehr M, Nürnberger A (2013) Introducing Docear's research paper recommender system. In: *Proceedings of the 13th ACM/IEEE-CS joint conference on digital libraries*, pp 459–460. ACM
24. Zhang X, Jiang S (2012) A splitting criteria based on similarity in decision tree learning. *J Softw* 7(8):1775–1782
25. Bhargava N, Sharma G, Bhargava R, Mathuria M (2013) Decision tree analysis on j48 algorithm for data mining. *Proc Int J Adv Res Comput Sci Softw Eng* 3(6)
26. Anyanwu MN, Shiva SG (2009) Comparative analysis of serial decision tree classification algorithms. *Int J Comput Sci Secur* 3(3):230–240
27. Gates G (1972) The reduced nearest neighbour rule. *IEEE Trans Inf Theory* 18:431–433
28. Alpaydin E (1997) Voting over multiple condensed nearest neighbors. *Artif Intell Rev* 11:115–132
29. Kubat M, Jr M (2000) Voting nearest-neighbour subclassifiers. In: *Proceedings of the 17th international conference on machine learning, ICML-2000*, pp.503–510, Stanford, CA
30. Wilson DR, Martinez TR (2000) Reduction techniques for exemplar-based learning algorithms. *Mach learn* 38–3:257–286
31. Mitchell T (1997) *Machine learning*. In: Bishop CM *Neural networks for pattern recognition*. Oxford university press, MIT press and McGraw-Hill 11. UK

A Review of Solar Refrigeration for Cooling Applications



Sudhanshu Sharma, Aayush Tiwari, Abdur Rehman, Arbaz Ahmad Siddiqui, and Himanshu Yadav

Abstract The need for total energy is fast increasing as the standard of living and global population rise, and it is expected that existing fossil fuels will be depleted by the middle of this century. Energy consumption per capita per year is increasing every day around the world, and the pace of increase in sophisticated countries is even faster. Therefore, more attention has been focused on developing the potential methods to use solar energy, which is considered an unlimited source of energy. This study explores several solar refrigeration systems, with a particular focus on solar absorption refrigeration systems. The different parts of solar power refrigeration systems are illustrated by considering their basic working principles. Many review papers have been studied based on the investigation of performance, life cycle cost analysis, solar thermal cooling and refrigeration method, etc. This study shows the consumption of energy and fossil fuels can be minimized by increasing the coefficient of performance of solar power absorption system by using generator temperatures in the range of 60 °C to 80 °C, using lithium bromide as the absorbent and water as the refrigerant, as well as a higher evaporator and generator temperature, a lower condenser temperature, a double liner heat exchanger, a gravity heat pipe, and a single-effect vapor absorption refrigeration system.

Keywords Solar power refrigeration · Coefficient of performance · Solar thermal cooling

1 Introduction

The process of eliminating heat from a substance or a restricted or enclosed place is known as refrigeration. Thus, refrigeration means pumping of heat from lower to higher temperature. The refrigerant is pressed into the capillary tube and condenser for that reason increasing its pressure and temperature inside the cooled refrigerator

S. Sharma (✉) · A. Tiwari · A. Rehman · A. A. Siddiqui · H. Yadav
Department of Mechanical Engineering, Galgotias College of Engineering and Technology, Uttar Pradesh, Gr. Noida 201306, India
e-mail: sudhanshu.shr@gmail.com

depending on the present ambient temperature. Refrigeration is used in many places such as to avoid spoiling of food and to provide cooling, etc.

1.1 Solar Power Refrigerator

It is the refrigeration system that runs on the solar energy where the power is supplied not by the electrical supply system, but from the solar panel. In this process we produce refrigeration effect with the help of energy of sun and thermal energy or photovoltaic may be included in this. Solar power refrigerators are mostly used in rural locations where there is a lack of reliable grid access or unavailability of AC power.

1.2 Uses of Solar Power Refrigerator

Solar power refrigerators are used in the making of ice, freezer, cooling, for the preservation of food, to build an air conditioning system, etc. In this, direct current electricity using semiconducting materials is used directly by the conversion of solar radiation. Solar power refrigeration is used in off-grid rural areas for the preservation of food and vaccine. For transportation, solar power refrigeration is used in cars, buses, etc.

1.3 Working of Solar Power Refrigerator

Solar power refrigerator uses natural sunlight and converts it into energy which we finally use this energy to chill its storage compartment as shown in Fig. 1. There is no requirement for an electrical source, the only requirement is sunshine. The refrigerant solution is converted into the liquid through thermal energy.

Solar refrigerators uses several refrigerant solutions. Water and ammonia or water and lithium bromide remain the most common solution.

For the cooling of the storage compartment, the coolant converts into the liquid from vapor or vice-versa. In the solar refrigerator, the thermal energy gets created by the conversion process. This thermal energy can be used for supplying the power to the DC electrical systems. In the beginning, refrigerants in gaseous form are supplied to solar refrigerators. Due to heat produced by the sunlight, more pressure acts on the gases until they condense into a liquid.

Heavy insulation is applied to the solar-power refrigerator around the lining to maintain the cooling for hours. The items inside the fridge stay cool and is in good condition even when the device is left out in the sunlight.

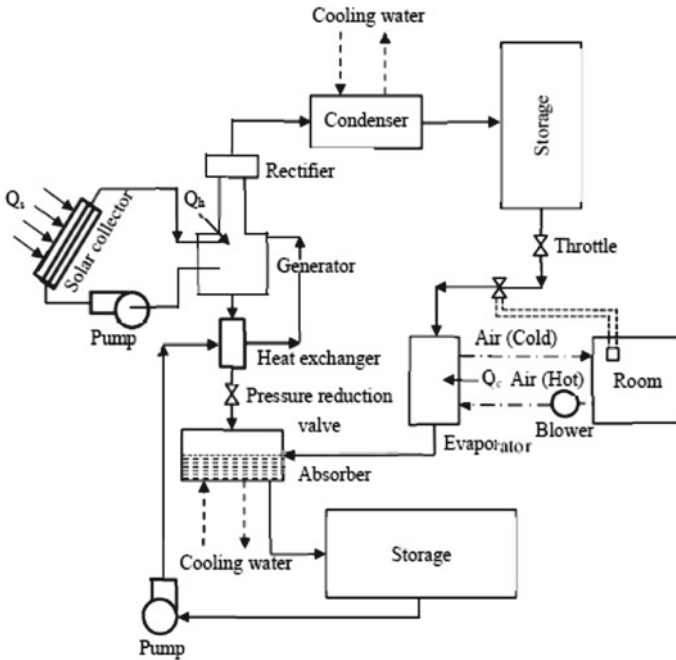


Fig. 1 Solar absorption refrigeration system schematic diagram

The change in refrigerant from gas phase to liquid phase produces enough thermal energy to give power to the fridge even if it is not in direct sunlight. In this way, no batteries are required to power solar refrigerators at night.

1.4 Types of Solar Power Refrigeration Systems

The three types of solar power refrigeration systems are:

- Photovoltaic operated refrigeration system
- Solar mechanical refrigeration system

Absorption refrigeration system.

1.5 COP of Solar Power Refrigeration System

$$\text{COP (refrigerator)} = \frac{Q_c}{W} = \frac{Q_s}{Q_r - Q_c} = \frac{T_c}{T_a - T_c}$$

where T_h , T_a and T_c are the temperatures of source, sink (atmosphere) and refrigeration respectively.

The overall COP of the system is given by.

$$\begin{aligned} \text{COP} &= \frac{Q_c}{Q_s} = W \left(\frac{T_c}{T_a - T_c} \right) \times \left(\frac{T_h - T_a}{W_{\text{Th}}} \right) \\ &= \left(\frac{T_c}{T_h} \right) \left(\frac{T_h - T_a}{T_a - T_c} \right) \end{aligned} \quad (1)$$

where $T_c < T_a < T_h$.

The absorption system's COP is calculated as follows:

$$\text{COP} = \frac{Q_e}{Q_s}$$

where Q_s is the heat withdrawn from the evaporator and Q_s is the incident energy on the collector. But the actual heat given in the generator is Q_h which is less than Q_s , (where Q_s is incident energy on collector therefore net COP will be reduced by the factor (Q_h/Q_s)).

$$(\text{COP}) = \frac{Q_c}{Q_s} \times \frac{Q_h}{Q_s} = \frac{Q_h}{Q_s} \left(\frac{Q_c}{Q_s} \right) \quad (2)$$

But the (Q_c/Q_s) is the COP of the system as shown. Substituting the value of (Q_c/Q_s) from Eq. (1) into Eq. (2).

$$\text{COP} = \left(\frac{Q_h}{Q_s} \right) \left(\frac{T_c}{T_s} \right) \left(\frac{T_h - T_a}{T_a - T_c} \right) \quad (3)$$

$$Q_h = Q_s - \text{Loss in the collector} = Q_s - U(T_h - T_a) \quad (4)$$

where T_h is the collector temperature and T_a is atmosphere temperature.

Substituting the value of Q_h in Eq. (3)

$$\text{COP} = \left[1 - \left(\frac{U}{Q_s} \right) (T_h - T_a) \right] \left(\frac{T_c}{T_h} \right) \left(\frac{T_h - T_a}{T_a - T_c} \right) \quad (5)$$

The equation shows that for the fixed atmospheric temperature T_a and required evaporator temperature T_c , the COP is dependent on T_h . Therefore, the COP will be maximum when

$$\left(\frac{d}{dT_h} \right) (\text{COP}) = 0$$

$$\left(\frac{d}{dT_h}\right)\left\{\left[1 - \left(\frac{U}{Q_s}\right)(T_h - T_a)\right]\left(\frac{T_c}{T_h}\right)\left(\frac{T_h - T_a}{T_a - T_c}\right)\right\} = 0$$

$$\frac{T_h}{T_a} = \frac{1}{\frac{T_c(T_h - T_a)}{Q_s} - T_h} \quad (6)$$

The COP of the system increases with increasing T_h while the output of the collector falls as per the Eq. (4).

2 State of the Art Review

2.1 Performance Investigation

In 2021, the performance of a solar adsorption cooling system was investigated by adding a SAPO-34 zeolite and comparing the optimal performance of the silica gel system to the SAPO-34 zeolite system that was operated throughout the experiment [1]. The cooling capacity and performance coefficient of the silica gel system were found to be more substantially influenced by adsorption time than those of the SAPO-34 zeolite system. The Munters and Platen cycle was used to test a diffusion absorption refrigeration machine (DAR) [2]. The global heat transfer coefficient of the evaporator (UA) is calculated using static and dynamic state approaches. It was discovered that the global heat transfer coefficient is 0.3 W/°C. To ensure the desired condition of this device, the required heating power supply for the generator should be in the range of 35–45 W. In 2017, results on the performance of an ice-storage system in a solar absorption cooling system for workplace cooling were presented [3]. The outcome showed that chiller average COP is 0.43 during charging for the months of March and 0.47 for month of October. An electron diffusion model was used to determine the current voltage characteristics of the DSSC [4]. The optimum values of this film thickness, current density, and structure parameter were about 5.62 μm , 11.7 Acm^{-2} , and 0.000465 cm^{-1} , respectively for parametric design. Performance investigation of a thermoelectric solar cell refrigerator was done in 2008 [5]. This was done by installing a conventional thermal cooler, which represents its own autonomous photovoltaic system for domestic use. The effect of opening the door on cooling, the temperature of which is produced by the sun element driving the thermoelectric refrigerator, was studied.

2.2 Cooling Capacity Increase

A dynamic model was created to predict the behavior of the variable speed photovoltaic direct-current refrigerator (VSPVDR) system [6]. The impact of the

compressor speed control method, radiation intensity, and ambient temperature were examined using this model. A multi-stage traveling-wave thermo-acoustic refrigerator using SAGE software the working mechanism was studied numerically. The calculation results shows that in multi-stage traveling-wave thermos-acoustic refrigerator three to five stages is more appropriate by striking a balance inside the temperature range of cooling efficiency and cooling power [7]. As a zero energy cool chamber, a system with two cooling systems, a solar-driven adsorption refrigerator and evaporative cooling, were developed (ZECC). The outcome suggested that new ZECC which is proposed is more useful for storing vegetables and fruit [8].

2.3 Enhanced Economic Performance

The effect of nano-sized oil droplets was studied in order to determine the effectiveness of a diffusion absorption refrigerator (DAR) [9]. In the absorption refrigeration cycle, a solar double product system was proposed [10]. Through the proposed system with matched system output, the energy saving achieved was 25.64%. The proposed system had an external energy efficiency of 9.83%, which was 2.97% higher than the reference systems. An optimized roll channel evaporator/collector was used to develop, build, and test the Direct Expansion—Solar Assisted Heat Pump Water Heating System (DX-SAHP) [11, 12]. Solar Vapor Absorption C.O.P. Improvement, a study of the refrigeration system was conducted. The efficiency of a steam absorption system can be improved by utilizing a generator set between 65 and 80 °C, as well as using lithium bromide as an absorbent and water, as in a refrigerator. [13, 14].

2.4 Refrigerator Analysis

Theoretical and practical evaluation of a small-scale ammonia water absorption refrigerator powered by a solar condenser was done. The results demonstrated that a parabolic concentrator (P.C.) with an average power supply and an efficiency of 530 W and 26 percent, respectively, can give a temperature above roughly 200 °C for around 6 h [15]. Annual performance of Absorption-compression solar driven cascade refrigeration system is investigated [16]. Void tube analysis on solar energy absorption system for process optimization in hot regions was carried out [17]. Cooling the water temperature below 40 °C will considerably diminish the unit's performance, which is necessary when the outside temperature is excessively hot. The first and second laws of thermodynamics were used to analyze a single stage absorption refrigeration cycle [18]. Under the steady state condition, the proposed model (first and second law analysis) was tested. Circulation Ratio (CR), Coefficient of Performance (COP), and Carnot Coefficient of Performance are the parameters considered (COPc). A computational model was used to conduct a theoretical analysis of the Lithium Bromide/Water Absorption Refrigeration system [19]. The

single-effect and series flow double-effect water lithium bromide absorption refrigeration systems were investigated using this model. With the help of three condensers, a thermodynamic analysis of the triple effect parallel flow water/lithium bromide chiller was performed [20]. The conservation equation that governs the cycle was stated like this, and the cycle was explored using the first and second laws.

2.5 Prototype Model

To create a cold storage refrigerator car model, SolidWorks was used, and analysis was performed to run simulations. The results reveal that as the temperature rises, the melting process of the storage plate accelerates and the time it takes for thermal energy to be discharged decreases [21]. Powered by an activated carbon/methanol pair, a multifunctional solar-powered kitchen appliance was constructed and tested [22]. Field experiments revealed that the prototype can produce 5 kg of ice with a COP of 0.08. TRANSYS was used to create a simulation model for the PV hybrid system, and the performance of the 1.44 kW PV hybrid system was assessed [23].

2.6 Effect on System Performance

An experimental refrigerator was constructed and tested of 1 kW cooling capacity [24]. The effect of a cylindrical adsorber on the operation of a solar adsorption refrigeration machine has been determined. The experimental results reveal that the primary nozzle geometry has a significant impact on the ejector performance and, as a result, on the system COP [25] outcome has shown that the adsorber with fins has optimal diameter larger than one without fins.

2.7 Engine Exhaust Gas as an Energy Source

An absorption refrigeration system that utilizes fumes gas by the motor and a LiBr water arrangement have been tried [26]. This test was carried out at various motor speeds of 1000, 1200, 1400, and 1600 rpm, with development valve opening levels of 54.5%, 72.7%, and 90.9% at the power source separator and 3.41%, 4.55%, and 5.68% at the power source condenser, respectively.

3 Conclusion

This review indicates the following research opportunities in the area of solar refrigeration.

3.1 Increase in COP

Methods of increasing COP.

- Using a roll-bond panel with an optimum channel layout can improve COP.
- When the refrigerator is operated at boiler temperature of 110 °C, evaporator temperature of 17 °C, and cooling capacity of 3000 W, the maximum COP of 0.45 is attained.
- To get the highest possible COP, the refrigeration system should be designed with current density, film thickness, and structure characteristics of 11.7 Acm^{-1} , $5.62 \text{ }\mu\text{m}$, and 0.000165 cm , respectively.
- The use of binary nanoemulsion fluid will improve the COP of the Diffusion Absorption Refrigerator (DAR). A binary nanoemulsion is defined as a nanoemulsion with a binary base liquid, such as an $\text{NH}_3/\text{H}_2\text{O}$ solution.
- The C.O.P. of a Vapor Absorption system will be improved by using generator temperatures ranging from 65–80 °C, using Lithium Bromide as an absorbent and water as a refrigerant, using higher evaporator and generator temperatures, low condenser temperatures, double liner heat exchangers, gravity heat pipes, and a single effect vapor absorption refrigeration system.

3.2 Increase in Cooling Power

Methods of increasing cooling power.

- Using multi-stage traveling-wave cooling will boost cooling capacity (three to five stages may be most suitable) refrigerator with a thermos-acoustic system.
- When photovoltaic (PV) cells are directly connected to the compressor without batteries or inverters, cooling power increases, and the DC compressor speed changes with radiation intensity in the VSPVDR system.

3.3 Enhance Performance

Methods of enhancing performance.

- When the evaporator temperature is set to 7.5 °C and eight primary nozzles with different shapes are employed, performance improves.

- Using a cylindrical adsorber will improve the performance of a solar adsorption refrigeration machine.
- To improve the multi-generation system's economic performance, the absorption chiller is increased, along with liquid desiccant dehumidification, which can result in cooling and water without the use of a desalination unit.
- The use of phase transition materials that increase the latent heat of fluid will improve performance.
- When SAPO-34 zeolite system is employed as a working pair, the performance of solar adsorption cooling system will improve.
- Using nanoparticles will considerably improve the performance of a vapor absorption refrigeration system.

3.4 *Decrease in Cost and Energy Saving*

Method of decrease in cost.

- The cost of a refrigerator with two cooling systems, a solar-driven adsorption refrigerator and an evaporative cooling system, will be lower.

Method of saving energy.

- LiBr-H₂O and R134a are used as working pairs in the absorption cycle and refrigerant in the compression cycle, respectively, and evacuated tube collectors are used to feed the refrigeration system.

References

1. Liu YM, Yuan ZX, Wen X, Du CX (2021) Evaluation on performance of solar adsorption cooling of silica gel and SAPO-34 zeolite. *Appl Therm Eng* 182:116019
2. Jemaa RB, Mansouri R, Boukholda I, Bellagi A (2016) Experimental investigation and exergy analysis of a triple fluid vapor absorption refrigerator. *Energy Convers Manage* 124:84–91
3. Ibrahim NI, Khan MMA, Mahbulul IM, Saidur R, Al-Sulaiman FA (2017) Experimental testing of the performance of a solar absorption cooling system assisted with ice-storage for an office space. *Energy Convers Manage* 148:1399–1408
4. Su S, Chen X, Wang J, Chen J (2015) Performance evaluation and parametric optimum design of a thermoelectric refrigerator driven by a dye-sensitized solar cell. *Int J Refrig* 60:62–69
5. Ullah KR, Saidur R, Ping HW, Akikur RK, Shuvo NH (2013) A review of solar thermal refrigeration and cooling methods. *Renew Sustain Energy Rev* 24:499–513
6. He D, Zhao L, Chang Z, Zhang Z, Guo P, Bai B (2021) On the performance of a centrifugal pump under bubble inflow: effect of gas-liquid distribution in the impeller. *J Petrol Sci Eng* 203:108587
7. Wang X, Wu Z, Zhang L, Hu J, Luo E (2020) Traveling-wave thermoacoustic refrigerator for room temperature application. *Int J Refrig* 120:90–96
8. Islam MP, Morimoto T (2014) A new zero energy cool chamber with a solar-driven adsorption refrigerator. *Renewable Energy* 72:367–376

9. Lee JK, Lee KR, Kang YT (2014) Development of binary nanoemulsion to apply for diffusion absorption refrigerator as a new refrigerant. *Energy* 78:693–700
10. Su B, Han W, Jin H (2017) An innovative solar-powered absorption refrigeration system combined with liquid desiccant dehumidification for cooling and water. *Energy Convers Manage* 153:515–525
11. Sun X, Wu J, Dai Y, Wang R (2014) Experimental study on roll-bond collector/evaporator with optimized-channel used in direct expansion solar assisted heat pump water heating system. *Appl Therm Eng* 66(1–2):571–579
12. Dhindsa GS (2021) Review on performance enhancement of solar absorption refrigeration system using various designs and phase change materials. *Mater Today Proc* 37:3332–3337
13. Wang J, Chen G, Jiang H (1998) Study on a solar-driven ejection absorption refrigeration cycle. *Int J Energy Res* 22(8):733–739
14. Thongtip T, Ruangtrakoon N, Aphornratana S (2014) Development of a steam jet refrigeration cycle for the actual application driven by low grade thermal energy. *Energy Procedia* 52:110–119
15. Busso A, Franco J, Sogari N, Cáceres M (2017) Attempt of integration of a small commercial ammonia-water absorption refrigerator with a solar concentrator: experience and results. *Int J refrig* 34(8):1760–1775
16. Bellos E, Tzivanidis C, Tsifis G (2017) Energetic, exergetic, economic and environmental (4E) analysis of a solar assisted refrigeration system for various operating scenarios. *Energy Convers Manage* 148:1055–1069
17. Saleh A, Mosa M (2014) Optimization study of a single-effect water–lithium bromide absorption refrigeration system powered by flat-plate collector in hot regions. *Energy Convers Manage* 87:29–36
18. Kaynakli O, Yamankaradeniz R (2007) Thermodynamic analysis of absorption refrigeration system based on entropy generation. *Curr sci*, 472–479
19. Arora A, Kaushik SC (2009) Theoretical analysis of LiBr/H₂O absorption refrigeration systems. *Int J Energy Res* 33(15):1321–1340
20. Sedigh S, Saffari H (2013) Exergy analysis of the triple effect parallel flow water-lithium bromide absorption chiller with three condensers. *Scientia Iranica* 20(4):1202–1212
21. Xiaofeng X, Xuelai Z, Munyalo JM (2017) Simulation study on temperature field and cold plate melting of cold storage refrigerator car. *Energy Procedia* 142:3394–3400
22. Santori G, Santamaria S, Sapienza A, Brandani S, Freni A (2014) A stand-alone solar adsorption refrigerator for humanitarian aid. *Sol Energy* 100:172–178
23. Bilal M, Arbab MN, Afridi MZUA, Khattak A (2016) Increasing the output power and efficiency of solar panel by using concentrator photovoltaics (CPV). *Int J Eng Works* 3(12):98–102
24. Ruangtrakoon N, Aphornratana S, Sriveerakul T (2011) Experimental studies of a steam jet refrigeration cycle: effect of the primary nozzle geometries to system performance. *Exp Thermal Fluid Sci* 35(4):676–683
25. Louajari M, Mimet A, Ouammi A (2011) Study of the effect of finned tube adsorber on the performance of solar driven adsorption cooling machine using activated carbon–ammonia pair. *Appl Energy* 88(3):690–698
26. Kaewpradub S, Sanguandean P, Katesuwan W, Chimres N, Punyasukhananda P, Asirvatham LG, Mahian O, Dalkilic AS, Wongwises S (2018) Absorption refrigeration system using engine exhaust gas as an energy source. *Case Stud Therm Eng* 12:797–804

Experimental Analysis on Different Terrains Using Proprioceptive Information of One Leg of Quadruped Robot



Avinash Bhashkar and Anuj Kumar Sharma

Abstract The animal used to maneuver on every terrain very efficiently and have the capability to survive on earth. In order to perform agile motions on concrete, sand, soil, sponge, and hard surfaces, a biological system must have the capability to recognize the terrains through its legs and sensing capabilities. For making decisions to navigate through these terrains, one must have to differentiate between these surfaces. This study proposes a novel technique to understand and differentiate the terrains using robot legs. In the present study, we propose to use the proprioceptive information of leg joints and record on different terrains. The results were analyzed to understand the behavior of robotic legs in different terrains. The developed leg is found to recognize the different terrains efficiently.

Keywords Legged robot · Terrains analysis · Quadruped · Robot · Leg proprioceptive leg

1 Introduction

This study concentrates on the experimentation of an animal-inspired robotic leg on different terrains and analysis it. The robot leg can realize the dynamic behavior and shows agile capabilities, which are tested on different terrains. This aim has the most critical, yet immature technological components in the legged system. We performed an agile hopping motion on the leg. To obtain this kind of motion by the leg, high force performance actuators are required while making and breaking contact with the ground then swinging. Two types of actuators have been introduced to fulfill the requirement of such dynamical behavior in the robotics literature proprioceptive and series elastic actuators. The robot leg is capable of position, velocity, and torque control. Hence we recorded the joint information while experimenting

A. Bhashkar (✉) · A. K. Sharma
Centre for Advanced Studies, Lucknow, India
e-mail: 19mech02@gmail.com

A. K. Sharma
e-mail: Anujksharma@cas.res.in

in different environments and analyzed it. Such information can be used to classify the terrains in order to make some decisions for the robot while traversing the terrains. In order to mitigate the problem, the proprioceptive actuation process is designed and fabricated. The proposed method of using proprioceptive information like joint angle, velocity, and phase voltage can be utilized in order to study different terrains. This phenomenon is to be used without ground contact feedback. This system does not cancel out the natural dynamical performance. Legged locomotion has been a fascinating study among scientists and engineers. Terrain identification is required in order to choose the correct gait to enhance locomotion. Researchers have performed methods using high-resolution pressure images [1], tactile sensing [2], machine learning algorithms [3]. Adaptive and natural locomotion requires robust design as well as active sensing abilities [4–7]. Since MIT Cheetah’s [8] proprioceptive actuation process was introduced, now legged robots have become very advanced in design, control, and intelligence. Quasi-Direct-drive has been investigated in Stanford’s Doggo robot and MIT Cheetah 3 [9, 10]. Single-leg experimentation has been done in order to gain acrobatic behaviors [11]. Seok et al. Bioinspiration [12, 13] gave an argument to mimic principles over appearance. Since many of the locomotion principles [14], energy-efficient locomotion [15] has been investigated for over two decades.

After getting dynamic behaviors of walking, trotting, galloping a recent trend has been studied to achieve real agile motions as animals exhibit. Motions like explosive jumping and compliant landing were investigated in Goat robots [13], few studies like optimized jumping and mixed-integer convex optimization [16] showed promising results. Underactuated spine behaviors for dynamic locomotion and planar dynamic leap were studied in [17, 18]. Most of the dimensions of design thinking of legged systems have been authored in [19]. Design for highly efficient hardware and composite force-sensing stated an approach of actuator design in order to generate higher efficiency in terms of proprioception *p*13, *p*14, *p*15. Novel single-leg design [20] open-sourced quadruped design [21], torque-controlled architecture [22] have made impact robotics research community. However, to the best of the author’s knowledge, the terrain study using proprioception has not been yet investigated, therefore, in the present paper, the author has done the terrain analysis with the help of proprioception. The authors discussed a brief introduction in Sect. 1. Related work has been mentioned about legged robots which have made a huge impact on research and industry. Section 2 consists mechanical and electronic system of the robot and its specifications similarly performed the experiments hence describing the process. We discussed proprioceptive and sensing capability in Sect. 2.1. Section 3 consists results of experiment, conclusion, and future work [23].

2 Methodology and Experimental Setup

In order to mitigate the problems in the identification of different terrains, this study approaches a novel method to sense proprioceptive information and analyze different terrains at open-loop frequency of 2.5 Hz. This experiment has been performed on terrains like concrete, hard surface, sand, soil, and elastic sponge as shown in Figs. 1 and 2. In this section, hardware specification and experimental test rig have been discussed as shown in Table 1. The robot consists of two co-axial quasi-direct-drive actuators. The robot leg is capable of showing proprioceptive information using

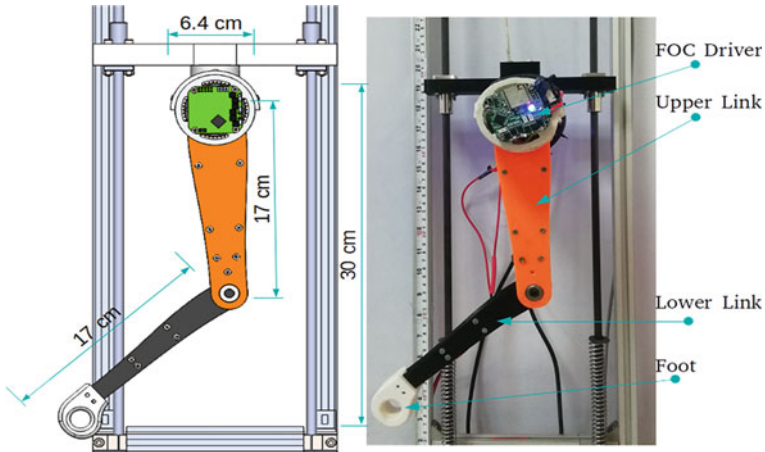


Fig. 1 CAD model (left) and prototype (right) of the leg

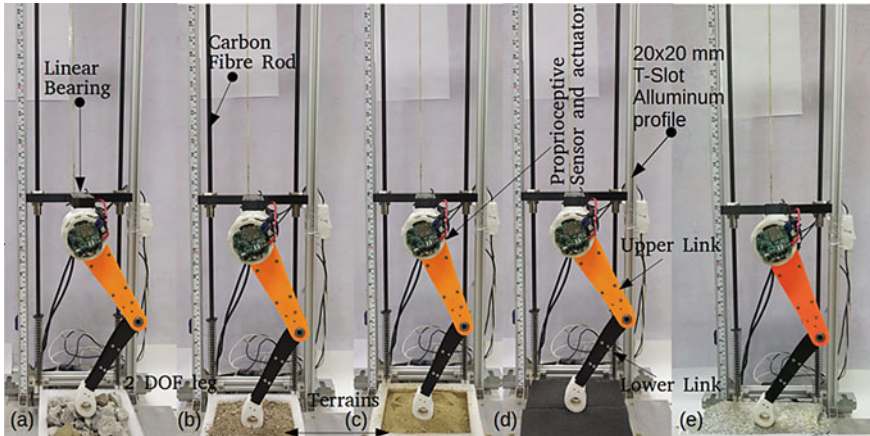


Fig. 2 Experimental setup on different terrains. Figure from left to right represents experiments on a concrete, b sand, c soil, d sponge and e hard surface

Table 1 Hardware specification and performance of the robot

Parameter	Symbol	Value	Unit
Total leg length	L	30	cm
Total leg mass	m	780	gm
Hip link	l_1	17	cm
Knee link	l_2	17	cm
Max. hip angle	θ_1	2.9	rad
Max. knee angle	θ_2	4.1	rad
Max. hip speed	ω_1	12.11	rad/sec
Max. knee speed	ω_2	8.56	rad/sec

sensors embedded in actuator. The robot leg has 35 cm and 780 gm leg length and mass, respectively. The range of motion is maximum of 2.9 rad and 4.1 rad on hip joint and knee joint, respectively. Maximum angular velocity of hip joint is 12.11 rad/sec at 1:6 gear reduction and 8.56 rad/sec of knee joint angular velocity at 1:12 gear reduction. Hardware parameters are described in Table 1. The leg is mounted on test rig and constrained in vertical direction so that a leg can jump at a certain height by gaining the kinetic energy and exert forces on the terrains. The test rig is built using linear 20×20 T-slots, linear bearing, and 8×1000 mm carbon fiber rod as shown in Fig. 2. The driver board consists of necessary sensors like position of the shaft and current sensing capabilities hence collecting the data points at 100 cycles at different loop frequencies. The control of the leg is open-loop hopping motion is being generated in python environment. This experiment collected 1,200,000 data sets on each terrain. We analyzed initial 500 data points in order to understand values over the time. The detailed experimental setup, plots, and validation it has been discussed in Sect. 3. The performance of the system could be seen in terms of agility and robustness. The leg was able to produce about 12 rad/sec hip joint and 8.56 rad/sec knee joint angular velocity. As mentioned in Table 1 total leg length is 30 cm and leg mass is around 780 gm. The hip, knee link lengths are 17 cm and 17 cm, respectively. Low mass and design lead the leg to low inertial effect on the system. The hip joint can rotate up to 2.9 rad while knee joint can rotate maximum of 4.1 rad. Such parameter makes the robot robust and agile.

2.1 Proprioception and Sensor Module

This study approaches experimental validation of legs on different terrains using proprioceptive information. In proprioception, it is suggested to have the capability of torque control and sensing abilities of the actuator in closed-loop with the micro-controller along with the driver, while the name refers to its mechanical design. Proprioceptive sensors are mainly utilized to measure joint position, rate of change of angles, joint torques, and body position with respect to an inertial frame. The QDD

Table 2 Electronics hardware specification

Equipment	Details
Magnetic encoder	AS5147
Microcontroller chip-set	ESP32
Driver	DRV8305
Hardware control	FOC
USB to UART bridge	CP22102

proprioceptive actuators consist of planetary gear reduction. A hall effect magnetic encoder AS5147 has been embedded on each driver module. It helps to measure the joint angle and velocity as mentioned in Table 2. The field-oriented control has been implemented in actuator control.

3 Results and Discussion

The test has been performed at voltage limit of 1.5 V, current limit of 0.2, and 2.5 Hz frequency of the loop. The following terrain samples had taken in different containers for the test. The leg generated vertical hopping motion on the terrains one by one on terrains which are concrete, hard surface, sand, soil, and sponge. In this part of the work, different terrains have been utilized in order to record its features with the help of proprioception as mentioned in the above section. The average size of stones is about 8 cm³. Real-world terrains are mostly unlike and uneven in size, concrete is one of them. We recorded the voltage drop, joint angle, and joint velocities while performing the test on concrete. The voltage drop of hip and knee actuator is represented by a blue curve with respect to time is scaled by $T/5$ s as shown in Fig. 3. As shown in Figs. 3, 4, 5, 6, and 7, the experiment results are plotted in a sequence as concrete, hard surface, sand, soil, and sponge at a frequency of the loop of 2.5 Hz. The hard plane surface does not deform when the leg makes an impact on it, this is why the curves are smoother than on other terrains.

In this part of the work, different terrains have been utilized in order to record its features with the help of proprioception as mentioned in the above section. The average size of stones is about 8 cm³. Real-world terrains are mostly unlike and uneven in size, concrete is one of them. We recorded the voltage drop, joint angle, and joint velocities while performing the test on concrete as shown in Fig. 4. The voltage drop of hip and knee actuator is represented by a blue curve with respect to time is scaled by $T/5$ s as shown in Fig. 3. As shown in Figs. 3, 4, 5, 6, and 7, the experiment results are plotted in a sequence as concrete, hard surface, sand, soil, and sponge at a frequency of the loop of 2.5 Hz. The hard plane surface does not deform when the leg makes an impact on it, this is why the curves are smoother than on other terrains.

We compare the average value of different parameters of the data set. Average V_{d1} and V_{d2} on every terrain are different from each other. Since legged systems

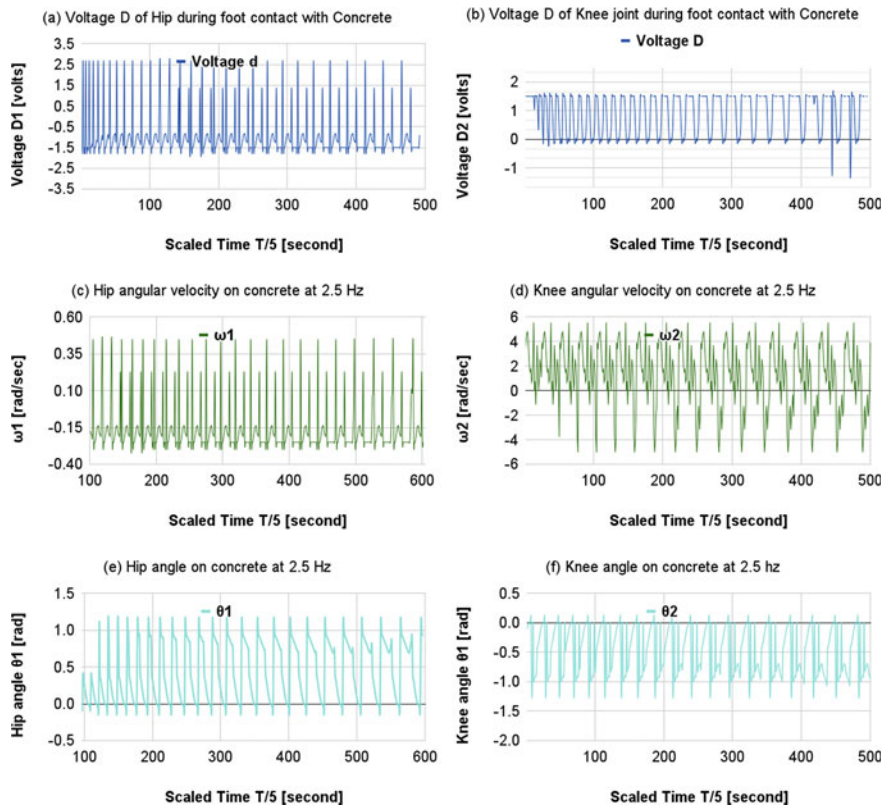


Fig. 3 Experimental results on concrete at 2.5 Hz frequency. **a–b** represents voltage drop at both actuators with respect to scaled time, and **c–d** represents joint angular velocity while **e** and **f** represent joint angles. The concrete terrain properties are affecting each parameter

are used to work on kinetic loss principle which tends to lose actuator energy in order to exert force. This leads to voltage drop because of different ground reaction forces. Different terrains exhibit different shapes, sizes, and material properties. The joint angle θ_1 at the hip and joint angle θ_2 at the knee have different averages, maximum, minimum, and plots. These parameters are visualized in graphs due to ground reaction forces acting on the leg. Similarly, joint angular velocities ω_1 and ω_2 are having differences in average, maximum, minimum, and graphs. This shows how different terrains are affecting joint velocities while making and breaking contact with the ground. The sponge has elastic properties hence the joint angle will be greater than on hard surfaces.

While sand and soil are more penetrable than in other environments, so the maximum and minimum values of parameters in such environments are higher than in others. Since sand and soil have similar properties hence they show similarities in parameters as shown in graphs. All Figs. 3, 4, 5, 6, 7 exhibits differences in

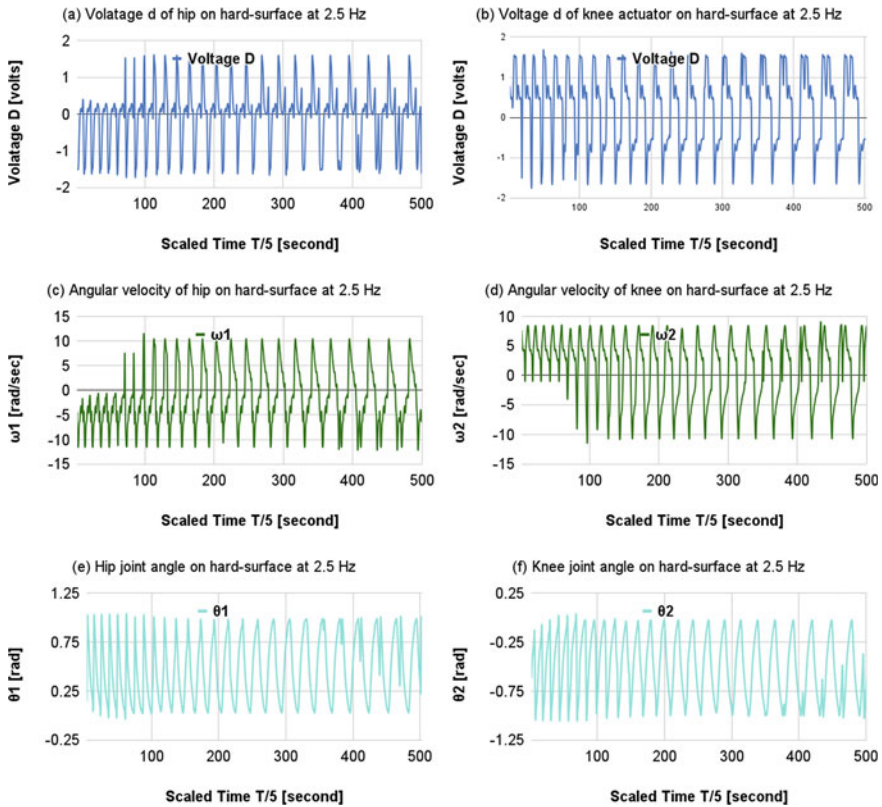


Fig. 4 Experimental results on hard surface at 2.5 Hz frequency. **a–b** describe voltage drop of hip and knee actuators with respect to scaled time, and **c–d** represents joint angular velocity while **e** and **f** represent joint angles

patterns in sensor readings collected in different environments. The leg can penetrate the sand terrain and can deform this is why the curves are repeating nature but are not smooth while making contact. Similarly, the soil shows almost the same behaviors in signals but can be seen in graphs. Hence it shows the possible classification of different terrains using proprioceptive information. The hard surface does not deform while making and breaking the contact resulting in the signals being much smoother than other curves. While concrete has the tendency to shift itself and unstable the reaction forces. Such tendency exhibits differences in pattern while repeating the same motion. The sponge has elastic and deformable properties. This leads to increase higher amplitudes in signals but smooth and exhibits pattern. While making contact. Similarly, the soil shows almost the same behaviors in signals but can be seen in graphs. Hence it shows the possible classification of different terrains using proprioceptive information.

The hard surface does not deform while making and breaking the contact resulting in the signals are much smoother than other curves. While concrete has the tendency

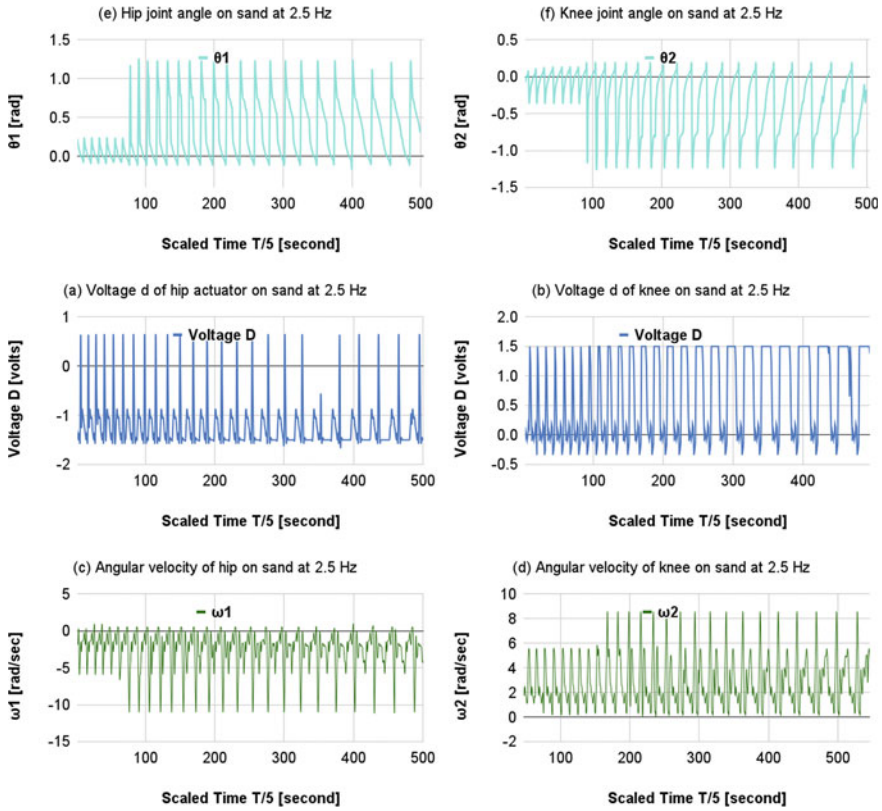


Fig. 5 Experimental results on sand at 2.5 Hz frequency. **a–b** represents voltage drop at both actuators with respect to scaled time, and **c–d** represents joint angular velocity while **e** and **f** represent joint angles

to shift itself and unstable the reaction forces. Such tendency exhibits differences in pattern while repeating the same motion. The sponge has elastic and deformable properties. This leads to increase higher amplitudes in signals but smooth and exhibits pattern.

4 Conclusions

This study emphasizes proprioception and its applicability in terrain identification. This methodology helps to identify differences in a different ground environment which is the most critical information for legged systems in order to make some decisions while walking in different environments simultaneously. The difference between sand and soil is pretty small in data because their grain sizes are almost similar,

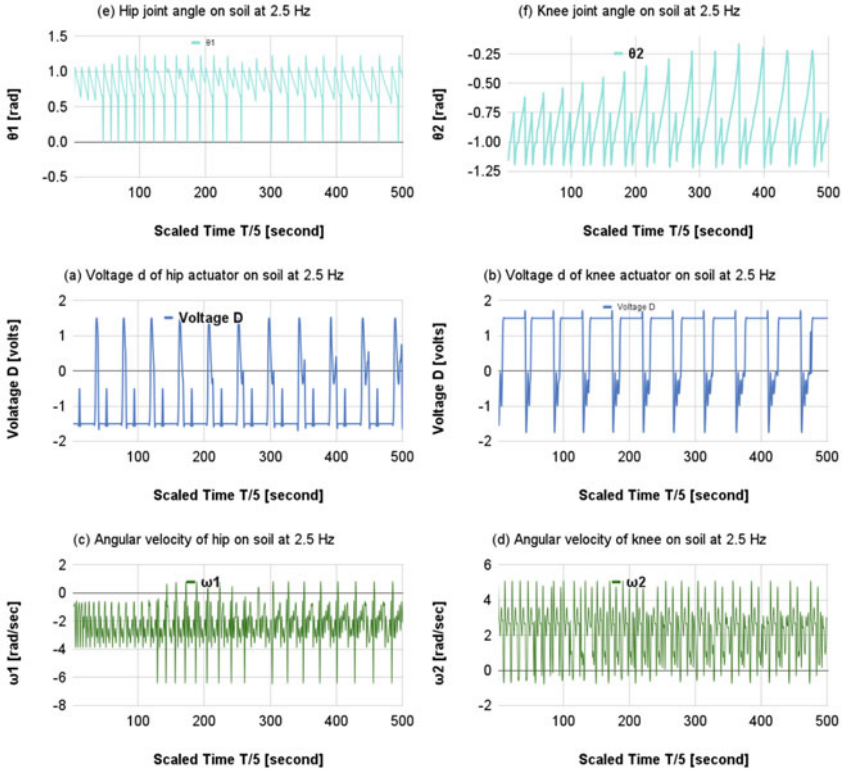


Fig. 6 Experimental results on soil at 2.5 Hz frequency. **a–b** represents voltage drop at both actuators with respect to scaled time, and **c–d** represents joint angular velocity while **e** and **f** represent joint angles

This is why the foot has a tendency to penetrate the environment. The hard surface is plane and shows very smooth curves which means the reaction forces from the ground are equally acting on foot. Concretes are different in size and can shift from their places while feet used to interact with them. Also, it produces more reaction forces than sand, soil, and sponge. The result section describes the sensor reading and found that our method can give efficient evidence to recognize the terrain. The author found evidence as discussed in Sect. 3 of the paper, that how exactly terrain can affect the proprioception and give the feedback to the system. It is found that the leg can get enough information about terrains without any external sensors like LIDAR, Cameras, and other sensing methods. Such a method of sensing may help in highly dynamic motion. The experiments generate an enormous amount of data points that lead to complications in analyzing the data statistically. Here comes the role of the machine learning approach to solve the problem and classify the terrains using proprioceptive information.

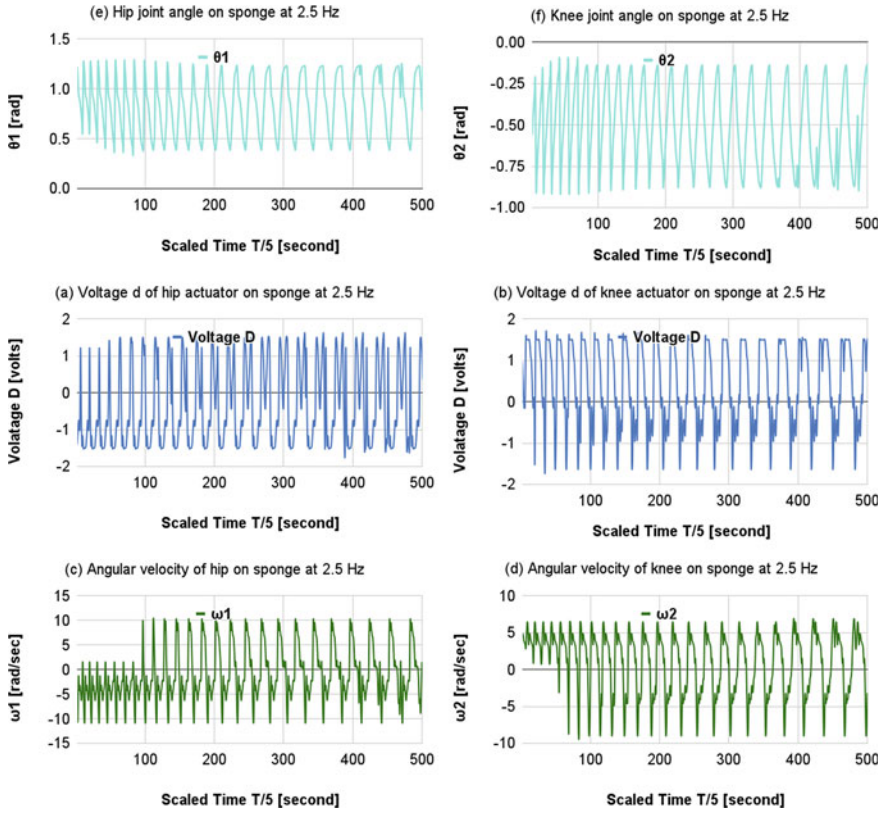


Fig. 7 Experimental results on sponge at 2.5 Hz frequency. **a–b** represents voltage drop at both actuators with respect to scaled time, and **c–d** represents joint angular velocity while **e** and **f** represent joint angles

Acknowledgements The authors are thankful to Mithilesh Kumar Koiri and Anurag Chaubey for helping in the investigation.

References

1. Shill J, Collins E, Coyle E, Clark J (2014) Terrain identification on a one-legged hopping robot using high-resolution pressure images, pp 4723–4728
2. Stone EA, Lepora NF, Barton DA (2020) Walking on tactip toes: a tactile sensing foot for walking robots. In: 2020 IEEE/RSJ international conference on intelligent robots and systems (IROS), pp 9869–9875
3. Zhao Y, Gao F, Sun Q, Yin Y (2021) Terrain classification and adaptive locomotion for a hexapod robot Qingzhui. *Front Mech Eng* 16(2):271
4. Biswal P, Mohanty PK (2021) Development of quadruped walking robots: a review. *Ain Shams Eng J* 12(2):2017–2031

5. Čížek P, Zoula M, Faigl J (2021) Design, construction, and rough-terrain locomotion control of novel hexapod walking robot with four degrees of freedom per leg. *IEEE Access* 9:17866–17881
6. Christie J, Kottege N (2016) Acoustics based terrain classification for legged robots. In: 2016 IEEE international conference on robotics and automation (ICRA)
7. Ngamkajornwivat P, Homchanthanakul J, Teerakittikul P, Manoonpong P (2020) Bio-inspired adaptive locomotion control system for online adaptation of a walking robot on complex terrains. *IEEE Access* 8:91587–91602
8. Wensing PM, Wang A, Seok S, Otten D, Lang J, Kim S Proprioceptive actuator design in the mit cheetah: impact mitigation and high-bandwidth physical interaction for dynamic legged robots. *Ieee Trans Robot* 33(3)
9. Kau N, Schultz A, Ferrante N, Slade P (2019) Stanford doggo: an open-source, quasi-direct-drive quadruped. In: 2019 international conference on robotics and automation (ICRA). IEEE, pp 6309–6315
10. Bledt G, Powell MJ, Katz B, Di Carlo J, Wensing PM, Kim S (2018) Mit cheetah 3: design and control of a robust, dynamic quadruped robot. In: 2018 IEEE/RSJ international conference on intelligent robots and systems (IROS). IEEE, pp 2245–2252
11. Ding Y, Li C, Park H-W (2018) Single leg dynamic motion planning with mixedinteger convex optimization. In: 2018 IEEE/RSJ international conference on intelligent robots and systems (IROS). IEEE, pp 1–6
12. Seok S, Wang A, Otten D, Kim S (2012) Actuator design for high force proprioceptive control in fast legged locomotion. In 2012 IEEE/RSJ international conference on intelligent robots and systems. IEEE, pp 1970–1975
13. Kalouche S (2017) Goat: a legged robot with 3d agility and virtual compliance. In: 2017 IEEE/RSJ international conference on intelligent robots and systems (IROS). IEEE, pp 4110–4117
14. B'ottcher S (2006) Principles of robot locomotion. In: Proceedings of human robot interaction seminar
15. Seok S, Wang A, Chuah MY, Hyun DJ, Lee J, Otten DM, Lang JH, Kim S (2014) Design principles for energy-efficient legged locomotion and implementation on the MIT cheetah robot. *IEEE/ASME Trans Mechatron* 20(3):1117–1129
16. Ding Y, Park HW (2017) Design and experimental implementation of a quasidirect-drive leg for optimized jumping. In: 2017 IEEE/RSJ international conference on intelligent robots and systems (IROS). IEEE, pp 300–305
17. Bhattacharya S, Singla A, Dholakiya D, Bhatnagar S, Amrutur B, Ghosal A, Kolathaya S (2019) Learning active spine behaviors for dynamic and efficient locomotion in quadruped robots. In: 2019 28th IEEE international conference on robot and human interactive communication (RO-MAN). IEEE, pp 1–6
18. Bhattacharya S, Chitta S, Kumar V, Lee D (2008) Optimization of a planar quadruped dynamic leap. In: International design engineering technical conferences and computers and information in engineering conference, vol 43260, pp 1101–1110
19. Kim S, Wensing PM (2017) Design of dynamic legged robots. *Found Trends Robot* 5(2):117–190
20. Grimminger F, Meduri A, Khadiv M, Viereck J, Wüthrich M, Naveau M, Berenz V, Heim S, Widmaier F, Flayols T et al (2020) An open torque-controlled modular robot architecture for legged locomotion research. *IEEE Robot Autom Lett* 5(2):3650–3657
21. Ananthanarayanan A, Azadi M, Kim S (2012) Towards a bio-inspired leg design for high-speed running. *Bioinspiration biomimetics* 7(4):046005
22. Zeng X, Zhang S, Zhang H, Li X, Zhou H, Fu Y (2019) Leg trajectory planning for quadruped robots with high-speed trot gait. *Appl Sci* 9(7):1508
23. Neha E, Orlando FM, Suhaib M, Shrivastava Y (2020) An effort for resolving redundancy of a multi-finger robotic hand in straight-line motions. *J Braz Soc Mech Sci Eng* 42(11):1–27

Advanced Cooling System Using Graphite Foam Heat Exchangers for Automobile



Kapil Rajput, Nayan Kumar Roy, and Aakash Crispin Martin

Abstract In this paper, we will analyze all aspects of graphite foam for cooling in heat exchanger. The primary purpose of an automobile's cooling system is to keep the engine cool and in good working order without overheating or overcooling it. Overheating the engine will result in the melting of engine parts and, eventually, the engine seizing. And, in the event of engine overcooling, the whole engine system will shut down. The advanced cooling system was achieved by using carbon foam as the fin material for radiator construction, then replacing the ordinary centrifugal pump with a sliding vane rotary pump, and finally using nanofluids as coolants in the radiator. We will improve the cooling performance of the engine as well as the mechanical efficiency of the engine by applying these three methodologies.

Keywords Graphite foam · Heat exchanger · Cooling system · Temperature drop · Simulation

1 Introduction

Transportation of goods and passengers on modern highways, where the speed requirement is much higher and the vehicle is loaded heavily, as well as problems in hot summers, necessitates an advanced engine cooling system [1]. The research aims to create a new cooling system for heavy vehicles in order to reduce fuel consumption and CO₂ emissions. This study is divided into two parts, flow field, and heat transfer. Cooling is a critical event that must provide the best working environment for the engine without compromising its mechanical effectiveness. The advanced cooling system outperforms the conventional cooling system in terms of cooling performance. This advanced cooling system also improves the engine's overall mechanical performance. A motor vehicle's engine cooling system is cooled by this equipment. An instrument required for an undertaking or to perform a service is referred to as equipment [2].

K. Rajput (✉) · N. K. Roy · A. C. Martin
Department of Mechanical Engineering, Galgotias University, Greater Noida, India
e-mail: kapil.rajput@galgotiasuniversity.edu.in

1.1 Engine Cooling

For engine cooling, we use radiator to ensure that the engine is operating at its ideal temperature (80–90 °C) and Intercooler to cool the fresh air, which has had its temperature raised by a Turbocharger [2].

2 Methods for Saving Energy

We can store mechanical energy during braking and use it to drive the vehicle later. During the braking process, the kinetic energy is used to produce a high pressure gas, which is then used to drive vehicles as shown in Fig. 1. About 80% of the kinetic energy lost during braking can be recovered [3]. Vehicles are becoming more powerful, and electric or hybrid vehicles are becoming more common. Less heat can be dissipated in the exhaust gas from hybrid electric vehicles. The cooling system would have to remove more heat [4] Fig. 2.

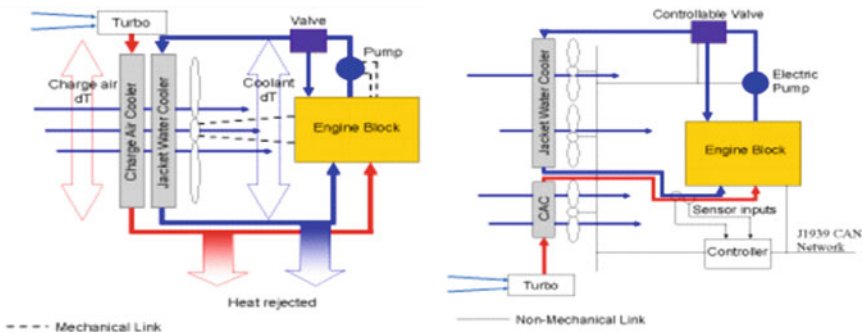
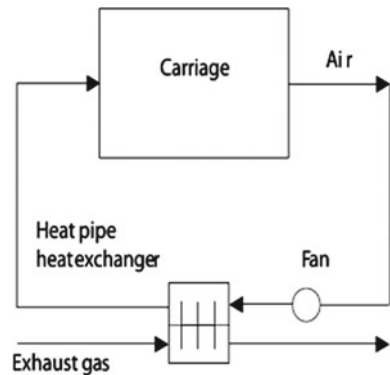


Fig. 1 Methods for saving energy

Fig. 2 Compartment for heating



3 New Material for Heat Exchangers

With the advancement of thermal control by aluminum and copper heat exchanger 180 W/mK for aluminum 6060 and 400 W/mK for copper, the cooling power increases further by utilizing microcellular foam material such as metal or graphite foams [5, 6]. The properties of graphite foam are shown in Fig. 3.

The problems that rises with new material for heat exchangers are the decrease in high pressure, Heat transfer’s effective area is reduced. Pumping power input is high, but output eco-efficiency is poor. Mechanical properties are poor, Graphite foam with a porosity of 75% has a tensile strength of just 0.69 MPa. Nickel foam of the same porosity, on the other hand, has a tensile strength of 18.44 Mpa and blocks the dust [7]. The different types of foam shapes are analyzed for graphite foam as shown in Fig. 4 (Table 1).

The current simulation model’s Nusselt numbers are significantly higher than the previous one in the outcomes of the experiment (Figs. 5 and 6).

The Forchheimer pressure loss model is used to calculate the pressure loss by graphite foam.

Darcy’s expanded equation [8]:

$$\frac{Dp}{dx} = -\left(\mu f * \frac{ui}{\alpha} + \frac{\rho f C f}{\sqrt{\alpha}} |ui|ui\right)$$

Because of the limited flow length, corrugated and pin-finned foams have a lower pressure drop (corrugated) and a non-corrugated flow direction (pin-finned) (Fig. 7).

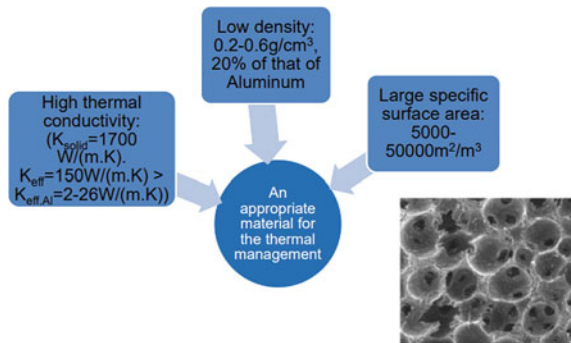
The setup has a significant impact on foam pressure drop.

More cold air will flow through the corrugated and pin-finned foams because of their low flow resistance.

To remove the heat from the foam, hit the surface within the foam. As a result, the efficient heat transfer surface in corrugated and pin-finned foams is larger (Fig. 8).

$$Q_{removed} = h.A_{eff}\Delta T$$

Fig. 3 Graphite foam



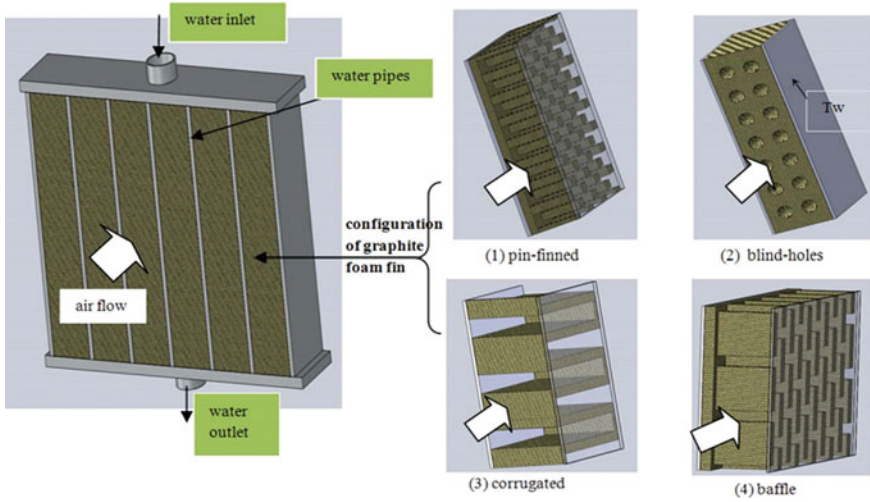


Fig. 4 Four different foam shapes (pin-finned, blind-holes, corrugated, and baffle) are investigated in order to minimize the pressure drop of graphite foams

Table 1 Properties of the graphite foam

Graphite foam	Porosity (ϵ)	Pore diameter (Dp) (Um)	Specific surface are(β) (m^2/m^3)	Effective thermal conductivity (keff) (W/m•K)	Permeability (α) (m^2)	Forchheimer coefficient (CF)
POCO	0.82	500	5240	120	6.13×10^{-10}	0.4457

Fig. 5 Verification of the simulation model

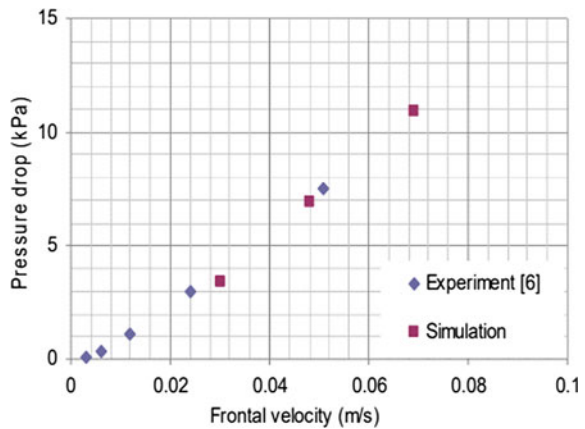


Fig. 6 The current simulation model's pressure drop values are justified as comparable to trying new things

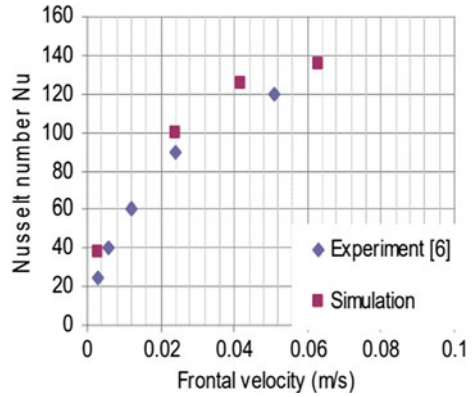


Fig. 7 Pressure drops of graphite foam

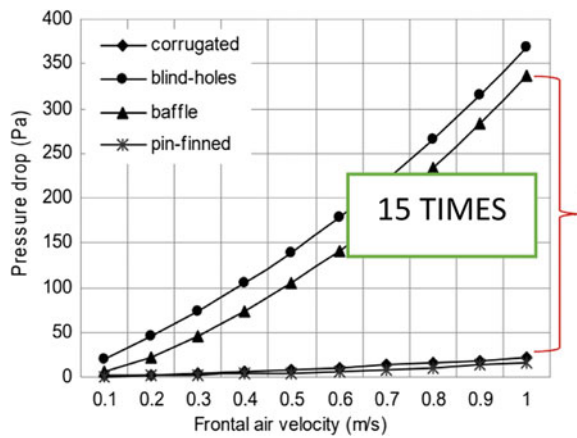
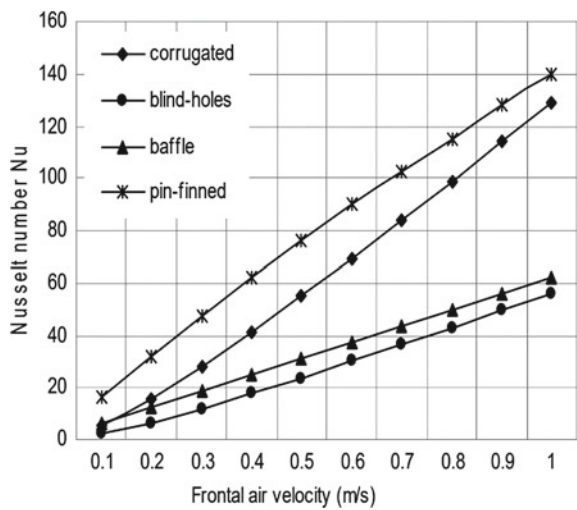


Fig. 8 Thermal performance of graphite foam



The Nusselt number (Nu) is determined as follows [8]:

$$Nu = hp \frac{D}{kf} = Dh \frac{Q_{removed}}{kfAb\Delta T_{base - inlet}}$$

The Nu content of corrugated and pin-finned foams is higher (Fig. 9).

Thus by using an acceptable graphite foam configuration, it is possible to reduce the input pumping power while maintaining a COP value comparable to that of an aluminum louver fin (see Fig. 10).

This indicates that the graphite is corrugated or pin-finned. The louver fin heat exchanger is heavier than the foam heat exchanger [10–12]. When the extracted heat is the same, use a heat exchanger. (Due to its low density) When the amount of heat removed is the same, the volume of the container is the same. The corrugated or pin-finned foam is much thinner than the corrugated or pin-finned foam fin louver [13–15]. The heat transfer surface in corrugated or pin-finned foam is larger than in louver fin foam due to the open cells in the foam [16–18] (Fig. 11).

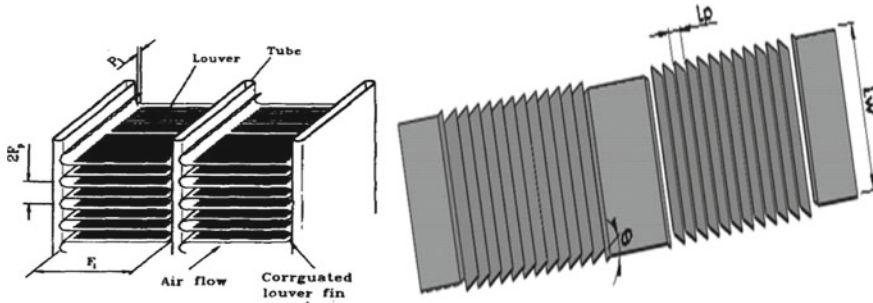


Fig. 9 Graphite foam and aluminum louver fins are compared [9]

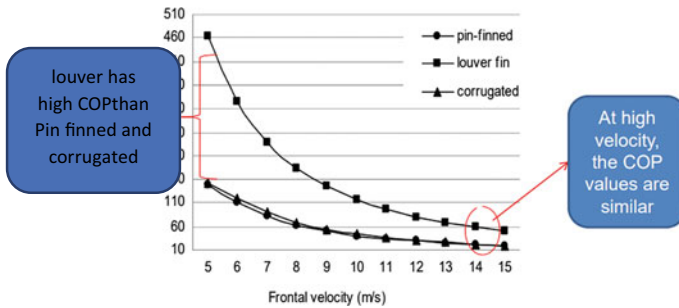


Fig. 10 Comparison of COP (coefficient of performance)

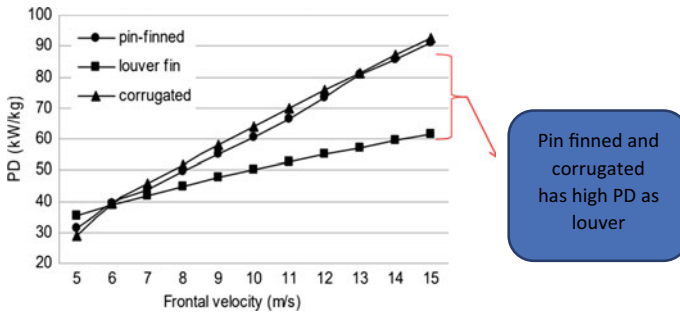


Fig. 11 Comparison of PD (power density)

4 Conclusion

From the above analysis, we conclude that corrugated and pin-finned graphite foams have a low-pressure drop and a high thermal efficiency. The PD and CF values of the corrugated and pin-finned graphite foams are higher than the aluminum louver fin. This refers to a vehicle’s cooling system being light or compact. It is possible to achieve a comparable COP value to the aluminum louver fin by using a suitable graphite foam configuration.

Heat exchangers have a new structure. Due to a lack of space, it may be necessary to relocate the heat exchanger. However, if the heat exchanger’s position is altered, a new heat exchanger structure can be required to accommodate the new position. A counter-current exchanger for the radiator on top of the driver compartment may be a smart idea. When designing a new heat exchanger system, the aluminum heat exchanger will be considered and analyzed first. The graphite foam heat exchanger will be considered in the future.

References

1. Klett JW (2000) Process for making carbon foam, US Patent 6033506
2. Yu Q, Thompson BE, Straatman AG (2006) A unit cube-based model for heat transfer and fluid flow in porous carbon foam. *J Heat Transfer* 128:352–360
3. Straatman AG, Gallego NC, Thompson BE, Hangan H (2006) Thermal characterization of porous carbon foam—convection in parallel flow. *Int J Heat Mass Transfer* 49:1991–1998
4. Klett J, Hardy R, Romine E, Walls C, Burchell T (2000) High-thermal conductivity, mesophase-pitch-derived carbon foams: effect of precursor on structure and properties. *Carbon* 38:953–973
5. Paek WJ, Kang HB, Kim YS, Hyum MJ (2000) Effective thermal conductivity and permeability of aluminum foam materials. *Int J Thermophys* 21(2):453–464
6. Klett J, Ott R, McMillan A (2000) Heat exchangers for heavy vehicles utilizing high thermal conductivity graphite foams, SAE paper 2000–01–2207
7. Yu Q, Straatman AG, Thompson BE (2006) Carbon-foam finned tubes in air-water heat exchangers. *Appl Therm Eng* 26:131–143

8. Garrity PT, Klausner JF, Mei R (2010) Performance of aluminum and carbon foams for air side heat transfer augmentation. *J Heat Transfer* 132(121901):1–10
9. Straatman AG, Gallego NC, Yu Q, Thompson BE (2007) Characterization of porous carbon foam as a material for compact recuperators. *J Eng Gas Turbines Power* 129:326–330
10. Gallego NG, Klett JW (2003) Carbon foams for thermal management. *Carbon* 41:1461–1466
11. Leong KC, Jin LW, Li HY, Chai JC (2008) Forced convection air cooling in porous graphite foam for thermal management applications. In: 11th intersociety conference on thermal and thermomechanical phenomena in electronic systems, pp 57–64
12. Lin YR, Du JH, Wu W, Chow LC, Notardonato W (2010) Experimental study on heat transfer and pressure drop of recuperative heat exchangers using carbon foam. *J Heat Transfer* 132(091902):1–10
13. Yuan J, Huang Y, Sundén B, Wang W (2009) Analysis of parameter effects on chemical reaction coupled transport phenomena in SOFC anodes. *Heat Mass Transfer* 45:471–484
14. Lu W, Zhao CY, Tassou SA (2006) Thermal analysis on metal-foam filled heat exchangers. Part I: metal-foam filled pipes. *Int J Heat Mass Transf* 49:2751–2761
15. Pope SB (2000) *Turbulent flows*. Cambridge University, UK
16. Versteeg HK, Malalasekera W (2007) *An introduction to computational fluid dynamics*, 2nd edn. Pearson Prentice Hall, UK
17. Chang Y, Wang C (1997) A generalized heat transfer correlation for louver fin geometry. *Int J Heat Mass Transf* 40:533–544
18. Chang Y, Hsu K, Lin Y, Wang C (2000) A generalized friction correlation for louver fin geometry. *Int J Heat Mass Transf* 43:2237–2243

Additive Manufacturing: A State of Art Review



Rahul Jain, Sudhir Kumar Singh, and Rajeev Kumar Upadhyay

Abstract In this study, an attempt is made to investigate the SWOT analysis on Additive Manufacturing by examining the research papers from past one decade (2010–2020). The reviewed paper illustrates how production methods and technology have evolved during the last decade. The organizations are searching better responsiveness for the clients in terms of counting capacity, minimum cost, recyclability or vigorously effective items. In order to address the latest industry problems and consumer requests, organizations are looking for better techniques. Organizations are exploring better techniques to meet the latest market challenges and demands of the clients. In the serious market, client-based manufacturing is the primary concern to improve and broaden strategies and methods in the industries. Today's market demands simplicity in manufacturing of intricate shapes, time savings, scrap reduction and efficient use of people, machines, money and resources. An industry can only exist today, if it meets every customer's desire quickly and cheaply. To keep up with the expanding market, industries transitioned from Industry 1.0 to Industry 4.0. According to study findings there are number of recommendations that can be made to practitioners in the business as well as academics, planners and administrators using additive manufacturing.

Keywords Additive manufacturing · 3D printing · Subtractive manufacturing · Powder metallurgy · Rapid prototyping · Aerospace · Medical

1 Introduction

The main methods for Additive Manufacturing (AM) opened up in the last part of the 1980s. It is for the most part thought about that the methodology was brought into the world in 1987 when 3D Systems built up the Stereo-Lithography Apparatus

R. Jain (✉) · S. K. Singh
Galgotias University, GB Nagar, Greater Noida, India
e-mail: rahul.jain_phd2019@galgotiasuniversity.edu.in

R. K. Upadhyay
Hindustan College of Science & Technology, Mathura, India

(SLA). They were first used to deliver model and prototype parts. Today, they are utilized for a lot more extensive scope of utilizations; from clinical gear to modern items yet in generally limited quantity. The development of the strategies for this strategy produced new techniques with improved capacity and material. In the past time the manufacturing was done using the Subtractive Manufacturing Technique in which the material is removed to get the desired shape, size and dimensions. A drastic change can be noticed from the 1800 century till now. The means of manufacturing and the method of production is getting easier and customer friendly from day by day. This era of revolution can be classified as Industry 1.0 to Industry 4.0 [1–8].

2 Literature Review

Additive manufacturing, also known as 3D printing, was introduced in the past decade. However, this seemingly latest technology has, in actuality, been around for nearly 40 years. In the traditional manufacturing, machining is done to get the desired shape, this process is based on the subtractive technology where material is removed in the form of scrap. Advanced machining almost uses numeric control (NC), numerical control (CNC) or direct numerical control (DNC) tools. On the other hand, 3D printing is an additive process in which material is gradually layered to get the desired shape and size. There are numerous techniques and technologies that are being used today, the end product and material helps in determining the method of additive manufacturing that should be used. Today there are many additive manufacturing technologies that are available in the market and tested under ISO/ASTM52900 “Standard Terminology for Additive Manufacturing” which categorize the additive manufacturing into 7 technological categories: Vat photopolymerization, material extrusion, binder jetting, directed energy deposition, powder bed fusion, sheet lamination and material jetting. Besides these 7 categories, there are multiple proprietary technologies, such as: Fusion Deposition Modeling (FDM), a form of material extrusion process and Direct Metal Laser Sintering (DMLS), a form of powder bed fusion [9–20].

The research progress in AM and the various techniques used to enhance process efficiency over the last decade depending on methodology have been shown in the Tables 1, 2, and 3 (Fig. 1).

From the Table 1 depending upon various experiments performed on additive manufacturing this was seen that the smart materials that are difficult to machine by the conventional processes without disturbing the microstructure of the material can be manufactured easily with the use of additive manufacturing. The use of additive manufacturing in medical or health industry improves the success rate and reduces the complication in treatment. High accuracy and tolerance with good surface finish are the basic requirements of today’s industry, machining of alloys and high-speed materials are hard nut to crack by the traditional machining methods but good quality products can be manufactured by using high speed additive manufacturing. An experiment proved that the stem cell manufactured by additive manufacturing has better

Table 1 Research progress in additive manufacturing based on various experiments performed

S. No.	Journal details	Methodology	Research findings
1	Ludwig [3]	Experiment (solvent free batteries)	The performance of solvent-free additive manufactured batteries was better and cheap as compared to the conventional slurry cast electrode batteries with similar specifications
2	Jansson [2]	Experiment (impact of gravity on scale factor)	Gravity has a very small impact on the scale factor and particle size affects shrinkage. Smaller particles sinters faster and results in high shrinkage and less porosity. The length in each direction has a greater impact on the scale factor
3	Tappa [4]	Experiment (novel bio material)	An ideal implant biomaterial that can be, inert, mechanically durable, and easily moldable can be easily manufactured by AM
4	Meiteoh [5]	Experiment (prototyping)	3D printing of smart materials and structures can be made possible by AM
5	Bansal [10]	Experiment (endodontic)	With growing advancement in 3D techniques like imaging, printing and planning improves the success rate of treatment outcomes and also improves patient’s comfort
6	Nazir [12]	Experiment (high speed additive manufacturing)	High Speed Additive Manufacturing (HSAM) can produce material with high accuracy and speed and of good surface finish with very little wastage. So, HSAM can be used in mass production for timesaving and high-quality product
7	Cronskar [13]	Experiment (orthopedics)	EBM produces the metal which has high strength and elastic properties which are very close to bone, hence the stem cell manufactured by AM has better life quality and can be given to young THA patient and feels like more active after surgery
8	Klein [14]	Experiment (transparent glass)	Optically transparent glass, manufactured by AM has the strength 60% greater than the conventional glass with improved transparency
9	Patel [15]	Experiment (portable centrifuge)	The portable centrifuge made by the AM is light in weight and can be operated by the solar panel

(continued)

Table 1 (continued)

S. No.	Journal details	Methodology	Research findings
10	Panesar [17]	Experiment (topology optimization)	The graded strategy is a robust strategy in which explored design strategies. When it's enforced in AM through topology optimization it indicates lattice designation points to develop complex structure lattice which enhances the mechanical functionalities in terms of high resilience and variability in loading, through superior stiffness
11	Chang [18]	Experiment (micro fluids)	With the help of AM microfibers, carriers based on micro fluids generation through droplet micro fluids spinning technology in the medical industry can be made. It also open doors to make 3D cellular structures with the gain of benefits in terms of catching mechanical characteristics outstanding process ability and good bio-compatibility
12	Arora [19]	Experiment (production of medical equipment)	The AM is also used in covid-19 pandemic scenario, with the help of this mass production of all medical equipment's which are used by medical professional and nursing staff are in use at instantaneous moment at low cost and very rapidly with effective and efficient supply chain facilities
13	Yong Da [20]	Experiment (thermo electric material)	The drawback of using AM in fabrications of thermoelectric materials is that it does not provide a smooth surface in comparison to traditional manufactured. Hot pressing and many other techniques were used. The reason is the resolution used in AM is limited, so it should be enhanced
14	Wai [21]	Experiment (bio material meta material)	It doesn't need any extra process like bonding mechanical fitting because it gives unnecessary materials while making and fabricating the coefficient of thermal expansion in meta materials. This is the advantage of using AM to program thermal expansion in making bi-material

(continued)

Table 1 (continued)

S. No.	Journal details	Methodology	Research findings
15	Chen [22]	Experiment (dynamic deformation)	With the use of AM, the fabrication of alloy of stainless steel attains higher mechanical property in a characterized manner by progress. In this matter, average thickness and flow behavior is the parameter to evolve microstructures by using a fitted empirical equation
16	Yuan [23]	Experiment (voxel design)	AM can give complex 3D structures in the form of products by controlling processing parameters to construct digital material by manipulating and stimulating the thermodynamic properties in terms of size and space
17	Derakda [24]	Experiment (friction forging)	AM is used in 3D printing of tubular components using friction–stir, forging or hydrostatic pressing. It enables fabrication by detecting solidification defects and enforce to produce a tube having tensile strength which is the highest ever and decreased elongation with fracture surface in compatible form
18	Betlers [25]	Experiment (dynamic stiffness modification)	The product manufactured and design using a metal wire arc AM through open channel structure gives less magnitude in modified component at a natural frequency. Through this performance, the dynamic stiffness can be increased
19	Frey [26]	Experiment (thermoplastic forming)	With the laser powder bed fusion technique to decrease surface roughness by applying thermoplastic forming to give structured surface pattern by providing thermal stability and detecting a small amount of crystalline prove bulk metallic glass has unique amorphous characteristic, the name of net shape creating method

(continued)

quality and the patient was more active and comfortable after the surgery, another experiment shows that the glass manufactured by AM has 60% more strength than the traditional glass with good transparency. Hence it plays vital role in dentistry, orthopedics, manufacturing, reverse engineering, product development and design, rapid tooling etc. With the help of AM, complex shapes can be quickly and easily fabricated directly from the CAD model (Fig. 2).

Table 1 (continued)

S. No.	Journal details	Methodology	Research findings
20	Plotowski [27]	Experiment (Si-transformer core)	A novel design is selected which is through Hilbert curve geometry to exploit AM complexity in 3D structure so, cores are printed. Heat treated assembled showed performance which is better than non-oriented sheet due to which higher power losses due to variation in grain structure and defects during assembly indicate high silicon content led to deformation during machining
21	Chai [28]	Experiment (martensitic stainless steel)	It is done to evaluate face stability and microstructure by using heating and cooling neutron diffraction. Results are based on two components which are austenite having more thermal stability by more thermal cycles and martensite have higher compressive stress by more thermal cycles due to changeable strain and miss-fit strain
22	Blindheim [29]	Experiment (RP and physical modelling)	By this experiment, an attempt has been made to produce Spindle, Extruder which titled from axis vertically in feed direction by changing their configuration
23	Pappas [30]	Experiment (alumina ceramics)	In this paper by the laser direct deposition, the doping of Zirconia on alumina ceramics is done and found that the Zirconia doping reduced the crack formation, meanwhile, the porosity increased. It is also found that the bending strength increases by four times that of the base material alumina and the fracture toughness increased by 1.5 times of the base material alumina
24	Atzeni [31]	Experiment (vibro finishing technology)	The surface finishing of AM components is done from both sides internally and externally. The material used is vibro finishing technology. The material whose finishing is done is alsil0mg which is fabricated by laser powder-based fabrication (l-puff). The deepest valley can also be reduced by this technology and the cost is also low

(continued)

Table 1 (continued)

S. No.	Journal details	Methodology	Research findings
25	Hel [32]	Experiment (X-ray tomography)	It is done to detect the deformation effects which affect the performance of the material in terms of mechanical properties. It provides a rapid approach to predict damageable defects instantly
26	Unsal [33]	Experiment (material properties)	The outcomes are lack of fusion is not detected. Reduction in ductility shows a difference in comparison to conventional material. The main effect is to reduce porosity and heat intake into it
27	Arbeiter [34]	Experiment (damage tolerance)	The lifetime of a component by utilizing crack growth kinetics under loading conditions which are based on damage tolerant fracture mechanics by applying this can reduce the time between component designs
28	Knapik [35]	Experiment (rapid prototyping)	Rapid Prototyping can control objects by using complex algorithms through wireless communication by projecting a real-time controlled system that is embedded in an external computer
29	Rivas [36]	Experiment (metrology)	With the use of AM design artifact having some great outcomes which is measured by measuring systems compatible with AM technique due to some uncertainties while undergoing various processes which is treated by trace ability having complex features and rough surface textures
30	Colditz [37]	Experiment (experimental investigation)	The product component of AM through hot forming, cold forming heat treated in cold forming their hardness is raised due to work hardening while in hot and heat processes, the micro structure change at micro level caused by temperature induced recrystallization process

(continued)

The above graph shows the production of parts manufactured by AM. It can be seen from the graph that from 1994 to 2020 there is a big change in the amount spent on AM. This proves that the industries are welcoming this latest trend and increasing the profit day by day [57, 58].

Table 1 (continued)

S. No.	Journal details	Methodology	Research findings
31	Oliveira [38]	Experiment (process parameter of PBFMAM)	Additive Manufacturing is a great technique to optimize, utilize, controlled, manipulate, and simulate the process parameters through various approaches in terms of building qualities and material characteristics regarding their designation structure
32	Catalano [39]	Experiment (cardio vesicular stents)	It shows that the use of laser micro cutting in process to design metal sheets provides large flexibility and in mesh geometrics and process materials
33	Ahmed [40]	Experiment (molded interconnect devices)	It is used because it replaces MID-technology which is expansion and time consuming having needed shape forming tools. While RP, easily manipulates and designs complex 3D prototype components regarding their technical configuration having surface quality is important in the metallization process
34	Popesue [41]	Experiment (bio sensor)	Using light scribe photo thermal reduction method, interdigitated, arrays of electrodes used in reduced graphene oxide were manufactured on flexible show electro-chemical properties have low temp., low cost, major production of sensor
35	Carless [42]	Experiment (bone deformities)	This method has better technique to provide bone changes in deformities and permissible accurate planning that indicates minimized complication results. It has limitation due to absence of control group
36	Shreepad [43]	Experiment (biomaterial fabrication)	Using this method bone and teeth can be manufactured in the form scaffolds having mechanical and structural properties through processed methods by optimization of operating parameter to overcome hindrance as the natural teeth and bone

(continued)

Table 1 (continued)

S. No.	Journal details	Methodology	Research findings
37	Budding [44]	Experiment (ceramics)	It is made to printing the material in 3D complex structure in ceramic membranes and reactors deposit the powder with bulk density used to alter the properties
38	Brkic [45]	Experiment (spectrometer)	With making of Quadrupole mass spectrometer, using digital light processing i.e., this is good processing method which is implemented in the making, providing smaller size indicate high degree accuracy by potential to make spectrometer with single mass analyzer
39	Rlichewin [46]	Experiment (agile development)	AM helpful in Agile software development for hardware working from CAD model to compete the need of tooling
40	Schesh [47]	Experiment (agile measuring network)	Agile Manufacturing has high management cost in manufacturing network in designation which is overcome by reducing and modify the fixed cost by apply various methods in terms of cost evaluation factors

It has always been a hard task to use SLS and FDM both together but when they are used in AM, they provide a wide range of design options [55] (Fig. 3).

Industries are investing a handsome amount on the AM from the past 10 years, this shows that market is welcoming AM and the industries are earning profit by replacing the conventional manufacturing process with AM processes.

3 Conclusion

In the end of eighteenth century, the concept of Industry 1.0 was introduced in which mechanical and production equipment driven by water and steam were used. After this at the end of nineteenth century second industrial revolution i.e. Industry 2.0 came into existence where mass manufacturing production lines powered by electric energy was majorly adopted by the industries. At the end of twentieth century Industry 3.0 gave the gift of electronics, PLC devices, robots and IT to automate the production. Currently IoT and Cyber-Physical Systems driven by Augmented Reality and Real-Time Intelligence are used and known as the fourth revolution i.e. Industry 4.0.

Table 2 Research progress in additive manufacturing based on tool, survey and advancements

S. No.	Journal details	Methodology	Research findings
1	Zegard [1]	Tools FDM And SLS	Both of the techniques FDM and SLS has their strength and weakness but when used together in AM it provides valuable information of the optimal structural mechanism while providing the user a wider range of design options
2	Biedermann [9]	Tool	Using the computational design synthesis technique is easy to design and produce complex and intricate 3D printable materials through multi-flow nozzles
3	Nandy [16]	Tool development and testing AMTT	The aim to develop AMTT is to reduce the cost of testing which is 99% cheaper than the commercial labs which help in performing scientific research at a lower cost
4	Babcinsh [48]	Tool	Interoperability is a medium to share data between the department and different stages of given technological process. In this, an integrated and interoperable automation ml-based platform is prepared to sort out the problem of unavailability of data for exchange. This exchanged data can be edited at different sub stages from CAD design to robot simulation and production
5	Schuh [49]	Tool	In this, the additively manufactured 3D printed PLA tool is manufactured for the sheet metal operation. In this, the tool used for the deep drawing operation found good results like it is stable for sheet metal and in terms of formability it is same as metallic tools. PLA tools have good frictional properties
6	Panesar [50]	Tool	In this paper to produce a multi-functional part in a single operation, a method is introduced which is called couple optimization formulation. With this development, we can design a multi material part embedded with various systems

(continued)

Table 2 (continued)

S. No.	Journal details	Methodology	Research findings
7	Parab [51]	Advancement in additive manufacturing	Ultrafast x-ray imaging technique help in recording the changes which takes place during the additive manufacturing process, this recording helps in study of the dynamic behavior of the material which is used in the manufacturing process
8	Thakar [52]	Advancement in AM	The main aim of this research is to use waste papers instead of plastic filaments which are harmful for the environment. With the use of waste papers, the manufacturing cost can be reduced and the profits with 3D printing can be increased
9	Reza [53]	Survey	This experiment shows stiffness and strength which is a mechanical property and it's dependent on raster angle
10	Guo [54]	Advancement in AM	All methods like SLS/SLM exhibit relationship between materials features and processing method
11	Siraj [55]	Survey	With the help of Red X theory determine that the quality aspects FDM which makes stable and reliable
12	Fercellese [56]	Advancement of AM	The applied load increases with displacement during compression test of the ISO grid panel until, it shows high value and then due to which buckling falls until fracture

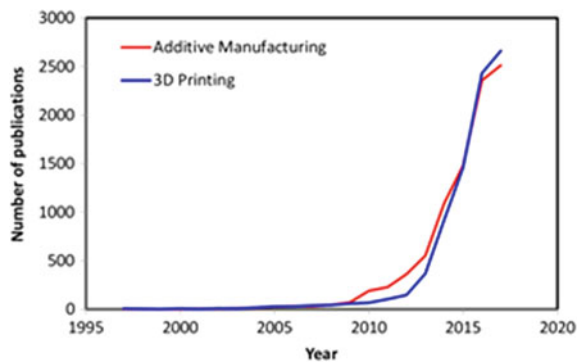
Research findings of reviewed paper based on various experiments, analysis, surveys and advancements performed on additive manufacturing concludes that.

1. Compared to the conventional battery manufacturing, additive manufactured batteries are better and cheap.
2. The biomedical parts required in implants manufactured by Additive Manufacturing are durable and user-friendly.
3. Use of computational design synthesis, Advanced Machine Tool Testing (AMTT), interoperability, Polylactic Acid (PLA) makes the Additive Manufacturing easier and helpful in designing and manufacturing of intricate shapes that were difficult to manufacture by the conventional manufacturing.
4. AM is a disruptive technology that can be fruitful in the coming future because this technology reduces the complexity in production.

Table 3 Research progress in additive manufacturing based on technology advancement

S. No.	Journal Details	Methodology	Research findings
1	Chen [6]	Technology	Ceramic components with highly complex structures that are impossible to be fabricated using conventional techniques can now be prepared by using 3D printing technology like slurry based, powder-based, bulk solid based that can demonstrate the great potential and value of ceramics using AM
2	Dawood [7]	Technology	Using 3D printing and technologies like cone beam computed tomography & intraoral scanning AM has a huge scope in dentistry, as it makes the surgery less invasive and more predictable
3	Srisainam [8]	Technology	Rapid Prototyping is an ideal method for manufacturing intricate shapes. AM reduces the complexity in the manufacturing to increase production
4	Vendra [11]	Technology	AM as a transformative technology can provide advantages in terms of efficiency, sustainability and cost reduction. In oil and gas industry, the additive design results in cost reduction reliability
5	Herzog [47]	Technology	The interrelationship between process, micro-structure and properties
6	Knulst [57]	Technology	The characteristic awareness, low-tech and fragmentation are most important for accepting technology
7	Cleveland [58]	Technology	The use of FIA technology in Additive Manufacturing is to produce parts with similar strength to the parts made by forging

Fig. 1 Year wise publications on AM and 3D printing [1]



- Glass manufactured by AM has 60% more strength than the traditional glass with good transparency.
- In the health industry, it makes surgery more successive, reduce manufacturing cost of the medical product and improves the strength and life of the implants.

Fig. 2 Production of AM parts from independent service providers (In millions of dollars) [59]

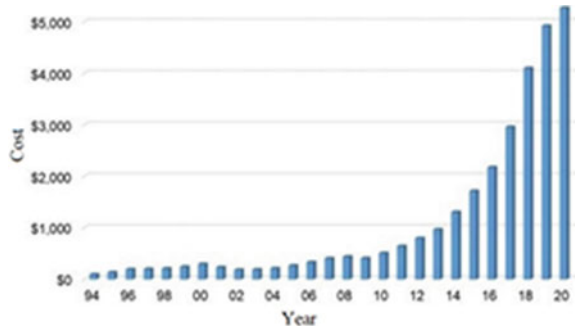
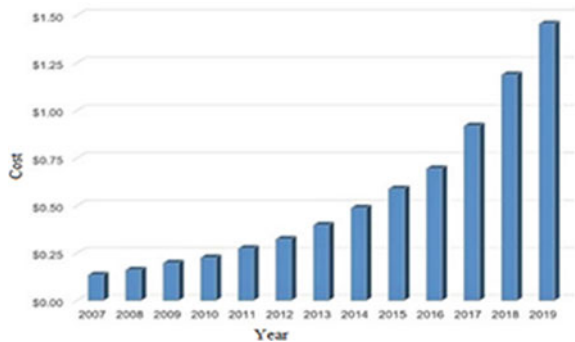


Fig. 3 Money spent annually on final part production by AM worldwide [59]



7. It plays vital role in dentistry, orthopedics, manufacturing, reverse engineering, product development and design, rapid tooling etc.
8. Additive Manufacturing helps in mass production with time saving and complex shapes can be quickly and easily fabricated directly from the CAD models used in AM.

References

1. Zegard T, Paulino GH (2020) Bridging topology optimization and AM. Springer
2. Jansson A, Edholm O (2016) Scale factor and shrinkage in AM using binder jetting. *Mo S T Sci Rep J*
3. Ludwig BJ (2019) Solvent free AM of electrodes for Li-ion batteries. *Examensarbete Inom Teknik*, 15
4. Tappa K, Jammalamadaka U (2018) Novel bio materials used in medical 3D printing technique. *J Funct Biomater*
5. Meiteoh ZE, Liu Y, Chua CK, Yang S, An J, Leong KF, Yeong WY (2015) Virtual and physical prototyping. Taylor & Francis
6. Chen Z, Li Z, Li J, Liu C, Lao C, Fu Y, Liu C, Li Y, Wang P, He Y (2014) 3D printing of ceramics. AM Institute, Shenzhen University

7. Dawood A, Marti BM, Sauret-Jackson V, Darwood A (2015) 3D printing in dentistry. *Br Dent J*
8. Srisainam V, Manthan Kumar CD (2015) Rapid prototyping—additive solid free form manufacturing in automobile engineering. *Int J Eng*
9. Biedermann M, Meboldt M (2020) Computational design synthesis of additive manufactured multi-flow nozzles. *Addit Manuf Elsevier*
10. Bansal A, Kukreja N, Trivedi S, Verma J (2020) 3D Printing: a paradigm shift in endodontic. *IJOSR*
11. Vendra L, Achanta A (2015) Metal AM in the oil and gas industry. *Enterprise additive manufacturing*
12. Nazir A, Jeng JY (2019) A high speed AM approach for achieving high printing speed and accuracy. *Sage J*
13. Cronskar M (2011) The use of AM in the custom design of orthopedic implants. *Mittuniversitetet*
14. Klein J, Stern M, Franchin G, Kayser M, Inamura C, Dave S, Weaver JC, Houk P, Colombo P, Yang M, Oxman N (2015) AM of optically transparent glass. *3D Printing Addit Manuf*
15. Patel AK, Jha A, More P, Henry R (2019) Design and development of low cost portable centrifuge using AM. *Int J Appl Eng Res*
16. Nandy K, Collinson DW, Scheftic CM, Brinson LC (2018) Open source micro tensile testers via AM for mechanical characterization of thin films and papers. *Plos One*
17. Panesar A, Abdi M, Hickman D, Ashcroft I (2017) Strategies for functionally graded lattice derived using topology optimization for AM. *ScienceDirect*
18. Chang JW, Yuetong M, Sun WL, Zhao YI (2020) Micro fluids for medical AM. *Elsevier*
19. Arora PK, Arora R, Haleem A, Kumar H (2020) Application of AM in challenges posed by COVID-19. *Elsevier*
20. Da Y, Chen J, Meng Q, Dou Y, Jiayuxue, Z-Shen J (2020) Thermo electric materials and devices fabricated by AM. *Elsevier*
21. Wei K, Xiao X, Chen J, Wu Y, Li M, Wang Z (2020) Additively manufactured bio-material meta material to program wide range of thermal expansion. *Elsevier*
22. Chen J, Wei H, Zhang X, Peng Y, Kong J, Wang K (2020) Flow behavior and microstructure evolution during dynamic deformation of 36l stainless steel fabricated by wire and arc additive manufacturing. *ScienceDirect*
23. Yuan C, Wang F, Rosen DW, Ge Q (2020) Voxel design of additive manufactured digital material with customized thermo chemical properties. *ScienceDirect*
24. Derazkola HA, Khodabakhshi F, Gerlich AP (2020) Friction forging additive manufacturing (FFTAM): a new route of solid state layer upon layer metal deposition. *ScienceDirect*
25. Betters ED, West J, Noakes M, Nycz A, Smith S, Schmitz TL (2020) Dynamic stiffness modification by internal feature in additive manufacturing. *ScienceDirect*
26. Frey M, Wegner J, Neuber N, Reiplinger B, Bochtler B, Adam B, Ruschel L, Riegler SS, Jiang HR (2020) Thermoplastic forming of additively manufactured Zr-based bulk metallic glass: a processing route for surface finishing of complex structure. *ScienceDirect*
27. Plotkowski A, Carver K, List F, Pries J, Li Z, Rossy AM, Leonard D (2020) Design and performance of an additively manufactured high Si-transformer core. *ScienceDirect*
28. Chae H, Huang EW, Woo W, Kang SH, Jain J, An K, Lee SY (2020) Unrevealing thermal history during additive manufacturing of martensitic stainless steel. *ScienceDirect*
29. Blindheim J, Welo T, Steinhest M (2019) Rapid prototyping and physical modeling in the development of a new additive manufacturing for aluminum alloys. *ScienceDirect*
30. Pappas JM, Thakur AR, Dong X (2020) Effects of zirconia doping on additively manufactured alumina ceramics by laser direct deposition. *Mater Des John. Elsevier*
31. Atzeni E, Balestrucci A, Catalano AR, Iuliano L (2019) Performance assessment of a vibro finishing technology for additively manufactured components. *Elsevier ScienceDirect*
32. Hu D, Pan J, Mao J, Hu S, Liu X, Fu Y (2020) Mechanical behavior prediction of additively manufactured components based on defect evolution by synchrotron radiation x-ray tomography. *ScienceDirect*

33. Ünsal I, Hirtler M, Sviridov A, Bambach M (2020) Material properties of features produced fusion EN AW 6016 by wire arc additive manufacturing. ScienceDirect
34. Arbeiter F, Trávníček L, Petersmann S, Dlhý P, Spoerk M, Pinter G, Hutař P (2020) Damage tolerance based methodology for fatigue lifetime estimation of a structural component produced by material extrusion—based additive manufacturing. ScienceDirect
35. Knapik D, Kotek K, Maciej, Rasot, Turnace A (2020) Autonomous, reconfigurable mobile with rapid prototyping functionality. ScienceDirect
36. Santos VM, Thompson A, Sims-Waterhouse D, Maskery I, Woolliams P (2020) Design and characteristic of an additive manufacturing bench marking artifact a design for metrology approach. ScienceDirect
37. Colditz P, Graf M, Hälsig A, Härtel S, Awiszus B (2020) Experimental investigation on the forming of additively components with regard to forming behavior and component properties. ScienceDirect
38. Oliveira JP, LaLonde AO, Ma J (2020) Processing parameters in laser power bed fusion metal additive manufacturing. ScienceDirect
39. Catalano G, Demir AG, Furlan V, Previtali B (2020) Use of sheet material for rapid prototyping of cardio vascular stents. ScienceDirect
40. Amend P, Pscherer C, Rechtenwald T, Frick T, Schmidt MA (2020) A fast and flexible method for manufacturing 3D molded interconnect devices by use rapid prototyping technology. ScienceDirect
41. Carl SP, Kugan N, Ghosh B, Kaner R, Hedley J (2017) Rapid prototyping of a low cost graphene based impedimetric bio sensor. ScienceDirect
42. Mothes FC, Britto A, Matsumoto FM (2018) Marco tending, application of 3D prototyping in planning the treatment of proximal humerus bone deformities. ScienceDirect
43. Shreepad S, Ravi W (2015) New revolutionary ideas of material processing a path to bio material fabrication by rapid prototyping. ScienceDirect
44. Budding A, Vaneker TH (2013) Open source powder based rapid prototyping machine for ceramics. ScienceDirect
45. Brkić B, France N, Clare AT, Sutcliffe CJ, Chalker (2009) Development of quadrupole mass spectrometers using rapid prototyping technology. ScienceDirect
46. Reichwein J, Vogel S, Schork S, Kirchner E (2020) On the applicability of Agile development methods to design for additive manufacturing. ScienceDirect
47. Herzog D, Seyda V, Wycisk E, Emmelmann C (2016) Additive manufacturing of metals. Elsevier
48. Babcinski M, Freire B, Ferreira L, Señaris B (2020) An integrated interoperable automation ml-based platform for the robotic process of metal additive manufacturing. Procedia Manuf. Elsevier
49. Schuh G, Bergweiler G, Colag C (2020) Sheet metal forming using additively manufactured polymer tool. Elsevier Procedia CIRP
50. Panesar A, Ashcroft I, Brackett D, Wildman R (2017) Design framework for multifunctional manufacturing: coupled optimization strategy for structures with embedded functional system. Elsevier Addit Manuf
51. Parab ND, Zhao C, Cunningham R, Escano LI (2018) Ultrafast x-ray imaging of laser metal additive manufacturing process. J Synchrotron Radiat
52. Thakar CM, Thakar C, Deshmukh SP, Mulla MT (2020) Design and development of 3D components manufacturing system using waste paper. IRJET
53. Khosravani MR, Reinicke T (2020) Effect of raster layup and printing speed on strength of 3D printed structural components. Procedia Struct Integrity. Elsevier
54. Guo H, Lv R, Bai S (2019) Recent advances on 3D printing graphene based composites. Nano Mater Sci Elsevier
55. Imran Siraj, Pushpendra Singh Bharti, Reliability analysis on 3D printing process. Procedia Comput Sci. Elsevier
56. Forcellese A, Simoncini M, Vita A (2020) Manufacturing of isogrid composite structures by 3D printing. Procedia Manuf. Elsevier

57. Knulst R (2016) 3D printing of marine spares. Open Universities. Netherlands
58. Cleveland, Schwan O D, Silwal B (2017) Application of additive manufacturing in forging-case western reserve university
59. Wohlers report 2020, 2021

Investigation of Machining Parameters in Turning of AISI 316 Steel Using Palm Oil-Enriched Cutting Fluid



Tushar Singh, Prameet Vats, Vineet Dubey, Pawan Kumar Arora, Harish Kumar, and Anuj Kumar Sharma

Abstract Turning operation is widely used in industries for manufacturing different kinds of products. To cope with global market in this era of globalization, industries need manufacturing processes to be economical and would give best quality products and they should have high production rate. In order to achieve these needs, machining is done at high cutting speed, high feed, and depth of cut. At these machining parameters, large amount of heat is generated and high cutting temperature is produced. This results in reduction in tool life, poor dimensional accuracy, and surface integrity of the product are reduced. Thus, it becomes essential to apply cutting fluid for improving the machining performance. Machining is performed on AISI 316 steel by use of tungsten carbide insert. Palm oil-based MQL is used as the cutting fluid. Cutting velocity, feed rate, and depth of cut are taken as input parameters. ANOVA is performed to find the most significant input parameter which affects the response. Results show that depth of cut has significant effect as cutting parameter in both the machining environment. It is found that cutting forces were reduced by 11.945% when machining with palm oil when compared with dry machining.

Keywords Steel · Force · Optimization · Fluid · Machining

1 Introduction

Considerable amount of heat is generated while performing turning operations at high speed, due to friction between the tool and workpiece. The heat generated at time of machining operation affects the tool geometry and also the physical properties of tool and workpiece. The hardness of tool gets reduced which results in reduced

T. Singh · P. Vats · V. Dubey (✉) · A. K. Sharma
Centre for Advanced Studies, Lucknow 226031, India
e-mail: dubey.vin1324@gmail.com

P. K. Arora
Galgotias College of Engineering & Technology, Greater Noida 201310, India

H. Kumar
National Institute of Technology, New Delhi 110040, India

tool life. It hampers the surface characteristics and dimensional accuracy of the machined surface. To prevent large heat generation during machining, cutting fluid is used. Flood cooling has been a common practice used for cooling and lubrication in which continuous supply of cutting fluid is maintained. Cutting fluids helps in reducing the cutting temperature and also flush away the chips produced during the machining operation. There are various techniques and cutting fluids used for cooling and lubrication purposes. One of the major problems that arise during flood cooling is that it harms the environment as well as the health of the worker, therefore it is not environment friendly and discharge of cutting fluid is a major challenge faced by the industries. Minimum Quantity Lubrication commonly known as MQL is an alternative for flood cooling which supplies less amount of cutting fluid in mist form and has gained popularity among researchers as an effective means of lubrication [1].

Hussain et al. [2] investigated tribological characteristics of castor oil blended with mineral oil and compared it with mineral oil. The castor oil is mixed in ratio of 20–80% into commercial mineral oil. Results show that castor oil blended with mineral oil show reduced friction of coefficient and low wear scar diameter compared to mineral oil. Castor oil blended mineral oil show better tribological properties and can be used as a bio-lubricant rather than mineral oil. Gopal et al. [3] evaluated tribological characteristics of pongamia oil methyl ester mixed in diesel oil in concentration of 20, 50, and 80% by volume. Reciprocating wear tester and four-ball tribotester is used to measure wear and friction. The results reveal that with increase in concentration of biodiesel coefficient of friction and wear scar diameter reduced. 50% concentration of biodiesel gives 25% less wear than 20% concentration of biodiesel. Hassan et al. [4] performed investigation of tribological properties of RBD palm oil blended in jatropha oil and compared its performance with RBD palm oil and engine oil. RBD palm oil and jatropha oil blend in ratio of 40:60. Results show lower value of wear scar diameter and coefficient of friction of blended oil when compared with commercial lubricant and RBD palm oil. Pandey et al. [5] reviewed the tribological effect of nanofluids. The study discussed the effect of different nanofluids on friction and lubrication properties. Jabal et al. [6] investigated emissions and tribological characteristics of sunflower oil under different loads and compared it with SAE-40 which is petroleum-based oil. Four-ball tribotester is used for studying characteristics of lubricant and 4-stroke diesel engine for testing the emission. Results show that sunflower oil reduced emission of hydrocarbons, CO, and CO₂ and show better anti-friction and anti-wear properties than SAE-40. Burton et al. [7] performed milling operation on Al6061 and steel 1018 to evaluate the performance of canola oil in water emulsion prepared through ultrasonic atomization and compared its performance with dry cutting and 5% TRIM. It is found from result that by using ultrasonic atomization canola oil emulsion is prepared into water both having same concentration performed better compared to other cutting environments. Cutting forces are reduced in milling of both materials, reduction in chip thickness, and better lubrication is obtained by using canola oil emulsion in water. Dubey et al. studied different temperature machining techniques while machining.

The study revealed that the technique of using thermocouples is widely used for estimating temperature. Shukla et al. [8] performed milling operation on Al6061 under dry, flood, and canola oil-based MQL and compared their performance. TiAlN coated carbide PVD insert tool is used. Canola oil and water emulsifier is used as vegetable oil for MQL. Result show that by using MQL cutting performance improved and minimum tool wear is obtained. Improvement in surface finish is obtained when performing milling operations at high feed rate, high depth of cut, and low cutting speed. Bai et al. [9] evaluated the performance of five different vegetable oils as a lubricant while machining and compared their performance with synthetic cutting fluid. Palm, castor, soybean, cottonseed, and peanut are the five oils that are used in milling steel with grade 45. MQL is the mode of lubrication. Cutting forces, surface roughness is the response parameters. It is found that palm oil gives lowest milling force which is 7.76% less in horizontal direction and 13.6% in the vertical direction compared to synthetic cutting fluid. Best surface finish is obtained by cottonseed and palm oil while soybean gives the worst surface finish. From results it is concluded that palm and cottonseed oil are more suitable base fluid that can be used with MQL. Nareshbabu et al. [10] performed end milling operation on AISI 304 steel with olive oil as the lubricant in the experiment. Results show that by using MQL tool wear reduced by 70%. Reduction of 66% found in surface roughness due to fact that olive oil particles split into small components and penetrate deeper and provide ball bearing effect. Junior et al. [11] performed lubrication and cooling tests for six different vegetable oils, i.e., canola, corn, cottonseed, sunflower, soybean and babassu nut oil by performing their characterization and found that canola and cottonseed gives the best result. These two oils were further selected for lubrication on AISI 1045 steel and compared it with commercial lubricant, i.e., LB2000. Coated cemented carbide tool is used for milling. Tool life is the response parameter. Highest tool life is obtained in MQL by canola oil.

Shankar et al. [12] performed milling operation on AISI 1020 using kapok oil-based MQL and flank wear is selected as the response parameter. Lowest surface roughness and flank wear is obtained in kapok oil when compared to other oils. Minimum resultant vibration is obtained in mineral oil compared to others because of its higher viscosity than others. Zhang et al. [13] used MQCL (minimum quantity cooling lubrication) having advantage of MQL and cryogenic air for lubrication while performing end milling operation on Inconel 718 using coated tool insert and compared its performance with dry machining. Bescut 173 vegetable-based cutting oil is used for the lubrication. Results show that tool life increased by 1.57 times and cutting force reduced in MQCL compared to dry machining.

In this research work, turning operation is performed on AISI 316 steel by the help of tungsten carbide inserts using palm oil-based cutting fluid to investigate the performance of cutting fluid and compare its performance with dry machining on cutting force.

2 Materials and Methodology

Experiment is performed on AISI 316 steel. It is a stainless steel with chromium-molybdenum-nickel content. It is used in manufacturing of pharmaceutical equipment, valves, tanks, pumps, evaporators, furnace parts, jet engine parts, equipment used in chemical processing, photographic equipment, heat exchanger, and exhaust manifolds. Chemical composition of AISI 316 steel is given below in Table 1.

The turning operation is performed on AISI 316 steel using tungsten carbide insert. Turning is performed on central lathe machine. Palm oil-based cutting fluid is used as lubricant. Minimum quantity lubrication (MQL) is the mode of lubrication used for applying cutting fluid while performing turning operations. Taguchi $L9$ DOE method has been used for conducting the experiment. It is a three-level design having three factors. Each of the factors consists of three levels of values. It has been carried out with the help of MINITAB software. The input parameters selected for machining operation are cutting speed, feed rate, and depth of cut. Response parameter is cutting forces. The forces to be analyzed are measured using Kistler force measuring dynamometer along with an amplifier. Dynoware software is used for data acquisition and the input parameters and their levels are mentioned in Table 2.

Turning operation is performed on the workpiece using palm oil-based cutting fluids and the response obtained from it is compared with dry machining. Optimization has been performed using Taguchi method to measure the quality characteristics and significance level of the response parameters.

In Taguchi's approach, the objective of this method is to produce high-quality products at low cost. This is achieved by designing robust DOE which reduces variations during any process. By using Taguchi DOE, with the help of small number of experiments large number of variables are studied that help in reducing manufacturer's cost of production. For performing the turning operation, design of experiment has been made using Minitab software. The design made is a fractional factorial design with $L9$ orthogonal array. It consists of three factors with three levels. Cutting velocity, depth of cut, feed rate are the three factors. Table 3 shows the DOE made for performing experiment. It consists of nine rows. Number of rows indicates how

Table 1 Chemical constituents of AISI 316

Element	Mn	C	S	P	Si	Cr	Mo	Ni
Content (%)	0.0–2.0	0.0–0.07	0.0–0.02	0.0–0.05	0.0–1.0	16.50–18.50	2.00–2.50	10.00–13.00

Table 2 Input parameters

Factors/levels	1	2	3
Speed (rpm)	250	430	660
Feed (mm/rev)	0.06	0.09	0.12
DOC (mm)	0.1	0.3	0.5

Table 3 Design of experiment

S. No.	Depth of cut	Cutting velocity	Feed rate
1	0.1	250	0.06
2	0.1	430	0.09
3	0.1	660	0.12
4	0.3	250	0.06
5	0.3	430	0.09
6	0.3	660	0.12
7	0.5	250	0.06
8	0.5	430	0.09
9	0.5	660	0.12

many experiments need to be performed. Number of columns represents the number of input parameters.

3 Results and Discussions

In this research paper, cutting force is taken as response parameter. Since it is a non-desirable parameter, thus it should be minimum. To get minimum cutting forces, machining should be done at optimum machining parameters and use of lubricant and coolant helps in reducing it. In both the machining operations, i.e., under dry machining and under palm oil-based MQL machining cutting force is calculated and effect of palm oil-based machining is investigated and it is compared with the dry machining. Table 4 shows the response parameters.

Table 4 Response parameters

Experiment S. No.	Depth of cut (mm)	Cutting velocity (rpm)	Feed rate (mm/rev)	Force in dry Cutting	Force in palm oil-based MQL cutting
1	0.1	250	0.06	118.40	90.60
2	0.1	430	0.09	100.50	78.82
3	0.1	660	0.12	72.62	69.55
4	0.3	250	0.06	172.10	160.60
5	0.3	430	0.09	165.40	150.50
6	0.3	660	0.12	159.90	141.50
7	0.5	250	0.06	219.80	200.80
8	0.5	430	0.09	214.50	193.60
9	0.5	660	0.12	158.20	138.20

3.1 Taguchi Methodology

Taguchi uses orthogonal array for design of experiments. DOE made using orthogonal array are helpful in those experiments which have multiple level factors. Taguchi orthogonal array helps in studying entire parameter space with small number of experiments. In Table 3, L_9 orthogonal array is shown which indicates nine trials are needed to be performed. Number of factors, number of levels, and cost limitations are the items on which selection of orthogonal array is depending [14].

Signal-to-noise ratio (SN ratio) is measure of quality characteristics deviating from desired value. S/N ratio is comparison between desired signals to the undesired signal, i.e., ratio of signal power to noise power. After conducting the experimental trials, results obtained from the trials are converted into signal-to-noise ratio. When objective has goal of minimization of the response or output then Smaller-the-better S/N ratio is used. In this case, negative data characteristics are obtained. For objectives having goal of maximization of response or output then higher-the better S/N ratio is used. In this case, positive data characteristics are obtained.

Nominal-the-better is used when neither a larger nor a smaller output is required. In this case, data characteristics have positive, negative, and zero values. In this experiment, cutting force is to be analyzed. Thus, lower-the-better category should be selected. The value of SN ratio is obtained from Eq. 1.

$$S/N = -10 * \log(\Sigma(Y^2)/n) \quad (1)$$

ANOVA is used to check the significance level of the response parameters. It signifies the effectiveness of the process parameters on the response parameters. ANOVA marks on 95% confidence level, i.e., P -value should be less than or equal to 0.05 (P -value \leq 0.05). In ANOVA table, sum of squares signifies that maximum will be the value of sum of square of a parameter more will be the effectiveness of that parameter. Coefficient of determinant in the ANOVA table is used to check the effectiveness of experimental results. To get the desirable results coefficient of determinant should be close to 100% [15–17]. The analysis of response parameters is shown in Table 5. Similarly, Table 6 shows ANOVA analysis of response parameters at Palm oil-based MQL machining.

R^2 -98.73% and adjusted R^2 -94.93%

Table 5 Analysis of cutting forces (dry)

Source	D.O.F	Seq S.S	Adj.SS	Adj. MS	F -value	P
Depth of cut	2	15,779.9	15,779.9	7890.0	64.67	0.015
Cutting velocity	2	2581.8	2581.8	1290.9	10.58	0.086
Feed rate	2	644.2	644.2	322.1	2.64	0.275
Residual error	2	244.0	244.0	122.0		
Total	8	19,249.9				

Table 6 Analysis of variance for means of cutting forces (palm oil)

Source	D.O.F	Seq. S.S	Adj. S.S	Adj. MS	F-value	P
Depth of cut	2	15,361.8	15,361.8	7680.9	37.05	0.026
Cutting velocity	2	1870.1	1870.1	935.0	4.51	0.181
Feed rate	2	467.1	467.1	233.6	1.13	0.470
Residual error	2	414.6	414.6	207.3		
Total	8	18,113.6				

R^2 -97.71% and adjusted R^2 -90.84%

ANOVA analysis of response parameters in various cutting environments is shown in Table 5 and Table 6 which signifies the effect of input parameters on response parameters. From Table 5 in case of dry machining, it is found that depth of cut is dominant parameter that affects the cutting force followed by cutting velocity. Similarly, in Table 6 it can be inferred that depth of cut is the most significant input parameter.

S/N ratio signifies the optimum machining parameter for getting the best response. In this experimental work cutting forces is response which should be minimum thus, smaller is better is taken as the objective for getting the optimum machining parameter. From Fig. 1a, when machining is performed under dry conditions, minimum cutting force is obtained when depth of cut is 0.1 mm, cutting velocity is 660 rpm and feed rate is 0.12 mm/rev. Figure 1b shows that it in case of palm oil MQL based machining optimum machining parameter is depth of cut of 0.1 mm, cutting velocity of 660 rpm and feed rate of 0.09 mm/rev.

Figure 2a, b shows the contour plot of cutting forces in dry machining and MQL based machining. The depth of cut is represented on x-axis while cutting velocity is represented on Y-axis. The contour plot in the above figures shows the variation of cutting forces with depth of cut and cutting speed. In Fig. 2a the dark green region shows higher value of cutting forces due to high depth of cut and low cutting speed. The dark blue region shows lower value of cutting force due to high cutting speed and low depth of cut. From Fig. 2a it is clear that at depth of cut 0.5 mm and cutting

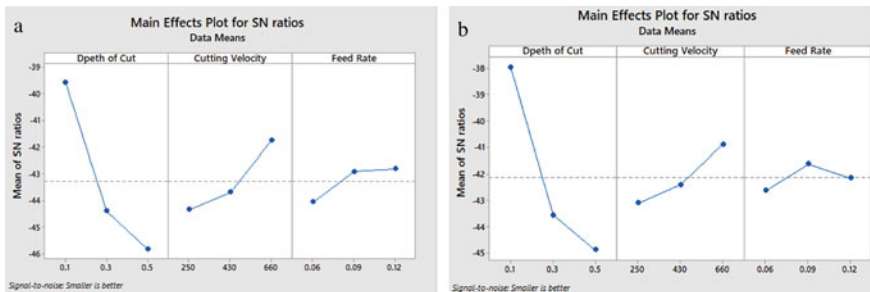


Fig. 1 Main effect plot for SN ratio for dry machining and MQL based machining

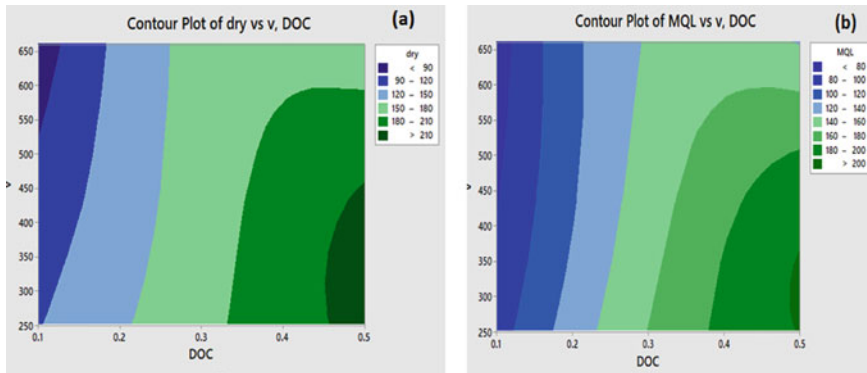


Fig. 2 a Contour plot for dry machining 3 b contour plot for MQL based machining

speed of 250–450 rpm high cutting forces are obtained and lower cutting forces are obtained above 550 rpm and 0.1 mm depth of cut. Similarly, in Fig. 2b MQL based on machining less cutting forces are shown by dark blue color at low depth of cut and high cutting speed for the value above 450 rpm cutting speed and 0.1 mm depth of cut and dark green region denotes high cutting forces for 0.5 mm depth and 250–350 rpm in Fig. 2b. The surface plot representing cutting forces shows higher elevation in case of depth of cut when compared to cutting velocity in both dry as well as MQL based turning. It is due to the fact that cutting forces are directly proportional to depth of cut [17].

4 Conclusions

- By using palm oil-based MQL cutting force is reduced by 11.945% when compared with dry machining because palm oil act as a lubricant and reduces the friction.
- ANOVA is performed to find the most significant factor which affects the response parameters. In both the cutting environment, i.e., in dry machining as well in MQL depth of cut is the most significant factor affecting the cutting forces.
- From SN most optimum machining parameter is investigated. In case of dry machining depth of cut is 0.1 mm, cutting velocity is 660 rpm and feed rate is 0.12 mm/rev is the optimum cutting parameter while in case of palm oil-based MQL depth of cut of 0.1 mm, cutting velocity of 660 rpm and feed rate
- Palm oil-based MQL performed better compared to dry environment because palm oil has larger content of unsaturated fatty acids in it which is the main reason for effective lubrication and reduced cutting forces.

References

1. Dubey V, Sharma AK, Singh RK (2020) Study of various cooling methodology used in machining processes. *Mater Today Proc* 21:1572–1576. <https://doi.org/10.1016/j.matpr.2019.11.092>
2. Hussain A, Mehdi SM, Ali A, Adeel M, Jabal MH, Ani FN (2018) Investigation of tribological characteristics of castor oil with mineral oil blends. *J Eng Appl Sci* 37(1):45–50
3. Nantha Gopal K, Mana AP, Ashok B (2018) Tribological characteristics of pongamia oil methyl ester. *J Tribol* 17:65–76
4. Hassan M, Ani FN, Syahrullail S (2016) The tribological characteristics of RBD palm olein with jatropa oil blend using four-ball tribotester with different normal loads. *Appl Mech Mater* 819(4):499–503. <https://doi.org/10.4028/www.scientific.net/amm.819.499>
5. Pandey K, Dubey V, Sharma AK, Mital A (2019) State of art on tribological behaviour of nanoparticle enriched cutting fluid. *Mater Today Proc* 26:2586–2589. <https://doi.org/10.1016/j.matpr.2020.02.547>
6. Jabal MH, Abdulmunem AR, Abd HS (2019) Experimental investigation of tribological characteristics and emissions with nonedible sunflower oil as a biolubricant. *J Air Waste Manag Assoc* 69(1):109–118. <https://doi.org/10.1080/10962247.2018.1523070>
7. Burton G, Goo CS, Zhang Y, Jun MBG (2014) Use of vegetable oil in water emulsion achieved through ultrasonic atomization as cutting fluids in micro-milling. *J Manuf Process* 16(3):405–413. <https://doi.org/10.1016/j.jmapro.2014.04.005>
8. Shukla A, Kotwani A, Unune DR (2020) Performance comparison of dry, flood and vegetable oil based minimum quantity lubrication environments during CNC milling of aluminium 6061. *Mater Today Proc* 21:1483–1488. <https://doi.org/10.1016/j.matpr.2019.11.060>
9. Bai X, Zhou F, Li C, Dong L, Lv X, Yin Q (2020) Physicochemical properties of degradable vegetable-based oils on minimum quantity lubrication milling. *Int J Adv Manuf Technol* 106(9–10):4143–4155. <https://doi.org/10.1007/s00170-019-04695-x>
10. Babu MN, Anandan V, Muthukrishnan N, Santhanakumar M (2019) End milling of AISI 304 steel using minimum quantity lubrication. *Meas J Int Meas Confed* 138:681–689. <https://doi.org/10.1016/j.measurement.2019.01.064>
11. Junior AS, Sales WF, da Silva RB, Costa ES (2017) Machado ÁR (2017) Lubri-cooling and tribological behavior of vegetable oils during milling of AISI 1045 steel focusing on sustainable manufacturing. *J Clean Prod* 156:635–647. <https://doi.org/10.1016/j.jclepro.2017.04.061>
12. Shankar S, Manikandan M, Raja G, Pramanik A (2020) Experimental investigations of vibration and acoustics signals in milling process using kapok oil as cutting fluid. *Mech Ind* 21(5) <https://doi.org/10.1051/meca/2020066>.
13. Zhang S, Li JF, Wang YW (2012) Tool life and cutting forces in end milling Inconel 718 under dry and minimum quantity cooling lubrication cutting conditions. *J Clean Prod* 32:81–87. <https://doi.org/10.1016/j.jclepro.2012.03.014>
14. Fernando WLR, Sarmilan N, Wickramasinghe KC, Herath HMCM, Perera GIP (2019) Experimental investigation of minimum quantity lubrication (MQL) of coconut oil based metal working fluid. *Mater Today Proc* 23:23–26. <https://doi.org/10.1016/j.matpr.2019.06.079>
15. Yang WH, Tarng YS (1998) Design optimization of cutting parameters for turning operations based on the Taguchi method. *J Mater Process Technol* 84(1–3):122–129. [https://doi.org/10.1016/S0924-0136\(98\)00079-X](https://doi.org/10.1016/S0924-0136(98)00079-X)
16. Dubey V, Sharma AK, Singh B (2021) Optimization of machining parameters in chromium-additive mixed electrical discharge machining of the AA7075/5%B4C composite. *Proc Inst Mech Eng Part E J Process Mech Eng*. <https://doi.org/10.1177/09544089211031755>
17. de Lacalle LN, Pelayo GU, Fernández-Valdivielso A, Alvarez A, González H (2017) Wear-dependent specific coefficients in a mechanistic model for turning of nickel-based superalloy with ceramic tools. *Open Eng* 7(1):175–184. <https://doi.org/10.1515/eng-2017-0024>

Real-Time Medical Infusion Set Drip Monitoring and Controlling Healthcare System



Praveen Kumar Maduri, Mohd. Alamgir Khan, and Rajesh Yadav

Abstract In this modern era, many advanced methods are implemented due to instrumentation and automation for quick treatment of patient in medical healthcare centers. There is a need for advanced facilities regarding good consideration of patients in medical field, also for measurement and evaluation of liquid and lipids which is most basic thing to treat patients. In all medical healthcare medical attendants has to check the liquid level in the bottle. Sometimes staff might be failed to change the bottle at right time to solve this problem, a real-time-based medical liquid drip monitoring and controlling system is proposed where load cell is used as a weight sensor. It works on the methodology that when liquid level the changes then also weight of bottle also changes data is collected for further controlling of flow of liquid. At point where fluid is low, will alert the staff member with trading notification on their designed platform. So, that medical plugs the bottle directly with in indication that might reverse the blood flow to the bottle from patient view in the proposed, medical staff can control the liquid flow from their designed dashboard online and can be accessed remotely. It will help in reducing this kind of incident in medical time and also no one has to monitor the bottle manually, these gadgets will be very helpful in the medical department.

Keywords Medical drip · Real-time · Infusion · Healthcare · Monitoring

1 Introduction

This system is used in the medical line when the infusion of liquid is taking place as there are many issues while monitoring and measuring of exact fluid which is to be injected into the patient's body. As more amount is to be infused which will take a fixed time interval in the cycle regular monitoring is required which needs

P. K. Maduri (✉) · Mohd. Alamgir Khan · R. Yadav
Galgotias College of Engineering and Technology (AKTU), Lucknow, India
e-mail: praveen.kumarmaduri@galgotiacollege.edu

Mohd. Alamgir Khan
e-mail: alamgir.khan@galgotiacollege.edu

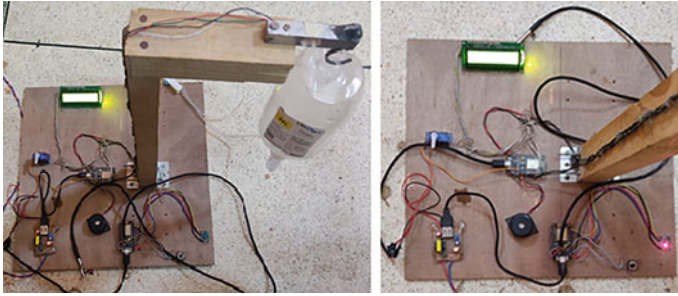


Fig. 2 Implemented system

with RGB lights as low, medium, and high, and this whole indication is fixed in that system medical staff can see the level on this system. The models only help to monitor the level of bottle only, it should be having some advanced features to be helpful and effective to the patient and some features to monitor the patient online with IoT based platform, with liquid bottle can be a part of improving medical system [2]. It also transmits data online to designed dashboard sometimes medical staff members may forget to manage flow of liquid. This alerting technology only detects the liquid through IR Sensors which shows inaccurate results sometimes and only alerting is available to indicate low liquid levels, so it is used for only alerting the concerned department for further actions [3].

This may be harmful to patient, drip flow should be managed according to the patient's condition otherwise any serious accident may occur considering these conditions designed system with alert specifications and share data to IoT platform with the interfacing with cloud, and then conditions are applied for the further transmission of data [4]. If there is no one to monitor the drip bottle then it will alarm the respective doctors/nurse, so they can control it accordingly with that blynk application online remotely it reduces any accident with the drip and patients' health. Some designed models are also available that work on both problems but they do monitor features to control the flow of fluid [5, 6].

3 Working

From load cell input is received in terms of weight later than defined in terms of volume (ml), and signal passed through load cell controller, then sent to Arduino microcontroller which applies the designed algorithm to compare predefined values with receiving values. Load cell provides liquid weight information after processing it will display on LCD screen. It fetches the liquid availability information and sends it to node MCU for further calculation and comparison of predefined conditions to show the results with command to know the fluid level and then check for maximum level (full bottle) if it is met with given condition the liquid level information is fetched

for further operations otherwise LCD will display an error message as (maximum level error) and it will stop the process of the given command. After fetching real-time fluid level, it follows the condition when predefined minimum level is reached. if matched an alert notification is sent on blynk application and also starts alarming for alerting the staff member else when condition does not match it will return to the step of checking maximum level and then again start to verify data for further operations. Body temperature, heartbeat rate, and oxygen level are measured and shared online with the medical team so that they can easily control the infusion drip value. It would help medical team to handle more patients from a single platform remotely after reviewing the health measuring instruments, they can manage the system according to the patients' health, which will also help to patient not to worry about his/her monitoring. Data is transmitted to blynk application for remote online controlling a monitoring the system.

For regular flow when conditions are met with automatic liquid flow in which it would be set to fixed value till the availability in the bottle, if minimum level of bottle is not reached then again repeats its value to the drip level condition when reached, it would start alarming automatically with the scalding of information to the blynk application so that medical staff can focus on the condition of patient. Remotely flow can be controlled by concerned staff members through slider seen on the blynk application with an available variable which can control speed of servo motor according it will turn. Clockwise/anticlockwise drip valve starts to lose of tight, the fluid flow will be controlled within this algorithm medical. Information set value is used with servo motor, whole operation will be carried out in the pressure of medical teams this process is recalled again to again in real-time, so that flow can be controlled ESP8266 and data is transmitted from blynk application to system easily as shown in Figs. 3 and 4.

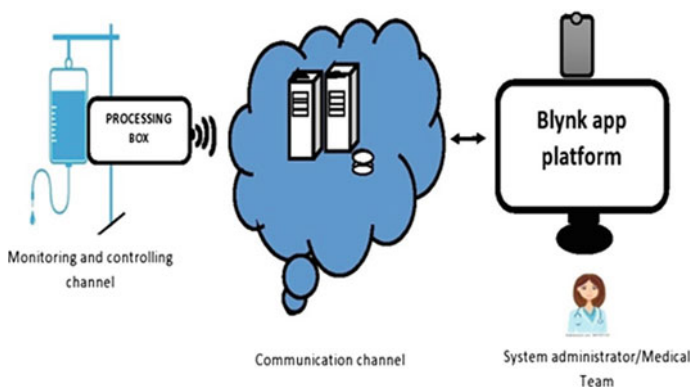


Fig. 3 Data communication

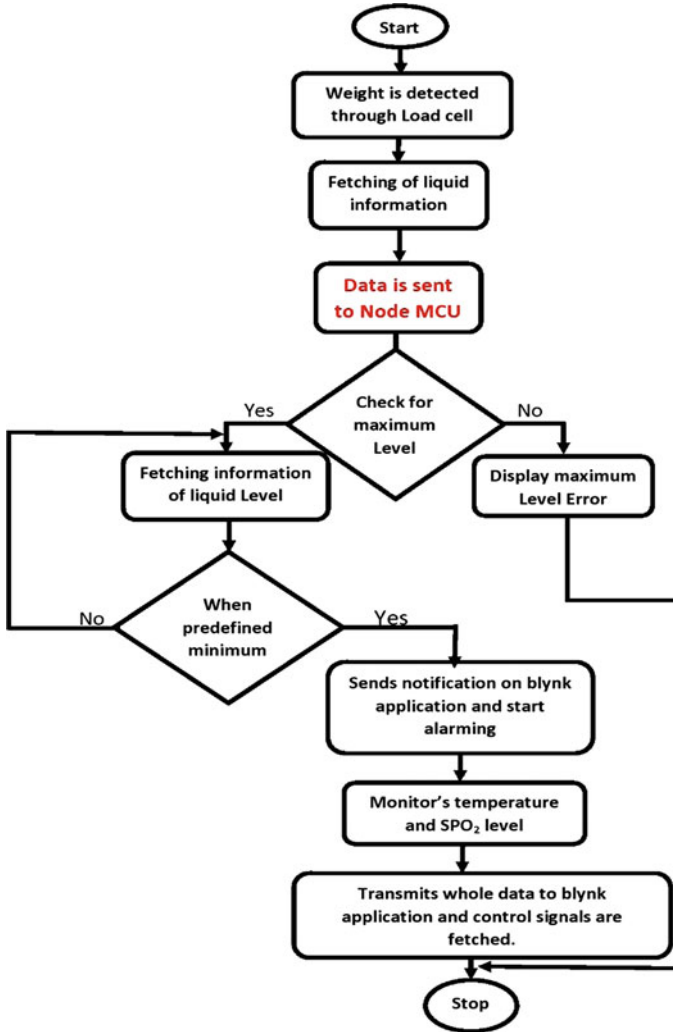


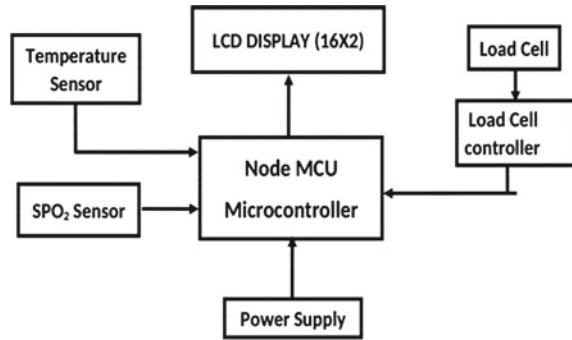
Fig. 4 Flowchart

4 Methodology

4.1 Monitoring of the System

Load sensor is used to measure weight of the liquid bottle and whenever the present liquid decreases and also weight of bottle also goes down, so the measured weight will be used as liquid level indication load cell controller takes data from load cell sensor and transfer it to Arduino microcontroller, as the liquid level decreased LCD

Fig. 5 Monitoring functional diagram



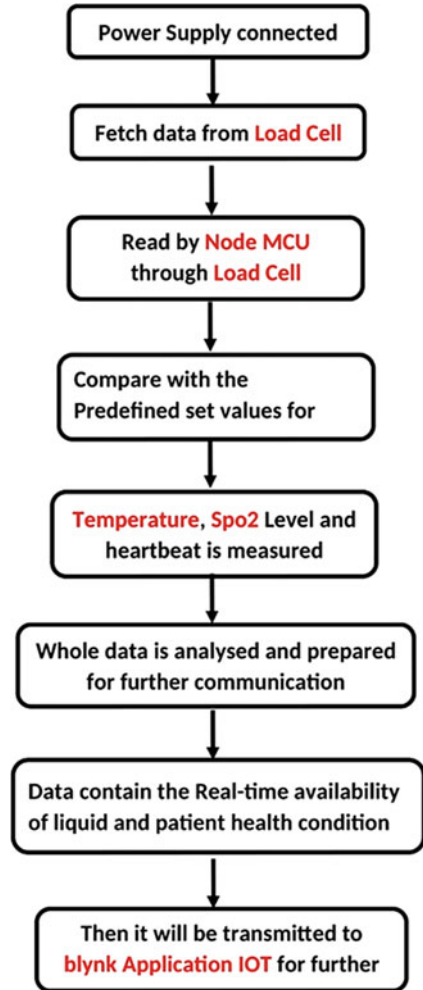
(16 × 2) will display the data in percentage of its availability. The weight will start decreasing as liquid levels turn to be down, this parameter will be used as perfect drip flow connected with load cell with gauge factor (2.05), creep (0.03) respectability (0.01), it is connected to Arduino microcontroller to analyze data and send through ESP 8266, It is used to exchange information with cloud through internet of things (IoT), and transmit it to the designed platform. Temperature sensor is used here to detect real-time body temperature of patient SPO2 sensor will analyze heartbeat and oxygen level available in the blood which would help doctors to free from manual measurements and also can be seen on blink app remotely so that exact treatment is given to the patient.

This device is integrated with all features with useful parameters that are needed to check in very short time period repeatedly, e.g., temperature check, heartbeat rate, oxygen level, etc. Accordingly in fusion set value is controlled remotely by doctors after seeing these parameters liquid flow will be measured and decision is finalized for further treatment. This weight of liquid is actually converted into the measurements of liters in ML so that level of liquid can easily be leveled in the program for calculation and applying comparison conditions, e.g., (>70%, <50%). This helps in alerting the concerned department from time to time as the liquid level falls from the defined conditions. The whole the data is sent to the designed blink application to monitor the drip level and flow of fluid at low level (e.g., less than 100 ml). It starts sending notifications to medical staff and alarming with the help of buzzer near-patient so that whole the help of buzzer near-patient so that whole bottle's information can be monitored easily, as shown in Figs. 5 and 6.

4.2 Controlling of System

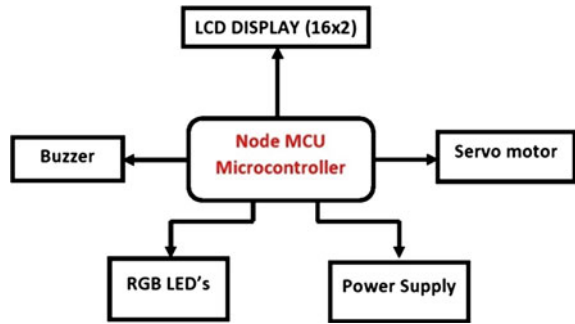
Whenever the liquid seems to be end in the bottle or any condition is matched, programmed based on the temperature, heartbeat rate, and oxygen level, it will notify medical staff so that they can monitor the condition and control the flow of the liquid accordingly. It will be an immediate process of controlling the flow with

Fig. 6 Monitoring algorithm



the help of infusion set value attached to servo motor, which rotates accordingly to the received command to control the fluid through it. System will be working in real-time from blynk application dashboard, which is designed with manual and automatic. In manual mode it is directly controlled under the supervision of medical team and in automatic mode, the flow will be controlled depending on the condition of patient automatically followed by the programmed cut-off values with conditional statements so that each action can be performed in minute. This technology will help to reduce the issues of less availability of staff members and patient can feel secure during night. Liquid flow can be easily controlled by drip whether to slow or fast the flow, it can be controlled online by any medical staff member remotely. ESP8266 transmits signal to Arduino microcontroller about liquid flow rate then it compares data and send to dashboard. Whole information will be displayed on the designed

Fig. 7 Monitoring block diagram



dashboard, so that staff can easily can change or set flow rates anytime with online controlling and monitoring system.

In this whole system 12 V power supply is used to power the whole mechanism and after receiving signal for dashboard, so that it can make sure to take further actions taken for drip flow management for with servo motor the liquid flow valve will be controlled through it according to the staff management, then servo motor will rotate the drip valve and control the flow rate. Servo motor will run slowly to manage the required flow with the drip valve attached to it whenever fluid will go less than 100 ml than it will start alarming for fluid control (slow or fast) then the Arduino Uno R3 sends signal to servo motor to run anticlockwise/clockwise to control fluid in the drip, with servo motor specification, operating speed (20 s/60°), stall torque (10 kg/cm), operating speed (4.8 V) specification it is used to control the fluid because of its less power consumption, as shown in Figs. 7 and 8.

5 Outcome

This system worked on proposed algorithm successfully for monitoring and controlling the infusion set and obtaining patients' health conditions online by controlling it remotely from blynk application. All the drip levels are displayed with the cut-off conditions for alerting and sending notifications to medical staff. When bottle is full, it shows its level according to flow in real-time as shown in Figs. 9 and 10. When the liquid level will reach to minimum level, then it will alert (bottle level low) as shown in Fig. 11. All measured values by sensors will be sent to blynk app and displayed in real-time to take care and supervision of patient as shown in Fig. 12.

6 Conclusion

With this proposed system, a perfect instrumentation will be reflected in medical field. It will help to reduce the efforts of staff members. It is real-time mechanism

Fig. 8 Controlling algorithm

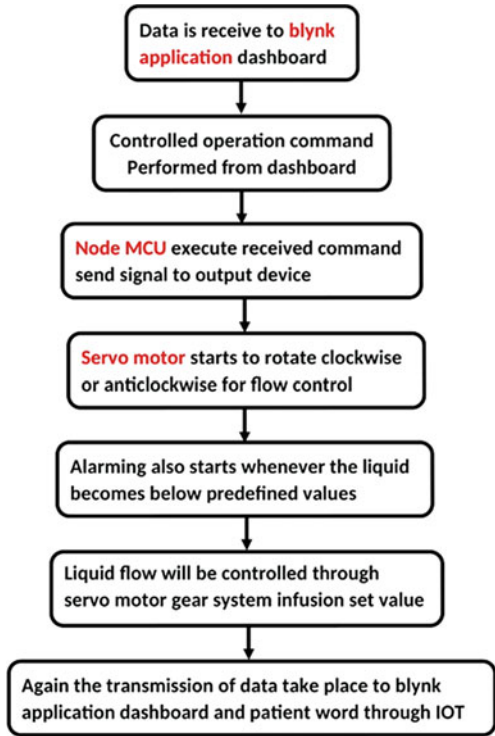


Fig. 9 Maximum liquid level with flow control

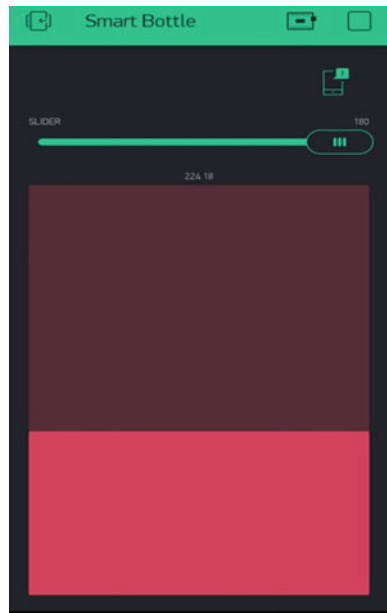


Fig. 10 Minimum liquid level with flow control

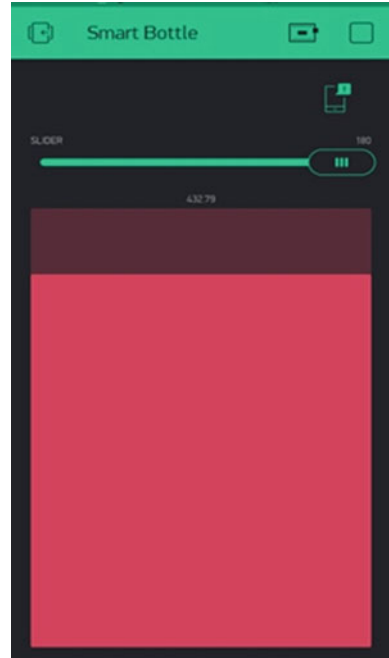


Fig. 11 Low liquid level alert and real-time values of temperature SPO2

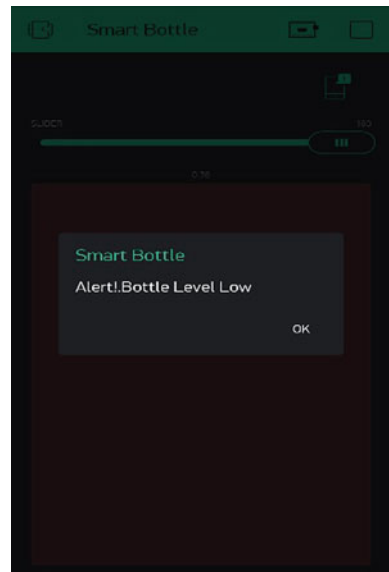
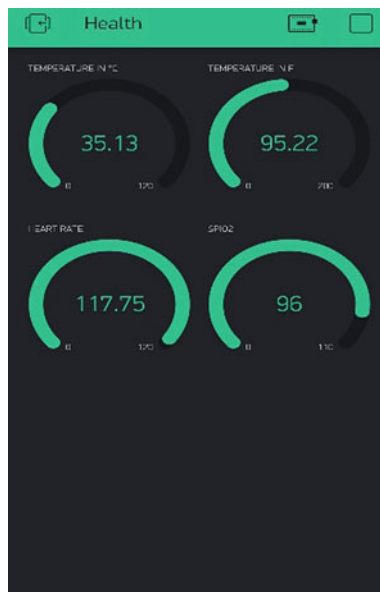


Fig. 12 Low liquid level alert and real-time values of temperature Heart Rate monitoring



that controls and monitors the whole operation of drip infusion. It will be proved as an intelligent system in medical field which is integrated with all health monitoring sensors and flow control with online dashboard remotely. It will help in reducing human intervention in monitoring and controlling the system manually. This system also can be set to automatic mode whenever there is lack of medical staff, all the operations are carried out automatically with the control of whole system. It can be an advanced technology by adding matching learning models to detect the patient's body situation with the implementation of rest position sleeping hours and other required actions can be detected through it so that medical staff can have full control of patient's health remotely. It will also alarm and send notification to the concerned staff member so that staff can respond easily to condition of patient immediately.

References

1. Hamidi H (2019) An approach to develop the smart health using internet of things and authentication based on biometric technology. *Future Genre Comput Syst* 91:434–449
2. Jagannathachari A, Nair AR Saline level indicator. *IOSR J Comput Eng (IOSRJCE)* e-ISSN: 2278–0661, p-ISSN: 2278–8727 PP 13–16
3. Priyadharshini R, Mithuna S, Kumar UV, Devi SK, Vanitha NS (2015) Automatic intravenous fluid level indication system for hospitals. *Int J Res Appl Sci Eng Technol (IJRASET)* N vol 3 Issue VIII, Value:13.98 ISSN: 2321–9653
4. Vaishnav K, Swamy N, Haidarali NB, Patil M (2017) IoT based saline level monitoring system. *Int J Innov Adv Comput Sci IJIACS* 6(10):2347–8616

5. Dharmale A, Mehare R, Bharti A, Meshram S, Deshmukh S (2019) Iot based saline level monitoring and automatic alert system. *Int J Adv Res Comput Commun Eng* 8(4)
6. Santos PM, Rodrigues JGP, Cruz SB, Lourenço T, d'Orey PM, Luis Y, Rocha C, Sousa S, Crisóstomo S, Queirós C (2018) PortoLivingLab: an IoT-based sensing platform for smart medical machines. *IEEE Internet Things J* 5:523–532

Design and Fabrication of CNC Lathe Fixture for Cone



Sanjay Rathaur, Rishi Sanoria, Syed Haider Abbas Abidi, and Abdul Gani

Abstract Fixture is a device that supports, and holds the workpiece for operation or process but does not guide the cutting tool. It allows only a reference to a surface or a tool. Fixtures are unique because each of them is built to fit a specific part or shape. This paper presents design and fabrication of fixtures for tapered or conical workpieces. Operations that can be performed with this fixture are front-facing, drilling and boring. Fixture is designed with minimum number of components. Mild steel is selected for manufacturing because of its composition which is Fe 98.0%, C 0.04%, Mg 1.03%, Si 0.280%, Cu 0.20% P 0.04. There are various types of fixtures are available to hold various shapes of workpieces. The aim is to design and fabricate a fixture that can hold a conical or tapered body. Fixture design process is done on SolidWorks and stress, strain and displacement analysis are also carried out. The results are $2e+011$ N/m² maximum stress. 0.0153602 mm maximum resultant displacement and 0.000484712 is maximum equivalent strain. After desired results are analyzed, manufacturing of designed fixture is performed on lathe machine. This research has discussed design and manufacturing in-depth in different types of terminology. This terminology shows the study, goals, methodology and design analysis as well as the outcome, result and conclusion.

Keywords Cone fixture · CNC machine · Fixture · Facing and boring · Solidworks

1 Introduction

The mass production method always demands a fast and effortless method of work positioning for precise operations on it. Jigs and fixtures are devices used in production for manufacturing accurately duplicate and interchangeable parts. Fixture is unique because it is designed and built to fit a specific part, shape and size. During an operation or process, the fixture's purpose is to locate and hold the workpiece. Fixtures are designed to hold, support and locate each part to make sure that part

S. Rathaur (✉) · R. Sanoria · S. H. A. Abidi · A. Gani
School of Mechanical Engineering, Galgotias University, Greater Noida, India
e-mail: sanjay.rathaur03@gmail.com

is machined within the specified limits. The fixture design process and manufacturing are a very complicated processes in which knowledge of various areas, such as dimensions, geometry, procedures, tolerances, and manufacturing processes is required.

The target is to build a fixture that can hold a tapered or conical shape workpiece. Usually, chucks can easily hold a square, round or hexagonal shapes but it is hard to make grip on tapered objects as they will slide during the machining as the heavy force is applied. So, the aim was to design a fixture that can offer better grip and can hold the tapered object tightly during the machining process. The machining processes like facing, drilling and boring can be performed using this fixture [1, 2].

1.1 Literature Review

After going through various literature published on fixture in reputed journals of mechanical engineering and gathering a brief knowledge on designing, material selection and different types of fixtures and finding different research papers on similar topics. Below are the research papers which have assisted or been found to be helpful for the present work. After studying these researches useful information was found on fixtures and their uses, manufacturing, parameters, etc. Shubham et al. [1] emphasized the need for a fixture that can hold a square block. Designing this fixture mainly focused on reducing the total cost. The study identified that this fixture can be useful for enhancing the production. Corrado and Polini [3] recognized the need for comparison of three tools used for analysis of tolerance to approximate the position difference of a drilled hole on a body due to random error of locater position. And the three tools he compared are vector loop, cat software and variation modal and he found the different root of errors. Maniar and Vakharia [4] reviewed design and development and its future directions. To hold a different shape or size or workpiece requires a different fixture. The design of fixture needs to be evaluated and tested in real environment of manufacturing. An optical fixture solution results in different consideration such as machining process, stiffness and tolerance configuration.

Roy and Kumar [5] emphasized the need for a lathe attachment. A lathe component is designed using CAD modeling and then fabricated. Components are successfully attached to CNC lathe and performed various operations. The CNC lathe becomes multifunctional with the existing lathe by attaching addition components. Kumara and Ram [6] recognized the need for developing fixtures for brake drums by new design by neglecting the gap available in the old fixture instead of button brake drum was seated on fixture. The main objective is to hold the brake drum in a way in a single setup of lathe these should facilitate brake surface diameter as well as machining of rake drum bore. Pachbhai and Raut [7] reviewed on design of fixtures to satisfy high performance and perform multiple functions that can be approached by optimum design requirements. Fixture reduces the time requirement and increases the productivity. Kamble and Tom Mathew [8] emphasized the need to design cohesive fixtures to perform different variety of tasks in a single workbench. Scope of this

research in future is to shorten the time and new areas such as expert structure and artificial intelligence.

2 Problem Description

Selecting a chuck for manufacturing processes depends upon the design, size and shape of the component or part which is to be manufactured. For cylindrical components three jaw chucks are used, for square components, four jaw chucks or independent jaw chucks, etc. can be used. In industries, a problem is faced of purchasing four jaw chucks for processing of cone component which is in batch production type. Till now companies processing mainly cylindrical components so they only have three jaw chuck and for some batch production of cone or square components they want to use four jaw chuck whose market price is around 10,000–80,000 which is not affordable. The purpose of this research is to design and fabricate a fixture to three jaw chuck so that it will be processed cone component also in minimum cost of three thousand. Tapered products have various diameters that are why they get failed on these fixtures. But here this paper is focused on a taper product. The designed fixture can easily hold a cone and perform various operations like facing, drilling, boring, etc.

The objectives of this project are:

1. Design a fixture that can hold and process cone or tapered components on three jaws and four jaw chucks.
2. Evaluate and analyze the design of fixtures in solid works.
3. Fabricate the final design and implement the fixture for manufacturing.

3 Materials and Methodology

The proposed design, a cylindrical body is taken as supporting part and it will be main body of fixture. From the backside some space is given for jaws to hold the fixture. Fixture will be suitable for both three jaw/4 jaw chuck. On the other end, tapered openings and holes in four directions are given. The holes are threaded from inside in which bolts can be screwed. The bolts will exert pressure from different points so that they will hold at fixed position. The body is tapered from inside under the holes so the head of cone can be inserted and can be tightened with the help of bolts. After the workpiece is fixed with fixture, fix it in chuck of CNC or lathe and can perform various operations like facing, drilling, boring, etc. on its body without any problem.

These are the consideration for fixture design processes [9].

- (a) Study the dimensions and material of tapered workpiece.
- (b) The type and capability of machine on which operation to be performed.

- (c) Better grip to be provided for avoiding slip or slide of workpiece.
- (d) Understand the strength and properties of the fixture material.
- (e) Accuracy in the work and desired level of quality to be produced.

3.1 Material Selection

There is vast range of different materials from which a fixture can be built. Different materials have different specific qualities. Fixture material should resist wear and tear because it is frequently tempered and hardened and non-ferrous metals like phosphor bronze and other metals are used to wear reduction for the part that mate and prevent damage. In this fixture, mild steel is used due to its material properties [10].

Mild steel: Mild steel is a part of carbon steel known as low carbon steel which carries around 0.3% of carbon because of its easy availability it is frequently the first-choice material for manufacturing fixtures and they are very cheap as well.

Advantages of mild steel are

1. Mild Steel is cheaper than other materials like aluminum, phosphor bronze, etc.
2. Mild Steel has excellent machinability. It can be easily shaped in any form.
3. It has high thermal conductivity, and electrical conductivity and is light in weight.
4. High tensile and impact strength.
5. Good Ductility and malleability.

The less amount of carbon makes the mild steel more ductile and machinable which gives advantage of changing raw material to desired shape of fixture. The property of high malleability and does not crack as opposed to the high carbon steel that is very susceptible to breaking. The mild steel also has magnetic properties because of high amount of Iron and Ferrite. Its versatility, easily moldable into any shape and cost-effective as compared to other carbon steel make it excellent choice for manufacturing. Mechanical and physical properties of mild steel and its element are given in Table 1.

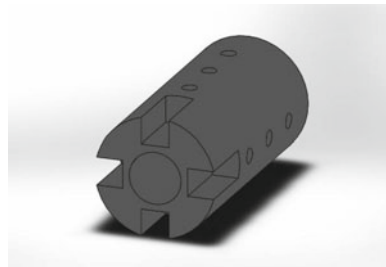
3.2 Construction

Here a cylindrical body fixture is constructed which is tapered from inside. The inner part has two different diameters one of which makes the inside area taper where a conical body can be held for machining as well as drilling as shown in Fig. 1. The back part is open for gripping area which is provided for four jaws chuck as well as it can hold by other chucks too. Screw of 8 mm diameter in four directions is given at three different areas to hold the workpiece accordingly. It consists of following parts.

Table 1 Composition and properties of mild steel [11]

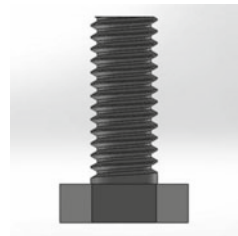
Mechanical properties	Metric
Bulk modulus	140 Gpa
Tensile strength, yield	250 Mpa
Tensile strength, ultimate	400–550 Mpa
Shear modulus	79.3 Gpa
Modulus of elasticity	200 Gpa
Poisson’s ratio	0.260
Density	7.85 g/cm ³
<i>Element</i>	<i>Content</i>
Carbon (C)	0.04–0.3%
Iron (Fe)	98.0%
Phosphorus (P)	0.040%
Copper (Cu)	0.20%
Silicon (Si)	0.280%
Manganese (Mg)	1.03%
Sulfur, S	0.050%

Fig. 1 Actual fixture drawing (SolidWorks 2016)



Cylindrical body. The main fixture body with a standard length and cylindrical body which is hollow from inside and tapered from one end to another the front part has bigger diameter while back has diameter for drilling size.

Fig. 2 Head bolt (4 × 3)



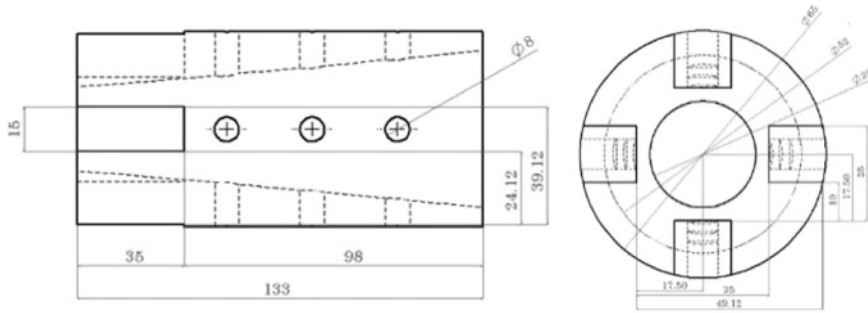


Fig. 3 Drawing of fixture (2D with top view and front view)

Head bolts. There are 12 head bolts as shown in Fig. 2 available for tightening the workpiece in this fixture. The four of them will tight the workpiece from the front, four from the middle, and four from the back, depending on the size of the workpiece. It can be designed for a particular part with an accurate measurement and used for quality control since it is tapered.

Engineering Drawing for designed fixture as shown in Fig. 3. Drawing of fixture (2D with top view and Front View) shows the 2D drawing with top and front view with all the dimensions provided in designing the fixture. Dimensions provided in the given design are in mm.

4 Analysis

During the operation, different forces will act on the fixture body which will be found by analyzing processes like stress, strain and displacement. Following information is provided during the analysis process as given in Table 2. Solid works software used in the analysis process.

Table 2 lists the different terms used in analysis that are derived from the results. This terminology demonstrates the use of a solid form of mesh and mesher is standard mesh. In order to perform a simulation analysis or create a digital model, meshing is frequently used to divide the framework into cells. A fixed volume mesher is used in the standard mesher process form which is used in tetrahedral and hexahedral elements. In this operation, the outcomes of Jacobian points are four. Its point in two dimensions, a Jacobian matrix would be a measure of how much distortion and entity experiences when moving from Cartesian to Natural coordinates. After that element size is 2 mm it is a size of mesh that is directly connected to improve accuracy of model. In this operation, the total no of elements is 284,499 and the total no of nodes 414,990. The degrees of freedom (DOFs) is described at a node, which is a coordinate position in space. The degrees of freedom (DOFs) for this point reflects the potential movement of this point as a result of the structure's loading. The degree of freedom (DOF) of a node refers to different set of forces and constraints that are transferred

Table 2 Condition for stress, strain and displacement analysis for the proposed fixture

Mesh type	Solid mesh
Mesher used	Standard mesh
Automatic transition	Off
Include mesh auto loops	Off
Jacobian points	4 points
Element size	2 mm
Tolerance	0.1 mm
Mesh quality	High
Total nodes	414,990
Total elements	284,499
Maximum aspect ratio	6.0888
% of elements with aspect ratio < 3	99.9
% of elements with aspect ratio > 10	0
% of distorted elements (Jacobian)	0
Torque	250 nm
Rpm	2000

to the component through the node. In this operation, it contains high-quality mesh. The result of analysis is appropriate on 250 nm torque and 2000 rpm.

5 Implementation

Final working design as shown in Fig. 4 is fabricated with mild steel and tested on lathe 3 and 4 jaws chuck. The fixture is fully functional and can able to hold a conical or tapered workpiece.

Fig. 4 Fabricated working fixture



6 Results

The analysis results in figures with table showing the working parameters and safety of the fixture in working environment. Solid mesh of entire fixture body with 2 mm element size has been done. Different results are obtained in analysis which shows stress as critical stage of fixture as shown in Fig. 5 but elastic modulus of this fixture confirms the two times safety of the material. Von mises stress is used to find whether the given material will yield or fracture. Displacement of fixtures is safe as shown in Fig. 6. When displacement vectors are added, the result is a resultant displacement. Results show fixture is safe during machining there is negligible displacement between chuck and fixture, as shown in Table 3, 4 and 5. In Fig. 7 strain is analyzed for maximum and minimum deformation. There is no deformation occurred during the machining. Selected material is safe. There is no change in length or crack occurs and strain value is under safety. The results show the safety of material through different analysis processes as well as cost reduction as shown in Table 6.

Fig. 5 Assem1 fixture-static 1-stress-stress

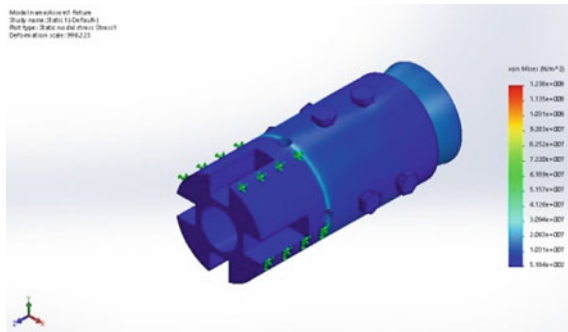


Fig. 6 Assem1 fixture-static 1-displacement-displacement

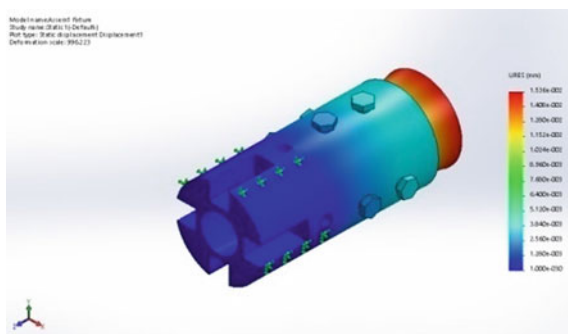


Table 3 Study results assem1 fixture-static 1-stress-stress

Name	Type	Min	Max
Stress	VON: von Mises stress	518.363 N/m ² Node: 148,644	1.23772e+008 N/m ² Node: 139,028

Table 4 Study results assem1 fixture-static 1-displacement-displacement

Name	Type	Min	Max
Displacement	URES: resultant displacement	0 mm Node: 139,084	0.0153602 mm Node: 129,551

Table 5 Study results assem1 fixture-static 1-strain-strain

Name	Type	Min	Max
Strain	ESTRN: equivalent strain	2.45517e-009 Element: 54,408	0.000484712 Element: 6872

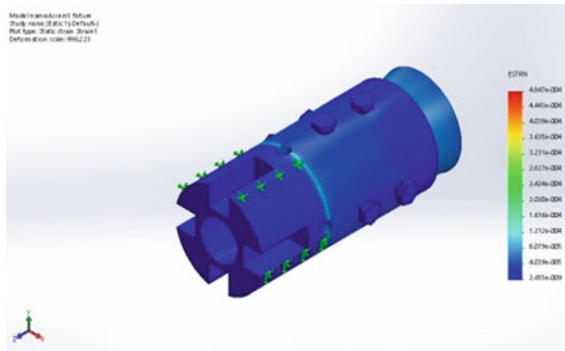


Fig. 7 Assem1 fixture-static 1-strain-strain

Table 6 Fixture specification

Specification	Fabricated fixture
Material	Mild steel
Weight	2.250 kg
Speed	2000 rpm
Components	2
Operation	One sided
Cost	3000

7 Conclusion

After finalizing the design and fabrication of this fixture it can be concluded that this fixture can hold a tapered or conical body and is ideal for 3 and 4 jaws chuck after finalizing the design and manufacturing the fixture. The loading and unloading of workpieces are simple in this fixture model because it is made up of just two parts: a cylindrical body and head bolts. The both fixture parts are manufactured using slandered manufacturing machine with process of rolling, drilling and finishing. The force acting on this fixture's body is analyzed, strain, stress and displacement are carried out in the analysis and the results show that the fixture's configuration is within the safe limit. Fixtures are important because their nature has a direct impact on efficiency and manufacturing quality. The fixture can comfortably accommodate conical bodies, allowing you to avoid purchasing several types of chucks specifically for tapered products. This would result in cost savings, increased accessibility, and the ability to perform a variety of machining processes.

References

1. Design & fabrication of a CNC lathe machine fixture for a square 7:15286–15289 (2017)
2. Apoorva MV (2016) Design and fabrication of Cnc fixture for a spring sheet component 4:106–110
3. Corrado A, Polini W (2020) Tolerance analysis tools for fixture design: a comparison. *Procedia CIRP* 92:112–117
4. Maniar NP, Vakharia DP (2012) Design & development of rotary fixture for CNC 1:32–43
5. Roy V, Kumar S (2013) Development of Lathe attachment for a CNC Machine. *J Inst Eng Ser C* 94:187–195
6. Kumara B, Ram MM (2014) Design and fabrication of lathe fixture for brake drum (cargo) machining 4:1–5
7. Pachbhai SS, Raut LP (2014) A review on design of fixtures. *Int J Eng Res Gen Sci* 2:126–146
8. Kamble VD, Tom Mathew A (2019) Brief review of methodologies for creation of cohesive fixture design. *Mater Today Proc* 22:3353–3363
9. Boyle I, Rong Y, Brown DC (2011) A review and analysis of current computer-aided fixture design approaches. *Robot Comput Integr Manuf* 27:1–12
10. Khurmi RS, Gupta JK (2005) A textbook of Garden 14
11. Sultana MN, Hasan F, Islam M (2014) Analysis of mechanical properties of mild steel applying various heat treatment. *Int Conf Mech Ind Energy Eng* 1–4

Utilization of Reinforced Palm Fibers Used for Composite Materials—A Review



Shailendra Kumar Verma, Vijay Kumar Dwivedi, and S. P. Dwivedi

Abstract Researchers and scientists have recently focused on developing a green composite material to replace traditional materials like metals, polymer, metal matrix composites, alloys, etc. Natural fibers as reinforcing materials for constructions have gotten attention in recent years because of their lower cost, environmental-friendliness, and bio-compatibility compared to fabricated fiber composite materials. This study focuses on current palm fiber investigations, collating, and reviewing data from a variety of sources. Finally, the findings from previous research were collated and analyzed, using visual, chemical, physiological, mechanical, and thermal considerations. Sugar palm, oil palm, date palm, as well as other palm species, as well as leaf extract, were included in this study. Physiological, mechanical, morphological, and thermal properties are all investigated. Palm fibers have been proven to be compatible with a wide range of reinforcing materials, such as polymer composite materials, epoxy, polypropylene, polyethylene, and high-density Portland cement, among others.

Keywords Palm fiber · Date palm fiber · Matrix composite · Green composite

S. K. Verma (✉) · V. K. Dwivedi
Department of Mechanical Engineering, Institute of Engineering & Technology GLA University,
Mathura 281406, India
e-mail: shailendra.niet@gmail.com

S. K. Verma
Department of Mechanical Engineering, Noida Institute of Engineering and Technology, Greater
Noida 201306, India

S. P. Dwivedi
Department of Mechanical Engineering, G. L. Bajaj Institute of Technology and Management,
Greater Noida 201310, India

1 Introduction

Academicians are concerned about the inclusion of natural fibers in advanced engineering endeavors attributed to the increasing requirement and necessity to reduce the use of synthetic materials in composite materials generated by petroleum resources. Natural compounds are available in all organisms, and they also have superb, interconnected, graded structures with remarkable characteristics. Engineers can benefit much by imitating these interconnected morphologies and micro-mechanisms throughout the development and continuous enhancement of composite structure's effectiveness. DPF, or date palm fiber, is a byproduct of the farming sector that is commonly grown in Saudi Arabia and Asia. After pineapple and citrus, date (*dactylifera*) was discovered to become the most vital tropical fruit available commercially around the globe. Date leaves of this plant are classified as date palm trash and are mostly utilized for the production of natural fibers [1]. The components of DPF are holocellulose (range 60–75%), lignin (around 20%), and ash (around 1.18%), which are similar to those of other lignocellulosic fibers [2]. Palm fibers are readily available in large quantities in the Mideast, but little is known about their mechanical qualities. As a result, as shown in Fig. 1, the present study will focus on the impact of palm fiber on the material characteristics of green composite, metal matrix composite, polymer composite materials. In addition, this study could provide academics with a basis for encouraging them to be using eco-friendly materials that damage the environment and cost much less conventional materials.

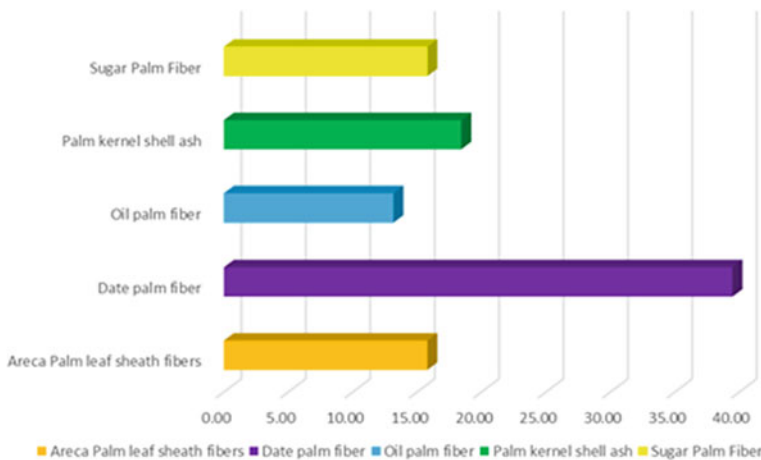


Fig. 1 Percentage utilization of palm fiber as a reinforced in various application

2 Date Palm Fiber and Its Extraction

Since ancient history, the date palm, as a part of *Palmae* (*Arecaceae*) species, has been cultivated in tropical and subtropical locations. Dates are usually generated in Egypt (1,352,950 metric tons), Saudi Arabia (1,078,300 metric tons), Iran (1,023,130 metric tons), the United Arab Emirates (775,000 metric tons), and Algeria (710,000 metric tons), all of which report significant improvements in date industrial development, producing, and utilization [3]. *Phoenix dactylifera* seems to be the longest date palm variety, reaching a height of even more, about 30 m and coming to fruition of varying sizes from 100 mm through 40 mm. The stem of a tropical date palm tree is positioned behind gray leaf bases and has several branches at its bottom. Fruits that are both luscious and nourishing. Date palms also have a specific style that makes them susceptible to a variety of situations. Date palm trees flourish on sand, but since their roots include air spaces, they may also grow in areas when moisture content is present on the surface. Date palms are usually encountered in saline environments, and their development is mostly dependent on good water and soil. Date palm fibers have been removed from leaf surfaces and plant trunks using a variety of ways. It is possible to obtain a bunch of the bast stem, leaves, and kernel from plant species, which is why it is called bundles of fibers. In both the stapled and the leaf, seed fiber extraction is the same, while in the purification stage, cotton dust is extracted. The band is obtained from stem and leaf to extract strip fiber. For separation, the decorticator method, followed mostly by the dry retting method, with chemical compounds and bioremediation, is advised for trying to remove fibers from the stem [4]. The majority of researchers have discovered useful properties for date natural fibers that rely on the fibers properties in the creation of lightweight materials for the vehicle industry. These fibers have been used in thermosetting and thermoplastic materials as an appropriate reinforcement material. Researchers have reported the ability to compete with palm fiber dates in developing biodegradable polymers appropriate for manufacturing automotive components, bio-composite materials, and green composites.

3 Literature Review of Reinforced Palm Fibers Used for Composite Materials

The consolidated review on the impact of palm fiber on the properties of the composite as a reinforcement material. A full study on the physicochemical characteristics of palm fibers was undertaken and their properties compared with those of other metal matrix materials. In addition, the mechanical characteristics of the composite based on palm fiber were discussed in Table 1. This review is important to identify the information gap and to highlight the gaps in other aspects for future research.

Table 1 Literature review of reinforced palm fibers used for composite materials

Types of palm fiber	Conclusion and result	References
Palm shell activated carbon	Aluminum matrix composite with palm shell activated carbon were fabricated by using powder metallurgy technique. Also study the worn surface analysis by using SEM and EDX	[5]
Palm oil clinker	Palm oil clinker particle reinforced aluminum matrix composites were manufactured through the powder metallurgy technique. Also investigated the sliding wear, surface morphology, and wear resistance performance of composite	[6]
Date palm fiber	DPF reinforcement polyester resin matrix composites were manufactured through resin transfer molding (RTM) processing technique. Also evaluated the mechanical properties like tensile strength, impact strength, and various critical analysis	[7]
Oil palm fiber	Fiber Metal Laminate was manufactured through oil palm fiber reinforced polypropylene and aluminum 6061. Also investigated the bond strength and share strength	[8]
Palm kernel shell ash	Palm kernel shell ash as reinforcement aluminum matrix composites was fabricated by casting technique. Also investigated the characteristics of mechanical properties through a various tests	[9]
Windmill palm fiber	The fiber board was made from windmill palm fiber (SEWPF) through the steam exploded technique. Also investigated the effect of surface morphology and chemical composition through SEM and FTTR	[10]
Oil palm fiber	Oil Palm fiber reinforced geo-polymer was investigated. Improves physical and mechanical properties of it. Also studies their microstructure through SEM	[11]
Sugar palm fiber	Cassava bagasse (CB) and SPF reinforced hybrid composite were fabricated by casting method. Also, investigates its thermal, physical, mechanical, and structural properties	[12]
Date palm fiber	Polypropylene (PP) matrix composite reinforced with date palm fiber was fabricated through heat treatment and extrusion. Also, evaluates the water absorption characteristics and the degradation phenomenon	[13]

(continued)

Table 1 (continued)

Types of palm fiber	Conclusion and result	References
Date palm fiber	Green composites with a HDPE matrix with reinforced DPF were prepared through a melt blending technique using a Laboratory Mixing Extruder instrument. Also, investigates the thermal and melt rheological properties in different loading conditions	[14]
Palm fiber	Brake composite materials reinforced with palm fiber were investigated through various testing procedures. The tribological properties were analyzed through performance parameters like pressure–speed sensitivity and temperature sensitivity	[15]
Oil palm fiber	A polypropylene (PP) matrix composite reinforced with oil palm fiber was fabricated through a thermos-kinetic mixer followed by hot pressing. Also investigated the thermomechanical properties by Testing and SEM	[16]
Sugar palm fiber (SPF)	Thermoplastic polyurethane (TPU) composites reinforced with sugar palm fiber (SPF) were fabricated by the melt-mixing compounding method. Also investigated the thermal and mechanical properties by using various fiber loadings and silane treatments	[17]
Sugar palm fiber (SPF)	Tensile tests were used to determine the tensile strength of concrete composites reinforced with sugar palm fiber. When compared to normal concrete, tensile strength rose by 19.5%	[18]
Palm fiber	The hand lay method was used to make the Ceramic Palm fiber composite out of epoxy resin. Researchers used various experiments to assess mechanical and tribological qualities	[19]
Palm fiber	The hand lay method was used to create a polymeric hybrid with epoxy coating as the matrix reinforced (Bio-composites) with glass and palm fiber. Different testing methods were used to determine the material's mechanical properties, impact strength, and hardness	[20]
Date palm tree trunk fiber	Date palm trunk fiber reinforced phenolic resin composite fiber sheet was fabricated by compression molding and investigated the mechanical properties, water absorption, flammability, and thermal gravimetric	[21]

(continued)

Table 1 (continued)

Types of palm fiber	Conclusion and result	References
Date palm fiber	The polylactic acid (PLA) reinforced with date palm fibers (bio-composite) was fabricated by solution blending using a melt compounding technique. Also, investigate the characterization by FTIR and SEM	[22]
Date palm fiber	Fourier transform infrared spectroscopy (FTIR), thermal analysis (TGA), differential scanning (DSC), and X-ray diffraction were used to evaluate the thermally and mechanical characteristics of date palm fiber (DPF) reinforcement for green composites	[23]
Date palm fiber	A mixture of cement, water, and sand was used to make cement composites reinforced with date palm fiber. The features of moisture absorption, thermal transfer, compressive, and acoustic transmission were also examined	[24]
Date palm fiber	Concrete cement reinforced date palm fiber was prepared for a specific design. and also investigate the effects of compressive strength, flexural strength, and water absorption	[25]
Date palm fibers	Epoxy composites were reinforced with fabricated date palm fiber through a three step technique. The tensile, flexural, and compression characteristics of the EDPL, EDPB, and EDPC composites were all outstanding	[26]
Palm kernel shell	Aluminum alloy 6063 was fabricated by palm kernel shell as a reinforcement through double stir casting. The density and weight of the composite can decrease with increasing palm kernel shell	[27]
Date palm fiber	Vacuum bagging technology was used to strengthen a polymeric composite with date palm fibers. The Taguchi method was also used to investigate the various mechanical characteristics	[28]
Palm kernel shell	The stir casting process was used to create AA6063 matrix composites reinforced with palm kernel shell. Dry sliding wear was also examined, as well as microstructure characterization using an optical microscope	[29]
Palmyra palm petiole fiber	Palmyra palm petiole fiber reinforced epoxy composites were fabricated by using the hand layup process in cold press molds. Also investigated the mechanical characteristics by performing various tests	[30]

(continued)

Table 1 (continued)

Types of palm fiber	Conclusion and result	References
Areca palm leaf sheath fibers	Fibers from the Areca Sheath-palm Leaf Sheath Reinforcement Epoxy. The hand lay approach was used to create Reinforcement Epoxy. The ultimate tension, bending, compressive, and toughness values of 46 MPa, 51 MPa, 54 MPa, and 87 MPa, respectively, were evaluated. SEM was used to emphasize the fiber bonding and void properties	[31]
Areca palm leaf sheath fibers	The hand lay approach was used to make green polymeric materials of areca leaf sheath (ALS) fiber with epoxy resin. Mechanical qualities (such as tensile strength and flexural strength) were also enhanced. FTIR, XRD, and SEM analyses were also explored	[32]
Date palm fiber	A surface coating procedure was used to create coated date palm fiber based on bio composite (Cs/Mt-Tbz). The impact of coating on the biomechanical, thermodynamic, morphology, and microbiological characteristics of composite materials was also examined	[33]
Date palm fiber	Composite materials were prepared using a polymer matrix and date palm fiber as reinforcement. Also, the investigation performs at a macro and micromechanical level	[34]
Date palm fiber	The Polypropylene (PP) matrix composite reinforced with date palm fiber was fabricated through a compounding process. Also investigated the FTIR studies, XRD and SEM analysis	[35]

4 Conclusions

The current investigations found that very little study has been carried in the literature to evaluate the surface properties of palm fiber reinforced composite materials, including such physical properties, mechanical properties, electrochemical characteristics, thermal expansion, scanning electron microscopy, and microstructure. The number of conclusion and findings are as follows—

- Due to reinforcement of Areca Sheath-palm Leaf Sheath Fibers the composites have improved various properties such as ultimate tensile strength, flexural strength, compression strengths, and hardness.
- Composite materials using polymer matrix and reinforced with date palm fiber are fabricating through various processing methods like resin transferred molding processing technique, melt blending technique using a Laboratory Mixing Extruder instrument, three step technique, heat treatment, and extrusion.

- Due the reinforcement of date palm fiber the composite has shown excellent mechanical properties (like impact strength, critical stress intensity factor, and Tensile strength), improve morphological and antibacterial properties.
- A hybrid composite reinforced with sugar palm fiber are fabricating through melt-mixing compounding method and molding technique.

References

1. Mahdavi S, Kermanian H, Varshoei (2010) A comparison of mechanical properties of date palm fiber-polyethylene composite. *Bio Resources* 5:2391–2403
2. AL-Oqla FM, Allothman OY, Jawaid M, Sapuan SM, Es-Saheb MH (2014) processing and properties of date palm fibers and its composites. *Biomass Bioenergy* 1–25
3. Chandrasekaran M, Bahkali AH (2013) Valorization of date palm (*Phoenix dactylifera*) fruit processing by-products and wastes using bioprocess technology–review. *Saudi J Biol Sci* 20:105–120
4. Foulk JA, Akin DE, Dodd RB, McAlister DD III (2002) Flax fiber: potential for a new crop in the Southeast. In: Janick J, Whipkey A (eds) *Trends in new crops and new uses*. ASHS Press, Alexandria, VA, pp 361–370
5. Zamri Y, Shamsul JB (2011) Analysis of worn surfaces of palm shell activated carbon (PSAC) reinforced aluminium matrix composite. *Eng e-Trans* 6(2):164–168
6. Zamri Y et al (2011) Potential of palm oil clinker as reinforcement in aluminum matrix composites for tribological applications. *Int J Mech Mater Eng* (6):10–17
7. Wazzan AA (2005) Effect of fiber orientation on the mechanical properties and fracture characteristics of date palm fiber reinforced composites. *Int J Polymeric Mater Polymeric Biomater* 54:3:213–225
8. Hussain NF, Sivakumar D, Daud MA, Selamat MZ (2015) Study of interfacial shear of aluminum/oil palm empty fruit bunch fiber reinforced polypropylene fiber metal laminates. *Appl Mech Mater* 789–790; *Trans Tech Publications, Ltd.*, pp 131–135
9. Oyediji E, Dauda M, Yaro S, Abdulwahab M (2021) The effect of palm kernel shell ash reinforcement on microstructure and mechanical properties of Al-Mg-Si metal-matrix composites. In: *Proceedings of the institution of mechanical engineers, Part C: journal of mechanical engineering science*
10. Luo H, Zhang H, Yue L et al (2018) Effects of steam explosion on the characteristics of windmill palm fiber and its application to fiberboard. *Eur J Wood Prod* 76:601–609. <https://doi.org/10.1007/s00107-017-1259-7>
11. Kroehong W, Jaturapitakkul C, Pothisiri T et al (2018) Effect of oil palm fiber content on the physical and mechanical properties and microstructure of high-calcium fly ash geopolymer paste. *Arab J Sci Eng* 43:5215–5224
12. Ahmed Edhirej SM, Sapuan MJ, Zahari NI (2017) Cassava/sugar palm fiber reinforced cassava starch hybrid composites: physical, thermal and structural properties. *Int J Biol Macromol* 101:75-83
13. Boukettaya S, Alawar A, Almaskari F, Ben Daly H, Abdala A, Chatti S (2018) Modeling of water diffusion mechanism in polypropylene/date palm fiber composite materials. *J Compos Mater* 52(19):2651–2659
14. Chafidz A, Rizal M, Kaavessina M, Hartanto D, Alzahrani SM (2018) Processing and properties of high density polyethylene/date palm fiber composites prepared by a laboratory mixing extruder. *J Mech Eng Sci* 12(3):3771–3785
15. Bernard SS, Jayakumari LS (2018) Pressure and temperature sensitivity analysis of palm fiber as a biobased reinforcement material in brake pad. *J Braz Soc Mech Sci Eng* 40:152

16. Simão JA, Marconcini JM, Mattoso LHC, Sanadi AR (2019) Effect of SEBS-MA and MAPP as coupling agent on the thermal and mechanical properties in highly filled composites of oil palm fiber/PP. *Compos Interf* 26:8:699–709
17. Atiqah A, Jawaid M, Sapuan SM, Ishak MR (2018) Mechanical and thermal properties of sugar palm fiber reinforced thermoplastic polyurethane composites: effect of silane treatment and fiber loading. *J Renew Mat* 6(5):477–492
18. Lumingkewas RH, Setyadi R, Yanita R, Akbar S, Yuwono AH (2018) Tensile behavior of composite concrete reinforced sugar palm fiber. *KEM* 777:471–475
19. Devaraju A, Murali P (2020) Experimental investigation of mechanical and tribological properties of palm fiber composite with Al₂O₃ ceramic particles. *Mater Today Proc* 22, Part 3:1161–1166, ISSN 2214-7853
20. Raju K, Balakrishnan M (2020) Evaluation of mechanical properties of palm fiber/glass fiber and epoxy combined hybrid composite laminates. *Mat Today Proc* 21, Part 1:52–55, ISSN 2214-7853
21. Kashizadeh R, Esfandeh M, Rezadoust AM, Sahraeian R (2019) Physico-mechanical and thermal properties of date palm fiber/phenolic resin composites. *Polym Compos*. <https://doi.org/10.1002/pc.25228>
22. Semlali Aouragh Hassani FZ, Ouarhim W, Raji M (2019) N-silylated benzothiazolium dye as a coupling agent for polylactic acid/date palm fiber bio-composites. *J Polym Environ* 27:2974–2987
23. Amroune S, Bezazi A, Dufresne A, Scarpa F, Imad A (2021) Investigation of the date palm fiber for green composites reinforcement: thermo-physical and mechanical properties of the fiber. *J Natural Fibers* 18(5):717–734. <https://doi.org/10.1080/15440478.2019.1645791>
24. Lahouioui M, Ben Arfi R, Fois M (2020) Investigation of fiber surface treatment effect on thermal, mechanical and acoustical properties of date palm fiber-reinforced cementitious composites. *Waste Biomass Valor* 11:4441–4455
25. Aljalawi NMF (2019) Effect of sustainable palm fiber on high strength concrete properties. In: *IOP conference series: materials science and engineering*, 518:022004
26. Alarifi IM (2020) Investigation into the morphological and mechanical properties of date palm fiber-reinforced epoxy structural composites. *J Vinyl Additive Technol*
27. Edoziuno FO, Adediran AA, Odoni BU, Utu OG, Olayanju A (2020) Physico-chemical and morphological evaluation of palm kernel shell particulate reinforced aluminium matrix composites. *Mat Today Proc*. [j.matpr.2020.03.641](https://doi.org/10.1016/j.matpr.2020.03.641)
28. Sadik, T., Muthuraman, S., Sivaraj, M., & Rajkumar, S, Experimental evaluation of mechanical properties of polymer matrix composites reinforced with date palm frond fibers from Oman. *Materials Today: Proceedings*, [j.matpr.2020.09.216](https://doi.org/10.1016/j.matpr.2020.09.216) (2020).
29. Edoziuno FO, Odoni BU, Alo FI, Nwaeju CC (2020) Dry sliding wear and surface morphological examination of an aluminium matrix composite reinforced with palm kernel shell. *Acta Metal Slovaca* 26(2):54–62
30. Mohan Kumar A, Gowthaman M, Harikrishnan M, Kesava Nanthanan A (2020) Investigation of mechanical behavior of .palmyra palm petiole fiber reinforced epoxy composites. *Mat Today Proc*. [j.matpr.2020.07.174](https://doi.org/10.1016/j.matpr.2020.07.174)
31. Ganesh S, Gunda Y, Mohan SRJ, Raghunathan V, Dhillip JDJ (2020) Influence of stacking sequence on the mechanical and water absorption characteristics of areca sheath-palm leaf sheath fibers reinforced epoxy composites. *J Natural Fibers* 1–11
32. Ashok RB, Srinivasa CV, Basavaraju B (2020) Study on morphology and mechanical behavior of areca leaf sheath reinforced epoxy composites. *Adv Comp Hybrid Mat*
33. Hassani FZSO, El Bourakadi K, Merghoub N, Qaiss AEK, Bouhfid R (2020) Effect of chitosan/modified montmorillonite coating on the antibacterial and mechanical properties of date palm fiber trays. *Int J Biol Macromol* S0141813019399829
34. Chihaoui B, Serra-Parareda F, tarrá@s Q, Espinach FX, Boufi S, Delgado-Aguilar M (2020) Effect of the fiber treatment on the stiffness of date palm fiber reinforced pp composites: macro and micromechanical evaluation of the Young's Modulus. *Polymers* 12(8):1693

35. Sh. Al-Otaibi M, Alothman OY, Alrashed MM, Anis A, Naveen J, Jawaid M (2020) Characterization of date palm fiber-reinforced different polypropylene matrices. *Polymers* 12(3):597
36. Bezazi A, Amroune S, Scarpa F, Dufresne A, Imad A (2020) Investigation of the date palm fiber for green composites reinforcement: quasi-static and fatigue characterization of the fiber. *Ind Crops Prod* 146:112135

Development of Mathematical Model of Chiller System Considering Pressure as Well as Heat Losses Using C++ Programming



Pradeep Barnwal, Anil. P. Singh, Subhash Mishra, Neeraj Kumar, Sourabh Joshi, and Vikas Tiwari

Abstract The use of chillers has been increased day by day for fulfilling various purposes. However, this increased use of chillers causes increased in energy consumption. So, it is unavoidable to enhance the performance of chillers. For achieving that goal, this study has been done, to analyze the different parameters such as refrigeration effect, COP, compressor work, etc. by comparing practical vapor compression cycle with the ideal Carnot cycle considering the different types of practical losses which occur in system. A mathematical model is developed for reaching the objective. Furthermore, the outcomes are verified by experimental data taken from a research paper. This study helps in improvement and maintenance of chiller system. The purpose of this project is to develop mathematical model of chiller system which is based on V.C.R.S. by taking heat as well as pressure losses. This system is generally based on familiar equations and parties based on parametrical and empirical correlation. The C++ programming language is used to determine the model predictions. In such way, the system allows for validating the Experimental results with Mathematical Results.

Keywords Mathematical model · V.C.R.S · COP · Mass flow rates · Validation

Nomenclature

COP	Coefficient of performance
h_j	Enthalpy of the refrigerant at point j in kJ/kg
m	Mass flow rate
ΔP_{cond}	Condenser pressure loss (kpa)
ΔP_{evap}	Loss of pressure in evaporator (kpa)
Q_{cond}	Heat rejected by condenser (kj)
Q_{evap}	Heat gain by evaporator

P. Barnwal (✉) · Anil. P. Singh · S. Mishra · N. Kumar · S. Joshi · V. Tiwari
Department of Mechanical Engineering, IPEC, U.P, GZB, India
e-mail: pradeep.barnwal@ipeec.org.in

$Q_{\text{suc}}^{\text{loss}}$	Heat lost in suction line
$Q_{\text{pc}}^{\text{loss}}$	Heat loss due to pressure loss in condenser (kj)
$Q_{\text{dis}}^{\text{loss}}$	Heat loss in discharge line (kj)
W_{comp}	Compressor work (kj/sec)
$Q_{\text{comp}}^{\text{loss}}$	Heat loss in compressor (kj/sec)
T_{wine}	Inlet water temperature of evaporator in K
T_{woe}	Outlet water temperature of evaporator in K

1 Introduction

In recent years, there is a massive increase in heat in our environment, which increases the manufacturing of chiller systems and air conditioning systems that consume high energy, most of the systems are based on the VCR system. To minimize the losses, it is essential for both of them to have effective systems and to perform them correctly. In similar manner, there is also requirement for models having low-performance costs, to evaluate the execution of any resource and that can be applied to upgrade the system performance and simulate its operation easily. Chiller model comprises a condenser, a compressor, an expansion valve and an evaporator. The condensers are mostly a shell and tube heat exchangers which exchange heat between the system and cooling water or to the atmosphere. The evaporator is most often a shell and tube type heat exchanger which transfers heat to evaporate the refrigerant. The expansion device is normally some type of regulating valve (ex-temperature, pressure) according to the type of control system used [1]. In VCR cycle, the refrigerant undergoes change of phase from vapor to liquid and then liquid to vapor in a low-grade cycle by rejecting the heat loss in the condenser and absorbing the heat in the evaporator. The COP, is a ratio of refrigeration effect to the input power by the compressor in the VCR system. The COP can be increased either by increasing the refrigeration effect or by decreasing the compressor input work [2].

By eliminating pressure losses, irreversibility losses in the compressor and heat exchangers of the model, the mathematical model considering the actual properties of cycle can be reduced to an ideal refrigeration cycle system. The Carnot cycle model is considered to be a design goal for actual systems. The main merits of theoretical study via mathematical model are that the model can be used to forecast all output variables under any conditions. Ongoing with the main aspirations of this work, this paper presented a model to forecast the execution of a VCR cycle including the various heat as well as pressure losses.

2 Literature Review

In the obtainable literature review, there is a wide variety of work that deals with modeling vapor compression cycle [3, 4]. Different type of method has been tried out for upgrading the chiller systems, as reported in literature. Focusing on the models based on Physics laws, Buzelin et al. [1] was pointed out different ways to deal with the problem of high energy consumption in commercial refrigeration systems. Performed a simulation in which the temperature is measured at various points of system and this typical “off–on” system displayed that the closed-loop power law-controlled system is having little disparity of cold chambered internal temp. allows a sharp tuning of the real temperature around setpoint temperature. In one day of testing, the 35.24% was achieved while comparing the typical system of “on–off” which is operated in same scenario.

Navarro-Esbrí et al. [2] introduced the model, which studies the variation in speed of a V.C.R.S. The model used secondary fluid variables and many other inputs, by using these parameters it produced energy performance. The model has been investigated on the different mathematical equations for each component which gives desirable results. It was proposed to predict accurately the systems performance with the help of data easily collected from commercial factories. Various predictions are based on secondary fluid input conditions temp, pressure and power consumed by compressor and the overall performance of a model of error is lower than 10%.

Cabello et al. [3] presented the work which is about the steady-state model of single-stage V.C.R.S. plant. The model has been investigated on equations that are based on actual and parametrical connections. Experiments are conducted on the model by using three refrigerants (R134a, R407C and R22). This way the model is accurately studied about the energy consumption and performance. It was observed that difference of $\pm 5\%$ for mass flow rate and $\pm 10\%$ for other energy specification.

Browne et al. [4] carried out steady-state system that is basically for the centrifugal liquid chillers. In this model, there is use of “elemental” NTU- ϵ method to both the shell and tube condenser and the overflow evaporator. In this proposal, there is division of waterside region and refrigerant side region to obtain improved heat transfer. The model has been investigated on empirical equations which are based on manufacturers and experimental data. The system is validated with the parameters from a 450 kW open drive centrifugal chiller and it was observed the difference of $\pm 10\%$.

Klein [5] stated that the Carnot Coefficient of Performance for a refrigeration system does not provide a practical maximum limit for design considerations. Another expression was obtained for the COP of a simple internal Carnot refrigeration cycle. It is also stated that limitation of drawing rule for the ideal dispersal of heat exchangers. This Coefficient of Performance considers heat transfer procedures to and from the cycle which are a necessarily an irreversible process and the study assumes that the transfer of heat occurs isothermally.

Qureshi et al [6] had worked on the combination of different coolant which is used in vapor compression refrigeration systems. The refrigerant, R134a is used in upper

and lower cycles of vapor compression system to form the best outcomes in terms of COP and other parameters and equipment of both cycles are connected in closed-loop. After modification, there is combination of refrigerant R717 with (R410A and R407C) which is considered for sub-cooler cycle and resulted in decrement in COP and other parameters. It was that found that dedicated mechanical sub-cooling was suitable for refrigerant R134a as compared to refrigerant R717.

Akintunde [9] derived a validation model that based on vapor compression refrigeration system. In this model working refrigerant (R134a) and reciprocating compressor capacity of 0.746 kW capacity are used. The model has been investigated experimentally water circulation on condenser which leads to evaporator pressure was relatively constant while the condensing pressure increases slightly. There is the variation in COP and other variables of the model and the experimental rig. The design model was validated by using test results to compare the experimental results with model-predicted results. By using the same operational conditions mass flow rates and other parameters the maximum deviations are within range of 16%.

Ongoing with the main aim of these works, this paper suggests a model forecast the performance of a vapor compression refrigeration system including the various heat losses as well as pressure losses [7–15].

Figure 1 shows the component network diagram of a VCR system considering pressure as well as heat losses in which low-pressure vapor refrigerant enters the

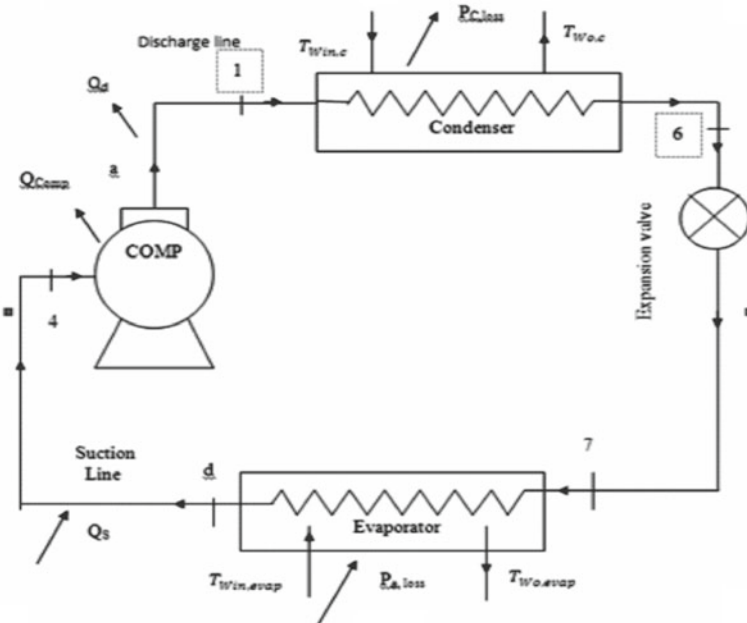
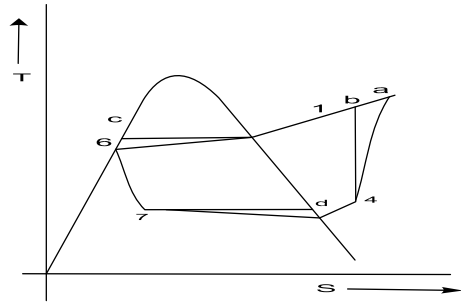


Fig. 1 Component network diagram of a vapor compression refrigeration considering losses

Fig. 2 Temperature entropy diagram of simple refrigeration cycle considering losses



compressor which compresses the refrigerant to high-pressure high temperature vapor refrigerants.

Figure 2 shows the temperature entropy diagram of simple vapor refrigeration cycle considering losses where there is a pressure loss in compressor from state *a* to *b* and in condenser from state *c* to *6*. There is also a pressure drop in evaporator from state *4* to *d*.

3 Model Development and Validation

In this part, the justification of the system utilizing experimental calculations of various steady-state is introduced. Assuming the steady-state cycle working of the model shown in Figs. 1 and 2, sat. liquid exits condenser at point 6 and refrigerant vapor enters the compressor at point 1.

$$Q_{\text{cond}} + Q_{\text{dis}}^{\text{loss}} + Q_{\text{pc}}^{\text{loss}} - (Q_{\text{evap}} + Q_{\text{suc}}^{\text{loss}} + Q_{\text{pc}}^{\text{loss}}) - (W_{\text{comp}} - Q_{\text{comp}}^{\text{loss}}) = 0 \quad (1)$$

Expansion Valve:

Process 6–7 is an isenthalpic process therefore

$$h_6 = h_7$$

h_6 is calculated from table at $(P_{\text{cond}} - \Delta P_{\text{cond}}) = P_6$

$$\Delta P_{\text{cond}} = 25\% \text{ of } P_{\text{cond}}$$

$$h_6 = h_f \text{ at } p_6, \quad t_6 = t_{\text{sat}} \text{ at } p_6$$

Evaporator:

Heat transfer from and to the system takes place by convection to the fluid streams flowing with finite rate of mass flow and specific heat. So, heat transfer rate related to effectiveness is given by

$$\begin{aligned} \epsilon &= Q_{\text{evap}}/Q_{\text{max}} \\ &= m_w \cdot C_{\text{pw}}(T_{\text{wine}} - T_{\text{woe}})/m_w \cdot C_{\text{pw}}(P_{\text{wine}} - T_7) \end{aligned} \quad (2)$$

T_7 is calculated from at.

$$T_7 = T_{\text{sat}} \text{ at } P_7, P_7 = P_{\text{evap}} + \Delta P_{\text{evap}}$$

$$\Delta P_{\text{evap}} = 30\% \text{ of } P_{\text{evap}}$$

It is assumed that the heat leaking into the suction line is

$$Q_{\text{suc}}^{\text{loss}} = m_r \times (h_4 - h_d) \quad (3)$$

$$(Q_{\text{suc}}^{\text{loss}})_{\text{evap}} = 50\% \text{ of } (Q_{\text{evap}})_{\text{ref}}$$

$$50\% \text{ of } (Q_{\text{evap}})_{\text{ref}} = (Q_{\text{evap}})_{\text{ref}} - (Q_{\text{evap}})_w$$

$$.05m_{\text{ref}} \times (h_4 - h_7) = m_{\text{ref}} \times (h_4 - h_7) - m_w \cdot C_{\text{pw}}(T_{\text{wine}} - T_{\text{woe}})$$

h_4 Can be calculated from eqn, above.

T_4 Can be calculated at h_4, P_4 from table

$$\text{RE} = m_{\text{ref}} \times (h_4 - h_7) \text{ in kW} \quad (4)$$

$$\text{Also } \epsilon = 1 - \exp^{-\text{NTU}} \quad (5)$$

$$\text{UA} = C \min . \ln(1/1 - \epsilon_{\text{cond}})$$

U_{evap} in watt/m²°C.

Compressor:

The power input to compressor is given in terms of isen. efficiency which is as follows:

$$h_a = h_4 + (h_b - h_4)/\eta_{\text{isentrope}} \quad (6)$$

$S_4 = S_b$ and $P_b = P_c$, h_b can be calculated from table.

Thus, h_a can be calculated in kJ/kg.

Heat loss in compressor:

$$Q_{\text{comp}}^{\text{loss}} = m_s(h_a - h_4) - (h_b - h_4) \quad (7)$$

Assume, $Q_{\text{comp}}^{\text{loss}} = Q_{\text{discharge}}^{\text{loss}}$

The leakage of heat from the discharge can be given as

$$Q_{\text{comp}}^{\text{loss}} + Q_{\text{discharge}}^{\text{loss}} = m_{\text{ref}}(h_a - h_1)$$

h_1 can be calculated in kJ/kg.

T_1 can be calculated in kJ/kg.

T_1 can be calculated at h_1 , P_1 , from table.

$$(W_{\text{comp}})_{\text{act}} = m_{\text{ref}}(h_a - h_4) \text{ in kW} \quad (8)$$

The Coefficient of Performance is termed as the refrigerating cooling effect by the total work input,

$$\text{COP} = \text{RE}/(W_{\text{comp}})_{\text{act}} \quad (9)$$

Condenser:

The heat transfer rate between the VCR cycle and the condenser is given by

$$(W_{\text{comp}})_{\text{ref}} = m_{\text{ref}}(h_1 - h_6) \text{ kW} \quad (10)$$

$$(Q_{\text{cond}})_{\text{ref}} = (Q_{\text{cond}})_w$$

$$m_w \cdot C_{pw}(T_{\text{woc}} - T_{\text{winc}}) \quad (11)$$

T_{woc} calculated in K.

Now, $\varepsilon = 1 - \exp(-\text{NTU})$

It is known that if one fluid is experiencing a change of phase, but the reality is that a large part of the heat exchanger in this model is in two-phase domains, we can indite from the theory of heat exchanger.

$$U_{\text{cond}} = (1/A)(C_{\text{min}} \cdot \ln(1/1 - C_{\text{cond}})) \quad (12)$$

The above equations are solved by “C++” program. The program provides the Coefficient of performance and all other parameters of model as output for the given set of input parameters given below.

Input Parameters:

Case 1:

Operating pressure of condenser and evaporator: 1385.4 kPa and 179 kPa.
 Mass flow rate of water and refrigerant (\dot{m}): 0.046 kg/sec and 0.008 kg/sec.
 Inlet water temperature in condenser and evaporator: 18.3°C.

Case 2:

Operating pressure of condenser and evaporator (P_c, P_e): 1200 and 170 kPa.
 Mass flow rate of water and refrigerant (\dot{m}): 0.046 kg/sec and 0.008 kg/sec.
 Inlet water temperature in condenser and evaporator (T_{winc}, T_{wine}): 18.3°C.

Validation of Experimental Results with Mathematical Model Result

Outputs	Mathematical result	Experimental result	Error (%)
T_1 (°C)	70	70.1	0.014
T_6 (°C)	39.5	40.8	3.18
T_7 (°C)	-7.8	-6.9	11.53
T_4 (°C)	5	10.3	51.45
COP	2.138	2.2	2.81
RE (kW)	1.159	1.134	2.20
W_{comp} (kW)	0.542	0.555	2.34
U_{cond} (watt/m ² °C)	130.951	152.2	13.9
U_{evap} (watt/m ² °C)	68.859	75.69	9.02
T_{woe} (°C)	12.575	12.4	1.41
T_{woc} (°C)	22.676	26	12.78

4 Results and Discussion

With the help of model, the performance of the VCR system can be analyzed by varying the rate of mass flow at constant inlet water temperature.

The variation also simulates the fouling condition. The study further can help in evaluating the fouling effect on various performance parameters. To prove the nature of these curves in a precise manner, all of them were fitted to perceive how close each resembles logarithmic behavior.

Figure 3 shows the refrigeration effect variation with the rate of mass flow at different inlet temperatures of water. By increasing the mass flow rate the behavior of refrigeration effect is logarithmic. Also, there is increase in refrigeration effect because the temperature difference of water also increases.

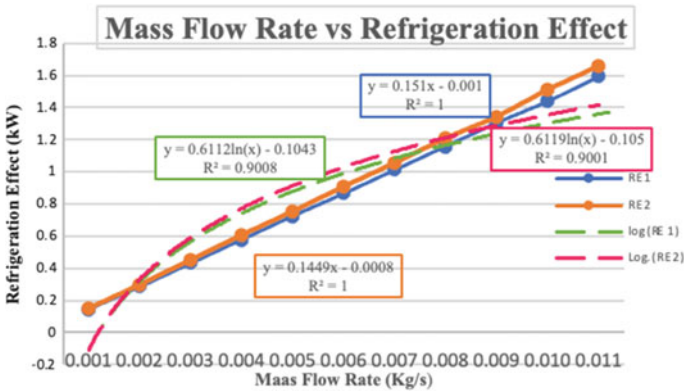


Fig. 3 Refrigeration effect versus mass flow rate

Figure 4 shows the variation of compressor work with the mass flow rate at different inlet temperatures. By increasing the mass flow rate the variation of compressor work is logarithmic and with increase in temperature, the compressor work will also increase.

Figure 5 shows the Overall Heat Transfer Coefficient variation with the rate of mass flow of water. Graph indicates the overall heat transfer coefficient of condenser and evaporator decreases with increase in rate of mass flow because the value of temperature difference decreases with mass flow rate and also reduces the amount of heat transfer.

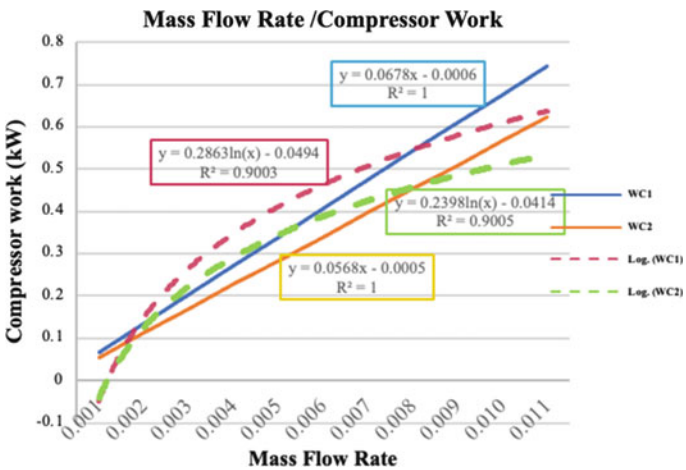


Fig. 4 Compressor work versus mass flow rate

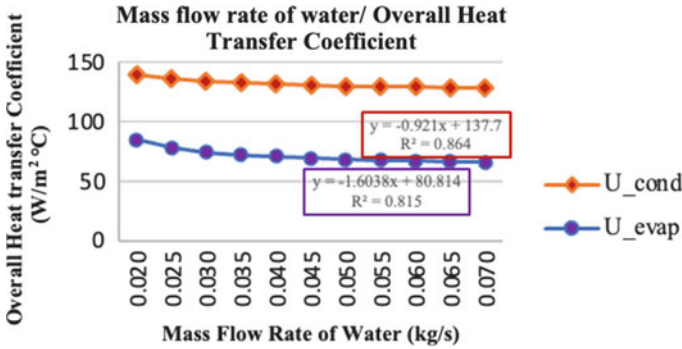


Fig. 5 Overall heat transfer coefficient versus mass flow rate of water

5 Conclusion

1. To know the reliability of developed system, the results of observed experimental data were compared with the forecasted mathematical results from the simulation by the same input parameters.
2. The computed statistical parameters show that the developed mathematical model of chiller system is promising.
3. The average value of work input to compressor, refrigeration cooling effect and COP is 0.555 kW, 1.134 kW and 2.2, respectively and error in experimental and mathematical models observed minimal.
4. The overall heat transfer coefficient of condenser and evaporator are 152.2 W/m²°C and 75.69 W/m²°C.

References

1. Kaya D, Alidrisi H (2016) Energy savings potential in air conditioners and chiller systems. *Turk J Elec Eng Comp Sci* 24:935–945
2. Sairamakrishna B, Rao TG, Krishna NR (2021) Cop enhancement of vapour compression refrigeration system. *Indian J Prod Therm Eng (IJPTE)* 1(2):2582–8029
3. Gordon JM, KC Ng (2000) *Cool thermodynamics*. Cambridge international science publishing
4. Bourdouxhe JP, Grodent M, Silva KL, Lebrun JJ, Saavedra C (1994) A toolkit for primary HVAC system energy calculation. Part 2: Reciprocating Chiller Models, *ASHRAE Transactions* 100:774–786
5. Braun JE, Mitchell JW, Klein SA, Beckman WA (1966) Models for variable speed centrifugal chillers. System simulation in buildings. In: *Proceedings of the international conference in Liege, Belgium*, pp. 83–111.
6. Beyene A, Guven H, Jawdat Z, Lowrey P (1994) Conventional chiller performance simulation and field data. *Int J Energy Res* 18:391–399
7. Zubair SM (1999) Design and performance evaluation of reciprocating refrigeration systems. *Int J Refrig* 22:235–243

8. Browne MW, Bansal PK (2001) An elemental NTU-e model for vapour compression liquid chillers. *Int J Refrig* 24:612–627
9. Jabardo JS, Mamani WG, Ianella MR (2002) Modelling and experimental evaluation of an automotive air conditioning system with a variable capacity compressor. *Int J Refrig* 25:1157–1172
10. Gordon JM, Chua HT, Ng KC (1996) Experimental study of the fundamental properties of the reciprocating chillers and their relation to the thermodynamic modelling and chiller design. *Int J Heat Mass Transfer* 39(11):2195–2204
11. Stoecker WF, Jones JW (1982) Refrigeration and air conditioning. McGraw-Hill, New York
12. Kuehn HT, Liang H (1991) Irreversibility analysis of a water-to-water mechanical-compression heat pump. *Energy* 16(6):883–896
13. Cabello R, Torrella E, Navarro-Esbri J (2004) Experimental evaluation of a vapour compression plant performance using R134a, R407C and R22 as Working Fluids. *Appl Therm Eng* 24:1905–1917
14. Cabello R, Navarro J, Torrella E (2005) Simplified steady-state modelling of a single stage vapour compression plant. Model development and validation. *Appl Therm Eng* 25:1740–1752
15. Cabello R, Navarro-Esbri J, Llopis R, Torrella E (2007) Analysis of the variation mechanism in the main energetic parameters in a singlestage vapour compression plant. *Appl Therm Eng* 27:167–176

Generation of Electricity from Sound Waves



Praveen Kumar Maduri, Avinash Kaushal Awasthi, Sachin Pandey,
and Rajneesh Mishra

Abstract This research paper traverses a very capable of being endured less standard wellspring of clean energy. Recently we have some energy harvesting methods from sound waves. Firstly, we have by creating apparatus using curtain (diaphragm), magnet, and conductor. Second, we have by converting sound energy into heat energy and then heat energy into electrical energy. Disturbance (sound) energy can be changed over into sensible wellspring of electric power by using a suitable transducer. This ought to be conceivable by using a transducer by changing over vibrations achieved by uproar into electrical energy. Piezoelectric transducers are used for change of sounds into electric energy. The conveyed electric energy from various piezoelectric transducers is taken care of in various super capacitors which are then summed up and improved through voltage multiplier circuits. In this way, unpredictable sound energy from different sources around us can be taken care of as electric energy which can be used later to pass on electric capacity to drive feasible little loads. The proposed thought can give another wellspring of harmless to the ecosystem power energy and can contribute in overall mission for maintainable force.

Keywords Sound · Piezoelectric · Electrical energy · Rectification · Amplification · Super capacitor

1 Introduction

The heart part of this device is piezoelectric crystals which is made up of quartz. In this device the sound directly fall on the very thin curtain like diaphragm through which the sound noise is converted into vibration which will directly fall on piezoelectric crystals, then these crystals generated a charge Q . Numerous sorts of sounds are regularly delivered around us from different sources. These irregular sounds assume no part aside from delivering clamors for us. In this work, irregular sound energy around

P. K. Maduri · A. K. Awasthi · S. Pandey (✉) · R. Mishra
Galgotias College of Engineering and Technology (AKTU), Greater Noida, India
e-mail: sachinpandeyei@gmail.com

us is treated as a wellspring of electric force after their productive change through appropriate transducer. A successful method of creating usable electric force from accessible irregular sound energy is introduced. Piezoelectric transducers are utilized for transformation of sounds into electric energy. The delivered electric energy from different piezoelectric transducers is put away in numerous super capacitors which are then summarized and intensified through viper and voltage multiplier circuits. The resultant electric force was used to charge a battery-powered DC battery in order to store this energy. The change circuit was tried in outside with different sound sources like train whistle in rail route station, sound delivered from a running water powered siphon, and sound delivered from development heaping. Taking all things together cases, it was discovered that battery can assume responsibility from these sound sources through the proposed change circuit from a sensible separation from the source. This distance fluctuates contingent upon the nature and power of the tried sound sources [1]. The current generated by this device is in sinusoidal form because when we applied pressure on piezoelectric crystals compressed which generated a positive pulse and when the piezoelectric crystals expand then it generated a negative pulse which leads to a sinusoidal wave. As we know that we cannot store an alternating current then this alternating current is passed through a quadruple voltage multiplier by which this alternating current is converted into DC. The current we get is smaller in amount so after passed through voltage multiplier. This current is directly stored in many super capacitors. Conductor versus superconductor versus battery. A capacitor does not hold as much charge as a battery, but it can release the charge it holds much, much faster. A battery can't hold or supply the high voltages that a capacitor can, but it can hold more charge. So basically, for voltage capacitor and for current battery, for short-term bursts a capacitor, for the long-haul a battery. Depends on what you need. Lastly, a capacitor can be charged over and over without degradation while the battery will degrade over time. But a battery will hold its energy longer than a capacitor. From this audit, clear features have been given for the late improvement on the uncommon earth materials based super capacitors to comprehend energy science of uncommon earth materials. Specifically, the uncommon earth metal oxides and hydroxides-based cathodes show better electrochemical exhibitions, and henceforth uncommon earth metal oxides/hydroxides have been composited with carbon to accomplish better capacitances. Additionally, the option of uncommon earth metals oxides joined with leading polymers and progress metal oxides has been accounted for to improve the generally speaking super capacitive exhibition, for example, energy and force densities. A nitty gritty record on various uncommon earth-based materials has been utilized as uncommon earth metal-doped, rare-earth oxides/hydroxides, uncommon earth chalcogenides, rare-earth/carbon composites, uncommon earth/metal oxide composites for super capacitor applications. Other than that, the assessment strategies for the cathode materials and super capacitor gadget exhibitions have likewise been talked about. In any case, still numerous difficulties yet exist to be addressed to control size, shape, and so on new amalgamation techniques are required for getting rare-earth-based terminal materials with controlled size and structure. These are the boundaries that must be taken care and upgraded to defeat the impediments, which thusly the uncommon

earth materials can create higher electrochemical exhibitions. In this manner, inside and out research endeavors are being completed to foster better uncommon earth-based anode materials [2]. And really lastly, capacitors are primarily intended to maintain a constant voltage in a circuit rather than being a primary supply of power. All the current stored in super capacitor is directly stored in battery through which we used our appliances.

2 Literature Review

Eco-friendly and renewable sources of production of electricity recently are wind and solar. Nowadays, there are various conventional sources to generate electricity using different natural resources such as fuels are non-renewable in nature and there is a huge scarcity of these fuels therefore, we must use these fuels wisely for sustainable development, so to overcome this challenge and with the advancement of technology, so here we proposed a device which will generate electricity using sound waves. The converter accomplished a decent productivity when contrasted with the past proposed designs [3]. Electricity will be generated by two different methods by magnets and by heat. By using magnets, we need more power to generate more electricity and by using heat method sound producing less heat due to which the output is low.

So here we proposed the third method by piezoelectric crystals in this method sound noise is used as vibrations using diaphragm and these vibrations directly fall on piezoelectric crystals then piezoelectric crystals generate ac current then using a step-up transformer then the ac current will pass through rectifier to convert ac current to dc current, then stored in super capacitors because in super capacitors current is stored faster than the battery. After storing in super capacitors, the current will finally be stored in battery which is used for any purpose. The exhibition of the circuit for various frequencies of sound was tried and it was seen that the circuit functions admirably for frequencies generally accessible from train wheels [4]. If you have an AC input, you can make a circuit out of diodes and capacitors that “stacks” the input on top of itself. This is usually what people are talking about when they talk about voltage multipliers. There’s also a circuit called a charge pump that does something like what you’re describing from a DC input. It does this by using capacitors like buckets of charge to move the charge to a higher voltage to charge up more capacitors. This requires active switching elements to control the flow of electrons into and out of the capacitors. There are also all sorts of switching converters that use a combination of inductors, capacitors, and switching elements to produce an output with a higher voltage than the input. These don’t really look anything like the feedback topology you’re imagining. The piezoelectric impact exists in two areas: the first to direct piezoelectric impact that depicts the material’s capacity to change mechanical strain into electrical charge; the second structure is the opposite impact, which is the capacity to convert an applied electrical potential into mechanical strain energy. When a material’s capacity is to change the electrical energy into mechanical strain and vice versa [5].

Past examinations on clamor are basically to control and retain commotion. There are a couple different ways to get a higher voltage out than in. AC to AC is easy. You can use a transformer to boost the voltage as high as you need. The practical limits of transformer voltage come down to the breakdown voltage of insulation. AC to DC is also pretty easy. This is probably closest to what you were describing. There are many designs but most use a ladder of rectifiers and capacitors to increase voltage. An example would be the Marx generator. DC to DC is tricky because it requires some type of active switching. There are two main types I can think of, but there are probably more. The first is the boost converter circuit. This circuit uses the kick of an inductor to generate higher voltages. It requires some type of active component to switch the inductor. The second type is called a charge pump and relies on active switching and capacitors. The input voltage is allowed to charge at least two capacitors in parallel. Depends what you mean by "better". The yield current that is produced from the piezoelectric sensor might be less, which may build the time taken for charging a battery. Yet, it very well may be utilized for charging an electronic gadget battery for crisis reason where there is no immediate wellspring of power. This can be utilized as an effective hotspot for compact electric force for versatile gadgets. This work is a minimal expense way to deal with exhibit the utilization of piezoelectric sensor to address the issue for compact electric force [6]. They can be charged and discharged much faster than batteries, but they can't store as much charge per unit mass. They are well suited applications where you want to store up charge and then release it quickly (such as camera flashes), and they can replace batteries in low-power applications, but existing lithium batteries can store much more energy for the same size device.

The dc-dc multipliers and are dependent on these cells which we are investigated. For the dc-dc multiplier, a rotational charging plan is proposed subsequently, the huge yield capacitor needed by conventional exchanged capacitor geographies can be disposed of. To increment the proficiency, a delicate exchanging plan without adding additional parts is embraced, and a variable recurrence control for the inverter is proposed to acknowledge full-range delicate exchanging. The proposed geographies and control strategies can be utilized in applications with a force range from sub kilowatts to many kilowatts [7]. Then the switching components reconnect the charged capacitors in series so that the voltage across the two is doubled. Charge pumps usually have multiple stages, so charge is pumped through the circuit, increasing in voltage as it goes along. As of late, a specific measure of exploration on clamor has been leading all around the globe. For instance, dust evacuation through commotion, clamor weapons, clamor spellbinding, commotion weeding, clamor analysis, estimating temperature through clamor, clamor refrigeration, etc. Chinese specialists have additionally acquired striking accomplishments in sound energy application, for example, the ultrasonic machining, weld dab cleaning, dust evacuation and thermos acoustic refrigeration innovation, etc. [8]. In any case, as to commotion age, it is as yet in examination stage.

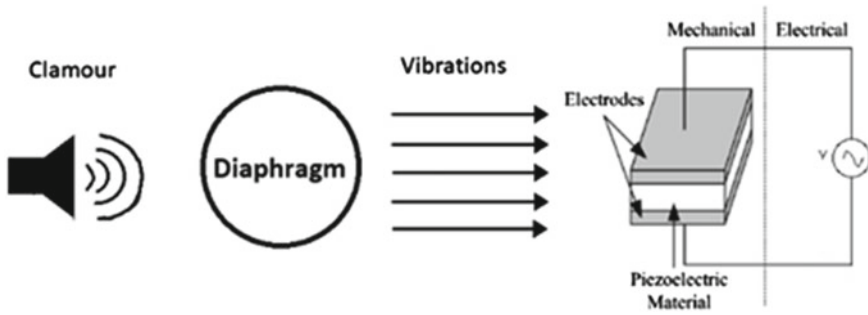


Fig. 1 Conversion of mechanical wave into sinusoidal form

3 Methodology

3.1 Conversion of Mechanical Strain into Sinusoidal Form

The clamor directly falls into a thin curtain (diaphragm) through which the sound waves is converted into vibrations which will directly fall on a parallel combination of 20 number of piezoelectric crystals. In this circuit the parallel circuit is for summing of voltage. The piezoelectric crystals work on compression and expansion method. During compression the positive cycle is generated and, in the expansion, a negative cycle is produced which will produce an electrical sinusoidal waveform. The maximum output voltage of this sinusoidal wave by a piezoelectric is 0.3 V, so the maximum output comes from the parallel combination is 6 V, as shown in Fig. 1.

3.2 Rectification and Amplification

The electrical sinusoidal waveform is passed through a quadruple voltage multiplier circuit. A quadruple voltage multiplier circuit is a combination of capacitors and diodes in such way that it converts AC electrical power from a lower voltage to a four times DC voltage of given AC voltage.

In this stage electrical sinusoidal waveform is converted into DC voltage with four times of coming AC voltage. Here we have the maximum input voltage is 6 V which means the maximum resultant voltage is obtained is 24 V, as shown in Fig. 2.

3.3 Storage

The generated voltage is directly stored in super capacitors. Super capacitors are used here due to its rapid charging and discharging property as shown in Figs. 3 and

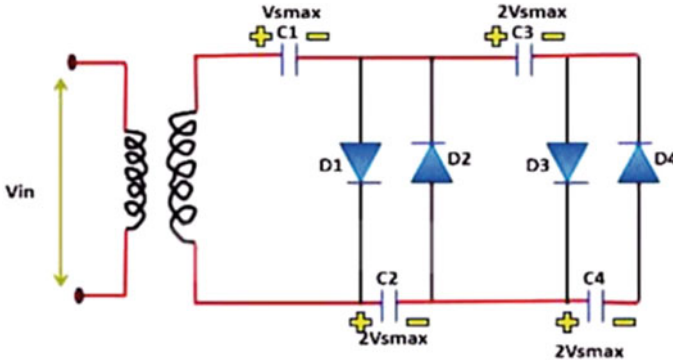


Fig. 2 Rectification and amplification circuit

4, due to which the generating DC is easily stored in super capacitors. Now all the super capacitors are directly connected to a battery through which in discharging process all the current is stored in battery. Super capacitors are better than batteries at charging quickly and then shoving out a ton of power. But batteries are better at holding large amounts of energy and releasing it slowly over time. So, if you want your laptop to last a long time without charging, you'll want to use batteries. Super capacitors are useful when you want short bursts of extra power. They store more than standard capacitors but still $100\times$ less than even conventional batteries, not to even compare to lithium ions. Battery capacities are measured in milliamp hours or amp hours for big one. Capacitors are measured in farads. Super capacitors in hundreds of farads. Historically, capacitors haven't been able to have the energy density of batteries. So chemical batteries hold more juice. Also, capacitor's voltage is directly proportional to the amount of charge they have on them. So, when they're halfway discharged, their voltage goes down to one-half of fully charged. But the voltage from a battery dip much more slowly during discharge, as shown in Figs. 3 and 4.

Fig. 3 Capacitor charging by dc supply and then stored in battery

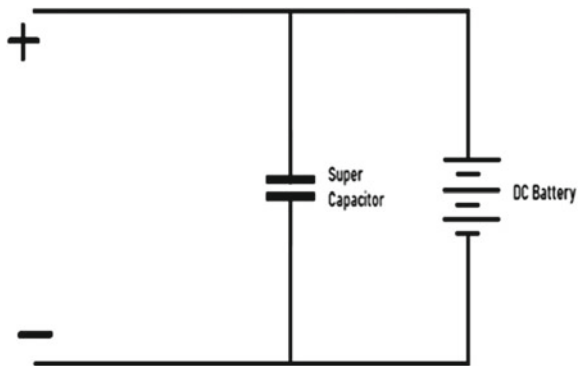
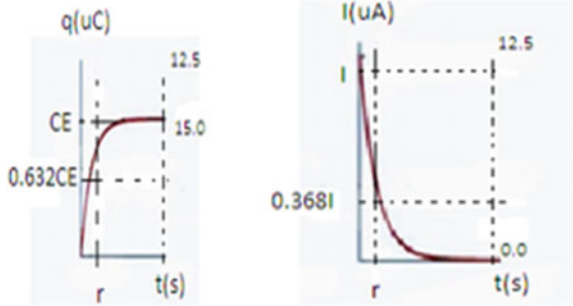


Fig. 4 Graph plotting



4 Block Diagram

Block diagram representing the flowchart has been shown in Fig. 5.

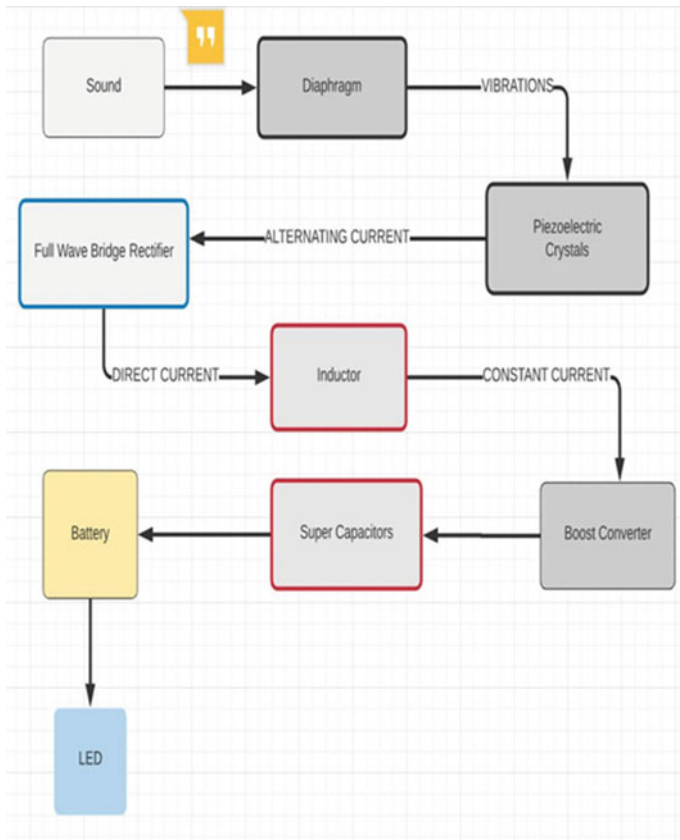


Fig. 5 Block diagram

5 Conclusion

From this project we conclude that we can harvest the electrical energy from absurd sound waves by the help of piezoelectric quartz crystals. These irregular sounds assume no part aside from delivering clamors for us. In this work, irregular sound energy around us is treated as a wellspring of electric force after their productive change through appropriate transducer. The delivered electric energy from different piezoelectric transducers is put away in numerous super capacitors which are then summarized and intensified through viper and voltage multiplier circuits. The resultant electric force was used to charge a battery-powered DC battery in order to store this energy. Taking all things together cases, it was discovered that battery can assume responsibility from these sound sources through the proposed change circuit from a sensible separation from the source. This distance fluctuates contingent upon the nature and power of the tried sound sources.

References

1. Jamal GR, Ahmed et al (2013) Generation of usable electric power from available random sound energy. In: 2013 international conference on informatics, electronics and vision (ICIEV). IEEE
2. Arunachalam S et al (2020) Research progress in rare earths and their composites-based electrode materials for supercapacitors. *Green Energy Environ* 5(3):259–273
3. Alcazar, Acosta YJ et al (2008) High voltage gain boost converter based on three-state switching cell and voltage multipliers. In: 2008 34th annual conference of IEEE industrial electronics. IEEE
4. Arnab MMB et al (2014) Generation of electrical energy using piezoelectric material from train wheels: Bangladesh perspective. In: 2014 9th international forum on strategic technology (IFOST). IEEE
5. Sodano HA, Inman DJ, Park G (2004) A review of power harvesting from vibration using piezoelectric materials. *Shock Vib Digest* 36(3):197–206
6. Livingston J, Hemlatha M (2014) Charging an electronic gadget using piezo-electric material. *Indian J Sci Technol*
7. Zou K, Scott MJ, Wang J (2012) Switched-capacitor-cell-based voltage multipliers and DC–AC inverters. *IEEE Trans Ind Appl* 48(5):1598–1609
8. Halper MS, Ellenbogen JC (2006) Supercapacitors: a brief overview, 1. The MITRE Corporation, McLean, Virginia

Identification of Process Parameter Combination for Maximum Tensile Strength in 3D Printed Polylactic Acid Specimens Using Regression and ANOVA



Manohar Singh and Pushpendra S. Bharti

Abstract This work aims at studying the effect of various inputs like infill density, layer thickness, speed of printing, and nozzle temperature on tensile strength of the Poly Lactic Acid (PLA) specimen printed using Fused Deposition Modeling (FDM) process technique. Experiments have been conducted using a variety of different combinations of influencing parameters chosen from Taguchi's L16 orthogonal array. A regression-based mathematical model has been developed to establish relationship between output and input variables. The significance of input parameters in terms of degree of influence on tensile strength has been determined using Analysis of variance (ANOVA). It has been observed that the input parameters in layer height, print speed, and nozzle temperature are more significant than other parameters. Additionally, factorial plots have been utilized to determine the effect of each input parameter on the output, namely the tensile strength. Moreover, Taguchi analysis was done to find the best combination of input parameters for maximum Tensile strength. It has been observed that maximum value of Tensile Strength can be obtained at print speed of 50 mm/s, layer thickness of 0.2 mm, infill density of 100%, and nozzle temperature of 220 °C. The results obtained from Taguchi Analysis have been experimentally validated.

Keywords Analysis of variance (ANOVA) · Fused deposition modeling (FDM) · Poly lactic acid (PLA) · Regression analysis (RA)

1 Introduction

Additive Manufacturing is gaining momentum mainly because of ease of printing complex parts. Among the available methods, fused deposition modeling (FDM) is preferred due to its low cost and ability to employ filaments made of a variety

M. Singh (✉) · P. S. Bharti
U.S.I.C.T., Guru Gobind Singh Indraprastha University, Delhi 110078, India
e-mail: manoharmnr@gmail.com

M. Singh
Galgotias College of Engineering and Technology, UP 201310, India

of thermoplastics, including polylactic acid (PLA). The mechanical properties of the printed objects vary with process parameters, thus attracting the interest of numerous researchers for optimization of parameters for best mechanical properties. The parameters studied by prominent researchers include layer thickness [1–7], orientation [1, 2, 5, 7–9], raster angle1, [3, 5, 9, 10], raster width [1, 3], air gap1, feed rate [2], print speed [9, 10], filling ratio [4, 9, 10], nozzle temperature [9], nozzle diameter [9] and shell number [9]. Sood et al. found that strength decreases with decrease in layer thickness while smaller raster angle results in better strength. Chacon, et al. noticed increase in mechanical characteristics as layer thickness is increased while it decreased when feed rate was reduced. According to Rajpurohit et al. raster angle and width have significant effect on tensile strength of PLA specimens. Mustafa et al. found tensile strength to be influenced most by filling ratio followed by raster angle and speed of printing. Camargo et al., Valena et al., and Boni et al. found that mechanical qualities rise as layer thickness increases. Yao et al. discovered that increasing the layer thickness results in a decrease in tensile strength. According to Gonabadi et al., orientation of build and infill density are critical parameters.

2 Proposed Methodology

The proposed methodology consists of four stages. In the first stage, process parameters, machine, and material has been identified. Second stage consists of design of the experiment. The third stage is printing of specimens. Following that, the tensile strength of the printed specimen is determined. In the last stage, data has been analyzed by generating mathematical model using regression using the data obtained by experiments. The significant and non-significant process parameters are identified by using ANOVA. Then the optimum combination of process parameters is observed for maximum tensile strength using ANOVA. Finally, the obtained combination is verified experimentally. The recommended methodology is shown in Fig. 1.

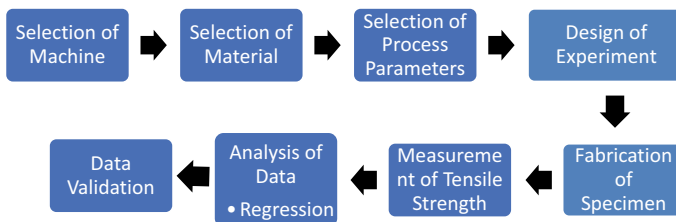


Fig. 1 Methodology

Fig. 2 Printed Samples



3 Material and Methods

The specimens for tensile test were printed as per ASTM D638 [11] standards. For this, the 3D model has been generated and converted to .stl (Stereolithography) file format using Autodesk Inventor. Flash Print software has been used for slicing and controlling the machine parameters of Flash forge Dreamer NX printer. Four levels of the four input variables, i.e., print speed, layer thickness, infill density, and nozzle temperature [12] have been identified. One set of printed specimens is shown in Fig. 2.

4 Fabrication and Testing

Three specimens each for combinations as per L16 orthogonal array, as per the design of experiments, have been printed. The testing of the specimens has been done using NTF Tensile, Compression, and Flexural Strength Tester (Fig. 3). This type of machine is generally used for measuring the tensile s, flexural and compressive strengths. For tensile test, the specimen has been gripped at both ends and one end has been pulled, at constant rate, by ever-increasing load until failure. The peak force, elongation at peak, and tensile strength have been recorded for each test. Table 1 shows various combinations of parameters and their respective tensile strengths.

5 Mathematical Modeling

A mathematical model has been generated using regression analysis. The model can be used to figure out the relationship between output-input parameters. It can also be used for predicting the output for any given set of parameters.

Fig. 3 NTF tensile, compression, and flexural strength tester



Table 1 Test results of all specimens

Specimen no	Layer thickness (mm) A	Print speed (mm/s) B	Infill density (%) C	Nozzle temperature (°C) D	Tensile strength (Kg/mm ²)
1	0.2	50	70	190	3.735
2	0.2	100	80	200	4.025
3	0.2	150	90	210	3.988
4	0.2	200	100	220	3.400
5	0.25	50	80	210	3.688
6	0.25	100	70	220	3.366
7	0.25	150	100	190	1.615
8	0.25	200	90	200	2.452
9	0.3	50	90	220	4.576
10	0.3	100	100	210	3.567
11	0.3	150	70	200	1.904
12	0.3	200	80	190	1.291
13	0.35	50	100	200	3.585
14	0.35	100	90	190	1.558
15	0.35	150	80	220	2.945
16	0.35	200	70	210	1.751

5.1 Regression Modeling

Many researchers have employed regression modeling to identify the input–output relation with MINITAB17 software while maintaining the correction factor as 95. Equation 1 and Table 2 show the developed model and related ANOVA with an R sq value of 86.08%. The ANOVA table shows that the regression model has a P-value of less than 0.05, which is extremely significant [13]. Also, P values are less than 0.05 for input parameter thicknesses, speed of print, and nozzle temperature, suggesting that they are significant parameters. Figure 4 shows the normal regression analysis probability plot. The image in Fig. 4 indicates that the data distribution is normal over the range.

Table 2 Analysis of variance

Source	DF	Adj SS	Adj MS	F-value	P-value
Regression	4	14.1562	3.5391	17.01	0.00
Layer thickness (A)	1	3.0851	3.0851	14.82	0.003
Print speed (B)	1	6.1239	6.1239	29.43	0.00
Infill density (C)	1	0.295	0.295	1.42	0.259
Nozzle temperature (D)	1	4.6523	4.6523	22.36	0.001
Error	11	2.2892	0.2081		
Total	15	16.4454			

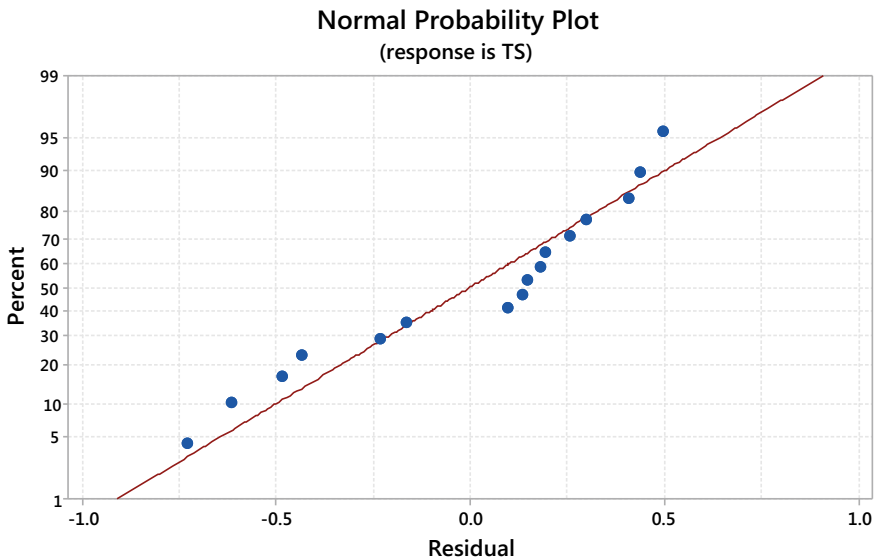


Fig. 4 Normal probability plot

Table 3 Response table for signal-to-noise ratio

Level	Layer thickness (A)	Print speed (B)	Infill density (C)	Nozzle temperature (D)
1	11.546	11.77	8.112	5.42
2	8.458	9.384	8.758	9.142
3	8.017	7.788	9.217	9.816
4	7.297	6.376	9.232	10.941
Delta	4.249	5.394	1.12	5.521
Rank	3	2	4	1

$$\begin{aligned} \text{TensileStrength} = & -4.41 - 7.86 \times A - 0.01107 \times B \\ & + 0.0121 \times C + 0.0482 \times D \end{aligned} \quad (1)$$

5.2 Taguchi Analysis

Taguchi analysis [12, 14] has been carried out for L16 orthogonal array. The response table for signal-to-noise ratio is shown in Table 3. It is evident from Table 3 that any change in nozzle temperature impacts the Tensile strength most followed by speed of printing, layer thickness, and infill density. Main effect plot for signal-to-noise ratio is shown in Fig. 5. It is observed from Table 3 that the optimum value of Tensile Strength can be obtained at layer thickness of 0.2 mm, print speed of 50 mm/s, infill density of 100%, and nozzle temperature of 220 °C. From Table 3 it is noticed that a layer thickness of 0.2 mm, print speed of 50 mm/s, infill density of 100%, and nozzle temperature of 220 °C offer the optimal value of tensile strength.

6 Results and Discussion

The mathematical model has been developed using regression using which we can predict the value of tensile strength for any given set of parameters. In order to understand the effect of individual parameters on the output, i.e., tensile strength, main effect plot for tensile strength has been plotted (Fig. 6). As seen in the figure, the tensile strength decreases with increase in layer thickness and speed of printing while it increases with increase in infill density and nozzle temperature. When the layer thickness is kept minimum then the number of layers will be more and hence it will increase the tensile strength. An increase in the speed of printing will allow less time for solidification and bonding between two successive layers will be weaker leading to decrease in tensile strength. Similarly, higher infill density increases the tensile strength as the mass of the specimen increases. Higher nozzle temperature

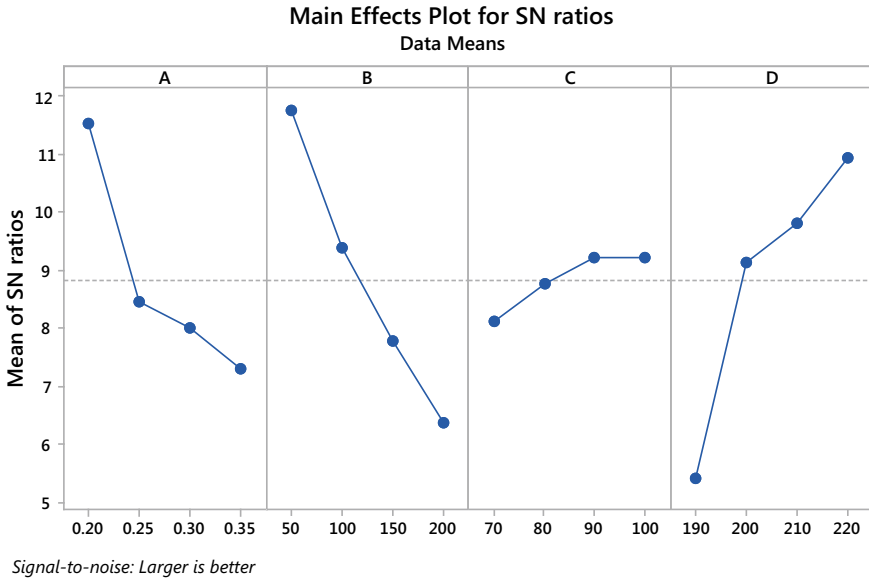


Fig. 5 Main effect plot for SN ratios

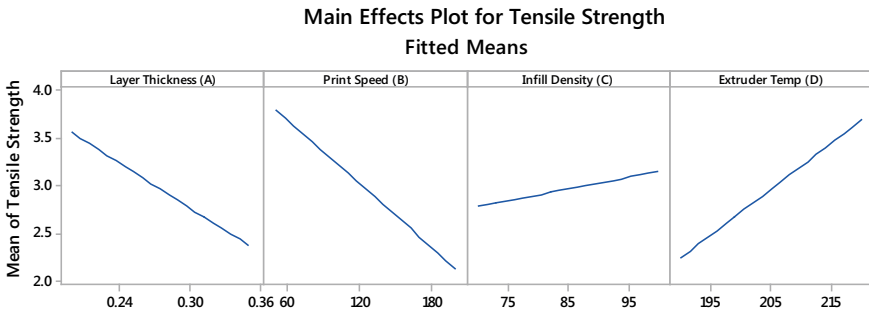


Fig. 6 Main effect plot for tensile strength

ensures proper melting of the filament leading to smooth flow and better adhesion properties as a result tensile strength increases with increase in nozzle temperature.

From Taguchi analysis it was observed that maximum value of Tensile Strength can be obtained at layer thickness of 0.2 mm, print speed of 50 mm/s, infill density of 100%, and nozzle temperature of 220 °C. To validate this a sample has been printed for above parameters and the value of tensile strength measured is 4.896 kg/mm², which is the highest.

7 Conclusions

In this study, an effort is being made to determine the input parameter values that give optimum tensile strength to PLA sample prepared on an FDM-based printer. Taking into consideration L16 orthogonal design, the samples were produced. For the development of regression and ANN models, experimental values of tensile strength have been used. The analysis reveals that:

1. The regression analysis demonstrates that the thickness of each layer, printing speed, and nozzle temperature have a greater influence on the output than the other input factors.
2. 86.08% of the R-sq regression score shows that the tensile value for a given set of input parameters can be anticipated quite accurately.
3. Taguchi Analysis shows that a maximum tensile strength value may be achieved at a thickness of each layer (0.2 mm), 50 mm/s printing speed, 100% infill density, and a temperature of the nozzles (220 °C).
4. The validation result shows that the obtained value of tensile strength is maximum for the parameters obtained from Taguchi analysis.

References

1. Sood AK, Ohdar RK, Mahapatra SS (2010) Parametric appraisal of mechanical property of fused deposition modelling processed parts. *Mater Des* 31(1):287–295. <https://doi.org/10.1016/j.matdes.2009.06.016>
2. Chacón JM, Caminero MA, García-Plaza E, Núñez PJ (2017) Additive manufacturing of PLA structures using fused deposition modelling: effect of process parameters on mechanical properties and their optimal selection. *Mater Des* 124:143–157. <https://doi.org/10.1016/j.matdes.2017.03.065>
3. Rajpurohit SR, Dave HK (2018) Analysis of tensile strength of a fused filament fabricated PLA part using an open-source 3D printer. *Adv Manuf* 6(4):430–441. <https://doi.org/10.1007/s40436-018-0237-6>
4. Camargo JC, Machado ÁR, Almeida EC, Silva EFMS (2019) Mechanical properties of PLA-graphene filament for FDM 3D printing. *Int J Adv Manuf Technol* 103(5–8):2423–2443. <https://doi.org/10.1007/s00170-019-03532-5>
5. Yao T, Deng Z, Zhang K, Li S (2019) A method to predict the ultimate tensile strength of 3D printing polylactic acid (PLA) materials with different printing orientations. *Compos B Eng* 163:393–402. <https://doi.org/10.1016/j.compositesb.2019.01.025>
6. Boni R, Martelli L, Massa M, Mascandola C, Petronio L (2020) Novel mechanical models of tensile strength and elastic property of FDM AM PLA materials: experimental and theoretical analyses. *Eng Geol* 105722. <https://doi.org/10.1016/j.enggeo.2020.105722>
7. Vălean C, Marşavina L, Mărghitaşl M, Linul E, Razavi J, Berto F (2020) Effect of manufacturing parameters on tensile properties of FDM printed specimens. *Procedia Struct Integr* 26(2019):313–320. <https://doi.org/10.1016/j.prostr.2020.06.040>
8. Gonabadi H, Yadav A, Bull SJ (2020) The effect of processing parameters on the mechanical characteristics of PLA produced by a 3D FFF printer. *Int J Adv Manuf Technol* 111(3–4):695–709. <https://doi.org/10.1007/s00170-020-06138-4>

9. Hikmat M, Rostam S, Ahmed YM (2021) Investigation of tensile property-based Taguchi method of PLA parts fabricated by FDM 3D printing technology. *Results Eng* 11(100264):1–10
10. Günaya M (2019) Modeling of tensile and bending strength for Pla parts produced by Fdm. *Int J 3D Print Technol Digital Ind* 3(3):204–211
11. ASTM D638-14, Standard Test Method for Tensile Properties of Plastics, ASTM International, West Conshohocken, PA, 2014, www.astm.org
12. Singh M, Bharti PS (2021) Parametric influence of process parameters on the wear rate of 3D printed polylactic acid specimens. *Indian J Pure Appl Phys* 59(03):244–251
13. Bharti PS, Maheshwari S, Sharma C (2012) Multi-objective optimization of die-sinking electric discharge machining. *Appl Mech Mater* 110–116:1817–1824. <https://doi.org/10.4028/www.scientific.net/AMM.110-116.1817>
14. Pant M, Singari RM, Arora PK, Moona G, Kumar H (2020) Wear assessment of 3-D printed parts of PLA (polylactic acid) using Taguchi design and artificial neural network (ANN) technique. *Mat Res Express* 7(11). <https://doi.org/10.1088/2053-1591/abc8bd>
15. Kumar S, Ghoshal SK, Arora PK (2020) Optimization of process variables in electric discharge machining (EDM) using Taguchi methodology. *Indian J Eng Mat Sci* 27(4):819–825

Flammability and Moisture Absorption Behavior of Sugarcane Bagasse with Epoxy-Based Composite



Nitin Mukesh Mathur, Yashpal, and Akshay Jain

Abstract Ease of availability and due to various specific properties of composite materials, their demand is increasing day by day. Composites are used in various applications such as in food packaging, building construction, etc. that is why various analysis is necessary before use. In his paper, we studied flammability and moisture absorption behavior without treated sugarcane bagasse fiber composite with low temperature curing epoxy resin (AW 106) chemically belongs to the “epoxide” family and corresponding hardener (HV 953U) for different fiber volume fractions as 0, 6, 12, 18% and for 5 mm constant thickness. Samples of size 300 mm × 300 mm were fabricated by hand layup process. The fire resistance test has been performed according to ASTM D 635-03 standards. The burning rate is calculated in mm/min. The moisture absorption test has been conducted as per ASTM D 570-98 standard. It has been observed that with the increase in volume fraction, fire resistance and moisture absorptions increase.

Keywords Sugarcane Bagasse · Epoxy resin · Composite materials · Hand lay method · Flammability test · Moisture resistance property

1 Introduction

Due to regular increasing demand for traditional materials, their depletion attracts researchers to find alternate sources of materials that do not harm environment, which are reusable, recyclable, and biodegradable [1–3]. Green composite plays a vital role with its specific properties and abundance in nature. Various works have done on natural fibers such as orange fiber, banana fiber, sisal fiber, wood fiber,

N. M. Mathur (✉)
Poornima University, Jaipur, Rajasthan 302020, India
e-mail: nitinmukesh@poornima.org

Yashpal
School of Engineering & Technology, Poornima University, Jaipur, Rajasthan 302020, India

A. Jain
Poornima College of Engineering, Jaipur, Rajasthan 302020, India

[4, 5]. Composites based on natural fibers are easily available, light weight, have, etc. acceptable tensile, flexural, and other mechanical properties, inexpensive and easy to produce [6–8]. They are extensively used in various applications such as in aerospace, marine, automobile parts, and structure and in nonstructural applications like window and door frames, panels, roof tiles, partition walls, deck materials, etc. Although they have commendable properties they have also some limitations such as moisture content [9, 10]. Natural composite materials are although hydrophobic in nature yet they have poor bonding between matrices and fiber. This effect can be minimized by various chemical treatments [7]. Natural fiber based composites are also poor in fire resistance properties, which can be improved by adding magnesium hydroxide [11, 12].

2 Materials and Methods

2.1 Materials

Resin and hardner have been purchased from Mahaveer hardware, Jaipur. Sugarcane bagasse fibers have been procured from sugarcane.

2.2 Preparation of Fiber

Sugarcane bagasse fibers have been left in sunlight for 48 h. Then washed with hot water to remove impurities and other dust particles. It has been crushed into small particles by using hand grinder. To maintain uniformity of thickness, sieve shaker machine has been used. After performing the operation on sieve shaker Particle of size 3–5 mm has been extracted and used for experimental purposes [13].

2.3 Fabrication of Composites

Samples of composite have been fabricated by hand layup technique. Composite has been fabricated of size 300 mm × 300 mm as per ASTM standard. Resin and hardener (10:8) are properly mixed with different volume fractions of filler materials like 0, 06, 12, 18%. It was observed that at the above percentage amalgamation of fiber took place in samples. The samples have been cured at room temperature for 48 h. After curing process specimen has been prepared as per ASTM standards for testing.



Fig. 1 Flammability sample testing of a horizontal specimen

3 Experimentation

3.1 Flammability Test

Toper form fire resistance test, samples have been prepared with size 125 mm × 13 mm × 5 mm. The test has been performed as per ASTM D 635 standards. For the test, First sample has been hold in horizontal direction and distances has been marked at 25 mm apart from free edge [3, 14]. Stop watch has been used for time calculation. Fire resistance capacity has been calculated in mm/min. The burning rate has been calculated by dividing total marked burned length with the time taken into burning process. Figure 1 represents the flammability test (Table 1 and Fig. 2).

3.2 Moisture Absorption Test

Moisture absorption test has been performed as per ASTM D 670 standard. Samples of size 76.4 × 25.4 x 5 mm have been prepared. Weight of samples has been taken

Table 1 Time taken and burning rates of different volume fractions

Filler percentage (A) (%)	Flammability rate at mm/min (B)	Time taken for burning	Time taken for burning	Time taken for burning	Time taken for burning
		0–25 mm in Second (C)	25–50 mm in Second (D)	50–75 mm in Second (E)	75–100 mm in Second (F)
0	19.3	57	151	245	316
6	19.1	65	143	223	311
12	16.6	80	144	255	362
18	12.04	348	674	801	932

Fig. 2 Burning rates of different volume fractions samples

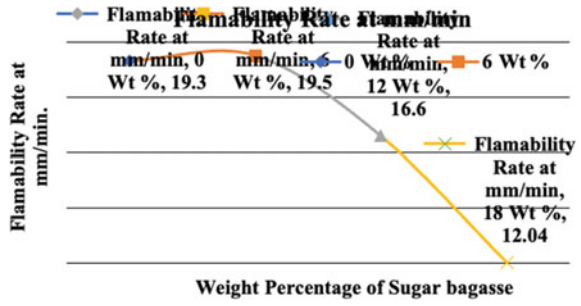


Table 2 Weight taken (Before and after) of different volume fractions

Filler percentage (%)	Moisture absorption (%)	Weight before test	Weight after test (g)
0	49.19	9.45	9.76
6	49.25	11.97	12.33
12	49.34	11	11.29
18	49.52	14.71	14.99

in vertical position in distilled water for 24 h. After 24 h, sample has been wiped properly with cotton cloth after that weight has been taken. Then difference between the two weights has been calculated for calculation of absorbed moisture [15–28] (Table 2, Figs. 3 and 4).



Fig. 3 Sample for water absorption test

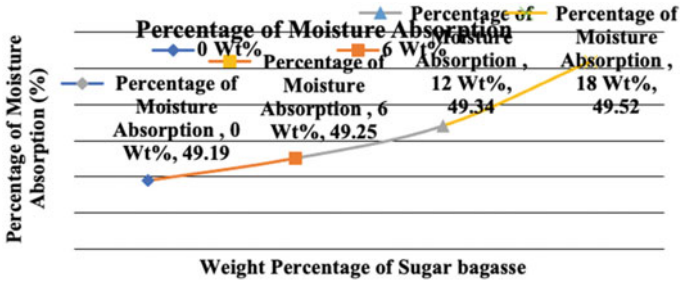


Fig. 4 Moisture absorptive rate for different fiber volume fractions

4 Results and Discussions

Sugarcane bagasse as a natural filler has been used in epoxy and sample has been tested for fire and moisture absorption test. Results show that rate of burning decreased with the increased percentage of fiber volume. At 18% volume fraction burning rates are found lower due to compactness of fibers with epoxy. Samples burned with blackish smoke with unpleasant smell and finally converted into ash.

Moisture absorption test is also shown by graph, which indicated that with increasing volume fraction percentage, moisture absorption also increases due to good absorption capacity of natural fibers. This shows that to reduce water absorption, chemical treatment is necessary. Chemical treated composites are less moisture absorber due to reduction in hydroxyl groups in fiber cell walls. Moisture absorption can be increased by proper chemical treatment of the filler materials.

5 Conclusions

In this study, Testing of partial green composite based on sugarcane bagasse with epoxy-based composite with different volume fractions has been conducted. Fire resistance and water absorption tests have been performed as per ASTM standards. Graph indicates that burning rates demonstrated decreasing trend with increasing fiber volume percentage. In water absorption test, graph shows an increasing movement with increase in fiber volume fraction. An optimum fiber volume fraction must be chosen to balance all properties including mechanical and other properties. Sugarcane fiber composites can be used in various applications such as in aerospace, marine, automobile parts, and structure and in nonstructural applications like window and door frames, panels, roof tiles, partition walls, deck materials but limiting their use in bathroom and kitchen which are disposed to water and fire, respectively.

Acknowledgements The authors would like to thank CRED, Poornima University for providing us Support.

References

1. Tutuşluk H Improvement of flame retardant characteristic of raw silk fabric. The evaluation of Balkan countries clothing trade with eu-28 based on the analysis of comparative advantages indices, p 199
2. Ganesh S, Gunda Y, Mohan SRJ, Raghunathan V, Dhillip JDJ (2020) Influence of stacking sequence on the mechanical and water absorption characteristics of areca sheath-palm leaf sheath fibers reinforced epoxy composites. *J Natural Fibers* 1–11
3. Dhibar B, Singh SV, Anwar S, Singh A (2018) Sugarcane bagasse reinforced polyester composites
4. Nanthakumar K, Yeng CM, Chun KS (2020) Tensile and water absorption properties of solvent cast biofilms of sugarcane leaves fibre-filled poly (lactic) acid. *J Thermoplast Compos Mater* 33:289–304
5. Agung E, Hamdan M, Siregar JP, Bachtiar D, Tezara C, Jamiluddin J (2018) Water absorption behaviour and mechanical performance of pineapple leaf fibre reinforced polylactic acid composites. *Int J Autom Mech Eng* 15:5760–5774
6. Wirawan R, Sapuan S (2018) Sugarcane bagasse-filled poly (Vinyl Chloride) composites: a review. In: *Natural fibre reinforced vinyl ester and vinyl polymer composites*. Elsevier, pp 157–168
7. Tripathi P, Kumar D (2016) Study on mechanical behaviour of sugarcane bagasse fiber reinforced polymer matrix composites. *SAMRIDDHI J Phys Sci Eng Technol* 8:34–42
8. Cerqueira E, Baptista C, Mulinari D (2011) Mechanical behaviour of polypropylene reinforced sugarcane bagasse fibers composites. *Procedia Eng* 10:2046–2051
9. Al Bakri A, Liyana J, Norazian M, Kamarudin H, Ruzaidi C (2013) Mechanical properties of polymer composites with sugarcane bagasse filler. In: *Advanced materials research*, pp 739–744
10. Mulinari DR, Voorwald HJ, Cioffi MOH, Da Silva MLC, da Cruz TG, Saron C (2009) Sugarcane bagasse cellulose/HDPE composites obtained by extrusion. *Compos Sci Technol* 69:214–219
11. Ramlee NA, Jawaid M, Zainudin ES, Yamani SAK (2019) Tensile, physical and morphological properties of oil palm empty fruit bunch/sugarcane bagasse fibre reinforced phenolic hybrid composites. *J Market Res* 8:3466–3474
12. Aigbodion V, Hassan S, Agunsoye J (2012) Effect of bagasse ash reinforcement on dry sliding wear behaviour of polymer matrix composites. *Mater Des* 33:322–327
13. Ribeiro Filho SLM, Oliveira PR, Panzera TH, Scarpa F (2019) Impact of hybrid composites based on rubber tyres particles and sugarcane bagasse fibres, *Compos Part B Eng* 159:157–164
14. Candido VS, da Silva ACR, Simonassi NT, da Luz FS, Monteiro SN (2017) Toughness of polyester matrix composites reinforced with sugarcane bagasse fibers evaluated by Charpy impact tests. *J Market Res* 6:334–338
15. Bansal G, Singh V, Patil P, Rastogi S (2016) Water absorption and thickness swelling characterization of chicken feather fiber and extracted fish residue powder filled epoxy based hybrid biocomposite. *Int J Waste Res* 6:1–6
16. Mulinari DR, Voorwald HJ, Cioffi MOH, Rocha GJ, Da Silva MLCP (2010) Surface modification of sugarcane bagasse cellulose and its effect on mechanical and water absorption properties of sugarcane bagasse cellulose/HDPE composites. *BioResources* 5(2):661–671
17. Paiva JM, Frollini E (2002) Sugarcane bagasse reinforced phenolic and lignophenolic composites. *J Appl Polym Sci* 83(4):880–888
18. Loh YR, Sujun D, Rahman ME, Das CA (2013) Sugarcane bagasse—the future composite material: a literature review. *Resour Conserv Recycl* 75:14–22
19. Leman Z, Sapuan SM, Saifol AM, Maleque MA, Ahmad MMHM (2008) Moisture absorption behavior of sugar palm fiber reinforced epoxy composites. *Mater Des* 29(8):1666–1670
20. Hu RH, Sun MY, Lim JK (2010) Moisture absorption, tensile strength and microstructure evolution of short jute fiber/polylactide composite in hygrothermal environment. *Mater Des* 31(7):3167–3173

21. Ferguson T, Qu J (2003) Moisture absorption analysis of interfacial fracture test specimens composed of no-flow underfill materials. *J Electron Packag* 125(1):24–30
22. Chen X, Zhao S, Zhai L (2005) Moisture absorption and diffusion characterization of molding compound
23. Shen CH, Springer GS (1976) Moisture absorption and desorption of composite materials. *J Compos Mater* 10(1):2–20
24. Li Y, Sun Y, Qiu J, Liu T, Yang L, She H (2020) Moisture absorption characteristics and thermal insulation performance of thermal insulation materials for cold region tunnels. *Construct Build Mat* 237:117765
25. Wong EH, Rajoo R (2003) Moisture absorption and diffusion characterisation of packaging materials—advanced treatment. *Microelectron Reliab* 43(12):2087–2096
26. Wong KJ, Johar M, Koloor SSR, Petrú M, Tamin MN (2020) Moisture absorption effects on mode II delamination of carbon/epoxy composites. *Polymers* 12(9):2162
27. Cruz J, Leitão A, Silveira D, Pichandi S, Pinto M, Figueiro R (2017) Study of moisture absorption characteristics of cotton terry towel fabrics. *Procedia Eng* 200:389–398
28. Lundgren JE, Gudmundson P (1999) Moisture absorption in glass-fibre/epoxy laminates with transverse matrix cracks. *Compos Sci Technol* 59(13):1983–1991

Progressive Collapse: A Review and Bibliometric Analysis



Md Osaid Arshad, Shilpa Pal, and Mohammad Umair

Abstract Progressive collapse is a promising field for structural engineers and researchers, earning the attention, especially after 9/11 incident. The aim of this paper is to use bibliometric techniques and network analysis tools to critically examine and review the documented work in the larger framework of progressive collapse. To develop a clear understanding and evaluate the study area linked with progressive collapse, this study uses a comprehensive literature approach followed by bibliometric analysis. The analysis of keywords and their co-occurrence network depicts critical approach to understanding topics in trends in this field. The three fields plot illustrates main elements, i.e., researchers, keywords, sources, and their interconnectivity. The bibliographic coupling and co-citations analysis depict correlation degree between articles and intellectual structure as well as the evolution and research variations over the span of time. In addition, this study makes recommendation for future research in the area of progressive collapse.

Keywords Progressive collapse · Bibliometric analysis · Biblioshiny · Vosviewer · Co-citation · Three field plot

1 Introduction

Progressive collapse can be described as a series of smaller events that end in partial collapse or entire structure collapse disproportionate to the original local damage. The early local damage could be loss or damage of a vertical load-carrying element such as column or load-bearing wall. There are many worldwide catastrophic progressive collapses that drew the attention of structural engineers as well as researchers. Few of them are Ronan Point Apartment in 1968, Alfred P. Murrah Building, Oklahoma city in 1995, and World Trade Center, New York in 2001 [1].

Md Osaid Arshad (✉) · S. Pal
Department of Civil Engineering, Delhi Technological University, Delhi 11042, India
e-mail: osaid.sepc@gmail.com

M. Umair
Department of Civil Engineering, Jamia Millia Islamia, Delhi, New Delhi 110025, India

Despite the fact that research in the field of progressive collapse is on the rise, bibliometric analysis approaches have not been used to review and analyze the topic of progressive collapse. To fill this void, this paper examines the available literature in the broader field of progressive collapse dating back to 2002 using bibliometric analysis. Bibliometric report reveals prominent participating authors, territories, associations, publications, and primary keywords. It detects and classifies significant specific research on citations and total link strength. It suggests future study directions related to numerous sub-disciplines of concerned research areas.

Marjanishvili [1] applied four different methods for the analysis of progressive collapse and compared each other in terms of advantages and disadvantages. The methods are linear elastic static, linear elastic time history, nonlinear static, and nonlinear time history analysis. Out of which nonlinear time history analysis is the most comprehensive and exhaustive method whereas static linear elastic is the simplest one. Xiao et al. [2] employed new method “virtual thermal pushdown analysis” in progressive collapse of RC structure. In it, displacement-temperature curve is produced that shows the real nonlinear relation between the structural performance (vertical displacement) and quantity of reinforcement. The quantity of reinforcement at the specified performance target is thus directly determined using this curve. Lim et al. [3] developed an analytical model to predict the resistance of affected structures under progressive collapse and provided a quick check for suitability of progressive collapse resistance in order to avoid remaining structure damage by propagation of local failure. Tsai et al. [4] reported that with the rise-time effect in consideration, an approximate analytical formulation for the maximum dynamic response is obtained based on the work-energy principle. The correctness and validity of the suggested formulation are evaluated using displacement and the force-based dynamic increase factors (DIFs) of a single-degree-of-freedom model and a clamped steel beam. The DIFs decrease as the rise-time increases and with higher ductility demand, the rise-time effect also drops according to the results of the analysis. Mohajeri et al. [5] presented a simpler theoretical model for assessing RC frames after the removal of the middle column. The suggested model predicts the general behavior of an RC frame in four stages when the middle column is removed. It is observed that the practical and theoretical results accord well. The suggested model is straightforward, practical, and easy to grasp, which reduces computation time and simplifies the prediction of RC frame ultimate capabilities. Elsanadedy et al. [6] reported the progressive collapse-resistant capacity of steel moment-resisting frames using alternate path methodologies prescribed in US General Services Administration (GSA) and Department of Defense (DoD) guidelines. For comparison, linear static and nonlinear dynamic analysis methodologies were used. The nonlinear dynamic analysis provided bigger structural reactions than the linear analysis, and the findings changed considerably based on factors such as location of column removal, number of building stories, or applied load, as compared to the linear analysis results. Gombeda et al. [7] used external blast threats in a threat-dependent progressive collapse assessment on building frames for mapping structural damage. The studied behavior of structural components (especially the columns) to a blast-induced pressure and time history is used to map structural damage. For direct shear, flexure, and breach failure

modes, this model can be utilized to analyze the ultimate damage status of crucial column locations. Feng et al. [8] performed sensitivity analysis on RC structure under column removal case. They used Tornado diagram for capacity of tensile catenary action and compressive arch action with respect to compressive strength of concrete, diameter of bar, and yield strength of reinforcement, these parameters depicted significant effect on the capacity of progressive collapse behavior. Azim et al. [9] predicted capacity of RC building behavior in terms of catenary action using gene expression programming (GEP). In this study, the input influential parameters were selected as stiffness of relative rotational restraints and relative axial restraints, ratio of double beam length to depth, and longitudinal rebar's yield strength. For pre-design objectives, GEP's recommended formulation is found to be simple, sturdy, and straightforward to use. Li et al. [10] investigated robustness analysis of RC structure based on building height influence. They found that high-rise building is more robust with respect to lower stories building with initial column removal of corner column on lowest floor. Li et al. [11] proposed probability index of collapse to evaluate the resistance of progressive collapse in RC structures. Instead of assessing any specific beginning local failures, such an index can measure all usual initial local failures. The fragility curve of collapse is further defined by this index, which fluctuates as nominal gravity increases. Feng et al. [12] proposed a new method named probability density evolution method (PDEM) to investigate structural reliability and structure response in terms of progressive collapse behaviour. Under pushdown method of column removal case, structure's robustness and reliability indices are calculated and the effects of position of first damage scenarios on the robustness are examined. Sasani [13] performed finite element method (FEM) and Applied energy method (AEM) based analysis employing the removal case of simultaneous two outer columns to evaluate local as well as global deformations on a six-story RC frame structure. As per the response, the displacement is around 1.8 times that achieved when the infills are modeled using shell elements and element cracking is taken into account.

Adam et al. [14] performed the experimental analysis on a full-scale RC cast-in-situ building structure exposed to a sudden column failure for corner location is described in their work. After the corner column was abruptly removed, the structure was able to discover effective alternate load routes, and the observed dynamic amplification did not cause substantial structural damage. The peak dynamic values were significantly greater than the stabilized residual values following the time-history test, according to the results. For the case under investigation, the flexural and Vierendeel beam actions were the most common alternate load paths (ALPs) in the test whereas slab membrane action was not an important ALP. To investigate the differences between the UDL's resisting mechanisms, Tuan et al. [15] performed progressive collapse experiments under a corner column removal scenario on a two-fifth scale RC frame with slab by quasi-static loading. For evaluation of the resilience of beam-slab substructures to progressive collapse, Kai and Li [16] conducted practical research on three quarter-scale samples for RC frames with slabs. To forecast the dynamic displacement of specimens in dynamic phase, single degree of freedom (SDOF) models are used. It was discovered that SDOF could accurately forecast peak

dynamic displacement while overestimating vibration and underestimating permanent residual deformation. Yu et al. [17] conducted an experiment on two specimens, made of seven beams and two square slabs under column removal case of penultimate exterior and middle perimeter. Progressive collapse resistance, as well as the mechanism of load transfer of the frame, were shown using proper instrumentation. Sadek et al. [18] examined the performance of steel and reinforced concrete beam-column assemblies under monotonic vertical movement of a middle column, representing a column removal scenario experimentally as well as computationally. The assemblies are parts of ten-story structural framing systems intended for seismic design categories C and D, respectively, as intermediate moment frames (IMFs) and special moment frames (SMFs). Lim et al. [19] performed experiment to investigate the role of slabs in the resistance and behavior of frame-slab systems exposed to point loads for corner column loss has been studied. It is found that on top of the frame's maximum flexural capacity, the slab flexural capacity added roughly 55 percent more capacity, and tensile membrane action could not be activated which is indicated by no compressive ring formation. Joshi and Patel [20] used precast dry connection with one-third scale of the assembly and compared its performance with that of monolithic dry connection in their experiment. They concluded that the building did not respond dissimilar to the monolithic construction and thus, this could be used as a good option for the cast-in-situ construction.

2 Research Methodology

The primary focus of this research is on the exploration of bibliography used to analyze and classify the field of progressive collapse of RC structure literature. The goal of the bibliometric study is to employ network maps to quantitatively analyze a research, particularly on progressive collapse in order to provide meaningful insights into how this topic has evolved over time. The current study used vosviewer and biblioshiny for bibliometric and network analysis.

3 Data Source

The research data is taken from scopus database by searching keywords like “progressive collapse analysis”, “RC building”, “Nonlinear dynamic analysis”, etc. Initially, documents sources were journals, book chapters, books, conference reviews, review papers, and later books chapters and books are excluded and time span is limited to 2002–2021. Here, Table 1 depicts basic information on data source and its type.

Table 1 Primary information of data

Description	Outcomes
Time duration	2002:2021
Sources	203
Documents	531
Average years from publication	5.75
Mean citations/paper	13.14
Mean citations/year/paper	1.883
References	11,758
Article	362
Conference paper	143
Conference review	21
Review	5

4 Result Analysis

Using biblioshiny in R package bibliometrix and vosviewer are employed for network and bibliometric analysis [21, 22] to show the following key results which are elaborated with relevant figures.

4.1 Three Fields Plot

Using a Sankey diagram, three fields plot represents the important elements in three fields namely authors, keywords, and journals and it also shows the way they are linked. The left field shows the source or journal name and middle one represents author’s name who contributes to the research publication. The right field element depicts research topic. The size of rectangle reflects the huge number of research articles linked to each of these parts. It is shown in Fig. 1.

Most cited countries in the field of progressive collapse in construction engineering are USA, China, and Singapore among the top three in the list based on data analysis in biblioshiny.

4.2 Bibliographic Coupling

The term bibliographic coupling was first introduced by M. M. Kessler in 1961 and it is defined as “a single item of reference shared by two documents and it is defined as a unit of coupling between them” [23]. The current study focused on bibliographic coupling of sources with weightage of documents and coupling of documents based

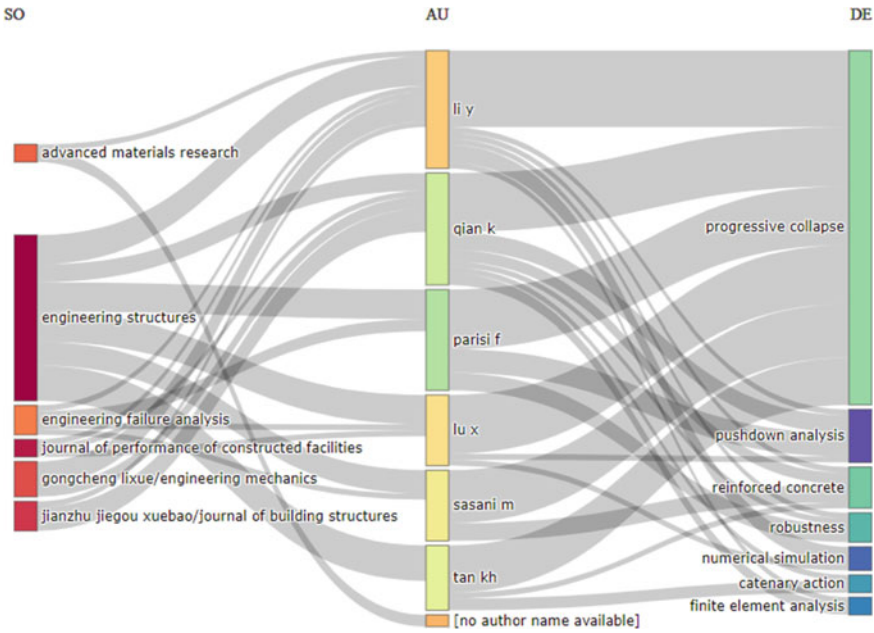


Fig. 1 Three fields plot

on citations. Here 22 sources are clustered into six groups with different color codes and threshold limit of five documents as shown in Fig. 2.

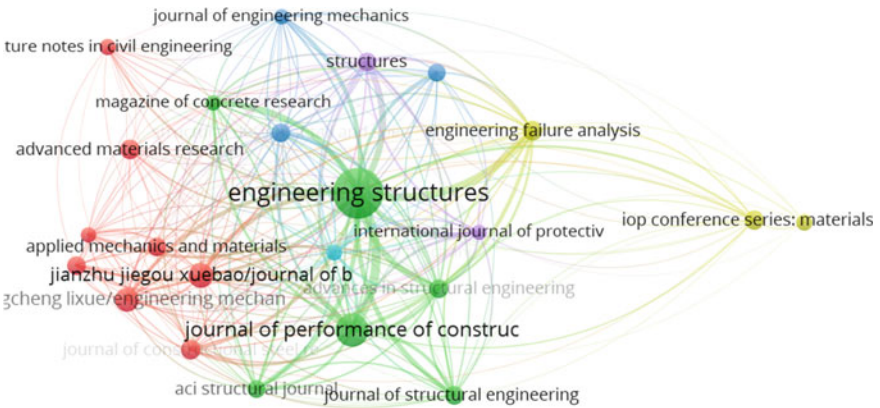


Fig. 2 Bibliographic coupling of Sources

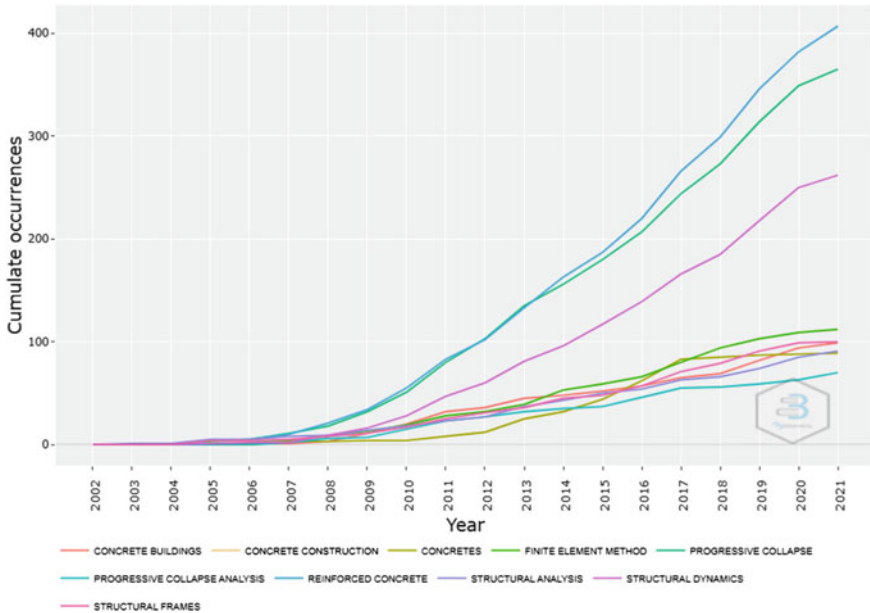


Fig. 3 Word growth

4.3 Keywords Analysis

The keyword analysis in paper is a critical approach for understanding the trend in the field and name of academics concentrating their efforts [24]. This inquiry is required since keywords of publication help in quickly establishing a publication topic and its focus areas. Figure 3 depicts the word dynamics of the title, abstract as well as writer’s most frequently used keywords.

4.4 Co-citation Analysis

The term “co-citation analysis” refers to a method of determining that authors, journals, keywords, and themes all have a link. It is used to determine the correlation degree between two different articles. When two papers contain one or more of the same references, this is known as a co-citation [25]. If this technique is employed in publications, it reveals a field’s intellectual structure as well as the evolution and research variations over the span of time. On the other hand, when applied to writers, co-citation analysis reveals the structure of their social interactions [26].

in R package and vosviewer tool. The following conclusions have been reached based on the current research.

- The respective top three sources, i.e., engineering structures, journal of performance of constructed facilities, and engineering failure analysis have been identified on the basis of bibliographic coupling with weightage of total document counts.
- As per the word growth analysis, reinforced concrete, progressive and structural dynamics are fastest growing keywords in structural engineering. The sub-research areas of progressive collapse are robustness, reliability, numerical simulation, and finite element analysis.
- USA, China, and Singapore, respectively are the top three among the most cited countries with main research topic of progressive collapse.

The limitations of the current study are that book chapters and book materials are excluded and research span is taken from 2002 to 2021. Apart from it, data is taken from scopus database, thus some peer-reviewed documents might have been missed. More comprehensive research connections between intellectuals and institutions may be required to have a more effect on progressive collapse possibilities for improved educational opportunities.

References

1. Marjanishvili S (2004) Progressive analysis procedure for progressive collapse. *J Perform Constr Facil* 18. [https://doi.org/10.1061/\(ASCE\)0887-3828\(2004\)18:2\(79\)](https://doi.org/10.1061/(ASCE)0887-3828(2004)18:2(79))
2. He X-H-C, Yi W-J, Yuan X-X (2019) A non-iterative progressive collapse design method for RC structures based on virtual thermal pushdown analysis. *Eng Struct* 189:484–496. ISSN 0141-0296, <https://doi.org/10.1016/j.engstruct.2019.03.102>
3. Lim NS, Tan KH, Lee CK (2018) A simplified model for alternate load path assessment in RC structures. *Eng Struct* 171:696–711. <https://doi.org/10.1016/j.engstruct.2018.05.074>
4. Tsai M-H, Lin B-H (2008) Dynamic amplification factor for progressive collapse resistance analysis of an RC building. *Struct Des Tall Special Build* 18:539–557. <https://doi.org/10.1002/tal.453>
5. Mohajeri Nav F, Usefi N, Abbasnia R (2017) Analytical investigation of reinforced concrete frames under middle column removal scenario. *Adv Struct Eng* 21(9):1388–1401. <https://doi.org/10.1177/1369433217746343>
6. Elsanadedy HM, Al-Salloum Y, Almusallam T, Ngo TD, Abbas H (2019) Assessment of progressive collapse potential of special moment resisting RC frames—experimental and FE study. *Eng Failure Anal* 105. <https://doi.org/10.1016/j.engfailanal.2019.07.045>
7. Gombeda MJ, Naito CJ, Quiel SE, Fallon C (2016) Blast-induced damage mapping framework for use in threat-dependent progressive collapse assessment of building frames. *J Perform Constr Facil* 31:04016089. [https://doi.org/10.1061/\(ASCE\)CF.1943-5509.0000949](https://doi.org/10.1061/(ASCE)CF.1943-5509.0000949)
8. Feng D-C, Xie S-C, Deng W-N, Ding Z-D (2019) Probabilistic failure analysis of reinforced concrete beam-column sub-assembly under column removal scenario. *Eng Fail Anal* 100:381–392. ISSN 1350-6307. <https://doi.org/10.1016/j.engfailanal.2019.02.004>
9. Azim I, Yang J, Iqbal MF, Mahmood Z, Javed MF, Wang F, Liu Q-F (2021) Prediction of catenary action capacity of RC beam-column substructures under a missing column scenario using evolutionary algorithm. *KSCE J Civ Eng* 25:891–905. <https://doi.org/10.1007/s12205-021-0431-0>

10. Shan L, Petrone F, Kunnath S (2019) Robustness of RC buildings to progressive collapse: Influence of building height. *Eng Struct* 183:690–701. ISSN0141-0296, <https://doi.org/10.1016/j.engstruct.2019.01.052>
11. Li Y, Lu X, Guan H, Ren P, Qian L (2016) Probability-based progressive collapse-resistant assessment for reinforced concrete frame structures. *Adv Struct Eng* 19(11):1723–1735. <https://doi.org/10.1177/1369433216649385>
12. Feng D-C, Xie S, Xu J, Kai Q (2020) Robustness quantification of reinforced concrete structures subjected to progressive collapse via the probability density evolution method. *Eng Struct* 202(109877):2019. <https://doi.org/10.1016/j.engstruct.109877>
13. Sasani M (2008) Response of a reinforced concrete infilled-frame structure to removal of two adjacent columns. *Eng Struct* 30:2478–2491. <https://doi.org/10.1016/j.engstruct.2008.01.019>
14. Adam JM, Buitrago M, Bertolesi E, Sagaseta J Moragues JJ (2020) Dynamic performance of a real-scale reinforced concrete building test under a corner-column failure scenario. *Eng Struct* 210. <https://doi.org/10.1016/j.engstruct.2020.110414>
15. Tuan PA, Lim N, Tan K-H (2017) Investigations of tensile membrane action in beam-slab systems under progressive collapse subject to different loading configurations and boundary conditions. *Eng Struct* 150:520–536. <https://doi.org/10.1016/j.engstruct.2017.07.060>
16. Kai Q, Li B (2017) Dynamic and residual behavior of reinforced concrete floors following instantaneous removal of a column. *Eng Struct* 148:175–184. <https://doi.org/10.1016/j.engstruct.2017.06.059>
17. Yu J, Tang J-H, Luo L-Z, Fang Q (2020) Effect of boundary conditions on progressive collapse resistance of RC beam-slab assemblies under edge column removal scenario. *Eng Struct* 225:111272. <https://doi.org/10.1016/j.engstruct.2020.111272>
18. Sadek F, Main JA, Lew HS, Bao Y (2011) Testing and analysis of steel and concrete beam-column assemblies under a column removal scenario. *J Struct Eng* 137(9):881–892
19. Lim NS, Tan KH, Lee CK (2017) Experimental studies of 3D RC substructures under exterior and corner column removal scenarios. *Eng Struct* 150:409–427. ISSN 0141-0296, <https://doi.org/10.1016/j.engstruct.2017.07.041>
20. Joshi DD, Patel PV (2019) Experimental study of precast dry connections constructed away from beam–column junction under progressive collapse scenario. *Asian J Civ Eng* 20(209–222):2019. <https://doi.org/10.1007/s42107-018-0099-z>
21. Aria M, Cuccurullo C (2017) Bibliometrix: an R-tool for comprehensive science mapping analysis. *J Informetrics* 11(4):959–975. ISSN 1751-1577, <https://doi.org/10.1016/j.joi.2017.08.007>
22. Van Eck NJ, Waltman L (2010) Software survey: VOSviewer, a computer program for bibliometric mapping. *Scientometrics* 84(523–538):2017. <https://doi.org/10.1007/s11192-009-0146-3>
23. Kessler M (2017) An experimental study of bibliographic coupling between technical papers (Corresp.). *IEEE Trans Inf Theory* 9(1):49–51, January 1963. <https://doi.org/10.1109/TIT.1963.1057800>
24. Song Y, Chen X, Hao T, Zhinan L, Lan Z (2019) Exploring two decades of research on classroom dialogue by using bibliometric analysis. *Comput Educ* 137. <https://doi.org/10.1016/j.compedu.2019.04.002>
25. Walter C, Ribiere V (2013) A citation and co-citation analysis of 10 years of KM theory and practices. *Knowl Manage Res Pract* 11. <https://doi.org/10.1057/kmnp.2013.25>
26. Haleem A, Khan MI, Khan S, Jami AR (2020) Research status in Halal: a review and bibliometric analysis. *Modern Supply Chain Res Appl*. Ahead-of-print. <https://doi.org/10.1108/MSCRA-06-2019-0014>
27. Esfahani HJ, Tavasoli K, Jabbarzadeh A (2019) A Big data and social media: a scientometrics analysis. *Int J Data Netw Sci* 145–164. <https://doi.org/10.5267/j.ijdns.2019.2.007>

Analysis of Double Wishbone Suspension System Using MechAnalyzer



Abhay Dhar Dubey, Shubham Verma, and Pramod Kumar

Abstract Double wishbone suspension system is generally used to avoid any defect on the body of a vehicle from irregularities on the roads. This helps comfort the people and can obviate the shocks that come from wheel through the lower body of vehicle's shaft. It transfers the force from wheel to the wishbone suspension system which works on the basis of four-bar mechanism. By using MechAnalyzer software the four-bar mechanism of the system analysis has been done. Analysis of how it can be reduced in size by using different materials. The size of linkage and selection of material has been decided on the basis of result from analysis done on the software.

Keywords Double wishbone suspension system · Four-bar mechanism · MechAnalyzer

1 Introduction

The double wishbone suspension system works on the basis of four-bar mechanism, it consists of linkage, springs, and shock absorbers which obviate the shock of wheel by absorbing the force which produces due to irregularities on roads. It is independent suspension system which means both the wheels are independent of one another. It provides height from the surface of road to the body, it acquires all the load of the body of the vehicle, it provides smooth traveling for the people, and it sets apart from the shocks [1]. The life of the material used in suspension systems increased by using better material which will analyze calculation of their mechanical value like fatigue, torsional effect, young's modulus, etc. Double wishbone system is known for providing comfort to the people who drive the vehicle. Due to the quality of independent suspension system, there is no connection between one wheel to another one. If one makes up down one manages to be smooth oneself. There are many obstacles on the road especially in India what we have to do as mechanical engineers, add suspension systems to the vehicles it will become easy life.

A. D. Dubey (✉) · S. Verma · P. Kumar
Department of Mechanical Engineering, Galgotias University, Greater Noida, Uttar Pradesh, India
e-mail: abhaydubey484@gmail.com

In this research paper what has been done is to accentuate the size of the suspension system which is not considered in the other literature, and also the strength of material on the basis of their mechanical properties by using some mechanical formula like fatigue, torsional effect and young's modulus, etc.

In this paper, the analysis of the double wishbone suspension system is done using the MechAnalyzer. The positions, velocity acceleration, and the force of suspension system are analyzed [2]. The graphs for the various links and joints are analyzed in the results and discussions. MechAnalyzer is a software developed by IIT Delhi to perform the kinematics and dynamics analysis of the different mechanisms. It is being used in this work to perform kinematic analysis of the four-bar mechanism on which the double wishbone suspension system is based. The four-bar mechanism applied in the system is described as follows.

It consists of four linkages that connect each other and move in a parallel plane. It is the simplest movable closed chain linkage. It has three moving links, one fixed link, and four pinpoints. There is only one constraint on the linkage, which defines a definite motion. This mechanism has many applications, that is, to convert reciprocating motion to the rotational motion and constrain motion [3]. In this system, the mechanism is used to convert the reciprocating motion to constraint one.

The suspension systems play very crucial role in the overall performance of an automobile. There are numerous types of suspension systems here the use of most common and major types of the suspension system. Now the explanation of functions of suspension system has been done as follows.

1.1 Functions of Suspension System

The functions of suspension system need to be understood to analyze it and hence those are discussed below.

Maximizing the traction: Maximizing the traction is one of the functions of suspension system. The contact of all wheels with the ground by enabling the wheels to move independently with respect to the body or frame of the vehicle. Hence, maximizing the control and the power utilization [4]. If suspension were not there, there would have been the scenarios wherein one of the wheels would lose contact with the ground hence losing power.

Improving steering stability: The vehicle, while steering a car or taking a turn, is pushed outside due to the centrifugal force and hence it tends to topple sideways. This tendency can result in loss of handling and control over the vehicle. The suspension systems reduce these unwanted movements and hence enhance handling. If there were no suspension system there would be simply toppling off while turning hard and could go rolling away with vehicle.

Providing passenger comfort: The passenger can take nap or drink water or work on a laptop while riding a vehicle. The suspension system dampens the shocks that

are generated from the ground reactions due to the bumps on the road and hence increases the passenger's comfort [5]. Without suspension, there would be going all over the up and downs even on the slightest rough road.

Summarizing all the functions in one sentence, the suspensions keep the vehicle body and frame stable by absorbing the forces imposed because of different road scenarios and vehicle motion.

As we discussed in the introduction, the space from road to body of the vehicle sometimes becomes very large due to the suspension system. We are trying to reduce this by decreasing the size of the linkage connected in the suspension systems without affecting its result which will be analyzed on MechAnalyzer software.

1.2 Motions of Frame and Body

To perform different tasks the suspension system must control the dynamics of the vehicle by overcoming four main motions of the frame and body of the vehicle namely dive, squat, roll, and yaw. Let us understand these four motions with respect to the cartesian system shown in Fig. 1.

Motion with respect to X-axis runs in the direction of motion of the vehicle the Y-axis runs perpendicular to the direction of vehicle motion that is from the driver to the co-driver and the Z-axis runs perpendicular to the road plane.

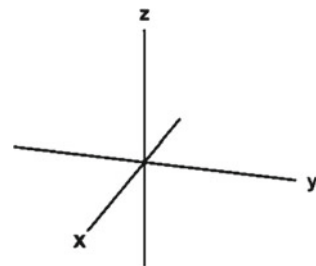
Dive: Dive occurs due to longitudinal weight transfer toward the front of the vehicle that is in motion about Y-axis. The motion during longitudinal weight transfer toward the rear of the vehicle again about Y-axis which occurs during acceleration and it is known as squat.

Roll: Roll is the motion due to lateral weight transfer which means rotation about X-axis this occurs during cornering or turning as the vehicle mass gets thrown outside due to the centrifugal force.

Yawn: The motion of vehicle about Z-axis which generally occurs if wheels lose traction that is their grip on the road surface like during drifting, known as yawn.

There are three main components of the suspension systems such as Spring, Damper, and Linkages or control arms. Through spring it can absorb force which

Fig. 1 The cartesian coordinate system used in the work



is produced due to aberrant nature of road, spring absorbs the force in the form of potential energy, $W = F \cdot d$ [2], higher the displacement smoother can be the vehicle. It also acquires linkages that move continuously because small movements will be there due to friction or aberrant nature of the road which causes the motion of linkages which is joints to one other.

Now, we like to introduce the double wishbone suspension system. In this system, there are two control arms shaped as an “A” they are also called as wishbone arms because they are also shaped as the wishbone of a bird so the two control arms are connected to the knuckle using ball joint and to the frame of the vehicle using a pivot. The strut, that is, the coil-over that is a spring plus damper is connected on either of the two-arm upper or lower generally it is connected to the lower arm and can also be connected to the upper arm.

The material selection process to very important for analyzing the suspension system. Some basic methods to select material are discussed below.

1.3 Selection of Materials

Price and availability: The price of material will be selected as also keep in mind that the nature and quality of the material, is it suitable for the system or not, can people find ease with the material which are going used because transportation of material and price of material will depend on the availability of the material.

Mechanical properties of materials: The mechanical properties have played big role in selecting the material, there have been used Pugh’s concept for selecting the material in which the calculation of the net score is by adding individual scores of the material on the basis of their total weight, yield strength, tensile strength, cost of the material and factor of safety this is called scoring matrix of Pugh’s concept [6–8]. The Pugh matrix helps to find out which items or potential solutions are more important or better than others. It is employed after capturing voice of the customer (VOC). It is a scoring matrix used for concept selection in which options are assigned scores relative to criteria.

Ease of manufacturing, texture, feel: This is one of the reasons for the selection of the materials. As the manufacturers need to have ease of operation and must care about the comfort of the customers.

Based on the above criteria, some of the materials are selected to be used in analyzing the suspension systems, shown in Table 1.

In the Table 1, the mechanical properties of different materials have been selected on the basis of their value of yield strength, elastic modulus, and fracture toughness. Which will give some idea about the selection of material for the suspension system.

Table 1 Mechanical properties of different materials

	Yield strength (MPa)	Elastic modulus (GPa)	Fracture toughness (MPam ^{1/2})
Maraging steel	1730	200	90
Ti-6Al-4V	900	114	57
2014-T3 Al alloy	385	72.4	26
7075-T6 Al	450	71.7	24
4340 steel	1470	200	46

1.4 Formulations and Calculations

In this section, the discussion about the parameters that are considered in the paper for analyzing the mechanism.

Factor of safety

$$\sigma = S_y / f_s \tag{1}$$

where σ is allowable load (stress), S_y is ultimate load, and f_s is factor of safety and the values for S_y is 315 m and factor of safety, $f_s = 1.2$ (as 4340 steel is a ductile material) taken. After the calculation,

$$\sigma = 262.33 \text{ MPa}$$

Torsional Stiffness is defined as torque per unit deflection, and it is significant in positional systems and describes a coupling’s resistance to torsional deflection.

Torsional stiffness = Applied torque/ angle of deformation

$$\text{Torsional stiffness} = (F \times L) / \Theta \text{ and } \text{Tan}(\Theta) = D / (L/2) \tag{2}$$

where, F is force, L = distance between diagonally opposite suspension mounts, D = vertical deformation in suspension mounts.

The maximum deformation was at the rear suspension mount and the other values are taken as

$$F = 2500 \text{ N}, L = 300 \text{ mm}, \text{ and } D = 0.823 \text{ mm.}$$

After calculation, we get

$$\text{Torsional stiffness} = 2943.79 \text{ N m/degree}$$

This is the value of allowable stress in wishbone. The designed wishbone is safe when the induced stress is lesser than the allowable stress value.

Table 2 Parameters of suspension system

Parameters	Dimension
Static ride height	10 in.
Front track width	45 in.
Rear track width	45 in.
Wheelbase	47 in.
Front roll center	12 in.
Length of upper wishbone	15 in.
Length of lower wishbone	20 in.
Motion ratio	0.69

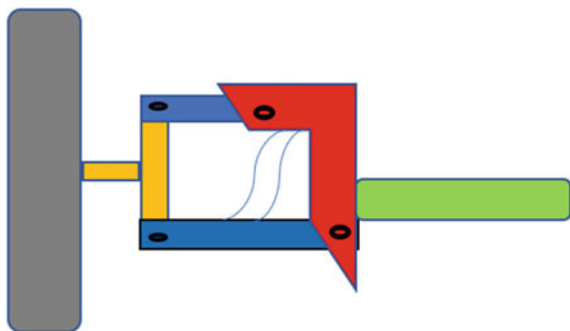
1.5 Analysis Using MechAnalyzer

The parameters, as shown in Table 2, are selected as input parameters in the MechAnalyzer. Taking these parameters, the different graphs were obtained and analyzed in the subsequent sections. The graph, of velocity of link 2 with time, is shown in Fig. 3, which shows that the velocity makes a complete cycle in one second with zero velocity at mid of the cycle. To minimize the size of the system by the use of MechAnalyzer software by putting different parameters related to the linkage and angles. As given in Table 1, the parameters of the suspension system are selected which will further analyze the MechAnalyzer software by putting these values to get better output.

1.6 Analysis of 4-bar Mechanism of Double Wishbone Suspension System

The four-bar mechanism taken for the analysis of the suspension system is shown in the Fig. 2. It is schematic representation of the double wishbone suspension system.

Fig. 2 Schematic figure of linkages and spring in suspension system



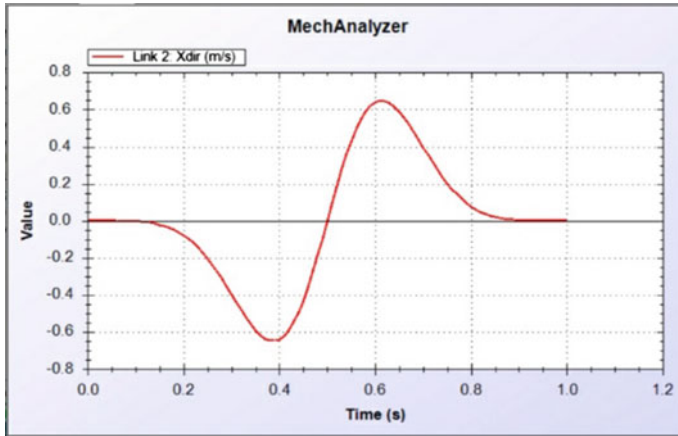


Fig. 3 Graph between the velocity of link 2 with the time in suspension system

The given figure is showing the connection of linkages at different joints with the wheel, this is independent of wheel at other one, the spring is connected between the smaller and longer linkage which will move accordingly.

MechAnalyzer software helps to find out best way to connect linkages for better output. At which length should be the first linkage connected and at what angle should be joint at it so that from fluctuating length and angle of linkages and the spring connected in double wishbone suspension system gives best output. The analytical conclusion has found that longest length of linkage has to be 150 cm so it can operate easily at low gap between surface and the body of the car, as shown in above graph the different value of velocity is given on Y-axis with respect to the time as time increasing it acquires maximum velocity and then at its lowest with the time as in suspension system with time the connected linkage achieve its highest velocity with force exerted on it externally which absorb the forces and converted into the motion. At link 2 the velocity has been counted and analyzed that with time value is increasing and then decreasing and again after the moment it achieves its peak in other direction because the direction of velocity has changed frequently [9–12, 12].

In the graph two different types of wave have been shown in Fig. 3 tells that one in positive direction and another in negative direction that is what process occurs in suspension system when it goes up the one wave follow that equation, and it goes down it shows the positive one wave equation as shown in the Fig. 3.

The analysis of different linkage of wishbone system on MechAnalyzer software has done, by putting their length to find out maximum force and velocity which can derive better output from the system, putting the value of first linkage approx. 1.5 times and giving the output better than other lengths. The length is adjusting as to moderate the range of motion of triangle with linkage-5 and linkage-6 which will help in to select the size of wishbone suspension system if the size of linkage is proper and range of motion so as then it contains some better spring between the linkage. Here L-1 is fixed just like suspension system. L-2 and L-4 have angular

motion which will transfer linear motion to the spring when force is applied as input on the linkages.

1.7 Force and Velocity Experience by Joint 1 in 4-bar Mechanism

We observe in Fig. 4, the graph the force on the joint-1 is applied due to which the velocity has been in the scene at joint-1 and L-2 as one is fixed velocity can be produced only at the other linkage.

With change of the velocity increase, it shows all depends on the length of the linkage and the angle of L-1 and L-2, one linkage is fixed and one is connected with spring in the wishbone suspension system just like other side of suspension system it helps to achieve maximum velocity with time. Joint-1 and joint- 2 have different values of velocity because of length of linkage between the wheel.

The force exerted on the suspension system is absorbed by the suspension system and it converts into the motion which is shown in the graph with the help of value at join of force and the time for which amount of time is acted on it as time increasing the force increases but it only for fleeting time, in which occurs its maximum point.

There is another different suspension system independent and dependent but it does not have graph like double wishbone suspension system which absorbs forces most of it without damaging the suspension system because of material selection and the parameter of the linkages and the spring which is most important part of the system.

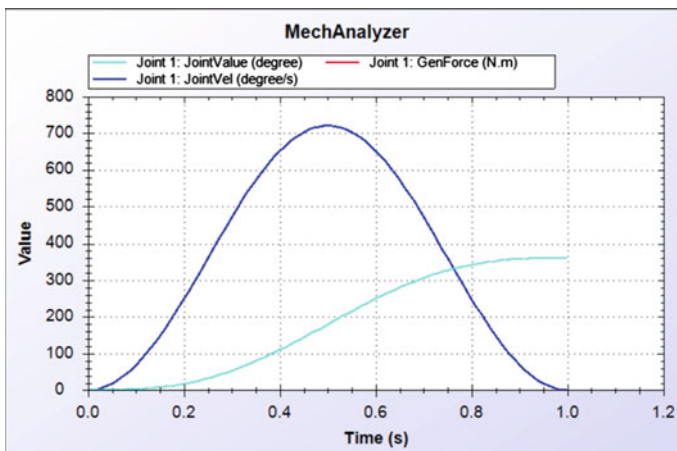


Fig. 4 The graph between force, velocity with the time

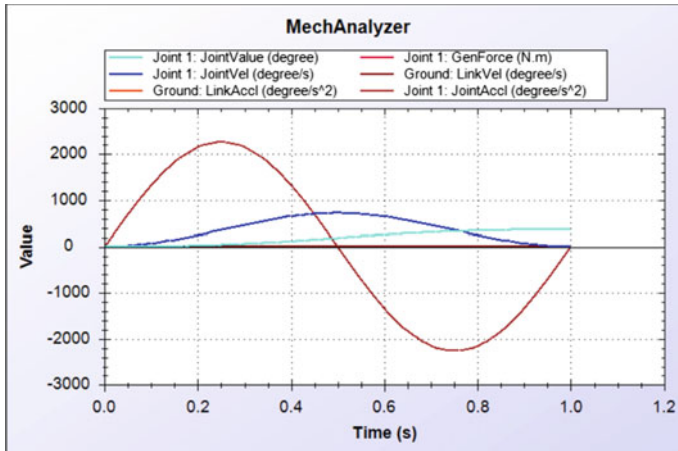


Fig. 5 The graph of force, acceleration, joint value with the time

1.8 Force, Velocity, and Acceleration Exerted on Movable Joint of Wishbone Suspension System as Shown in Graph

The given below graph shows the force on the joint one which connected L-1 and L-2 that derives and can obviate the accident which can approximate the value of factor of safety otherwise when force will increase with time or velocity it can cause suddenly broke of material. And on the other hand, acceleration gives sinusoidal graph which s with time the value becomes zero. The acceleration which is shown in the graph has covered maximum area with respect to other parameters which indicate the alteration in the velocity of system during the motion of the vehicle (Fig. 5).

Due to camber change characteristics, desired under steer qualities are maintained under high lateral acceleration which is the goal for this car [6]. Double wishbone suspension system is more costly as compared to Macpherson strut-type suspension system but double wishbone suspension system is best suited for race cars.

Double wishbone suspension system vastly has been used in race cars but nowadays luxury vehicles also have it. But only difference is the distance between surface and the body of the vehicle. In the graph that is mentioned clearly if the upper linkage which is over the spring can be altered but for maximum absorption of force it should be enough space for the spring to move up down at the end of the day it makes sure that the smoothness of the vehicle should be at it best if it possible at desire cost and life of suspension system.

2 Results and Discussions

After analysis of MechAnalyzer software have found out at which length of linkages will give best output and also using Pugh's concept have selected the material which gives longest life for the system. According to analysis done on software at 130 cm of longest linkage gives better velocity, acceleration and can absorb force easily and by the help of Pugh's concept of material selection and selected the 4340 steel which has best torsion effect, modulus value and have better factor of safety. On the basis of four-bar mechanism, it has been decided that analysis of system can be done on MechAnalyzer software whereby putting parameters of different linkages.

3 Conclusion

After performing various analyses, it concluded that double wishbone system is used for avoiding any defect on the body of vehicle from irregularities of the roads. The double wishbone suspension system works on the basis of 4-bar mechanism, it consists of linkage, springs, and shock absorbers which obviate the shock of wheel by absorbing the force. After some theoretical calculation, it concluded that 4340 steel has better factor of safety value and torsion effect which can be perfect for the suspension system. Analysis of the system including 4-bar mechanism has been done on MechAnalyzer software which gives the parameter of linkage to get best output from the system. The prospective on this literature is that it can reduce the space from surface to the body of vehicle by using different parameters like its connecting rod, springs, etc. but for maximum absorption of the vibration or shock due to rough surfaces, trying to be maximum which will result in better driving experience. And also have been considered that the life of the system should be up to the mark which has been done by the use of selecting process of better material to be used in the system.

References

1. Jain A, Suryawanshi A, Sharma R (2019) Double wishbone suspension system of BAJA ATV. Available at SSRN 3377582
2. Arikere A, Kumar GS, Bandyopadhyay S (2010) Optimisation of double wishbone suspension system using multi-objective genetic algorithm. In: Asia-Pacific conference on simulated evolution and learning. Springer, Berlin, Heidelberg
3. Patil KS, Gambhire VR (2014) Design and development of double wishbone electro-hydraulic active suspension system. *Int J Sci Eng Technol* 3(6):760–764
4. Patil AM et al (2013) Experimental & finite element analysis of left side lower wishbone arm of independent suspension system. *IOSR J Mech Civil Eng* 7(2):43–48
5. Kewat R et al Dynamic analysis of double wishbone and double wishbone with s-link and toe link. *Int J Eng Res Appl (IJERA)* ISSN: 2248-9622

6. Woods DE, Jawad BA (1999) Numerical design of racecar suspension parameters. SAE Trans 3156–3161
7. Riordan C, Tovar A, Renaud J (2010) Topology optimization of a formula SAE upright using Optistruct. No. 2010-01-0396. SAE Technical Paper
8. Yang L et al (2017) Loads analysis and optimization of FSAE race car frame. No. 2017-01-0423. SAE Technical Paper
9. Deakin A et al (1998) Design of a single seater racing car suspension system. SAE Trans 2507–2511
10. Robertson D, Delagrammatikas GJ (2010) The suspension system of the 2009 cooper union fsae vehicle: a comprehensive design review. SAE Int J Passenger Cars-Mech Syst 3.2010-01-0311, 366–380
11. Subedi S, Logan J, Zahui M (2017) Simplified approach for formula sae car suspension design and component size optimization using finite element method. In: ASME 2017 international mechanical engineering congress and exposition. American Society of Mechanical Engineers Digital Collection
12. Sert E, Boyraz P (2017) Optimization of suspension system and sensitivity analysis for improvement of stability in a midsize heavy vehicle. Eng Sci Technol Int J 20(3):997–1012
13. Sert E, Boyraz P (2017) Optimization of suspension system and sensitivity analysis for improvement of stability in a midsize heavy vehicle. Eng Sci Technol Int J 20(3):997–1012
14. Lai CY, Liao W-H (2002) Vibration control of a suspension system via a magnetorheological fluid damper. J Vib Control 8(4):527–547

A Review and Emphasis on the Relevance of the Aluminum Based Hybrid Composite



Mohammad Arshad Jamal, Praveen Pachauri,
and Shailendra Kumar Verma

Abstract The need for relatively inexpensive composite hybrid materials with many different characteristics has grown in recent years for innovative matrix composites. Aluminum's primary qualities interest the user since it is relatively cost-effective, widely accessible and lightweight, and durable. It can be processed to high strengths and is also characterized as becoming one of the materials that are easily manufactured and have cheaper prices. In that perspective, the work that has been carried out over the previous couple of decades is indeed deemed suitable for consolidation. This analysis examines the turning of the facts, usage and upcoming capabilities of Al-MMCs in numerous materials and commercial applications, coupled with the existing challenges that prevent their complete market entry. The comparison analysis shows that the hybrid composites presented have such a reduced friction coefficient, a lower increase in temperature and reduced noise level. It is determined that the tribological properties with a dark and smoother texture are satisfactory in the hybrid composite.

Keywords Aluminum 5083 · Stir casting · Friction stir casting · Hybrid composite

1 Introduction

The need for relatively inexpensive composite hybrid materials with many characteristics has grown in recent years for innovative matrix composites. Aluminum's primary qualities interest the user since it is relatively cost-effective, widely accessible and lightweight and durable. It can be processed to high strengths and is also characterized as becoming one of the materials that are easily manufactured and have cheaper prices. In that perspective, the work that has been carried out over the previous couple of decades is indeed deemed suitable for consolidation. This analysis examines the turning of the facts, usage and upcoming capabilities of Al-MMCs in numerous materials and commercial applications, coupled with the existing challenges that prevent their complete market entry. The comparison analysis shows that

M. A. Jamal (✉) · P. Pachauri · S. K. Verma

Department of Mechanical Engineering, Noida Institute of Engineering and Technology, Greater Noida 201306, India

e-mail: arshadjamal284@gmail.com

the hybrid composites presented have such a reduced friction coefficient, a lower increase in temperature and reduced noise level. It is determined that the tribological properties with a dark and smoother texture are satisfactory in the hybrid composite.

1.1 Aluminum Based Hybrid Composite

The integration of two or more different types of reinforcing, such as fibers, microfibrates, particles, whiskers, and nanostructures, may be engineered using hybrid composites. The materials for strengthening such as (SiC, Al₂O₃), (Graphite, SiC) and (Graphite, Al₂O₃) might be varied. For example, motor car blocks are utilized in particulate form with graphite and alumina. Composites with hybrid matrix phases have enhanced mechanical characteristics by reducing penetrative defects in meniscus and by reducing inter-metallic element development at interfaces by increasing the interfacial interaction. Manufacturing of Metal Matrix Composites (MMCs) is largely divided into two different groups: ex-situ synthesis and in-situ synthesis. Ex-situ synthesis is used to add the granules to an external metal matrix and reinforced in situ synthesis by chemical reactions or exothermic reactions, e.g., exothermic dispersions, reactive hot pressings, reactive infiltration and direct melting reactions [1]. Strengthening in hybrid shape to increase composite characteristics, which offers significant flexibility in design techniques. As a result of the combined hybrid efficiency of reinforced-in-hybrid composites, the characteristics of composite materials are greater than those of hybrid reinforcing. When strengthened by a hybrid mixture of SiC and graphite particles, the composite matrix gives outstanding mechanical and physical characteristics. SiC. Al matrix supports the development of graphite and lubricating support. However, SiC decreases composite elasticity and decreases graphite's whole mechanical hybrid capacity. Thermal treatment with Al/SiC + Gr composites at 630 °C improves hardness due to interaction reactions in the matrix and reinforces interaction in conjunction with the response production process Al₂O₃ [2].

2 Literature Review Emphasis on the Relevance of the Aluminum Based Hybrid Composite

The effect on an aluminum hybrid composite is analyzed in this article by the metal matrix as a reinforcement. Compared to the quality of other metal matrix components, complete research was conducted on the tribological features and attributes of enhanced particles. Table 1 further revealed the mechanical characteristics of the composite hybrid metal-matrix. The review is essential in order to identify the knowledge gap and to identify more aspects for future investigations.

Table 1 Literature review of reinforced palm fibers used for composite materials

Composition of hybrid composites	Summary/Conclusions	Refs.
Al5083/SiCp/Fly ash	The stir casting method was used to create aluminum (Al5083) based hybrid composites. Tensile strength, compressive strength, and hardness of aluminum alloy (Al5083) composites increase with the weight percentage of reinforced silicon carbide up to 5% SiCp, and then gradually decrease with the weight percentage of reinforcement	[3]
Al5083/CNT/Ni/MoS ₂	Al5083 based hybrid composites were manufactured by the traditional stir casting process. Investigate whether tensile strength increases with an increase in weight percentage until a certain value and then decreases as hardness increases. With increasing MoS ₂ with Ni up to 5%, wear rate decreases, corrosion rate decreases, and compressive strength increases	[4]
Al5083/SiC/TiO ₂	Aluminum alloy (Al5083) based hybrid surface composite was prepared by the friction stir process. By using the RSM technique, the modeling equation was created and verified by ANOVA. The ultimate tensile strength of the specimen improved by approximately 50%	[5]
Al5083/SiCP/Fly ash	Aluminum alloy (Al5083) based hybrid surface composite was prepared by the electromagnetic stir casting process. Optimum mechanical strength was obtained for Al5083, a 5% SiC, 2% Fly Ash hybrid composite. Microstructure and SEM of specimens were performed	[6]
Al5083/Fly ash/SiC	Al5083-based hybrid composites were manufactured by the liquid casting process. Hardness and tensile strength show SiC has more effect than fly ash. Microstructure analysis shows a uniform distribution of SiC	[7]
Al-6063/TiB ₂ /Gr	Aluminum alloy (Al6063) hybrid composite was prepared by the stir casting process. The mechanical properties like tensile strength improved by approximately 67%, hardness increased by 80%, impact strength 24.3% compared to the base material. Wear resistance improved with an increase in reinforcement percentage	[8]

(continued)

Table 1 (continued)

Composition of hybrid composites	Summary/Conclusions	Refs.
Al5083/ZrSiO ₄ /TiO ₂	Aluminum alloy (Al6063) hybrid composite was prepared by the stir casting process. SEM, EDAX were performed on the microstructure of the hybrid composite, mechanical properties like tensile and hardness increased	[9]
Al5083 and fly ash	Microstructure is observed by SEM, using Brinell testing and universal testing machine hardness and tensile test performed respectively, result shows mechanical properties improved	[10]
Al 6063-cotton shell ash and SiC	Hybrid composites were prepared by mechanical stir casting. The hybrid composite shows improved mechanical strength like hardness, compressive strength, and density decreases. Microstructure was also analyzed	[11]
Al 6063/B ₄ C/SiO ₂	A hybrid composite was fabricated through the use of the friction stir process. The EDS analysis was performed. The microstructure analyzed by SEM shows a uniform distribution of reinforcement and there is a decrease in specific wear rate	[12]
SiC and RE oxides reinforced Al-6063 alloy	Stir casted hybrid composite morphology was analyzed by SEM, XRD, EBSD, EDS and mechanical properties by Brinell hardness, Rockwell micro hardness, tensile strength and impact strength	[13]
Al6063/SiC-Cr	EIS technique study shows 3% by weight of Cr has optimal corrosion performance of hybrid composite	[14]
Al6063 alloy with silicon, graphite and fly ash	Hybrid mechanical properties improved with increment of graphite and decrement of fly ash with weight percentage	[15]
Al5083/SiC	Using the stir casting process and ultrasonic stir casting, the Al5083 alloy composite was developed. also investigated the mechanical properties like, tensile and compressive tests	[16]
Al6063/SiC/ZrO ₂	Al6063 base hybrid composite was prepared by the stir casting process. This forming process analysis shows that at 1%wt. SiC and 1% wt. ZrO ₂ particles improved impact strength by 23.5%, wear rate decreased with increment of SiC, debris, dilatation, and cleavage decreased with increment of SiC	[17]

(continued)

Table 1 (continued)

Composition of hybrid composites	Summary/Conclusions	Refs.
SiC/rare earth particulates	A hybrid composite of aluminum alloy was prepared using SiC and REP ($\text{CeO}_2 + \text{La}_2\text{O}_3$) by the stir casting process in varying amounts. The result showed mechanical strength improved by up to 2wt.% mixture of rare earth particles, and further, up to 3% it decreased. Morphology analyzed by EBSD, SEM, EDS, test	[18]
Palm kernel shell ash and SiC	Aluminum alloy hybrid fabricated through the double-stir casting process. The optimization of parameters was done using Taguchi and Grey's relational analysis methods. The results were validated through ANOVA. Optimal conditions for volume loss and wear index had been obtained	[19]
SiC/PKSA	The Agro-residue palm kernel shell ash (PKSA) (0–8 wt.%) and SiC (2 wt.%) reinforced aluminum alloy hybrid composite was fabricated using the double stir casting process. The result shows an increment in hardness of 10.3%, yield strength of 18.5%, and ultimate tensile strength of 10.4% with an increase in PKSA. When compared to the base alloy, percent elongation and fracture toughness decrease	[20]
Al5083/CNTs/B ₄ C	The Al5083 base hybrid composite was fabricated using a powder metallurgy process. The mechanical test of the specimen evaluated that the increment in B ₄ C amount, increased hardness, wear resistance, delamination mechanism, and abrasion mechanism found at higher percentage of B ₄ C and CNT, increment in creep rate because of CNTs and decrement in creep rate because B ₄ C	[21]
Al–Mg/Si/B ₄ C	The pure aluminum based hybrid composite with varying amounts of B ₄ C was fabricated with the stir casting process. The result obtained is decreased nucleation temperature and grain growth temperature. Mechanical testing at 5% B ₄ C composite UTS increased maximum 217 MPa, elongation 7%, hardness 100 Hv, and wear rate 46%. SEM, EDS, XRD test were performed	[22]
CNT/MoB/Ni	Aluminum based hybrid composite was fabricated by combo casting. Tensile strength and fatigue life improved by up to 0.75%wt. due to grain refinement, but decreased due to CNT cluster. Tensile strength improved by 25.4%, and microstructure was analyzed using SEM	[23]

(continued)

Table 1 (continued)

Composition of hybrid composites	Summary/Conclusions	Refs.
B ₄ C and Al ₂ O ₃ reinforcement	The Al5083 hybrid composite was created by stir casting with a fixed amount of Al ₂ O ₃ and varying amounts of B ₄ C by weight percent. The wear resistance increased with increments in reinforcement	[24]
Al5083/B ₄ C and TiC	Al5083 based hybrid surface composite was fabricated by FSP. The processed surface was analyzed by XRD, SEM. The results obtained show that mechanical properties improved, wear resistance improved	[25]
Al5083/CNTs/SiC	The aluminum alloy-based hybrid surface composite was fabricated using the FSP methodology. The mechanical properties analyzed and morphology were studied by TEM, EBSD. In the processed zone, an equal concentration of SiC & CNT obtained. Maximum tensile strength was obtained for Al5083/CNTs/SiC and hardness for Al5083/SiC	[26]
TiO ₂ / Al-15% SiC	An aluminum-based hybrid composite was manufactured through powder metallurgy. Wear resistance, micro hardness, density increase, and mean size of debris reduced with increment of debris were the results obtained	[27]
B ₄ C/coconut shell ash	Hybrid Composite was fabricated from reinforced aluminum based alloy (Al6061) using stir casting. The result obtained decreased in tensile strength, and hardness with increased amounts of reinforcement. Only fracture toughness improved compared to base material	[28]
Al ₂ O ₃ /MoS ₂	Aluminum based hybrid composite was manufactured using microwave sintering in a domestic microwave oven. The result obtained was an improved wear rate et al. 4% Al ₂ O ₃ /2% MoS ₂ , plastic deformation and oxide formation on surfaces reduce wear loss	[29]
TiO ₂ -Gr	Using the powder sintering technique, aluminum based hybrid composite was developed. At 5% wt. of TiO ₂ and 4 wt.% Gr we obtained maximum axial stress, the true hoop stress, and the true hydrostatic stress. The strength coefficient (K) and strain hardening index of the composite increased, reducing densification and deformation characteristics due to the presence of TiO ₂ and Gr	[30]

(continued)

Table 1 (continued)

Composition of hybrid composites	Summary/Conclusions	Refs.
Ni/SiCp	Hybrid composite of aluminum alloy was fabricated by the sintering process. At the temperatures of 400 °C and 600 °C, the result obtained is maximum hardness et al. -Mg-Mn-5%SiCp-6%Nip, optimum temperature is 400 °C	[31]
B ₄ C/MoS ₂	An aluminum based hybrid composite with varying wt.% of reinforcement was fabricated by stir casting process. Also, the comparative result obtained shows that the cutting surface and surface roughness on increase in cutting speed	[32]
SiC and Fly Ash	Al5083 based hybrid composite was prepared by stir casting with varying amounts of reinforcement composition. The result obtained was an increase in tensile strength, hardness, and wear resistance properties with increments of reinforcement of up to %wt. microstructure observed by SEM	[33]
Gr/Al ₂ O ₃	Aluminum based self-lubricating hybrid composite was prepared by the powder metallurgy process. The result analyzed was mechanical and tribological properties improved, maximum result obtained is for Al + 3%Gr + 10% Al ₂ O ₃	[34]
SiC/WC	Al6061 based hybrid composites were manufactured by the stir casting process. The varying amounts of reinforcement percentage by weight improved the mechanical properties and microstructure of the SEM, XRD performed	[35]
RHA and fly ash	Aluminum A536 based hybrid composite was manufactured by the double stir casting process. The reinforcement increased mechanical properties, maximum hardness was obtained at 10% fly ash and 10% RHA	[36]

3 Conclusion

Based on study of various research articles following conclusions can be made

- The most common fabrication process for aluminum 5083 based hybrid composites is the stir casting process. Some other processes like friction stir casting, double stir casting, electromagnetic casting, and powder metallurgy can also be used for aluminum based hybrid composites.
- There are lots of reinforcements like SiC, Al₂O₃, B₄C Graphite, TiO₂, and MoS₂ can be used for fabrication up to a certain limit to increase mechanical properties, but after a certain point it decreases properties.

- Agro waste like fly ash, RHA, and palm fiber are used for processing the hybrid composite for increasing tribological properties.

References

1. Zhao YT, Zhang SL, Chen G (2010) Aluminum matrix composite reinforced by in-situ Al_2O_3 and Al_3Zr particles fabricated via magneto-chemistry reaction. *Trans Nonferrous Metals Soc China* 20:2129–2133
2. Ge D, Gu M (2001) Mechanical properties of hybrid reinforced aluminum based composites. *Mat Lett* 49:334–339
3. Kempaiah UN, Santhosh N, Harshith Kumar D, Chelgeri AH, Vishnu P, Raorane S (2017) Characterization of high performance Al 5083/SiCP/Fly ash hybrid metal matrix composite for advanced aerospace applications. *Int J Adv Innov Res* /# 311 3(10), 2278–7844
4. Robinson Smart DS, Pradeep Kumar J, Sanjit Cyrus R (2019) Development and investigations of Al5083/CNT/Ni/MoS2 metal matrix composite for offshore applications, pp 2214–7853. <https://doi.org/10.1016/j.matpr.2019.07.753>
5. Devanathan C, Boopathi S, Giri R, Shankar E, Sivanand A (2020) Development of Al 5083 based hybrid surface composites via friction stir processing. *Mat Today Proc*. <https://doi.org/10.1016/j.matpr.2020.07.445>
6. Manish TS, Harshvardhan VK, Ramini S, Rudra Naik M, Avinash L, Avvari M (2016) Development of aluminium based hybrid (AA5083/FLYASH/SiCp) MMCs for ship building applications, 5th world conference on applied sciences, engineering & technology 02–04 June 2016. HCMUT, Vietnam
7. Vijaya kumar K, Prabhu L, Subin BS, Satheen S, Vaishnav K (2020) Development of hybrid aluminium metal matrix composites for marine applications. In: ICMECE 2020 IOP conference series: materials science and engineering 993 012016 IOP Publishing. <https://doi.org/10.1088/1757-899X/993/1/012016>
8. Idrisi AM, Singh VD, Saxena V (2014) Development and testing of Al5083 alloy reinforced by SiC particles. *Int J Sci Res Eng Technol (IJSRET)* 2(11):697–704. www.ijsret.org, ISSN 2278-0882 IJSRET @ (2014)
9. Hariprasad T, Srinivasan K, Channankaiah, Rajesh kumar S Evaluation of mechanical and tribological properties of Al5083/ZrSiO₄/TiO₂ hybrid composite. *Int J Appl Eng Res* 13(6):3754–3758 (2018). ISSN 0973-4562
10. Ganesh K, Justin antony raj I, Kamaraj P, Sebastin joyal J (2018) Experimental investigation of microstructure and mechanical characteristics of Al5083 & fly ash composite. *Int Res J Eng Technol (IRJET)* 05(01). e-ISSN: 2395-0056
11. Akash N, Harish P, Veeranki Mohan Srikanth P, Ravindra Babu MRC, Sastry (2019) Analysis of mechanical behavior of AL 6063-cotton shell ash and SiC METAL matrix composites using stir casting. *J Mechatron Mach Des Manuf* 1(1):23–33
12. Dinesh D, Megalingam A, Rajamurugan G, Arundeeep M, Tajdeen A (2019) Evaluation of microstructure and tribological characterization of friction stir processed Al 6063/B4C+SiO₂ composites. In: International conference on materials, manufacturing and machining, AIP conference proceedings 2128, 020030-1-020030-9; <https://doi.org/10.1063/1.5117942>. Published by AIP Publishing. 978-0-7354-1870-7/\$30.00 020030-1
13. Sharma VK, Kumar V, Joshi RS, Sharma D (2020) Experimental analysis and characterization of SiC and RE oxides reinforced Al-6063 alloy-based hybrid composites. *Int J Adv Manuf Technol*. <https://doi.org/10.1007/s00170-020-05228-7>
14. Idusuyi N, Ojide OO, Oluwole OO, Arotiba OA (2016) Electrochemical impedance study of an Al6063/12%SiC-Cr composite immersed in 3% wt. Sodium chloride; International conference of sustainable materials processing and manufacturing, SMPM 2017, 23–25 January 2017, Kruger National Park, Procedia Manufacturing

15. Loganathan M, Dinesh S, Vijayan V, Karuppusamy T, Rajkumar S (2020) Investigation of mechanical behaviour on composites of Al6063 alloy with silicon, graphite and fly ash. *J New Mat Electrochem Syst* 23(1):36–39. <http://new-mat.org> <http://iieta.org/journals/jnmes>
16. Manoj Kumar G (2020) Characterization of Al-6063/TiB₂/Gr hybrid composite fabricated by stir casting process. *Met Powder Rep.* <https://doi.org/10.1016/j.mprp.2020.06.063>
17. Sekar K, Vasanthakumar P (2020) Mechanical and tribological properties of Al6063 hybrid composites reinforced with SiC/ZrO₂ by stir casting and thixoforming process. *Materials Science Forum* Submitted: 2019-04-28, vol 979, pp 47–51. Revised: 2019-07-30. <https://doi.org/10.4028/www.scientific.net/MSF.979.47>. Accepted: 2019-08-02 © 2020 Trans Tech Publications Ltd, Switzerland Online
18. Sharma VK, Aggarwal D, Vinod K, Joshi RS (2021) Influence of rare earth particulate on the mechanical & tribological properties of Al-6063/SiC hybrid composites. *Particulate Sci Technol* <https://doi.org/10.1080/02726351.2021.1871691>
19. Ikubanni PP, Oki M, Adeleke AA, Agboola OO (2021) Optimization of the tribological properties of hybrid reinforced aluminium matrix composites using Taguchi and Grey's relational analysis. *Scientific African* 12
20. Ikubanni PP, Oki M, Adeleke AA, Omoniyi PO (2021) Synthesis, physico-mechanical and microstructural characterization of Al6063/SiC/ PKSA hybrid reinforced composites. *Sci Rep* 11:14845. <https://doi.org/10.1038/s41598-021-94420-0>
21. Alizadeh A, Abdollahi A (2015) Creep behavior and wear resistance of Al 5083 based hybrid composites reinforced with carbon nanotubes (CNTs) and boron carbide (B₄C). *J Alloy Compd.* <https://doi.org/10.1016/j.jallcom.2015.07.214>
22. Ghandvar H, Jabbar MA, Kolor SSR, Petru M, Bahador A, Bakar TAA, Kondoh K (2021) Role B₄C addition on microstructure, mechanical, and wear characteristics of Al-20%Mg₂Si hybrid metal matrix composite. *Appl Sci* 11:3047. <https://doi.org/10.3390/app11073047> <https://www.mdpi.com/journal/applsci>
23. Sajeeb Rahiman AH, Robinson Smart DS (2020) Study on low cycle fatigue and tensile behavior of Al 5083/CNT/ MoB/Ni hybrid composite. *Int J Manuf Mat Mech Eng* 10(4). <https://doi.org/10.4018/IJMMME.2020100102>
24. Hariprasad T, Varatharajan K, Ravi S (2014) Wear characteristics of B₄C and Al₂O₃ reinforced with Al 5083 metal matrix based hybrid composite. *Procedia Eng* 97:925–929. <https://doi.org/10.1016/j.proeng.2014.12.368>
25. Yuvaraj N, Aravindan S, Vipin (2017) Wear characteristics of Al5083 surface hybrid nano-composites by friction stir processing. *Trans Indian Inst Met.* <https://doi.org/10.1007/s12666-016-0905-9>
26. Vikram Kumar S, Jain KU, Yazar S, Muthukumaran (2019) Development and characterization of Al5083-CNTs/SiC composites via friction stir processing. <https://doi.org/10.1016/j.jallcom.2019.05.232,0925-8388>/Elsevier B.V. All rights reserved
27. C. Antony Vasantha Kumar, Selwin Rajadurai J (2016) Influence of rutile (TiO₂) content on wear and microhardness characteristics of aluminium-based hybrid composites synthesized by powder metallurgy. *Trans Nonferrous Met Soc China* 63–73
28. Nithyanandhan T, Rohith K, Sidharath CG, Sachin C, Jagadesh S (2017) Investigation of mechanical properties on aluminium based hybrid composites. *Int J Innov Res Sci Eng Technol ISO 3297: 2007 Certified Org* 6(7)
29. Raghavendra Pai K, Hebbale AM, Vishwanatha JS, Sachin B (2021) Study of tribological properties on aluminium based hybrid composite developed through microwave energy. *Mat Today Proc* 44:4245–4250
30. Ravichandran M, Naveen Sait A, Ananda Krishnan V (2014) Synthesis and forming behavior of aluminium-based hybrid powder metallurgic composites. *Int J Minerals Metal Mater* 21(2):181. <https://doi.org/10.1007/s12613-014-0883-z>. University of Science and Technology Beijing and Springer Berlin Heidelberg
31. Naeem HT (2020) The mechanical properties of aluminium metal matrix composite (AIMMCs) reinforced with Ni and SiCp. In: *ZICMSE 2020 IOP conference series: materials science and engineering* 987 012004. IOP Publishing <https://doi.org/10.1088/1757-899X/987/1/012004>

32. Siddesh Kumar NG, Shiva Shankar GS, Ganesh MN, Vibudha LK (2017) Experimental investigations to study the cutting force and surface roughness during turning of aluminium metal matrix hybrid composites. *Mater Today Proc* 4:9371–9374
33. Ramgopal Reddy B, Srinivas C (2018) Fabrication and characterization of silicon carbide and fly ash reinforced aluminium metal matrix hybrid composites. *Mater Today Proc* 5:8374–8381
34. Zamani NABN, Asif Iqbal AKM, Nuruzzaman DM (2020) Tribo-mechanical characterization of self-lubricating aluminium based hybrid metal matrix composite fabricated via powder metallurgy. *Materialia*. <https://doi.org/10.1016/j.mtla.2020.100936>
35. Fenghong C, Chang C, Zhenyu W et al (2019) Effects of silicon carbide and tungsten carbide in aluminium metal matrix composites. *SILICON* 11:2625–2632. <https://doi.org/10.1007/s12633-018-0051-6>
36. Vinod B, Ramanathan S, Ananthi V et al (2019) Fabrication and characterization of organic and in-organic reinforced A356 aluminium matrix hybrid composite by improved double-stir casting. *SILICON* 11:817–829. <https://doi.org/10.1007/s12633-018-9881-5>

Descriptive Analysis of Performance and Emissions Characteristics of Diesel with Palm Oil and WCO



Sunny Kumar, Param Verma, Ranjeet Sharma, Satendra Choudhary, and Raj Kumar

Abstract Nowadays the energy demand is ceaselessly expanding and the genuine explanation is Population, industrialization, and metropolitan turn of events. All activities in metropolitan regions depend upon energy like force, Transportation. The main wellspring of energy is oil, coal, and combustible gas. These energies are non-sustainable, which is decreasing step by step in view of the appeal of people. Step by step consumption of petroleum products and their developing contamination has become a genuine worry for scientists around the world. Developing concern in regards to energy assets and the climate has expanded interest in the investigation of elective wellsprings of energy like breeze energy, solar-powered energy, biomass, biodiesel, and so on Presently a-days individuals are getting interested in biodiesel to give an appropriate diesel oil substitute for interior burning motors. Biofuels are amazingly the most ideal decision to defeat the energy crisis. Since we have the waste feedstock at the home for creating the biofuels. The techniques we use to make biofuel are picked with the goal that it cannot pollute nature. We can unreservedly create biofuel (biodiesel, bioethanol, biogas, etc.) by using an unmistakable substance and organic transformation advancements.

Keywords Energy · Biofuel · WCO · Palm oil · POD

1 Introduction

Nowadays demand for energy is continuously increasing and the real reason is Population, industrialization, and metropolitan development. All exercises in metropolitan urban areas rely upon energy like power, Transportation. The main source of energy

S. Kumar · P. Verma · R. Sharma · S. Choudhary
ME Department, Golgotia's College of Engineering & Technology, Greater Noida, India

R. Kumar (✉)
ME Department, GCET, Greater Noida, India
e-mail: raj.kumar@galgotiacollege.edu

DTU, Delhi, India

is oil, coal, and flammable gas. These energies are non-renewable, which is diminishing day by day because of the high demand of individuals. For transportation and power generation we need to rely upon oil which is the main source of energy. In the ongoing time, the cost of oil has been setting a record high in history. At the same time, excess use of these sources of energy is likewise a reason for the rise in temperature worldwide, additionally because of increment in contaminations in nature makes the living being unhealthier. Ailment like breathing and cancer are common these days. This is the reason for picking the substitute source of energy. Both the issue of contamination in the atmosphere and decrement in the number of conventional energy sources drives us to take an alternative to satisfy all the interests of people and to keep the surrounding from an unnatural weather change. An alternative source of energy tends to satisfy all the demands of people and keep the environment clean. Both energy and ecology are the significant issue, which could be decreased by adopting alternative sources, for example, biofuel which is produced from sustainable sources, also the adoption of sustainable and environment-friendly methods for the production of biodiesel. Biofuels are extremely the best choice to overcome the energy emergency. Since we have the waste feedstock at the home for producing the biofuels. The strategies we use to create biofuel are chosen so that it cannot contaminate nature. We can freely produce biofuel (biodiesel, bioethanol, biogas, and so on), by utilizing distinct chemical and biological conversion technologies [1–5]. The generation of biodiesel has increased internationally because of a decrement in the amount of Fossil fuel. As we can create different biofuel. Among all the biofuels, biodiesel is the best choice which has great properties and chemical nature. WCO can be utilized as a mix with diesel to various extents (B10, B20). There is no adjustment in the particular of the conventional engine while utilizing biodiesel. Biodiesel has properties of biodegradability and is inexhaustible and carbon impartial nature. In contrast with regular diesel, biodiesel is perfect and does not pollute nature. Synthetically, biodiesel is unsaturated fat methyl esters (FAME), which can be incorporated by compound response among liquor and oil in presence of a suitable catalyist. For the creation of biodiesel, we utilize feedstock like energy crops, animal fats, kitchen waste, insects, and microalgae. The fundamental obstacle in creating biodiesel is the expense of generation. Biodiesel creation requires a lot of investment of money. Thus we can utilize the waste cooking oil for the generation of biofuel which might be helpful to lessen the feedstock cost, which makes the procedure economical. As we are utilizing waste cooking oil as a biofuel which is generally thrown into the environment and makes it contaminate yet we can change over it in the item which can create require energy and do not contaminate the earth. Also, the change of WCO into biodiesel will be a precious gathering of energy. Besides, it can satisfy the present environmental situation [6–11].

2 Experimental Setup

Experimental setup as shown below is Research Diesel Engine of 3.50 kW and 1500 rpm. It is one cylinder 4-stroke constant Speed engine that is water-cooled. The cylinder bore is 87.50 mm, length of stroke 110 mm, length of connecting rod is 234 mm, compression ratio 18, and swept volume 661.45 cc.

3 Results

3.1 Brake Explicit Fuel Utilization (Bsfu) Using Palm Oil

Brake explicit fuel utilization indicates the fuel flow in accordance with force applied. Clearly, lower bsfu is attractive and for pressure start motor it is about 205 g per kWh. The bsfu test is conducted at various brake powers and its experimental setup is shown above (Fig. 1) [11]. The value of bsfu begin to diminish dramatically as motor was stacked and expanded to get appraised power. The bsfu was possibly higher for Palm oil diesel (POD) because of lower calorific value [11].

In the same way, to keep up with a similar bp yield, the bsfu of POD is enhanced to decrease compound energy of fuel. The most reduced qualities accomplished in the experiments were estimated as 445 g/kWh for Pal oil diesel and roughly 410 g/kWh for diesel at all velocities and it is observed that bsfu of POD was 11% more in comparison to diesel.

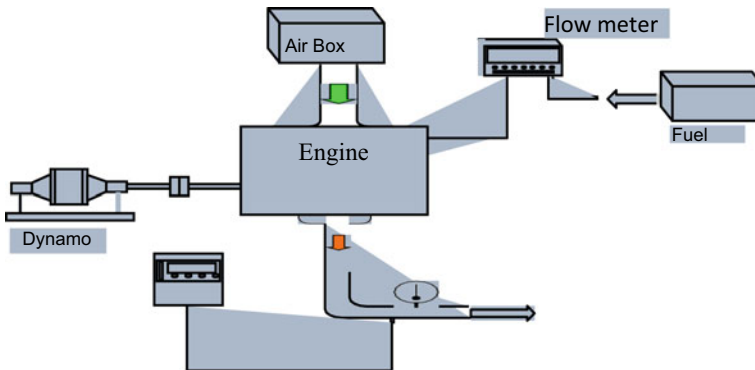


Fig. 1 Experimental setup

SFC & Fuel Consumption

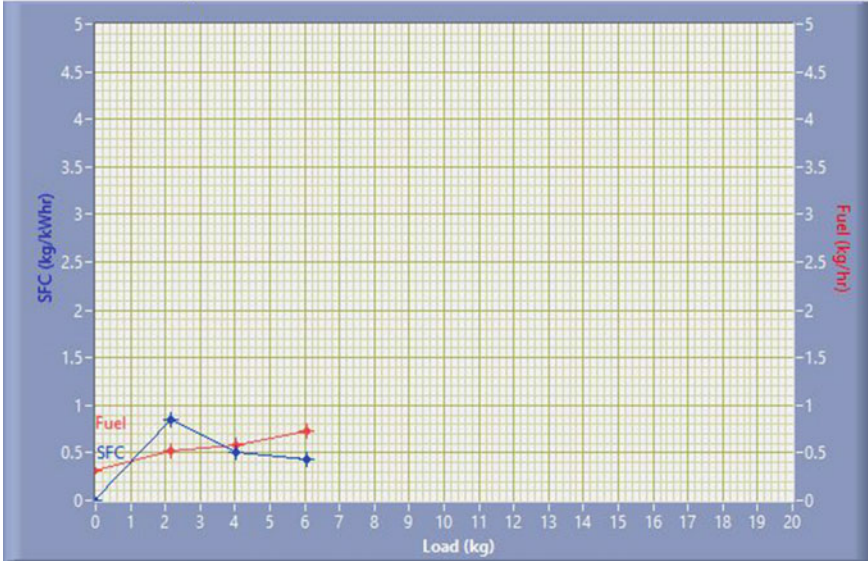


Fig. 2 Fuel consumption (B5)

3.2 Brake Torque Using Palm Oil

The variety of plots for sfc and load on motor has been drawn in Figs. 2, 3, and 4. It is observed that the brake force of a motor is straightforwardly corresponding to the brake force and a comparable direct pattern is displayed in this experiment. The brake forces for palm oil diesel (POD) were 5.3% lower than those of diesel fuel [11].

3.3 Brake Specific Fuel Consumption (Bsfu) Using Waste Cooking Oil

The brake explicit fuel utilization (bsfu) and brake warm productivity (BTE) for various WCOME mixes (arranged utilizing KOH reagent) at various burden is accounted for in Fig. 2. Additionally, Fig. 3 shows the variety of biodiesel mixes arranged to utilize NaOH reagent. The brake explicit fuel utilization is the mass of fuel devoured by motor per unit time. The brake explicit fuel utilization (g/kWh) diminishes as the heap increments for all kinds of fuel blends. The purpose for that might be, at a high burden, the chamber divider temperature builds, which lessens the start delay. So shortening of start delay further develops burning and diminishes fuel utilization. It is seen that brake explicit fuel utilization for various mixtures

SFC & Fuel Consumption

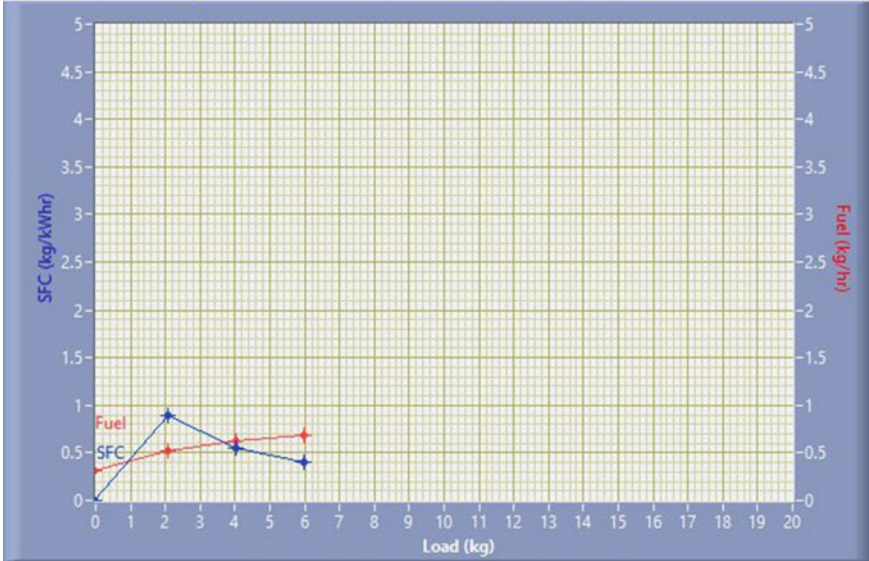


Fig. 3 Fuel consumption (B10)

SFC & Fuel Consumption

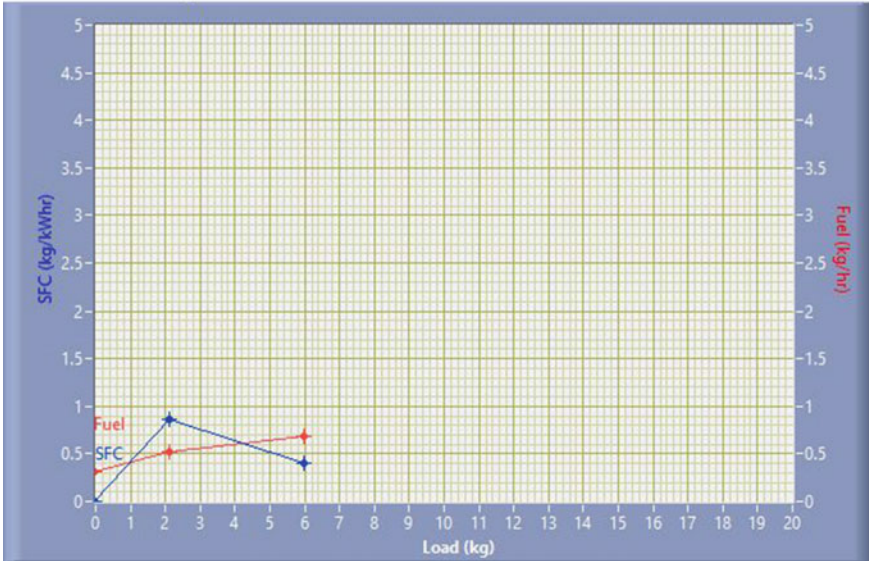


Fig. 4 Fuel consumption (B15)

with biofuel formed by waste cooking oil to various extents is more when contrasted with diesel. This is because of lower calorific value upsides of the mixtures of waste cooking oil biodiesel when concentrated with diesel.

3.4 Brake Thermal Efficiency Using POD

It is found that brake sp. fuel utilization for various blends of WCO and POD is more in comparison to conventional diesel. This is due to the lower CV of various blends of waste cooking oil biodiesel in comparison to diesel. It is found that brake thermal efficiency of waste cooking oil biodiesel (prepared using KOH) and its blends are slightly lower than that of diesel fuel. The maximum value of brake thermal efficiency of diesel is 36% and those of biodiesel blends as 34%. The brake thermal efficiency of WCO (prepared using NaOH reagent) at different loads shows that the variation of brake thermal efficiency for this biodiesel for all blends range (B10–B40) was found almost comparable to the efficiency of diesel fuel (Figs. 5, 6 and 7).

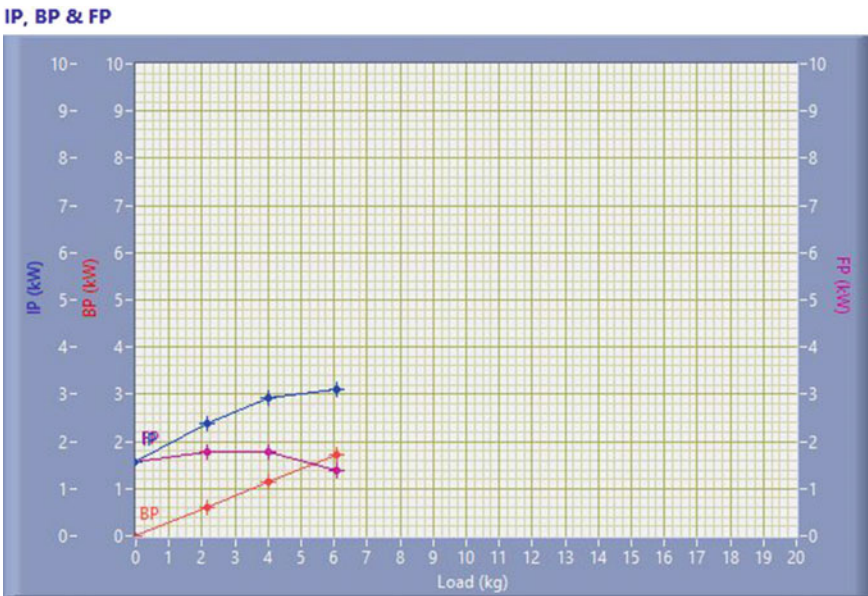


Fig. 5 Indicated power, brake power with load (B5)

IP, BP & FP

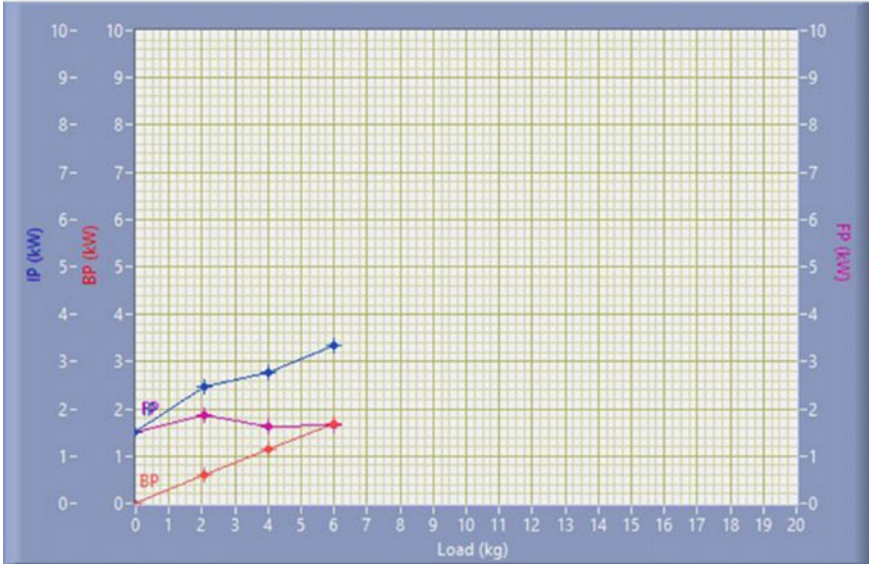


Fig. 6 Indicated power, brake power with load (B10)

IP, BP & FP

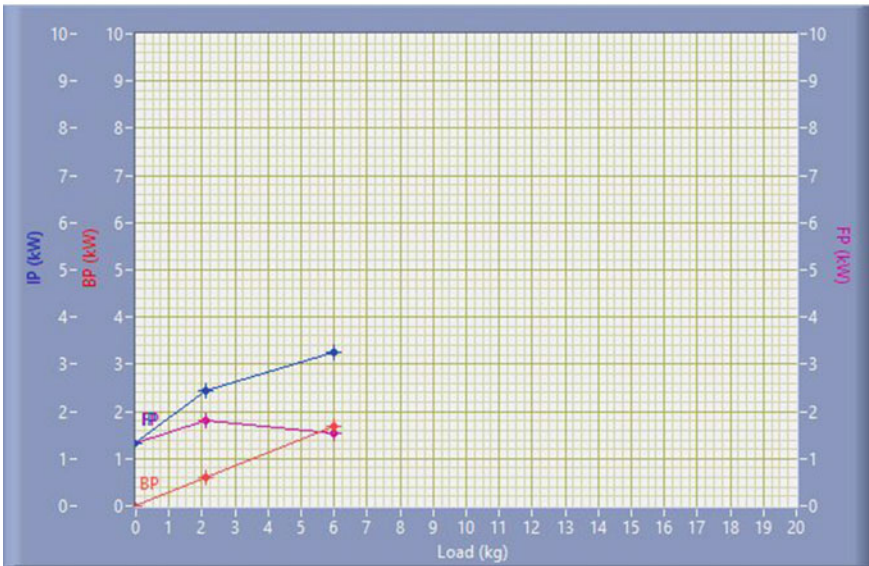


Fig. 7 Indicated power, brake power with load (B15)

4 Emission Analysis

4.1 Emission

Outflows are fundamentally synthetic substances in fumes gases that are destructive to air quality mostly CO, HC, and oxides of nitrogen (NO). Solid motors produce less emanations, and more established or undesirable motors produce more. Some motor plans like rotational motors for instance produce a greater amount of specific emanations than others.

Outflows from autos are rising worldwide as vehicle proprietorship increments within the creating scene and normal vehicle size increments within the created world. Expanding proficiency through diminished size mileage builds crossover vehicles and diesel motors is a method of diminishing nursery discharges from autos. Likewise, auto use might be diminished through open and elective vehicle drafting in urban communities and different settlements so on limited driving and gridlock, and other measures. Biofuels which do not make an on-the-spot commitment to gas outflows are another choice for lessening car emanations. Biofuels are questionable anyway on the grounds that the rural area (which would offer the feedstocks with which to make the biofuels) is itself petroleum derivative concentrated and causes other natural harm also like soil misfortune and maritime no man's lands.

Outflow in autos implies utilized to restrict the release of harmful gases from the inward burning motor and different segments. The exhaust pipeage releases consumed and unburned hydrocarbons, CO, oxides of nitrogen and sulfur, and hints of different acids, alcohols, and phenols.

Main focus on these parameters is reduction of CO, hydrocarbon, and oxides of nitrogen.

4.2 CO Emission

The boundaries like lacking stockpile of air and low fire temperature prompt this harmful surge. Since the lacking air brings about deficiency of adequate proportion of oxygen amid the start method prompts deficient consumption in the engine.

It is ordinarily seen that at low burden paying little heed to fuel there is ascend in CO sum in exhaust gases in light of rich fuel-air mix in the chamber. From the graph it is seen that at low burden diesel has higher rate followed by B10 then B20 at higher weight blends of WCO have a high pace of outpouring as the difference with diesel may be a direct result of insufficient oxidation. A bit of the CO conveyed during consumption changed over to CO₂ by taking extra oxygen by virtue of diesel which prompts a lower rate if an instance of diesel.

4.3 NO_x Emission

Due to the nature of O₂ and N₂ at high temperatures in the copying chamber, it prompts the release of nitric oxides. NO_x percentage depends on consuming chamber temperature, weight, air-fuel extent in the midst of start system, and properties. Generally, it is seen that there is a straight association between NO_x outpourings with the untidy combustion gases inside engine cylinder. With increase in load, the overall fuel-air extent increases achieving addition in the typical gas temperature in the combustion chamber, and in this way NO_x formation increases rising temperature.

4.4 Hydrocarbon Emission

The hydrocarbon emission found from the experiments shows that the average unburnt hydrocarbon for palm oil diesel oil and diesel fuel are 48 parts per million and 108 parts per million, respectively for full speed engine and bp. It was found that HC emission was reduced by approximately up to 55% for POD than conventional diesel. This indicates better hydrocarbon oxidation which is due to the higher value of CN and O₂ in case of palm oil diesel.

5 Conclusions

The focus of this analysis is on using WCO and POD in varied proportions of diesel and reducing harmful pollutants through exhaust. The Palm oil diesel and its blend with conventional diesel and WCO reduces emission of hydrocarbon, CO, CO₂, and oxides of nitrogen as well. It is also observed that at lower load brake thermal efficiency is higher than that of biodiesel of different blends as compared to diesel. On other side, at higher load, it is higher followed by blends since there is a higher concentration of oxygen which successfully increases the brake thermal efficiency of engine.

References

1. Abed KA et al (2018) Effect of waste cooking-oil biodiesel on performance and exhaust emissions of a diesel engine
2. Madheshiya AK et al (2018) Energy exergy analysis of biodiesel fuels produced from waste cooking oil and mustard oil
3. Roy R et al (2017) Performance, combustion and emission characteristics of diesel engine fueled with waste cooking oil
4. Kataria J et al (2017) Biodiesel production from waste cooking oil using heterogeneous catalysts and its operational characteristics on variable compression ratio CI engine

5. Belokar V et al (2016) Effect of compression ratio, injection pressure and injection timing on performance and smoke emissions of CI engine fueled with waste fried oil methyl esters—diesel blend
6. Rajak U et al (2018) Effect of emission from ethylic biodiesel of edible and non-edible vegetable oil, animal fats, waste oil and alcohol in CI engine
7. Bhuiya M et al (2016) Performance and emission characteristics of a binary mixture of poppy and waste cooking biodiesel
8. Yamin JA et al (2013) Environmental and performance study of a 4-stroke CI engine powered with WCO biodiesel
9. Agarwal D, Sinha S, Agarwal AK (2006) Experimental investigation of control of NOX emissions in biodiesel-fueled compression ignition engine. *Renew Energy* 31:2356–2369
10. Carraretto C, Macor A, Mirandola A, Stoppato A, Tonon S (2004) Biodiesel as alternative fuel: experimental analysis and energetic evaluations. *Energy* 29:2195–2211
11. Singh B, Kaur J, Singh K (2010) Production of biodiesel from used mustard oil and its performance analysis in internal combustion engine. *J Energy Resour Technol* 132(3):031001
12. Cardone M, Prati MV, Rocco V, Senatore A (1998) Experimental analysis of performances and emissions of a diesel engine fuelled with biodiesel and diesel oil blends. In: *Proceedings of MIS–MAC V, Roma*, pp 211–225

Influence of Process Parameter of Die-Sinking Electric Discharge Machining on Machining of Grade-2 Type Titanium



Kuwar Mausam

Abstract Electro discharge Machining has become increasingly popular in terms of effective non-conventional machining processes in recent times. It has capability to effectively machining material with conductive properties regardless of property related to mechanical strength. MRR increases with increase in current Sluggish behavior of EDM for mass production-based targets. Reduced external quality, residual stresses are the main disadvantage of the process. Researchers have suggested numerous results to improve EDM machinability by optimization of process parameters. In this paper researcher investigate the effect of process parameter of EDM over MRR and TWR for Titanium work-pieces, Titanium is widely used in aeronautic industry, its MRR has to be optimized hence various optimization methods are being used. Researchers found out that as the current increase the MRR increase and TWR is also high, but at the mean value range of voltage TWR is at minimum level. Increment of T_{on} leads to high MRR and T_{off} optimum value responsible for the low TWR.

Keywords Electro discharge machining · Tool wear rate · Machinability · Material removal rate

1 Introduction

The use of Titanium (Ti) as alloying element in steel to decrease grain size, in Stainless Steel to decrease the content of carbon, etc. is widely used all over the world. Almost 96% of titanium ore is destined for refined titanium dioxide (TiO_2) to be used as pigments, additives, and coatings [1]. In Aerospace and marine field also titanium alloys are widely used due to their high tensile strength to density ratio and their ability to withstand high temperatures [2]. Titanium alloys are also used in automotive applications as consumer and architectural advancements. However, machining

K. Mausam (✉)

Department of Mechanical Engineering, GLA University, Mathura, Uttar Pradesh, India
e-mail: kuwar.mausam@gla.ac.in

IIT(ISM), Dhanbad, Jharkhand, India

of titanium also presents unique challenges. The properties that make titanium such an important element, the same properties make it difficult to get machined [2, 3]. Because of its high work hardening tendency and long continuous chips are formed during turning and drilling, which can entangle tools and impede function. Our experimental study, reveals the peculiar mechanical and chemical changes that occur when using nanofluid (Graphene) is used instead of Dielectric fluid (Transformer oil) while machining of Titanium takes place via EDM machine. EDM removes metal by means of electric spark erosion in a controlled manner. Dielectric fluid plays a major role in determining material removal rate and surface finish during operation. It basically controls electric discharge and absorbs heat during process. Our research is done using both dielectric fluid (transformer fluid) and nanofluid (graphene). We eventually found the increase in the thickness of recast layer when using Graphene instead of Transformer oil as lubricant fluid. Our study is based on Taguchi method for reducing the possibility of defects and failures in correct reading. Our research and study can enhance the surface finish and the mechanical properties of Titanium which can be further commercialized. The experiments were performed to improve the machining process parameter of EDM while machining Titanium material. There have been many models by various researchers to optimize the process parameter of EDM. Some of them are Bhattacharyya et al. presented a response surface methodology-based mathematical model for prediction of surface crack density, white layer thickness, and surface roughness [4]. Some of the researchers have proposed a model that utilized some other integrated optimization methods like Taguchi's parameter design, RSM (response surface methodology), neural network, GA (genetic algorithm), etc. in the prediction of optimal process parameters for die-sinking EDM and wire-cut EDM for single response value and double response value. There have been other simple methods for optimization of process parameters like Taguchi, TOPSIS. Taguchi takes the help of signal-to-noise ratio for getting the optimum level of process parameter [5, 6]. However, it does not present the optimal results as it only focuses on discrete variables. TOPSIS (Technique of order of preference by Similarity to Ideal solution) is a multi-factor decision-making algorithm. The most widely used method is Genetic Algorithm. It is quite popular and has wide engineering application. To overcome the drawbacks of non-traditional techniques some of the new techniques like the algorithm based on biological genetics is also used by some of the researchers. These techniques are more robust as compared to the previous technique as instead of using functional derivatives fitness information is used in these techniques.

1.1 Need for Optimization

In this era of technical modernization, even a small optimization can cause drastic enhancement in industries in terms of reduced time and saved money. Former researchers came across numerous limitations incorporated in EDM like large floor space, high cost of initial investment, and power consumption at higher rate, [2].

Also, only conductive materials can be machined and are costlier in comparison to traditional processes such as turning and milling. So, it is recommended to select process parameters very carefully. EDM is known for its Material Removal Rate (MRR) and Roughness Parameter, average Roughness (Ra) [2, 7]. Hence, to obtain optimum machining results, suitable process parameters are critical to achieving. Many researchers and industries are taking pains to maximize MRR and minimize Ra via EDM.

In this paper, our optimization in process parameters on Titanium will drastically improve the titanium machining optimum results to be effectively used in industries. Also, the use of nanofluid instead of dielectric fluid will improve the thickness of recast layer by 2.5 times that generated by conventional EDM.

2 Investigation Setup

Mitsubishi makes EA-8 Model Spark EDM utilized for experimental works. The experiment was to calculate the MRR (Material Removal Rate) by modifying the process parameters and finally obtaining the optimum results for the defined process parameters. Important process parameters of EDM that we have optimized are Current, Voltage Gap, Working Voltage, Pulse on time, Pulse off time, Gap between workpiece and tool, Polarity, and Dielectric Medium.

Material removal from workpiece and tool is taken place due to the thermoelectric process, in this process discrete spark series between the tool and workpiece is responsible for the material removal [3, 4]. EDM being a thermal process, optimized tools and process parameters are used during experiments [5–7]. The tool used here was electrolytic copper. Polarity used was NEGATIVE POLARITY, i.e., workpiece was connected to negative terminal and the tool was linked to positive terminal during this experimentation via EDM. This was done because of high tool wear in positive polarity due to high energy distribution at the cathode.

For the process parameters mentioned above, these parameters basically affect the spark origin in the EDM thermal process. The variables as a response to these parameters are supposed to be MRR (Material Removal Rate) and TWR (Tool Wear Rate). The process parameters values for few machining parameters as an example are mentioned in the Table 1.

Table 1 Parameters and their example values used for optimum results

Machining parameters	Level 1	Level 2	Level 3
Current (Ig)	6	8	10
Voltage (Vg)	50	60	70
Time-ON	200	360	280
Time-OFF	5	6	7
Machining time	30	30	30

Table 2 Experimental condition for EDM on titanium

S. No.	Particulars	Details
1	Work piece	Titanium plate (20 mm * 3 mm)
2	Electrode	Electrolytic Cu
3	Dielectric fluid	Dielectric oil
4	Polarity	Negative

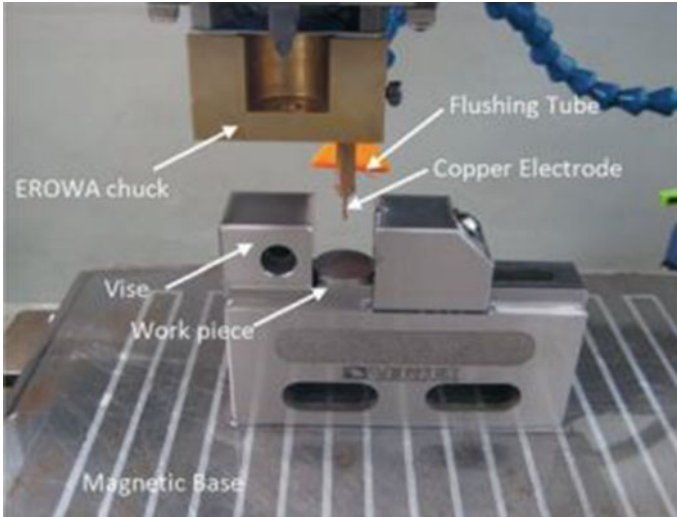


Fig. 1 EDM setup used in experimentation

Table 1 clearly reveals the example of values taken for few parameters pertaining to machining time as constant throughout the investigation. The experiments were conducted various times for different values of parameters. Finally, results were recorded for statistical analysis. The detailed investigational settings are mentioned in the Table2.

Before and after each test, the workpiece is carefully weighed for content calculation of material removal and wearing of the tool. The experimental setup is shown in Fig. 1.

3 Results and Discussions

See Table 3.

Table 3 Experimental values for MRR and TWR

S. No.	Time	(I_p)	(V_g)	T_{on}	T_{off}	MR	TR	MRR	TWR
1	30	6	50	200	5	0.024	0.003	0.0008	0.0001
2	30	6	50	280	6	0.036	0.004	0.0012	0.000133
3	30	6	50	360	7	0.038	0.003	0.001267	0.0001
4	30	6	60	200	5	0.024	0.006	0.0008	0.0002
5	30	6	60	280	6	0.031	0.004	0.001033	0.000133
6	30	6	60	360	7	0.033	0.003	0.0011	0.0001
7	30	6	70	200	5	0.012	0.004	0.0004	0.000133
8	30	6	70	280	6	0.024	0.003	0.0008	1E-04
9	30	6	70	360	7	0.019	0.003	0.000633	0.0001
10	30	8	50	280	5	0.045	0.009	0.0015	0.0003
11	30	8	50	360	6	0.044	0.011	0.001467	0.000367
12	30	8	50	200	7	0.005	0.002	0.000167	6.67E-05
13	30	8	60	280	5	0.03	0.006	0.001	0.0002
14	30	8	60	360	6	0.05	0.014	0.001667	0.000467
15	30	8	60	200	7	0.052	0.012	0.001733	0.0004
16	30	8	70	280	5	0.028	0.006	0.000933	0.0002
17	30	8	70	360	6	0.037	0.004	0.001233	0.000133
18	30	8	70	200	7	0.043	0.012	0.001433	0.0004
19	30	10	50	360	5	0.04	0.007	0.001333	0.000233
20	30	10	50	200	6	0.055	0.02	0.001833	0.000667
21	30	10	50	280	7	0.07	0.016	0.002333	0.000533
22	30	10	60	360	5	0.045	0.01	0.0015	0.000333
23	30	10	60	200	6	0.052	0.017	0.001733	0.000567
24	30	10	60	280	7	0.064	0.014	0.002133	0.000467
25	30	10	70	360	5	0.041	0.007	0.001367	0.000233
26	30	10	70	200	6	0.048	0.018	0.0016	0.0006
27	30	10	70	280	7	0.046	0.009	0.001533	0.0003

3.1 Effect of Voltage and Current on MRR

As shown in the contour plot in Fig. 2. At an average value of voltage the MRR increases with increase in current. For getting the optimal value we can say that the optimum MRR can be found at a voltage between 60 and 65 and the current of 10 A will give highest MRR.

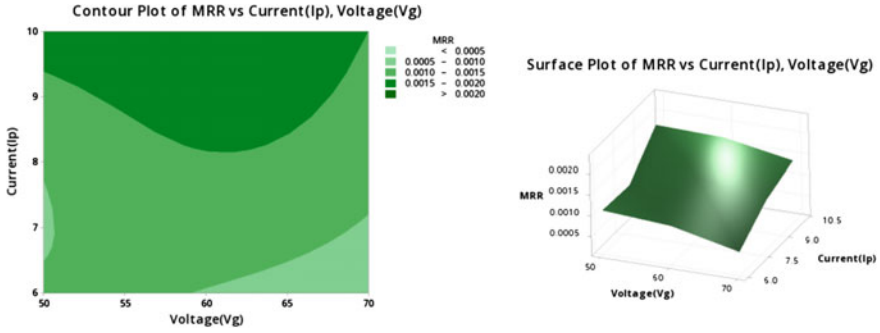


Fig. 2 Contour and surface plot of MRR versus I versus V

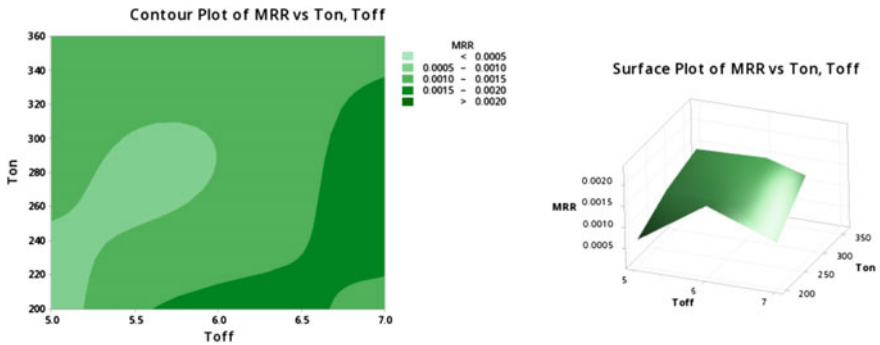


Fig. 3 Contour and surface plot of MRR versus T_{on} versus T_{off}

3.2 Effect of T_{on} and T_{off} on MRR

On increasing the value of T_{on} , MRR increases but an optimal value of T_{off} drastically increases the MRR so we can say that we should a T_{off} at some constant value (6–7 μ s) and then increase the T_{on} so we will get a high MRR (Fig. 3).

3.3 Effect of Voltage and Current on TWR

As the trends are shown in graph as we increase the current the tool wear rate also increases with the increase in current but at the mean position or at a voltage of 60–65 V we see the lowest tool wear rate but highest MRR so it can be inferred from the graph to have an optimal value of voltage to get high MRR but low TWR (Fig. 4).

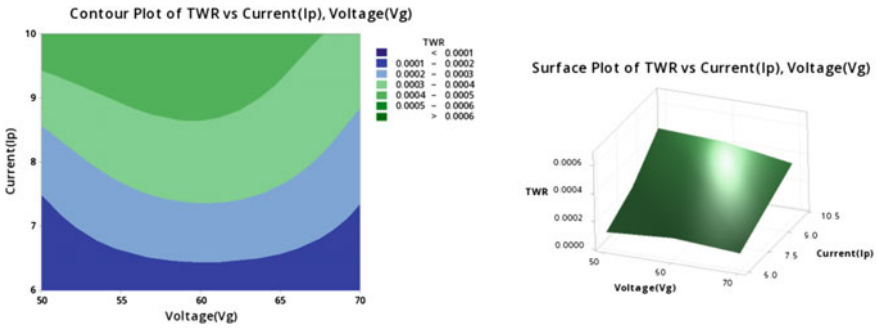


Fig. 4 Contour and surface plot of TWR versus V versus I

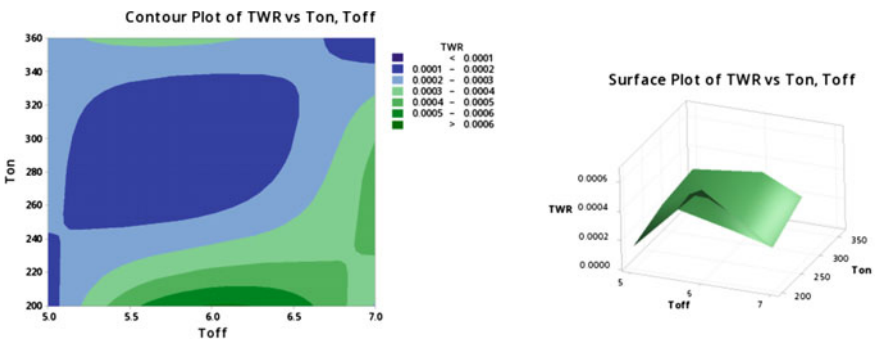


Fig. 5 Contour and surface plot of TWR versus T_{on} versus T_{off}

3.4 Effect of T_{on} and T_{off} on TWR

The lowest value of TWR was at average value of T_{on} and T_{off} . When T_{on} is between 260 and 320 and T_{off} is between 5.5 and 6.5 we get the lowest value of TWR so we can say that at $T_{off} = 6.5$ and $T_{on} = 320$ we get the highest value of MRR and lowest value of TWR.

4 Conclusion

In this experiment, various process parameters were used to get their optimal value while machining titanium grade 2 on electron discharge machine. The process parameter which was used for this experiment is voltage, current, T_{on} , T_{off} . The experimental parameter which was generated using Taguchi method in our range has shown some optimal value in the given range as expected. The main concluding results are

1. At a voltage of 60–65 V and the current ranges between 8 and 9 A we get the highest MRR at the expense of the lowest TWR so this can be regarded as an optimal value of voltage and current for machining of Titanium.
2. As for as T_{on} and T_{off} are considered the optimal value of T_{on} ranges between 300 and 320 μ s while T_{off} is 6–7 μ s. In this range, we get most optimum result, A high MRR at a low TWR.

References

1. F.: Article title. Journal 2(5), 99–110 (2016). Dauw DF et al (1990) Surface topography investigations by fractal analysis of spark eroded electrically conductive ceramics. CIRP Annals Manuf Technol 39(1):161–165
2. Shankar Singh S et al (2004) Some investigations into the electric discharge machining of hardened tool steel using different electrode materials. J Mat Process Technol 149:272–277
3. Haron C et al (2001) Investigation on the influence of machining parameters when machining tool steel using EDM. J Mat Process Technol 116:84–87
4. Dave KV et al (2012) Influence of electrode geometry and process parameters on surface quality and MRR in electrical discharge machining (EDM) of AISI H13. Int J Eng Res Appl (IJERA) 2(3):1498–1505
5. Tiwari M et al (2013) Experimental analysis of electro-discharge machining parameters for minimum tool wear rate on machinability of carbon fiber/epoxy composites using Taguchi method. Int J Eng Res Technol (IJERT) 2(10):3182–3188. ISSN: 2278-0181
6. singh RP et al Selection of optimum honing parameter for surface roughness using design of experiment. In: International conference on frontiers in engineering, applied science and technology, March 31–April, 2017, NIT, Trichy, Tamilnadu
7. Mausam K et al (2019) Multi-objective optimization design of die-sinking electric discharge machine (EDM) machining parameter for CNT-reinforced carbon fibre nanocomposite using grey relational analysis. J Braz Soc Mech Sci Eng 41:348. <https://doi.org/10.1007/s40430-019-1850-4>

A Broad Review of Biodiesel Feedstocks with Competency to Replace Diesel



Ashish Dewangan , Anand Bahadur Singh, Anurag Srivastava, Amartya Srivastava, Ankush Patel, and Ashok Kumar Yadav 

Abstract An ever-increasing dependency on fossil fuels is driving them to the verge of depletion, thus requiring a better alternative. Biodiesel has the best similarity to conventional fuel, hence incorporating it will surely decrease the reliance on fossil sources. The current paper has a thorough review of various biodiesel feedstocks while pointing over each aspect of it, including the production, extraction, qualities, properties, and production to compensate for the demerits of different biodiesel feedstocks and a discussion on their future practices as well. A thorough study has been done on six different non-edible feedstocks available like the Pongamia, Mahua, Manilkara Zapota, Algae, Jojoba, and Moringa Olifera oils along with properties namely kinematic viscosity, density, flash point, fire point, cloud point, pour point, cetane number, calorific value, and oxidation stability. Mahua and Jojoba biodiesel can be proved to be a promising feedstock as mahua has least kinematic viscosity of 3.9 mm²/s and jojoba biodiesel has the best calorific value of 47.12 MJ/kg. Economic viability and efficiency are the major parameters to be checked before commercializing a fuel and thus the blended biodiesel fuel of mahua and jojoba will certainly replace the conventional diesel fuel in near future.

Keywords Biodiesel · Kinematic viscosity · Cetane number · Calorific value · Density · Performance · Emission

1 Introduction

Diesel fuel is the conventional fuel which is a mixture of hydrocarbons obtained by distillation of crude oil. India's demand for diesel is always on a higher side with consumption of 40 million tons in 1998–99 to nearly 80 million tons in 2019–20

A. Dewangan (✉) · A. B. Singh · A. Srivastava · A. Srivastava · A. Patel
Department of Mechanical Engineering, Galgotias College of Engineering and Technology,
Greater Noida, India
e-mail: ashish.dewangan@galgotiacollege.edu

A. K. Yadav
Department of Mechanical Engineering, Raj Kumar Goel Institute of Technology, Ghaziabad,
India

© The Author(s), under exclusive license to Springer Nature Singapore Pte Ltd. 2023
S. Yadav et al. (eds.), *Advances in Mechanical and Energy Technology*, Lecture Notes
in Mechanical Engineering, https://doi.org/10.1007/978-981-19-1618-2_28

285

[1]. With the advancement of automobile industry day by day, more cars and trucks are using diesel as fuel. Owing to more usage, there is a risk of extinction of diesel fuel, and also it adds to the pollution level to great extent. Various countries across world are planning to ban the usage of diesel and petrol and adopt the alternate fuels in coming 30–40 years. The exhaust of diesel produces thousands of gases and fine particles (commonly called soot) that contain several toxic air contaminants. These may include hazardous substances such as benzene, arsenic acid, and formaldehyde. Another emission like nitrogen oxides, CO_2 , etc. affects environment adversely. Also due to more demand and less availability, the cost of diesel is increasing day by day.

So, to counter the cons of the diesel various researches have been done to appreciate usage of biodiesel which can be alternative source of fuel in CI engines. It can be easily derived from various edible and non-edible sources of oil and from microalgae. In the technical terms, biodiesel is long-chained mono-alkyl fatty acid ester that is extracted from the animal fats or vegetable oils. Biodiesel is renewable, bio-degradable, environment friendly, and can be viable alternative to the limited fossil fuels in the near future. It has reduced emission of NO_x , Sulfur, and Carbon monoxide and due to the proper combustion, the unburnt HC emission is also restricted [2]. It has positive economic impact on the country that the land and the soil condition favor the growth of such resources.

Out of different edible and non-edible oils available, attention has been given toward the non-edible ones because the former is consumed by the humans, and using them will lead to a sudden rise in the good's prices.

1.1 Production

Oils can be of two types edible and non-edible type. The FFA content on the oil starts formation of soap with alkali, which is required to minimize its presence in non-edible oils. Acidic ion conversation resins can be very productive in decreasing FFA levels [3]. Four different processes can be accommodated in converting these oils and fats into pure biodiesel namely transesterification, blending, micro-emulsion, and pyrolysis. Out of these, Transesterification process is popularly used. If FFA (Free Fatty Acid) content in oil is more than 2–3%, 2-stage transesterification process for conversion into biodiesel is applied. The 2-stage process involves the reduction of FFA contents by acid-catalyzed esterification followed by base-catalyzed transesterification for conversion of vegetable oil into FAME (Fatty Acid Methyl Ester) [4].

Transesterification is a process of reducing high viscosity without affecting the CV (calorific value) of fuel and as a result improves the fuel atomization, combustion, and exhaust emissions of oil and is also known as alcoholizes. It is the process in which alcohol is replaced by an ester, this reaction is same as hydrolysis. Ethanol and methanol are most suitable for this process. In this reaction, triglycerides are

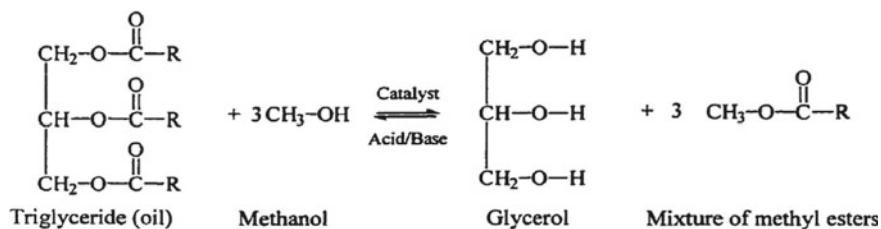


Fig. 1 Transesterification reaction

subsequently reacting with alcohol and produce diglycerides, then monoglycerides, and finally ester and glycerol as final product. Figure 1 shows the transesterification reaction.

1.2 Properties

The fuel qualities must adhere to the ASTM 6751-3 or EN14214 standards and the qualities include calorific value, density, flash point, pour point, cloud point, acid value, oxidation stability, and kinematic viscosity. These physiochemical properties of the fuel basically depend on FFA contents. Kinematic viscosity is ability of any material to flow. The max. limit of biodiesel according to the ASTM standards is around 1.9–6.0 mm²/s. Under the ASTM D1298 and EN3675/12185 density of biodiesel should be under 880 kg/m³ at a testing temperature of 15 or 20 °C. For the safe transport and storage handling, ASTM D93 limits are 93 °C whereas for the diesel fuel, it is around 55–66 °C but generally biodiesel fuels have more than 150 °C [5]. The Cloud Point (CP) is the temp. at which wax crystals are started to form and the lowest temp. at which the fuel can flow or becomes wax gel solution is known as the Pour Point (PP). Cold Filter Plugging Point (CFPP) can be defined as the fuel's limit of filterability or the temp at which filter starts to plug due to the gel-like nature of the fuel or the crystal formation and it is measured with the ASTM D6371 [6]. According to ASTM D613 minimum, CN of biodiesel can be 47 and minimum 51 according to the EN ISO 5165 whereas diesel fuel can have CN between 44 and 55 [7]. ASTM D6751 has a minimum limit of 3 h of oxidation stability and EN 14214 has a greater 6 h minimum limit and while these are measured at a testing temperature of 110 °C by Rancimat method EN ISO 14112.

2 Review of Feedstocks

2.1 *Pongamia pinnata* (Karanja)

Pongamia pinnata is also known as *Derris indica*. It belongs to the family of Leguminosae and has flexible benefits conferring to weather and seasons. 200 MMT/year of *Pongamia* oil is produced in India which can be considered as a decent feedstock for biodiesel blend. The seed comprises 28–34% oil with large percentage of polyunsaturated fatty acids. In history, *Pongamia* had been used for medicinal purposes, majorly in Ayurveda medicine [3]. Every part of this plant can be used for treatment of diseases such as tumors, piles, skin itches, and many other infections. Naturally, *Pongamia* is found over the shores and riversides of Myanmar and India and also found in humid tropical lowlands around Philippines, Malaysia, Australia, the Seychelles, the United States of America, and Indonesia. *Pongamia Pinnata* plantation is done around every state of India which comprises the major producers like Andhra Pradesh, Karnataka, Kerala, Jharkhand, Chhattisgarh, Bihar, Orissa, Madhya Pradesh, and West Bengal [3].

Pongamia pinnata vegetable oil can yield up to 99% when treated in ideal conditions. Table 1 shows the properties of *pongamia* biodiesel of B100, B40, B20, and conventional diesel. As only up to B40 blend similarities can be seen with diesel.

From Table 1 it was found that the B20 blend has similar CV as diesel and the B40 blends also show the comparable results after some post-processing. The possible reason for the decreased calorific value is the greater oxygen content in the blend which also helps in the complete combustion of the biodiesel [3, 5]. Transesterification lowers the flashpoint of biodiesel but is still over that of diesel. The acid methyl ester present in the *pongamia* or any biodiesel is more disposed to oxidation at room temperature. Poor oxidation stability consequences for the filter clogging, fuel congealing, creation of gums, and injector fouling. Conversion of R-H group

Table 1 *Pongamia* biodiesel fuel properties [3, 5]

Fuel Properties	B100	B40	B20	Diesel
Specific gravity	0.876–0.939	0.856	0.848	0.8
Kinematic viscosity (mm ² /s) at 40 (°C)	3.99–11.82	3.51–4.63	3.01–3.49	1.3–4.1
Flashpoint (°C)	147–196	81–99	76–96	60–80
Calorific value (MJ/Kg)	35.56–42.17	37.85–43.15	38.28–43.6	44.8
Cloud point (°C)	–3 to 22.5	10.9–18	7.1–14.1	–15 to 5
Pour point (°C)	–4 to 15	3.6–5.7	1.8–3.6	–35 to –15
Density	869–884	854	851–862	830
Cetane number	47.78–57.9	–	51	40–55
Oxidation stability at 110 °C, h	2.3–11.6	–	–	–
Acid value (mg KOH/gm)	0.62–0.80	–	–	–

to hydroperoxide group (ROOH) occurs during autoxidation which again reduces to carbonyl and carboxylic acid by chain oxidation reaction. Researchers have found that synthetic phenolic antioxidants can affect the storage oxidation stability of pongamia biodiesel and standards have also been set to a minimum of 6 h induction period at 110 °C. Rancimat method is taken into action for determining the oxidation stability. By using this Rancimat experiment researchers have found that Pyrogallol (PY) has the antioxidants properties when used for pongamia biodiesel and increases the induction time to 34.35 h at a PY concentration of 3000 ppm at 110 °C [3, 5, 6].

2.2 Mahua Oil (*Madhuca Indica*)

Botanical name of Mahua oil is *Madhuca Indica* and it belongs to the family of Spotaceae. These are up to 15 m tall deciduous trees, with dense and shady canopy with a brown rough bark [7]. These are mainly found in South Indian forests, West Bengal, Maharashtra, and Orissa. Research figures show that possible maximum yield of 90% can be obtained from Mahua oil [8]. Oil is extracted from the kernel of seeds containing 50–55% oil. At present, 4,00,000 tons/year of these oils are estimated to be produced. FFA content of mahua oil extracted is above 15% which is why esterification is done which is followed by the transesterification process. Its physiochemical properties were found to meet the ASTM standards. On the basis of different literature available, properties of Mahua biodiesel is shown in Table 2.

Table 2 Comparison of properties of Mahua biodiesel and diesel [7–9]

Properties	ASTM D6751	Mahua biodiesel	Straight diesel
Kinematic viscosity at 40 °C (mm ² /s)	1.9–6.0	3.9	3.18
Density at 15 °C (Kg/m ³)	860–900	872	839
Flash point (°C)	Min 130	205	68
Calorific value (MJ/Kg)	–	39	44.8
Ash content (%)	<0.02	0.02	0.01
Fire point (°C)	Min 145	218	103
Carbon residue (%)	–	0.2	0.1
Cetane number	–	52	51
Acid value, mg KOH	<0.8	0.5	0.35

2.3 *Moringa olifera*

Moringa olifera is commonly known as moringa, benzoil, horseradish tree, drumstick trees and comes from a family of Moringaceae which is indigenous to sub-Himalayan part of north-western India. *Moringa Olifera* possesses significant quantity of behenic acid (docosanoic) thus commercially also called “behen oil” or “ben oil” and also has more resistance to oxidative degradation. *M.olifera* has also been showing significant medicinal uses and nutritional value to it. An average growth of tree is about 10 m in height and is best cultivated in dry sandy soil or drought-prone areas withstanding poor soil pH ranging between 5 and 9. Spreading the cultivation from Australia, Africa, Asia, Latin America, and other oceanic countries with major producers from Queensland, Northern Territory, and Western Australia. Apart from Himalayan foothills in India cultivation of *Moringa Olifera* can also be found in the southern states of Tamil Nadu, Kerala, Andhra Pradesh, and Karnataka [9–11].

Rashed et al. [10] found 35% w/w biodiesel from *M. Olifera* seed with a high acid value of 2.9. This high content of acid results in demanding a two-step transesterification process. The maximum yield from the crude oil after transesterification process is about 94.30%. The value of different standard properties of *Moringa Olifera* can be seen in Table 3 and are compared to the standard ASTM standards.

From Table 3, it can be concluded that the flashpoint of moringa biodiesel is 162 °C which is quite greater than the ASTM standards also, it is not a demerit as it arises a beneficial point to conclude that this biodiesel can be stored safely at room temperature. Higher values of cloud point (CP) and pour points (PP) can be seen as a major problem of biodiesel rising from the lower temperature flow possessions (cloud point & pour point) as it is the temperature at which the primary solids are underway to form in liquid fuel [11, 12]. Cetane number can be a major deciding parameter for any feasible biodiesel production which in case of *Moringa Olifera*, was found to be 67 which is greater than the conventional diesel. Oxidative stability stands to be 3.61 h at 110°C as per the Rancimat test which however is sufficient by

Table 3 Properties of *Moringa Olifera* biodiesel as compared to ASTM and conventional diesel fuel [3, 10–12]

Fuel properties	Moringa biodiesel	Diesel	ASTM standards
Kinematic viscosity (mm ² /s) at 40 °C	4.8	1.3–4.2	1.9–6
Flash point (°C)	162	60–80	130 max
Calorific value (MJ/Kg)	43.28	44.8	–
Cloud point (°C)	17	–15 to 5	–3 to 12
Pour point (°C)	17	–35 to –15	–15 to 16
Density	875	830	880 max
Cetane number	67	40–55	47 min
Oxidation stability at 110°C, h	3.61	58.2	3 min
Acid Value (mg KOH/gm)	0.38	0.24	0.5 max

ASTM standards of 3 h but it is not fulfilling the European standard EN14214 of 6 h. This, however, is the major demerit of any biodiesel fuel but still, some exceptions are also present and research is ongoing on how to increase the oxidative stability [3, 10–12].

2.4 *Manilkara Zapota (Chikoo)*

Manilkara Zapota is the scientific name of commonly used fruit known as Chikoo or Sapodilla. An evergreen tree that can grow up to 5–20 m is basically native to countries like Mexico and West Indies and other parts of Central America but is now widely cultivated in tropical and subtropical areas. It is fruit-bearing tree is found in South East Asia and grown in households, and plantations. The largest producing countries are India, Thailand, Philippines, and Malaysia. It is rich in sugar, protein, and minerals like iron, copper, calcium, and potassium. Its leaves have high medicinal value. Various results have shown the oil yielding of 90% from the seeds of zapota fruit. Biodiesel from its seed is mainly composed of methyl esters of oleic, stearic, and palmitic acids. Hence, it was found that the biodiesel derived from *M. Zapota* would be a good alternative to conventional diesel [13, 14].

Table 4 shows the physical properties of biodiesel. Comparing different properties of *M. Zapota* biodiesel and normal diesel, it was found that the effectiveness of using biodiesel as replacement for diesel. The viscosity of oil before transesterification was found to be 11.74 times that of diesel. After the transesterification, it is found to be 1.57 times which is well within the limits of use of biodiesel standards. CP and PP are important parameters to measure the cold weather characteristics of any fuel. Both oil and biodiesel satisfy minimum criteria of below 1 °C. The flashpoint of oil was measured as 1.4 times more than that of biodiesel and five times more than that of

Table 4 Physical Properties of *M. Zapota* Biodiesel as per EN 14214 standards [14, 15]

Sr. no.	Property	EN 14214	Units	MZME	Diesel
1	Ester content	Min 96.5	% (m/m)	96.8	
2	Density at 15 °C	0.86–0.90	g/cm ³	0.875	0.861
3	Kinematic viscosity	3.5–5	mm ² /s	4.67	2.96
4	Acid value	Max 0.50	mg KOH/g	0.15	0.18
5	Flash point	Min 120	°C	174	48
6	Pour point	Max 0	°C	–6	–12
7	Iodine value	Max 120	g iodine/100 g	65.28	–
8	Cetane number	Min 51	–	52	51
9	Glycerol	Max 0.25	% (m/m)	0.17	–
10	Heating value	Min 35	MJ/kg	37.2	44.8
11	Sulfur content	Max 10	mg/kg	0	350

conventional diesel. Iodine number shows the stability of oxidation of biodiesel. The iodine number of the biodiesel is within the limit. The Acid value of oil was 1.96 and after transesterification, it was reduced to 0.15 which can be compared with diesel. The emission of CO is less for biodiesel and its blends as compared to diesel [15, 16]. However, all blends show high CO₂ and NO_x emissions which can be curbed by identification of suitable nano additives. [15, 17, 18].

2.5 Algae

Algae can be found in freshwater, sea, and slightly wetlands. On the basis of pigmentation, they can be broadly classified into three groups, i.e., green seaweed (*Chlorophyceae*), brown seaweed (*Phaeophyceae*), and red seaweed (*Rhodophyceae*). These micro-organisms generally convert water, carbon dioxide, and sunlight to algal biomass. Microalgae did not demand irrigation and fertile land as compared to the terrestrial plants. On the basis of abundance, they are classified into three important categories that are the golden algae, the green algae, and the diatoms (*Bacillariophyceae*) [19]. The algae fuel is considered to be a better alternative when compared with various other sources of the biodiesel available such as sugarcane, corn, etc. The algal biomass has high oil yield which makes it suitable to convert into biodiesel. The microalgae species such as *Kirchneriella lunaris*, *Ankistrodesmus fusiformis*, *Chlamydocapsa bacillus*, and *Ankistrodesmus falcatus* have high levels of polyunsaturated fatty acid which is used for biodiesel production. Algae multiply themselves by double in a day and oil content is found to be very high, which can exceed up to 80%. Algae has potential to produce about 5000–15,000 gallons of biodiesel from algal biomass per acre per year, which shows its potential. One limitation of algal biodiesel is that the high degree of polyunsaturated fatty acids which makes it prone to oxidation [19].

From Table 5, it can be concluded that properties tested from different microalgae biodiesel are comparable to conventional biodiesel and are also fulfilling the standard criteria from ASTM. Kinematic viscosity of algae oil is at an upper range of around 5.5 mm²/s for a standard biodiesel of 6 mm²/s. Pour point is at –12 °C which is good for running engine with this microalgae biodiesel at colder temperatures without any freezing problem [20]. Handling storage challenges for this biodiesel are at minimum due to the higher oxidation stability of about 7 h during the Rancimat test and also due to the better cold flow properties. Heating value is also quite comparable with petroleum diesel at 41 MJ/kg and is also satisfying the ASTM D6751 criteria. Density is still at an alarming range however much research is still going to reduce the density of algal oil and make it replace the conventional diesel fuel [21].

Table 5 Comparison of algae fuel with diesel and ASTM standards [19–21]

Fuel properties	Algae biodiesel (B100)	Diesel	ASTM D6751
Kinematic viscosity (mm ² /s) at 40 (°C)	5.2	1.3–4.1	1.9–6
Flash point (°C)	65–115	60–80	130 max
Calorific value (MJ/Kg)	41	44.8	–
Cloud point (°C)	4	–15 to 5	–3 to 12
Pour point (°C)	–2	–35 to –15	–15 to 16
Density	864 to 912	830	880 max
Cetane number	46.5	40–55	47 min
Oxidation stability at 110 °C, h	2.3	–	3 min
Acid value (mg KOH/gm)	0.14 to 0.38	–	0.5 max

2.6 *Simmondsia chinensis* (Jojoba)

Jojoba is given the botanical name *Simmondsia chinensis*, it belongs to the species of the family Simmondsiaceae. Different names are given to jojoba as gray box bush, goat nut, pignut, wild hazel, coffeeberry, quinine nut, and deer nut. These are the long-lasting and evergreen shrubs that can grow in parched and drylands of the country. The shrubs range from 3 to 6 feet high and somewhere they can grow up to 10 feet tall. Jojoba plant grows 0.4 inches to 0.8 inches with dark brown-colored seeds. The seeds take the shape of a corn. It has greenish-yellow small-sized flowers and there can be up to six sepals without any petals in the flower [22]. Lipid content of Jojoba seed varies between 45 and 55 wt. %, which is present in the long-chain fatty acid esters. Instead of triacylglycerols (TAG) encountered in the animal fats and other vegetable oils, alcohol (wax esters) is present in the oil [23].

As being a dry, arid type growth conditions favorable plant, it is planted in various semi-desert and desert regions, mainly in Australia, Mexico, Israel, Peru, Argentina, and the United States. It demands a soil pH value to lie between 5 and 8 [23].

Jojoba oil wax is processed to make biodiesel. The conversion reaction tends to give the 79% FAME along with 21% fatty alcohols and different other compositions of FAME and Fatty Alcohols under slightly different operating conditions [22].

From Table 6, it can be inferred that the jojoba has a high cetane number value which will reduce the ignition delay as well as increase the combustion quality. The flashpoint is also in the required range as per the diesel standards, i.e., between 60 and 80, thus providing a considerable ignition point to the fuel mixture. It also has high calorific value thus ensuring a proper combustion and thus reducing the carbon deposits in the engine and making it a better fuel substitute with lesser harmful emissions [24]. Thus, jojoba biodiesel has some promising attributes which can be used in order to counter the demerits of the non-renewable standard biodiesel and thus can substitute it in the upcoming future.

Table 6 Properties of Jojoba Biodiesel [22–24]

Property	Jojoba biodiesel
Flash point (°C)	154
Pour point (°C)	4.4
Kinematic viscosity at 40 (°C) (mm ² /sec)	19.2
Density at 23 (°C) (g/cm ³)	0.86
Cetane no	63.5
Calorific value (MJ/kg)	47.38
Iodine value (g/100 g)	82
Saponification value	92
Sulfur content % by mass	Nil
Carbon content % by mass	86.98
Ash content % by mass	0.002

3 Results and Discussion

A thorough study of different feedstocks has been conducted with their properties (Table 7). Some demerits were found but also have contrasting pros such that they can be mixed with each other and can be used to produce different blends which will incapacitate the demerits of each other. In this detailed theoretical discussion, different data was collected, and with the help of this, it can be predicted that the blending of biodiesels coming from different feedstocks can be done.

Table 7 Properties of selected feedstock

Fuel properties	Pongamia	Mahua	Moringa	Jojoba	M. Zapota	Algae	ASTM standards
Kinematic viscosity (mm ² /s) at 40 °C	3.99	3.9	4.8	19.2	4.67	5.2	1.9–6
Specific gravity	0.876	0.872	0.83	0.863	0.902	0.84	–
Flash point (°C)	147	205	162	154	174	110	–
Calorific value (MJ/Kg)	35.56	39	43.28	47.38	37.27	41	–
Cloud point (°C)	–3	16	17	7	–	4	–3 to 12
Pour point (°C)	–4	2	17	4.4	–6	–2	–15 to 16
Density	869	882	875	869	875	890	880 max
Cetane number	47.78	52	67	63.5	52	46.5	47 min
Oxidation stability at 110 °C, hours	2.3	–	3.61	–	–	2.3	3 min
Acid Value (mgKOH/gm)	0.62	0.5	0.38	0.4	0.15	0.28	0.5 max

- Mahua biodiesel has best kinematic viscosity of $3.9 \text{ mm}^2/\text{s}$ tested at 40°C which is under ASTM standards but still not less than conventional diesel fuel. Pongamia Pinnata has similar kinematic viscosity of $3.99 \text{ mm}^2/\text{s}$ tested at 40°C and can also be placed second after Mahua biodiesel. Kinematic viscosity directly affects the engine combustion efficiency and results in prolonged ignition delay.
- It can be inferred that Moringa (CN-67), Jojoba (CN-63.5), Mahua, and M. Zapota (CN-46.5) biodiesels have appreciable values for Cetane Number when compared with the ASTM Standards for diesel and biodiesels. CN affects the ignition delay and auto-ignition timing of the fuel and thus becomes the important parameter to be discussed. Thus, these can be blended to obtain a promising result in terms of fuel combustion properties.
- It can be inferred that Jojoba biodiesel has the highest calorific value of 47.12 followed by moringa, mahua, jatropha, and algae biodiesels, calorific value provides information regarding the fuel's burning quality.

4 Conclusion

This literature survey over different biodiesel feedstocks concludes several points which are prominent for selecting biodiesel to replace conventional diesel fuels-

- Mahua biodiesel has the least kinematic viscosity which further promotes the engine life; Moringa biodiesel stands out from others when selecting a fuel on the criteria of cetane number; Jojoba biodiesel releases higher thermal energy from the fuel and greater fuel efficiency as compared to other feedstocks.
- Blending mahua biodiesel and Jojoba biodiesel will result in better overall fuel, which will surpass all the required parameters as mahua has an edge of having least kinematic viscosity which increases the overall lifespan of engine, and Jojoba on the other hand has the best calorific value which produces better thermal efficiency and therefore becoming a suitable fuel to replace conventional diesel fuel without modifying the engine.

References

1. India's annual diesel consumption trend. <https://www.reuters.com/article/india-diesel-demand-idINKBN1Y80B9>
2. Dewangan A, Mallick A, Yadav AK, Kumar R (2020) Combustion-generated pollutions and strategy for its control in CI engines: a review. Mater Today Proc 21:1728–1733
3. Atabani AE, Silitonga AS, Badruddin IA, Mahlia TMI, Masjuki HH, Mekhilef S (2012) A comprehensive review on biodiesel as an alternative energy resource and its characteristics. Renew Sustain Energy Rev 16(4):2070–2093
4. Dewangan A, Yadav AK, Mallick A, Tyagi A (2020) Optimisation of biodiesel production and engine performance from Simarouba oil in compression ignition engine. Int J Oil Gas Coal Technol 25(3):357–376

5. Dwivedi G, Sharma MP (2014) Prospects of biodiesel from Pongamia in India. *Renew Sustain Energy Rev* 32:114–122
6. Yadav AK, Dewangan A, Mallick A (2018) Synthesis and stability study of biodiesel from Kachnar seed oil. *J Energy Eng* 144(5):04018053
7. Abdelmoez W, Tayeb AM, Mustafa A, Abdelhamid M (2016) Green approach for biodiesel production from jojoba oil supported by process modeling and simulation. *Int J Chem Reactor Eng* 14(1):185–193
8. Yadav AK, Khan ME, Pal A, Dubey AM (2017) Experimental investigations of performance and emissions characteristics of Kusum (*Schleicheraoleosa*) biodiesel in a multi-cylinder transportation diesel engine. *Waste Biomass Valorization* 8(4):1331–1341
9. Puhan S, Vedaraman N, Rambrahamam BV, Nagarajan G (2005) Mahua (*Madhuca indica*) seed oil: a source of renewable energy in India
10. Rashid U, Anwar F, Moser BR, Knothe G (2008) Moringa oleifera oil: a possible source of biodiesel. *Biore Technol* 99(17):8175–8179
11. Rashed MM, Masjuki HH, Kalam MA, Alabdulkarem A, Rahman MM, Imdadul HK, Rashedul HK (2016) Study of the oxidation stability and exhaust emission analysis of Moringa olifera biodiesel in a multi-cylinder diesel engine with aromatic amine antioxidants. *Renew Energy* 94:294–303
12. Oni BA, Sanni SE, Ibegbu AJ, Adujo AA (2021) Experimental optimization of engine performance of a dual-fuel compression-ignition engine operating on hydrogen-compressed natural gas and Moringa biodiesel. *Energy Rep* 7:607–619
13. Jayaraman J, Karthik M, Krishna BM, Joy N, Mariadhas A, Appavu P (2021) Impact of titanium oxide nano additives on the performance characteristics of a CI engine fuelled with manilkarazapota methyl ester blends. *Mater Today Proc* 44:3601–3605
14. Dewangan A, Mallick A (2017) Ultrasonic-assisted production of biodiesel from Manilkara Zapota (L.) seed oil. *Energy Sour Part A* 39(15):1594–1601
15. Kumar RS, Sivakumar S, Joshuva A, Deenadayalan G, Vishnuvardhan R (2019) Data set on optimization of ethyl ester production from sapota seed oil. *Data Brief* 25:104388
16. Dewangan A, Yadav AK, Mallick A, Pal A, Singh S (2019) Comparative study of Manilkara zapota and Karanja based biodiesel properties and its effect on diesel engine characteristics. *Energy Sour Part A*, pp 1–11
17. Dewangan A, Mallick A, Yadav AK, Richhariya AK (2020) Effect of metal oxide nanoparticles and engine parameters on the performance of a diesel engine: a review. *Mater Today Proc* 21:1722–1727
18. Yadav AK, Dewangan A, Mallick A (2018) Effect of n-butanol and diethyl ether on performance and emission characteristics of a diesel engine fueled with diesel–Pongamia biodiesel blend. *J Energy Eng* 144(6):04018062
19. Behera S, Singh R, Arora R, Sharma NK, Shukla M, Kumar S (2015) Scope of algae as third generation biofuels. *Front Bioeng Biotechnol* 2:90
20. Khan S, Siddique R, Sajjad W, Nabi G, Hayat KM, Duan P, Yao L (2017) Biodiesel production from algae to overcome the energy crisis. *HAYATI J Biosci* 24(4):163–167
21. Joshi MP, Thipse SS (2019) An evaluation of algae biofuel as the next generation alternative fuel and its effects on engine characteristics: a review. *Int J Mech Prod Eng Res Dev (IJMPERD)* 9:435–440
22. Abdelgadir HA, Van Staden J (2013) Ethnobotany, ethnopharmacology and toxicity of *Jatropha curcas* L. (Euphorbiaceae): a review. *S Afr J Bot* 88:204–218
23. Huzayyin AS, Bawady AH, Rady MA, Dawood A (2004) Experimental evaluation of diesel engine performance and emission using blends of jojoba oil and diesel fuel. *Energy Convers Manage* 45(13–14):2093–2112
24. Raja SA (2011) Biodiesel production from jatropha oil and its characterization. *Res J Chem Sci* 1:81–87

Aerodynamic Drag Reduction Using Biomimics Inspired Surface



Shubhesh Ranjan and Faisal Shameem

Abstract Paper that we are discussing about the aerodynamics drag reduction using Bionics inspired surface. It is one of the growing field of Bionics which allow these to imitate and created by the natural biology to develop nanomaterial, nano devices, and the technique which allow fascinating goods. In this work the computational technique is used to understand the aerodynamic drag reduction on the bio-inspired shark bumps on a flat plate. The CFD approach is given to the 3D-dimensional shark bumps and flat plate to predict the aerodynamics characteristics for the following model. This computational analysis of this bumps profile is done and completed using Ansys 19.1 Design modellar (workbench) and fluent software for simulation drag result of this model. The simulation run of this model on Reynolds Number Re (10,000). These all efforts aimed to enhance the aerodynamic representation of flat plate with bumps by the customization in their surface and inspired by drag reducing effects of the bumps which may sleeve the skin of sharks. This simulation based investigation in the aerodynamics effect of inspired design of bumps is placed on flat plate surface. The computational simulation extracts result from this model with this design constraints. The aim of this paper is based on the grip of Bionics reduction of drag and also provide new exposure to emphasize the current criteria for rating of bionic creature for the reduction of drag. Finally, computational results is validated with the theoretical results.

Keywords Ansys · Fluent · CFD · Workbench drag · Lift · Boundary layer · Reynolds number · Bio-inspired design · Bumps · Sharkskin · Solid works

S. Ranjan (✉) · F. Shameem
Department of Mechanical Engineering, Galgotias University, Greater Noida, Uttar Pradesh
203201, India
e-mail: shubhesh4u@gmail.com

F. Shameem
e-mail: faisal.shameem@galgotiasuniversity.edu.in

1 Introduction

Methods used for Drag Reduction:

Active Method: Active control is a technique which is a device that increases the actual frontal area of the vehicle, this method is used to reduce the drag reduction.

Passive Method:-Passive control is a method which is exerted through modification to the shape of the body. This method is used to reduce the drag reduction.

Biomimicry

Bio mimicry is the study of nature and natural wonders in order to learn about the fundamental components, to gain ideas from nature, and to apply those concepts to science, design, and medicine.

Bumps

Bumps, also called serrations, are little impacts on a tooth's surface that give it a serrated edge. In fossil research, similar-sized and-thickened bumps (bumps per unit distance) are used to depict and describe fossilized teeth, particularly those of dinosaurs.

2 Literature Review

The main aim for the most of the literature is to minimization of aerodynamic drag. The situation of current fuel rate increases high prices, in heavy vehicle the drag reduction is so much important factor because in heavy vehicle they consume very high amount of fuel and gives low mileage, so that the one of the most crucial factor in auto mobile is drag reduction and this factor directly affect the consumption of fuel. There are many techniques or method that researchers do to reduce drag reduction in this field. After observing or studying all these things in this field then I decided to complete my effort in "Biomimics inspired surface area" for drag reduction. Some of the literature showed, In Yu et al. reviewed different work in the field of drag reduction based inspired from biological surface of artificial function. In this review researcher worked on the bio inspired drag reduction. The work on the five different kind of nature organism is used to reduce the drag reduction. Jung et al. [1] in this paper, they investigate the drag reduction biomimetic surface structure, with micro and nano hierarchical, in this shark skin rib pattern surface is created. The pressure dropped by the process was measured through the water flow of laminar and turbulent, and it is explained in terms of the measuring value of the fluid models for surface pressure through different way and also quantify the air flow through this. Duo et al. [2] in this paper, skin friction drag reduction has been re-emphasized, in the last decades several management strategies and technologies are prompt to scale back the drag

friction, but mostly the unit area that need extra input of power for their active ones and complicate the devices. Khan et al. [3] worked on bio mimicry surface of dragon fly mimicked corrugated airfoil which is 2D-dimension. Ansys simulation run on Re 15,000–75,000. They also perform experimental test perform on 3D-Printer tested in subsonic wind tunnels and different speed and angle. Arunvinthan [4] et al. performed the test with the help of vortex generator with shark scales duction. The work on the five different kind of nature organism which is used to reduce the drag reduction. Jung et al. [1] in this paper, they investigate the drag reduction biomimetic surface structure, with micro and nano hierarchical, in this shark skin rib pattern surface is created. The pressure dropped by the process was measured through the water flow of laminar and turbulent, and it is explained in terms of the measuring value of the fluid models for surface pressure through different way and also quantify the air flow through this. Duo et al. [2] in this paper, skin friction drag reduction has been re-emphasized in the last decades several management strategies and technologies are prompt to scale back the drag friction, but mostly the unit area that need extra input of power for their active ones and complicate the devices. Actually, to explore the underlying drag reduction mechanism and to any reveal the exceptional options of animals in nature to reduce drag reduction. Khan et al. [3] worked on bio mimicry surface of dragon fly mimicked corrugated airfoil which is 2-d dimension. Ansys simulation run on Re 15,000 to 75,000. They also perform experimental test perform on 3D-Printer tested in subsonic wind tunnels and different speed and angle. Arunvinthan et al. [4] performed the test with the help of vortex generator with shark scales. The NACA 0015 symmetric airfoil's aerodynamic characteristics: The Shark scale based vortex generator models were extracted to base of NACA 0015 symmetric airfoil. Yakkundi et al. [5] created model of a car with wing spoiler in the rear and found result around 8.2% in ΔC_d at speed of 70 km/h. Kim et al. [6] review in that paper he designed golf ball but they don't have dimple surface on the ball but there is micro grooved surface on the balls and after that measuring the drag and lift force and compare with the velocity and rotational speed of the ball. After result they found that both drag and lift coefficient of micro-grooved surface is higher than dimpled surface ball. Kozlov et al. [7] reviewed in their paper the behaviour of boxfish using computational and experimental method. They tested on wind tunnel at some range of Reynolds number and Yaw angle to check the drag, lift and side forces. They found on the result with boxfish shape is approx 0.1 is quite low than drag coefficient of a passenger car. In result they found that in a bluff geometry the drag reduction is so favourable in case of boxfish. There is slight variation between two parameter $k-\epsilon$ and $k-\omega$. Chen [8] et al. reviews in their paper the mechanism and the morphology of the shark skin and method to fabricating the morphology surface. In result they found various fabrication method is used to reduce drag reduction and potential applications antifouling is an anticipated part from drag reduction. [9] Mariko Miyazaki review in this paper the study of biomimetic riblets structure that is inspired by bumps of sharkskin to combine the 3D model of digitizing clean computational fluid model of turbulent flows with a rough surface with bumps and round pattern grooves. In this they study the advance measuring and digital technique to see the computerized computational fluid dynamics model with X-Ray CT to see the micro structure of grooves. Dai et al.

[10] review in their paper they study the effect of fluid behaviour of water, there are several morphological parameter in this methodology for the orientation of shark skin to define the flow direction and ridges. This fluid performance is obtained by rheometer. Result find that at 90° scale orientation low velocity gradient at uniform particles. Li Wen et al. [11] review in this paper and investigate about the change of surface of biomimetic shark skin bumps and changing the effect of its spacing and arrangements in two criteria, these are static and dynamic locomotors performance [12].

3 Governing Equation

Computational Fluid Dynamics (CFD) model is crucial element to determine the appropriate arrangement technique. Navier-Stokes expression considered as the best approach to handle the airflow issue & examine the variation in the stream. The Navier-Stokes equation is the conventional approach which is utilized in all turbulence models and can be determine as a “standard” approach. The three conservation equations derived from the Navier stokes equation, based on the concept of Reynolds. The conservation equations technique under is the apex5 of Navier-Stokes conditions [13].

(a) **Continuity of mass**

$$\frac{\partial p}{\partial t} + \frac{\partial y}{\partial x_i}(pu_i) = 0 \quad (1)$$

(b) **Momentum equation**

$$\frac{\partial pu_i}{\partial t} + \frac{\partial}{\partial x_j}(p \cdot u_i u_j) = \frac{\partial p}{\partial x_i} + \frac{\partial \tau_{ij}}{\partial x_j} + pq \quad (2)$$

(c) **Energy equation**

$$\frac{\partial pc_p T}{\partial t} + \frac{\partial}{\partial x_j}(pc_p u_j T) = \frac{\partial p}{\partial x_i} \left(\lambda \frac{\partial T}{\partial x_i} \right) + \frac{\partial}{\partial x_j}(u_i \tau_{ij}) \quad (3)$$

The, x_i stands for coordinate direction, u_i velocity component denotes by u_i , τ_{ij} indicates the stress tensor factor. P indicates density and g indicates gravity.

Turbulent heat of flux of the eddy viscosity can be modelled is shown below

$$q_j^{\text{Re}} = -\bar{p}c_p u_j'' T'' = \frac{u_t c_p (T) \partial T}{\text{Pr}_t \partial x_j} \quad (4)$$

3.1 *K-ε Turbulence Model*

The procedure to represent the stream field to show the turbulence subsequent value of the stream field which can be mathematically revealed as [13]:

$$\frac{\partial u_i}{\partial t} + u_j \frac{\partial u_i}{\partial x_j} = -\frac{1}{\rho} \frac{\partial \bar{p}}{\partial x_i} + \frac{\partial}{\partial x_j} \left(\nu \frac{\partial \bar{u}_i}{\partial x_j} - \tau_{ij} \right); i = 1, 2, 4; j = 1, 2, 3; \quad (5)$$

4 Methodology

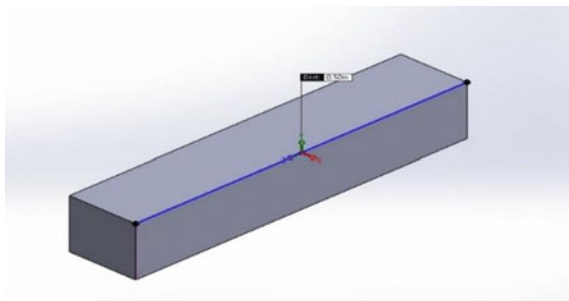
This model with proper dimension was designed in CAD software solid works. Various parameter like edges, faces were regulate and refined for improving the aerodynamics of the design model. This design model was meshed with suitable inputs and simulated at different speed variation in Ansys Fluent software [1, 14, 15], Bumps is designed and scaled according to the flat plate where the model of bumps to be placed on the flat plate. The final model is meshed and simulated as same as geometry or base model. Results recorded and observed for the final conclusion.

4.1 *Description of Biomimetic Model*

The biomimetic bumps with flat plate created utilized a detailed feature of given dimension in Figs. 1 and 2.

Bumps is designed in solid works with sweep, loft, boundary, trim, and untrim feature. The geometrical construction of this model is $X = 10 \text{ mm}$, $Y = 7 \text{ mm}$ and thickness of the model is approx. 3.5 mm. Especially bumps is also known as serration in other lan-guage. Deniticle is designed in that way where number of bumps placed on the bottom surface of flat plate with proper distance. Bumps, additionally called

Fig. 1 Flat plate without bumps



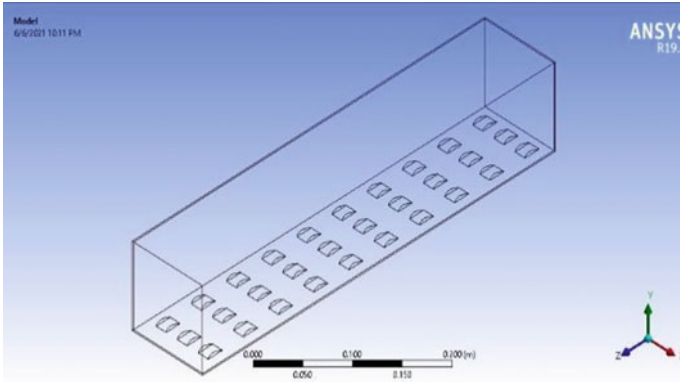
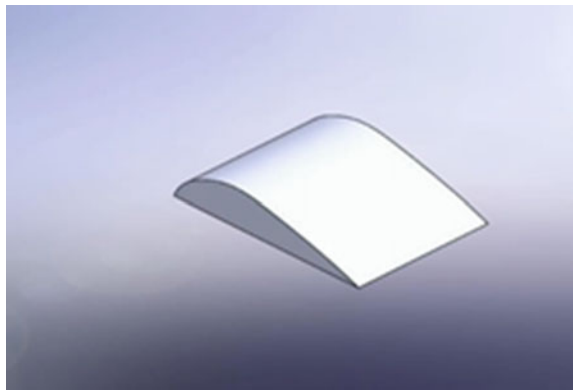


Fig. 2 Flat plate with bumps

Fig. 3 Ansys model of bumps



serrations, are little strike on a tooth that serve to give the tooth a serrated edge (Figs. 3 and 4).

4.2 Meshing

The meshing was done in a linear fashion with a default element size of 1.2 and no inflation at the boundary layer. Because of mesh refinement, the resolution has been increased to 7. The edge size is converted to number of divisions, with 200 divisions on the Z side. The total number of mesh elements in a flat plate without bumps is 76,480, and the total number of nodes is 85,281, or the total number of nodes in a flat plate with bumps is 85,281, as shown in Table 1.

Fig. 4 Side view of shark bumps

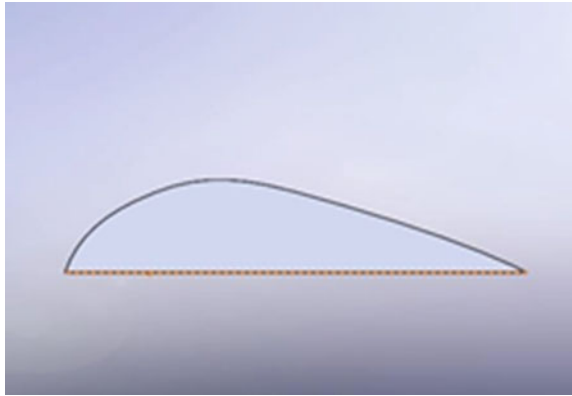


Table 1 Different models and configurations

Model	Cells	Faces	Nodes
1. Flat plate with bumps	581,132	1,251,808	257,289
2. Flat plate without bumps	76,480	1,189,997	6,448,378

4.3 Analysis of Final Model

The simulation was done at the given velocity for getting better result for the base model. Solver used in this setup is “Pressure Based” whereas velocity formation is “Absolute” and the Time is “Steady”. The viscous model was taken as the laminar and steady flow for the simulation. The solution method scheme is used to set up as “SIMPLE” and the special discretization “Gradient” is the “Least square cell based”. The pressure was taken as the “Second order” and the momentum was “Second order upwind, as shown in Figs. 5, 6, 7 and 8.

This is a contour map flat plate with pressure and velocity bumps of 0.0001. The generated figure in this plot depicts the attachment of bumps to a flat plate. This model’s mesh size is specified. The total number of cells is 581,132, the total number of faces is 1251,808, and there are 153,280 nodes. The total number of bumps is 30, all of which are equal in number and spaced evenly to reduce drag. At a certain number of iterations, a scaled residual graph is plotted between x, y, z, and the continuity value.

5 Results and Discussion

At velocity 0.0001, the model of flat plate with bumps show the skin friction drag-coefficient value is approx. 0.0165, when compared to the simple flat plate with or without bumps. The value of drag is 0.013 which is quite as same as the theoretical value at same velocity. This simulation results completely show that the value of drag

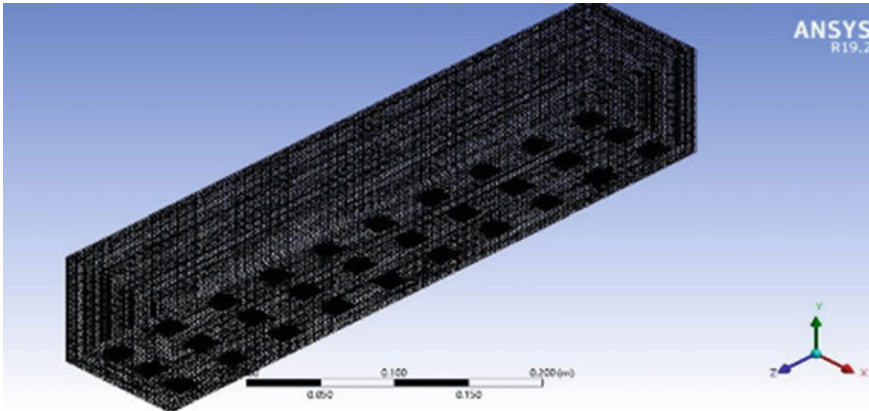


Fig. 5 Mesh display of model in fluent

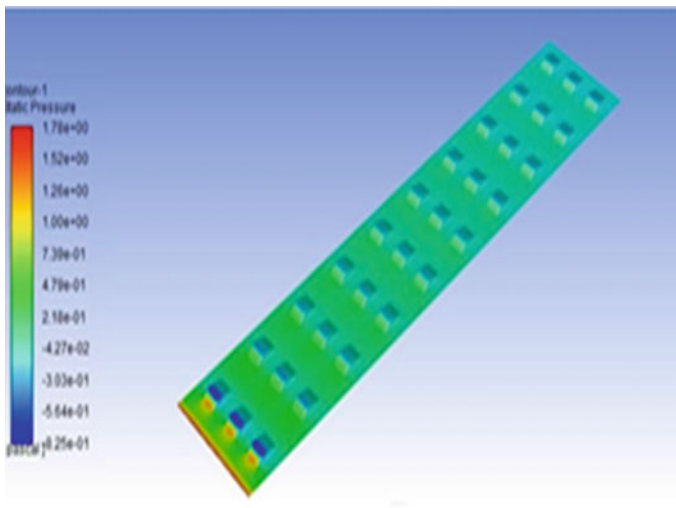


Fig. 6 Contour plot of bumps with flat plate

increase in the case of flat plate with bumps. So the drag coefficient will increase from the 0.003%. With the aerodynamic feature like bio-inspired structure surface the value of c_d is rise by 0.003% with the speed given to the body or model. The authentication gives the result of computational and theoretical value is adjacent. These results of simulation gives better grip and depiction about bio-inspired surface with drag reduction and able to design the structure of biomimics surface. In this case the element six is default for fine mesh structure. Actually air pressure comes from inlet boundary side, so I decide to increase the number of nodes at each edges and refine the mesh in proper way for better simulation results but number of elements

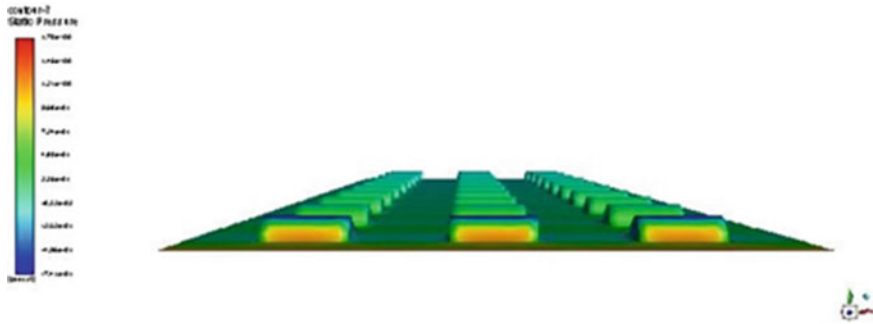


Fig. 7 contour plot flat plate with bumps

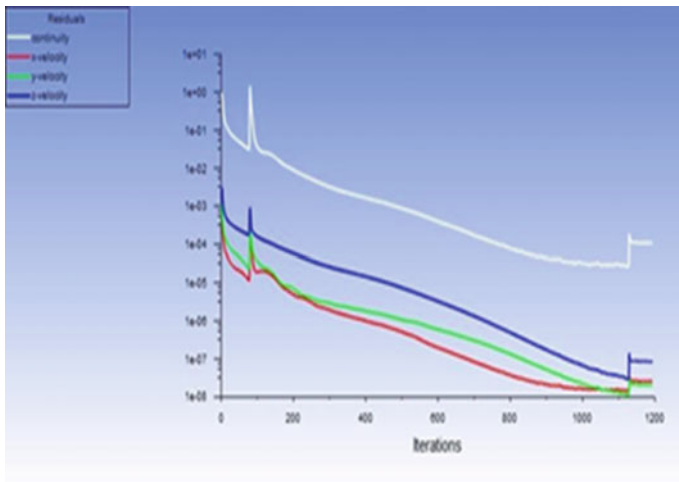


Fig. 8 Scaled Residual value of the mode

and nodes will increase, it depends on the size of mesh. In my case there are number of bumps attached on the bottom of plate and the bumps have number of faces, so the high number of faces takes more time to mesh the complete model and it also takes more time in simulation also, one thing is also important in the simulation result the same value which is given in geometry as same data feed into fluent setup profile like reference value etc.

6 Conclusion

This type of study appears the value when c_d is obtained from the model which is being designed. At being speed of 0.0001 when the bumps are attached with the plate there is 0.003% drag increase if we compare to the theoretical model. In the inclusion of bumps that is the reason for increasing of c_d value with many number of bumps body is attached on the plate that's why the reason behind the increasing of drag in this manner. After this result verification or validation we can use this concept for automobile drag reduction with the help of that type of structure placed on the vehicle surface.

References

1. Jung YC, Bhushan B (2009) Biomimetic structures for fluid drag reduction in laminar and turbulent flows. *J Phys Condens Matter* 22(3):035104
2. Dou Z, Wang J, Chen D (2012) Bionic research on fish scales for drag reduction. *J Bionic Eng* 9(4):457–464
3. Khan MA, Padhy C (2020) Aerodynamic and Experimental Analysis of Bio-mimic corrugated dragonfly aerofoil. *INCAS Bull* 12(2):73–85
4. Yu C et al (2020) Bio-inspired drag reduction: from nature organisms to artificial functional surfaces. *Giant*, pp 100017
5. Kim J, Choi H (2014) Aerodynamics of a golf ball with grooves. *Proc Inst Mech Eng Part P J Sports Eng Technol* 228(4):233–241
6. Kozlov A et al (2015) Bio-inspired design: aerodynamics of boxfish. *Procedia Eng* 105:323–328
7. Chen D et al, Bio-inspired drag reduction surface from sharkskin. *Biosurf. Biotribol* 4(2):2
8. Steinfeld B et al (2015) The role of lean process improvement in implementation of evidence-based practices in behavioral health care. *J Behav Health Serv Res* 42(4):504–518
9. Dai W et al (2019) Drag-reduction of 3D printed shark-skin-like surfaces. *Friction* 7(6):603–612
10. Willermet C (2016) Biological anthropology in 2015: open access, biocultural interactions, and social change. *Am Anthropol* 118(2):317–329
11. Prabhu L et al (2020) Aerodynamics analysis of the car using Solidworks flow simulation with rear spoiler using CFD. In: *IOP conference series: materials science and engineering*, vol 993, no 1. IOP Publishing
12. Sen W, Rahman KA, Tanim IK (2019) Experimental and CFD analysis on car with several types of vortex generators. In: *Proceedings of the international conference on mechanical engineering and renewable energy*
13. Elewe AM (2020) Numerical simulation of surface curvature effect on aerodynamic performance of different types of airfoils. In: *IOP conference series: materials science and engineering*, vol 928, no 3, IOP Publishing
14. Tsai C-H et al (2009) Computational aero-acoustic analysis of a passenger car with a rear spoiler. *Appl Math Modell* 33(9):3661–3673
15. Kumar VN et al (2015) Investigation of drag and Lift Forces over the Profile of Car with Rear Spoiler using CFD. *Int J Adv Sci Res* 1(8):331–339

Effect of Social Network System (Peer Inputs) in Influencing the Consumer Conformity Behavior in Product Customization System



Anitha Nallasivam, C. Selvaraj, K. S. Kalavathy, Prabha Kiran,
and Trupti Dandekar Humnekar

Abstract Conformity needs individuals to respond to other people's actions and decide for themselves about proper behavior, particularly those who aspire to similar characteristics. This research seeks to explore the impact of customer conformity on the final configuration of a product and the degree to which peer feedback impacts the final configuration of an individual's clothes. Also, to understand the significant variables underlying the behavior consequences of the customer due to peers. The convenient sample size of 300 was taken through a questionnaire and analyzed with relevant Statistical tools. With the largest beta value, peer group effects have the most substantial and beneficial influence on conforming behavior, supporting both Hypothesis 1 and Hypothesis 2. Using these findings, we will be able to better understand how the design of social product modification platforms affects customers' views of customized clothing. Few limitations include that the research is only about apparel and not for any other product categories.

Keywords Consumer conformity · Customization process · Peer inputs · Apparel

1 Introduction

Many businesses have come to depend on social-customization platforms. The linking of social groupings to these systems must become a widely accepted technique. The modern study, which was based on either the similarity attraction theory or the social impact theory, investigated how the two dominant mechanisms for offering interactions between users and their peers in social-customization systems

A. Nallasivam · K. S. Kalavathy · T. D. Humnekar
Jain CMS Business School, Bangalore, India

C. Selvaraj (✉)
Saveetha College of Liberal Arts and Sciences, SIMATS (Deemed to be University), Chennai,
India
e-mail: selvaraj1971@gmail.com

P. Kiran
Westminster International University, Tashkent, Uzbekistan

influence their product configurations in order to influence their product configurations. In many industries, creating one global product modification program rather than tailoring it to various regions or cultures is de facto norm [1–7]. For example, Adidas lets customers create their own running shoes and then get feedback from other customers on their designs. Notably, Adidas employs the same shoe configurator everywhere, regardless of customer culture. This paper recommends modifying these methods to individual markets to support or inhibit peer input compliance. Conforming model configurations lower the amount of variants and hence the company's cost of offering a system of social customization. Companies will so profit financially from complying with product revisions. The lower prices are due to lower sales of more robust features, which are used to earn larger profits [8–13].

2 Literature Review

To satisfy our psycho-physiological and sociological needs, we engage in social interactions with other people [14]. Peers, according to consumer socialization research, are the major means through which people make new friends outside of their immediate family [6]. For example, constant engagement with peers on consumer concerns leads to more substantial incentives for social consumption [8, 13]. Interpersonal communication rates between agents and learners may have a considerable influence on the purchasing decisions of consumers [3]. As part of a social learning cycle, we suggest that peers function as socializing agents via social media and that peers have an impact on those they come into touch with. Someone or a group that is intended to have a major effect on an individual's beliefs, expectations, and behaviors is referred to as an influencer [9]. Individuals' behavior, lifestyle, hobbies, and purchasing patterns may be easily compared to those of reference groups [7]. As a result, the individual's self-image and behavior are influenced by social reference groups. Their social background, age, domicile, work and interests and hobbies are often linked to them. People in the same demographic group might be used as a reference point for this purpose. Furthermore, Stanton, et al. [4] predicated on the assumption that the power of the reference group, a term indicating the social constituency to which a person belongs or appears to belong, has an impact on customer perceptions, priorities, expectations, views, and brand or product knowledge. When it comes to purchasing products and services, real-world or theoretical "models" of consumer conventions and expectations may be utilized as reference classes in any decision-making process involving such purchases [9]. The research on scents took into consideration the effect of the reference group on consumer buying decisions for branded products [11, 14].

3 Methodology

3.1 Research Questions

- Is it appropriate to tailor social product-customization structures to a specific market?
- What is the extent to which the peer input influences the decision of the final configuration of the apparel of the respondent?
- What are the significant variables (factors) that contribute to the behavior consequences due to peers, and how does that impact each other?

3.2 Objectives

- To find how consumer compliance affects the market. When a peer group influences a consumer’s decision during the final configuration of customization of a product.
- To know the extent to which the peer input influences the decision of the final configuration of an individual’s apparel.
- To understand the significant variables underlying the behavior consequences of the customer due to peers.

3.3 Research Model

The theoretical model of social customization by Schlager et al. [12] explains the similarity attraction theory wherein the consumers feel pressured to do so, rather than because they anticipate adhering to peer feedback will enhance product configurations, customers may diverge from their distinctive preferences, as shown in Fig. 1.

As a result of this, their assessment of the final product configurations should be reduced over time. On the contrary, a consumer’s judgment of final product configurations will be enhanced if the product conforms to peer feedback from close peers.

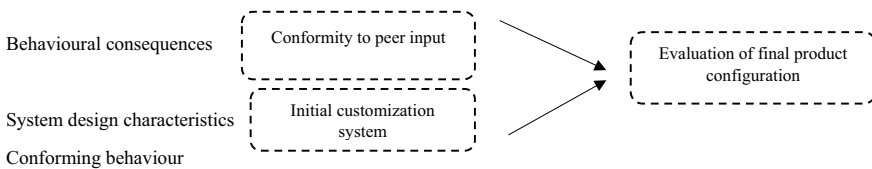


Fig. 1 Theoretical model of social customization due to peer groups

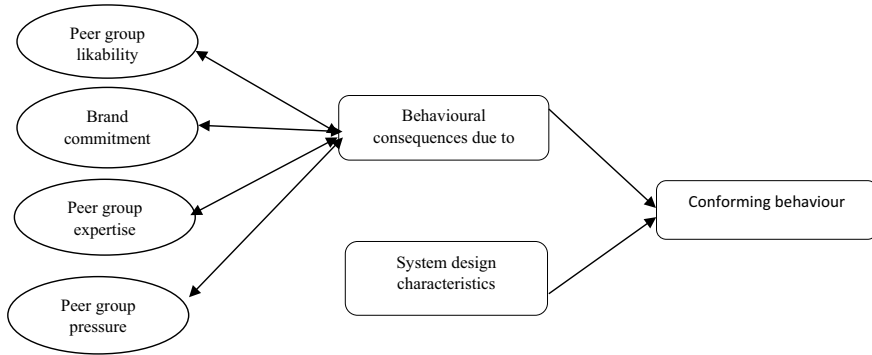


Fig. 2 Proposed research model of the study

1. Proposed Research Model,

Proposed methodology has been shown in Fig. 2.

The proposed model follows both the similarity attraction theory and social impact theory wherein the peer group influencing nature was explained by social impact theory wherein the peer group pressure, expertise, likability makes the consumer follow the peer person and end up changing their decision in buying or customizing a product.

4 Data Analysis and Interpretation

4.1 Reliability Test

Reliability refers to how replicable the outcomes obtained through a test and process can be. A lack of reliability can result from differences between observers or measuring instruments, such as a questionnaire or measuring attribute instability which inevitably affects the validity of that questionnaire, as shown in Table 1.

The reliability test was conducted with a total of 300 responses. In the end, the Cronbach’s alpha was 0.956, which is in the upper range of acceptable values. Between 0.9 and 1 is considered more reliable by many studies, while others believe that the 0.7–0.9 range provides the best results. The variables are more consistent inside. Because the test we have devised precisely measures the variable of interest, it is more trustworthy.

Table 1 Reliability test of the data

Reliability test	
Cronbach’s Alpha	N of items
0.956	36

4.2 Measurement Model—CFA Loadings

Cronbach’s alpha coefficient is used to measure the reliability of multi-item scales, and composite reliability is a good counterpart. The internal consistency of the metrics used to evaluate a component is measured by the composite reliability. Fornell and Larcker [5] proposed that showing estimates of 0.50 or greater would be suitable for the project, as shown in Fig. 3 metrics used to evaluate a component are measured by the composite reliability. Fornell and Larcker [5] proposed that showing estimates of 0.50 or greater would be suitable for the project.

The loadings give us some hint of which of the underlying factors in which of the variables we observed appear. The range of 0–1 should not exceed one as there is no model fit. Also, from the diagram, the factor loadings were in the range of 0–1. This proves that the model is fit enough. The measurement model shows that the value for all the variables is more significant than 0.7. Of which, each peer group’s pressure and expertise variables have given above 80% to the model.

Model Validity Measures

- **Cronbach Alpha**—Used to calculate the reliability of two or more measures for the building. A healthy Cronbach Alpha will generally be more than 0.7. A good measure indicates the dimension of stability that the variables have in them.
- **Reliability in Composite**—There is much internal consistency between the scale products, much more like a Cronbach Alpha. It shows the consistency aspect of the

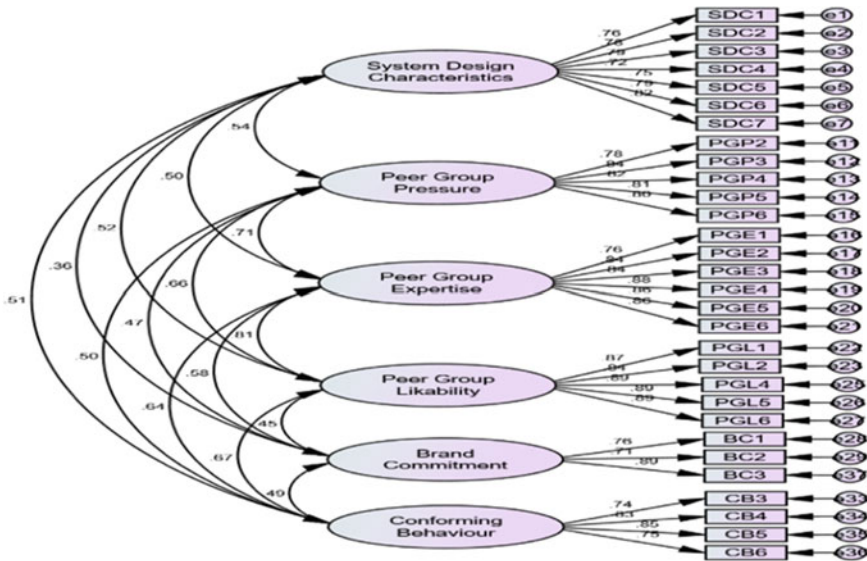


Fig. 3 Measurement model

Table 2 Model validity measures

Construct	CR	AVE	MSV	1	2	3	4	5	6
SDC	0.912	0.598	0.293	0.773					
PGP	0.906	0.659	0.499	0.542***	0.812				
PGE	0.936	0.709	0.658	0.504***	0.706***	0.842			
PGL	0.942	0.766	0.658	0.518***	0.662***	0.811***	0.875		
BC	0.831	0.624	0.336	0.363***	0.465***	0.580***	0.445***	0.790	
CB	0.870	0.627	0.453	0.512***	0.500***	0.641***	0.673***	0.492***	0.792

*** $p < 0.001$

scale items. Most researchers have concluded that 0.6 and above composite reliability is considered much of a better source for understanding the inner accuracy of the scale products.

- **Average Variance Derived**—Based on the “thumb rule,” the computed average variance is commonly used to establish discriminant validity. In the CFA model, the AVE of any latent construct should be greater than the squared correlation with any other latent variable. As a result, researchers believe that AVE should be more than 0.50 to achieve a more accurate assessment of the variance, as shown in Table 2.

The results of the variance tests taken from the safety measure construct are shown in the Table 2. Again, each square correlation supports discriminating validity less than the estimates extracted from both applicable variances, as shown in Table 3.

One-way ANOVA talks about the difference between the demographic variable and the research constructs such as system design characteristics, Peer group pressure, peer group expertise, peer group likability, brand commitment, conforming behavior.

Demographic Variable 1: Age

H0—There is no significant difference between age and research constructs.

H1—There is a significant difference between age and research constructs, as shown in Table 4.

Table 3 Model fit measures for measurement

Measure	Estimate	Threshold	Interpretation
CMIN	1130.268	–	–
DF	390.000	–	–
CMIN/DF	2.898	Between 1 and 3	Excellent
CFI	0.898	> 0.95	Acceptable
SRMR	0.049	< 0.08	Excellent
RMSEA	0.080	< 0.06	Excellent

Table 4 Difference between demographic variable age and research constructs

Factors		N	Mean	F-value	P-value
System design characteristics	Below 15	3	3.97	0.916	0.455
	15-30	257	3.85		
	31-45	26	3.85		
	46-60	10	3.51		
	Above 60	3	3.16		
	Total	299	3.83		
Peer group pressure	Below 15	3	4.18	0.987	0.415
	15-30	257	3.56		
	31-45	26	3.54		
	46-60	10	3.29		
	Above 60	3	3.08		
	Total	299	3.55		
Peer group expertise	Below 15	3	4.44	1.765	0.136
	15-30	257	3.62		
	31-45	26	3.52		
	46-60	10	3.64		
	Above 60	3	2.88		
	Total	299	3.62		
Peer group likability	Below 15	3	4.69	1.762	0.136
	15-30	257	3.86		
	31-45	26	3.79		
	46-60	10	3.74		
	Above 60	3	3.01		
	Total	299	3.85		
Brand commitment	Below 15	3	4.05	1.355	0.250
	15-30	257	3.32		
	31-45	26	3.32		
	46-60	10	3.61		
	Above 60	3	2.75		
	Total	299	3.33		
Conforming behavior	Below 15	3	3.77	2.603	0.036*
	15-30	257	3.51		
	31-45	26	3.59		
	46-60	10	3.58		
	Above 60	3	2.24		
	Total	299	3.51		

** $p < 0.01$; * $p < 0.05$

From the table, it appears that the age group above 60 were not susceptible to peer influence, which is indicated by the mean value, which is lower than the rest of the age groups and the age group below 15 was very much influenced by the peer groups.

A one-way ANOVA test was conducted to find the difference between the demographic variable age and research constructs. The ANOVA was not significant in all the research constructs with $p > 0.01$. Thus, there is no significant difference between demographic variable age and research constructs.

Demographic Variable 2: Occupation

H0—There is no significant difference between occupation and research constructs.

H1—There is a significant difference between occupation and research constructs, as shown in Table 5.

From the table, it is clear that the occupation group of government officials were not susceptible to peer influence, and this has been indicated by the mean value, which is lower than the rest of the groups and the working professional and student group has very high mean value whom the peer groups very much influenced.

A one-way ANOVA test was conducted to find the difference between the demographic variable occupation and research constructs. The ANOVA was significant in all the research constructs as $p < 0.01$. Thus, there is a significant difference between demographic variable occupation and research constructs.

Demographic Variable 3: Income

H0—There is no significant difference between income and research constructs.

H1—There is a significant difference between income and research constructs, as shown in Table 6.

The table shows that the people falling under the income group above Rs. 40,000 are very much influenced by the peer groups. A one-way ANOVA test was conducted to find the difference between the demographic variable income and research constructs. The ANOVA was significant in all the research constructs as $p < 0.01$. Thus, there is a significant difference between demographic variable income and research constructs.

Demographic Variable 4: Gender

H0—There is no significant difference between gender and research constructs.

H1—There is a significant difference between gender and research constructs, as shown in Table 7.

Both men and women are susceptible to peer group influence, but comparatively, females get highly influenced by their peers. Also, females are more loyal to the brands.

A one-way ANOVA test was conducted to find the difference between the demographic variable occupation and research constructs. The ANOVA was significant in

Table 5 Difference between demographic variable occupation and research constructs

Factors		N	Mean	F-value	P-value
System design characteristics	Student	120	3.77	6.510	0.000**
	Working professional	127	3.98		
	Business professional	30	3.81		
	Government official	8	2.54		
	Other	14	3.81		
	Total	299	3.83		
Peer group pressure	Student	120	3.50	5.549	0.000**
	Working professional	127	3.66		
	Business professional	30	3.61		
	Government official	8	2.35		
	Other	14	3.52		
	Total	299	3.55		
Peer group expertise	Student	120	3.57	7.004	0.000**
	Working professional	127	3.79		
	Business professional	30	3.30		
	Government official	8	2.66		
	Other	14	3.58		
	Total	299	3.62		
Peer group likability	Student	120	3.82	7.583	0.000**
	Working professional	127	4.03		
	Business professional	30	3.44		
	Government official	8	2.82		
	Other	14	3.96		
	Total	299	3.85		
Brand commitment	Student	120	3.24	3.730	0.006**
	Working professional	127	3.50		
	Business professional	30	3.23		
	Government official	8	2.64		
	Other	14	3.15		
	Total	299	3.33		
Conforming behavior	Student	120	3.43	5.168	0.000**
	Working professional	127	3.66		
	Business professional	30	3.36		
	Government official	8	2.66		
	Other	14	3.59		
	Total	299	3.51		

** $p < 0.01$

Table 6 Difference between demographic variable income and research constructs

Factors		N	Mean	F-value	P-value
System design characteristics	Below Rs. 10,000	86	3.77	3.444	0.009**
	Rs. 10,000–Rs. 20,000	40	3.61		
	Rs. 20,000–Rs. 30,000	43	3.73		
	Rs. 30,000–Rs. 40,000	40	3.73		
	Above Rs. 40,000	90	4.09		
	Total	299	3.83		
Peer group pressure	Below Rs. 10,000	86	3.50	3.258	0.012*
	Rs. 10,000–Rs. 20,000	40	3.44		
	Rs. 20,000–Rs. 30,000	43	3.32		
	Rs. 30,000–Rs. 40,000	40	3.48		
	Above Rs. 40,000	90	3.79		
	Total	299	3.55		
Peer group expertise	Below Rs. 10,000	86	3.65	7.411	0.000**
	Rs. 10,000–Rs. 20,000	40	3.32		
	Rs. 20,000–Rs. 30,000	43	3.34		
	Rs. 30,000–Rs. 40,000	40	3.47		
	Above Rs. 40,000	90	3.91		
	Total	299	3.62		
Peer group likability	Below Rs. 10,000	86	3.93	4.777	0.001**
	Rs. 10,000–Rs. 20,000	40	3.63		
	Rs. 20,000–Rs. 30,000	43	3.64		
	Rs. 30,000–Rs. 40,000	40	3.61		
	Above Rs. 40,000	90	4.09		
	Total	299	3.85		
Brand commitment	Below Rs. 10,000	86	3.31	7.372	0.000**
	Rs. 10,000–Rs. 20,000	40	3.14		
	Rs. 20,000–Rs. 30,000	43	3.23		
	Rs. 30,000–Rs. 40,000	40	2.94		
	Above Rs. 40,000	90	3.65		
	Total	299	3.33		
Conforming behavior	Below Rs.10,000	86	3.51	5.953	0.000**
	Rs. 10,000–Rs. 20,000	40	3.23		
	Rs. 20,000–Rs. 30,000	43	3.36		
	Rs. 30,000–Rs. 40,000	40	3.33		
	Above Rs. 40,000	90	3.77		
	Total	299	3.51		

** $p < 0.01$; * $p < 0.05$

Table 7 Difference between demographic variable gender and research constructs

Factors		N	Mean	F-value	P-value
System design characteristics	Female	180	3.85	0.202	0.654
	Male	119	3.81		
	Total	299	3.83		
Peer group pressure	Female	180	3.59	1.185	0.277
	Male	119	3.49		
	Total	299	3.55		
Peer group expertise	Female	180	3.70	5.318	0.022*
	Male	119	3.49		
	Total	299	3.62		
Peer group likability	Female	180	3.97	9.877	0.002**
	Male	119	3.68		
	Total	299	3.85		
Brand commitment	Female	180	3.43	6.820	0.009**
	Male	119	3.18		
	Total	299	3.33		
Conforming behavior	Female	180	3.62	11.268	0.001**
	Male	119	3.34		
	Total	299	3.51		

** $p < 0.01$; * $p < 0.05$

the research constructs such as peer group likability, brand commitment, and conformity as $p < 0.01$. Thus, there is a significant difference between demographic variable gender and these research constructs. At the same time, there is no significant difference between gender and research constructs such as system design characteristics, peer group pressure, peer group expertise as $p > 0.01$. Hence, for these constructs, ANOVA was not significant.

Hypothesis Testing

H1: The system design characteristics have a significant impact on consumer’s conforming behavior.

H2: The behavioral consequences due to peer groups have a significant impact on consumers’ conforming behavior, as shown in Fig. 4 and Table 8.

The overall behavioral consequences due to peer groups influenced by the four different conformity peer inputs namely peer group pressure (beta = 0.752; $p < 0.01$), peer group likability (beta = 0.939; $p < 0.01$), peer group expertise (beta = 0.904; $p < 0.01$) and brand commitment (beta = 0.701; $p < 0.01$). All four conformity peer inputs lead to overall behavioral consequences due to peer groups and peer group likability. Peer group expertise is the most significant predictor of overall behavioral consequences due to peer groups with the highest beta values. The above table concludes

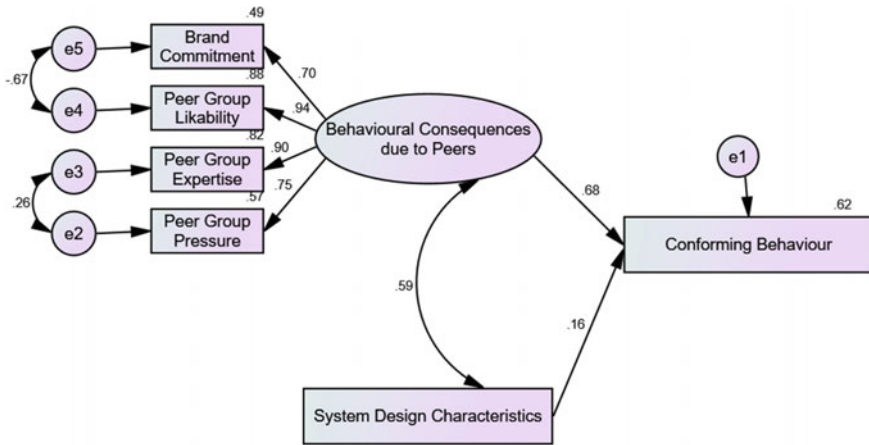


Fig. 4 Hypothesis testing of the model

Table 8 A path analysis of the model

Parameter			β -value	p-value	Result
Peer group pressure	←	Behavioral consequences due to peer groups	0.752	0.001**	H2 supported
Peer group expertise	←		0.904	0.001**	
Peer group likability	←		0.939	0.001**	
Brand commitment	←		0.701	0.001**	
Conforming behavior	←		0.681	0.001**	
Conforming behavior	←	System Design characteristics	0.157	0.012*	H1 supported

** $p < 0.01$; * $p < 0.05$

that the system design characteristics have a significant impact on a consumer’s conforming behavior ($\beta = 0.157$; $p < 0.05$), and the behavioral consequences due to peer groups have a significant impact on a consumer’s conforming behavior ($\beta = 0.681$; $p < 0.01$). 62% of behavioral consequences due to peer groups are explained by both system design characteristics and behavioral consequences due to peer groups. However, the behavioral consequences due to peer groups have a more significant and positive impact on conforming behavior with the highest beta value. This concludes both H1 and H2 supported, as shown in Table 9.

Table 9 Model fit measures for structural model

Measure	Estimate	Threshold	Interpretation
CMIN	28.642	–	–
DF	6.000	–	–
CMIN/DF	4.774	Between 1 and 3	Acceptable
CFI	0.981	>0.95	Excellent
SRMR	0.037	<0.08	Excellent
RMSEA	0.113	<0.06	Acceptable

The results tested by the conceptual model show that the CMIN/DF is 4.774. The Comparative Fit Index (CFI) is 0.981, which shows a good model fit. RMSEA is 0.052, and the Root Mean Square Residual (SRMR) is 0.037, which shows a good model fit.

5 Findings

All four conforming peer inputs impact behavior. Peer group likability and competence are the most significant predictors of total behavioral consequences. Both system design variables and individual influences of peer groups explain 62% of the effects of peer groups on a person’s behaviors. With a beta value of 0.68, there are more significant and favorable impacts on conforming behavior. Determinants of conforming behavior include system design factors (about 16% of With a beta value above 0.7, the four factors that underpin the customer’s behavioral repercussions due to peer group have an influence on individuals’ behavior. Preferred peer group likability is about 0.94, expert peer group likability is 0.90, and peer group pressure is at 0.75. With a beta value of around 0.49, the variable brand commitment seems to have little influence on the behavior consequences. The interaction between two separate study constructs, such as system design attributes and behavior repercussions, was also studied in detail. With a beta score of 0.59, the client is more likely to be swayed by the peer group’s opinion and alter their mind. This supports H1 and H2. Peer group pressure is not an issue for those over 60. Peer pressure does not sway government leaders. Peer group influence affects people of all socioeconomic levels. However, female respondents were more influenced than male ones. The one-way ANOVA shows significant differences in all demographic and research parameters. The model also fits the study. The questionnaire’s design demonstrates the model’s reliability.

5.1 *Managerial Implication and Recommendation*

Customizing items using social media is risky because businesses cannot control client feedback. Clothing customization interfaces show how many individuals have a certain product configuration. Consumers benefit from more consistent product modifications, and corporations may construct social product customization programs to encourage or prohibit conforming product changes (i.e., increasing or decreasing the satisfaction). Create a global product modification program rather than one for each region and culture. To maximize savings, research proposes customizing consumer goods distribution tactics to diverse markets.

5.2 *Limitations*

The study does not look at other products. So simple. A shop that understands personalization is more accurate. To save time, the model was quantified. This research does not characterize thinking styles. Peer feedback was also ignored. It does not matter how near feedback sources and receivers are to one other. The research is meaningless outside India due to consumer perceptions and peer influence. Due to scheduling, only 300 samples were prepared. Phase one included analyzing the customer's thinking style and behavior. Due of budget restrictions, the research examined conformity rather than cognitive processes. Demands and demands vary throughout time, shortening the research's lifespan.

6 Conclusion

- Advancing cooperation, empowering shared encounters, and coordinating with clients dependent on accessible client data, clothing organizations giving social customization frameworks will put resources into more grounded associations among purchasers.
- The discovery of this exploration shows that the similarity relies upon framework context-oriented variables, individual attributes, and companion social connections.
- The current work gives new bits of knowledge into how organizations can successfully foster social item customization projects to either work with or debilitate adjusting item alterations, regardless of whether these item changes /customizations are helpful or destructive to purchasers and the organization.

References

1. Batra R, Homer PM, Kahle LR (2001) Values, susceptibility to normative influence, and attribute importance weights: a nomological analysis. *J Consum Psychol* 11(2):115–128
2. Chow S, Celsi RL, Abel R (1990) The effects of situational and intrinsic sources of personal relevance on brand choice decisions. *ACR North Am Adv*
3. De Gregorio F, Sung Y (2010) Understanding attitudes toward and behaviors in response to product placement: a consumer socialization framework. *J Advert* 39(1):83–96
4. Etzel MJ, Walker BJ, Stanton WJ (1994) Fundamentals of marketing
5. Fornell C, Larcker DF (1981) Structural equation models with unobservable variables and measurement error: algebra and statistics
6. Köhler CF, Rohm AJ, Ko R, Wetzels M (2011) Return on interactivity: the impact of online agents on newcomer adjustment. *J Mark* 75(2):93–108
7. Long MM, Schiffman LG (2000) Consumption values and relationships: segmenting the market for frequency programs. *J Consumer Market*
8. Moschis GP, Churchill Jr GA (1978) Consumer socialization: a theoretical and empirical analysis. *J Mark Res* 15(4):599–609
9. Park CW, Lessig VP (1977) Students and housewives: differences in susceptibility to reference group influence. *J Consumer Res* 4(2):102–110
10. Ratner RK, Kahn BE (2002) The impact of private versus public consumption on variety-seeking behaviour. *J Consumer Res* 29(2):246–257
11. Ratneshwar S, Shocker AD (1991) Substitution in use and the role of usage context in product category structures. *J Mark Res* 28(3):281–295
12. Schlager T, Hildebrand C, Häubl G, Franke N, Herrmann A (2018) Social product-customization systems: peer input, conformity, and consumers' evaluation of customized products. *J Manag Inf Syst* 35(1):319–349
13. Shim S (1996) Adolescent consumer decision-making styles: the consumer socialization perspective. *Psychol Mark* 13(6):547–569
14. Ward S (1974) Consumer socialization. *J Consumer Res* 1(2):1–14

CFD Based Investigation of Thermophoresis Effect on Microparticles in Micro Channel



Niraj Kumar , Ashok Kumar Yadav , Ashish Dewangan ,
and Mukesh Kumar 

Abstract Present research work deals with the investigation of thermophoresis effect on microparticles in liquid media. In this work, microfluidic thermophoresis was simulated on a COMSOL based CFD platform. A three-dimensional microchannel of 750 μm width, 500 μm depth and 50mm length was constructed and a fluid flow inside this channel was simulated considering a flow rate of 420 $\mu\text{l}/\text{min}$. The model uses the Navier–Stokes equations with no-slip conditions. As a first step of the simulation process, a particle tracing model was implemented in a laminar flow domain with isothermal conditions. Later a temperature gradient was imposed normal to the flow direction and the field was solved under non-isothermal conditions. Results reveal that the particles motion is significantly influenced by the presence of thermal field. Variation of temperature gradient and its effect on thermophoresis phenomenon was presented in detail.

Keywords Microchannel · Thermophoresis · Temperature gradient · Movement of microparticle size · CFD

N. Kumar

Department of Mechanical Engineering, Ghani Khan Choudhury Institute of Engineering & Technology, Malda 732141, India

A. K. Yadav

Department of Mechanical Engineering, Raj Kumar Goel Institute of Technology, Ghaziabad 201003, India

A. Dewangan (✉)

Department of Mechanical Engineering, Galgotias College of Engineering and Technology, Greater Noida 201306, India
e-mail: ashdew15@gmail.com

M. Kumar

Mechanical Engineering Department, IEC-CET, Greater Noida 201306, India

1 Introduction

Microfluidics is a new area of research that studies fluid flow through microchannels and lab-on-chip technologies, among other things. Such microscale transport phenomena offer a lot of advantages in biomedical and biochemical applications of lab-on-chip systems, including heat and mass transfer, controlled mixing, and so on. Particle transport generated by a temperature gradient is known as thermophoresis. Thermophoresis is still a topic of theoretical and practical interest, despite the fact that it was discovered roughly 150 years ago.

Many investigations of thermal diffusion have been conducted since Ludwig [8] reported the first observations of the phenomena toward the end of the nineteenth century. Thermophoresis (also known as Thermo migration, Thermo diffusion, the Soret effect, or the Ludwig–Soret effect) is a phenomenon that occurs in mixtures of mobile particles when various particle types respond differently to the force of a temperature gradient. Thermophoretic force is defined as the force that a particle experiences due to the temperature gradient and thermophoretic velocity are defined as the velocity that particle moves through the fluid due to thermophoretic force [1]. Figure 1 shows the schematic diagram of the thermophoresis process.

The term thermophoresis is most usually used to describe the occurrence in aerosol mixtures. The Soret effect is most commonly associated with liquid mixtures, which behave in ways that are less well understood than gaseous mixtures. Rectangular channels are widely utilized in microfluidic devices for boosting heat transfer, increasing mixing efficiency, and modifying fluid flow direction. As a result, in the design and process control of microfluidic devices, a fundamental understanding of flow properties such as velocity distribution and temperature distribution is required [3]. Microfluidics deal with very small volumes of fluids, and fluids behave significantly differently on the micrometric scale than they do in ordinary life: these distinguishing characteristics constitute the foundation for new scientific breakthroughs. Understanding thermodiffusion may increase our ability to regulate such systems [2] and help us utilize its potential in the characterization of biological fluids, according to a number of studies. Some early research has recently revealed that thermodiffusion could be used as a control parameter in separation processes in micro-scale devices [4–9]. Despite this, the majority of theoretical and experimental findings [7,

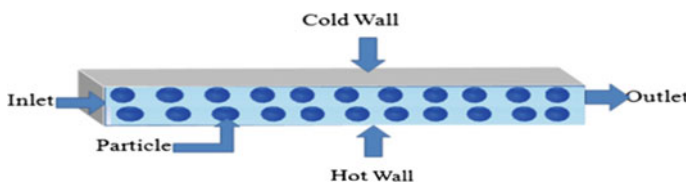


Fig. 1 Schematic of the thermophoresis inside a microchannel

9] suggest that thermophoretic velocity in colloidal suspensions is inversely proportional to fluid viscosity. On the basis of current experimental results and theoretical notions, a novel expression for thermophoretic mobility is proposed.

1.1 Methodology and Governing Equation

The commercial code COMSOL multiphysics was utilized to analyse the behavior of velocity distribution, temperature distribution, and particle trajectory characteristics inside rectangular microchannels in this work by establishing the 3-D computational domain. The governing equations in vector form for the research state are as follows. A fluid flow inside a 3-D microchannel with a width of 750 μm , a depth of 500 μm , and a length of 50 mm were simulated using a flow rate of 420 l/min first of all, water is flowing inside microchannel whose upper and lower walls are kept at same temperature after solving velocity and temperature field we add the particle tracing module and here we add drag force, gravity force and thermophoretic force but here temperature gradient is zero so thermophoretic force is insignificant and 10micron sized polystyrene particles move with the effect of flow velocity of water but the velocity of particle is less than the flow velocity of water because of applying drag force. After that water is flowing inside micro channel whose upper wall is hot and lower wall is cold are kept at different temperatures after solving velocity and temperature field we add the particle tracing module and here we add drag force, gravity force and thermophoretic force but here temperature gradient is applied so thermophoretic force is significant and 8 micron-sized polystyrene particles move with the effect of flow velocity of water and we will see the effect of thermophoresis inside microchannel. The steady-state governing equation in vector form written as Minea [10]

$$\nabla \cdot \rho_f u = 0 \quad (1)$$

$$\rho_f u \cdot (\nabla \cdot u) = -\nabla p + \nabla \cdot \mu_f [\nabla u + (\nabla u)^T] \quad (2)$$

Here, u is the velocity field (m/s), p is the static pressure; ρ_f and μ_f are the fluid density and the viscous dissipation effect.

- The Fluid flow is incompressible and laminar
 Particle density (ρ_p) = 1040 kg/m³.
 Particle diameter (d_p) = 10 μm

$$F_D = m_p(u - v)/\tau_p \quad (3)$$

$$\tau = \rho_p d_p^2 / 18\mu \quad (4)$$

where F_D is drag force and m_p is particle mass, τ_p is particle velocity response time, v is the velocity of particle and u is the fluid velocity.

- Thermophoretic force for stationary study

$$F_t = 6d_p\mu^2C(k_f/k_p)\nabla T/\rho(2(k_f/k_p) + 1)T \quad (5)$$

where F_t is Thermophoretic force, k_f is thermal conductivity of fluid, k_p is thermal conductivity of particle, ρ is the density of fluid,

- Gravity force for stationary study

$$F_g = m_p g(\rho_p - \rho)/\rho_p \quad (6)$$

All the equations were solved using finite element based solver of COMSOL multiphysics 4.3a.

1.2 Results and Discussion

In the present study, an attempt has been made to know about the effect of thermophoresis inside three-dimensional straight rectangular microchannels using CFD. Navier–Stokes and continuity equation at steady state were solved considering laminar flow throughout the channel at isothermal condition by applying suitable boundary conditions and it gives the velocity and temperature field of the entire flow domain. After that particle tracing algorithm was implemented to know the particle trajectory which is time-dependent and it has been computed for 10 s. After the computation with particle tracing, particle trajectory has been obtained along with the velocities of the particles. In the following section, results of the simulation are presented where 125 numbers of particles were considered. Temperature difference (ΔT) in this study means the temperature difference between the upper and lower wall of the considered microchannel. Here temperature of the lower face is always kept constant (300 K) and the temperature of the upper face changes from 302.5 K to 307.5 K, 315 K, 330 K, 350 K and 400 K. Figure 3 shown the cross-section wise velocity contour along the length of the channel. It shows zero velocity at the wall and maximum velocity at the center of the channel which is expected in the laminar flow condition. Our Results shown below are in the form of simulation result that has been obtained by Comsol-4.3a which is CFD based software and another result in the form of graph has been made by result obtained from simulation. Figure 4a. Contour of particle velocities along YZ direction from the CFD simulation of a particular case when the number of particle is 125 and temperature difference between lower and upper surface is only 0 K. As we have already described our coordinate system in Fig. 2 of model geometry where the length, width and height are represented in x, y and z directions, respectively. In Fig. 4a red particle containing at middle section it having maximum velocity and blue particles at wall it having very low velocity

which is expected to result in laminar flow coupled with particle tracing module. So we can say if the 125 particles are released at inlet then red particles first reach at outlet because it has high velocity and consequentially other particles this is clearly seen in Fig. 4b, c represents all the upper and lower quadrants of channel along with particles. In Fig. 4 there is no temperature gradient so in laminar flow the curve of velocity profile is parabola and it is symmetry from center to either side of wall so number of particles contained in lower quadrant of channels is almost same that can clearly be represented in Fig. 6a. Figures 4 and 6 represent (a) Contour of particle velocities along YZ direction. (b) Position of particle when particle moving it just reach the outlet at time $t = 1.4$ s (c) Represents all the upper and lower quadrants of the channel along with particles. For $\Delta T = 0$ K, and 100 K. That means here the temperature gradient increases then we found that after seeing the simulation result in Figs. 4 and 6 the number of particles increases toward the cold wall of microchannel and the number of particles decreases from heated wall of microchannel. Our discussion is clearly rectified in Fig. 6, which is obtained with the help of simulation results carried out in Figs. 4 and 6. It shows the cross-sectional planes along with particles in each quadrant or sub-cell. In order to understand the effect of thermophoresis, particle number of each sub-cell is calculated and particle number of upper half of the channel and lower half of the channel was plotted against time such plots at different temperature differences are shown in Fig. 6. Each plot of Fig. 6 shows temporal variation of two-particle numbers, upper half particle numbers and lower half particle numbers. Difference in particle numbers between both these portions of the channel is an indicator of the effect of thermophoresis. Figure 6b, c show the similar type of particle distribution when very small thermal gradient has been applied across the cross-section of the channel. In comparison to Fig. 6a–c show slight differences between the particles numbers in upper and lower sections of the channel. However, the difference is not large since the applied thermal gradient is too small. To enhance the effect of thermal gradient, in Fig. 6d–g, the temperature difference is gradually increased from 7.5 K to 15 K, 30 K, 50 K and 100 K, respectively (Fig. 5).

The results clearly show that as the temperature difference increases, the difference in particle numbers between the upper and lower section of the channel is

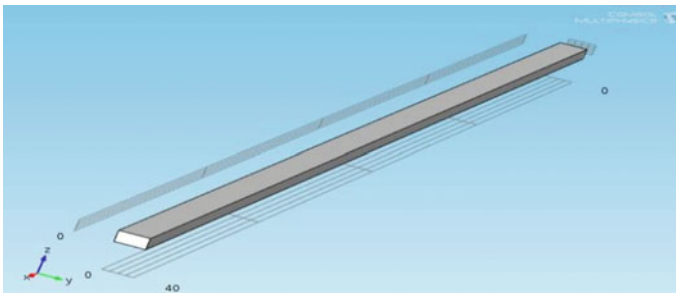


Fig. 2 3-D rectangular geometry straight rectangular microchannels

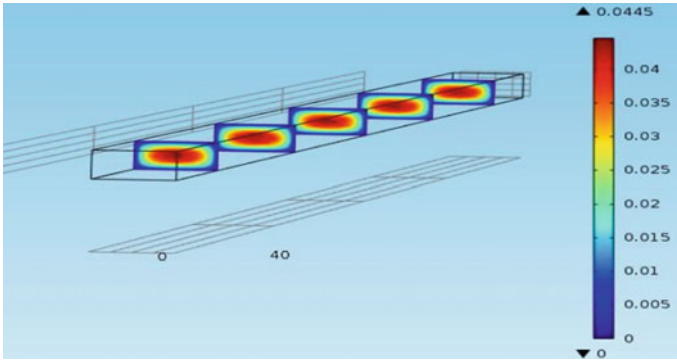


Fig. 3 *c/s* planes showing the velocity contour at different locations

Fig. 4 For $\Delta T = 0$ K **a** Contour of particle velocities along YZ direction. **b** Position of particle when particle moving it just reach the outlet at time $t = 1.4$ s and **c** represents all the upper and lower quadrants of the channel along with particles

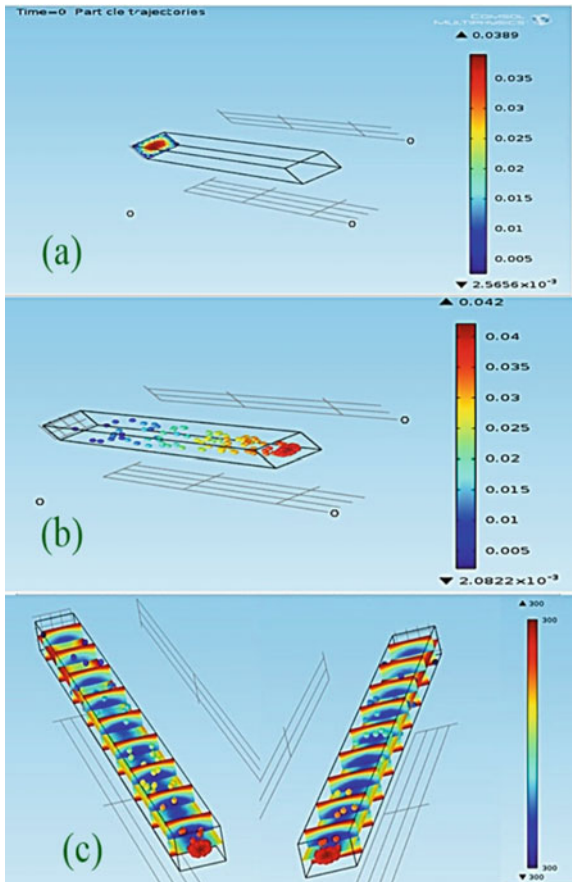
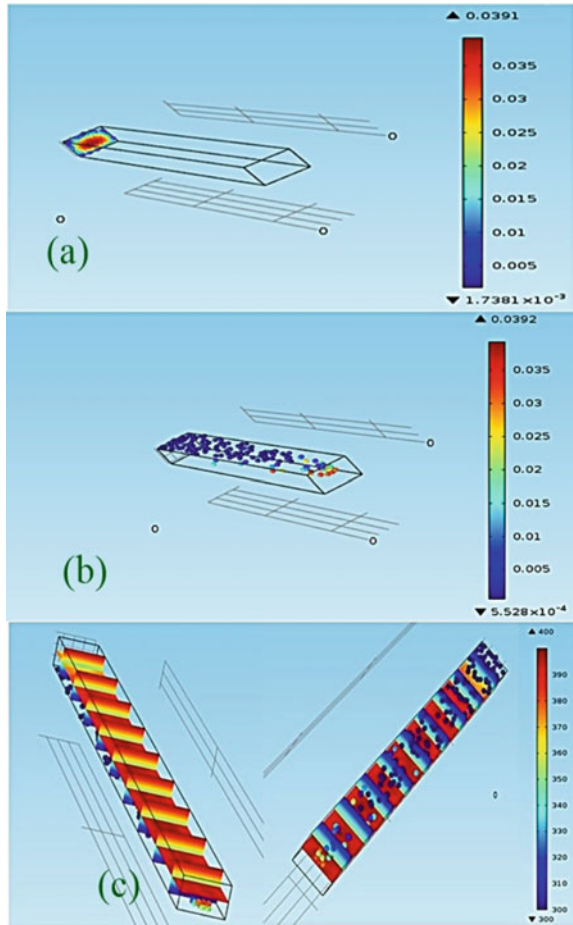


Fig. 5 For $\Delta T = 100$ K **a** Contour of particle velocities along YZ direction. **b** Position of particle when particle moving it just reach the outlet at time $t = 1.4$ s and **c** upper and lower quadrants of the channel along with particles



gradually increased and from 7.5 K onwards, this difference becomes prominent. It was also observed that with higher degree of temperature difference, the attainment of equilibrium particle concentration in each half of the channel becomes faster. For example, when the temperature difference is as high as 100 K (as shown in Fig. 6g), the equilibrium particle concentrations in lower and upper half of the channel are reached almost instantaneously with maximum difference in particle numbers. These results clearly show the influence of thermal gradient in the movement of particles in a liquid-filled microchannel.

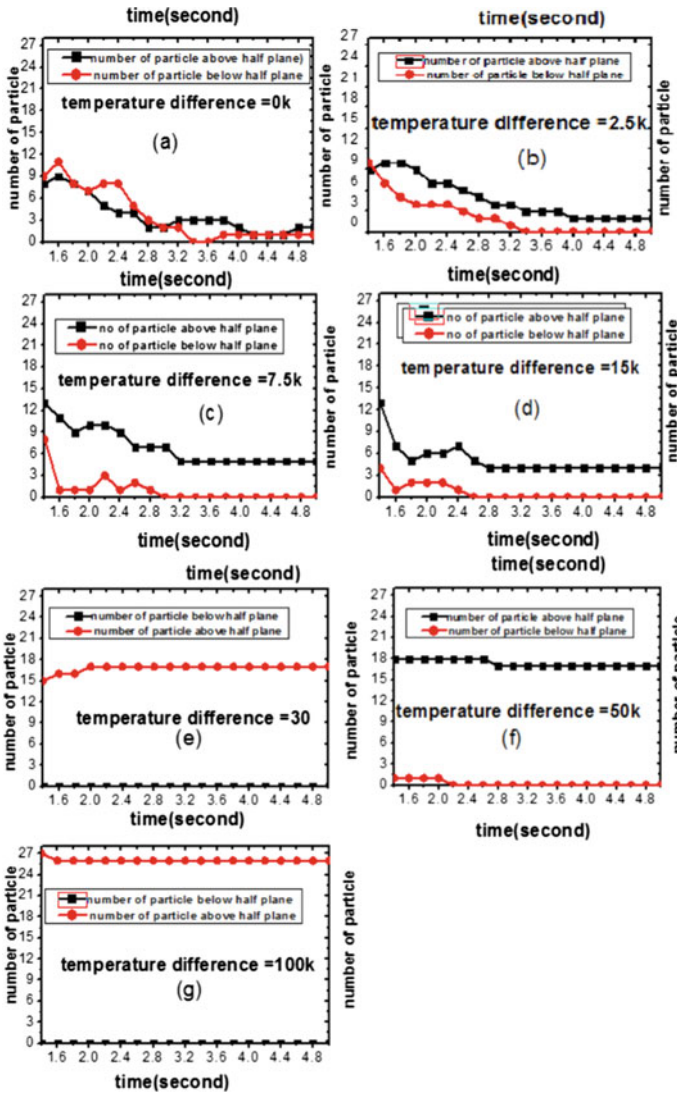


Fig. 6 a Variation of number of particle with given time at $T = 0$ K, **b** at $T = 2.5$ K, **c** at $T = 7.5$ K, **d** at $T = 15$ K, **e** at $T = 30$ K, **f** at $T = 50$ K and **g** at $T = 100$ K

1.3 Conclusions

In the present work migration of polymeric microparticles inside a liquid-filled microchannel has been studied under the influence of a thermal gradient applied to the normal direction of the flow. The results reveal that movement of particles is significantly influenced by the external thermal gradient and it shows that up

to a certain value of temperature difference, the extent of particle migration shows approximate linear relationship and after reaching a limiting higher value, the particle migration becomes complete and further increase in temperature difference do not show any significant change. Such control of particle movement with the application of thermal gradient can be used in a number of futuristic lab on-chip devices such as circulating tumor cell isolation inside microchannel. Although our study is in liquid media. Variation of temperature gradient and its effect on thermophoresis phenomenon was presented in detail.

- Thermophoretic velocity is increasing with increase in temperature gradient so the particle moves quickly toward the cold face.
- In all above cases, the shifting of particles from hot side to cold side will increase with increasing temperature gradient because, as we know that the thermophoretic velocity and thermophoretic force directly dependent on temperature gradient.

References

1. Aitken J (1884) XV. On the formation of small clear spaces in dusty air. *Earth Environ Sci Trans R Soc Edinburgh* 32(2):239–272
2. Astumian RD (2007) Coupled transport at the nanoscale: the unreasonable effectiveness of equilibrium theory. *Proc Natl Acad Sci USA* 104(1):3–4
3. Crookes W (1876) XIII. On repulsion resulting from radiation. Parts III. & IV. *Philos Trans R Soc Lond* 166:325–376
4. Jerabek-Willemsen M, Andre T, Wanner R, Roth HM, Duhr S, Baaske P, Breitsprecher D (2014) MicroScaleThermophoresis: interaction analysis and beyond. *J Mol Struct* 1077:101–113
5. Keng EY, Orr JC (1966) Thermal precipitation and particle conductivity. *J Colloid Interf Sci* 22(2):107–116
6. Kumaran G, Sandeep N (2017) Thermophoresis and Brownian moment effects on parabolic flow of MHD Casson and Williamson fluids with cross diffusion. *J Mol Liq* 233:262–269
7. Liang G, Mudawar I (2019) Review of single-phase and two-phase nano fluid heat transfer in macro-channels and micro-channels. *Int J Heat Mass Transf* 136:324–354
8. Ludwig C (1856) Diffusion zwischen ungleich erwärmten Orten gleich zusammengesetzter Lösungen. *Sitz. Ber. Akad. Wiss. Wien Math-Naturw* 20:539
9. Lusebrink D, Yang M, Ripoll M (2012) Thermophoresis of colloids by mesoscale simulations. *J Phys Condensed Matter* 24(28):284132
10. Minea AA (2013) *Advances in industrial heat transfer*, CRC press

Design and Analysis of the Effect Through Different Aspect Ratio on Performance of VAWT



Ashish and P. Suresh

Abstract This paper aims to analyze the effect of the aspect ratio, which is the ratio between the height of the blade to the radius of the rotor on the turbine's performance. A vertical wind turbine is different from a traditional wind turbine; the axis of rotation of the blade for vertical axis wind turbine is in the vertical direction, as its name suggests, whereas a traditional wind turbine or horizontal wind turbine has an axis of rotation in a horizontal manner. Many researchers have found that the performance of VAWT is more efficient than HAWT. Their performance factors solely depend upon the design of the turbine and its blade for better drag coefficient, aerodynamicity, and aerofoil which generates more Reynolds numbers. Pressure found at inlet or outlet. So, we will conclude this study and see through the result. The model is designed using SOLIDWORKS and analyzed through flow simulation. The angle of the blade is taken as 22° (efficient). The model is tested at different aspect ratios, and the variation in torque generation has been studied. Inside SOLIDWORKS flow simulation, BEM analysis is performed. From the results, it can be concluded that for the angle of attack at 22° , the optimum aspect ratio ranges in-between 1.30 and 1.35. Table 1 shows torque variation with the aspect ratio at that point pressure calculated for the blade; these are plotted with the help of Figs. 3, 4, 5, 6, 7, and 8 that shown and discussed below.

Keywords VAWT · HAWT · SOLIDWORKS flow simulation · BEM

1 Introduction

The turbine blade flexibility crucially increases due to the large scale and uses alloy material with lower elastic stiffness and modulus, the strong aerodynamic coupling between the aerodynamic blade load and dynamic of structure. At that time, the

Ashish (✉) · P. Suresh

Department of Mechanical Engineering, Galgotias University, Greater Noida, Uttar Pradesh, India
e-mail: vashish612@gmail.com

wind turbine designer must take into consideration of flexible long blades' aeroelasticity. The Analysis of the VAWT blade and the torsional behavior of a rotor blade. Generally, BEM is used majorly for analysis.

The (BEM) model is also known as blade element momentum; BEM has a more accurate aeroelasticity model and structural, in aerodynamics analysis and structural for both aspects. But has minor limitations in Three Dimensional effect [1]. Theory of Blade Element Momentum equates binary methodology of examining wind turbine operation. The primary method is to balance on a rotating angular stream tube using the momentum that passes through a turbine. The Secondary method is at various sections along the blade forces are generated by the drag coefficients, and aerofoil lift will be examined. As described, iteratively can be solved by the two methods give a series of equations [2, 3].

Design variables take the size and location of the turning mass along the blade span and the disadvantage of the increasing structural mass. Furthermore, rapid research is going on to improve the design of wind turbines as compared to conventional turbines because an efficient design not only increases performance but also is more cost economic [3]. Design nonlinearity in blades shape has three major effects, increment in flap deflection, gradual increment in time shift in nodal displacement, and shivering of blades [4, 5]—the different shapes of the blade through stiffness and mass modification to make computing to the air-load.

The interior construction is designed to achieve maximum strength while weighing as little as possible; the spars are the most significant structural component of the wings since they carry the air loads during blade rotation. Box spars are placed at 40% of the blade chord and function as structural reinforcement for the blade, making it more efficient at resisting out-of-plane shear stresses and bending moments. There is also some boundary condition applied to an inlet; boundary condition was established at the upstream end of the stationary domain to simulate the incoming wind velocity [6–15].

In the present time work rate, the maximizing strategy of the overall level of the behavior of these frequencies and their variation with the second optimization variables are researched briefly. The symmetrical airfoil-shaped of the blade. The thin-walled spar is the main supporting the skin and nonstructural rib. A finite element approach based on 3-dimensional elements including shear and warping deformation of the welded beam [6, 12]. It is shown to be successful in this analysis of the finite element applied for the test problems. Aerofoil drags and lifts performance will determine the exact chord length and angle of twist for better aerodynamic.

As we know wind turbine machine is used to convert kinetic energy into electrical energy. Wind turbine blades are generally made of a wide range of side which is vertical and horizontal axes. The place where a large number of wind turbines are installed is known as a wind farm; it is estimated that hundreds to thousands of turbines are generated meanwhile 650 GW of power, with 60 GW added each year. They are the best renewable energy sources and are used in many countries because of low energy costs and reduce air pollution, and it helps to reduce the low consumption of fossil fuels. In 2009, one study claimed that wind turbine emission lowers the



Fig. 1 The working model of vertical axis turbine view

amount of greenhouse gas. Some wind turbine is smaller in size which is used for mainly charging a battery for auxiliary power for boat and power traffic warning Sign.

1.1 Vertical Axis Wind Turbine (VAWT)

As per data, VAWT is more efficient compared to HAWT according to researchers. Performance of VAWT depends on many factors like material used, angle of attack, dynamic-wind viscosity, aspects ratios, Reynolds number, design, etc. Today, most VAWT are made up of composite materials or glass fibers. Glass fiber provides strength and has less weight compared to other materials of the same strength [7, 8]. When the flow is unsteady, wind turbine performance reduces and may develop aerodynamic instability on wind turbine blades [9, 10, 13] like stall generation, stall flutter, etc. In addition, the stall induced in turbine results in the development of vibration edge-wise [11, 14] (Fig. 1).

2 Methodology

Creating a 3D model of a vertical axis turbine is preferable for the first step. Solid Works is used for this task because it is easy to learn and use. It has many features that make the designing process simple and fast. The initial dimension of the turbine is set to 1400 mm in radius and 1750 mm in height, which makes the aspect ratio 1.25. Further, the height of the turbine is changed to different aspect ratios (Fig. 2).

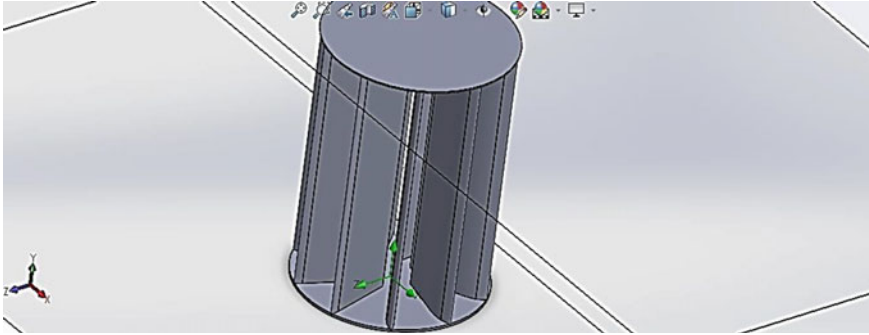


Fig. 2 The model of vertical axis turbine on SOLIDWORKS in isometric view

2.1 Meshing

Meshing is an essential task in analysis. The quality of mesh determines the accuracy of the result obtained. Meshing divides the model into small subparts. The more the number of subparts, the more fine mesh becomes and reduces the percentage of error in the result. Solid Works provide a simple and easy way to mesh the model. Meshes are generally rendered to the screen of computer and for a physical simulation such as (CFD) computational fluid dynamics (FEA) finite element analysis. Meshings are the composition of the simple cell of like a triangle, e.g., one may know how to perform operations such as calculation of FEA (i.e., engineering) or tracing ray (i.e., computer graphics) on a triangle, but one did not know how to perform these operations on complicative spaces and shapes. Here, blades are messed up simply by using software for better results to prevent any problem in design and practical uses.

2.2 Analysis Settings

For analysis, the contour or air region model is created around in mm^3 unit. The air velocity is taken as 50 m/s on the positive z-axis. The goal is set to determine the torque in the y-direction. Torque can be found as $(T = F \cdot r \cdot \sin A)$. The first 1.4 aspect ratio is taken, then values are set for once then after for variance get by increasing and other by decreasing to measure the change in torque. Finally, by getting the graph of torque versus time is plotted.

3 Results

All the plot obtained from flow analysis is shown in Figs. 3, 4, 5, 6, 7 and 8. In Fig. 3 at aspect ratio; the flow near the blade edge is between 102,683 and 103,166, which shows that the pressure at the inlet is much as compared to the rest part of the turbine.

The least pressure region is near the outlet from where wind flows exit at approximately 100,264 then again, pressure starts increasing as it moves further toward the z-axis. While in Fig. 4, at the 1.5 aspect ratio, the region at the inlet of flow, the pressure region is much smaller than the 1.4 aspect ratio. Also, as in the positive z-axis, the pressure is lower than that of 1.4. At 1.4 aspect ratio, the torque starts to decrease, so further the lower aspect ratio is considered. From Fig. 5 shows that the pressure region is most remarkable among all six cases. In Fig. 6, with an aspect ratio of 1.3, the pressure is similar to Fig. 5, but at the outlet region, the flow is uniform when compared with aspect ratio of 1.35. From Fig. 7 at 1.25 aspect ratio, the pressure is less, and at the outlet, the flow is uniform, and pressure is also significantly less. Figure 8, at 1.2 aspects the result slightly vary from Fig. 5.

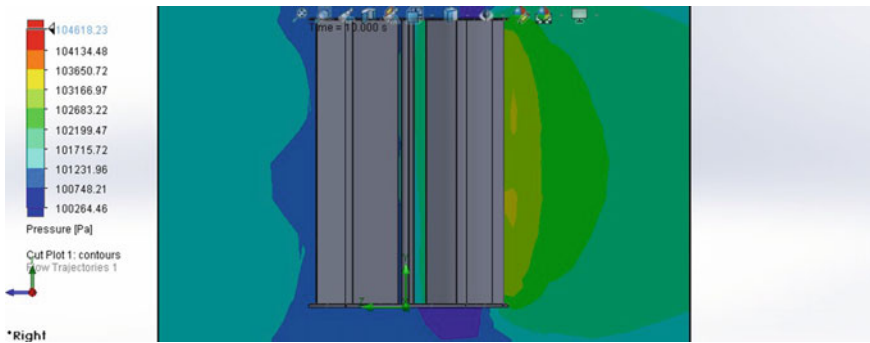


Fig. 3 The pressure at the blade is 1.4 aspect ratio

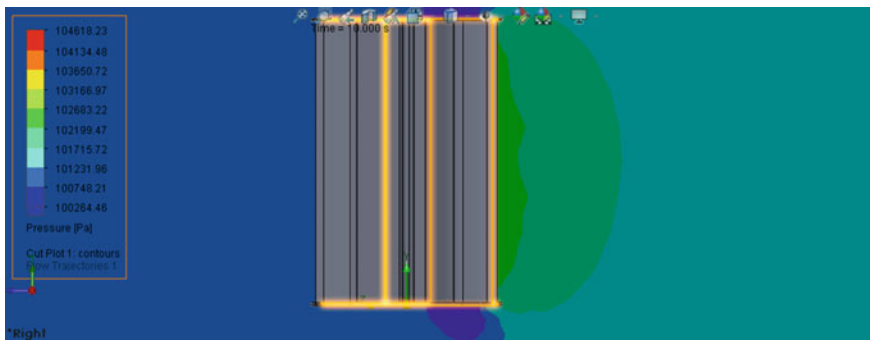


Fig. 4 The pressure at the blade is 1.5 aspect ratio

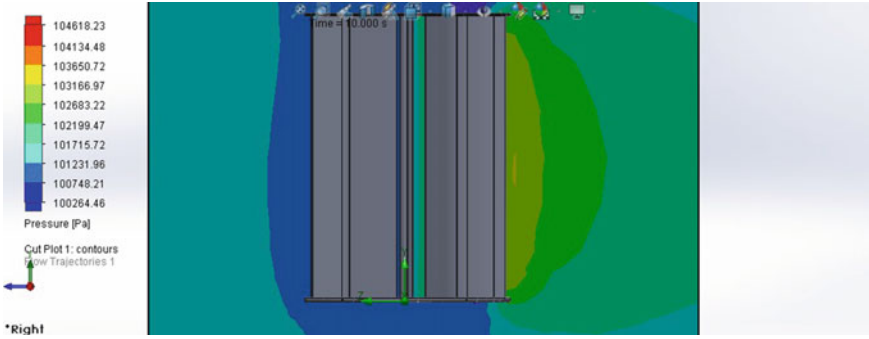


Fig. 5 The pressure at the blade is 1.35 aspect ratio

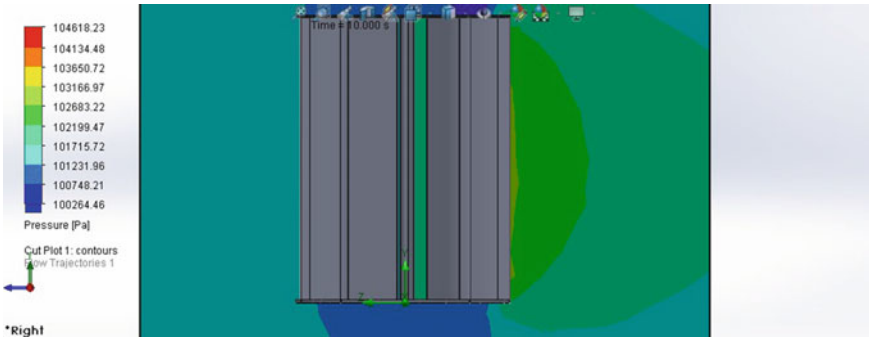


Fig. 6 The pressure at the blade is 1.3 aspect ratio

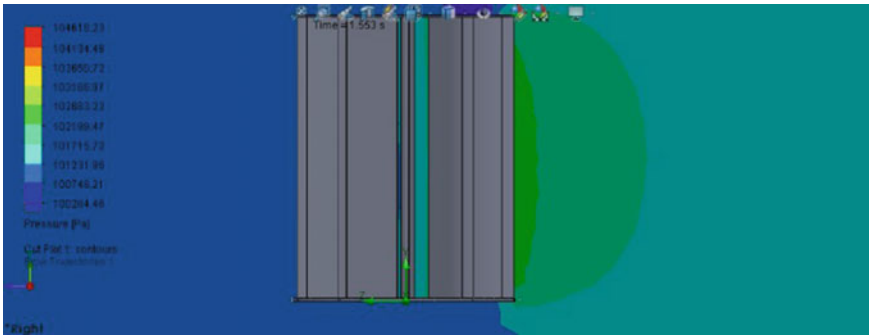


Fig. 7 The pressure at the blade is 1.25 aspect ratio

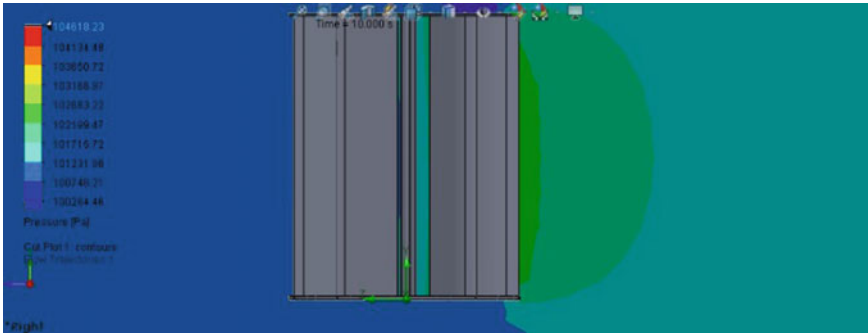


Fig. 8 The pressure at the blade is 1.2 aspect ratio

Table 1 Torque at a different aspect ratio

Aspect ratio	1.5	1.4	1.35	1.3	1.25	1.2
Torque	71.263	48.829	84.217	98.165	52.693	50.387

Table 1 shows torque variation with the aspect ratio. The result shows that on increasing the aspect ratio, the torque generated starts decreasing. On the other hand, it is seen that at a lower aspect ratio, Reynolds Number is much higher, which ultimately results in an increase in performance. On decreasing the aspect ratio, the torque generated goes on increasing, as shown by the results. Nevertheless, this is valid up to a certain aspect ratio; on further decreasing the aspect ratio, the torque also decreases. So, after summing up all the results this paper concludes that for the angle of attack at 22°, the optimal aspect ratio found is between 1.3 and 1.35 ratio.

4 Conclusion

This paper successfully analyzed the effect of the aspect ratio on the performance of vertical axis wind turbine. The result has shown that on changing the aspect ratio, the performance also varies, using SOLIDWORKS flow simulation design of blade main factor of performance and aerodynamicity. It is observed that on increasing the aspect ratio, the performance decrease, and on reducing the aspect ratio, the performance increase. Reynolds number is also responsible for the performance of wind turbines. The Aspect ratio also affects the Reynolds number, and as a consequence, the commission also gets affected. The study suggests that it is possible to design the airfoil to generate different Reynolds number according to the needs. The advantages of using a turbine with a lower aspect ratio are greater power output and ease of maintenance, less risk of fracture or breakage because the blades are thicker. Also, it is found that the airfoils with the thicker blade or low aspect ratio, the larger radius

of the blade maintains the laminar flow at the leading edge of the upper surface. Further, the study can be made if the optimal aspect ratio varies for different angles of attack.

Acknowledgements The author gratefully acknowledges the partial support for this study by the mechanical engineering faculty from Galgotias University, Uttar Pradesh, India.

References

1. Chen J, Shen X, Liu P, Zhu X, Du Z (2017) Design tool for aeroelastic analysis of wind turbine blades based on geometrically exact beam theory and lifting surface method, pp 1–18. <https://doi.org/10.2514/6.2017-0450>
2. Hunt A, Stringer C, Polagye B (2020) Effect of aspect ratio on crossflow turbine performance. *J Renew Sustain Energy* 12(5)
3. Grant Ingram (2011) Wind turbine blade analysis using the blade element momentum method, [//creativecommons.org/licenses/by-sa/3.0/](https://creativecommons.org/licenses/by-sa/3.0/)
4. Staino B, Basu A (2013) Dynamics and control of vibrations in wind turbines with variable rotor speed. *Eng Struct* 56:58–67
5. Kumar A (2020) Modal analysis of helical gear train using Ansys, pp 604–607
6. Navadeh N, Goroshko I, Zhuk Y, Moghadam FE, Fallah AS (2021) Finite element analysis of wind turbine blade vibrations, pp 310–322
7. Kong JBC (2005) Structural investigation of composite wind turbine blade considering various load cases and fatigue life 30(11–12):2101–2114
8. Lin H (2011) Layup analyzing of a carbon/glass hybrid composite wind turbine blade using finite element analysis, vol 87, pp 49–54
9. Song F, Ni Y, Tan Z (2011) Optimization design, modeling and dynamic analysis for composite wind turbine blade, vol 16, pp 369–375. <https://doi.org/10.1016/j.proeng.2011.08.1097>
10. Sørensen JN, Voutsinas S, Sørensen N, Madsen HA (2007) State of the art in wind turbine aerodynamics and aeroelasticity. *Prog Aerosp Sci* 42(2006):285–330
11. Hansen MH (2007) Aeroelastic instability problems for wind turbines. *Wind Energy* 10:551–577
12. Holierhoek JG (2013) An overview of possible aeroelastic instabilities for wind turbine blades 37(4)
13. Shamsoddin S, Porté-Agel F (2020) Effect of aspect ratio on vertical-axis wind turbine wakes. *J Fluid Mech* 889, Cambridge University Press
14. Sobczak K (2018) Numerical investigations of an influence of the aspect ratio on the Savonius rotor performance. *J Phys Conf Ser* 1101, XXIII fluid mechanics conference (KKMP 2018) 9–12 September 2018, Zawiercie, Poland
15. Sriganapathy AJ, Sudhan S, Sundarmagalingam T, Nijilabinash E, Siva T (2020) Design and Analysis of vertical axis wind turbine blade, vol 02, Issue 05. www.rspsciencehub.com

Parametric Optimization of Fused Filament Fabrication Process



Sourabh Anand and M. K. Satyarthi

Abstract The process of making three dimensional solid objects from a CAD model with the help of layer upon layer deposition is termed additive manufacturing (AM) or also known as 3D printing. In the present work, test specimens will be manufactured by fused filament fabrication process (FFF) process and the quality of manufactured product depends upon various process parameters. Out of these various process parameter, layer thickness, orientation, and infill% has been used for experimental analysis. In this work, experimental analysis is done to see the impact of layer thickness, infill%, and orientation on performance parameters. Experiment is conducted with Taguchi L₉ orthogonal array. Finally, the process parameter will be optimized by calculating the grade and coefficient with the help of GRA to increase the high tensile strength and compressive strength and reduce the surface roughness.

Keywords Additive manufacturing · 3D printing · DOE · GRA Taguchi · L₉ orthogonal array

1 Introduction

In the generation of industry 4.0, the term AM is very popular among various industries because it rapidly creates the model or part prior to final release or commercialization. AM is a layer upon layer deposition manufacturing process which is completely automated manufacturing process for building 3D physical objects directly from 3D CAD model produced by CAD software. At the early stage of development, it was known by various names such as Automated fabrication (Autofab) further developments took place with time in this technology, and in current it is called 3D printing, Additive manufacturing, Rapid prototyping [1].

S. Anand (✉) · M. K. Satyarthi
University School of Information, Communication & Technology, Guru Gobind Singh
Indraprastha University, New Delhi 110078, India
e-mail: sourabh.17216490020@ipu.ac.in

M. K. Satyarthi
e-mail: mksssrewa@ipu.ac.in

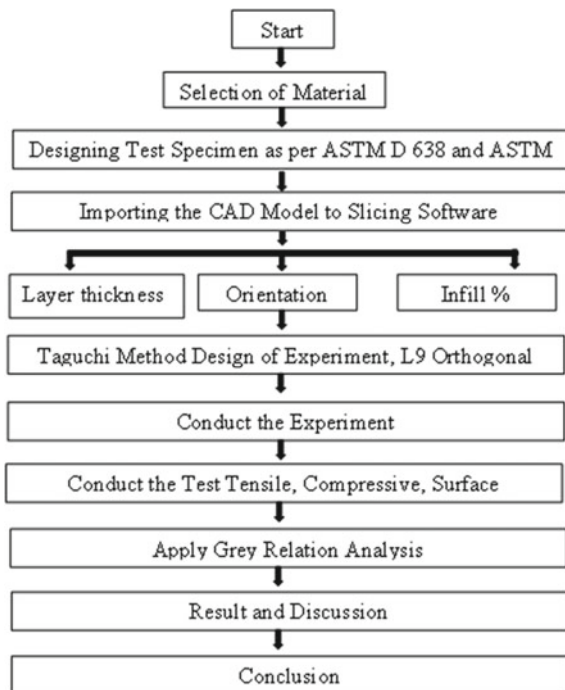
1.1 Printing Material of FDM

FFF's best printing material is highly dependent on its application and each printing filament has its advantages and disadvantages. At present eight standard filaments PLA, ABS, PETG, nylon, carbon fiber composite, PFA, hips, flexible filament (TPU), and polypropylene are used. In this work only, PLA has been used to print test samples because PLA is thermoplastic polyester and it is most popular as it is produced from economically renewable sources and is biodegradable. The maximum tensile strength of PLA is 37mpa, its density is 1.3 g/cm³, and the glass transition temperature is 60 °C [2].

1.2 Methodology

The flow chart of methodology is shown in Fig. 1.

Fig. 1 Flow diagram of methodology



1.3 FFF Machine Tool

FFF is one of the 3D printing processes among various available 3D printing processes. In the present work, CADX FDM machine tool has been used. In this machine, the thermoplastic filament (PLA) is fed to the heated nozzle of the machine with the help of extruder. The speed of filament is controlled by the help of drive wheel present in the extruder. The movement of nozzle is according to the G code which is provided by the slicing software.

1.4 Sample Preparation Process

To test the tensile strength of build part tensile test specimen is designed according to ASTM D638 standards [3] used for testing thermoplastic material. The design is performed on CAD software. Similarly, for compression tests, test specimen is designed according to ASTM D695 [3]. After completing the 3D drawing, part is saved into STL file format. STL file is imported to the slicing software and part is divided into number of small layers. According to G code generated in slicing software the FDM machine is going to print the part. The tensile test specimen is divided into 114 layers.

1.5 Process Parameters

To manufacture FFF build parts different process parameters are required to achieve an optimum quality according to the requirement of application. To achieve high mechanical properties three process parameter is selected. Orientation: It is an inclination of build part with respect to X-axis, Y-axis, and Z-axis of build platform. Layer Thickness: After slicing of build part with the help of slicing software the build part is divided into number of layers and each layer has its specific height along Z direction, this specific height along Z direction is known as layer thickness. Varying the layer thickness has significant effect on mechanical strength. Infill: It is the amount of material that is deposited into the internal structure of build part. With zero infill hollow part is manufactured and with 100% infill, a solid part is manufactured. So, mechanical properties of build part are highly dependent upon infill % [4].

1.6 Introduction to 3D Printing Methodology

Parameters Levels as shown in (Table 1) three parameters, i.e., layer thickness (micron), orientation (degree), and infill (%) has been taken as process parameters. Therefore, this experiment is a three factor 3 level Taguchi method of design of experiment.

2 Literature Review

The FFF process is very popular among industries due to its ability to produce complex functional parts. The FFF process can be used for a variety of applications ranging from model prototyping to functionally working parts. The FFF process begins with the production of a CAD model, followed by the conversion of the CAD model into a standard tessellation language file format (STL). The STL file is then translated into a number of thin layers using slicing software, and the product is then printed using an FFF machine. Finally, post-processing and cleaning are carried out in order to obtain the desired product. Mechanical attributes such as tensile strength, compressive strength, flexural strength, and surface quality are regarded as key characteristics for the majority of the products generated by the FFF process. Despite this, achieving the best quality part manufactured using the FFF process without understanding the impact of input parameters is extremely challenging. Consequently, optimizing input parameters are critical for achieving required quality attributes in FFF-produced product [5, 6]. The research attempts carried out in recent past in the field of Additive manufacturing are summarized below.

Anitha et al. utilize the taguchi approach to look at the effect of road width, layer height, and deposition rate on the surface roughness of FDM components at three different levels. According to the findings, layer thickness has the largest influence on surface finish, followed by road width and deposition rate [7], Sood et al. used the Taguchi approach to evaluate the effects of inclination angle, layer height, raster angle, raster breath, and raster to raster gap on dimensional accuracy. The taguchi technique is used to identify significant variables and their interactions. The optimal parameter settings are discovered such that all three dimensions exhibit the smallest divergence from real value settings at the same time, and the common factor settings are investigated [8]. According to the research of Pradhan et al., product quality has a significant impact on material properties. The impact of process factors on surface

Table 1 Orthogonal factor level (3 × 3) table for PLA FFF process

Levels	1	2	3
Layer thickness (μ) A	100	200	300
Orientation ($^{\circ}$) B	0	45	90
Infill (%) C	100	90	80

roughness is studied using method of response surface methodology. The application of RSM allows for the establishment of a correlation between the process variable and the response. The surface response is strongly affected by pulse current, discharge duration, and the pulse current’s interaction term with other factors, according to a second-order response model of these parameters [9]. From the literature review, it was viable to study mechanical and topological features viz tensile, compressive strength, and surface quality for layer thickness, orientation, & infill %.

3 Design of Experiment

Taguchi’s experimental design uses orthogonal arrays to systematically arrange process parameters that affect variation in output parameters [8]. Under Taguchi method the testing is done in pairs of combinations, hence saving some time over conventional factorial design method (testing all possible combinations. So, with minimum amount of experimentation, required data can be collected and used for calculating the factors that affect product quality the most. This saves time and resources [10], and the orthogonal array is shown in Table 2. The performance measure of the array is shown in Table 3.

3.1 Optimization

Process parameters optimization of fused filament fabrication process not only increases the product quality but also reduces the cycle time of building product to greater extent. Multiple performance characteristics optimization is substantially more difficult than single performance characteristic optimization. This is due to a number of issues that arise when optimizing a process parameter with multi-performance characteristics, such that each performance characteristic’s category

Table 2 L9 orthogonal array

No. of expt	Layer thickness (μ)	Orientation ($^{\circ}$)	Infill (%)
1	100	0	100
2	100	45	90
3	100	90	80
4	200	0	90
5	200	45	80
6	200	90	100
7	300	0	80
8	300	45	100
9	300	90	90

Table 3 The performance measure of a L9 OA according to experimental setup

Specimen no	Levels of parameters			Higher the better	Higher the better	Lower the better
	Layer thickness	Orientation	Infill %	Tensile strength (N/mm ²)	Compressive strength (N/mm ²)	Surface roughness
1	100	0	80	47.20416667	54.071625	4.188930556
2	100	45	90	51.74029167	40.8465	4.173315972
3	100	90	100	55.79666667	36.793375	4.156013889
4	200	0	90	47.25729167	53.5175	4.368086806
5	200	45	100	54.43666667	41.878625	3.989472222
6	200	90	80	42.98579167	51.377875	3.359920139
7	300	0	100	52.67891667	52.609375	3.924180556
8	300	45	80	44.60029167	55.806875	3.456815972
9	300	90	90	48.54691667	50.63925	3.362263889

may not be the same. Each performance characteristic may be specified in its own engineering unit, and the significance of each performance characteristic may vary [11].

3.2 *Gray Relational Analysis (GRA) of Multi-performance Characteristics*

3.2.1 *Data preprocessing*

Data processing is very important for GRA when multi-performance characteristics are analyzed because each data sequence's unit and range may differ from the other data sequences. Data preprocessing is defined as the process of converting data from the original sequence to data from a comparable sequence. The experimental results have been standardized in the range between 0 and 1 for this purpose. Tensile and Compressive strength is the dominant mechanical properties in fused filament fabrication process that determine the quality of the built product under consideration. The original sequence can be standardized as follows for the larger-the-better characteristics like Tensile Strength and Compressive Strength [12–14].

$$X_i^* = \frac{a_i(n) - \min a_i(n)}{\max a_i(n) - \min a_i(n)} \quad (1)$$

Table 4 After data processing, the sequences of each performance measure

Tensile strength (N/mm ²)	Compressive strength (N/mm ²)	Surface roughness
0.329281	0.329281	0.670719
0.683365	0.683365	0.316635
1	1	0
0.333428	0.333428	0.666572
0.89384	0.89384	0.10616
0	0	1
0.756633	0.756633	0.243367
0.126026	0.126026	0.873974
0.434094	0.434094	0.565906

where, $x_i^*(n)$ and $a_i(n)$ represent the ordered sequence after the data preprocessing and equivalence sequence, respectively; $n = 1$ and 2 for Tensile and compressive Strength, respectively; $i = 1, 2, 3, \dots, 9$ for experiment numbers 1 to 9.

Surface the lower the better value has been utilized to minimize surface roughness in order to achieve optimal surface roughness. The original sequence should be standardized as follows when the lower the better characteristics are applied [12–14]. Table 4, shows the processed data. Table 5 shows the deviation sequences.

$$X_i^* = \frac{\max a_i(n) - a_i(n)}{\max a_i(n) - \min a_i(n)} \tag{2}$$

Now $\Delta_{0i}(n)$ is the deviation sequence of the reference sequence $x_0^*(n)$ and the comparability sequence $xi^*(k)$ i.e.

Table 5 The deviation sequences

Deviation sequences		
Tensile strength (N/mm ²) $\Delta_{0i}(1)$	Compressive strength (N/mm ²) $\Delta_{0i}(2)$	Surface roughness $\Delta_{0i}(3)$
0.670719	0.670719	0.329281
0.316635	0.316635	0.683365
0	0	1
0.666572	0.666572	0.333428
0.10616	0.10616	0.89384
1	1	0
0.243367	0.243367	0.756633
0.873974	0.873974	0.126026
0.565906	0.565906	0.434094

Table 6 The computed GRG and the sequence in the optimization procedure

Tensile strength	Compressive strength	Surface roughness	GRG γ	Rank
0.427088	0.427088	0.602932	0.485703	9
0.612268	0.612268	0.422524	0.54902	5
1	1	0.333333	0.777778	1
0.428606	0.428606	0.599932	0.485715	8
0.824865	0.824865	0.358721	0.669484	2
0.333333	0.333333	1	0.555556	4
0.672615	0.672615	0.397889	0.58104	3
0.363908	0.363908	0.798689	0.508835	6
0.469085	0.469085	0.535278	0.491149	7

$$\Delta_{0i} = |x_0^*(n) - x_i^*(n)|$$

$$\Delta_{\max} = \Delta_{06}(1) = \Delta_{04}(2) = \Delta_{02}(3) = 1.00$$

$$\Delta_{\min} = \Delta_{03}(1) = \Delta_{06}(2) = \Delta_{01}(3) = 0.00$$

3.2.2 Data preprocessing Computing the Gray Relational Coefficient (GRC) and the Gray Relational Grade (GRG)

The GRC is defined as follows:

$$\xi_i(n) = \frac{\Delta_{\min} + \alpha \Delta_{\max}}{\Delta_{0i}(n) + \alpha \Delta_{\max}} \tag{4}$$

where γ is GR Grade calculated by averaging the GR coefficient. Table 6. represents the GR Grade for each experiment that has been designed by L9 OA. The highest GR Grade value indicates that the experimental results are closer to the optimally normalized value.

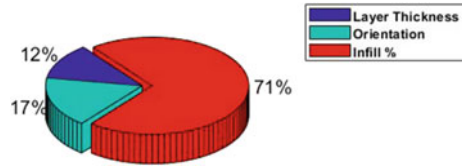
4 Results

Using the Taguchi method’s response table, the GRA has been proposed as a tool for exploring the optimization of FFF process parameters for Additive manufacturing. For multiobjective measurements including tensile strength, surface roughness, and compressive strength, the gray relational grade was utilized to determine the optimum process settings. There have been nine OA-based experimental runs conducted. It

Table 7 Analysis of variance

Source	DF	Adj SS	Adj MS	F-value	P-value	Contribution %
Layer thickness	2	0.008974	0.004487	3.24	0.236	11.9392
Orientation	2	0.012669	0.006334	4.57	0.179	16.8538
Infill %	2	0.053521	0.026761	19.32	0.049	71.2070
Error	2	0.002771	0.001385			
Total	8	0.077934				

Fig. 2 Factor contributions as a percentage of the GRG



was found that according to the response table of the average GRG, the greatest value of GRG for layer thickness, orientation, and infill is 100 μ, 90°, and 10%, correspondingly. These would be the proposed levels of modifiable process variables when better tensile and compressive strength, as well as improved surface quality, are generated together. It was also established that with utilization of this approach as described in this work, the multiobjective performance measures of the FFF process such as tensile strength, surface roughness, and compressive strength are all enhanced simultaneously.

Table 7 represents the results of an ANOVA for GRG. Figure 2 shows the factor contributions as a percentage for each term impacting GRG. The figure clearly illustrates that infill percent is one of the most important factors that influence GR Grade and so helps to improve tensile strength, compressive strength, and surface quality. Layer Thickness and Orientation, in addition to infill percent, are important. The best process parameters are infill % at first level, Orientation at 2nd level, and layer thickness at 3rd level based on the preceding discussion. In actual value, the optimal parameters are layer thickness, Orientation, and Infill % 100μ, 90°, and 100%, respectively.

5 Conclusions

In this analysis, the Taguchi technique was combined with GRA to optimize the Fused Filament Fabrication process parameters while considering several performance factors such as tensile strength, compressive strength, and surface roughness. Analyzing the response table of the gray relational grade yielded the optimal parameters. The largest value of gray relational grade for layer thickness, Orientation, and Infill percent is 100μ, 90°, and 100%, respectively, according to the response table

for gray relational grade. When improved Tensile Strength, Compressive Strength, and reduced surface roughness have to be achieved simultaneously, these are the suggested levels of controllable process parameters. The Infill percent is the most influential parameter impacting Tensile Strength, Compressive Strength, and surface roughness, according to the ANOVA Table of GR Grade for various performance measures. Further, the study of defects produced in this experimentation process is proposed for the future work.

References

1. Villalpando L, Eiliat H, Urbanic RJJPC (2014) An optimization approach for components built by fused deposition modeling with parametric internal structures. *Procedia CIRP* 17:800–805
2. Baumann FW, Roller D (2017) Survey on additive manufacturing, cloud 3D printing and services
3. Letcher T, Waytashek M (2014) Material property testing of 3D-printed specimen in PLA on an entry-level 3D printer. In: ASME international mechanical engineering congress and exposition, vol 46438. American Society of Mechanical Engineers, p V02AT02A014
4. Fatimatuzahraa A, Farahaina B, Yusoff W (2011) The effect of employing different raster orientations on the mechanical properties and microstructure of Fused Deposition Modeling parts. In: 2011 IEEE symposium on business, engineering and industrial applications (ISBEIA). IEEE, pp 22–27
5. Kumar S, Kannan VN, Sankaranarayanan G (2014) Parameter optimization of ABS-M30i parts produced by fused deposition modeling for minimum surface roughness. *Int J Curr Eng Technol* 3:93–97
6. Masood SH, Mau K, Song W (2010) Tensile properties of processed FDM polycarbonate material. In: *Materials science forum*, vol 654. Trans Tech Publ., pp 2556–2559
7. Anitha R, Arunachalam S, Radhakrishnan P (2001) Critical parameters influencing the quality of prototypes in fused deposition modelling. *J Mater Process Technol* 118(1–3):385–388
8. Sood AK, Ohdar RK, Mahapatra SS (2009) Improving dimensional accuracy of fused deposition modelling processed part using grey Taguchi method. *Mater Des* 30(10):4243–4252
9. Pradhan MK, Biswas CK (2011) Effect of process parameters on surface roughness in EDM of tool steel by response surface methodology. *Int J Precis Technol* 2(1):64–80
10. Pereira AC, Romero F (2017) A review of the meanings and the implications of the Industry 4.0 concept. *Procedia Manuf* 13:1206–1214
11. Bagchi TP (1993) Taguchi methods explained: practical steps to robust design. Prentice-Hall
12. Chang S-H, Wu JH, Li Z (1996) Frequency synthesizer product or/and process optimization using the grey relational analysis. *J Grey Syst* 8(3):235–260
13. Deng JL (1990) A course on grey system theory. Huazhong University of Science and Technology Press, Wuhan
14. Ju-Long D (1982) Control problems of grey systems. *Syst Control Lett* 1(5):288–294

A Perspective on Third-Generation Medium-Mn Steels for Automotive Application



Isha Apurwa, Jeetendra Kumar Yadav, and Ashok Kumar

Abstract Medium-Mn steels are one of the potential advanced high strength steels (AHSS) of third-generation, having an exceptional combination of high strength-elongation and crashworthiness. They have Mn in the range of 3–12 wt.% and consist of so-called “ultrafine-grained (UFG)” equiaxed or lath-like ferrite/martensite and retained austenite microstructure. The retained austenite content and its stability play a dominating role in influencing the properties of medium Mn steel as it delays the fracture or failure of the steel during deformation or event of a crash, via strain hardening mechanisms like “Transformation Induced Plasticity (TRIP)” and “Twinning Induced Plasticity (TWIP)” effects. The retained austenite amount and its stability can be tuned by adopting an appropriate intercritical annealing schedule, as it is influenced by various factors like the elemental composition of austenite, its grain size, morphology, etc. This article illustrates the evolution of medium-Mn steel, its microstructure, properties, and model for optimizing the retained austenite fraction, and factors influencing it.

Keywords Medium Mn steel · AHSS · TRIP · Intercritical annealing

1 Introduction

Steel continues to remain the most dominant material in the automotive industry because of its high strength, ductility, safety, and recyclability. Stringent norms for reducing CO₂ emissions have compelled steelmakers and automotive manufacturers to adopt a new grade of steel that has a high strength to weight ratio and is also cost-effective and feasible for large-scale industrial production [1–5]. Steelmakers are striving to develop various new grades of steel that are lighter and stronger.

I. Apurwa (✉) · A. Kumar
Department of Metallurgical and Materials Engineering, National Institute of Technology,
Jamshedpur 831014, India
e-mail: isha.apurwa@gmail.com

J. K. Yadav
Department of Mechanical Engineering, Galgotias College of Engineering and Technology,
Greater Noida 201306, India

© The Author(s), under exclusive license to Springer Nature Singapore Pte Ltd. 2023
S. Yadav et al. (eds.), *Advances in Mechanical and Energy Technology*, Lecture Notes
in Mechanical Engineering, https://doi.org/10.1007/978-981-19-1618-2_34

351

Now the trend is toward lightweight materials to enhance the fuel economy of the vehicles without compromising strength, durability, corrosion, and wear resistance so as to meet safety requirements. This has directed the research community toward the development of advanced high strength steel (AHSS) [6]. AHSS possesses an excellent combination of strength and formability obtained from a thinner gauge as compared to conventional steel thus making it suitable to meet the challenges of the demanding automobile industry.

2 AHSS Evolution and the Need for Medium-Mn Steel Development

Figure 1 shows the various grades of AHSS with respect to strength and elongation. The first-generation of AHSS typically consists of martensitic steels, dual-phase (DP) steels, and lean alloyed transformation induced plasticity (TRIP) steels. These first-generation steels have a strength and elongation product (PSE) in the range of 10–20 GPa% [7]. Though the tensile strength obtained in the first-generation AHSS is higher than conventional steel grades, it had limited formability to meet the safety standards. Thereafter, the next progress in AHSS was the development of high Mn (>15 wt. %) second-generation twin induced plasticity (TWIP) steels for use in critical automotive components for enhanced passenger safety. The TWIP steels possessed a fairly good strength-ductility combination with PSE exceeding 50 GPa% [7]. Despite their advantages in strength-ductility over the first-generation AHSS, these steels had severe limitations for practical applications. Firstly, the requirement of high alloying content, esp. Mn increases the production cost and poses manufacturing challenges at an industrial scale. Secondly, due to high alloying content, they have poor weldability. Thirdly, these steels have relatively lower yield strength

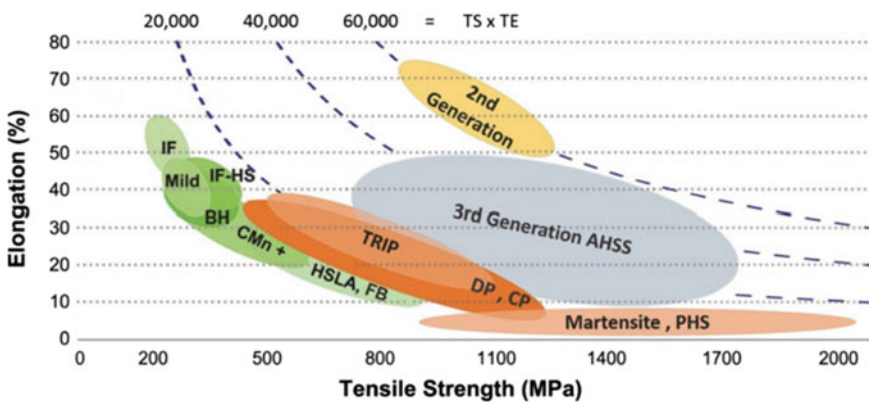


Fig. 1 Elongation vs tensile strength of existing automotive-grade steels and prospective “third-generation” steel grades. Adapted from Ref. [9]

(<550 MPa), as it has a fully austenitic microstructure. To overcome the drawbacks of second-generation AHSS, research is being carried out worldwide toward the development of steel grades with relatively lower alloying content, good weldability, ease of production, and having high strength-ductility combination. This steered to the development of third-generation AHSS, like medium-Mn steel. The medium Mn steels have lower Mn content (Mn in range of 3–12 wt.%) [1] and have mechanical properties intermediate to first-generation and the second-generation steels. These steels exhibit increased energy absorption compared to the first-generation AHSS and possess an outstanding combination of strength-elongation products in the range of 30–60 GPa% [8].

Besides the strength-ductility attributes of steel, the strength-to-weight ratio of steel also has a crucial role. Automobiles are one of the major sources of greenhouse gas emissions globally, due to which strict environmental norms to restrict emissions have been implemented worldwide. Also, the automotive sector is moving toward the adoption of electric vehicles (EV); to compensate for the additional weight of batteries in EVs, it requires a considerable weight-saving approach in the body-in-white (BIW) and other automotive parts. Also, in traditional automobiles, weight-saving would maximize fuel efficiency. It has been reported that with every 10% reduction in the weight of vehicles, there is an improvement in fuel efficiency by 6–8% and a subsequent decrease in emission by 5–6% [10]. With the advent of medium Mn steel, having very high strength and ductility, the de-gauging of the steel sheet in automotive components is quite possible, thus decreasing the overall weight of the vehicle.

3 Microstructure

The medium Mn steels possess a microstructure of ultrafine-grained (UFG) or lath ferrite/martensite phases along with a significant amount of film and/or blocky retained austenite (RA) phase (generally >15 vol.%) [3]. Excellent strength-ductility combination in medium Mn steel is ascribed to the presence of RA in the ultrafine ferrite/martensite (α) matrix. Stabilization of austenite to room temperature is one of the key steps in the annealing treatment of medium Mn steel. It is achieved through austenite reverted transformation (ART) annealing, commonly known as intercritical annealing (IA) [1, 11], wherein the steel is heated to a temperature between A_{c1} and A_{c3} and held for a considerable time duration for partitioning of alloying elements as illustrated in Fig. 2.

The IA parameters (temperature and time) are crucial for determining austenite fraction, its thermal and mechanical stability, morphology (lath or equiaxed), stacking fault energy (SFE), and crystallographic orientation, all of which will directly or indirectly influence the properties and performance of the steel. Therefore, a detailed understanding of the intercritical annealing parameters and their effect is essential in the design of medium Mn steels. The intercritical annealing temperature needs to be appropriate such that austenite with optimum content and mechanical stability is

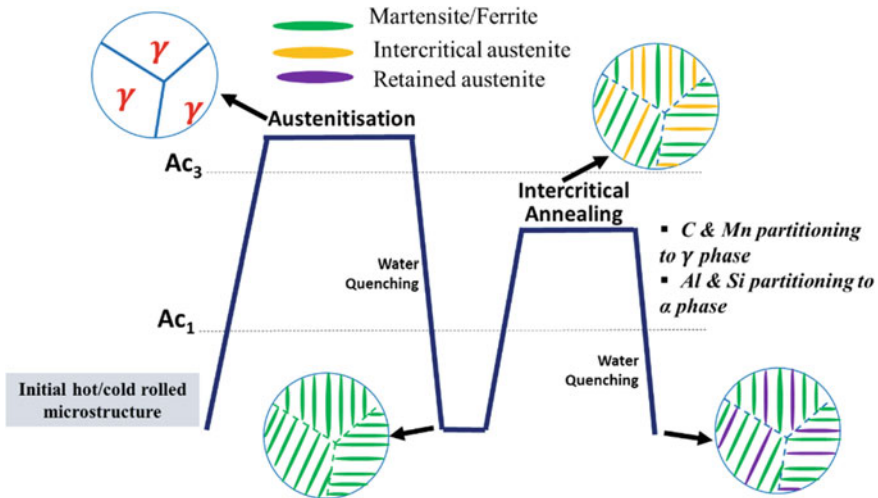


Fig. 2 Illustration of the intercritical annealing treatment and microstructure in medium-Mn steels

retained. Additionally, the IA temperature should be high enough, so as to prevent the formation of low-temperature carbides and intermetallics [13].

4 Thermodynamic Model for Prediction of Retained Austenite and Factors Affecting It

As the retained austenite directly affects the properties in medium Mn steels, it becomes quite important to devise an approach to predict the fraction of RA after intercritical annealing (IA) at different temperatures between Ac_1 and Ac_3 . In order to predict the amount of austenite retained (γ_{ret}) at room temperature, after intercritical annealing followed by quenching to room temperature, a thermodynamic model given by Moor et al. [12] is illustrated below:

- (i) Prediction of equilibrium amounts of austenite (γ_{IA}) as a function of IA temperature using a commercial thermodynamic software package like Thermo-Calc™ [13].
- (ii) Prediction of equilibrium austenite compositions at different intercritical temperatures, using Thermo-Calc™. The composition of austenite would vary with IA temperature. During the IA, the austenite stabilizing elements like Mn and C would selectively partition to the intercritical austenite phase, while ferrite stabilizing elements like Al and Si would partition to intercritical ferrite resulting in a gradient in composition between ferrite and austenite.
- (iii) The C, Mn partitioning to austenite would subsequently decrease the martensite start (M_s) and martensite finish (M_f) temperature of austenite such that

the M_f lies below the room temperature (RT), and subsequently, some amount of austenite will remain untransformed and retained at RT. Using the equilibrium composition of the austenite phase, predicted above by ThermoCalc, the martensitic start (M_s) temperature is calculated using Eq. (1) [14]:

$$M_s(^{\circ}\text{C}) = 539 - 423 * \%C + 30 * \%Al - 7.5 * \%Si - 30.9 * \%Mn \quad (1)$$

As the elemental composition of austenite would be varying with IA temperature, the M_s temperature would subsequently vary. The M_s temperature usually decreases with the decrease in IA temperature, as at lower IA temperature the amount of equilibrium austenite fraction is low, and Mn, C composition in austenite will be higher. It is pertinent from the above equation (i) that increases the amount of C and Mn will decrease the M_s temperature and increase retained austenite fraction. However, increasing the carbon content leads to the formation of low-temperature carbides. The addition of Si and Al is done in these steels, which prevents the formation of carbides and increases the activity of carbon thereby enriching C content in austenite and increasing its retention and stability.

- (iv) The amount of thermal martensite that would form upon quenching the sample to RT, from a particular intercritical annealing temperature is estimated using the empirical Koistinen-Marburger (KM) equation [15]:

$$f_m = 1 - \exp(-0.011 * (M_s - QT)) \quad (2)$$

where, M_s is the martensitic start temperature and QT is the final quenching temperature, which is RT (25 °C) in this case. The final retained austenite γ_{ret} is obtained by subtracting f_m from γ_{IA} .

5 Mechanical Properties

The medium Mn steel possesses an outstanding combination of mechanical properties as compared to first-generation AHSS, and is also not much inferior to the second-generation AHSS. However, it has an edge over the second-generation AHSS in terms of low alloying elements, ease of manufacturing, and improved weldability. Medium Mn steels have higher yield strength, tensile strength as high as 1200–1500 MPa, and an elongation greater than 50% [6]. The high strength in these steels is due to contribution from the solid-solution strengthening of alloying additions, grain size strengthening from the ultrafine ferrite/martensite and austenite grains (lath or equiaxed morphology in the range of 150–800 nm). In addition, the austenite exhibits work hardening phenomena during deformation like the TRIP effect and TWIP effect. In TRIP effect, strain-induced α - and/or ε -martensite is formed during deformation which releases the stress concentration in the material and imparts exceptional ductility. While, in the TWIP phenomenon, fine deformation twins are formed in

austenite, which imparts the necessary hardening effect along with improvement in elongation. Some medium Mn steels are known to simultaneously exhibit both TRIP and TWIP effects during deformation [2, 5]. This invariably depends on the stacking fault energy (SFE) of the austenite. It has been reported that the austenite having $SFE < 18 \text{ mJ/m}^2$ exhibits TRIP effect, while the TWIP effect is exhibited in the austenite having SFE between 20 and 45 mJ/m^2 . Above $SFE > 45 \text{ mJ/m}^2$, the deformation is primarily via Slip [1, 3]. The SFE of the austenite should be such, that it could impart progressive work hardening effect during deformation. The SFE of the austenite phase can be tuned to suit the mechanical property requirement as it depends on austenite composition, morphology, grain size, and temperature.

6 Concluding Remarks

The medium Mn steels look to be quite promising for future automotive applications in terms of performance, crash resistance, and ease of industrial scalability. However, these steels are yet to see the light of the day owing to a few challenges ahead:

- (a) Production of medium Mn steel would require special steel-making practices to produce inclusion-free clean steel grades. The castability of these steels also requires special attention to minimize casting defects.
- (b) As these steel have very high strength, cold rolling of these steels in industrial mill poses challenges as it may require high strength-high stiffness rollers to sustain the high rolling load. During the forming operation of medium Mn steel at the automotive component manufacturer end, a high spring-back effect is encountered due to its high strength.
- (c) The medium Mn steels may require specialized welding techniques for the fabrication of the automotive structure. Several investigations are being carried out worldwide to address the above challenges for the successful production and application of these steels.

Despite the above predicaments, the advantageous effect these steels impart are immense with regard to passenger safety, and vehicle weight reduction and this drives the future medium Mn steel design philosophy.

References

1. Lee YK, Han J (2015) Current opinion in medium manganese steel. *Mater Sci Technol* (United Kingdom) 31:843–856. <https://doi.org/10.1179/1743284714Y.0000000722>
2. Sahoo BK, Sadhu S, Chandan AK, Bansal GK, Srivastava VC, Chowdhury SG (2022) Microstructure evolution in medium Mn, high Al low-density steel during different continuous cooling regimes. In: Kumari R, Majumdar JD, Behera A (eds) Recent advances in manufacturing processes. Lecture notes in mechanical engineering, pp 99–101

3. Chandan AK, Bansal GK, Sahoo BK, Chakraborty J (2022) Medium manganese steel: revealing the high sensitivity of microstructure and mechanical properties on intercritical annealing temperature and time. In: Kumari R, Majumdar JD, Behera A (eds) Recent advances in manufacturing processes. Lecture notes in mechanical engineering, pp 229–240
4. Sahoo BK, Srivastava VC, Mahato B, Ghosh Chowdhury S (2021) Microstructure-mechanical property evaluation and deformation mechanism in Al added medium Mn steel processed through intercritical rolling and annealing. *Mater Sci Eng A* 799. <https://doi.org/10.1016/j.msea.2020.140100>
5. Sahoo BK, Srivastava VC, Chandan AK, Chhabra HS, Ghosh Chowdhury S (2021) Evolution of microstructure and deformation behavior in Al–Ni added medium-Mn steel processed through intercritical/cold rolling and annealing. *Mater Sci Eng A* 824:141852. <https://doi.org/10.1016/j.msea.2021.141852>
6. Keeler S, Kimchi M, Advanced High-strength steels application guidelines 6.0, World Auto Steel
7. Nanda T, Singh V, Singh V, Chakraborty A, Sharma S (2019) Third generation of advanced high-strength steels: processing routes and properties. *Proc Inst Mech Eng Part L J Mater Des Appl* 233:209–238. <https://doi.org/10.1177/1464420716664198>
8. Ghosh M, Bansal G, Chandan A, Shah M, Tripathy S, Murugaiyan P, Sahoo B, Mukherjee K, Srivastava VC, Ghosh Chowdhury S (2017) Functionally driven steels: a review. *Steel Tech* 12:13–36
9. Fonstein N (2015) Advanced high strength sheet steels: physical metallurgy, design, processing, and properties. In: Advanced high strength sheet steels: physical metallurgy, design, processing, and properties, p 12
10. Energy, U.S.D. of (2015) Advancing clean transportation and vehicle systems and technologies
11. Zackay VF, Parker ER, Fahr D, Busch R (1967) The enhancement of ductility in high-strength steels. *ASM Trans Quart* 60:252–259
12. De Moor E, Matlock DK, Speera JG, Merwin MJ (2011) Austenite stabilization through manganese enrichment. *Scr Mater* 64:185–188. <https://doi.org/10.1016/j.scriptamat.2010.09.040>
13. Andersson JO, Helander T, Höglund L, Shi P, Sundman B (2002) Thermo-Calc & DICTRA, computational tools for materials science. *Calphad Comput Coupling Phase Diagrams Thermochem* 26:273–312. [https://doi.org/10.1016/S0364-5916\(02\)00037-8](https://doi.org/10.1016/S0364-5916(02)00037-8)
14. Mahieu J, Maki J, De Cooman BC, Claessens S (2002) Phase transformation and mechanical properties of Si-free CMnAl transformation-induced plasticity-aided steel. *Metall Mater Trans A Phys Metall Mater Sci* 33:2573–2580. <https://doi.org/10.1007/s11661-002-0378-9>
15. Koistinen DP, Marburger RE (1959) A general equation prescribing the extent of the austenite-martensite transformation in pure iron-carbon alloys and plain carbon steels. *Acta Metall* 7:59–60. [https://doi.org/10.1016/0001-6160\(59\)90170-1](https://doi.org/10.1016/0001-6160(59)90170-1)

Review on Drag Reduction Using Biomimics Surface



Shubhesh Ranjan and Faisal Shameem

Abstract This paper focuses on biomimetic drag reduction techniques as well as the growing field of biomimetics, which allows scientists to create macro materials, macro devices, and processes with intriguing qualities by mimicking biology or nature. Characteristics of species that have evolved in nature over a long period of time provide a diverse set of ideas for grouping to address engineering issues. Biotechnology has made an indelible mark on my mind. In order to tackle engineering challenges, characteristics of organisms that have evolved over a long period of time in nature provide a wide range of suggestions for grouping. A biological principle served as inspiration. The recent attention given to bio-inspired surfaces for minimizing fluid resistance, such as the microgroove surface of shark skin, the self-cleaning and protective surface Class-conscious structures with dimensions ranging from the macro to the micro-scale are common in nature and have unique qualities. These surfaces with a high contact angle and a low contact angle physical phenomenon have low adhesion and drag reduction when it comes to fluid movement. An associate degree aquatic animal, such as a shark, is another natural example of lowering sweep fluid flow. In this work's CFD simulation procedure, a drag reduction by Bionic Non-smooth surface is required.

Keywords CFD computational fluid dynamics · BNSS (bionic non-smooth surface) · Drag reduction · Boundary layer

S. Ranjan (✉) · F. Shameem
Department of Mechanical Engineering, Galgotias University, Greater Noida, Uttar Pradesh
203201, India
e-mail: Shubhesh4u@gmail.com

F. Shameem
e-mail: faisal.shameem@galgotiasuniversity.edu.in

1 Introduction

Bionic drag reduction is essential for preserving energy by reducing air surface rate and preventing cross-sectional airspeed. As a result, the model's pressure is unaffected. A similar situation can occur in the case of a turtle body for drag reduction, resulting in an effective decrease of skin friction drag with remarkable drag reduction performance. Engineers are drawn to biomimetic materials and systems because they resemble natural organisms. One of the most important aspects of fluid flow is drag reduction, which occurs in all-natural specimens. The researchers discovered nano, micro, and layered structures in lotus plant surfaces, which are comparable to shark skin replication and therefore the rib pattern surface for sharkskin structure simulation. They have to be made. On the water flow, surface drag reduction studies were required. The experimental flow channel was used to live the pressure drop in stratified and turbulent flows, and it provided the dynamic models' expected worth. The length of slip for a variety of surfaces in a streamlined flow was also calculated to support the pressure drop measurement.

2 Literature Survey

Due to the current condition of high fuel prices, drag reduction is a highly important element in heavy vehicles. Jung et al. in this paper, they examine the drag reduction biomimetic surface structure, which is generated in the form of a sharkskin rib pattern surface, using micro and nano hierarchical techniques. The pressure lowered by the process was measured using laminar and turbulent water flows, and it is described in terms of the measuring value of fluid models for surface pressure in various ways, as well as quantifying air flow [1]. Duo et al. in this paper in recent decades, the need of reducing skin friction drag has been reemphasized. Several management tactics and technologies are prompting to reduce drag friction, but most notably the unit area that requires additional power input for their active devices, which complicates the devices. Specifically, to investigate the underlying drag reduction mechanism and to identify any unique possibilities that animals in nature have for reducing drag [2]. Khan et al. the biomimicry surface of a dragonfly mimicked a two-dimensional corrugated airfoil. Ansys simulation was done on a range of Re 15,000 to 75,000. They also conduct experimental tests using a 3D printer in subsonic wind tunnels at various speeds and angles [3]. Arunvinthan et al. performed the test was carried out using a vortex generator and shark scales. The aerodynamic properties of the NACA 0015 symmetric airfoil. The vortex generator models based on the Shark scale were extracted and applied to the basis of the NACA 0015 symmetric airfoil [4]. Yakkundi et al. At a speed of 70 km/h, a model of an automobile with a rear wing spoiler was produced, and the result was roughly 8.2% in Cd [5]. Kim et al. reviewed in that paper he constructed a golf ball with no dimples but a tiny grooved surface, and then measured the drag and lift force and compared it to the ball's velocity and

rotational speed. They discovered that the drag and lift coefficients of microgroove surfaces are higher than those of dimpled surfaces [6]. Kozlov et al. reviewed that they used computational and experimental methods to study the behavior of boxfish. They investigated the drag, lift, and side forces in a wind tunnel at various Reynolds numbers and yaw angles. They discovered that the drag coefficient of a boxfish is approximately 0.1, which is remarkably low compared to a passenger car's drag coefficient. As a result, they discovered that in the case of boxfish, a bluff geometry provides the best drag reduction. Two parameters, k - and k - ω , have a minor difference [7]. Chen et al. review in their paper the process and morphology of shark skin, as well as the way of creating the morphological surface. As a result, they discovered a variety of fabrication techniques for reducing drag and potential uses. Drag reduction is expected to result in antifouling [8]. Mariko Miyazaki reviews in this paper that the shape of biomimetic riblets is inspired by the bumps on sharkskin, and it combines a 3D model of digitizing a clean computational fluid model of turbulent flows with a rough surface with bumps and round pattern grooves. They investigate advanced measuring and digital techniques to examine a computerized computational fluid dynamics model with an X-Ray CT to examine the microstructure of grooves [9]. Dai et al. review in their paper, In this methodology for the orientation of shark skin to define the flow direction and ridges, they analyze the effect of fluid behavior of water. There are various Morphological parameters in this methodology for the orientation of shark skin define the flow direction and ridges. The rheometer is used to determine the fluid performance. The results show that uniform particles have a minimal velocity gradient at 90 degrees scale orientation [10]. Wen et al. review this paper and investigate the effect of modifying the spacing and arrangement of biomimetic shark skin bumps on two criteria: static and dynamic locomotor performance [11]. Prabhu et al. review in the paper, perform an examination of the car body using a solid works simulation of the rear spoiler to ensure that the aerodynamics simulation is correct [12]. Sen et al. investigate in their paper using several types of vortex generators, to determine the reduction in drag [13]. Elewe et al. worked on the through the technology and adjustment of the air foil's aerodynamic performance they also studied the NACA 0012 and a variety of other airfoils to determine efficiency based on shape and AOA (Angle of Attack) [14]. Tsai reviewed the Analysis of a vehicle using the rear spoiler's aeroacoustic. This rear spoiler is a wing style that uses a grid system to evaluate the car. The solver chosen for this project is Ansys fluent [15]. Muthukumar et al. reviews in their paper a collection of fish skins a turbulent boundary layer is used to make the transition. This is set up in such a way that the fish arrays overlap each other, resulting in a potential 27% reduction in drag [16]. Ibrahim et al. reviewed about Sharkskin has a lower drag coefficient. The sharkskin denticles were inspired by riblets surface and the change in the design structure of marine vessels. After calculating the drag reduction result, it decreased by roughly 3.75% [17]. Oeffner reviews in that paper two biomimicry applications that mimic the function of shark skin they employ two types of profiles, one of which is a flapping foil robotic device for self-propelled swimming [18]. Launder et al. reviewed fluid dynamics and the formation of fish skin surfaces they worked on a new manufacturing process for foil-like surfaces that resemble fish, then tested

the dynamics of surface texture [19]. Muthukumar et al. says that The formation streak inflow across fish scale arrays is the subject of an article. A digital microscope technique was used to measure the geometry and modeling. The surface oil-flow simulation findings derive from a physical model with a flow channel [20]. Kim et al. review in their paper the goal of this work is to construct a parametric shape modification of biomimetic design and apply it. From the standpoint of biomimetic structural design, this is a relatively typical design. Following the results, the bio-model is verified and changed using a quantitative manner [21]. Wang et al. review that the aerodynamics noise around the bionic structure's air foil be checked for drag reduction the performance of the Airfoil NACA 0012 profile with a 0-degree angle of attack is shown below [22]. Pirzzoli et al. review in their paper for the eddies velocity spectra, use paper for the outer turbulent wall layer. They looked at the flow at high spectra increase as a function of wall distance. As a result, the outer layer's momentum is uniform with regard to the outer wall layer [23]. Wu et al. about the features of airflow bionic microgrooves with the help of bionic micro surface and lessen the vortex structure near the wall zone [24]. Heidarian et al. review in their paper examines the effect of reducing drag on a flat using riblets. It is covered with riblets and smooth ones, and it performs velocities in various ways, with the riblets reducing drag by 11% [25]. Dyan et al. describe in their chapter the intricate and slippery surface of a fish they worked on a three-dimensional structure of protective and hydrodynamic scales of function for displaying fish scale morphology *a/c* to shape size and structure [26]. Son et al. worked on the Experiment by reducing the drag of a sphere surface for a tripwire. For free stream velocity and diameter *d*, the Reynolds Number is $Re = 0.5105-2.8105$. The main source of tripwire drag reduction is the backside delay [27]. Bhatia et al. reviewed drag reduction for boundary layer laminar flow employing biomimetic structure facing stages through the result on boundary layer thickness at ratio (δ/h) for the boundary layer laminar flow and the result of transition delay is 20% and 6% drag reduction, respectively [28]. Subramanian et al. investigate the dimple pattern on an aircraft wing and its characteristics are studied using the ($K-\epsilon$) turbulence model in CFD on a NACA 2412 airfoil construction. The main goal was to assess for delayed flow separation [29]. Fu et al. review their paper on shark skin drag reduction for riblet surface the evaluation was based on the riblets' performance. Not only does it reduce marine drag, but it also improves the riblet evaluation criterion [30–33] (Figs. 1, 2 and 3).

3 Future Scope of Biomimics

Modern aerodynamics' approach for reducing drag is bio mimics. Biomimetic engineering has developed a new area of flow control research by combining two different ideas of biology and fluid mechanics. Because living entities fluctuate and have qualities that are beyond the scope of a single scientific theory, it is obvious that integrating two scientific concepts could aid our understanding of nature. There are various opportunities to design simple and effective biomimetic flow control

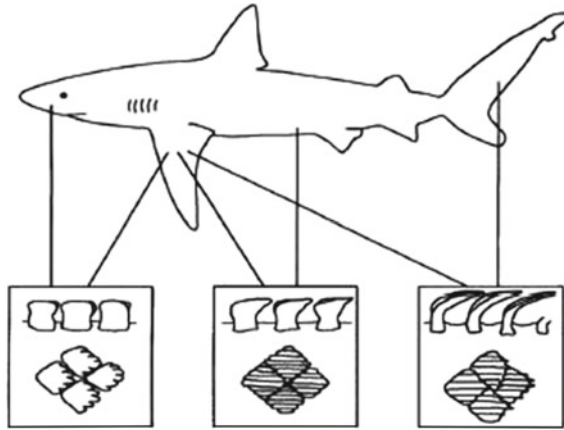


Fig. 1 Sharkskin is covered by small-tooth

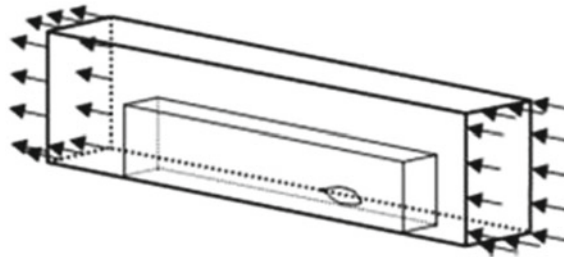


Fig. 2 Schematic diagram of boxfish like elements are dermal denticles [9] domain [7]

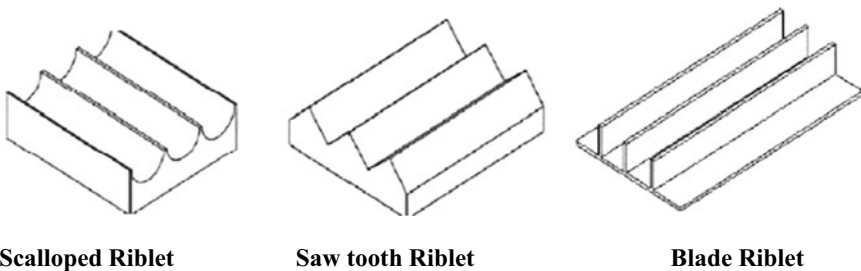


Fig. 3 Different types of riblet [31]

technologies that are inspired by nature. Biomimetic technology could help wind turbines, for example. Surface coatings with the same properties could be applied to wind turbine blades. The remarkable performance features on its surface have a significant research value. We observed that there is a widespread Non-smooth Surface structure with a certain geometry structure unit that is regularly distributed

in biological body parts after studying and analyzing the biological surfaces of sharks, worms, beetles, moles, lotus leaves, and other organisms. The structural unit has a dimpled shape and a convex hull form, as well as corrugated and flake shapes, stripes and bristles, and other characteristics.

4 Conclusion

In turbulent flows, a study was conducted to assess the impact of two different types of roughness elements on the boundary layer, and hence on the wall shear stresses. There are three types of turbulent roughness: hydrodynamically smooth, transitional, and totally rough. However, in our investigation, we reproduced turbulent roughness, which is commonly assumed to lower drag. We first simulated turbulent flow over riblets using computational fluid dynamics. Although roughness that is hydrodynamically smooth has no effect on wall shear stress, turbulent roughness usually creates additional drag on the surfaces to which they are mounted. After going through the many literature reviews, the conclusion exists in the field of biomimetic surface structure: the velocity in the boundary layer is reduced by non-smooth structures. Because of the viscosity of air, small reverse-direction vortices were created in the riblet. The surface of the riblets interfered with the near-wall turbulent coherent structure. The streamwise and span-wise vortices were effectively controlled by the “secondary vortices” with an equal and opposite reaction created by the tip of riblets. The riblet structure increased the thickness of the viscous sublayer, resulting in a decrease in the thickness of the hybrid layer, reducing the impact of random and chaotic fluidity. Surface vortices are reduced by non-smooth structures. The eddy’s lateral migration was hindered by the non-smooth surface, and the air could only flow streamwise along with the model. To reduce drag caused by dolphin inspiration, bionic flexible coatings with features such as smoothness, softness, and viscoelasticity are used. The surface microstructure of birds’ feathers was examined, and a microstructure bionic surface matching birds’ feathers was made using hot roll pressing technology to investigate the prospect of lowering friction drag with a bionic approach in a practicable method.

References

1. Jung YC, Bhushan B (2009) Biomimetic structures for fluid drag reduction in laminar and turbulent flows. *J Phys Condens Matter* 22(3):035104
2. Dou Z, Wang J, Chen D (2012) Bionic research on fish scales for drag reduction. *J Bionic Eng* 9(4):457–464
3. Khan MA, Padhy C, Aerodynamic and experimental analysis of bio-mimic corrugated dragonfly airfoil. <https://doi.org/10.13111/2066-8201.2020.12.2.7>
4. Arunvinthan S et al (2021) Aerodynamic characteristics of shark scale-based vortex generators upon symmetrical airfoil. *Energies* 14(7):1808

5. Yakkundi V, Mantha SS (2018) Effect of spoilers on aerodynamic properties of car effect of spoilers on aerodynamic properties of a car. 7:271–280
6. Kim J, Choi H (2015) Aerodynamics of a golf ball with grooves. *Procedia Eng* 105:323–328. <https://doi.org/10.1177/1754337114543860>
7. Kozlov A, Chowdhury H, Mustary I, Loganathan B, Alam E, Bio- inspired design: aerodynamics of boxfish
8. Chen D, Liu Y, Chen H, Zhang D, Bio-inspired drag reduction surface from sharkskin. ISSN 2405-4518. <https://doi.org/10.1049/bsbt.2018.0006>
9. Miyazaki M, Hirai Y, Moriya H, Shimomura M, Miyauchi A, Liu H (2018). Biomimetic riblets inspired by sharkskin denticles: digitizing, modeling and flow simulation. *J Bionic Eng* 15(6):999–1011. <https://doi.org/10.1007/s42235-018-0088-7>
10. Dai W, Alkahtani M, Hemmer PR, Liang H, Drag-reduction of 3D printed shark-skin-like surfaces. ISSN 2223-7690. <https://doi.org/10.1007/s40544-018-0246-2>
11. Wen L, Weaver JC, Lauder GV (2014) Biomimetic shark skin: design, fabrication and hydrodynamic function. 217:1656–1666. <https://doi.org/10.1242/jeb.097097>
12. Prabhu L, Krishnamoorthi S, Gokul P, et al (2020) Aerodynamics analysis of the car using solid works flow simulation with rear spoiler using CFD. *IOP Conf Ser Mater Sci Eng* 993. <https://doi.org/10.1088/1757-899X/993/1/012002>
13. Sen W (2020) Experimental and CFD analysis on car with several types of icmere2019-pi-185 experimental and CFD analysis on car with several types of vortex generators
14. Elewe AM (2020) Numerical simulation of surface curvature effect on aerodynamic performance of different types of airfoils. *IOP Conf Ser Mater Sci Eng* 928. <https://doi.org/10.1088/1757-899X/928/3/032003>
15. Tsai CH, Fu LM, Tai CH (2009) Computational aero-acoustic analysis of a passenger car with a rear spoiler. *Appl Math Model* 33:3661–3673. <https://doi.org/10.1016/j.apm.2008.12.004>
16. Muthuramalingam M, Villemin LS, Bruecker C (2019) Streak formation in flow over biomimetic fish scale arrays. *J Exp Biol* 222(16):jeb205963
17. Ibrahim MD et al (2018) The study of drag reduction on ships inspired by simplified shark skin imitation. *Appl Bionics Biomech*
18. Oeffner J, Lauder GV (2012) The hydrodynamic function of shark skin and two biomimetic applications. *J Exp Biol* 215(5):785–795
19. Lauder GV et al (2016) Structure, biomimetic, and fluid dynamics of fish skin surfaces. *Phys Rev Fluids* 1(6):060502
20. Muthuramalingam M et al (2020) Transition delay using biomimetic fish scale arrays. *Sci Rep* 10(1):1–13
21. Kim S-J, Lee J-H (2015) Parametric shape modification and application in a morphological biomimetic design. *Adv Eng Inform* 29(1):76–86
22. Wang J et al (2017) Numerical study on reduction of aerodynamic noise around an airfoil with biomimetic structures. *J Sound Vibr* 394:46–58
23. Pirozzoli S, Grasso F (2006) Direct numerical simulation of impinging shock wave/turbulent boundary layer interaction at $M = 2.25$. *Phys Fluids* 18(6):065113
24. Wu ZR, Cheng YL, Wang SL (2006) Numerical study on effect of waving bed on the surface wave. *J Hydrodyn Ser B* 18(4):464–468
25. Zhang MM, Zhang L, Zhao M (2020) Investigation on the mechanism of drag modification over triangular Riblets. *J Appl Fluid Mech* 13(4)
26. Wainwright DK, Lauder GV (2017) Mucus matters: the slippery and complex surfaces of fish. In: *Functional surfaces in biology III*. Springer, Cham, pp 223–246
27. Son K et al (2011) Mechanism of drag reduction by a surface trip wire on a sphere. *J Fluid Mech* 672:411
28. Bhatia D et al (2020) Laminar flow control and drag reduction using bio mimetically inspired forward facing steps. *J Appl Comput Mech Articles in Press*
29. Subramanian V et al (2020) Investigation on the aerodynamics characteristics of dimple patterns on the aircraft wing. *Int J Ambient Energy*, pp 1–9

30. Fu YF, Yuan CQ, Bai XQ (2017) Marine drag reduction of shark skin inspired riblet surfaces. *Biosurface Biotribol* 3(1):11–24
31. Heidarian A, Ghassemi H, Liu P (2018) Numerical analysis of the effects of riblets on drag reduction of a flat plate. *J Appl Fluid Mech*
32. Gu YQ et al (2015) Overview of the technology of bionic surface drag reduction. *J Biomimetics Biomater Biomed Eng* 23. Trans Tech Publications Ltd
33. Liu W et al (2019) Investigation on drag reduction performance of pipeline with bio inspired micro grooved surface. *Beilstein Arch* 1:17

Solar Industrial Process Heating Prospects in Indian Cement Industries



Niranjan Sahoo , Anil Kumar , and Samsher 

Abstract This article presents a preliminary study of solar industrial process heating (SIPH) potential for the Indian cement industry. To begin, data was gathered for (i) categorization of cement plants based on industrial categories (ii) yearly cement production capacity and actual output (state-by-state), (iii) specific thermal energy requirements for process heating (iv) Global horizontal irradiance (GHI) and direct normal irradiance (DNI) of plant sites, and so on. The annual process heating demand for cement production at cement mills in India has been calculated (based on real cement output). Further potential was estimated depending on the solar resource available at different plant locations in the country. Some techniques suitable for cement production with the application of solar energy are investigated and analyzed. The majority of cement factories in India are located in states where DNI is readily available. In India, the cement industry's annual process heating potential is estimated to be 664 PJ.

Keywords Solar energy · Industrial process heating · Cement industry

1 Introduction

Cement industry in India is the world's second-biggest, accounting for roughly 7.1% of global cement output. In the financial year (FY) 20, cement output reached 329 million tons (MT), with a capacity of 537 MT. Because of the need for highways, urban infrastructure, and commercial real estate is anticipated to reach 550–600 MT by 2025. Over 350 mini-cement plants have an estimated production of capacity 11.10 MT, while 210 big cement plants have a combined installed capacity of over

N. Sahoo (✉)

Galgotias College of Engineering and Technology, Greater Noida, Delhi, India

e-mail: niranjan.sahoo@galgotiacollege.edu

N. Sahoo · A. Kumar · Samsher

Department of Mechanical Engineering, Delhi Technological University, New Delhi, Delhi, India

A. Kumar · Samsher

Centre for Energy and Environment, Delhi Technological University, New Delhi, Delhi, India

410 MT. In India, 77 of the 210 major cement factories are located in Andhra Pradesh, Rajasthan, and Tamil Nadu states [1]. Figure 1 depicts the installed capacity and important markets in each of the geographic areas. Figure 2 depicts real cement use and output in various geographic locations. Domestic cement output fell 18.3% during 9 M-FY21, compared to 13.9% and 0.7% increase in 9 M-FY19 and 9 M-FY20, respectively. The COVID-19 epidemic that erupted across the Indian subcontinent, forcing the government to declare a nationwide lockdown from March 25, 2020, onwards, has significantly impacted total domestic cement output. The national lockdown occurred at a time when building activity is at an all-time high.

Coal, fuel oil, and high-speed diesel oil are used to provide the thermal energy needs of the Indian cement industry. Ninety-four percent of the thermal energy requirement is fulfilled by coal, with the remainder need to be fulfilled by fuel oil and high-speed diesel oil. In India, there is not enough natural gas for the cement industry [2]. While meeting the growing energy demand of the cement industry, it is desirable to reduce fossil fuel usage. This may offer the dual effect of reducing fossil fuel usage while also cutting greenhouse gas emissions. In India's cement industry, reducing fossil fuel consumption may be accomplished by (i) enhancing fuel usage efficiency and (ii) substituting fossil fuels with renewable energy sources in appropriate processes. The former technique undoubtedly enhances the reduction of fossil fuel consumption but will bring significant advantages in the short term. While adoption of the latter technique satisfies the energy demands of the country's cement sector as well as it would have many long-term benefits like boosting the Indian economy, reduction of greenhouse gas emissions, etc.

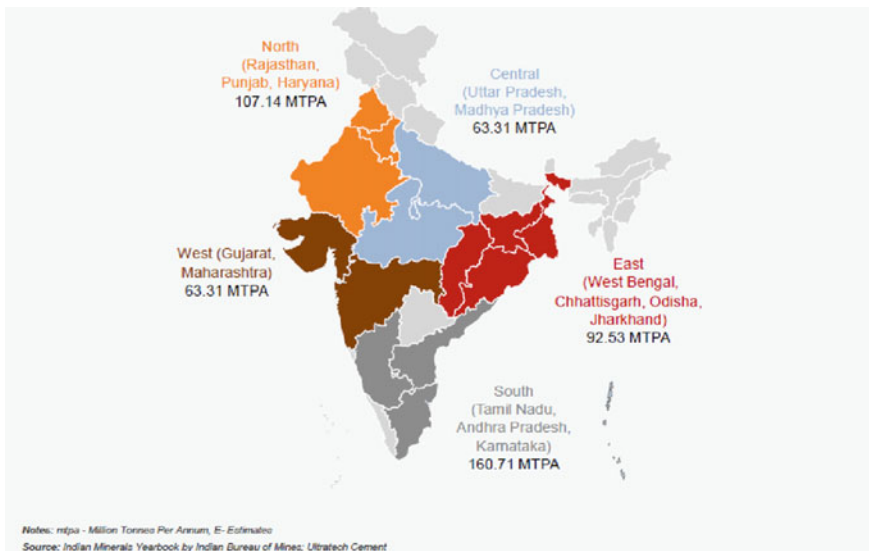


Fig. 1 Installed capacity & key markets in each of the geographic regions

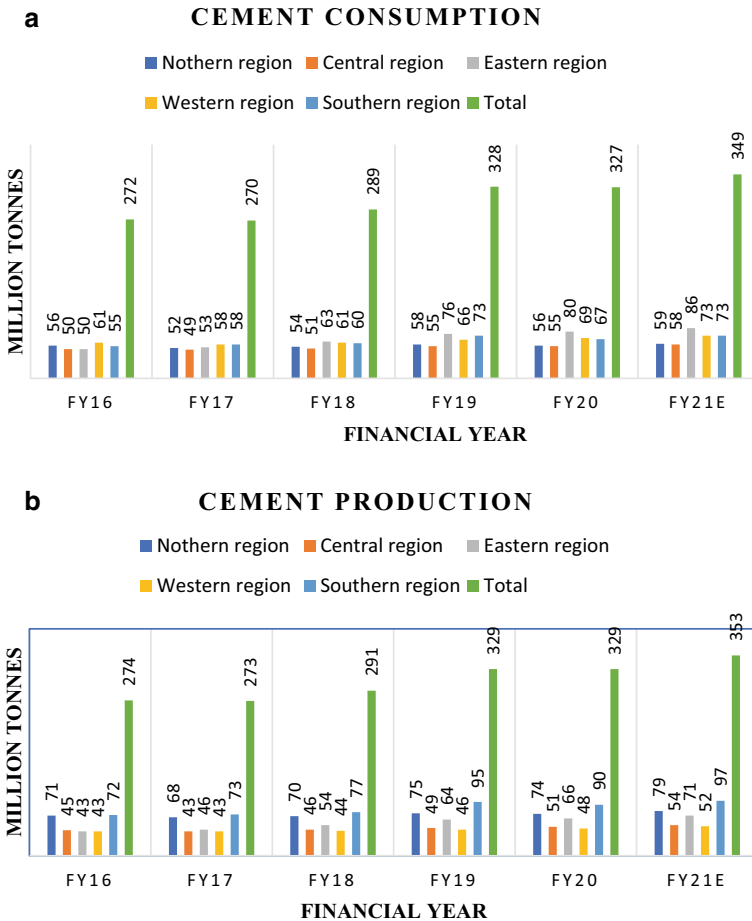


Fig. 2 a Cement consumption of the geographic regions. **b** Cement production of the geographic regions.

The cement industry generally uses two types of energy: electrical and thermal. The burning process consumes the preminent thermal energy, whereas grinding cement consumes electrical energy [3]. Processes like calcination and clinkering consume the majority of the process heat in a typical cement plant. In blending silos, raw material is mixed and then heated in the pre-heating system. This technique is termed calcination, in which calcium carbonate (CaCO₃) decomposes and produces calcium oxide (CaO) and liberates carbon dioxide (CO₂). This is carried out at a temperature of 900 °C. The calcium oxide (CaO) is then fired with silica, alumina, and ferrous oxide in a kiln. The process is termed clinkering, carried out at temperatures ranging from 1400 °C to 1500 °C. Clinker (silicates + aluminates + ferrites) is the

result of this process. The clinker is then crushed with gypsum, limestone, and ashes to make a fine product known as cement [4].

Several studies on the possibilities of SIPH in cement sectors have been published in the literature. The adoption of solar heat for the process heating of a clinker factory (3000 t/d) was examined by Imhof [5]. A hybrid method was studied, in which thermal energy can be obtained through a fossil calciner and solar calciner. The minimum solar irradiation required for obtaining heat is expected to exceed 2000 kWh/m²a, and the efficiency of the solar calciner is set at 86%. The research did not involve thermal storage. The author's study reveals that use of solar calciner can reduce 9% of carbon dioxide emissions with 28% of total fossil fuel inputs. A solar lime factory with a daily production limit of 50 tons was studied by Meier et al. [6]. A solar reactor replaces the single shaft lime kiln in the reference facility. The beam-down (BD) and top-of-tower (TT) process designs are studied with solar incident power of 1, 5, and 25 MWth on the reactor. The researchers utilize a Direct Normal Irradiation (DNI) of 2300 kWh/m² for the plant site and indicate that at least 500–600 W/m² of irradiation is required for plant start-up. A feasibility study (technological + economical) on hybrid (solar energy + fossil fuel) cement factory, which is based on the application of concentrated solar energy was done by Gonz Alez and Flamant [7]. The hybrid cement plant produces 3000 tons of cement clinker per day. The use of fossil fuels to replace the calciner in the 40–100% range is addressed and assessed. The assessment utilized a DNI of 2550 kWh/m². The use of calcined hot raw material at 900 °C (calcination temperature) is proposed for a thermal storage silo. Solar reactor runs for 9 h per day (on average) and produces calcined meals for use in the cement manufacturing process as well as heat storage. Based on the heat and mass balances of the process the researcher calculates the area requirement and equipment cost for solar setup. In light of the foregoing, this study makes a first approach to analyzing the potential of SIPH in the Indian cement sector.

2 Methodology

Cement plants are categorized according to their industrial types (Table 1). Both integrated cement plants and clinker cement plants are appropriate for SIPH applications since they produce clinker. SIPH is not applicable to cement grinding mills or secondary industrial units since thermal energy is not required.

SIPH potential for Indian cement plants was calculated by following several steps. The steps are given as follows:

Step 1: Study the different types of cement plants

Step 2: State-by-state list of cement plants with their locations

Step 3: Annual cement production and consumption in various geographical regions

Step 4: Annual thermal energy requirement of each cement plant [8]

Step 5: Stagewise thermal energy requirement of cement plants

Step 6: GHI and DNI of all cement plants across India

Table 1 Classification of cement plants in India

Classification fundamentals	Types	Details	SIPH-related comments
Main industrial types	Integrated cement plant	Both clinkerization and grinding both carried out	Potentially suitable for SIPH
	Cement clinker plant	It solely produces clinker	Potentially suitable for SIPH
	Cement grinding plant	To create finished cement, clinker is ground, and gypsum is added	Since thermal energy is not required therefore SIPH is not relevant
Secondary industrial types	Cement terminal	Transports cement, clinker, and cement-based goods in bulk to large customers	Since thermal energy is not required therefore SIPH is not relevant
	Cement packing plant	Facilities that specialize in cement packaging	Since thermal energy is not required therefore SIPH is not relevant
	Fiber cement plant	Cement is combined with 10% fiber materials, primarily for roofing	Since thermal energy is not required therefore SIPH is not relevant
	Dry mortar plant	A dry mortar is a mixture of cement and additional ingredients such as sand, limestone powder, and hydrated lime	Since thermal energy is not required therefore SIPH is not relevant
	Pozzolan quarry	It is where Pozzolan rocks come from, which are used to manufacture that type of cement	Since thermal energy is not required therefore SIPH is not relevant

Step 7: Average GHI and DNI of each state [9].

Finally, various commercially available solar industrial process heating techniques that deliver process heat in cement plants within the needed temperature range (1000–1500 °C) were chosen and analyzed.

3 Results and Discussion

Using the technique described in the previous part, an attempt has been made to assess the potential of SIPH in Indian cement plants, with representative findings provided in this part. Table 2 shows the details of cement output and thermal energy requirements at cement plants in various Indian states. In the 2019–20 fiscal year, cement mills produced 217.01 million tons of cement. The yearly thermal energy consumption of these facilities for cement manufacture is estimated to be 664 PJ. Table 2 also shows the year average DNI availability calculated using the technique

Table 2 State-wise annual thermal energy demand and average GHI and DNI

State	Annual installed capacity (in million tons)	Annual production (in million tons)	Thermal energy requirement (PJ/annum)	Global horizontal irradiance (GHI) kWh/m ² /year	Direct normal irradiance (DNI) kWh/m ² /year
Maharashtra	27.15	12.45	38.097	1773.75	1310.25
Himachal Pradesh	10.09	5.1	15.606	1745.333	1488.333
Chhattisgarh	22.05	14.81	45.3186	1729.714	1291.286
Madhya Pradesh	35.32	9.9	30.294	1758.5	1383.75
Rajasthan	74.72	44.75	136.935	1798.722	1504.278
Tamil Nadu	37.43	21.43	65.5758	1836.308	1225.154
Karnataka	42.18	23.5	71.91	1801.375	1316.75
Andhra Pradesh	58.99	29.78	91.1268	1796.706	1270.235
Gujarat	35.36	19.72	60.3432	1835.444	1485.333
Meghalaya	9.96	2.03	6.2118	1548.667	1082.667
Telangana	35.48	19.75	60.435	1772.714	1240.462
Punjab	1.5	–	–	–	–
Assam	4.27	0.97	2.9682	–	–
West Bengal	8.34	1.61	4.9266	1621	1061
Bihar	7.1	1.9	5.814	1644	1122
Andaman Nicobar Islands	1.65	1.41	4.3146	–	–
J & K	0.83	–	–	–	–
Uttar Pradesh	10.93	3.16	9.6696	1677.5	1194.5
Kerala	0.66	0.4	1.224	1832	1266
Odisha	6.5	4.34	13.2804	1734.5	1286
Jharkhand	1.2	–	–	–	–
Total	431.91	217.01	664.0506	–	–

explained above. It is worth noting that most of India's cement mill clusters are concentrated in states with sufficient DNI. Figure 3 depicts the potential of SIPH in cement plants in various states.

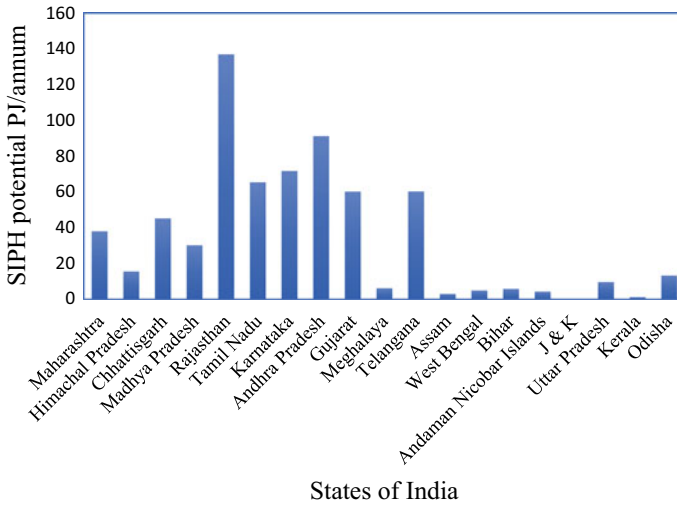


Fig. 3 SIPH potential of different states of India

4 Concluding Remarks

Preliminary evaluation conducted in the study confirms that solar energy has a great potential for addressing the need for process heating in the cement sector in India. According to a review of cement plant sites in India, factories are placed with enough sun irradiation, making solar calciner technology possible. The annual SIPH potential in Indian cement industries is estimated to be 664 PJ. It was determined that, based on the performance characteristics of commercially available solar technologies, some of them may be applied to fulfill the cement industry's process heating requirements with fair efficiency.

References

1. Cement Manufacturers Association (2018) Ministry of External Affairs, DPII, Heidelberg Cement Investors Presentation
2. Karwa DV, Sathaye J, Gadgil A, Mukhopadhyay M (1998) Energy efficiency and environmental management options in the Indian cement industry. For Knolls
3. Marciano EJ (2004) Sustainable development and the cement and concrete industries
4. Schorcht F, Kourti I, Scalet BM, Roudier S, Sancho LD (2013) Best available techniques (BAT) reference document for the production of cement, lime and magnesium oxide. European Commission Joint Research Centre Institute for Prospective Technological Studies, Luxembourg
5. Imhof A (2000) Solar cement plants-an interesting challenge for business and science. *ZKG Int* 53(8):448–456
6. Meier A, Gremaud N, Steinfeld A (2005) Economic evaluation of the industrial solar production of lime. *Energy Convers Manage* 46(6):905–926

7. Sebastián González R, Flamant G (2014) Technical and economic feasibility analysis of using concentrated solar thermal technology in the cement production process: hybrid approach—a case study. *J Solar Energy Eng* 136(2)
8. Indian Minerals Yearbook 2019 (part-III: mineral reviews)
9. <https://vedas.sac.gov.in/renewable-energy/index.html>

Recent Progress in the Design of Sustainable Thermoelectric Cooling Systems



Jitendra Mohan Giri  and Pawan Kumar Singh Nain 

Abstract The thermoelectric cooling (TEC) modules are electronic components that work on the principle of the Peltier effect. It functions as a heat pump moving heat from one side of the device to the other. The growing adoption of electric vehicles, growing inclination toward renewable energy sources, and increase in demand for energy-efficient consumer electronics are the key factors driving the thermoelectric devices market. However, the high cost of thermoelectric modules, design complexity and heat dissipation issues restrain the market growth. The reduced size of the thermoelectric elements is one goal for TEC module manufacturers. Various benefits can be achieved if TEC is made lighter and smaller. When the size of a TEC is reduced, however, we run into issues with heat transfer. It is difficult to transfer heat (source to sink) when end plates are small in cross-section. Increasing the gap between the TE elements would almost certainly solve the issue. But conduction, convection, and radiation heat losses increase substantially. In recent years, new techniques to design thermoelectric coolers have made significant progress. We summarize recent progress in the design of sustainable thermoelectric cooling devices in this review, which have been established to enhance various performance requirements and add new functionality.

Keywords Thermoelectric cooling · Peltier effect · Cooling capacity · Coefficient of performance · Exergy

1 Introduction

Worldwide, sustainable energy technologies are in huge demand. Conventional refrigerators employ sophisticated processes that need the synchronized functioning of numerous components, including the compressor, expansion valves, condensers,

J. M. Giri (✉) · P. K. S. Nain
Galgotias University, Greater Noida 201312, India
e-mail: jitendra.giri@galgotiasuniversity.edu.in

P. K. S. Nain
e-mail: pawan.kumar@galgotiasuniversity.edu.in

evaporator, and refrigerant. On the other hand, a thermoelectric cooler (TEC) utilizes the Peltier effect, eliminating the use of these complicated parts. This helps to prevent the release of chlorofluorocarbons (CFCs) and hydro-chlorofluorocarbons (HCFCs) into the environment, which contributes to global warming. TEC devices are also advantageous due to their compact size, dearth of moving parts, silent operation, and high reliability. Thermoelectric cooling devices are attractive alternatives to compressor-based cooling machines. TEC systems come in a variety of shapes and sizes, as well as various levels of heat pumping capability, so they can meet a wide range of industry needs. Industrial, military, aerospace, defense, radio-electronics, telecommunication, medical and scientific/laboratory organizations use these devices. However, the true performance of TEC devices is not very high at present, largely because of the material limitation and the suboptimal design. In recent years, researchers and scientists have shown a growing interest in studying and developing newer thermoelectric (TE) materials and optimum designs, in order to help enhance existing applications and discover whole new ones. In this work, we outline the current development of sustainable thermoelectric cooling devices designed to improve various performance demands and provide new functionalities. In this paper, the recent progress carried out on sustainable thermoelectric cooling devices designed to improve various performance demands and provide new functionalities are highlighted.

2 Working Principles

The Peltier effect, discovered by Jean Peltier is the physical basis for the thermoelectric cooling phenomena. Peltier demonstrated in 1834 that when an electric current (I) is driven across a junction between two distinct materials, heat is either dissipated or absorbed. The cooling or heating depends on the current direction. The rate of heat dissipation or absorption is proportional to the electric current. The coefficient of proportionality is termed the Peltier coefficient (Π).

$$Q_{\text{Peltier}} = \Pi \times I \quad (1)$$

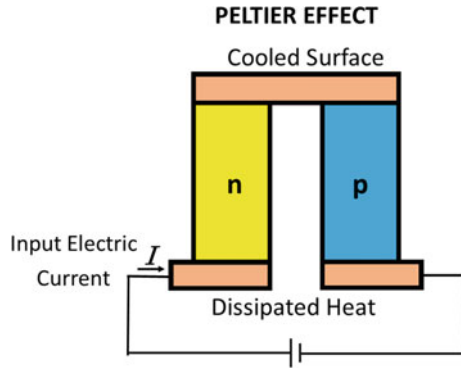
where Q_{Peltier} is the heat dissipation or absorption rate at the junction due to Peltier effect.

The Peltier coefficient is related to Seebeck coefficient (α). Lord Kelvin derived simple equation that relates the two coefficients using equilibrium thermodynamics.

$$\Pi = \alpha T \quad (2)$$

Standard TEC modules are mainly formed from n-type and p-type TE elements, known as TE couple. The TE cooling with a single couple is depicted in Fig. 1.

Fig. 1 Thermoelectric cooling



Two irreversible processes of Joule heating and thermal conduction are also involved in the TEC operation. The rate of heat transfer due to Joule effect (Q_{Joule}) and thermal conduction ($Q_{\text{conduction}}$) relates to I^2R and $K\Delta T$, respectively. In these expressions, R represents the electrical resistance, K refers to thermal conductance and ΔT is the temperature difference between hot and cold sides. Each junction receives half of the Joule heat, i.e., $0.5I^2R$. The following equations can be used to express the heat energy balance:

$$Q_c = Q_{\text{Peltier}} - Q_{\text{conduction}} - Q_{\text{Joule}} \tag{3}$$

$$Q_h = Q_{\text{Peltier}} - Q_{\text{conduction}} + Q_{\text{Joule}} \tag{4}$$

where Q_c is the cooling capacity or cold side heat absorption rate and Q_h refers to hot side heat rejection rate.

3 Advances in the Design of TEC Systems

Thermoelectric cooling (TEC) devices are attractive alternatives to compressor-based cooling machines. In recent years, researchers and scientists have shown a growing interest in studying and developing newer thermoelectric (TE) materials and optimum designs, in order to help enhance existing applications and discover whole new ones. In this review article, the recent research in the design of TEC devices is classified based on two criteria (i) methods to improve TEC performance (ii) TEC application areas.

3.1 Methods to Improve TEC Performance

Thermoelectric cooling systems could have different architectures based on the shapes of heat source and heat sinks, such as the traditional flat plate and annular structure. In addition, for high-temperature applications, segmented structure may be implemented, and cascaded structure has been suggested. In addition, various thermoelectric leg geometries, including standard rectangular and asymmetric geometric shapes, have been tested. Thermoelectric element's height/length, cross-sectional area of elements, number of TE elements, and shape of elements are the four major parameters that are paid much attention to during geometry optimization.

Analytical and Numerical Methods

The thermoelectric element length is a significant parameter that can be optimized to improve the thermoelectric cooler's performance. Cheng et al. [1] reported that the benefit of optimizing the dimensions of the thermoelectric cooler elements is that it increases the rate of cooling. Shen et al. [2] examined the efficiency of a segmented TEC device. The segment number appeared to be more susceptible to the thermal conductivity of TE material, according to the study. The two-segmented thermoelectric element using distinct thermoelectric materials of almost similar Seebeck coefficient value, with a significant difference in figure of merit, could get the better performance of cooling without enhancing the overall figure of merit of thermoelectric cooler. They observed that as element length increases, maximum temperature difference, maximum coefficient of performance, maximum cooling power, and all lower. Three separate double-stage TECs were optimized by Wang et al. [3]. To improve the cooling rate and coefficient of performance, they discovered that the number of TE elements on the hot side should be higher than the number of thermoelectric elements on the cold side. Besides this, the authors believed that the only way to reliably predict double-stage TEC output is to use temperature-dependent TE materials properties.

Lamba et al. [4] used a thermodynamic model to study a thermoelectric cooler and discovered that the Thomson effect improved the cooling rate of TEC. Lin et al. [5] improved a trapezoid-shaped thermoelectric cooler with two stages. To improve performance of device and reduce thermal resistance (inter-stage), ceramic plates (intermediate) were removed. The trapezoid leg shape ratio on the hot-stage had an effect on the maximum *COP* and maximum rate of cooling, they discovered.

A variety of publications have published studies on the experimental calculation and generalization of physical parameters of TEC systems. Fraisse et al. [6] have analyzed various modeling methods and measured the accuracy of certain simplified models while preserving the invariance of other parameters. Riffat et al. [7] used a small prototype device to build a computer model for simulating the efficiency of a novel TE heat pump. The thermoelectric parameters were determined using a quadratic empirical equation based on the cold side and hot side temperatures. In his classic textbook, Rowe [8] discussed temperature-dependent properties of physical

parameters. These parameters were validated by using them to solve a thermal resistance issue in TEC device [9]. The results showed that the errors remained below 5%. To define their module criteria, Chen et al. [10], Lineykin et al. [11], and Luo et al. [12] used curves for performances and many range values from TEC vendor datasheets. The key benefit of this approach is that the solutions can be found without having to use p-n-type pellet data. Huang et al. [13] and Mitrani et al. [14] looked at how a TEC's output changed as the cold and hot side temperatures changed, and how TEC performed under such thermoelectric conditions. The electrical resistance had been obtained from the voltage and current curves. The effective value of Seebeck coefficient was calculated by dividing the open circuit (measured) by the temperature difference (external). Theoretical study of a thermoelectric device fitted with an office space in Morocco was suggested by Allouhi et al. [15]. The number of TE modules needed to obtain a maximum *COP* of 2.0 was determined to be 12 in this study.

To simplify TEC system with totally temperature-dependent thermoelectric material properties, McCarty [16] reported a numerical technique of one-dimensional results. The precision of the numerical TEC model was further verified by experimental results. Finned arrangement of heat pipes could reach greater than 200 W/K values of *UA* (overall heat conductance \times area) for gas flow systems, according to existing technologies, since they have larger efficient areas for heat transfer. A novel TEC architecture was proposed by Owoyele et al. [17]. The effects of different geometry parameters were investigated, and it was discovered that the corrugated thermoelectric cooler worked better. It was more cost-effective for applications requiring low value of cooling power density. In a corrugated TEC, proper thickness selection was suggested for minimizing losses. Using simulated annealing, Khanh et al. [18] optimized the geometry of thermoelectric coolers. To increase the rate of refrigeration, the dimensions of thermoelectric coolers were optimized using simulated annealing. Lamba et al. [19] optimized the geometric parameters of a trapezoidal-shaped heat pump using a genetic algorithm. After 20 runs, the population of the GA converged rapidly, demonstrating that it is a cost and time-effective method. They noticed that the Thomson effect had a negative impact on the system's heating load and that contact resistance had a negative impact on the system's performance. Soprani et al. used topology optimization to improve TEC efficiency. Also, a three-dimensional finite-element approach was employed. The experimental outcome and the model predictions were very similar to each other. Electronic devices that were actively cooled were designed using the optimization process.

The finite-element approach was used to perform three-dimensional numerical simulation by Qiu et al. [20]. A sandwiched construction of thermoelectric cooler using uniform cross-section as well as non-uniform cross-section was used. To illustrate the working mechanism of the factors at play, a detailed mathematical model was built. For an input of smaller portion of thermoelectric element, non-uniform section type TEC is beneficial with more cooling capacity with 6–12% improvement. However, the coefficient of performance was identical. A modest element height (1.5 mm) will greatly boost the cooling rate of the thermoelectric cooler as compared to 3.0 mm height of TE element, with a 52.96% increase in peak cooling

rate. A -20.66% change in peak COP was evaluated. For the COP and cooling rate of the thermoelectric cooler, the contact layers provided different effect patterns and sensitivities. The TEC's output deteriorated as the solder thickness increased. The thickness of copper layer, on the other hand, had the opposite effect. The maximum COP and maximum cooling capacity were taken into consideration for a Pareto-optimal front with the help of NSGA-II by Lu et al. [21]. The effect of design variables like electric current and element structure on the performance of thermoelectric cooler has been demonstrated.

An electrically disconnected double-stage TEC's exergy, as well as exergoeconomic analysis, is reported by Nemati et al. [22]. The effects of electrode length, applied current, cross-sectional area ratio, and stage-wise number of electrodes were studied. In first stage, the optimum current is lower as compared to the current in second stage. The maximum second law efficiency is achieved at small values of current. The exergy efficiency improves with an increment in electrode numbers (both stages). Smaller optimal values of the cross-sectional area ratio and greater applied currents have better economic efficiency. The effects of electrical current, rate of flow of air, air inlet temperature, flow rate of water, and inlet temperature of water, were investigated using a Peltier air cooler by Dizaji et al. [23]. The exergetic performance has a minimum value when the DC voltage reaches an extreme. The exergetic performance was high for warmer temperatures of air inlet. The rate of airflow was also high. A theoretical evaluation of the optimum performance of a TE cooler was done by Tan et al. [24]. The optimization objectives were chosen to be cold exergy and second law efficiency. The effects of several main parameters on cooling performance, such as thermal conductance allocation ratio, electric current, and cooling temperature, were theoretically investigated. This was realized that there is an optimum cooling temperature that leads to maximum cooling rate and second law efficiency. A heat sink design optimization model for a TEC device was proposed by Zhu et al. [25]. The TEC system was optimized using an entropy generation minimization process. The cooling fluid's heat capacity rate is sensitive parameter and must be chosen appropriately to minimize entropy generation.

Maximum rate of refrigeration, maximum electric current, and voltage at different hot side temperatures were calculated using COMSOL[®] multiphysics by Panigrahi et al. [26]. At a given hot side temperature, the low cold side temperature attracted low rate of cooling. At a given cold side temperature, the rate of cooling increased with an increment in current followed by hot side temperature. The results have also shown that, regardless of cold side temperature, the COP for a given relative current value is higher in a higher hot side temperature. Analytically, the partial differential equations that control the function of a TEC were solved by Fong et al. [27]. It was carried out in order to calculate the temperature profile within the TE element and system's COP and cooling capacity. The thermoelectric cooler's transient behavior could be used as an optimization method for different design setups in order to satisfy particular packaging requirements. Using CFD, a TEC model with a heat sink was developed by Seo et al. [28]. As a result of the time-dependent characteristics revealed by the numerical solutions, the cooling capacity of TEC differs over time. Teixeira et al. [29] showed that a TEC can be made using cylindrical or cubic geometry of elements and

performs equally. According to simulations, increasing the cross-sectional area of the TE elements increases the power output of a TE device. Çağlar et al. [30] designed and fabricated a portable TE refrigerator. This refrigerator was tested at various ambient temperatures and for *COP*, a method for determining optimal operating conditions was defined. It was also observed that when the cooled space temperature drops from 293 K to 254.8 K, the system's *COP* drops from 0.351 to 0.011. Giri et al. [31] proposed a numerical method to enhance cooling rate and coefficient of performance of TEC within space restrictions by applying genetic algorithm. They showed that optimum values can be greatly achieved by selecting simultaneously taking input current, height, and area of cross-section of n-type and p-type TE elements. The GA results were validated through three-dimensional finite-element simulations.

Experimental Methods

Significant attempts have been made to boost device efficiency thereby lowering energy consumption. Cai et al. [32] built an air source TE heat pump device that can deliver cold air and hot water at the same time. The thermal conductance as well as sp. heat allocations in heat exchangers (cold and hot side), they found, could have a significant impact on *COP* and cooling capacity. Zhou et al. [33] proposed a TE-supported evaporative cooling device (indirect). The TEC units are located between many channels of the evaporative cooling device (cross-flow flat plate) to increase heat transfer capacity at the hot side of TEC. The performance of a heat sink-assisted TEC within a square duct was investigated numerically and experimentally by Seo et al. [28]. It was observed that the heat sink's various parameters affect the TEC system's efficiency. Liu et al. [34] developed a conceptual model for a PV-thermally-compound TE ventilator framework that generates electric power in the winter while also preheating the fresh air, allowing for full solar energy utilization.

Lal and Kumari [35] investigated the performance of a cost-oriented TEC in an experimental environment. With a minimum attainable temperature of 2.3 °C, the optimum amount of the *COP* was recorded to be 0.26. Desalination systems based on bubble column humidification-dehumidification have demonstrated encouraging results in terms of reduced quantum need for freshwater. Patel et al. [36] examined the effects of air and water temperature, hot water column height, circling tube holes diameter, and air mass rate of flow on freshwater production. An excellent experimental output of the device was observed at 12.96 L/d for 2 mm of hole diameter, 60 °C of water temperature, 0.016 kg/s of air mass rate of flow, and 27 °C of air temperature, and 7 cm of hot water column in the humidifier. Afshari [37] conducted an experiment to measure the relative efficiencies of air-to-water and air-to-air TECs. It was discovered that air-to-water method is more effective with the *COP* value 30–50% greater than that of the air-to-air TEC. The computational fluid dynamics results were utilized to depict the flow structure and heat transfer properties within the cooling box.

3.2 TEC Application Areas

Saifizi et al. [38] designed and tested a hybrid device. A direct air-to-air heat pump was used to hold vaccine packages at a low temperature. Dongareet al. [39] designed and updated a real-world TEC device with 18 L volume. From 33 °C to 22 °C, it took one hour to maintain this temperature with coefficient of performance of 0.2–0.6. Lv et al. [40] proposed a unique technique of PVRC-TE to enhance sky radiative cooling. With photovoltaic cells, some of the sun's radiation is used to produce electricity, decreasing the amount of solar radiation and heat absorbed, and improving diurnal radiant cooling. The PVRC-TE technology delivers significant power gains as well as cooling gains.

Ebrahimi et al. [41] developed a model with micro-combination of heating, cooling, and power generation features. They used a thermoelectric cooler as the cooling system. Shafee et al. [42] designed and tested a thermoelectric heating as well as cooling system that was cascaded and incorporated. For this cascading and integration configuration, the coefficient of performance were 0.02 and 0.294, respectively. Adeyanju et al. [43] investigated a fast drink cooler relying on TEC in attempt to chill water in a glass. The volumetric size of glass was 0.5 L and the time taken to chill was 2 min. It was done both experimentally and theoretically. Chiba et al. [44] investigated the Peltier and Seebeck effects in multistage thermoelectric coolers depending on hydrogen liquefier.

The refrigerants in traditional air conditioning systems with vapor-compression harm the global environment. Ma et al. [45] reported that TEC has the potential to be integrated into the framework of a building. Utilizing waste heat generated during cooling mode effectively will significantly increase the TE system's total *COP*.

4 Conclusions

TEC devices are attractive and in recent years have frequently been employed due to their easy operation and eco-friendly characteristics. Compact and quiet, they can switch between heating and cooling instantly and provide fine temperature control. They operate without the generation of greenhouse gases that damage ozone. But thermoelectric cooling technology is being confronted with performance challenges. In this review, the recent research on optimum design methods for TEC systems and their newer applications are summarized. Efficient TE cooling is a major way of reducing energy consumption and emissions of carbon. TE elements that can achieve limited cooling can be created thanks to the favorable growth in the semiconducting sector over the last decade. Up-scaling often goes at the expense of price, space, and efficiency of the system. Researchers are trying to improve TEC performance and applicability with innovative methods.

In summary, thermoelectric cooling devices have both industrial and personal applications. Growth in the market is positively influenced by the growing demand for

customized solutions with unique TEC systems for specific applications. The small size makes them a great choice when it comes to placing cooling equipment in small spaces. With additional advancements in system design, the future of TEC devices for commercial use appears bright. To maximize desired output, design methodologies that are more efficient are required and to realize the potential, modern manufacturing techniques must be employed. TE cooling approach thereby can effectively replace compressor-based cooling and new application fields can also be explored.

References

1. Cheng YH, Lin WK (2005) Geometric optimization of thermoelectric coolers in a confined volume using genetic algorithms. *Appl Therm Eng* 25:2983–2997
2. Shen L, Zhang W, Liu G, Tu Z, Lu Q, Chen H, Huang Q (2020) Performance enhancement investigation of thermoelectric cooler with segmented configuration. *Appl Therm Eng* 168:114852
3. Wang XD, Wang QH, Xu JL (2014) Performance analysis of two-stage TECs (thermoelectric coolers) using a three-dimensional heat-electricity coupled model. *Energy* 65:419–429
4. Lamba R, Manikandan S, Kaushik SC, Tyagi SK (2018) Thermodynamic modelling and performance optimization of trapezoidal thermoelectric cooler using genetic algorithm. *Therm Sci Eng Prog* 6:236–250
5. Lin S, Yu J (2016) Optimization of a trapezoid-type two-stage Peltier couples for thermoelectric cooling applications. *Int J Refrig* 65:103–110
6. Fraisse G, Ramousse J, Sgorlon D, Goupil C (2013) Comparison of different modeling approaches for thermoelectric elements. *Energy Convers Manag*
7. Riffat SB, Ma X, Wilson R (2006) Performance simulation and experimental testing of a novel thermoelectric heat pump system. *Appl Therm Eng* 26:494–501
8. Rowe DM (1995) CRC handbook of thermoelectrics
9. Astrain D, Vián JG, Martínez A, Rodríguez A (2010) Study of the influence of heat exchangers' thermal resistances on a thermoelectric generation system. *Energy* 35:602–610
10. Chen M, Snyder GJ (2013) Analytical and numerical parameter extraction for compact modeling of thermoelectric coolers. *Int J Heat Mass Transf* 60:689–699
11. Lineykin S, Ben-Yaakov S (2005) Analysis of thermoelectric coolers by a spice-compatible equivalent-circuit model. *IEEE Power Electron Lett* 3:63–66
12. Luo Z (2021) A simple method to estimate the physical characteristics of a thermoelectric cooler from vendor datasheets | Electronics cooling. <https://www.electronics-cooling.com/2008/08/a-simple-method-to-estimate-the-physical-characteristics-of-a-thermoelectric-cooler-from-vendor-datasheets/>. Last accessed 31 Mar 2021
13. Huang BJ, Chin CJ, Duang CL (2000) Design method of thermoelectric cooler. *Int J Refrig* 23:208–218
14. Mitrani D, Tomé JA, Salazar J, Turó A, García MJ, Chávez JA (2005) Methodology for extracting thermoelectric module parameters. *IEEE Trans Instrum Meas* 54:1548–1552
15. Allouhi A, Boharb A, Ratlamwala T, Kousksou T, Amine MB, Jamil A, Msaad AA (2017) Dynamic analysis of a thermoelectric heating system for space heating in a continuous-occupancy office room. *Appl Therm Eng* 113:150–159
16. McCarty R (2010) A comparison between numerical and simplified thermoelectric cooler models. *J Electron Mater* 39:1842–1847
17. Owoyele O, Ferguson S, O'Connor BT (2015) Performance analysis of a thermoelectric cooler with a corrugated architecture. *Appl Energy* 147:184–191
18. Khanh DVK, Vasant PM, Elamvazuthi I, Dieu VN (2017) Geometric optimisation of thermoelectric coolers using simulated annealing. *Int J Comput Sci Eng* 14:279–289

19. Lamba R, Kaushik SC, Tyagi SK (2018) Geometric optimization of trapezoidal thermoelectric heat pump considering contact resistances through genetic algorithm. *Int J Energy Res* 42:633–647
20. Qiu C, Shi W (2020) Comprehensive modeling for optimized design of a thermoelectric cooler with non-constant cross-section: theoretical considerations. *Appl Therm Eng* 176:115384
21. Lu T, Zhang X, Zhang J, Ning P, Li Y, Niu P (2019) Multi-objective optimization of thermoelectric cooler using genetic algorithms. *AIP Adv* 9:095105
22. Nemati A, Nami H, Yari M, Ranjbar F (2018) Effect of geometry and applied currents on the exergy and exergoeconomic performance of a two-stage cascaded thermoelectric cooler. *Int J Refrig* 85:1–12
23. Sadighi Dizaji H, Jafarmadar S, Khalilarya S, Pourhedayat S (2019) A comprehensive exergy analysis of a prototype Peltier air-cooler; experimental investigation. *Renew Energy* 131:308–317
24. Tan H, Fu H, Yu J (2017) Evaluating optimal cooling temperature of a single-stage thermoelectric cooler using thermodynamic second law. *Appl Therm Eng* 123:845–851
25. Zhu L, Yu J (2017) Optimization of heat sink of thermoelectric cooler using entropy generation analysis. *Int J Therm Sci* 118:168–175
26. Panigrahi N, Venkatesan K, Venkata Ramanan M (2019) Performance study of thermoelectric cooler using multiphysics simulation and numerical modelling. *Int J Ambient Energy*
27. Fong E, Lam TT, Fischer WD, Yuan SWK (2019) Analytical approach for study of transient performance of thermoelectric coolers. *J Thermophys Heat Transf* 33:96–105
28. Seo YM, Ha MY, Park SH, Lee GH, Kim YS, Park YG (2018) A numerical study on the performance of the thermoelectric module with different heat sink shapes. *Appl Therm Eng* 128:1082–1094
29. Ferreira-Teixeira S, Pereira AM (2018) Geometrical optimization of a thermoelectric device: numerical simulations. *Energy Convers Manag* 169:217–227
30. Çağlar A (2018) Optimization of operational conditions for a thermoelectric refrigerator and its performance analysis at optimum conditions. *Int J Refrig* 96:70–77
31. Giri JM, Nain PKS (2020) Performance optimization of thermoelectric cooler using genetic algorithm. *Math Model Eng Probl* 7:427–435
32. Cai Y, Zhang DD, Liu D, Zhao FY, Wang HQ (2019) Air source thermoelectric heat pump for simultaneous cold air delivery and hot water supply: full modeling and performance evaluation. *Renew Energy* 130:968–981
33. Zhou Y, Zhang T, Wang F, Yu Y (2018) Performance analysis of a novel thermoelectric assisted indirect evaporative cooling system. *Energy* 162:299–308
34. Liu Z, Zhang Y, Zhang L, Luo Y, Wu Z, Wu J, Yin Y, Hou G (2018) Modeling and simulation of a photovoltaic thermal-compound thermoelectric ventilator system. *Appl Energy* 228:1887–1900
35. Lal S, Kumari E (2017) Performance analysis of a low price thermoelectric cooler: an experimental approach. In: International conference on expo advances in power generation from renewable energy sources, pp 76–82
36. Patel V, Patel R, Patel J (2020) Theoretical and experimental investigation of bubble column humidification and thermoelectric cooler dehumidification water desalination system. *Int J Energy Res* 44:890–901
37. Afshari F (2021) Experimental and numerical investigation on thermoelectric coolers for comparing air-to-water to air-to-air refrigerators. *J Therm Anal Calorim* 144:855–868
38. Saifizi M, Zakaria MS, Yaacob S, Wan K (2018) Development and analysis of hybrid thermoelectric refrigerator systems. In: IOP Conference Series: Materials Science and Engineering. Institute of Physics Publishing, p 012036
39. Dongare V, Kinare R (2018) Design and development of thermoelectric refrigerator. *Int Res J Eng Technol* 5:2970–2974
40. Lv S, Ji Y, Qian Z, He W, Hu Z, Liu M (2021) A novel strategy of enhancing sky radiative cooling by solar photovoltaic-thermoelectric cooler. *Energy* 219:119625
41. Ebrahimi M, Derakhshan E (2018) Design and evaluation of a micro combined cooling, heating, and power system based on polymer exchange membrane fuel cell and thermoelectric cooler. *Energy Convers Manag* 171:507–517

42. Sm S, Gnanasekaran K, Johnson SA, Samuel J (2018) Performance study on thermoelectric cooling and heating system with cascaded and integrated approach. *Int J Chem Stud* 6:1348–1354
43. Adeyanju AA, Ekwue E, Compton W (2010) Experimental and theoretical analysis of a beverage chiller. *Res J Appl Sci* 5:195–203
44. Chiba Y, Marif Y, Boukaoud A, Brahim K, Tlemcani A, Henini N (2019) A multi stage study of thermoelectric device based on semi-conductor materials. In: *Lecture notes in networks and systems*. Springer, pp 560–565
45. Ma X, Zhao H, Zhao X, Li G, Shittu S (2019) Building integrated thermoelectric air conditioners—a potentially fully environmentally friendly solution in building services. *Futur Cities Environ* 5:12

Solar Photovoltaic System (SPV) Installation in Indian Rural Households



Suyash Sharma, Affan Khan, Kapil Rajput, and Shrikant Vidya

Abstract Conservative energy system, an alternative source for electrification in rural areas is needed. This is due to the advantages, rich availability of solar energy, and encouraging rural electrification policies in India. But India has still not accomplished the 100% rural electrification due to many technical, social, or financial reasons. In this paper, a wide possibility of solar photovoltaic system (SPV) Installation in rural households has been covered including the current scenario. Advantages of consuming solar energy that transforms the rural life into light were also highlighted including other projects and early implementation experience.

Keywords Solar energy · Solar photovoltaic system · Rural electrification · Rural households · Conservative energy system

1 Introduction

Due to shortage of remaining fuels and constantly increase in prices of fuels and demand in this decade, at some point it has shown a great opportunity to use sources of alternative energy [1]. But we need to reduce the sources of pollution in air worldwide and regulate the climate changes imperatively supports dependency on sustainable energies sources [2]. We could say that solar energy has been well chosen reliable and valuable source of energy to cover the restricted accessibility of the conventional energy sources [3]. SPV system covers wide range of applications and can shield rural/urban regions from pollution without any CO₂ emissions [4]. Countries including India utilize renewable sources of energy like solar, hydro, and wind energy, to compensate for their hefty energy requirement. Even though hydropower has nice possibility, it has not been exploited to its entire capability. India owns 6.4% of the earth's coal reserved, while oil sit is 0.55%. Basically, solar energy can easily be converted to thermal energy through solar collectors and electrical energy through photovoltaic (PV) cells, it is very eco-friendly.

S. Sharma · A. Khan · K. Rajput (✉) · S. Vidya
Department of Mechanical Engineering, Galgotias University, Greater Noida, India
e-mail: kapil.rajput@galgotiasuniversity.edu.in

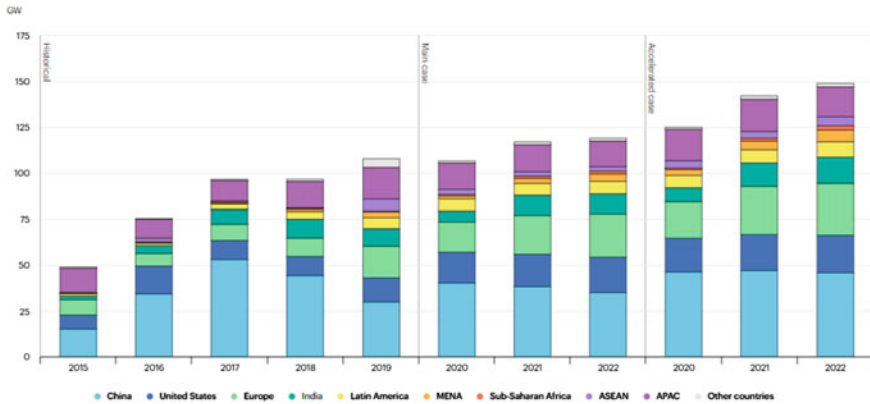


Fig. 1 Solar PV net capacity addition by country and region

Daylight seals the electromagnetic spectrum extending from visible light, infrared light, and ultraviolet light which might be used direct/indirect via transformation within electrical energy [5]. As reported in the Renewable Electricity Futures (RE futures) study by National Renewable Energy Laboratory in 2021, the technical and economical possibility of synthesizing 170 + gigawatts (GW) of solar energy into India's electricity network by 2022 [6]. Regardless of high-level early investing expenses, a home solar system (HSS) is a promising substitute for energy sources in many village areas in developing countries. Radiation-free and modesty features are the key benefits of HSSs. Furthermore, the total cost of SPV systems has weakened drastically, but their effectiveness had improved substantially with innovations in technology. Figure 1 depicts growth of solar PV net capacity on global level since 2015. China has an effective addition in the capacity and leading in accelerated graphs as well (Source: IEA). Conversely, in developed countries, currently, almost all of the rural residents have the reach of grid electricity. In conflict, in the countries which are developing, small scale (40–100 W) household solar systems are more important. About 1.7 billion people, mostly in Asia and Africa, are living without any electricity [7]. The HSS initiative initially called solar home systems (SHS) has achieved a great success in Bangladesh. Impacts of HSS's of rural households can be reviewed after the installation of the HSS's and may help to improve the living specifications of off-grid rural populations in the globe.

2 Working Principle of an HSS

Solar panels are contrived of numerous specific solar panels antennae known as solar photovoltaic (PV) or solar cells which transform daylight instantly into electricity known as photovoltaic effect [8]. Solar cells are generally substrate-type thin-film cells or translucent silicon cells on silicon or cadmium telluride substratum [9].

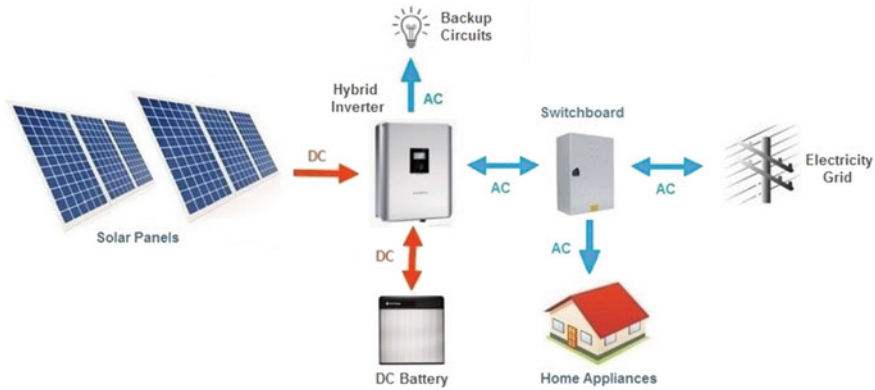


Fig. 2 Typical home solar system

These cells are lean (about one-hundredth of an inch), usually around 22 s to 25 cm², and have an average life of 25–30 years [10]. An HSS is consist of a solar panel, a controller or charge regulator, cables, batteries, an inverter to transform DC to AC for grid-based AC equipment, and switchboard for safety as shown in Fig. 2. An HSS normally conducted at a particular rated voltage of 12 V DC to deliver power for DC equipment that required less power like bulbs, lights, radio, and mini Televisions for around 2 to 5 h in one day [11]. The Photo Voltaic module is basically situated on rooftop at a particular angle at which it can accumulate maximum sunlight. The battery of the HSS could usually hold up storage capacity of 2–3 days in the occurrence of bad weather.

3 Significance and Showcases of Village Electrification

Significance of electrified villages while a critical built include for monetary growth of the nation had sometimes been recognized. Modern analysis data of village electrification signifies ensuing broad concord referring to the effect of electricity connections in village households [12]. Measurable advantages for the cost-saving and increased productivity include as usage of electricity for commercialization, household purpose, and agriculture. Village area electrification is an essential element of Multilingual Rural Advancement. In India, it has been assumed not as much significant because of the following grounds. Villages are situated from 4 to 70 km far-off from accessible grids or in two ways far away and are in challenging areas like hills, forests, and deserts. The quantity of households may be scaled between 3 and 120 with scattered dissemination of loads whose level of income is low hence paying capacity is also low [13]. Energy required in rural areas is very less and rural domestic buyers are mostly climax time consumers and donate for the poor load factors of 0.15–0.3.

4 Key Elements of Grid-Based Connection

In India rural electrification is borne out primarily by grid construction. The approach of linking an unelectrified rural area to nearby electrified rural areas has led to an ineffective, insurmountable distributing network [14–16]. Figure 3 shows that electricity connection to rural areas had been increased rapidly in last six decades. Government has organized many plans in these years for villages as rural areas have very low percentage of electricity connections. More than 5,00,000 villages have electricity connections to rural households. As per CEA (Central Electricity Authority) in India, approximately 597,464 villages have registered for electricity connections. The data below mentioned graph shows the number of villages got electrified from 1947 till 2020 in India. This graph clearly indicates the rise from nearly 3000 in 1950 to around 600,000 in 2020, which further keep on increases. Figure 4 clearly reflects the total Solar installed capacity of all the states within India till 2020. Karnataka is having the maximum capacity of 7328.86 followed by Rajasthan and Tamil Nadu. The top ten states namely Karnataka, Rajasthan, Tamil Nadu, Telangana, Gujarat, Andhra Pradesh, Madhya Pradesh, Maharashtra, Uttar Pradesh, and Punjab add in more than 90% of the total installed capacity [17–19]. Still, India has huge potential in the field of solar which can be harnessed in the near future by using proper policies and technology.

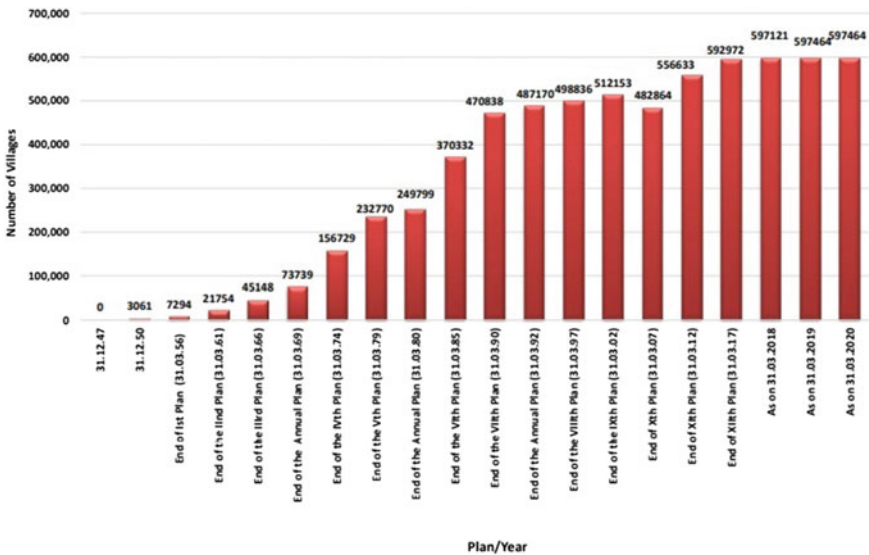


Fig. 3 Planwise growth of number of villages electrified in India

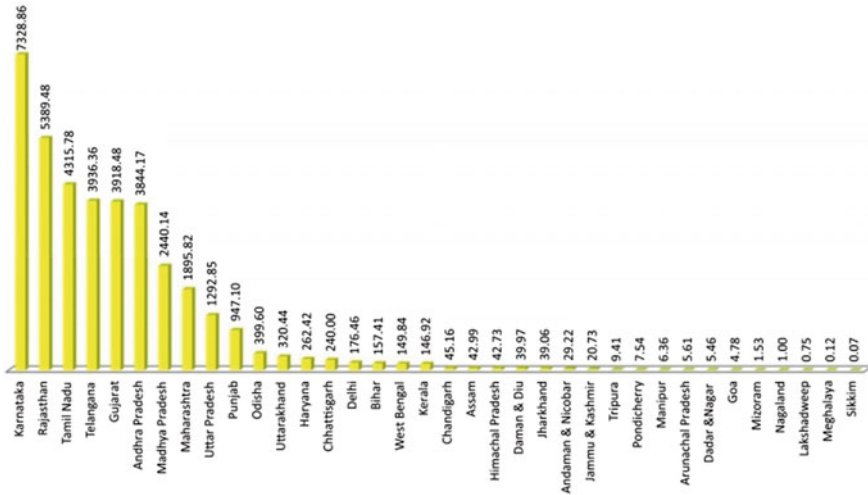


Fig. 4 Cumulative capacity of solar power installed till 31–12–2020. Source MNRE

5 Practicability of SPV for a Rural Household

Various factors such as construction and home size, weather, and family size affect a household’s regular energy consumption (ref: census 2017, average 5.4 persons in one house with three rooms). The cost of electricity in electrified areas has been estimated, ranging from 0.34 kWh per day per household for powerless houses to 0.83 kW per day per household on larger land for lighting purposes. For a family of five, a rural residence consists primarily of lighting, television, radio, and a fan.

According to IREDA, India’s waterless zone receives ample solar radiation (an average of six kilowatt-hour/m² in 24 h of solar insolation) having a potential of 20 megawatt/km². IREDA plans to electrify 78,500 communities by 2022, principally through solar photovoltaic (SPV) technology, with the goal of large-scale deployment of SPV technology by diverse industries in the next five years [20].

For various locations in India, daily solar radiation ranges from 4 to 7 KWh per square meter. The 22 years average of solar energy on occasion on latitude 15.47 and longitude 75.77 rural demonstrates that there is sufficient SPV in remote areas [21].

Most businesses have a minimum size for bottomless discharge batteries, which commonly range from 40 to 100 AH. In light of the higher price of a superior battery, it is extra cost-effective to choose for systems having panel capacities of ten or more (Figs. 5 and 6).

Solar machinery demonstrates an enormous capacity for reducing socioeconomic issues. Solar photovoltaic technology is unlike any other in terms of its compatibility with long-term growth. Solar energy has the potential to bring electricity to remote rural regions and improve rural living conditions.

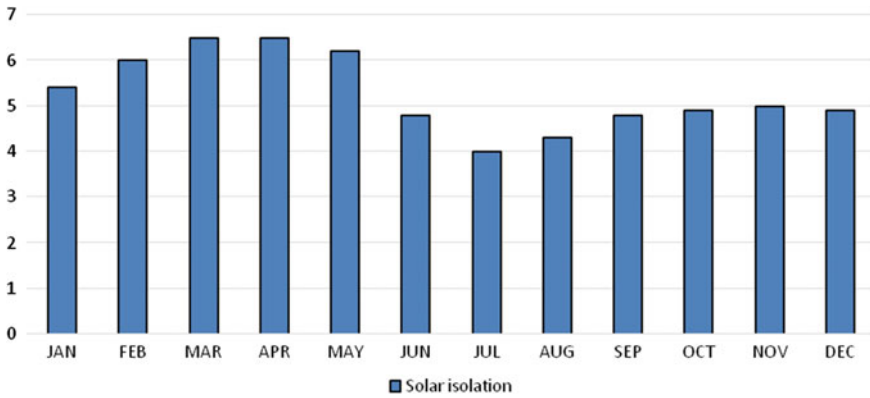


Fig. 5 Solar energy (KWh per day per m²)

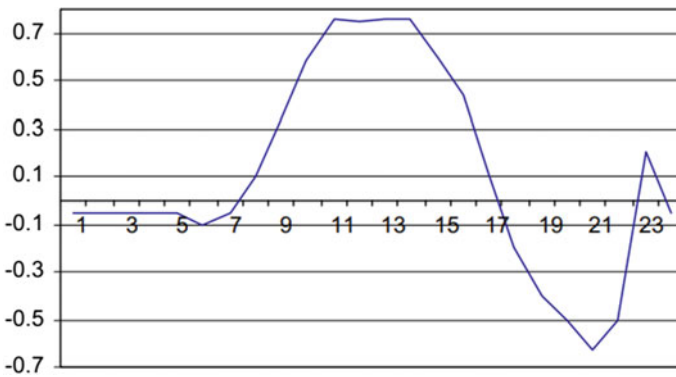


Fig. 6 Solar insolation (KWh) stored in a day

6 Conclusions

Countryside electrification may be a discerning catalyst to boost farming efficiency through modernization and is vital for several rural pursuits. Electrification cannot ensure economic process by itself, but it is a needed but inadequate situation. It performs best when it is in the midst of social and economic transportation expansion.

A sequence of small, medium, and durable approaches aids strategy makers to plan and execute the eco-friendly power programs for backward areas, shall bring the change in usual approach from just power usage to eco-friendly power generation assistance in step with, As per the Renewable Global Status Report 2020 update, about 3.5 million homes utilize HSS around the world. Until November 2017, 15 lakh HSSs had been installed in India. New initiatives will produce better results, yet more encouraging new approaches must be experienced to see if they will tackle

financial shortages, assets, environmental, and public health cares in the framework of the continuing worldwide reorganization of energy industries.

Here we have large opportunity for developing solar plates in India. Along with ongoing R&D and value cuts solar plates might become the foremost effective source of energy. With a strong inexhaustible energy strategy in situ, India is the predecessor in this particular field, there's room for firms, foreign money, regional monetary and institutional organizations, and others. solar power is often one in every of the main target areas because of its availability by the country in adequate amounts. We deserve and need to do something that will be good for ourselves and others to supply balanced growth to our ecosystem. Inexhaustible energy is the supply of nature, and it must be used for humankind in harmoniousness as well as congruence in our ecosystem.

References

1. Baghaee HR, Mirsalim M, Gharehpetian GB, Talebi HA (2016) Reliability/cost-based multi-objective Pareto optimal design of stand-alone wind/PV/FC generation microgrid system. *Energy* 115:1022–1041
2. Kabakian V, McManus MC, Harajli H (2015) Attributional life cycle assessment of mounted 1.8 kWp monocrystalline photovoltaic system with batteries and comparison with fossil energy production system. *Appl Energy* 154:428–437
3. Roohollahi E, Mehrabian M, Abdolzadeh M (2013) Prediction of solar energy gain on 3-D geometries. *Energy Build* 62:315–322
4. Shazly J, Hafez A, El Shenawy E, Eteiba M (2014) Simulation, design and thermal analysis of a solar Stirling engine using MATLAB. *Energy Convers Manage* 79:626–639
5. Khan S, Towfiq R, Hossain S (2012) A brief study of the prospect of solar energy in generation of electricity in Bangladesh. *JRSE*, pp 1–8
6. National Renewable Energy Laboratory (2012) U.S. Renewable Energy Technical Potentials: A GIS-Based Analysis; National Renewable Energy Laboratory, Golden, CO, USA
7. World Bank. Where does the world stand in reaching sustainable energy objective
8. International Energy Agency. Photovoltaic power systems program
9. Bangladesh Power Development Board (BPDB) (2014) Annual Report 2012–2013. Bangladesh Power Development Board (BPDB), Dhaka, Bangladesh
10. Mondal AH, Klein D (2011) Impacts of solar home systems on social development in rural Bangladesh. *Energy Sustain Dev* 15:17–20
11. Khan SA, Azad AKMAM (2014) Social impact of solar home system in rural Bangladesh: a case study of rural zone. *Energy Environ* 1:5–22
12. Munasinghe M (1990) Rural electrification in the third world. *IEEE Power Eng J*, pp 189–202; Wang J, Fundamentals of erbium-doped fiber amplifiers arrays (Periodical style—Submitted for publication). *IEEE J Quant Electron*, submitted for publication
13. Burt E, Peter O, Susan B (2013) Scientific evidence of health effects from coal use in energy generation. University of Illinois at Chicago, Chicago IL USA
14. Kharecha P, Hansen J, Coal and gas are far more harmful than nuclear power
15. Samad HA, Khandker SR, Asaduzzaman M, Yunus M (2013) The benefits of solar home systems: an analysis from Bangladesh. Policy Research Working Paper; No. 6724. World Bank, Washington, DC, USA
16. Renew Economy. Why solar costs will fall another 40% in just two years
17. Infrastructure Development Company Limited (IDCOL) (2016) Request for Expression of Interest (REoI) & Terms of Reference (ToR): selection of software development firm for developing enterprise resource planning (ERP) for automation of IDCOL solar home system program. Infrastructure Development Company Limited (IDCOL), Dhaka, Bangladesh

18. Li S, Haskew TA, Li D, Hu F (2011) Integrating photovoltaic and power converter characteristics for energy extraction study of solar PV systems. *Renew Energy* 36:3238–3245
19. An BI, Kim GB (2012) Development of structured hybrid illumination system and optimum illumination condition selection for detection of surface defects on silicon wafer in solar cell. *J Korean Soc Mech Eng A* 36:336–337
20. Neuhaus DH, Münzer A (2007) Industrial silicon wafer solar cells. *Adv OptoElectron* 2007:24521
21. Phadke A, Jacobson A, Park WY, Lee GR, Alstone P, Khare A (2015) Powering a Home with Just 25 Watts of Solar PV: super-efficient appliances can enable expanded off-grid energy service using small solar power systems. Berkeley, CA, USA, Lawrence Berkeley National Laboratory, pp 234–256